Pertanika Journal of

SCIENCE & TECHNOLOGY

JST

VOL. 28 (S2) 2020

A special issue devoted to
Applied Engineering and Sciences

Guest Editors
Hidayah Ariffin, Norhayati Ramli and Suhaidi Shafie

PERTANIKA JOURNALS

A scientific journal published by Universiti Putra Malaysia Press

Pertanika Journal of Science & Technology

About the Journal

Overview

Pertanika Journal of Science & Technology (PJST) is the official journal of Universiti Putra Malaysia published by UPM Press. It is an open-access online scientific journal which is free of charge. It publishes the scientific outputs. It neither accepts nor commissions third party content.

Recognized internationally as the leading peer-reviewed interdisciplinary journal devoted to the publication of original papers, it serves as a forum for practical approaches to improving quality in issues pertaining to science and engineering and its related fields.

PJST is a **quarterly** (January, April, July and October) periodical that considers for publication original articles as per its scope. The journal publishes in **English** and it is open to authors around the world regardless of the nationality.

The Journal is available world-wide.

Aims and scope

Pertanika Journal of Science and Technology aims to provide a forum for high quality research related to science and engineering research. Areas relevant to the scope of the journal include: bioinformatics, bioscience, biotechnology and bio-molecular sciences, chemistry, computer science, ecology, engineering, engineering design, environmental control and management, mathematics and statistics, medicine and health sciences, nanotechnology, physics, safety and emergency management, and related fields of study.

History

Pertanika was founded in 1978. A decision was made in 1992 to streamline *Pertanika* into three journals as Pertanika Journal of Tropical Agricultural Science, Pertanika Journal of Science & Technology, and Pertanika Journal of Social Sciences & Humanities to meet the need for specialised journals in areas of study aligned with the interdisciplinary strengths of the university.

After almost 28 years, as an interdisciplinary Journal of Science & Technology, the journal now focuses on research in science and engineering and its related fields.

Goal of *Pertanika*

Our goal is to bring the highest quality research to the widest possible audience.

Quality

We aim for excellence, sustained by a responsible and professional approach to journal publishing. Submissions are guaranteed to receive a decision within 14 weeks. The elapsed time from submission to publication for the articles averages 5-6 months.

Abstracting and indexing of *Pertanika*

The journal is indexed in SCOPUS (Elsevier), Clarivate-Emerging Sources Citation Index [ESCI (Web of Science)], BIOSIS, National Agricultural Science (NAL), Google Scholar, MyCite and ISC.

Future vision

We are continuously improving access to our journal archives, content, and research services. We have the drive to realise exciting new horizons that will benefit not only the academic community, but society itself.

Citing journal articles

The abbreviation for Pertanika Journal of Science & Technology is *Pertanika J. Sci. Technol.*

Publication policy

Pertanika policy prohibits an author from submitting the same manuscript for concurrent consideration by two or more publications. It prohibits as well publication of any manuscript that has already been published either in whole or substantial part elsewhere. It also does not permit publication of manuscript that has been published in full in Proceedings.

Code of Ethics

The *Pertanika* Journals and Universiti Putra Malaysia takes seriously the responsibility of all of its journal publications to reflect the highest in publication ethics. Thus all journals and journal editors are expected to abide by the Journal's codes of ethics. Refer to *Pertanika*'s **Code of Ethics** for full details, or visit the Journal's web link at http://www.pertanika.upm.edu.my/code_of_ethics.php

International Standard Serial Number (ISSN)

An ISSN is an 8-digit code used to identify periodicals such as journals of all kinds and on all media–print and electronic. All *Pertanika* journals have ISSN as well as an e-ISSN.

Pertanika Journal of Science & Technology: ISSN 0128-7680 (*Print*); ISSN 2231-8526 (*Online*).

Lag time

A decision on acceptance or rejection of a manuscript is reached in 3 to 4 months (average 14 weeks). The elapsed time from submission to publication for the articles averages 5-6 months.

Authorship

Authors are not permitted to add or remove any names from the authorship provided at the time of initial submission without the consent of the Journal's Chief Executive Editor.

Manuscript preparation

Refer to *Pertanika*'s **Instructions to Authors** at the back of this journal.

Editorial process

Authors are notified with an acknowledgement containing a *Manuscript ID* on receipt of a manuscript, and upon the editorial decision regarding publication.

Pertanika follows a **double-blind peer-review** process. Manuscripts deemed suitable for publication are usually sent to reviewers. Authors are encouraged to suggest names of at least three potential reviewers at the time of submission of their manuscript to *Pertanika*, but the editors will make the final choice. The editors are not, however, bound by these suggestions.

Notification of the editorial decision is usually provided within ten to fourteen weeks from the receipt of manuscript. Publication of solicited manuscripts is not guaranteed. In most cases, manuscripts are accepted conditionally, pending an author's revision of the material.

The Journal's peer-review

In the peer-review process, three referees independently evaluate the scientific quality of the submitted manuscripts.

Peer reviewers are experts chosen by journal editors to provide written assessment of the **strengths** and **weaknesses** of written research, with the aim of improving the reporting of research and identifying the most appropriate and highest quality material for the journal.

Pertanika Journal of Science & Technology
Pertanika Journal of Science & Technology
Pertanika Journal of Science & Technology

Operating and review process

What happens to a manuscript once it is submitted to *Pertanika*? Typically, there are seven steps to the editorial review process:

1. The Journal's Chief Executive Editor (CEE) and the Editorial Board Members (EBMs) examine the paper to determine whether it is appropriate for the journal and should be reviewed. If not appropriate, the manuscript is rejected outright and the author is informed.

2. The CEE sends the article-identifying information having been removed, to 2 or 3 reviewers who are specialists in the subject matter represented by the article. The CEE requests them to complete the review within 3 weeks.

   Comments to authors are about the appropriateness and adequacy of the theoretical or conceptual framework, literature review, method, results and discussion, and conclusions. Reviewers often include suggestions for strengthening of the manuscript. Comments to the editor are in the nature of the significance of the work and its potential contribution to the research field.

3. The Editor-in-Chief (EiC) examines the review reports and decides whether to accept or reject the manuscript, invites the author(s) to revise and resubmit the manuscript, or seek additional review reports. Final acceptance or rejection rests with the CEE and EiC, who reserve the right to refuse any material for publication. In rare instances, the manuscript is accepted with almost no revision. Almost without exception, reviewers' comments (to the author) are forwarded to the author. If a revision is indicated, the editor provides guidelines to the authors for attending to the reviewers' suggestions and perhaps additional advice about revising the manuscript.

4. The authors decide whether and how to address the reviewers' comments and criticisms and the editor's concerns. The authors return a revised version of the paper to the CEE along with specific information describing how they have answered' the concerns of the reviewers and the editor, usually in a tabular form. The author(s) may also submit a rebuttal if there is a need especially when the authors disagree with certain comments provided by reviewer(s).

5. The CEE sends the revised paper out for re-review. Typically, at least 1 of the original reviewers will be asked to examine the article.

6. When the reviewers have completed their work, the EiC examines their comments and decides whether the paper is ready to be published, needs another round of revisions, or should be rejected. If the decision is to accept, the CEE is notified.

7. The CEE reserves the final right to accept or reject any material for publication, if the processing of a particular manuscript is deemed not to be in compliance with the S.O.P. of *Pertanika*. An acceptance letter is sent to all authors.

   The editorial office ensures that the manuscript adheres to the correct style (in-text citations, the reference list, and tables are typical areas of concern, clarity, and grammar). The authors are asked to respond to any minor queries by the editorial office. Following these corrections, page proofs are mailed to the corresponding authors for their final approval. At this point, **only essential changes are accepted**. Finally, the manuscript appears in the pages of the journal and is posted online.

Pertanika Journal of

SCIENCE & TECHNOLOGY

A special issue devoted to

Applied Engineering and Sciences

VOL. 28 (S2) 2020

(Special Issue)

Guest Editors

Hidayah Ariffin, Norhayati Ramli and Suhaidi Shafie

PERTANIKA JOURNALS

A scientific journal published by Universiti Putra Malaysia Press

PJST

Pertanika Journal of Science & Technology

AN INTERNATIONAL PEER-REVIEWED JOURNAL

EDITOR-IN-CHIEF

LUQMAN CHUAH ABDULLAH

Chemical Engineering

CHIEF EXECUTIVE EDITOR

Abu Bakar Salleh

Biotechnology and Biomolecular Science

UNIVERSITY PUBLICATIONS COMMITTEE

Zulkifli Idrus, *Chair*

EDITORIAL STAFF

Journal Officers:

Kanagamalar Silvarajoo, *ScholarOne*

Siti Zuhaila, *ScholarOne*

Tee Syin Ying, *ScholarOne*

Ummi Fairuz Hanapi, *ScholarOne*

Editorial Assistants:

Ku Ida Mastura Ku Baharon

Siti Juridah Mat Arip

Zulinaardawati Kamarudin

PRODUCTION STAFF

Pre-press Officers:

Nur Farrah Dila Ismail

Wong Lih Jiun

WEBMASTER

IT Officer:

Munir Hayat

EDITORIAL OFFICE

EDITORIAL OFFICE

JOURNAL DIVISION
Putra Science Park
1st Floor, IDEA Tower II
UPM-MTDC Technology Centre
Universiti Putra Malaysia
43400 Serdang, Selangor Malaysia.
Gen Enq.: +603 9769 1622 | 1616
E-mail:
executive_editor.pertanika@upm.edu.my
URL: www.journals-jd.upm.edu.my

PUBLISHER

UPM Press
Universiti Putra Malaysia
43400 UPM, Serdang, Selangor, Malaysia.
Tel: +603 9769 8855
E-mail: penerbit@putra.upm.edu.my
URL: http://penerbit.upm.edu.my

EDITORIAL BOARD

2020-2022

Abdul Latif Ahmad
Chemical Engineering
Universiti Sains Malaysia, Malaysia

Adem Kilicman
Mathematical Sciences
Universiti Putra Malaysia, Malaysia

Ahmad Zaharin Aris
Hydrochemistry, Environmental Chemistry, Environmental Forensics, Heavy Metals
Universiti Putra Malaysia, Malaysia

Azlina Harun@Kamaruddin
Enzyme Technology, Fermentation Technology
Universiti Sains Malaysia, Malaysia

Bassim H. Hameed
Chemical Engineering: Reaction Engineering, Environmental Catalysis & Adsorption
Qatar University, Qatar

Biswajeet Pradhan
Digital image processing, Geographical Information System (GIS), Remote Sensing
University of Technology Sydney, Australia

Daud Ahmad Israf Ali
Cell Biology, Biochemical, Pharmacology
Universiti Putra Malaysia, Malaysia

Hari M. Srivastava
Mathematics and Statistics
University of Victoria, Canada

Ho Yuh-Shan
Water research, Chemical Engineering and Environmental studies
Asia University, Taiwan

Hsiu-Po Kuo
Chemical Engineering
National Taiwan University, Taiwan

Ivan D. Rukhlenko
Nonliner Optics, Silicon Photonics, Plasmonics and Nanotechnology
The University of Sydney, Australia

Lee Keat Teong
Energy Environment, Reaction Engineering, Waste Utilization, Renewable Energy
Universiti Sains Malaysia, Malaysia

Mohamed Othman
Communication Technology and Network, Scientific Computing
Universiti Putra Malaysia, Malaysia

Mohammad Jawaid
Polymers and Plastics, Colloid and Surface Chemistry, Composite and Hybrid Materials, Chemical Engineering
Universiti Putra Malaysia, Malaysia

Mohd. Ali Hassan
Bioprocess Engineering, Environmental Biotehnology
Universiti Putra Malaysia, Malaysia

Mohd Sapuan Salit
Concurrent Engineering and Composite Materials
Universiti Putra Malaysia, Malaysia

Najafpour Darzi Ghasem
Bioprocess Technology, Chemical Engineering, Water and Wastewater Treatment Technology, Biochemical Engineering and Biotechnology, Bioethanol, Biofuel, Biohydrogen, Enzyme and Fermentation Technology
Babol Noshirvani University of Technology, Iran

Nor Azah Yusof
Biosensors, Chemical Sensor, Functional Material
Universiti Putra Malaysia, Malaysia

Norbahiah Misran
Communication Engineering
Universiti Kebangsaan Malaysia, Malaysia

Roslan Abd-Shukor
Physics & Materials Physics, Superconducting Materials
Universiti Kebangsaan Malaysia, Malaysia

Wing Keong Ng
Aquaculture, Aquatic Animal Nutrition, Aqua Feed Technology
Universiti Sains Malaysia, Malaysia

INTERNATIONAL ADVISORY BOARD

2018-2021

Adarsh Sandhu
Editorial Consultant for Nature Nanotechnology and Contributing Writer for Nature Photonics, Physics, Magnetoresistive Semiconducting Magnetic Field Sensors, Nano-Bio-Magnetism, Magnetic Particle Colloids, Point of Care Diagnostics, Medical Physics, Scanning Hall Probe Microscopy, Synthesis and Application of Graphene
Electronics-Inspired Interdisciplinary Research Institute (EIIRIS), Toyohashi University of Technology, Japan

Graham Megson
Computer Science
The University of Westminster, U.K

Kuan-Chong Ting
Agricultural and Biological Engineering
University of Illinois at Urbana-Champaign, USA

Malin Premaratne
Advanced Computing and Simulation
Monash University, Australia

Mohammed Ismail Elnaggar
Electrical Engineering
Ohio State University, USA

Peter J. Heggs
Chemical Engineering
University of Leeds, U.K

Ravi Prakash
Vice Chancellor, JUIT, Mechanical Engineering, Machine Design, Biomedical and Materials Science
Jaypee University of Information Technology, Indian

Said S.E.H. Elnashaie
Environmental and Sustainable Engineering
Penn. State University at Harrisburg, USA

Suhash Chandra Dutta Roy
Electrical Engineering
Indian Institute of Technology (IIT) Delhi, India

Vijay Arora
Quantum and Nano-Engineering Processes
Wilkes University, USA

Yi Li
Chemistry, Photochemical Studies, Organic Compounds, Chemical Engineering
Chinese Academy of Sciences, Beijing, China

ABSTRACTING AND INDEXING OF PERTANIKA JOURNALS

Pertanika is over 40 years old; this accumulated knowledge has resulted in the journals being abstracted and indexed in SCOPUS (Elsevier), Clarivate-Emerging Sources Citation Index [ESCI (Web of Science)], BIOSIS, National Agricultural Science (NAL), Google Scholar, MyCite and ISC.

The publisher of Pertanika will not be responsible for the statements made by the authors in any articles published in the journal. Under no circumstances will the publisher of this publication be liable for any loss or damage caused by your reliance on the advice, opinion or information obtained either explicitly or implied through the contents of this publication.

All rights of reproduction are reserved in respect of all papers, articles, illustrations, etc., published in Pertanika. Pertanika provides free access to the full text of research articles for anyone, web-wide. It does not charge either its authors or author-institution for refereeing/publishing outgoing articles or user-institution for accessing incoming articles.

No material published in Pertanika may be reproduced or stored on microfilm or in electronic, optical or magnetic form without the written authorization of the Publisher.

Copyright © 2019 Universiti Putra Malaysia Press. All Rights Reserved.

Pertanika Journal of Science & Technology
Vol. 28 (S2) 2020

Contents

Applied Engineering and Sciences

Preface
Hidayah Ariffin, Norhayati Ramli and Suhaidi Shafie i

Detection of Muscle Activities in the sEMG Signal by Using Frequency Features and Adaptive Decision Threshold 1
Husamuldeen Khalid Hameed, Wan Zuha Wan Hasan, Suhaidi Shafie, Siti Anom Ahmad and Haslina Jaafar and Liyana Najwa Inche Mat

Proposal of Blood Glucose Control and Exercise Therapy Support System Using Non-invasive Blood Glucose Meter 13
Ryo Takeuchi, Kazuhiko Nagao and Hiroyuki Miyamoto

Application of Ecological Indices using Macroinvertebrate Assemblages in Relation to Aquaculture Activities in Rawang Sub-basin, Selangor River, Malaysia 25
Nadeesha Dilani Hettige, Rohasliney Binti Hashim, Ahmad Bin Abas Kutty, Nor Rohaizah Binti Jamil and Zulfa Hanan Binti Ash'aari

The Construction of Plant Expression Vector harbouring *Carica Papaya* L. *WRKY* Gene in *Escherichia coli* 47
Fauziah Abu Bakar, Pavitra Paramalingam and Kamariah Hasan

Regression Equation Between Required Force and Lumbar Load of Caregiver in Supporting Standing-up Motion via Computational Musculoskeletal Simulation 59
Kodai Kitagawa, Yoshiki Nishisako, Takayuki Nagasaki, Sota Nakano, Mitsumasa Hida, Shogo Okamatsu and Chikamune Wada

Linear Regression Technique for Improvement of Feet Position Estimation during Standing Balance Using a Cane with Millimeter Wave Radar 71
Ibai Gorordo Fernandez, Kodai Kitagawa, Kawthar Abdul Rahman, Azura Che Soh, Alpha Agape Gopalai, Siti Anom Ahmad and Chikamune Wada

Acetylcholine Receptor-based Biosensor Derived from Asian Swamp Eel, *Monopterus Albus* for Heavy Metals Biomonitoring 83
Siti Aishah Muhammad Khalidi, Mohd Khalizan Sabullah, Suraya Abdul Sani, Mohd Yunus Abd Shukor, Ain Aqilah Basirun, A'aishah Abd Gafar, 'Izazy Nur Mohd Jaafar and Noreen Nordin

Profiling of Cholinesterase Extracted from The Brain Tissue of Diodon hystrix and Its Inhibition Reaction Towards Carbamates 95
Akid Haris, Noreen Nordin, Nur Azizah Mustapa, Suraya Abd. Sani, Mohd Yunus Shukor and Mohd Khalizan Sabullah

Cholinesterase from the Liver of *Diodon hystrix* for Detection of Metal Ions 107
Noreen Nordin, Ronaldo Ron Cletus, Mohd Khalizan Sabullah, Siti Aishah Muhammad Khalidi, Rahmath Abdulla and Siti Aqlima Ahmad

Isolation and Characterisation of Thermophilic *Bacillus licheniformis* SUNGC2 as Producer of *α*-Amylase from Malaysian Hot Spring 121
Marwan Jawad Msarah, Ayesha Firdose, Izyanti Ibrahim and Wan Syaidatul Aqma

Effect of Steam and Bleaching Treatment on the Characteristics of Pineapple Leaves Fibre Derived Cellulose 135
Surenthiran Gnanasekaran, Siti Nur Najihah Muslih, Jun Haslinda Shariffuddin, and Noor Ida Amalina Ahamad Nordin

Physical and Mechanical Study of Palm Oil Fuel Ash (POFA) based Geopolymer as a Stabilizer for Soft Soil 149
Isam Adnan Khasib and Nik Norsyahariati Nik Daud

Deep Learning Object Detector Using a Combination of Convolutional Neural Network (CNN) Architecture (MiniVGGNet) and Classic Object Detection Algorithm 161
Asmida Ismail, Siti Anom Ahmad, Azura Che Soh, Mohd Khair Hassan and Hazreen Haizi Harith

Integrated Braking Force Distribution for Electric Vehicle Regenerative Braking System 173
Anith Khairunnisa Ghazali, Mohd Khair Hassan, Mohd Amran Mohd Radzi and Azizan As'arry

Design and Synthesis of a New Amphipathic Cyclic Decapeptide with Rapid, Stable, and Continuous Antibacterial Effects 183
Hisham N. Farrag, Khaled Metwally, Shinya Ikeno and Tamaki Kato

Enzyme Kinetics Study for Heterogeneous System of Pretreated Kenaf Hydrolysis 197
Nur Izyan Wan Azelee, Norhafiza Nordin, Rosli Md Illias, Nor Hasmaliana Abdul Manas and Mohd Nazlee Faisal Md Ghazali

Effect of Reaction Temperature on the Growth of Carbon Nanotubes from Waste Natural Rubber Glove 217
Mohammad Adib Hazan, Syazwani Mohamad, Mohamad Amin Hamid, Shahira Liza, Md Shuhazlly Mamat, Kar Fei Chan and Yazid Yaakob

Secured Electrocardiograph (ECG) Signal Using Partially Homomorphic Encryption Technique–RSA Algorithm 231
Muhammad Umair Shaikh, Wan Azizun Wan Adnan and Siti Anom Ahmad

Dark Fermentative Biohydrogen Production from Palm oil Mill Effluent: Operation Factors and Future Progress of Biohydrogen Energy 243
Fatin Sakinah Rosman, Mohd Zulkhairi Mohd Yusoff, Mohd Rafein Zakaria, Toshinari Maeda and Mohd Ali Hassan

Cellulose Nanofibers from Waste Paper and their Utilization as Reinforcement Materials in Poly((*R*)-3-Hydroxybutyrate-*co*-(*R*)-3-Hydroxyhexanoate Bionanocomposite 259
Tengku Arisyah Tengku Yasim-Anuar, Nur Sharmila Sharip, Liana Noor Megashah, Hidayah Ariffin and Nor Azlin Muhamad Nor

Nutritional Characteristics of Biochar from Pineapple Leaf Residue and Sago Waste 273
Norshidawatie Bohari, Hasmah Mohidin, Juferi Idris, Yoshito Andou, Sulaiman Man, Hushairy Saidan and Suraiya Mahdian

Static Mechanical, Thermal Stability, and Interfacial Properties of Superheated Steam Treated Oil Palm Biomass Reinforced Polypropylene Biocomposite 287
Muhammad Nazmir Mohd Warid, Tengku Arisyah Tengku Yasim-Anuar, Hidayah Ariffin, Mohd Ali Hassan, Yoshito Andou and Yoshihito Shirai

Parameters Optimization in Compression Molding of Ultra-high Molecular Weight Polyethylene/Cellulose Nanofiber Bio-nanocomposites by using Response Surface Methodology 299
Nur Sharmila Sharip, Hidayah Ariffin, Yoshito Andou, Ezyana Kamal Bahrin, Mohammad Jawaid, Paridah Md Tahir and Nor Azowa Ibrahim

Reducing Attribute Non-Attendance Risk in Choice Experiment: An application of Design Attribute Relative Importance Index for Waste Management Service Provision in Segmented Markets 317
Shehu Usman Adam, Shaufique F. Sidique and Mad Nasir Shamsudin

Preface

We are delighted to present the special issue of Pertanika Journal of Science and Technology (PJST). This special issue includes selected papers presented at the 7th International Symposium on Applied Engineering and Sciences (SAES2019), an international symposium jointly organized by Universiti Putra Malaysia (UPM) and Kyushu Institute of Technology (Kyutech), Japan. SAES2019 was held on 11th – 12th November 2019 at UPM, Malaysia. This annual international symposium serves as a unique platform for academics, researchers, students, scientists and engineers to share their research breakthrough, discuss the latest developments and innovations, as well as to share and interact among themselves on the current and emerging trends, and state-of-the-art technologies in the areas of Applied Engineering and Sciences.

SAES covers wide areas of Engineering & Technology, Materials Science, and Biomedical Sciences & Applied Biology. More than 300 papers were presented during SAES2019, and 24 of the papers were selected for publication in this special issue under a stringent peer-review process; 8 of the papers were categorized under Engineering & Technology, 8 Materials Science, 7 Biomedical Sciences & Applied Biology and 1 was from Environmental Science. All papers were reviewed by the experts in the areas from local and abroad.

We would like to take this opportunity to thank all the contributors for their contributions in this special issue. Congratulations to the authors whose papers are selected for publication! We are very grateful to have a full commitment from the dedicated reviewers in assisting the team to publish high quality articles. We also would like to extend our gratitude to the Pertanika JST Editor-in-Chief, Pertanika Chief Executive Editor and the publishing team for their support and guidance throughout the process. Special thanks to the members of SAES2019 Scientific Committee for their effort and assistance which have certainly making this publication a success.

It is hoped that this special issue would be beneficial to the readers in shaping their research and innovation strategies.

Enjoy reading!

Guest Editors

Hidayah Ariffin *(Professor Dr)*
Norhayati Ramli *(Assoc. Professor Dr)*
Suhaidi Shafie *(Assoc. Professor Dr)*

Pertanika J. Sci. & Technol. 28 (S2): 1 - 11 (2020)

PERTANIKA JOURNALS

SCIENCE & TECHNOLOGY

Journal homepage: http://www.pertanika.upm.edu.my/

Detection of Muscle Activities in the sEMG Signal by Using Frequency Features and Adaptive Decision Threshold

Husamuldeen Khalid Hameed[1]*, Wan Zuha Wan Hasan[1,2], Suhaidi Shafie[2], Siti Anom Ahmad[1] and Haslina Jaafar[1] and Liyana Najwa Inche Mat[3]

[1]Department of Electrical and Electronic Engineering, Faculty of Engineering, Universiti Putra Malaysia, 43400 UPM Serdang, Selangor, Malaysia
[2]Institute of Advanced Technology (ITMA), Universiti Putra Malaysia, 43400 UPM Serdang, Selangor, Malaysia
[3]Department of Medicine, Faculty of Medicine and Health Sciences, Universiti Putra Malaysia, 43400 UPM Serdang, Selangor, Malaysia

ABSTRACT

Reliable detection of muscle activities from the surface electromyography (sEMG) signal is an important factor that makes the sEMG controlled orthotic devices a practical tool for assisting disabled people. In spite of the advantages of employing the sEMG signal as a control signal, the changes in the amplitude characteristics of this signal due to many factors and consequent variations in the required decision threshold may impede this control paradigm from being a reliable control method for such devices. Therefore, the performance of the algorithms intended to detect muscle activities should be immune against the involuntary amplitude variations of the sEMG signal. Moreover, the decision threshold value must be adaptive to the changes in the sEMG signal characteristics to reduce the number of false alarms that may arise with the fixed threshold and lead to unintended movements to these devices. In this paper, an amplitude-independent algorithm had been developed with an adaptive decision threshold; the algorithm employed only frequency features of the sEMG signal to detect muscle activities. These features are the previously developed Adaptive Zero Crossing feature and the new proposed Adaptive Wilson Amplitude feature. The Mean Instantaneous Frequency value of the sEMG signal was used as an

ARTICLE INFO

Article history:
Received: 10 February 2020
Accepted: 13 November 2020
Published: 31 December 2020

DOI: https://doi.org/10.47836/pjst.28.S2.01

E-mail addresses:
husamuldeen72@gmail.com (Husamuldeen Khalid Hameed)
wanzuha@upm.edu.my (Wan Zuha Wan Hasan)
suhaidi@upm.edu.my (Suhaidi Shafie)
sanom@upm.edu.my (Siti Anom Ahmad)
jhaslina@upm.edu.my (Haslina Jaafar)
liyananajwa@upm.edu.my (Liyana Najwa Inche Mat)
*Corresponding author

ISSN: 0128-7680
e-ISSN: 2231-8526

© Universiti Putra Malaysia Press

adaptive decision threshold value to improve the detection performance and to minimize the number of false alarms produced with the utilization of inappropriate fixed decision threshold value. A comparison with an amplitude-independent algorithm that employed fixed decision threshold had revealed an improved performance regarding the resistance against false alarms.

Keywords: Adaptive decision threshold, false alarms, frequency features, muscle activity detection, sEMG

INTRODUCTION

Control of orthotic and prosthetic robotic devices by employing sEMG signals has acquired a lot of attention due to the advantages of this control method. One of the most important advantages is the naturalness, because this control method requires the same type of muscle activities used to move the limb which makes the control more natural (Meeker et al., 2017). Other advantages like simplicity in obtaining sEMG signal by surface electrodes as well as the little time delay between human intent and the real movement of the device (Rosen et al., 2001) have made this control method the most common type used to operate orthotic devices (Lobo-Prat et al., 2014). However, robust sEMG control is still a challenging process because of the variations in the amplitude characteristics of the sEMG signal due to many factors. Factors like electrode location, electrode movement, skin electrical impedance, fatigue, and sweat are affecting the amplitude of the sEMG over the time (Huang et al., 2015; Marchal-Crespo et al., 2009). Moreover, the amplitudes of the sEMG signals are not constant during the recording time due to the variations in the characteristics of the electrode-skin interface and due to the changes in the level of the ground reference signal (Severini et al., 2012). Therefore, the algorithms intended to detect muscle activities should be resistant against the involuntary amplitude variations of the signal and should have an adaptive decision threshold that adapts the algorithm detection to the variations in the sEMG signal level.

In the literature, various algorithms have been proposed to detect muscle activities from the sEMG signal. The conventional algorithms compare the amplitude features of the signal with a predefined threshold value, this threshold must be determined according to the amplitude of the measured signal during no activity period and must be modified whenever this amplitude changes. More complicated algorithms have been developed to overcome the problem of the predefined fixed threshold. Xu et al. (2013) had developed a detection algorithm based on the maximum likelihood method improved by an adaptive threshold, but this method depended on the signal amplitude features to report muscle activities. Yang et al. (2017) had enhanced the detection algorithm based on the Teager Kaiser Energy (TKE) operator by employing two image technologies to detect the amplitude variations in the

weak and noisy sEMG signal. Zhang and Zhan (2012) had developed a muscle activity detection algorithm against spurious background spikes by using sample entropy analysis of the sEMG signal, but this method required high computation efforts and therefore it was difficult to be implemented in real time. Moreover, it needed to preset threshold value for the muscle activity onset detection. Liu and Liu (2016) had developed a detection algorithm by employing the integrated profile of the sEMG signal in the presence of the spurious background spikes for the spinal cord injury patients, but this method depended on the changes in the amplitude of the sEMG signal to report the muscle activities. By using the continuous wavelet transform, Merlo et al. (2003) had developed a detection algorithm to detect the amplitude variations of the sEMG signal in order to report the muscle activities. Semmaoui et al. (2012) had developed an adaptive threshold for the Smoothed Teager Energy Operator detection method, but this method was amplitude dependent. Severini et al. (2012) had improved the Bonato double threshold detection method by making the decision threshold value adaptive to the variations in the sEMG signal to noise ratio, but still this method depended on the amplitude characteristics to report the muscle activities.

To our knowledge, only three amplitude-independent studies (D'Anna et al., 2019; Hameed et al., 2017, 2018) have been proposed in the literature to detect sEMG muscle activities, where the study in D'Anna et al. (2019) was an improvement to the algorithm presented in Hameed et al. (2017), but all these studies are with fixed decision threshold. In this paper, an amplitude-independent algorithm with an adaptive decision threshold value is proposed to detect muscle activities. The algorithm has the ability to detect muscle activities that have a low signal to noise ratio (SNR). The algorithm employs two frequency features in the detection process which are the Adaptive Zero Crossing (Hameed et al., 2017) and the new proposed feature which is the Adaptive Wilson Amplitude. In contrast to its name, the Wilson Amplitude is a frequency feature of the sEMG signal (Phinyomark et al., 2012). The algorithm utilizes the Mean Instantaneous Frequency of the sEMG signal as an adaptive decision threshold value to report muscle activities. It is hypothesized that the employment of the proposed Wilson feature will enhance the muscle activity detection process, as well as the use of the adaptive threshold, will reduce the number of false alarms compared to the fixed threshold algorithm presented in (Hameed et al., 2017). This research tests this hypothesis.

MATERIALS AND METHOD

The sEMG signal from the forearm muscle responsible for fingers flexion (Flexor Digitorum Superficialis muscle) of a healthy subject was obtained and amplified by using a muscle sensor (MyoWare from the Advancer Technology). The subject was ordered to generate a weak muscle activity every about two seconds, then to generate one weak muscle activity about every five seconds, then to stop generating muscle activities. The analog sEMG

signal was sampled at 1000 samples per second and converted to a digital signal by using an analog to digital converter (NI USB-6001 DAQ from National Instruments). The digital input samples were grouped into segments of 100 samples per segment and the proposed muscle activity detection algorithm developed by using LabVIEW software was applied in real time for each segment. The hardware setup used to conduct the experiments is illustrated in Figure 1. Figure 2 shows the flow diagram of the proposed algorithm.

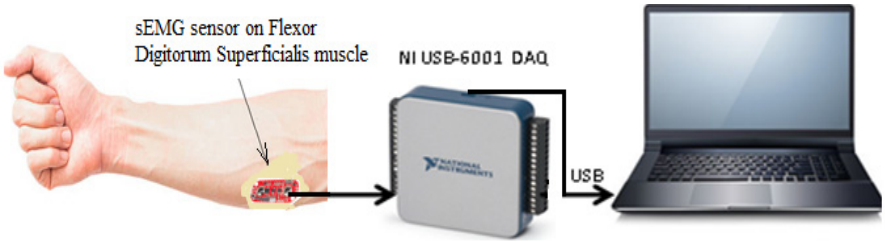

Figure 1. The hardware setup

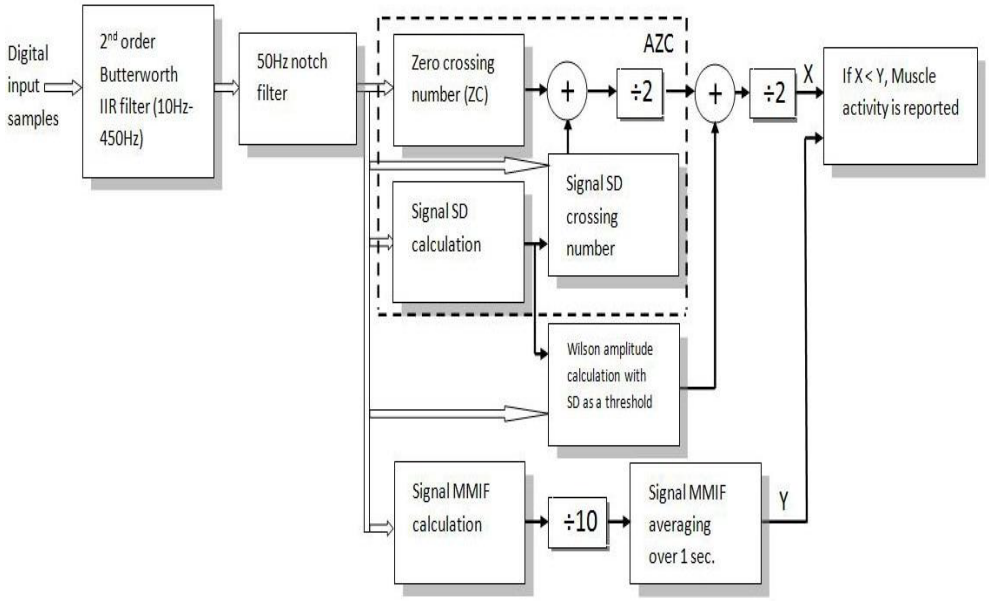

Figure 2. Muscle activity detection algorithm

A Bandpass filter was used to attenuate the artifact and high frequency noises, and then a notch filter was employed to remove the power line interference. The proposed Adaptive Wilson Amplitude (AWA) feature was extracted for each segment and averaged with the

Adaptive Zero Crossing (AZC) feature (dotted line in Figure 2). The result was compared with the adaptive threshold value; a muscle activity was declared if the (AZC+AWA)/2 value was less than the threshold value. To compute the adaptive decision threshold value, the Mean Instantaneous Frequency values for each segment were calculated by using the Gabor Transform, and then the mean of the Mean Instantaneous Frequency values (MMIF) for each segment was computed. The MMIF value is divided by 10 in order to make it within the same range of AZC and AWA values. These (MMIF/10) values were averaged over one second during no muscle activity period to represent the adaptive decision threshold value. The one second period is selected as a compromise between greater periods which leads to reduce adaptation ability and smaller periods which leads to reduce flatness of the threshold line, where this reduction in the flatness increases the possibility of misdetection and false alarms. Since the MMIF values were decreased during muscle activity periods, the averaging process took the last average (MMIF/10) value of the no muscle activity period as a threshold value during muscle activity period to prevent dropping in the threshold line. The proposed algorithm is adaptive and does not need to preset any value before the operation.

The proposed *AWA* feature was computed by using the signal Standard Deviation (SD) for each segment as a new threshold value instead of the fixed threshold value used in the traditional Wilson Amplitude feature (WA). This new threshold makes the *AWA* value independent of the sEMG signal amplitude and does not need to preset a threshold value based on the signal amplitude during no activity period. The proposed *AWA* feature is defined for each segment as:

$$AWA = \sum_{n=0}^{N-1} \quad f(|x(n) - x(n-1)|) \qquad [1]$$

$$\text{where } f(x) = \begin{cases} 1 & if\ x \geq SD \\ 0 & otherwise \end{cases}$$

where *x(n)* is input samples, *N* is the number of samples in each segment, *SD* is the standard deviation of the segment and it is calculated as:

$$SD = \sqrt{\left(\sum_{n=0}^{N-1} \quad (x(n) - \mu)^2\right)/N} \qquad [2]$$

where μ is the segment mean value and it is calculated as:

$$\mu = \left(\sum_{n=0}^{N-1} \quad x(n)\right)/N \qquad [3]$$

The *AZC* value for each segment is calculated by averaging the two values, *ZC* and *SDC*, as *(ZC+SDC)/2* (Hameed et al., 2017), where *ZC* value of the segment (number of times that sEMG signal crosses the zero volt line) is calculated as:

$$ZC = \sum_{n=0}^{N-1} \quad f(x(n) \times x(n-1)) \qquad [4]$$

where $f(x) = \begin{cases} 1 & if\ x \leq 0 \\ 0 & otherwise \end{cases}$

the *SDC* value of the segment (number of times that sEMG signal crosses the standard deviation of the segment) is calculated as:

$$SDC = \sum_{n=0}^{N-1} \quad f([x(n) - SD] \times [x(n-1) - SD]) \qquad [5]$$

where $f(x) = \begin{cases} 1 & if\ x \leq 0 \\ 0 & otherwise \end{cases}$

RESULTS

Figure 3 clarifies the difference in the behavior of AWA and WA values when the muscle activities are present. The AWA value decreased when the muscle activity was present,

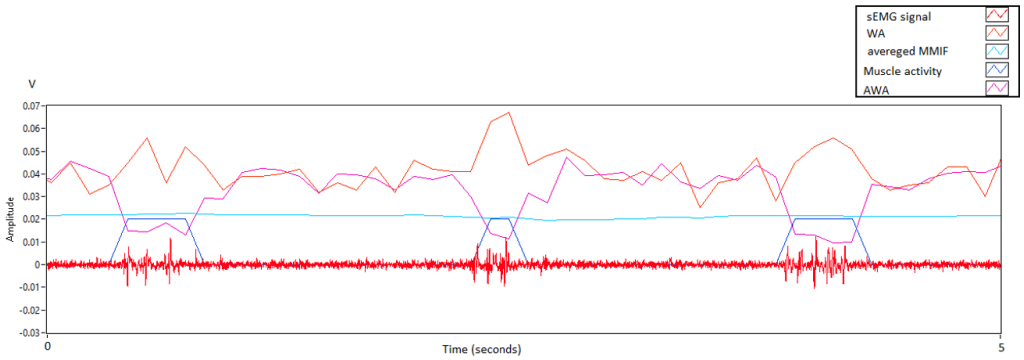

while WA value increased with the presence of muscle activity.

Figure 3. Comparison of the WA value (fixed threshold) and AWA value (SD as a threshold) for sEMG signal with three muscle activities (presented by the blue lines); WA, AWA and averaged MMIF are divided by 1000 to enable presenting in the same chart with the sEMG signal.

Averaging of AWA value with the AZC value was used to enhance the muscle activity detection process as shown in Figure 4, were employing the AZC alone had failed to detect the muscle activity. Moreover, the averaging process enhanced muscle activity detection in noisy sEMG signals as illustrated in Figure 5. Furthermore, the averaging enhanced muscle activity detection time and made it more accurate because the average value was more precise for detecting the period of muscle activity as clarified in Figure 6.

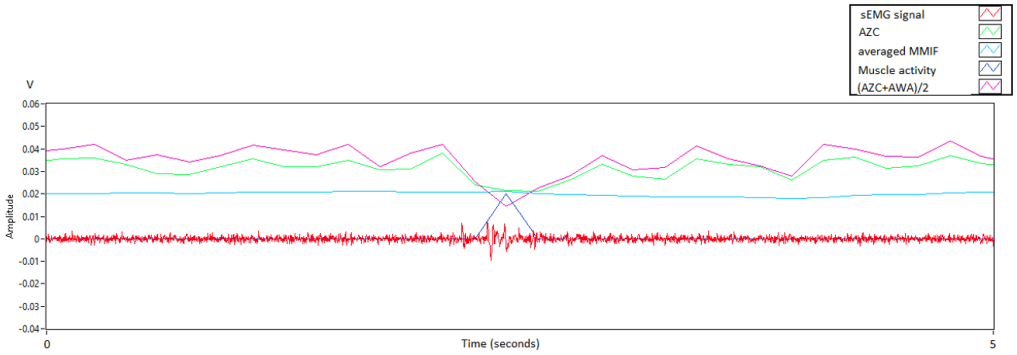

Figure 4. sEMG signal with one muscle activity (presented by the blue line); Employing of the (AZC+AWA)/2 instead of AZC alone enhances the muscle activity detection. AZC, (AZC+AWA)/2 and averaged MMIF are divided by 1000 to enable presenting in the same chart with the sEMG signal

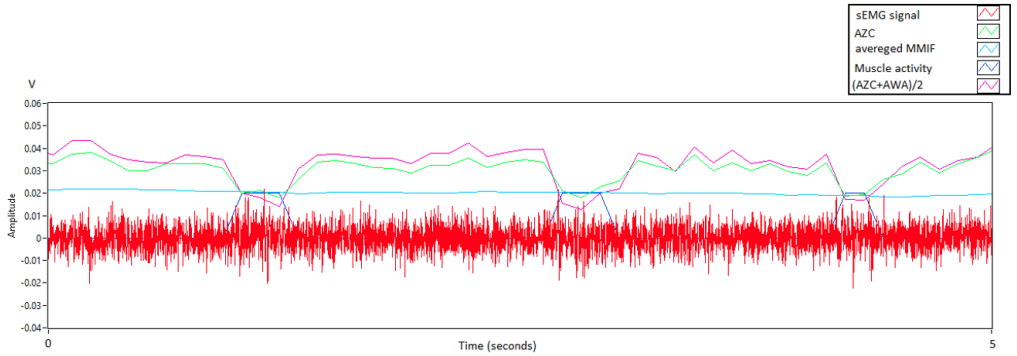

Figure 5. Noisy sEMG signal with three muscle activities (presented by the blue lines); Employing of the (AZC+AWA)/2 enhances the detection of muscle activities in the noisy signal. AZC, (AZC+AWA)/2 and averaged MMIF are divided by 1000 to enable presenting in the same chart with the sEMG signal

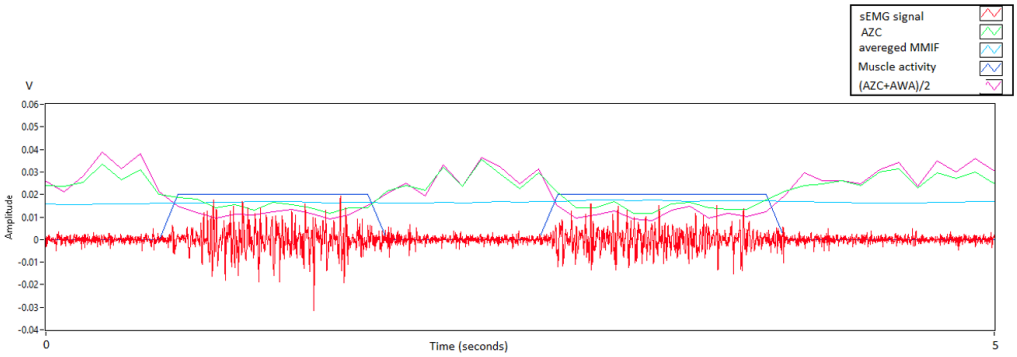

Figure 6. sEMG signal with two muscle activities (presented by the blue lines); Employing of the (AZC+AWA)/2 improves the accuracy of the muscle activity detection. AZC, (AZC+AWA)/2 and averaged MMIF are divided by 1000 to enable presenting in the same chart with the sEMG signal

Utilization of the averaged MMIF value as an adaptive decision threshold value reduces the possibility of generating false alarms. The adaptive threshold value decreased when the sEMG signal was contaminated by low frequency noise components as illustrated in Figure 7 and increased when the signal was contaminated by high frequency noise components as shown in Figure 8. This adaptation makes the threshold value to stay as close as to the (AZC+AWA)/2 value in order to detect muscle activities and far enough to avoid false alarms that may arise due to the presented noise components.

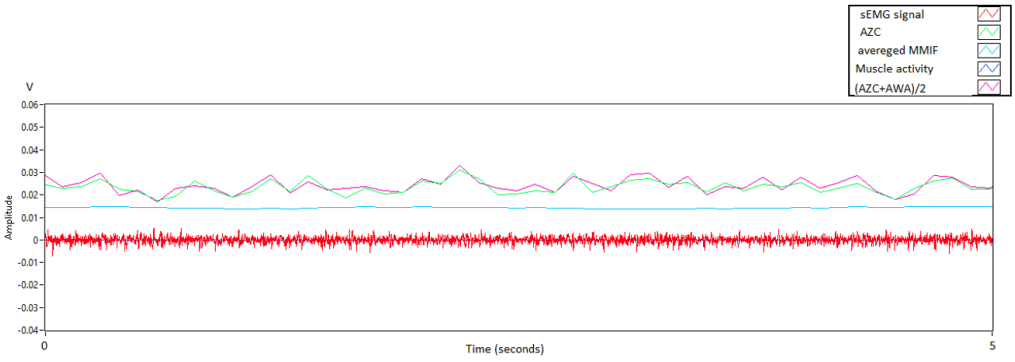

Figure 7. sEMG signal without muscle activities, the adaptive threshold value is about 15; AZC, (AZC+AWA)/2 and averaged MMIF are divided by 1000 to enable presenting in the same chart with the sEMG signal

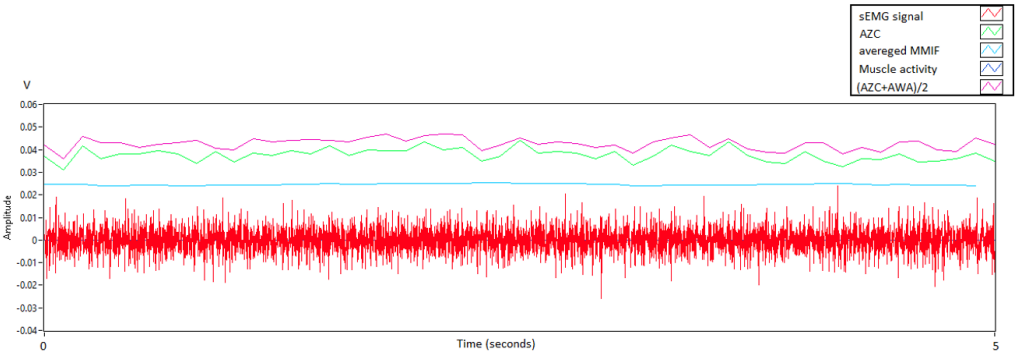

Figure 8. sEMG signal without muscle activities, the adaptive threshold value is about 25; AZC, (AZC+AWA)/2 and averaged MMIF are divided by 1000 to enable presenting in the same chart with the sEMG signal

DISCUSSION

Employing the proposed AWA feature as well as the adaptive decision threshold value had enhanced the muscle activity detection process because the average value (AZC+AWA)/2 was less than the AZC value during muscle activity period which increased the possibility

of detection as shown in Figures 4, 5 and 6. Moreover, the averaging process minimized the possibility of false alarms because the average value was greater than AZC value during no muscle activity period and therefore it was more distant from the threshold value.

The previous algorithm presented in Hameed et al. (2017) had employed the MMIF of the signal to enhance the detection process by multiplying the AZC value with the normalized MMIF value as ((MMIF/200) × AZC); the previous algorithm assumed that the average value of MMIF was 200Hz during no activity period, therefore it divided the MMIF by 200 to normalize it. Due to the imposed low or high frequency noise components, this process may lead to false alarms when the average value of MMIF is not 200Hz. Therefore, the proposed algorithm employs the MMIF feature as an adaptive decision threshold value by averaging the MMIF values over one second during no activity periods. This averaged value is used as a decision threshold value adapted to the variations in the sEMG signal characteristics as shown in Figures 7 and 8. Moreover, the previous algorithm employs a fixed decision threshold value to decide whether a muscle activity is reported or not, this process leads to false alarms when an inappropriate threshold value is chosen, consequently, the fixed threshold value must be predefined properly according to sEMG signal characteristics. In contrast, the proposed algorithm does not need to predefine a threshold value; it is defined automatically according to the MMIF of the sEMG signal.

A comparison was conducted by using real sEMG signal between the fixed threshold algorithm presented in Hameed et al. (2017) and the proposed adaptive threshold algorithm with respect to the resistance against false alarms (threshold value of 25 was chosen for the previous algorithm as was selected in Hameed et al. (2017). Since the sEMG signal used in the experiment was contaminated by low frequency noise components, the previous algorithm had produced many false alarms because of the high fixed threshold value of 25. In contrast, the proposed algorithm did not generate any false alarm due to the advantage of employing adaptive decision threshold as illustrated in Figure 9.

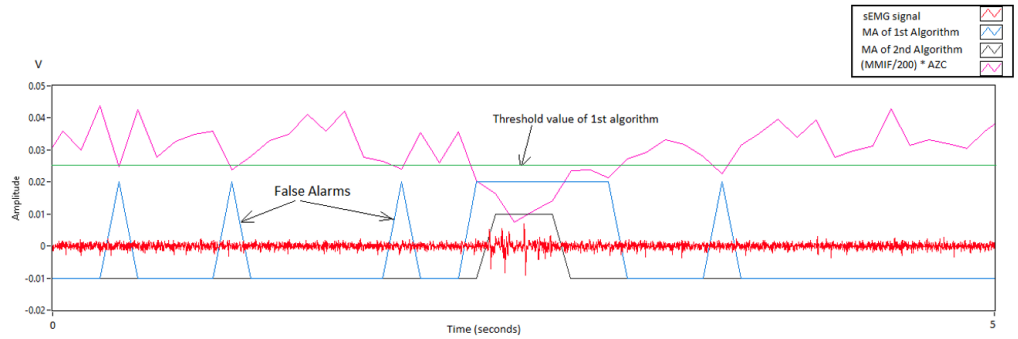

Figure 9. sEMG signal with one muscle activity (presented by the black line); A comparison between the performance of the previous algorithm (1st algorithm presented in [13] Hameed et al., 2017) and the proposed algorithm (2nd) regarding the resistance against false alarms. (MMIF/200)×AZC and the threshold value are divided by 1000 to enable presenting in the same chart with the sEMG signal. MA: Muscle Activity

CONCLUSIONS

An improved muscle activity detection algorithm with a new proposed frequency feature and adaptive decision threshold value has been successfully developed. The algorithm is amplitude-independent because it employs only frequency features to report muscle activities from the sEMG signal. In addition to the previously developed Adaptive Zero Crossing (AZC) feature, the algorithm employs the newly developed Adaptive Wilson Amplitude feature (AWA) to enhance the muscle activity detection process and improve resistance against false alarms. The algorithm employs an adaptive threshold value based on the Mean Instantaneous Frequency of the sEMG signal to improve the detection process and to reduce false alarms that may arise when unsuitable fixed threshold value is used. The efficacy of the algorithm has been evaluated in real time on a healthy subject by using the sEMG signal collected from the forearm muscle responsible for finger flexion (Flexor Digitorum Superficialis). A comparison between the proposed algorithm and the amplitude-independent algorithm that has a fixed decision threshold presented in Hameed et al., (2017) showed improved performance for the proposed algorithm in terms of resistance against false alarms.

For future work, the efficacy of the proposed algorithm will be verified on stroke patients to enable the utilization of this algorithm for controlling robotic devices devoted to disabled people.

ACKNOWLEDGEMENT

The authors would like to thank the Ministry of Education, Malaysia for supporting and funding this study under the MOE-FRGS scheme with grant number of 03-01-17-1893FR.

REFERENCES

D'Anna, C., Varrecchia, T., Schmid, M., & Conforto, S. (2019). Using the frequency signature to detect muscular activity in weak and noisy myoelectric signals. *Biomedical Signal Processing and Control,* 52, 69-76. doi:10.1016/j.bspc.2019.02.026

Hameed, H., Hassan, W., Shafie, S., Ahmad, S., & Jaafar, H. (2017, August, 23-25). An amplitude independent muscle activity detection algorithm based on adaptive zero crossing technique and mean instantaneous frequency of the sEMG signal. In *IEEE Regional Symposium on Micro and Nanoelectronics (RSM)*. Batu Ferringhi, Malaysia.

Hameed, H., Hassan, W., Shafie, S., Ahmad, S., & Jaafar, H. (2018, November 28-30). Soft robotic glove system controlled with amplitude independent muscle activity detection algorithm by using single sEMG channel. In *IEEE 5th International Conference on Smart Instrumentation, Measurement and Applications (ICSIMA 2018)*. Songkhla, Thailand.

Huang, J., Huo, W., Xu, W., Mohammed, S., & Amirat, Y. (2015). Control of upper-limb power-assist exoskeleton using a human-robot interface based on motion intention recognition. *IEEE Transactions on Automation Science and Engineering*, 12(4), 1257-1270. doi: 10.1109/tase.2015.2466634

Liu, J., & Liu, Q. (2016). Use of the integrated profile for voluntary muscle activity detection using EMG signals with spurious background spikes: A study with incomplete spinal cord injury. *Biomedical Signal Processing and Control*, 24, 19-24. doi:10.1016/j.bspc.2015.09.004

Lobo-Prat, J., Kooren, P., Stienen, A., Herder, J., Koopman, B., & Veltink, P. (2014). Non-invasive control interfaces for intention detection in active movement-assistive devices. *Journal of NeuroEngineering and Rehabilitation*, *11*(1), 1-22. doi: 10.1186/1743-0003-11-168

Marchal-Crespo, L., & Reinkensmeyer, D. (2009). Review of control strategies for robotic movement training after neurologic injury. *Journal of NeuroEngineering and Rehabilitation*, *6*(1), 1-15. doi: 10.1186/1743-0003-6-20

Meeker, C., Park, S., Bishop, L., Stein, J., & Ciocarlie, M. (2017, July, 17-20). EMG pattern classification to control a hand orthosis for functional grasp assistance after stroke. In *International Conference on Rehabilitation Robotics (ICORR)* (pp. 1203-1210). QEII Centre, London, UK.

Merlo, A., Farina, D., & Merletti, R. (2003). A fast and reliable technique for muscle activity detection from surface EMG signals. *IEEE Transactions on Biomedical Engineering*, *50*(3), 316-323. doi: 10.1109/tbme.2003.808829

Phinyomark, A., Phukpattaranont, P., & Limsakul, C. (2012). Feature reduction and selection for EMG signal classification. *Expert Systems with Applications*, *39*(8), 7420-7431. doi: 10.1016/j.eswa.2012.01.102

Rosen, J., Brand, M., Fuchs, M. B. & Arcan, M. (2001). A myosignal-based powered exoskeleton system. *IEEE Transactions on Systems, Man and Cybernetics, Part A: Systems and Humans*, *31*(3), 210-222. doi: 10.1109/3468.925661

Semmaoui, H., Drolet, J., Lakhssassi, A., & Sawan, M. (2012). Setting adaptive spike detection threshold for smoothed TEO based on robust statistics theory. *IEEE Transactions on Biomedical Engineering*, *59*(2), 474-482. doi: 10.1109/tbme.2011.2174992

Severini, G., Conforto, S., Schmid, M., & D'Alessio, T. (2012). Novel formelation of a double threshold algorithm for estimation of muscle activation intervals designed for variable SNR environments. *Journal of Electromyography and Kinesiology*, *22*(6), 878-885. doi: 10.1016/j.jelekin.2012.04.010

Xu, Q., Quan, Y., Yang, L., & He, J. (2013). An adaptive algorithm for the determination of the onset and offset of muscle contraction by EMG signal processing. *IEEE Transactions on Neural Systems and Rehabilitation Engineering*, *21*(1), 65-73. doi:10.1109/tnsre.2012.2226916

Yang, D., Zhang, H., Gu, Y., & Liu, H. (2017). Accurate EMG onset detection in pathological, weak and noisy myoelectric signals. *Biomedical Signal Processing and Control*, *33*, 306-315. doi: 10.1016/j.bspc.2016.12.014

Zhang, X., & Zhan, P. (2012). Sample entropy analysis of surface EMG for improved muscle activity onset detection against spurious background spikes. *Journal of Electromyography and Kinesiology*, *22*(6), 901-907. doi: 10.1016/j.jelekin.2012.06.005

Pertanika J. Sci. & Technol. 28 (S2): 13 - 24 (2020)

PERTANIKA JOURNALS

SCIENCE & TECHNOLOGY

Journal homepage: http://www.pertanika.upm.edu.my/

Proposal of Blood Glucose Control and Exercise Therapy Support System Using Non-invasive Blood Glucose Meter

Ryo Takeuchi[1]*, Kazuhiko Nagao[2] and Hiroyuki Miyamoto[1]

[1]Department of Human Intelligence Systems, Graduate School of Life Science and Systems Engineering, Kyushu Institute of Technology, in Japan, 2-4 Hibikino, Wakamatsu-ku, Kitakyushu, Fukuoka 808-0196, Japan
[2]Information Science and Technology Department, National Institute of Technology, Yuge College, in Japan, 1000,Yuge Shimoyuge, Ochi Gun Kamijima, Ehime 794-2593,Japan

ABSTRACT

According to WHO, 420 million adults worldwide are suffering from diabetes. The diabetic patient should regularly verify and control their blood glucose levels. However, the existing blood glucose meters use a needle to collect blood, thus causing problems such as pain and infections. A non-invasive blood glucose meter is a measuring instrument that can avoid these problems, but such an instrument has not been developed to date. Diabetic patients should ensure blood glucose control and exercise therapy: however, the difficulty of management and lack of guidance on exercise therapy are problematic issues that need to be overcome. In this study, a non-invasive blood glucose meter and blood glucose control system has been developed, which can be used along with a healthcare sensor equipped with a non-invasive blood glucose measurement function.

Keywords: Blood glucose, blood glucose monitoring, MHC, non-invasive

ARTICLE INFO

Article history:
Received: 10 February 2020
Accepted: 13 November 2020
Published: 31 December 2020

DOI: https://doi.org/10.47836/pjst.28.S2.02

E-mail addresses:
Takeuchi.ryo182@mail.kyutech.jp (Ryo Takeuchi)
nagao@info.yuge.ac.jp (Kazuhiko Nagao)
miyamo@brain.kyutech.ac.jp (Hiroyuki Miyamoto)
*Corresponding author

INTRODUCTION

Diabetes is one of the top ten causes of death. World Health Organization (WHO) has announced that 420 million adults worldwide suffer from diabetes. (World Health Organization [WHO], 2017). The treatment of diabetic patients is aimed at preventing the development and exacerbation of complications that are characteristic of diabetes and those that are

ISSN: 0128-7680
e-ISSN: 2231-8526

© Universiti Putra Malaysia Press

more likely to occur with diabetes, thus maintaining a quality of life similar to that of healthy people (Haneda et al., 2018). For diabetes management, blood glucose levels must be measured on a regular basis. Henson et al. (2016) studied changes in blood glucose levels in postmenopausal women at high risk for type 2 diabetes in three patterns. The pattern was 7.5 hours of continuous sitting (Pattern 1), 5 minutes of standing (Pattern 2) every 30 minutes, and 5 minutes of walking (Pattern 3) every 30 minutes. The area under the curve of blood glucose was reduced by approximately 30% in pattern 2 and pattern 3 compared to pattern 1 (Henson et al., 2016). The Honda et al. (2016) study also investigated whether short-term stair climbing at 60 and 120 minutes postprandial promoted postprandial hypoglycemia in patients with type 2 diabetes. As a result, the blood glucose level during stair ascent and the descent was significantly lower than that during postprandial rest (Honda et al., 2016). In addition, the effectiveness of physical exercise and aerobic exercise for treating and preventing diabetes has been confirmed, and exercise therapy is considered as the basic treatment of diabetes along with diet therapy. (Kodama et al., 2013; Sone et al., 2013). Therefore, diabetic patients must measure blood glucose levels, and control trends in blood glucose levels, exercise, and diet to prevent diabetes from worsening.

Currently, self-monitoring blood glucose meters that can measure blood glucose levels at home are available commercially. Using such meters, the blood glucose level can be confirmed: however current blood glucose self-monitoring devices require a blood sample from a fingertip using a needle: consequently, various problems have arisen (Patton & Clements, 2012; Vashist, 2012). First, because the measurement is performed using a needle, it is painful and the patient is stressed during each measurement. Both needles and test strips are expensive because they are disposable: however, they can cause infections when blood is drawn. Moreover, for diabetes management, depending on the severity of the disease, continuous blood glucose monitoring and blood glucose measurements are required several times a day, which may cause inflammation in the blood collection area. To solve these problems, an inexpensive measuring instrument is required, which does not require replacement of needle or test paper for each measurement, does not cause any sanitary problems, and does not require blood collection, and can be easily measured at home. For a long time, such devices are called noninvasive blood glucose meters and have been studied. Major noninvasive methods of measuring blood glucose include metabolic heat conformation (MHC) and optical techniques (Kit & Kassim, 2013; Megha & Joshi, 2015; Villena et al., 2019). In this study, MHC technology is used, which is advantageous in the miniaturization of the sensor. In addition to developing a non-invasive blood glucose meter, the simplification of blood glucose level management is another problem that needs to be solved. Arakawa et al. (2015) reported that patients receiving exercise therapy had lower levels of hemoglobin A1c (HbA1c) and frequent instructions. However, Arakawa et al. (2015) reported that exercise therapy for diabetes required less frequent instruction than

diet therapy and that there was no specialist in exercise instruction at medical institutions. Furthermore, it is impossible to provide support for exercise therapy for patients with diabetes who are being treated at home because of their health conditions. In this study, we focus on glycemic control in diabetic patients and develop a new system for glycemic control using smartphones and support of exercise therapy.

MATERIALS AND METHODS

Figure 1 shows the system configuration of this system, which is a configuration diagram of a new blood sugar management system developed by the authors. It comprises two systems: a healthcare sensor and a blood glucose control system, both of which have been developed by the authors.

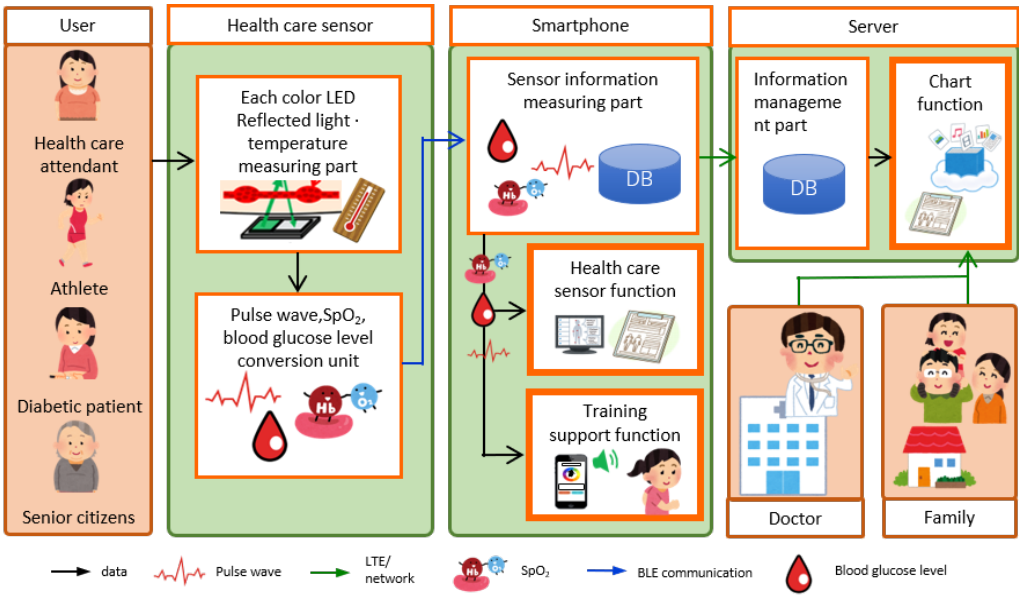

*Figure 1.*System configuration

Non-invasive Measurement of Blood Glucose

Figure 2 shows the appearance of the healthcare sensor and the equipment used is shown in Table 1. The sensor can measure blood glucose, blood oxygen (SPO2), and heart rate, and the results are used for a blood glucose management system. This sensor can be used by connecting the power supply. You can measure it by operating the measuring instrument from your smartphone and placing your finger on the sensor. The measurement result is transmitted to the smartphone and can be confirmed. MHC technology, which uses MHC

technology to measure blood glucose levels, is based on a correlation between glucose levels in the body and the amount of heat released by the body, both of which can be predicted from heat radiation and heat convection (Kit & Kassim, 2013). Heat radiation can be measured using Stefan–Boltzmann's law and is determined as follows:

$$hr = \rho \times \sigma \times (Ts^4 - To^4) \quad [1]$$

where hr (W/m2) is heat radiation, ρ is the reflection coefficient of the skin surface, σ is Stefan Boltzmann constant, Ts (° C) is the surface temperature, and To (° C) is the ambient temperature.

The thermal convection is obtained as follows.

$$hc = h \times (Ts - To) \quad [2]$$

where hc (W/m2) is heat convection and h is a heat transfer coefficient.

The formula for calculating the blood glucose level can be derived by performing a linear regression analysis based on the blood glucose level measured with an existing blood glucose meter.

$$\text{Glucose Level} = A + hr * x1 + hc * x2 \quad [3]$$

In this case, A, x1, and x2 are values derived using linear regression analysis.

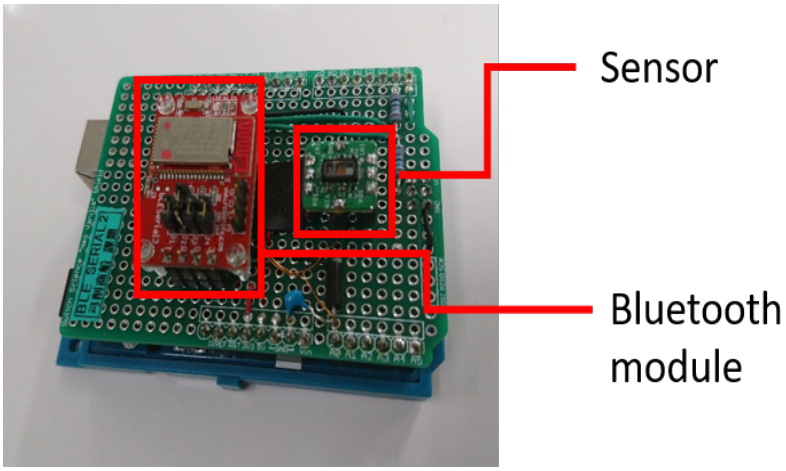

Figure 2. Healthcare sensor (appearance)

Table 1

Noninvasive blood glucose meter (equipment used)

Equipment name	Model number
Microcomputer	Arduino UNO
Reflective sensor	MAX30102
Temperature sensor	NTC thermistor
Communication	BLE Module

Accuracy Evaluation

In this study, we evaluated the accuracy of a non-invasive blood glucose meter mounted on a healthcare sensor. The EGA method of the ISO standard is used for accuracy evaluation. The EGA method is shown in Table 2. The EGA method can be evaluated on a scale of 5 from A to E, and used in medical applications if a value of 99% is plotted in zone A. When values are plotted in zones A and B, those levels can be used to measure daily life (Boren et al., 2010; Kit & Kassim, 2013).

Table 2

Definition of EGA method

Area	Description	Surveillance error grid (Degree of risk)
A	The estimated blood glucose level deviates about ± 20% from the actual value. (Clinically correct decisions)	No risk
B	Self-monitoring device giving predictive blood glucose level degree results differ by more than 20% from an actual value. (be available for daily use)	Mild risk
C	Poor results of self-monitoring equipment	Moderate risk
D	Dangerous failure to detect and treat	High risk
E	False blood glucose levels causing serious problems in diabetes management.	Extreme risk

Blood Glucose Control System

Table 3 shows a comparison with similar systems. The system can be linked to a non-invasive blood glucose meter to provide the visualization of measurement data and support

for exercise therapy. There is also no system that cooperates with a blood glucose meter to control blood glucose levels or support exercise therapy. This, therefore, is the first attempt.

Table 3
Comparison with similar systems

	Measurement of glucose levels	Noninvasive	Measurement of SPO2 and heart rate	Aerobic exercise support	Anaerobic exercise support
This system	○	○	○	○	○
Apple Watch	Unknown	○	×	×	×
MOCA heart	×	-	○	○	×
FreeStyle Libre	○	×	×	×	×
Run Keeper	×	-	×	○	×
KAATSU CYCLE	×	-	×	×	○

For glycemic control, HbA1c is the most important value for diabetics. This system also introduces HbA1c and calculates it as follows (Nathan et al., 2008):

$$HbA1c = (X + 46.7) / 28.7 \quad [4]$$

where X is the mean blood glucose level at 1 ~ 2 months.

RESULTS AND DISCUSSIONS

First, the measurement accuracy of the healthcare sensor is explained. Table 4 shows the parameters and error rates. For heart rate and blood oxygen concentration, 25 samples were taken from 1 male, and error rates were calculated. As a result, it was confirmed that these two parameters were very accurate and practical. Subsequently, 25 samples were taken from one male to investigate the accuracy of blood glucose measurements. On the blood sugar level, the accuracy evaluation was carried out using the EGA method of the ISO standard. The contents of zones A to E of the EGA method are shown in Table 2. In the graph of the EGA method, the vertical axis indicates the predicted blood glucose level, and the horizontal axis indicates the blood glucose level measured by an existing invasive blood glucose meter (true blood glucose level). This predicted blood glucose level was calculated using Equation 3 based on the temperature measured using the system. The results are shown in Figure 3. In Figure 3, values of 80% were plotted for Zone A and 20% for Zone B. The RMSE (Root Mean Squared Error) was 25.8. From Figure. 3, it was confirmed that the accuracy of this system is at a level usable in daily life.

Table 4

The error of each parameter

	Glucose Level	SPO2	Heart Rate
Error rate	9.7%	−0.04%	0.78%
subject	25 samples per man	25 samples per man	25 samples per man

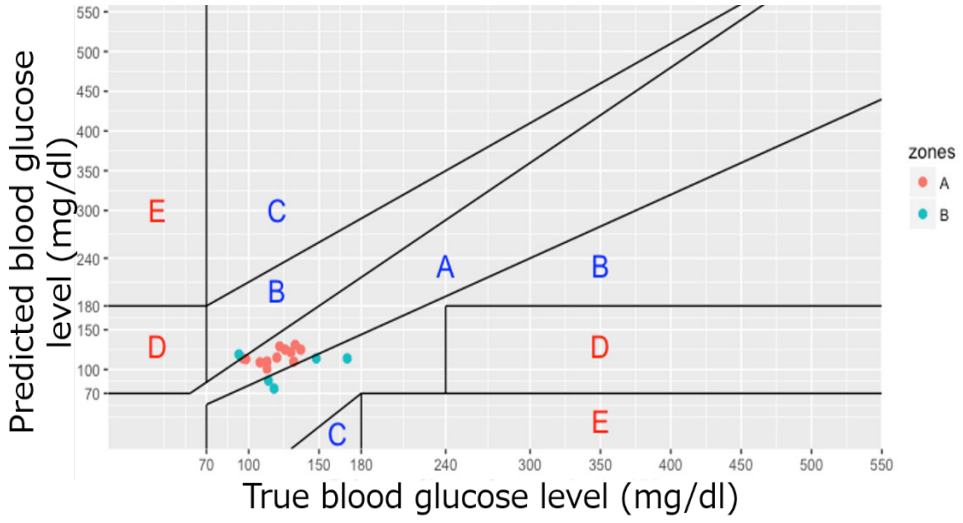

Figure 3. Accuracy evaluation using the EGA method

Next, the blood sugar management system is described. This blood sugar control system has three features. First, the data measured by the health sensor is automatically stored on the smartphone. When measuring blood glucose levels, we use a smartphone to operate a healthcare sensor. When measuring, one finger is placed on the health sensor. After about 10 seconds, the phone will show the results. The values measured here are blood glucose level, blood oxygen concentration, and heart rate. The results are stored on the smartphone and can be viewed at any time. Conventional blood glucose meters can only confirm blood glucose levels, and advice can be obtained from the state of blood glucose levels only when a person visits a hospital. In this system, as shown in Figure 4 and Figure 5, however, one can check at a glance whether the blood glucose level is high or low and make a simple comment according to the health condition. Consequently, one can grasp the state of oneself at the time of measurement without seeing a doctor. Since it is equipped with a memo function, it also becomes easy to explain the situation to the doctor at the hospital by noting the point of concern at the time of measurement.

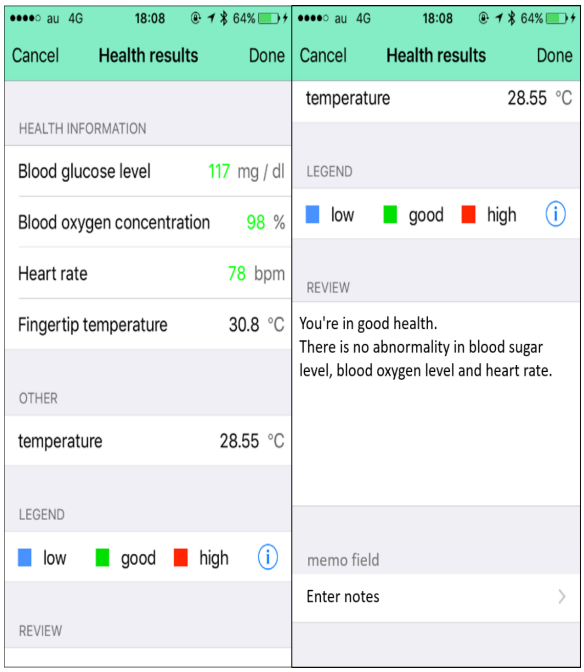

Figure 4. Diagnosis result screen

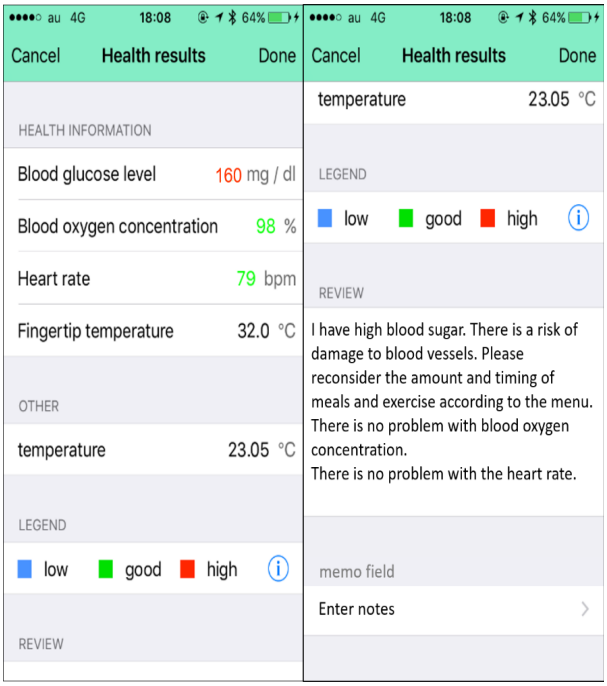

Figure 5. Diagnosis result screen (case of hyperglycemia)

The second is the training support function. Figure 6 shows a flowchart of the training support function, which is primarily based on exercise therapy in diabetics. First, we identify the patient's chronic illness and suggest a safe training menu based on the values obtained from the healthcare sensor. For example, if the previous blood sugar level is high, it is dangerous to do strenuous exercise and you should be advised to do light or no exercise. The same applies to cases of chronic diseases. This function also provides support during exercise. During exercise, it supports sugar, hydration, and pace. After exercise, save the day's distance traveled and time spent exercising, and use the healthcare sensor to reassess health. Consequently, it becomes possible to support exercise therapy that is currently not being performed due to insufficient guidance. It also proposes a menu to lower blood glucose levels based on the theory of exercise therapy, which is expected to spread among diabetic patients.

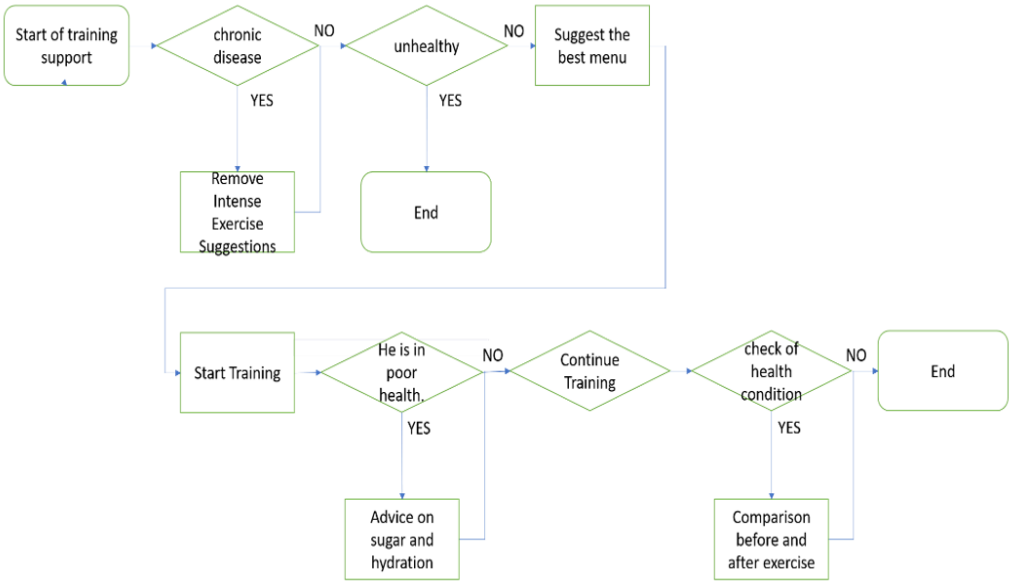

Figure 6. Exercise support flowchart

The third is the chart function. The contents of this function are different for each measuring object. In order to control diabetes, it is necessary not only to measure the blood sugar level but also to emphasize the change. Therefore, changes in blood glucose levels with time, changes before and after meals, and HbA1c are calculated. Figure 7 shows the display contents of the blood sugar level measurement result. As I explained

earlier, the measurement results so far can be checked graphically. The HbA1c, which is an important value for patients with diabetes, is also specifically calculated, and care is taken to make it easy for patients with diabetes to know their HbA1c levels even at home.

Figure 7. Chart function

Figure 8 shows the blood oxygen concentration. Since the blood oxygen concentration is dangerous when it is low in the exercise therapy in the diabetes mellitus treatment, it is possible to confirm the record of minimum value and average value. The progress graph of the graph is not displayed, because it is not necessary to control the time change of the blood oxygen concentration. The pulse rate is not continuously managed in this system, so there is no graph display function.

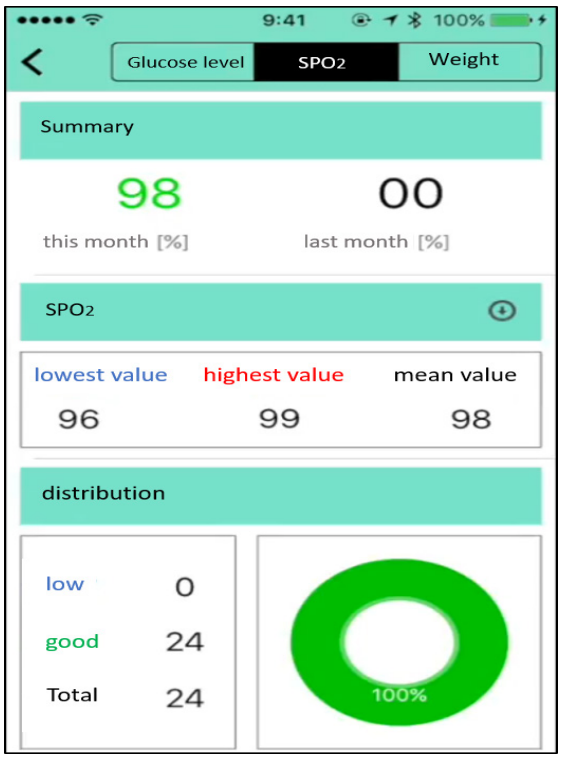

Figure 8. Diagnosis result screen (SPO2)

CONCLUSION

In this paper, we focus on glycemic control in diabetic patients and develop a new system to support glycemic control and exercise therapy using smartphones. Noninvasive blood glucose measurements of healthcare sensors cannot be used for medical purposes because of their accuracy in daily life. We, however, are confident that this system could support the currently insufficient exercise therapy and lead to the spread of health management and exercise therapy.

ACKNOWLEDGMENT

We want to express our gratitude to the participants who participated in the accurate evaluation of this system.

REFERENCES

Arakawa, S., Watanabe, T., Sone, H., Tamura, Y., Kobayashi, M., Kawamori, R., ... Sato, Y. (2015). The factors that affect exercise therapy for patients with type 2 diabetes in Japan: A nationwide survey. *Diabetology International, 6*(1), 19-25. doi:10.1007/s13340-014-0166-y

Boren, S., & Clarke, W. L. (2010) Analytical and clinical performance of blood glucose monitors. *Journal of Diabetes Science and Technology*, *4*(1), 84-97. doi:10.1177/193229681000400111

Haneda, M., Noda, M., Origasa, H., Noto, H., Yabe, D., Fujita, Y., ... Araki, E. (2018). Japanese clinical practice guideline for diabetes 2016. *Diabetology International*, *9*(1), 1-45.

Henson, J., Davies, M. J., Bodicoat, D. H., Edwardson, C. L., Gill, J. M., Stensel, D. J., ... Yates, T. (2016). Breaking up prolonged sitting with standing or walking attenuates the postprandial metabolic response in postmenopausal women: A randomized acute study. *Diabetes Care*, *39*(1), 130-138. doi:10.2337/dc15-1240

Honda, H., Igaki, M., Hatanaka, Y., Komatsu, M., Tanaka, S. I., Miki, T., ... Hayashi, T. (2016). Stair climbing/descending exercise for a short time decreases blood glucose levels after a meal in people with type 2 diabetes. *BMJ Open Diabetes Research and Care, 4*(1), 1-6. doi:10.1136/bmjdrc-2016-000232

Kit, S. Y. H., & Kassim, N. M. (2013). Non-invasive blood glucose measurement using temperature-based approach. *Jurnal Teknologi*, *64*(3), 105-110. doi:10.11113/jt.v64.2087

Kodama, S., Tanaka, S., Heianza, Y., Fujihara, K., Horikawa, C., Shimano, H., ... & Sone, H. (2013). Association between physical activity and risk of all-cause mortality and cardiovascular disease in patients with diabetes: A meta-analysis. *Diabetes Care, 36*(2), 471-479. doi:10.2337/dc12-0783

Megha, C. P., & Joshi, A. K. (2015). Non-invasive blood glucose measurement. *International Journal of Computational Engineering Research. 5*(4), 2250-3005.

Nathan, D. M., Kuenen, J., Borg, R., Zheng, H., Schoenfeld, D., & Heine, R. J. (2008). Translating the A1C assay into estimated average glucose values. *Diabetes Care*, *31*(8), 1473-1478. doi:10.2337/dc08-0545

Patton, S. R., & Clements, M. A (2012). Continuous glucose monitoring versus self-monitoring of blood glucose in children with type 1 diabetes-Are there pros and cons for both?. *US Endocrinology*, *8*(1), 27-29.

Sone, H., Tanaka, S., Tanaka, S., Suzuki, S., Seino, H., Hanyu, O., ... Yamada, N. (2013). Leisure-time physical activity is a significant predictor of stroke and total mortality in Japanese patients with type 2 diabetes: Analysis from the Japan Diabetes Complications Study (JDCS). *Diabetologia, 56*(5), 1021-1030. doi:10.1007/s00125-012-2810-z

Vashist, S. K. (2012). Non-invasive glucose monitoring technology in diabetes management: A review. *Analytica Chimica Acta*, 750, 16-27. doi:10.1016/j.aca.2012.03.043

Villena G. W., Mobashsher, A. T., & Abbosh, A. (2019). The progress of glucose monitoring—A review of invasive to minimally and non-invasive techniques, devices and sensors. *Sensors, 19*(4), 1-45. doi:10.3390/s19040800

WHO. (2017). *Global report on diabetes*. World Health Organization. Retrieved May 21, 2017, from https://apps.who.int/iris/bitstream/handle/10665/204871/9789241565257_eng.pdf;jsessionid=1B9E6B3DB0986FD75A9E03D6C5D8CFAD?sequence=1

Pertanika J. Sci. & Technol. 28 (S2): 25 - 45 (2020)

PERTANIKA JOURNALS

SCIENCE & TECHNOLOGY

Journal homepage: http://www.pertanika.upm.edu.my/

Application of Ecological Indices using Macroinvertebrate Assemblages in Relation to Aquaculture Activities in Rawang Sub-basin, Selangor River, Malaysia

Nadeesha Dilani Hettige[1, 3], Rohasliney Binti Hashim[1]*, Ahmad Bin Abas Kutty[2], Nor Rohaizah Binti Jamil[1] and Zulfa Hanan Binti Ash'aari[1]

[1]Faculty of Forestry and Environment, Universiti Putra Malaysia, 43400 UPM, Serdang, Selangor, Malaysia
[2]School of Environmental & Natural Resource Sciences, Universiti Kebangsaan Malaysia, 43600 UKM, Bangi Selangor, Malaysia
[3]Environmental Studies Division, National Aquatic Resource Research and Development Agency (NARA), Crow Island, Colombo 15, Sri Lanka

ABSTRACT

This study aimed to evaluate benthic macroinvertebrates assemblages using the application of ecological indices in the Rawang sub-basin of the Selangor River with reference to determining the impacts of aquaculture practices on benthic macroinvertebrates. In total, seven sampling sites were selected, namely Guntong (SR1), Guntong's tributaries (SR2, control site), Kuang (SR3 and SR7), Gong (SR4), Buaya (SR5) and Serendah (SR6) Rivers. Sites were selected using a random sampling technique and the accessibility and proximity to aquaculture farms. Macroinvertebrates were sampled from April 2019 to March 2020 using an aquatic kick net, a hand spade, and a D-frame dip net. Water samples were also taken. Twenty-seven families belonging to the Annelida, Mollusca and Athropoda phyla were identified using taxonomic keys. Tubificidae was found to be the most dominant family (36.79%) followed by Chironomidae (28.84%). The highest number of individuals from family Tubificidae was recorded in Gong River, where effluent was discharged from an aquaculture farm. The total abundance of benthic macroinvertebrates increased with increased proximity to the aquaculture farm. Based on Biological Monitoring Working

ARTICLE INFO

Article history:
Received: 10 February 2020
Accepted: 13 November 2020
Published: 31 December 2020

DOI: https://doi.org/10.47836/pjst.28.S2.03

E-mail addresses:
nadeeshahettige7@gmail.com (Nadeesha Dilani Hettige)
rohasliney@upm.edu.my (Rohasliney Binti Hashim)
abas@ukm.edu.my (Ahmad Bin Abas Kutty)
norrohaizah@upm.edu.my (Nor Rohaizah Binti Jamil)
zulfa@upm.edu.my (Zulfa Hanan Binti Ash'aari)
*Corresponding author

ISSN: 0128-7680
e-ISSN: 2231-8526

© Universiti Putra Malaysia Press

Party score value, the water quality of sampling sites in close proximity to the aquaculture farm was polluted as compared to the control location. Family Biotic Index score showed that all sites were substantially polluted with organic pollution, with the control site being much less polluted. In conclusion, benthic macroinvertebrates assemblage was affected by effluent originating from aquaculture farm outlets. It is therefore necessary to conduct aquaculture farming using methods that are deemed to be environmentally friendly.

Keywords: Benthic macroinvertebrates, biological monitoring working party, and family biotic index, diversity

INTRODUCTION

In recent years, the aquaculture industry has significantly expanded and become more efficient worldwide. This has been primarily to address increasing demands in food supply due to production limitations in capture fisheries (Saremi et al., 2013). Freshwater aquaculture, as one of the aquaculture industry activities, presents significant environmental problems for aquatic ecosystems worldwide (Kırkag et al., 2009). For instance, aquaculture activities nearby rivers generally discharge untreated wastewater into main water bodies. Over time, this leads to adverse changes in the water quality of aquatic environments including aquatic biota and their functional feeding traits (Minoo, 2015). The present situation has become a major concern in Malaysia (Hanafi et al., 1995; Kawasaki et al., 2016a; Yusoff, 2015). Previous reports had recorded the deleterious changes in water quality from aquaculture activities, among others, reduced diversity, replaced sensitive species, impacted native species and changed tropical structures of organisms (Diana, 2009). Karimi et al. (2016) in their studies in Dohezar Stream, Iran reported that populations of sensitive organisms had been reduced, and more tolerant species had survived and had become more dominant at fish farming sites. The effect diminished with increasing distance from discharge points of farm effluent.

Numerical values of several indices incorporating ecological responses of aquatic communities have been typically forming the basis of biological monitoring (Zhu & Chang, 2008). Among the most commonly used indices include diversity indices (species richness, Shannon index), abundance (coverage, density and biomass) and pollution tolerance (Biological Monitoring Working Party (BMWP) and Biological Monitoring Water Quality score systems). The preceding research summarised that biological monitoring of pollution originating from fish farms in aquatic ecosystems is possibly more appropriate for use in indices based on benthic macroinvertebrates (Camargo et al., 2011; Karimi et al., 2016). Studies on the effects of aquaculture effluent on benthic macroinvertebrates have previously been reported using BMWP index (Hatami et al., 2011). Benthic macroinvertebrates have been documented to respond to a wide range of environmental changes caused by various anthropogenic impacts (Kim et al., 2016), including those arising from aquaculture activities

(Hatami et al., 2011; Karimi et al., 2016; Minoo et al., 2016). Benthic macroinvertebrates have been considered as a good bioindicator in assessing river water quality (Oliveira & Callisto, 2010; Young et al., 2014).

Among the major rivers in the State of Selangor, Selangor River is renowned for its freshwater aquaculture production area which increases of nearly 20,000 tonnes per year from 2008 to 2013 (Lembaga Urus Air Selangor [LUAS], 2015). The Rawang sub-basin is an important sub-basin of the Selangor River in which freshwater aquaculture has been more prevalent (LUAS, 2014). In previous initiatives, environmental monitoring of Selangor River focused only on physiochemical parameters of water. Some researches had highlighted the impact of pollution in the area by using physiochemical water quality assessments (Chowdhury et al., 2018; Daniel & Kawasaki, 2016; Fulazzaky et al., 2010; Kawasaki et al., 2016a). According to Kawasaki et al. (2016a), it is cited that aquaculture ponds have been the major source of nutrients to the Selangor River. However, specific effects on aquatic organisms were not comprehensively discussed.

The influence of anthropogenic activities on benthic macroinvertebrates in streams and rivers in Malaysia have also been studied (Azrina et al., 2006; Hasmi et al., 2017; Ling, 2010; Rak et al., 2014, 2011). However, there has been no study focusing on the influence of aquaculture practices on benthic macroinvertebrates in streams using ecological indices. There has also been a lack of records on the diversity of benthic macroinvertebrates. It was against these backgrounds that the present multi-objective study was conducted. The first objective was to identify benthic macroinvertebrate assemblages in the Rawang sub-basin of the Selangor River using taxonomy keys. The second objective was to apply ecological indices to evaluate water quality status. The final study objective was to determine the impacts of aquaculture practices on benthic macroinvertebrates in selected rivers within the study area.

MATERIALS AND METHODS

Site Description

The Selangor River, one of the major rivers in the State of Selangor, flows from the Titiwangsa Range of Banjaran Titiwangsa (The Main Range in Peninsular Malaysia) beginning at the foothills of Fraser's Hill. Ultimately, the Selangor River makes its way west to the Straits of Malacca at Kuala Selangor town (Seyam & Othman, 2015). The catchment area of the river is nearly 2200 km^2 with a length of almost 110 km. The river flows through the districts of Hulu Selangor, Kuala Selangor and Gombak. It has seven main tributaries (Othman et al., 2014) and is divided into ten sub-basins based on hydrological boundaries (Chowdhury et al., 2018). Approximately 50% of the river basin is still covered by natural forests and 22% has agricultural activities (Othman et al., 2014). The upper part of the catchment consists mainly of granite and sedimentary bedrocks. Parts of the basin's

mid-section comprise granite rocks with meta-sedimentary face carboniferous rocks. The mid-section of the catchment is also underlined with limestone and interbedded schist (Hamzah et al., 2007). There is a rich aquatic and terrestrial life in the basin such as a firefly reserve, mangroves, migratory birds and peat swamp forests (LUAS, 2015). There exist approximately 300 freshwater and 50 brackish water aquaculture ponds along the Selangor River basin (Kawasaki et al., 2016b), including extensive aquaculture farming areas in the Rawang sub-basin.

Research Design

In the present study, site selection was done using a random sampling technique while taking into account a site's accessibility as well as its proximity to aquaculture farms. Accordingly, seven sampling sites (Figure 1) were selected along the following rivers: Guntong (SR1), Guntong's tributaries (SR2), Kuang (SR3 and SR7), Gong (SR4), Buaya (SR5) and Serendah (SR 6). SR2 served as the control site due to its minimal disturbance in its surrounding area and the absence of upstream aquaculture farms. The following are approximate downstream distances (in metres, m) from the sampling site to the nearest freshwater aquaculture farms: SR1 and SR3 (200 m), SR4 and SR5 (20 m), SR6 (400 m) and SR7 (400 m). There was no point source of pollution that discharged directly into the river between the aquaculture farm outlets and the sampling points. Sampling sites were located near to the riverbanks.

A sampling of benthic macroinvertebrates was carried out from April 2019 until February 2020. However, additional sampling visits were conducted until a proper rarefaction curve was attained in March 2020. Samples were collected using three types of sampling gears, namely a D-frame dip net, an aquatic kick net and a hand spade (N = 7 sampling × 1 river basin × 7 stations × 3 gear types × 5 replicates = 735 samples per river basin). To obtain samples from the D-frame net and aquatic kick net, the nets were placed against the flow of current and approximately one square meter of the substrate in front of the nets was disturbed for nearly two minutes using the kick sampling method (Merritt & Cummins, 1996). The hand-scooping method was used with a hand spade to collect sediment samples below (nearly 5 cm depth) the edge of the river's water level. Collected samples were then poured into polythene bags and transported directly to the Aquatic Laboratory, Faculty of Forestry and Environment, Universiti Putra Malaysia (UPM) for further analysis. In the laboratory, samples were wet-sieved using a 0.5 mm of fine mesh size sieve and separated according to particle size. After separation, benthic macroinvertebrates were sorted and preserved in 70% ethanol for storage prior to further analysis. Macroinvertebrates were identified to the nearest taxonomic unit using a dissecting microscope, a compound microscope and by using standard identification keys (Burnhill,

2006; Brinkhurst & Jamieson, 1971; Brinkhurst, 1971; Merritt & Cummins, 1996; Thorp & Lovell, 2014; Yong & Yule, 2004).

In addition to the benthic macroinvertebrates, water samples were taken from each sampling site at two-monthly intervals from April 2019 to February 2020. During the sampling work, three replicate samples were collected at each site for the purpose of physiochemical water quality analysis (N = 1 river basin × 7 sampling sites × 6 sampling trips × 3 replicates = 126 samples per river basin). Water temperature, dissolved oxygen (DO), electrical conductivity (EC), turbidity and pH were measured *in-situ* by using the following equipment: dissolved oxygen meter (YSI 52, USA), conductivity meter (Thermo Scientific Orion 3-Star, USA), turbidity meter (HACH 2100 P, USA) and pH meter (Thermo Scientific Orion 3-Star, Indonesia) respectively. All portable meters were duly calibrated before use.

Collected water samples were transported to the laboratory at 4°C for subsequent laboratory analysis. Chemical Oxygen Demand (COD) and ammoniacal nitrogen testing were performed using a DR 2800 spectrophotometer (HACH, 2007), while Biochemical Oxygen Demand 5 (BOD5) was measured using a BOD probe (Verma & Singh, 2013). Total suspended solids (TSS) were quantified using a standard method (American Public Health Association, 2012).

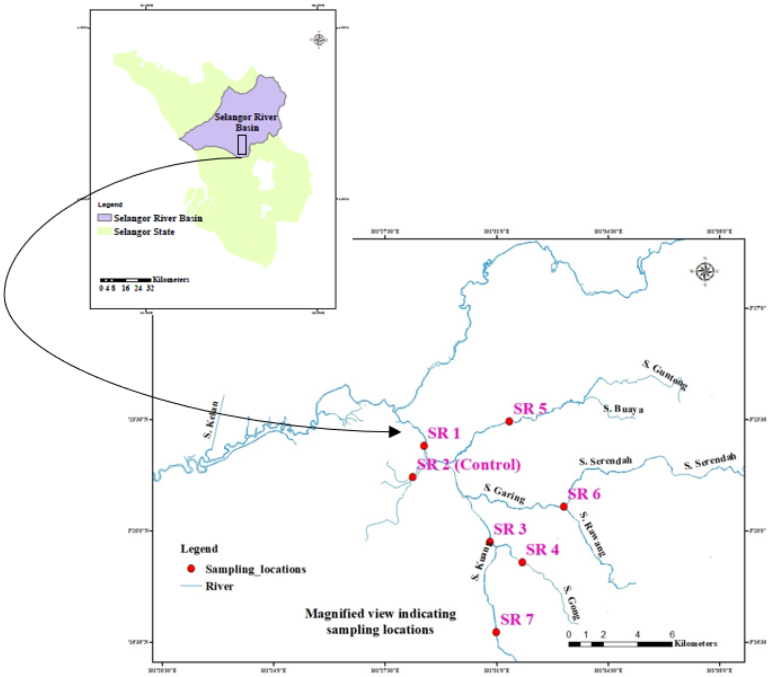

Figure 1. Map of the Selangor River in the State of Selangor and the chosen study area showing selected sampling locations

Data Analysis

The effects of land use and macroinvertebrate biotic indices on rivers have been studied by several researchers (Fierro et al., 2017; Hatami et al., 2011; Karimi et al., 2016; Kim et al., 2016; Kroll et al., 2009; Lalonde et al., 2016; Virbickas et al., 2011). In the present study, several ecological indices were used to express the diversity of benthic macroinvertebrates and water's pollution status, namely by Shannon's Diversity Index (H'), Simpson's Diversity Index (D), Biological Monitoring Working Party-Thailand ($BMWP^{Thai}$) and the Family Biotic Index (FBI). These indices were calculated based on the family level of benthic macroinvertebrates. The calculation methods for these indices are presented in Table 1.

The tolerance value of taxa was used to calculate the FBI following Mandaville (2002) and Hilsenhoff (1988) and the FBI table is presented in Table 2. Tolerance values ranged from 0 (very intolerant of organic wastes) to 10 (very tolerant of organic wastes). Table 3 presents the $BMWP^{Thai}$ score ranges and their corresponding water quality status. The tolerance value of each family was used to calculate the $BMWP^{Thai}$ (Mustow, 2002). It assigns scores to each family according to its sensitivity to organic pollution. The highest value was given to the most sensitive family.

Table 1

Ecological Indices used to determine benthic macroinvertebrates diversity and pollution status

Index Name	Formula used/Method	References
Shannon's index (H')	$-\sum_{i=1}^{S} pilnln\,(pi)$	Shannon (1948)
Simpson's Diversity Index (D)	$1-\left(\frac{\Sigma\, n(n-1)}{N(N-1)}\right)$	Simpson (1949)
Biological Monitoring Working Party - Thailand ($BMWP^{Thai}$)	Sum of the tolerance scores of macroinvertebrates families in the sample	Mustow (2002)
Family Biotic Index (FBI)	$\frac{\text{Total (n×a)}}{\text{Total (n)}}$	Hilsenhoff (1988)

Where,
pi : Proportion of species (i) relative to the total number of species
S : Number of taxa
n : Total number of organisms of a particular species
N : Total number of organisms of a particular species
a : Tolerance value

Table 2

Family Biotic Index (FBI) Informative table used to evaluate river water quality

FBI	Water Quality	Degree of pollution
0.00 – 3.75	Excellent	Organic pollution unlikely
3.76 – 4.25	Very Good	Possible slight organic pollution
4.26 – 5.00	Good	Some organic pollution probable
5.01 – 5.75	Fair	Fairly substantial pollution likely
5.76 – 6.50	Fairly poor	substantial pollution likely
6.51 – 7.25	Poor	Very substantial pollution likely
7.26 – 10.00	Very poor	Sever organic pollution likely

Source: Hilsenhoff (1988)

Table 3

$BMWP^{Thai}$ score values and corresponding water quality status

$BMWP^{Thai}$ Score	Category
>151	Excellent
101-150	Good
51-100	Moderate
17-50	Moderate Poor
0-16	Very Poor

Source: Mustow (2002)

Statistical analysis was performed using Statistical Package for Social Sciences (SPSS) 25.0. The Kolmogorov-Smirnov test (Mishra et al., 2019) was used to determine whether the ecological index data and water quality were normally distributed. As the data were subsequently determined to be normally distributed, Pearson correlation analysis was carried out to determine the relationship between water quality and ecological indices. Subsequently, Canonical Correspondence Analysis (CCA) was used to identify the relationships composition between macroinvertebrates and relevant environmental variables using Paleontological Statistics (PAST), a statistical software. Three taxa, namely Cladoceran, Dytiscidae and Ephydridae, recorded only one individual being sampled within the sub-basin during the study period. Therefore, they were excluded from the proceeding data analyses, except for percentage calculation.

RESULTS AND DISCUSSION

In the present study, a total of 7677 discrete individuals belonging to 27 families were identified. The families encompassed three phyla and five classes as shown in Table 4. Among the collected samples, Tubificidae was the most dominant family (36.79%) with Chironomidae as the second-most dominant (28.84%). Additionally, individuals from the Naididae family comprised 15.93% of the total abundance (Figure 2).

According to the results obtained, Tubificidae was found to be the dominant family within the sub-basin. It has been reported that Tubificidae is an effective biological indicator of water quality in streams (Martins et al., 2008). Tubificidae is also widely used as an indicator of organic pollution in rivers. Muddy sediments that are highly contaminated with organic matter facilitate the growth of the individual from the Tubificidae family. Therefore, an abundance of Tubificidae is an indicator of poor river water quality (Burnhill, 2006). In addition, based on a study conducted by Namin et al. (2013) on the impact of fish farm effluents on benthic macroinvertebrates of the Tajan River, Iran, members of the Tubificidae family were found in all of the selected locations including the control sites.

In the present study, the family Chironomidae was recorded to be the second most dominant family in the study area. The family had also been recorded at most other polluted areas (Al-Shami et al., 2010; Azrina et al., 2006) and recreational areas surrounding Malaysian streams and rivers (Ahmad et al., 2008; Muhazar et al., 2013; Rak et al., 2014). Chironomus larvae were the most dominant species found in the Tajan River in northern Iran, a river significantly impacted by aquaculture activities (Namin et al., 2013). Chironomidae has also been found in sampling stations downstream of a trout farm in Dohezar, Iran (Karimi et al., 2016). There has been no existing record of benthic macroinvertebrates in the Selangor River to compare with the results obtained from the present study.

The distribution and the total number of benthic macroinvertebrates at the family level from each sampling site are shown in Table 5. The highest total number of individuals from the dominant family (Tubificidae) was recorded from the Gong River (SR4), where aquaculture effluent was previously discharged. The lowest number of individuals from the family Tubificidae was recorded at the control site, that is, the Guntong River tributary sampling station (SR 2). Benthic macroinvertebrates from the Palaemonidae, Thiaridae and Caenidae families were most abundant.

Soonthornvipat et al. (2012) reported that oligochaetes constituted an ideal food source for various types of aquaculture fish including ornamental ones. They can survive in highly contaminated sites such as those with high turbidity, in the presence of toxic materials and high levels of organic matter content (Kang et al., 2017). Coldebella et al. (2018) recorded that COD, suspended and total solids in addition to the concentrations of some nutrients significantly increased during the time of harvest at aquaculture farms, which released

Table 4

Taxonomic list of benthic macroinvertebrates recorded at selected study sites

Phylum	**Class**	**Order**	**Family**
Annelida	Clitellata	-	Aeolosomatidae
Annelida	Clitellata	Haplotaxida	Naididae
Annelida	Clitellata	Haplotaxida	Haplotaxidae
Annelida	Clitellata	Haplotaxida	Tubificidae
Annelida	Clitellata	Lumbriculida	Lumbriculidae
Annelida		-	Unidentified Oligochaeta
Annelida	Clitellata	Rhynchobdellida	Glossiphoniidae
		Arhynchobdellida	Erpobdellidae
Arthropoda	Insecta	Diptera	Chironomidae
		Diptera	Ephydridae
Arthropoda	Malacostraca	Decopoda	Palaemonidae
Arthropoda	Insecta	Odonata	Gomphidae
			Libellulidae
			Corduliidae
			Protoneuridae
			Coenagrionidae
Arthropoda	Insecta	Ephemeroptera	Caenidae
			Baetidae
			Leptophlebiidae
Arthropoda	Insecta	Coleoptera	Dytiscidae
		Trichoptera	Hydropsychidae
	Branchiopoda	Cladocera	-
Mollusca	Gastropoda	Architaenioglossa	Viviparidae
		Hygrophila	Lymnaeidae
		Neotaenioglossa	Thiaridae
		Hygrophila	Planorbidae
Mollusca	Bivalve	Cardiida	Corbiculidae

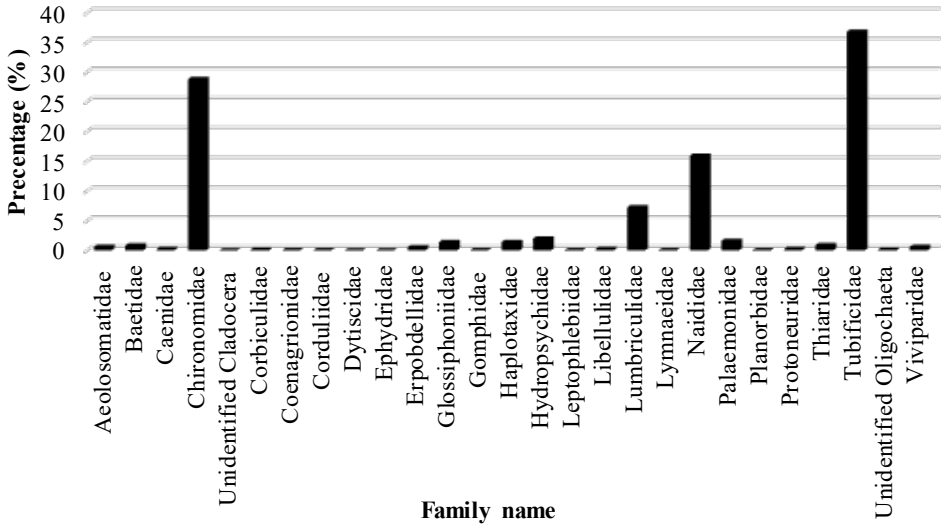

Figure 2. Percentage of individuals from families recorded at all sampling sites in the Rawang sub-basin

Table 5

Number of individuals at sampling sites distributed according to family

Family	**Number of Individuals**						
	SR 1	SR 2	SR 3	SR 4	SR 5	SR 6	SR 7
Aeolosomatidae	7	-	10	19	3	2	4
Baetidae	-	5	-	-	-	58	-
Caenidae	-	18	-	-	-	1	1
Chironomidae	180	8	202	287	810	414	313
Unidentified Cladocera	-	-	-	-	-	1	-
Corbiculidae	-	-	-	-	-	11	-
Coenagrionidae	1	-	2	-	-	-	-
Corduliidae	1	1	1	-	2	-	-
Dytiscidae	-	-	-	-	1	-	-
Ephydridae	-	-	-	1	-	-	-
Erpobdellidae	29	5	-	1	1	-	5
Glossiphoniidae	48	3	27	2	17	2	7
Gomphidae	-	3	-	-	-	2	-
Haplotaxidae	21	13	39	3	26	1	5

Table 5 *(Continued)*

Family	Number of Individuals						
	SR 1	SR 2	SR 3	SR 4	SR 5	SR 6	SR 7
Hydropsychidae	3	-	8	2	76	65	-
Leptophlebiidae	-	2	-	-	-	-	1
Libellulidae	1	2	-	-	10	-	5
Lumbriculidae	142	3	108	71	210	6	17
Lymnaeidae	-	1	1	-	-	2	-
Naididae	79	-	325	425	170	20	204
Palaemonidae	3	110	1	2	2	-	4
Planorbidae	-	-	1	3	-	-	-
Protoneuridae	1	-	1	2	11	-	4
Thiaridae	7	53	-	1	-	7	-
Tubificidae	598	16	734	956	351	21	148
Unidentified Oligochaeta	11	-	-	-	-	-	-
Viviparidae	11	26	1	2	-	5	1
Total Number collected	1143	269	1461	1777	1690	618	719
Number of families recorded	17	16	15	15	14	16	14

Key: SR1: Guntong; SR2: Guntong tributaries (Control); SR3& SR7: Kuang; SR4: Gong; SR5: Buaya; SR6: Serendah.

effluents into the environment. Effluents from aquaculture farms have been documented to facilitate the creation of suitable conditions for oligochaetes in receiving streams. In the present study, the sampling site at Gong River (SR 4) was in closest proximity to an aquaculture farm effluent outlet, which explained the high number of Tubificidae being recorded. Minoo et al. (2016) noted that the total abundance of benthic macroinvertebrates increased consistently near to and immediately downstream from effluent discharge points of aquaculture farms. The present study observed that the total number of individuals recorded at other sampling sites based on their proximity to other aquaculture farms was in the following descending order: Buaya River, Kuang River (SR3), Guntong River, Kuang River (SR7) and Serendah River. This observation suggests that water quality significantly improved at some distances away from the outfalls of aquaculture farms. Hatami et al. (2011) concurred with the present findings. Other studies reported that downstream inland

fish farms recorded lower diversity and taxa loss of macroinvertebrates (Lalonde et al., 2016). The recovery of stream fauna could occur even at long distances from aquaculture effluent outlets. From a spatial aspect, previous studies reported that at distances of up to 1,000 m downstream from a fish farm discharge point, changes in abundance and diversity have been detected (Camargo, 1992).

Table 6 shows the values of ecological indices sorted according to sampling sites and their respective water quality status. Highest values in both family richness level and Shannon Diversity Index (H') were found at the control sites of Guntong River tributary (SR2). Lower levels of family richness were recorded at sites just below the aquaculture farms (SR4 and SR5). This suggests a reduction in water quality when compared with the control site. Comparable findings were recorded in a preceding study by Loch et al. (1996) for EPT taxa richness due to fish farm effluent. However, family richness was observed to be higher in Kuang River (SR7) and Serendah River (SR6) than Guntong River (SR1) and Kuang River (SR3). This was because the sampling points of Kuang River (SR7) and Serendah River (SR6) were located further downstream from the aquaculture farm effluent discharge point as compared to the sampling sites at Guntong River (SR1) and Kuang River (SR3). The observation suggests that water quality of Kuang River (SR7) and Serendah River (SR6) were improving. However, the highest Simpson's Diversity Index was recorded from the control site (SR2) while Serendah River (SR6) showed the lowest. The highest value of FBI was recorded from Guntong River (SR1) sampling stations while the lowest was reported from the control site (SR2).

According to the H' index, all the sampling sites were classified as having moderately polluted water ($1< H'<2$) (Li-na et al., 2017). Guntong River, Kuang River, Gong River and Buaya River had very poor water quality status while Serendah River and Guntong's tributary were poor and fairly poor, respectively (Hilsenhoff, 1988). Therefore, the control site (SR2), which was located at Guntong River's tributaries, was also classified as having low water quality (Table 6).

Water quality evaluation results could change when integrated health monitoring is conducted. The classification of water quality status at sampling sites based on their corresponding $BMWP^{Thai}$ is also shown in Table 6.

The water quality of the Control river (SR2) was categorised as "Moderate" based on its $BMWP^{Thai}$ value. Because the site was located in a place with minimal disturbances and organisms from pollution-sensitive families (Leptophlebiidae, Corduliidae and Caenidae) were found here, the family level pollution-sensitive score for BMWP index was correspondingly high. Since there were differences in water quality levels for the same sampling site from BMWP and FBI, it was difficult to evaluate water quality accurately because biological analysis based on the composition of benthic macroinvertebrates could

Table 6

Species richness, diversity indices and biotic index at the study area's sampling sites

Sampling site	Family level richness	Shannon Diversity Index	Simpson's Diversity Index	Biological Monitoring Working Party Thai	Family Biotic Index
SR 1	0.50	1.54 Moderately polluted	0.68	57 Moderate	8.09 Very Poor
SR 2	0.98	1.92 Moderately polluted	0.78	70 Moderate	6.38 Fairly Poor
SR 3	0.39	1.42 Moderately polluted	0.67	50 Moderately poor	8.01 Very Poor
SR 4	0.33	1.22 Moderately polluted	0.63	41 Moderately poor	7.99 Very Poor
SR 5	0.32	1.51 Moderately polluted	0.70	41 Moderately poor	7.84 Very Poor
SR 6	0.60	1.23 Moderately polluted	0.53	47 Moderately poor	7.10 Poor
SR 7	0.52	1.40 Moderately polluted	0.69	53 Moderate	8.02 Very Poor

Key: SR1: Guntong; SR2: Guntong tributaries (Control); SR3& SR7: Kuang; SR4: Gong; SR5: Buaya; SR6: Serendah.

not be considered as a single factor to determine water quality status since it also depended on environmental factors (Surtikanti, 2016).

Pearson correlational analysis revealed that $BMWP^{Thai}$ was negatively correlated with TSS ($r = -0.768$; $P < 0.05$). Similar outcomes with regards to the correlation between $BMWP^{Thai}$ and suspended solids were reported by Kullasoot et al. (2017) based on studies conducted in Mae Klong River, Thailand. This further validated that macroinvertebrates could serve as an indicator for deteriorating water quality. A positive correlation was revealed between FBI and COD ($r = 0.786$; $P<0.05$), TSS ($r = 0.866$; $P < 0.05$), EC ($r = 0.960$; $P < 0.01$), BOD ($r = 0.877$; $P < 0.01$). Similar correlations were reported by Etemi et al. (2020) between FBI and BMWP with the above mentioned water quality parameters of

the Lepenci River basin in Kosovo. The family level richness was reported to be negatively correlated with EC ($r = -861$: $p < 0.05$), ammoniacal nitrogen ($r = -0.791$: $p < 0.05$), BOD ($r = -0.857$: $p < 0.05$), COD ($r = -0.826$: $p < 0.05$) and TSS ($r = -0.912$: $p < 0.01$). Based on a study conducted in the Tajan River in Iran by Namin et al. (2013), it was indicated that none of the correlational coefficients between water's physicochemical parameters and macroinvertebrates metrics and indices were insignificant. However, the correlational analysis conducted in the present study had allowed environmental variables to explain the variations of the indices due to aquaculture farming activities.

The CCA consisted of seven parameters, including pH, DO, water temperature, ammoniacal nitrogen, TSS, turbidity, EC. BOD, DO and COD, were significant in the composition of the benthic macroinvertebrate communities (*Figure 3*). The first and second CCA axes together accounted for approximately 89.17% of the relation between benthic macroinvertebrate communities and environmental variables. The length of the arrows in the CCA revealed that DO, TSS, turbidity, COD, ammoniacal nitrogen and BOD values were the main environmental factors affecting the distribution of benthic macroinvertebrates in the Rawang sub-basin of the Selangor River. Additionally, the arrow length for pH was the shortest in length which denoted a scant relationship between family and pH. However, pH was an important parameter for all organisms in any given aquatic ecosystem. As cited by the United States Environmental Protection Agency (USEPA), a pH range of 6.5 to 9.0 was suitable for bottom-dwelling macroinvertebrates (Prommi & Payakka, 2015). The number of individuals and taxa are very sensitive to the low pH of the aquatic ecosystem (Petrin et al., 2007). Both EC and water temperature also assert influence to some extent on variations in benthic macroinvertebrates communities.

The first quadrant of the CCA contained the families Baetidae, Corbiculidae, Corduliidae, Erpobdelliae, Gomphidae, Hydropsychidae, Libellulidae and Lymnaeidae. These families were influenced by high DO. DO concentration is an essential limnological factor for the characterisation of aquatic ecosystems and the survival of aquatic life (Moura et al., 2011). Preceding research conducted at the Teroi and Batu Hampar rivers of Gunung Jerai forest reserve, Kedah by Hamid et al. (2011) reported that genus *Baetis* (family Baetidae) had a positive correlation with DO. Nevertheless, based on a study conducted in the lower catchment of the Kinabatangan River, Sabah, Harun et al. (2015) reported that Coenagrionidae and Libellulidae were declined in the high concentrations of DO. The families in the second quadrant, especially Glossiphoniidae, Lumbriculidae, Protoneuridae, Chironomidae and unidentified Oligochaeta, were highly influenced by TSS, turbidity and COD. The said families had moderate relationship with water temperature. Sharma and Chowdhary (2011) reported that the presence of Lumbriculidae contributed to increase in TSS. Glossiphoniidae (some *Helobdella* sp.) can be considered as tolerant of physical water quality factors such as turbidity and TSS (Miserendino & Gullo, 2014).

Families located in the third quadrant were Aelosomadidae, Naididae, Coenagrionidae, Planorbidae and Tubificidae. All of these families had similar environmental selections and easily coexisted with high BOD, ammoniacal - nitrogen and EC. The said families had little relationship with pH. As pH increased, the recolonization of benthos occurred and pH positively affected benthic production in tropical waters (Vizakat et al., 1991). Based on a study conducted in Pauh River located at Cameron Highlands, Tan and Beh (2016) observed that Planorbidae and Tubificidae were positively correlated with EC, BOD and ammoniacal nitrogen. The fourth quadrant comprised families Caenidae, Haplotaxidae, Leptophlebiidae, Palaemonidae, Thiaridae and Viviparidae. No measured water quality parameters influenced the families.

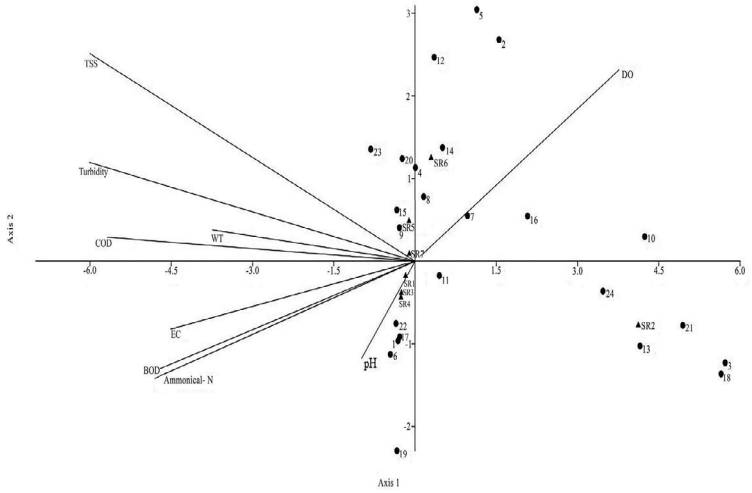

1.	Aeolosomatidae	7.	Corduliidae	13.	Leptophlebiidae	19.	Planorbidae
2.	Baetidae	8.	Erpobdellidae	14.	Libellulidae	20.	Protoneuridae
3.	Caenidae	9.	Glossiphoniidae	15.	Lumbriculidae	21.	Thiaridae
4.	Chironomidae	10.	Gomphidae	16.	Lymnaeidae	22.	Tubificidae
5.	Corbiculidae	11.	Haplotaxidae	17	Naididae	23.	Unidentified Oligochaeta
6.	Coenagrionidae	12.	Hydropsychidae	18.	Palaemonidae	24.	Viviparidae

Figure 3. Canonical Correspondence Analysis (CCA) diagram indicating the relationship between benthic macroinvertebrates families and correlations with environmental parameters

CONCLUSION

The present study revealed the occurrence of 27 families of benthic macroinvertebrates in the selected rivers of the Rawang sub-basin using taxonomic keys. Based on the values of ecological indices, the clear differences based on proximity to the aquaculture farming discharge point were not discernible because some organisms were able to tolerate environmental stresses fairly well. Consequently, based on BMWP, the findings of the present study indicated that the water quality from sampling sites near the aquaculture farm was polluted as compared to the control station. With respect to environmental quality, the FBI values indicated that all sites were substantially polluted with organic pollution. The control sites possessed the highest water quality, while the Buaya and Gong rivers which were near to aquaculture farm effluent discharge points exhibited the lowest quality of water in the Rawang sub-basin. Nevertheless, further studies are needed to better interpret the impacts of aquaculture farms on pollution levels through the development of the modelling approach.

ACKNOWLEDGEMENTS

The authors gratefully thank and acknowledge the research grant provided by the Ministry of Higher Education (MOHE), Malaysia for funding this work under Trans-Disciplinary Research Grant Scheme (TRGS/2016/5535713). The authors also express their gratitude to Miss Xeai Li Chai, a postgraduate student from the Faculty of Forestry and Environment, UPM and Miss Hanisah Binti Ibrahim, a PhD student from the School of Environmental & Natural Resource Sciences, UKM, for their assistance in fieldwork and laboratory work, respectively. Special thanks are also due to the technical staff, Faculty of Forestry and Environment, UPM, for their invaluable help in field sampling arrangements.

REFERENCES

Ahmad, A. K., Idris, A. B., Othman, M. S., Salwana, H., & Hamisah, H. (2008). A preliminary survey of chironomids diversity at headwater of Langat River, Selangor. *Serangga*, *13*(1–2), 1–18.

Al-Shami, S. A., Md Rawi, C. S., Ahmad, A. H., & Nor, S. A. M. (2010). Distribution of Chironomidae (Insecta: Diptera) in polluted rivers of the Juru River Basin, Penang, Malaysia. *Journal of Environmental Sciences*, *22*(11), 1718–1727. doi:10.1016 /S1001-0742(09)60311-9

American Public Health Association. (2012). *Standard methods for the examination of water and waste water* (22nd Ed.). Washington, USA: American Public Health Association (APHA), American Water Works Association (AWWA) and Water Environment Federation (WEF).

Azrina, M. Z., Yap, C. K., Rahim Ismail, A., Ismail, A., & Tan, S. G. (2006). Anthropogenic impacts on the distribution and biodiversity of benthic macroinvertebrates and water quality of the Langat River, Peninsular Malaysia. *Ecotoxicology and Environmental Safety*, *64*(3), 337–347. doi:10.1016/j.ecoenv.2005.04.003

Brinkhurst, R. O. (1971). *A guide for the identification of British Aquatic Oligochaeta* (2nd Ed.). Toronto, Canada: Titus Wilson & Sons LTD.

Brinkhurst, R. O., & Jamieson, B. M. G. (1971). *Aquatic oligochaeta of the world*. Edinburgh, Scotland: Oliver & Boyd.

Burnhill, T. (2006). *Identification of freshwater invertebrates of the Mekong River and its tributaries*. Vientiane, Laos: Mekong River Commission.

Camargo, J. A. (1992). Temporal and spatial variations in dominance, diversity and biotic indices along a limestone stream receiving a trout farm effluent. *Water, Air, and Soil Pollution, 63*(3-4), 343–359.

Camargo, J. A., Gonzalo, C., & Alonso, Á. (2011). Assessing trout farm pollution by biological metrics and indices based on aquatic macrophytes and benthic macroinvertebrates : A case study. *Ecological Indicators*, *11*(3), 911–917.

Chowdhury, S. U., Othman, F., Jaafar, W. Z. W., Mood, N. C., & Adham, I. (2018). Assessment of pollution and improvement measure of water quality parameters using scenarios modeling for Sungai Selangor Basin. *Sains Malaysiana*, *47*(3), 457–469. doi:10.17576/jsm-2018-4703-05

Coldebella, A., Gentelini, A. L., Piana, P. A., Coldebella, P. F., Boscolo, W. R., & Feiden, A. (2018). Effluents from fish farming ponds : A view from the perspective of its main components. *Sustainability*, *10*(3), 1–16. doi:10.3390/su10010003

Daniel, R., & Kawasaki, N. (2016). The distribution of heavy metals and nutrients along Selangor River and its adjacent mining ponds, Malaysia. *International Journal of Advances in Agricultural & Environmental Enginering*, *3*(2), 241–244. doi:10.15242/IJAAEE.A0516012

Diana, J. S. (2009). Aquaculture production and biodiversity conservation. *BioScience*, *59*(1), 27–38. doi:10.1525/bio.2009.59.1.7

Etemi, F. Z., Bytyçi, P., Ismaili, M., Fetoshi, O., Ymeri, P., Shala–Abazi, A., & Czikkely, M. (2020). The use of macroinvertebrate based biotic indices and diversity indices to evaluate the water quality of Lepenci river basin in Kosovo. *Journal of Environmental Science and Health - Part A Toxic/Hazardous Substances and Environmental Engineering*, *55*(6), 748–758. doi:10.1080/10934529.2020.1738172

Fierro, P., Bertrán, C., Tapia, J., Hauenstein, E., Peña-Cortés, F., Vergara, C., & Vargas-Chacoff, L. (2017). Effects of local land-use on riparian vegetation, water quality, and the functional organization of macroinvertebrate assemblages. *Science of the Total Environment*, *609*, 724–734. doi:10.1016/j.scitotenv.2017.07.197

Fulazzaky, M. A., Seong, T. W., & Masirin, M. I. M. (2010). Assessment of water quality status for the Selangor River in Malaysia. *International Journal of Water,Air, and Soil Pollution*, *205*(1-4), 63–77. doi:10.1007/s11270-009-0056-2

HACH. (2007). DR 2800 Spectrophotometer procedures manual (2nd Ed.). USA: Hach company.

Hamid, S. A., Md Rawi, C. S., Dieng, H., Ahmad, A. H., Satho, T., & Miake, F. (2011). Seasonal changes in mayfly communities and abundance in relation to water physicochemistry in two rivers at different elevations in northern Peninsular Malaysia. *Wetland Science*, *9*(3), 240–250.

Hamzah, U., Samsudin, A. R., & Malim, E. P. (2007). Groundwater investigation in Kuala Selangor using vertical electrical sounding (VES) surveys. *Envrionemntal Geology*, *51*(8), 1349–1359. doi:10.1007/s00254-006-0433-8

Hanafi, H. H., Arshad, M. A., & Yahaya, S. (1995). *Report on a regional study and workshop on the environmental assessment and management of aquaculture development*. Bangkok, Thailand. Retrieved November 08, 2019 from http://www.fao.org/3/ac279e/AC279E13.htm.

Harun, S., Al-shami, S. A., Ramzah, D., Mohamed, M., & Abdullah, M. H. (2015). Water quality and aquatic insects study at the Lower Kinabatangan River Catchment, Sabah: In response to weak La Niña event. *Sains Malaysiana*, *44*(4), 545–558. doi:10.17576/jsm-2015-4404-09

Hasmi, N. A., Ramlan, N., Musa, N. N., & Faizzainuddin, M. A. (2017). Influence of physiochemical parameters on abandance of aquatic insects in rivers of Perak, Malaysia. *International Journal of Advances in Science Engineering and Technology*, *5*(4), 68–72.

Hatami, R., Soofiani, N. M., Ebrahimi, E., & Hemami, M. (2011). Evaluating the aquaculture effluent impact on macroinvertebrate community and water quality using BMWP index. *Journal of Environmental Studies*, *37*(59), 13–15.

Hilsenhoff, W. L. (1988). Rapid field asessment of organic pollution with a family-level biotic index. *Journal of the North American Benthological Society*, *7*(1), 65–68. doi:10.2307/1467832

Kang, H., Bae, M., Lee, D., Hwang, S., Moon, S., & Park, Y. (2017). Distribution patterns of the freshwater oligochaete Limnodrilus hoffmeisteri influenced by environmental factors in streams on a Korean nationwide scale. *Water*, *9*(12), 1–11. doi:10.3390/w9120921

Karimi, J. M., Takami, G. A., Khara, H., & Abbaspour, R. (2016). Influence of trout farm effluents on water quality parameters and benthic macroinvertebrates. *Iranian Journal of Fisheries Sciences*, *15*(1), 133–143.

Kawasaki, N., Kushairi, M. R. M., Nagao, N., Yusoff, F., Imai, A., & Kohzu, A. (2016a). Release of nitrogen and phosphorus from aquaculture farms to Selangor River, Malaysia. *International Journal of Environmental Science and Development*, *7*(2), 113–116. doi:10.7763/IJESD.2016.V7.751

Kawasaki, N., Kushairi, M. R. M., Nagao, N., Yusoff, F., Imai, A., & Kohzu, A. (2016b). Seasonal changes of nutrient distributions along Selangor River, Malaysia. *International Journal of Advances in Chemical Engineering and Biological Sciences*, *3*(1), 113–116. doi:10.15242/ijacebs.a0516011

Kim, D. H., Chon, T. S., Kwak, G. S., Lee, S. B., & Park, Y. S. (2016). Effects of land use types on community structure patterns of benthic macroinvertebrates in streams of urban areas in the South of the Korea Peninsula. *Water*, *8*(5), 1–18. doi:10.3390/w8050187

Kırkag, M. U., Pulatsu, S., & Topcu, A. (2009). Trout farm effluent effects on water sediment quality and benthos. *Clean*, *37*(4–5), 386–391. doi:10.1002/clen.200800212

Kroll, S. A., Llacer, C. N., De La Cruz Cano, M., & De Las Heras, J. (2009). The influence of land use on water quality and macroinvertebrate biotic indices in rivers within Castilla-La Mancha(Spain). *Limnetica*, *28*(2), 203–214.

Kullasoot, S., Intrarasattayapong, P., & Phalaraksh, C. (2017). Use of benthic macroinvertebrates as bioindicators of anthropogenic impacts on water quality of Mae Klong river, Western Thailand. *Chiang Mai Journal of Science*, *44*(4), 1356–1366.

Lalonde, B. A., Garron, C., & Mercier, V. (2016). Analysis of benthic invertebrate communities downstream of land-based aquaculture facilities in Nova Scotia,Canada. *Cogent Environmental Science*, *2*(1), 1–11. doi:10.1080/23311843.2015.1136099

Lembaga Urus Air Selangor. (2014). *Sungai Selangor basin management plan 2015 – 2020*. Selangor, Malaysia: Lembaga Urus Air Selangor and Selangor Management Authority.

Lembaga Urus Air Selangor. (2015). *State of the river report 2015 Sungai Selangor*. Selangor, Malaysia: Lembaga Urus Air Selangor.

Li-na, D., Yan-e, J., Xiao-yong, C., Jun-xing, Y., & Aldridge, D. (2017). A family-level macroinvertebrate biotic index for ecological assessment of lakes in Yunnan, China. *Water Resources*, *44*(6), 864–874. doi:10.1134/S0097807817090020

Ling, E. G. L. (2010). *Macroinvertebrates in disturbed and undisturbed sites in Asap, Belaga*. (Unpublished B.Sc. Thesis). Universiti Malaysia Sarawak, Malaysia.

Loch, D. D., West, J. L., & Perlmutter, D. G. (1996). The effect of trout farm effluent on the taxa richness of benthic macroinvertebrates. *Aquaculture*, *147*(1-2), 37–55. doi:10.1016/s0044-8486(96)01394-4

Mandaville, S. M. (2002). *Benthic macroinvertebrates in taxa tolerance values, metrics, and protocols*. Nova Scotia, Canada: Soil & Water Conservation Society of Metro Halifax.

Martins, R. T., Stephan, N. N. C., & Alves, R. G. (2008). Tubificidae (Annelida : Oligochaeta) as an indicator of water quality in an urban stream in southeast Brazil. *Acta Limnologica Brasiliensis*, *20*(3), 221–226.

Merritt, R. W., & K.W. Cummins. (1996). *An introduction to the aquatic insects of North America* (3rd ed.). Dubuque, Iowa: Kendal/Hunt Publishing Company.

Minoo, C. M., Ngugi, C. C., Oyoo-okoth, E., Muthumbi, A., Sigana, D., Mulwa, R., & Chemoiwa, E. J. (2016). Monitoring the effects of aquaculture effluents on benthic macroinvertebrate populations and functional feeding responses in a tropical highland headwater stream (Kenya). *Aquatic Ecosystem Health and Management*, *19*(4), 1–10. doi:10.1080/14634988.2016.1258896

Minoo, M. C. (2015). *Impacts of aquaculture on water quality and economic benefits in central Kenya: A case study of Gatundu south constituency*. (Unpublished M.Sc. Thesis). University of Nairobi. Retrived November 25, 2019 from http://erepository.uonbi.ac.ke/handle/11295/90072.

Miserendino, M. L., & Gullo, B. S. (2014). Occurrence of Hirudinea species in a post urban reach of a Patagonian mountain stream. *Iheringia, Série Zoologia*, *104*(3), 308–313. doi:10.1590/1678-476620141043308313

Mishra, P., Pandey, C. M., Singh, U., Gupta, A., Sahu, C., & Keshri, A. (2019). Descriptive statistics and normality tests for statistical data. *Annals of Cardiac Anaesthesia, 22*(1), 67-72. doi:10.4103/aca.aca_157_18

Moura, R. De, Souto, G., Facure, K. G., Pavanin, L. A., & Jacobucci, G. B. (2011). Influence of environmental factors on benthic macroinvertebrate communities of urban streams in Vereda habitats, Central Brazil. *Acta Limnologica Brasiliensia*, *23*(3), 293–306. doi:10.1590/s2179-975x2012005000008

Muhazar, A., Othman, M. S., Kutty, A. A., & Desa, M. N. (2013). Mornitoring urban river water using macroinvertabrate and physico-chemical parameters: Case study of Penchala River, Malaysia. *Biological Sciences*, *13*(6), 474–482. doi:10.3923/jbs.2013.474.482

Mustow, S. E. (2002). Biological moritoring of rivers in Thailand: use and adaptation of the BMWP score. *Hydrobiologia*, *479*(1-3), 191–229.

Namin, J. I., Sharifinia, M., & Makrani, A. B. (2013). Assessment of fish farm effluents on macroinvertebrates based on biological indices in Tajan River (north Iran). *Caspian Journal of Environmental Sciences Assessment*, *11*(1), 29–39.

Oliveira, A., & Callisto, M. (2010). Benthic macroinvertebrates as bioindicators of water quality in an Atlantic forest fragment. *Journal Iheringia, Série Zoologia*, *100*(4), 291–300. doi:10.1590/s0073-47212010000400003

Othman, F., SadekUddin, M. C., & Sakai, N. (2014). Assessment of microorganism pollution of Selangor River, Malaysia. *International Journal of Advances in Agricultural and Environmental Engineering*, *1*(2), 203–206.

Petrin, Z., Laudon, H., & Malmqvist, B. (2007). Does freshwater macroinvertebrate diversity along a pH-gradient reflect adaptation to low pH?. *Freshwater Biology*, *52*(11), 2172–2183. doi:10.1111/j.1365-2427.2007.01845.x

Prommi, T., & Payakka, A. (2015). Aquatic insect biodiversity and water quality parameters of streams in Northern Thailand. *Sains Malaysiana*, *44*(5), 707–717. doi.org/10.17576/jsm-2015-4405-10

Rak, A., Said, I., & Mohamed, M. (2011). Effects of land use on benthic macroinvertebrate assemblages at three rivers in Endau catchment area, Kluang, Johor, Malaysia. *Journal of Applied Sciences in Envrionmental Sanitation*, *6*(2), 97–103.

Rak, A., Said, I., Mohamod, M., & Abas, A. (2014). A preliminary benthic macroinvertebrates survey of Gunung Belumut recreational forest, Kluang, Johor, Malaysia. *Journal of Wildlife and Parks*, *27*, 103–110.

Saremi, A., Saremi, K., Saremi, A., Sadeghi, M., & Sedghi, H. (2013). The effect of aquaculture effluents on water quality parameters of Haraz River. *Iranian Journal of Fisheries Sciences*, *12*(2), 445–453.

Seyam, M., & Othman, F. (2015). Long-term variation analysis of a tropical river's annual streamflow regime over a 50-year period. *Theoretical and Applied Climatology*, *121*(1-2), 71–85. doi:10.1007/s00704-014-1225-9

Shannon, C. E. (1948). A mathematical theory of communication. *Bell System Technical Journal*, *27*(3), 379–423.

Sharma, K. K., & Chowdhary, S. (2011). Macroinvertebrate assemblages as biological indicators of pollution in a Central Himalayan River, Tawi (J & K). *International Journal of Biodiversity and Conservation*, *3*(5), 167–174.

Simpson, E. H. (1949). Measurement of diversity. *Nature*, *163*(4148), 688.

Soonthornvipat, S., Soonthornvipat, P., & Chaibu, P. (2012, January, 10-12). Aquatic worms for aquaculture. In *Proceedings of the 1st Annual PSU Phuket International Conference* (pp. 1–5). Phuket, Thailand

Surtikanti, H. K. (2016). Uncertainty result of biotic index in analysing the water quality of Cikapundung river catchment area, Bandung. In T. Hidayat, A. B. D. Nandiyanto, A. Jupri, E. Suhendi, & H. S. H. Munawaroh (Eds.), *Proceedings of the 3rd International Seminar on Mathematics, Science, and Computer Science Education* (Vol. 1848). Bandung, Indonesia: AIP Publishing.

Tan, K. W., & Beh, W. C. (2016). Evaluation of water quality and benthic macrointervebrates fauna relationship using principal component analysis (PCA): A case study of Cameron Highlands Malaysia. *Environmental Management and Sustainable Development*, *5*(1), 187–208. doi:10.5296/emsd.v5i1.9399

Thorp, J. H., & Lovell, L. L. (2014). Phylum Annelida. In J. H. Thorp & D. C. Rogers (Eds.), *Thorp and Covich's Freshwater Invertebrates* (pp. 360–482). Amsterdam, Netherlands: Elsevier Publishing Company.

Verma, N., & Singh, A. K. (2013). Development of biological oxygen demand biosensor for monitoring the fermentation industry effluent. *ISRN Biotechnology*, *2013*, 1–6. doi:10.5402/2013/236062

Virbickas, T., Pliuraite, V., & Kesminas, V. (2011). Impact of agricultural land use on macroinvertebrate fauna in Lithuania. *Polish Journal of Environmental Studies*, *20*(5), 1327–1334.

Vizakat, L., Harkantra, S. N., & Parulekar, A. H. (1991). Population ecology and community structure of subtidal soft sediment dwelling macro- invertebrates of Konkan, West coast of India. *Indian Journal of Marine Science*, *20*(1), 40–42.

Yong, S. H., & Yule, C. M. (2004). *Fresh water Invertebrates of the Malaysian region*. Kuala Lumpur, Malaysia: Akademi Sains Malaysia.

Young, S. S., Yang, H. N., Huang, D. J., Liu, S. M., Huang, Y. H., Chiang, C. T., & Liu, J. W. (2014). Using benthic macroinvertebrate and fish communities as bioindicators of the Tanshui river basin around the greater Taipei area - Multivariate analysis of spatial variation related to levels of water pollution levels of water pollution. *International Journal of Environmental Research and Public Health*, *11*(7), 7116–7143. doi:10.3390/ijerph110707116

Yusoff, A. (2015). Status of resource management and aquaculture in Malaysia. In M. R. R. Romana-Eguia, F. D. Parado-Estepa, N. D. Salayo, & M. J. H. Lebata-Ramos (Eds.), *Resource enhancement and sustainable aquaculture practices in Southeast Asia: Challenges in responsible production of aquatic species: Proceedings of the International Workshop on Resource Enhancement and Sustainable Aquaculture Practices in Southeast Asi*a. Iloilo, Philippines: Aquaculture Dept., Southeast Asian Fisheries Development Center.

Zhu, D., & Chang, J. (2008). Annual variations of biotic integrity in the upper Yangtze River using an adapted index of biotic integrity (IBI). *Ecological Indicators*, *8*(5), 564–572. doi:10.1016/j.ecolind.2007.07.004

Pertanika J. Sci. & Technol. 28 (S2): 47 - 57 (2020)

PERTANIKA JOURNALS

SCIENCE & TECHNOLOGY

Journal homepage: http://www.pertanika.upm.edu.my/

The Construction of Plant Expression Vector harbouring *Carica Papaya* L. *WRKY* Gene in *Escherichia coli*

Fauziah Abu Bakar[1]*, Pavitra Paramalingam[2] and Kamariah Hasan[3]

[1]*Department of Crop Science, Faculty of Agricultural Science and Forestry, Universiti Putra Malaysia Bintulu Sarawak Campus, 97008 Bintulu, Sarawak, Malaysia*
[2]*Faculty of Biotechnology and Biomolecular Sciences, Universiti Putra Malaysia, 43400 UPM Serdang, Selangor Darul Ehsan, Malaysia*
[3]*School of Biological Sciences, Faculty of Science and Technology, Quest International University, 30250 Ipoh, Perak, Malaysia*

ABSTRACT

Carica papaya is a well-liked and economically important fruit with outstanding nutritional and medicinal values. Its susceptibility to abiotic stress which affects the growth and harvest, causes significant yield loss to farmers. In recent years, significant progress has been made to understand the genes that play critical roles in abiotic stress response, especially some transcription factor (TF) encoding genes. Among all TFs, WRKY TF gene family is one of the best-studied TFs involved in various stress responses. To date, only limited information on functionally characterised WRKY TFs is available for *C. papaya*. The aim of this study was to produce a recombinant construct harbouring *WRKY* gene in pGEM®-T Easy cloning vector. The presence of a DNA band of the expected size of 465 bp on agarose gel electrophoresis indicated that *WRKY* gene was successfully amplified from all treated samples. DNA sequencing analysis revealed that the amplified sequence isolated from the treated samples were closely related to *Carica papaya* species with 97% similarity. Following transformation, 4 out of 5 colonies that were randomly selected showed the *WRKY* gene had been successfully inserted into pGEM®-T Easy vector and transformed into *E. coli*. In future, the *WRKY* gene from pGEMT-*WRKY* recombinant construct will be cloned into

ARTICLE INFO

Article history:
Received: 10 February 2020
Accepted: 13 November 2020
Published: 31 December 2020

DOI: https://doi.org/10.47836/pjst.28.S2.04

E-mail addresses:
ab_fauziah@upm.edu.my (Fauziah Abu Bakar)
pavitra172@gmail.com (Pavitra Paramalingam)
kamariah@qiup.edu.my (Kamariah Hasan)
*Corresponding author

ISSN: 0128-7680
e-ISSN: 2231-8526

© Universiti Putra Malaysia Press

the plant expression vector pCAMBIA 1304 prior to transformation in the plant. The success of demonstrating the *WRKY* gene towards the response in abiotic stress will enable us to produce stress tolerant transgenic crops under unfavourable conditions via genetic engineering for sustained growth.

Keywords: Abiotic stress, carica papaya L., recombinant, salinity, WRKY transcription factor

INTRODUCTION

Papaya is a well-liked and economically important fruit crop in many countries including Malaysia due to its high nutritive value, production potentiality and many pharmacological benefits (Oliveira & Vitória, 2011). As a common climacteric fruit, papaya suffers many problems including susceptibility to abiotic environmental factors such as drought and high salinity, which could hamper its production worldwide. Up to date, traditional plant breeding has not been proven to be successful in mitigating abiotic stress problems. Hence, understanding how the papaya responds to these stresses at the molecular level could provide more effective strategy to tackle the problems.

Several significant attempts have been conducted to enhance abiotic stress resistance in crops. One of the successful attempts is by regulating the expression of a number of stress-responsive transcription factors (TFs) genes such as TFs from the bZIP, NAC, AP2 and WRKY. Many of these TFs have been shown to play significant roles in abiotic stress particularly to enhance plant adaptation to drought and salt stresses (Ma et al., 2019; Ullah et al., 2018). Among all TFs that have been studied so far, the *WRKY* TF gene family is among the well-known classes of plant TFs (Song et al., 2018; Xie et al., 2018). The earliest *WRKY* gene, known as SPF1 was characterised from sweet potato (Ishiguro & Nakamura, 1994). Since then, a number of WRKY proteins with various functions in many plants have been widely described, specifically playing role in biotic and abiotic stresses (Bai et al., 2018; Liu et al., 2019, 2016), as well as in the regulation of hormones (Chen et al., 2012; Johnson et al., 2002; Lagacé & Matton, 2004; Song et al., 2010).

Lately, the functional characterisation of WRKY proteins in response to abiotic stresses in plants was extensively studied. For example, overexpression of OsWRKY11 and OsWRKY42 in transgenic rice seedlings showed enhanced drought tolerance (Shen et al., 2012; Wu et al., 2009). Similarly, WRKY25 and WRKY26 from *Arabidopsis thaliana* exhibited substantially increased tolerance to heat stress when overexpressed (Li et al., 2011). Other than these two examples, various *WRKY* genes had also been characterised from other plants. For instance, overexpression of SpWRKY1 and GhWRKY41 from tomato and cotton, respectively, had shown remarkable improvement in salt and drought resistance in transgenic tobacco (Chu et al., 2016; Li et al., 2015). More *WRKY* genes

including TaWRKY2 and TaWRKY19 (wheat), VaWRKY14 (grapevine) and PeWRKY83 (moso bamboo) showed increased resistance to drought and/or salt stresses, respectively, when overexpressed in Arabidopsis (Niu et al., 2012; Wu M. et al., 2017).

While the research on the response of WRKY proteins to biotic stress has been widely reported, little information is available to understand the mechanism of WRKY proteins in plant abiotic stress (Niu et al., 2012). However, it is well known that abiotic stress such as high salinity could cause major damage in plants. Under stress conditions, the accumulation of second messengers such as ROS and IP3 modulates cytoplasmic Ca^{2+} and protein signaling pathways, resulting in stress-responsive gene expression and physiological changes in the plant (Huang et al., 2012; Xiong et al., 2002).

In addition, far less information is available to understand the function of WRKY proteins in *C. papaya*. As a major tropical crop consumed worldwide, various abiotic stresses such as drought, salinity and extreme temperature have caused a major hiccup in the papaya industry. Hence, the functional mechanisms on how *C. papaya* responds to abiotic stress need to be identified and genetic engineering could be one of the solutions to achieve this aim. Based on the genome-wide analysis of the *WRKY* gene family in *C. papaya* reported earlier by Pan & Jiang (2014), one of the *WRKY* candidate genes designated as TF807.3 was found to be involved in response to low temperature, drought, wound and PRSV pathogen. However, there has yet been any reports on the functionality of this *WRKY* gene in salinity stress. The current study reports the construction of recombinant construct harbouring *WRKY* gene in pGEM®-T Easy vector and the transformation into *Escherichia coli*. In the future study, the pCAMBIA 1304 plant expression vector harbouring WRKY gene will be constructed prior to transformation into *Arabidopsis thaliana*. The salt stress tolerance will be investigated to determine its response towards salt stress conditions. The success of demonstrating the response of *WRKY* gene towards the abiotic stress will enable us to produce stress tolerant transgenic crops to sustain its growth under unfavorable conditions.

MATERIALS AND METHODS

Plant Materials and Stress Treatment

Seedlings of *C. papaya* L. 'Sekaki' variety purchased from the local supermarket were grown under controlled greenhouse conditions, with a cycle of 16 h/day with three replications. For salt treatment, 30-day-old seedlings with four to five leaves were treated with 200 mM NaCl and leaves were harvested at 24 h following the stress treatment. The control used in this study was the plants treated with only water. Fresh leaves were harvested from each treated and control plants, then rapidly frozen in liquid nitrogen and stored at -80°C prior to RNA extraction. All the experiments were performed independently in triplicate.

RNA Isolation and cDNA Synthesis

Total RNA was extracted from leaves samples using a modified CTAB-based method (Rogers & Bendich, 1994). The quantity and quality of the RNA were examined using NanoDrop™ 2000/2000c spectrophotometer (Thermo Scientific, USA). The RNA was sequentially treated with DNase I (Invitrogen™, USA) to remove genomic DNA. One microgram of RNA was used for cDNA synthesis using QuantiTect® Reverse Transcription Kit (Qiagen, Germany) according to the manufacturer's instructions. Polymerase chain reaction (PCR) was performed to obtain a whole sequence of WRKY using the first-strand cDNA of *C. papaya* as a template. A pair of gene-specific primers, WRKY4_F: 5′-CCATGGATGGAGAAGTACCAAATTCTTTTCCCAGAC-3′ and WRKY4_R: 5′-AGATCTTTATACAATCAGGTTGAGCGATATTACAAT-3′, were designed based on the *C. papaya* WRKY coding sequence (GI 186140666) to amplify the full-length cDNA sequence. The *Nco*1 and *Bgl*II restriction sites were included at the 5′ end of the WRKY4_F and WRKY4_R respectively, to facilitate construction into plant expression vector pCAMBIA 1304 in the future. The *WRKY* was amplified using GoTaq® Flexi DNA Polymerase (Promega, USA) in a total volume of 25 µL in a thermal cycler (Biorad, USA) with the following conditions: initial denaturation at 95°C for 2 min, followed by 30 cycles of amplification (95°C for 1 min, 56°C for 1 min, and 72°C for 1 min) and a final extension at 72°C for 3 min. The resulting PCR products with an expected size of 465 bp was examined by agarose gel electrophoresis, then purified using the QIAquick Gel Extraction Kit (Qiagen, Germany) according to the manufacturer's instructions. The gel-purified DNA was later confirmed by DNA sequencing.

Bioinformatic Analysis of *CpWRKY*

The *CpWRKY* gene sequence was extracted from the local papaya database (GI 186140666) using BLAST with the CDS of *CpWRKY* as a query. BLASTn was performed to search for maximum identity and the number of bases of aligned sequence.

Cloning into pGEM®-T Easy Vector

The purified PCR product and pGEMT®-T Easy vector were digested with *Nco*1 and *Bgl*II restriction endonucleases. The digested PCR product was later cloned into pGEM®-T Easy vector according to the manufacturer's instructions and subsequently transformed into chemically competent *E. coli* DH5α cells using the heat shock method. In order to confirm the successful transformation of recombinant *E. coli* harbouring WRKY, colony PCR was performed using GoTaq® Green Master Mix (Promega, USA) in a total volume of 25 µL. The WRKY4 forward and reverse primers were used to amplify the transformed

gene with the same amplification conditions as described above. The positive recombinant *E. coli* harbouring *CpWRKY* were kept prior to further experiment.

RESULTS AND DISCUSSION

Previously, the functions of plant WRKY transcription factors were extensively reported to play a role in biotic stress responses (Li et al., 2006; Matsushita et al., 2012; Qiu & Yu, 2008; Shen et al., 2007; Xu et al., 2006). In recent years, a number of studies demonstrated that WRKY proteins play important role in abiotic stresses, such as drought and salinity (Chen et al., 2012; Jiang et al., 2012; Zhu et al., 2019). Although WRKY TFs have been reported in many plants, their roles in abiotic stresses are not well known in *Carica papaya*. Therefore, it is of interest to investigate if the WRKY protein from *C. papaya* would function in abiotic stress particularly salinity, as other WRKYs from other crops have been demonstrated to be functional in important crops such as rice, maize and wheat (Cai et al., 2014; Niu et al., 2012; Shen et al., 2012; Wu et al., 2009). To achieve the main aim of this study, WRKY4 primers were designed based on the *WRKY* gene sequence (GI 186140666), obtained from genome-wide analysis in *C. papaya* which has been reported earlier (Pan & Jiang, 2014). This sequence was chosen in this study because it has been shown to be involved in response to low temperature, drought, wound and PRSV pathogen. However, there has yet to be any report on the functionality of this *WRKY* gene in salinity stress. In this paper, we report our preliminary study on the cloning of *C. papaya WRKY* gene in pGEM®-T Easy vector.

Prior to amplification, a *WRKY* gene was isolated from *C. papaya* L. 'Sekaki' that had been treated with 200 mM NaCl and designated as *CpWRKY4*. Following treatment, total RNA was extracted from salt-treated and non-treated (control) plants. Intact total RNA extracted from these *C. papaya* leaves showed 28S rRNA band intensity about twice that of the 18S rRNA (Figure 1). *CpWRKY4* gene was amplified from salt-treated *C. papaya* leaves cDNA by RT-PCR. As a result from agarose gel electrophoresis, the PCR products amplified from the cDNA using WRKY4 primers showed a DNA band of the expected size of 465 bp (Figure 2).

A total of 4 PCR products (Figure 2 Lanes 1 – 4) were sent for sequencing and DNA analysis confirmed that these amplified sequences isolated from the treated samples were closely related to *C. papaya* WRKY sequences reported by Pan & Jiang (2014) with 97% similarity (Figure 3). Based on the results generated in NCBI database, this WRKY TF also showed close identity with other plant species including cotton, squash and grapevine, with 89%, 85% and 84% similarities, respectively (Figure 4). These results indicated that a completed sequence and deduced amino acid sequences of this gene showed homology with WRKY domain-containing proteins from other plants.

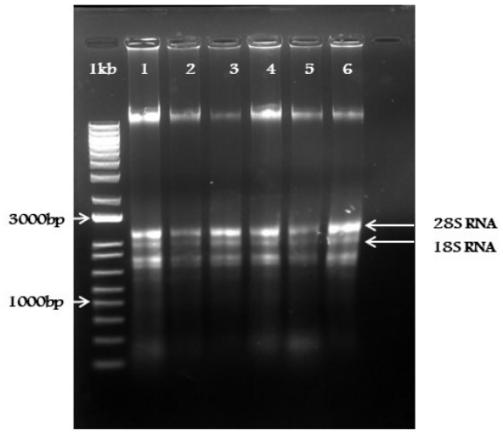

Figure 1. Total RNA extracted from treated and non-treated *C. papaya* following salt treatment. (Lanes 1 – 2: non-treated plant; Lanes 3 – 6: treated plants). 1kb: 1-kb DNA ladder (Fermentas). Molecular sizes are indicated.

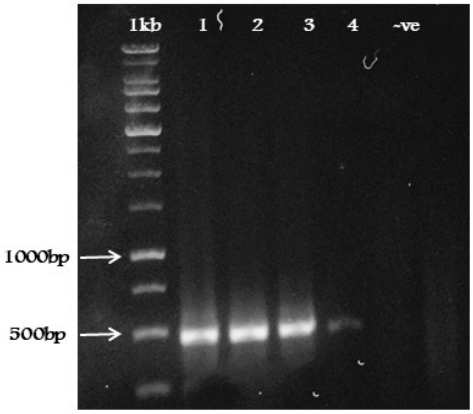

Figure 2. The amplification of full coding sequence of *CpWRKY4* gene using WRKY4 primers (Lanes 1 – 4: treated plants), resulted in the expected amplified product of 465 bp; lane -ve: non-treated plant (control); 1kb: 1 kbp DNA ladder (Fermentas). Molecular sizes are indicated.

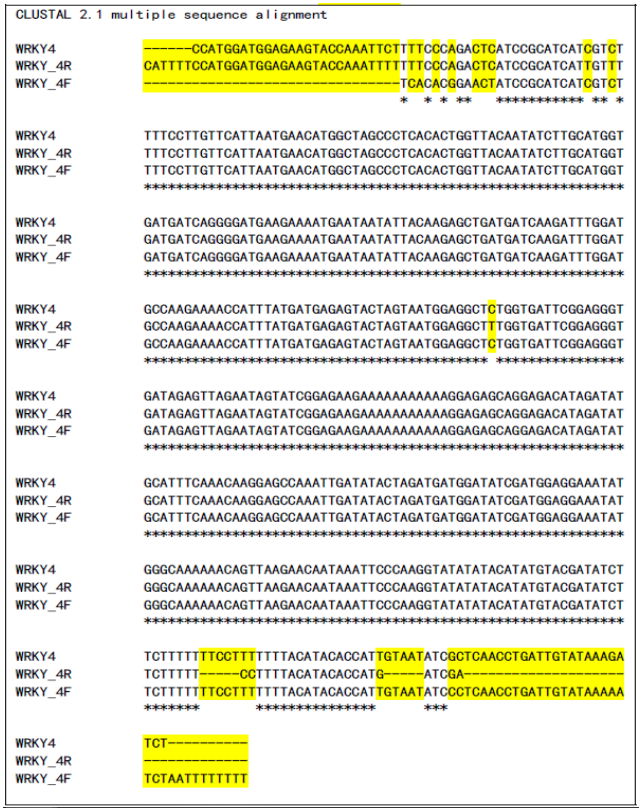

Figure 3. Comparison of the nucleotide sequences of the coding regions of WRKY from *Carica papaya.* The difference in nucleotides are highlighted in yellow and deletions are indicated by dashes.

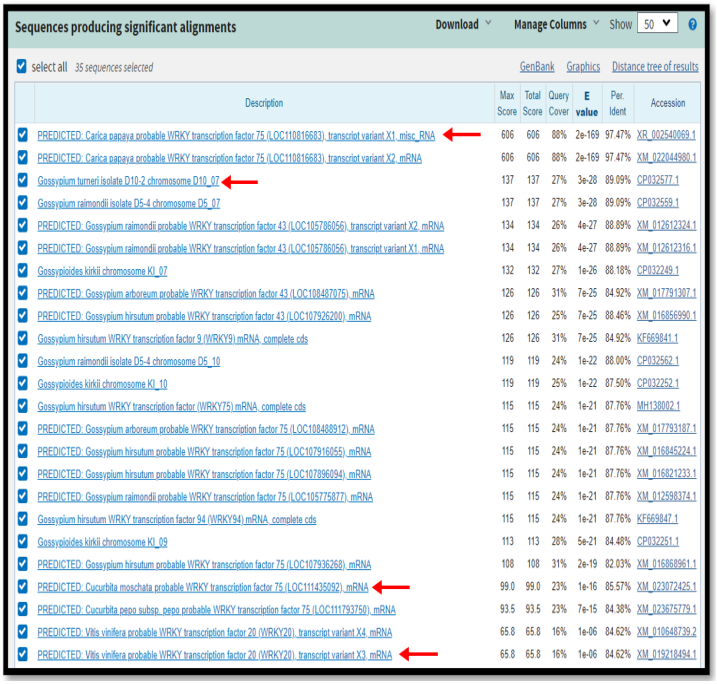

Figure 4. An excerpt of BLAST result, indicating top hits with significant homology to *CpWRKY4* gene from different plant species (indicated in red arrow).

The purified PCR product was cloned into pGEM®-T Easy vector and transformed into *E. coli* DH5α. Following transformation, five colonies were selected and the successful transformation was confirmed by using colony PCR using WRKY4 primers. The results showed that all the colonies except for colony 1 contained the correct WRKY amplified fragment, as indicated by the presence of DNA band of the expected size of 465 bp (Figure 5). In total, 4 out of 5 chosen colonies possessed the desired recombinant *WRKY* gene and these positive clones were selected to be cloned into the plant expression vector, pCAMBIA 1304 in a future experiment.

As a proof of concept, the plant recombinant construct harboring pCAMBIA1304_ *CpWRKY* will be transformed and expressed in a model plant *Arabidopsis thaliana* before generating transgenic *C. papaya* in the future. This is particularly important to investigate whether salt tolerance could be improved and gain further insights into the detailed mechanism of *CpWRKY* in response to salt stress conditions. The success of producing transgenic plants harboring *CpWRKY* in response to abiotic stress will provide fundamental knowledge in the agriculture industry, particularly for papaya in order to sustain its production under unfavourable environmental conditions.

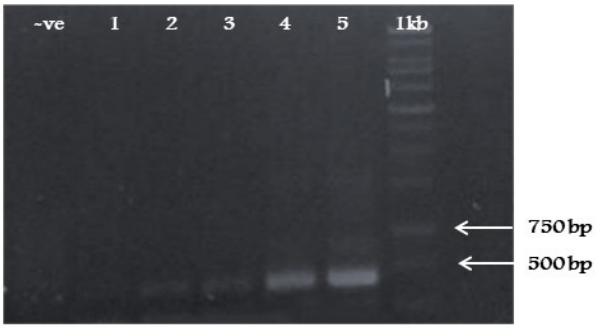

Figure 5. Colony PCR of pGEMT-*WRKY4* transformants. All colonies except No. 1 possessed the correct *WRKY* amplified fragment. Lanes 1 – 5: PCR of bacterial colonies using WRKY4 primers.

CONCLUSION

A full coding cDNA encoding WRKY has been isolated from *C. papaya* and designated as *CpWRKY4.* DNA sequencing analysis revealed that this isolated WRKY is closely related to *C.papaya* with 97% similarity. Cloning of the *CpWRKY4* into the plant expression vector pCAMBIA 1304 prior to transformation into *Arabidopsis thaliana,* for further functional studies, is currently in progress.

ACKNOWLEDGMENT

This work was supported financially by the Ministry of Higher Education (MOHE) FRGS (FRGS/1/2018/STG05/QUEST/03/1) and by the Universiti Putra Malaysia Grant (UPM/800-3/3/1/GP-IPM/2019/9681100). P.P performed the experiments. F.A.B designed the study. F.A.B, P.P and K.H wrote, edited and approved this manuscript.

REFERENCES

Bai, Y., Sunarti, S., Kissoudis, C., Visser, R. G., & Van der Linden, C. G. (2018). The role of tomato WRKY genes in plant responses to combined abiotic and biotic stresses. *Frontiers in Plant Science*, *9*, 1-7. doi:10.3389/fpls.2018.00801

Cai, R., Zhao, Y., Wang, Y., Lin, Y., Peng, X., Li, Q., ... & Cheng, B. (2014). Overexpression of a maize WRKY58 gene enhances drought and salt tolerance in transgenic rice. *Plant Cell, Tissue and Organ Culture (PCTOC)*, *119*(3), 565-577. doi:10.1007/s11240-014-0556-7

Chen, L., Song, Y., Li, S., Zhang, L., Zou, C. and Yu, D. (2012). The role of WRKY transcription factors in plant abiotic stresses. *Biochimica et Biophysica Acta (BBA)-Gene Regulatory Mechanisms*, *1819*(2), 120-128. doi:10.1016/j.bbagrm.2011.09.002

Chu, X., Wang, C., Chen, X., Lu, W., Li, H., Wang, X., ... & Guo, X. (2016). Correction: The cotton WRKY gene GhWRKY41 positively regulates salt and drought stress tolerance in transgenic. *Nicotiana benthamiana. PloS One*, *11*(6), 1-21. doi:10.1371/journal.pone.0157026

Huang, G. T., Ma, S. L., Bai, L. P., Zhang, L., Ma, H., Jia, P., ... & Guo, Z. F. (2012). Signal transduction during cold, salt, and drought stresses in plants. *Molecular Biology Reports*, *39*(2), 969-987. doi:10.1007/s11033-011-0823-1

Ishiguro, S., & Nakamura, K. (1994). Characterization of a cDNA encoding a novel DNA-binding protein, SPF1, that recognizes SP8 sequences in the 5′ upstream regions of genes coding for sporamin and β-amylase from sweet potato. *Molecular and General Genetics MGG 244*(6), 563–571. doi:10.1007/bf00282746

Jiang, Y. J., Liang, G. & Yu, D. Q. (2012). Activated expression of WRKY57 confers drought tolerance in Arabidopsis. *Molecular Plant, 5*(6), 1375-1388. doi:10.1093/mp/sss080

Johnson, C. S., Kolevski, B. & Smyth, D. R. (2002). TRANSPARENT TESTA GLABRA2, a trichome and seed coat development gene of Arabidopsis, encodes a WRKY transcription factor. *The Plant Cell*, *14*(6), 1359-1375. doi:10.1105/tpc.001404

Lagacé, M. & Matton, D. P. (2004). Characterization of a WRKY transcription factor expressed in late torpedo-stage embryos of Solanum chacoense. *Planta*, *219*(1), 185-189. doi:10.1007/s00425-004-1253-2

Li, J. B., Luan, Y. S., & Liu, Z. (2015). Overexpression of SpWRKY1 promotes resistance to Phytophthora nicotianae and tolerance to salt and drought stress in transgenic tobacco. *Physiologia Plantarum*, *155*(3), 248-266. doi:10.1111/ppl.12315

Li, J., Brader, G., Kariola, T. & Palva, E.T. (2006). WRKY70 modulates the selection of signaling pathways in plant defense. *The Plant Journal, 46*(3), 477-491. doi:10.1111/j.1365-313x.2006.02712.x

Li, S., Fu, Q., Chen, L., Huang, W., & Yu, D. (2011). *Arabidopsis thaliana* WRKY25, WRKY26, and WRKY33 coordinate induction of plant thermotolerance. *Planta*, *233*(6), 1237-1252. doi:10.1007/s00425-011-1375-2

Liu, X., Song, Y., Xing, F., Wang, N., Wen, F., and Zhu, C. (2016). GhWRKY25, a group I WRKY gene from cotton, confers differential tolerance to abiotic and biotic stresses in transgenic. *Nicotiana benthamiana*. *Protoplasma, 253*(5), 1265-1281. doi:10.1007/s00709-015-0885-3

Liu, Y., Yang, T., Lin, Z., Gu, B., Xing, C., Zhao, L., ... & Huang, X. (2019). A WRKY transcription factor PbrWRKY53 from *Pyrus betulaefolia* is involved in drought tolerance and AsA accumulation. *Plant Biotechnology Journal*, *17*(9), 1770-1787. doi:10.1111/pbi.13099

Ma, Q., Xia, Z., Cai, Z., Li, L., Cheng, Y., Liu, J., & Nian, H. (2019). GmWRKY16 enhances drought and salt tolerance through an ABA-mediated pathway in *Arabidopsis thaliana. Frontiers in Plant Science*, *9*, 1-18. doi:10.3389/fpls.2018.01979

Matsushita, A., Inoue, H., Goto, S., Nakayama, A., Sugano, S., Hayashi, N., & Takatsuji, H. (2012) Nuclear ubiquitin proteasome degradation affects WRKY45 function in the rice defense program. *The Plant Journal, 73*(2), 302-313. doi:10.1111/tpj.12035

Niu, C. F., Wei, W., Zhou, Q. Y., Tian, A. G., Hao, Y. J., Zhang, W. K., ... Chen, S. Y. (2012). Wheat WRKY genes TaWRKY2 and TaWRKY19 regulate abiotic stress tolerance in transgenic Arabidopsis plants. *Plant Cell & Environment, 35*(6), 1156–1170. doi:10.1111/j.1365-3040.2012.02480.x

Oliveira, J. G., & Vitória, A. P. (2011). Papaya: Nutritional and pharmacological characterization, and quality loss due to physiological disorders. An overview. *Food Research International*, *44*(5), 1306–1313. doi:10.1016/j.foodres.2010.12.035

Pan, L. J., & Jiang, L. (2014). Identification and expression of the WRKY transcription factors of *Carica papaya* in response to abiotic and biotic stresses. *Molecular Biology Reports*, *41*(3), 1215-1225. doi:10.1007/s11033-013-2966-8

Qiu, Y. P. & Yu, D. Q. (2008). Over-expression of the stress-induced OsWRKY45 enhances disease resistance and drought tolerance in Arabidopsis. *Environmental and Experimental Botany, 65*(1), 35-47. doi:10.1016/j.envexpbot.2008.07.002

Rogers, S. O., & Bendich, A. J. (1994). Extraction of total cellular DNA from plants, algae and fungi. In Gelvin, S. B. & Schilperoort, R. A. (Ed.), *Plant molecular biology manual* (pp. 183-190). Dordrecht, Netherlands: Springer.

Shen, H., Liu, C., Zhang, Y., Meng, X., Zhou, X., Chu, C., & Wang, X. (2012). OsWRKY30 is activated by MAP kinases to confer drought tolerance in rice. *Plant Molecular Biology, 80*(3), 241-253. doi:10.1007/s11103-012-9941-y

Shen, Q. H., Saijo, Y., Mauch, S., Biskup, C., Bieri, S., Keller, B. ... & Schulze-Lefert, P. (2007). Nuclear activity of MLA immune receptors links isolate-specific and basal disease-resistance responses. *Science, 315*(5815), 1098-1103. doi:10.1126/science.1136372

Song, H., Sun, W., Yang, G. & Sun, J. (2018). WRKY transcription factors in legumes. *BMC Plant Biology*, *18*(1), 1-13. doi:10.1186/s12870-018-1467-2

Song, Y., Al, C. R., Jing, S. J., & Yu, D. Q. (2010). Research progress on functional analysis of rice WRKY genes. *Rice Science*, *17*(1), 60-72. doi:10.1016/s1672-6308(08)60105-5

Ullah, A., Sun, H., Hakim, Yang, X., & Zhang, X. (2018). A novel cotton WRKY gene, GhWRKY6-like, improves salt tolerance by activating the ABA signaling pathway and scavenging of reactive oxygen species. *Journal of Plant Physiology*, *162*(4), 439–454. doi:10.1111/ppl.12651

Wu, M., Liu, H., Han, G., Cai, R., Pan, F., & Xiang, Y. (2017). A moso bamboo WRKY gene *PeWRKY83* confers salinity tolerance in transgenic Arabidopsis plants. *Scientific Reports, 7*(1), 1-16. doi:10.1038/s41598-017-10795-z

Wu, X., Shiroto, Y., Kishitani, S., Ito, Y. & Toriyama, K. (2009). Enhanced heat and drought tolerance in transgenic rice seedlings overexpressing OsWRKY11 under the control of HSP101 promoter. *Plant Cell Reports*, *28*(1), 21-30. doi:10.1007/s00299-008-0614-x

Xie, T., Chen, C., Li, C., Liu, J., Liu, C., & He, Y. (2018). Genome-wide investigation of WRKY gene family in pineapple: evolution and expression profiles during development and stress. *BMC Genomics, 19*(1), 1-18. doi:10.1186/s12864-018-4880-x

Xiong, L., Schumaker, K. S., & Zhu, J. K. (2002). Cell signaling during cold, drought, and salt stress. *The Plant Cell*, *14*(suppl 1), S165-S183. doi:10.1105/tpc.000596

Xu, X., Chen, C., Fan, B. & Chen, Z. (2006). Physical and functional interactions between pathogen-induced Arabidopsis WRKY18, WRKY40, and WRKY60 transcription factors. *The Plant Cell, 18*(5), 1310-1326. doi:10.1105/tpc.105.037523

Zhu, D., Hou, L., Xiao, P., Guo, Y., Deyholos, M. K., & Liu, X. (2019). VvWRKY30, a grape WRKY transcription factor, plays a positive regulatory role under salinity stress. *Plant Science*, *280*, 132-142. doi:10.1016/j.plantsci.2018.03.018

Pertanika J. Sci. & Technol. 28 (S2): 59 - 70 (2020)

PERTANIKA JOURNALS

SCIENCE & TECHNOLOGY

Journal homepage: http://www.pertanika.upm.edu.my/

Regression Equation between Required Force and Lumbar Load of Caregiver in Supporting Standing-up Motion via Computational Musculoskeletal Simulation

Kodai Kitagawa[1]*, Yoshiki Nishisako[1], Takayuki Nagasaki[2], Sota Nakano[3], Mitsumasa Hida[1,4], Shogo Okamatsu[1,5] and Chikamune Wada[1]

[1]Graduate School of Life Science and Systems Engineering, Kyushu Institute of Technology, 2-4 Hibikino, Wakamatsu-ku, Kitakyushu 808-0196, Japan
[2]Department of Rehabilitation, Faculty of Medical Science and Welfare, Tohoku Bunka Gakuen University, 6-45-1 Kunimi, Aoba-ku, Sendai 981-8551, Japan
[3]Department of Rehabilitation, Kyushu University of Nursing and Social Welfare, 888 Tomio, Tamana 865-0062, Japan
[4]Department of Physical Therapy, Faculty of Rehabilitation, Osaka Kawasaki Rehabilitation University, 158 Mizuma, Kaizuka 597-0104, Japan
[5]Department of Physical Therapy, Kitakyushu Rehabilitation College, 1575 Kamikatashima, Kanda-machi, Miyako-gun, 800-0343, Japan

ABSTRACT

Caregivers experience low back pain because of patient handling such as supporting standing-up. The lumbar load of a caregiver depends on the required force for patient handling motions. If the relationship between the required force and the lumbar load is quantitatively clarified, it may be useful for preventing low back pain in caregivers. In this study, we investigated the quantitative relationships between the required force and lumbar loads such as vertebral stress and muscle activity in supporting standing-up by computational musculoskeletal simulation. First, a musculoskeletal model of a caregiver was prepared, and then the model performed simulated supporting standing-up motions. The vertical load used as the required

ARTICLE INFO

Article history:
Received: 10 February 2020
Accepted: 13 November 2020
Published: 31 December 2020

DOI: https://doi.org/10.47836/pjst.28.S2.05

E-mail addresses:
kitagawakitagawa156@gmail.com (Kodai Kitagawa)
nishisako-yoshiki@edu.brain.kyutech.ac.jp (Yoshiki Nishisako)
nagasaki@rehab.tbgu.ac.jp (Takayuki Nagasaki)
nakano@kyushu-ns.ac.jp (Sota Nakano)
hidam@kawasakigakuen.ac.jp (Mitsumasa Hida)
shogo.okamatsu182505@gmail.com (Shogo Okamatsu)
wada@brain.kyutech.ac.jp (Chikamune Wada)
*Corresponding author

ISSN: 0128-7680
e-ISSN: 2231-8526

© Universiti Putra Malaysia Press

force was placed on the upper limb of the model. The compressive/shear stress of the vertebral (L4–L5) and muscle activities of spinae erector muscle group were recorded as the lumbar load. The results showed that there are highly significant correlations between the required force ($r > 0.9$, $p < 0.01$). In addition, regression equations for predicting each lumbar load by the required force with highly determination coefficients ($R^2 > 0.9$) were obtained from these relationships. Furthermore, we found that when the required force was more than 120 N, the compression stresses of the vertebral exceeded injury threshold (3400 N) by the regression equation. These regression equations contribute to quantitatively consider lumbar loads of caregiver during patient handling based on injury thresholds and the required force.

Keywords: Caregiver, lumbar load, musculoskeletal simulation, regression equation, required force, supporting standing-up

INTRODUCTION

Many caregivers experience low back pain because of frequent patient handling, such as transfer and supporting standing-up (Holtermann et al., 2013). Patient handling is considered to be the cause of low back pain because it involves heavy lifting, bending, and twisting (Schibye et al., 2003). There are assistive devices that reduce lumbar load during patient handlings, such as the sliding sheet and lifting robot (Iwakiri et al., 2016). However, these devices are not used in several facilities because there are limitations in time efficiency, cost, and workspace (Iwakiri et al., 2016). Therefore, it is necessary to assess the risk of low back pain due to patient handling without an assistive device.

Some studies have reported strategies for reducing the lumbar load (Ibrahim & Elsaay, 2015; Itami et al., 2010; Karahan & Bayraktar, 2004; Schibye et al., 2003). Schibye et al. (2003) reported that lumbar load during several patient handlings was reduced by pulling instead of lifting procedures (Schibye et al., 2003). Karahan and Bayraktar (2004) found that body mechanics theory was useful for reducing lumbar load during patient handling. The body mechanics theory provides suitable movements during common activities such as lifting and helps to prevent low back pain (Ibrahim & Elsaay, 2015; Itami et al., 2010; Karahan & Bayraktar, 2004). Furthermore, there is a wearable device that can assess lumbar loads during patient handling (Doss et al., 2018). The PostureCoach can assess lumbar spine flexion related to lumbar loads by two inertial measurement units (Doss et al., 2020). A previous study suggested that the PostureCoach could be applied for preventing lower back pain among caregivers (Doss et al., 2020). These studies provide reducing lumbar load, but these strategies and device are not enough for preventing lower back pain because these does not consider quantitative required force and lumbar loads. The required force is

important for preventing lower back pain since it is considered that lumbar loads eventually depend on required force because of the weight and remained the ability of the patient. Therefore, this study focused on the relationship between required force and lumbar loads for further prevention of lower back pain.

Figure 1 shows the required force while supporting standing-up, which is a kind of patient handling. In supporting standing-up, the required force is considered to be the difference between the patient's weight and ground reaction force exerted by the patient. Nakano et al. (2019) suggested that wearable force shoes could measure the required forces while supporting standing-up (Nakano et al., 2019). Regarding lumbar loads, stress of the vertebral (L4–L5) joint and activities of spinae erector muscle are considered as important factors. (Kitagawa et al., 2019; Ning, 2017; Schibye et al., 2003). There are quantitative injury thresholds for preventing low back pain in these lumbar loads (Daynard et al., 2001; McGill et al., 1998; Waters et al., 1993). For example, 3400 N was recommended as the injury threshold for the compression stress of L4–L5 by the National Institute of Occupational Safety and Health (NIOSH) (Waters et al., 1993). In addition, previous studies considered that 500 N is injury threshold for shear stress of L4-L5 (Daynard et al., 2001; McGill et al., 1998). Furthermore, previous studies recommend that the activity of spinae erector muscle during lifting is less than 50-70 % of maximum voluntary contraction (Weames et al., 1994).

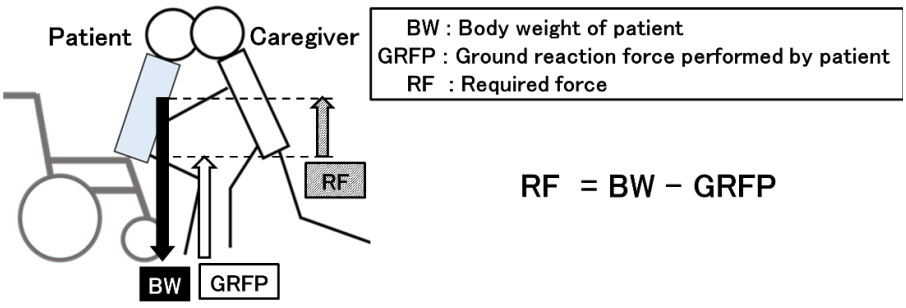

Figure 1. Required force for supporting standing-up

From these backgrounds, the quantitative relationships between the required force and lumbar loads are useful in preventing the low back pain of caregivers by wearable force shoes and injury threshold; however, these relationships were not quantitatively clarified. Therefore, this study investigated the quantitative relationships between the required force and lumbar loads during the support of standing-up motion, which caused the most lumbar load during patient handling (Schibye et al., 2003), using computational musculoskeletal simulation. Moreover, we present regression equations between the

required force and lumbar loads such as vertebral stress and muscle activity based on computational musculoskeletal simulation. These regression equations will be useful to predict quantitative lumbar loads based on the required force for preventing low back pain by wearable force shoes and injury thresholds.

MATERIALS AND METHODS

The AnyBody Modeling System (AnyBody Technology A/S, Denmark) is a musculoskeletal simulator that was used to investigate the relationship between the required force and lumbar loads during supporting standing-up motion. The system has an anatomically detailed biomechanical model and numerous muscles (Damsgaard et al., 2006; De Zee et al., 2007). The muscle strength and stress of the vertebral are calculated based on moment equilibrium equations using an optimization algorithm and inverse dynamics technique in the AnyBody Modeling System (Damsgaard et al., 2006). A study reported that the AnyBody Modeling System could predict the stress of L4–L5 joint during the lifting motion in closer agreement with *in vivo* data than other equation models and musculoskeletal simulators (Rajaee et al., 2015), suggesting that it is suitable to investigate the lumbar loads in supporting standing-up, which is similar to the lifting motion.

In this study, the simulated musculoskeletal model supported the standing-up motion based on a designated pelvic position in a computer environment. This musculoskeletal model was validated in our previous study (Kitagawa et al., 2019) and we found that it could evaluate the compression stress of L4–L5 joint while supporting standing-up by comparing with previous studies (Chaffin, 2005; Kitagawa et al., 2019; McGill & Norman, 1985). This model included characteristics of the muscles such as isometric force, fiber length, shortening velocity due to body based on body weight and height. Table 1 reveals the parameters of the simulated musculoskeletal model and supporting standing-up motion. Table 2 shows number of muscles in each body part of the musculoskeletal model. These parameters were determined based on the validations in our previous study (Kitagawa et al., 2019) and standard musculoskeletal model in the AnyBody Modeling System. Figure 2 reveals the supporting standing-up motion performed by the musculoskeletal model. The left foot was defined as the front foot and the right foot was defined as the rear foot. The arrows that are placed on the hands vertically in Figure 2 are the variable required force for this supporting standing-up motion. In this study, we investigated lumbar loads with different required forces (range: 0–630 N, interval: 90 N) by AnyBody Modeling System. The maximum, minimum and average values for compression stress, anterior/posterior shear stress and medial/lateral shear stress of the L4–L5 joint were calculated from time series data of each motion performed with different required force. In addition, average values for activity of spinae erector muscle of each side (left/right) were also evaluated.

These muscle activities were normalized by muscle physiological cross-sectional area based on body parameters such as height and weight defined by the AnyBody Modeling System. When this normalized index is more than 1.0, it is considered that muscle activity exceeds limits of the musculoskeletal model. These lumbar loads were calculated by inverse dynamics-based optimization.

Table 1
Parameters of the musculoskeletal simulation

Musculoskeletal Model	Body Height	1.8 m
	Body Weight	75 kg
Simulated Motion	Patient Handling	Supporting Standing
	Required Force	0-630 N
	Motion Time	0.8 seconds
	Sampling	100 Hz

Table 2
Number of muscles in each body part of the musculoskeletal model

Body Part	Number of Muscle
Neck	61
Upper Limb	284
Trunk	203
Lower Limb	330
Total	878

Correlation coefficients and regression equations were calculated as quantitative relationships between lumbar loads and the required force. Pearson's correlation coefficients between lumbar loads and the required forces were calculated using the EZR software (Kanda, 2013), which was developed by R programming language. The significant level was $p < 0.05$. The linear regression equations and determination coefficient between lumbar loads and the required forces were calculated by Microsoft Excel 2016 (Microsoft, USA).

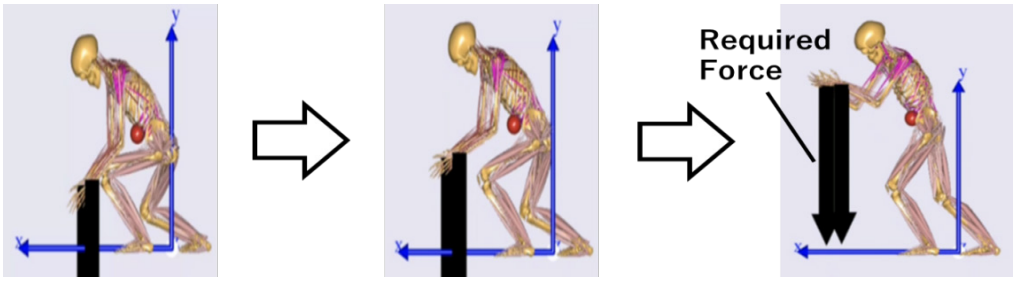

Figure 2. Supporting standing-up motion in computational simulation

RESULTS AND DISCUSSIONS

Table 3 shows correlation coefficients between the required force and each lumbar load. There were high significant correlations between the required force and all lumbar loads ($r > 0.9$, $p < 0.01$). Figure 3 – Figure 6 show scatter plots for the required force and each lumbar load. All lumbar loads had positive linear relationship with the required force. These high significant correlations and scatter plots suggest positive linear relationships between the required force and lumbar loads in the supporting standing-up motion. These trends are consistent with the result of a previous study related to common lifting task (Merryweather et al., 2009). Table 4 shows regression equations and determination coefficients for each lumbar load. Regression equations with high determination coefficients ($R^2 > 0.9$) were obtained for all lumbar loads. These high determination coefficients suggest that these regression equations obtained from computational musculoskeletal simulation could be used for prediction of lumbar loads of L4-L5 joint and erector spinae muscle.

Table 3

Correlation coefficients between the required force and lumbar load

Parameters Related to Lumbar Load	Correlation Coefficient (with Required Force)	p-value
Average of Compression Force of L4-L5	0.998	$p < 0.01$
Maximum Value of Compression Force of L4-L5	0.999	$p < 0.01$
Minimum Value of Compression Force of L4-L5	0.996	$p < 0.01$
Average of Anterior / Posterior Shear Force of L4-L5	0.999	$p < 0.01$
Maximum of Anterior / Posterior Shear Force of L4-L5	0.999	$p < 0.01$

Table 3 *(Continued)*

Parameters Related to Lumbar Load	Correlation Coefficient (with Required Force)	p-value
Minimum of Anterior / Posterior Shear Force of L4-L5	0.998	$p < 0.01$
Average of Medial / Lateral Shear Force of L4-L5	0.998	$p < 0.01$
Maximum of Medial / Lateral Shear Force of L4-L5	1.000	$p < 0.01$
Minimum of Medial / Lateral Shear Force of L4-L5	0.995	$p < 0.01$
Average of Muscle Activity in Left Sinae Erector Muscle	0.998	$p < 0.01$
Average of Muscle Activity in Right Sinae Erector Muscle	0.994	$p < 0.01$

Table 4

Regression equations and determination coefficients for lumbar load

Parameters Related to Lumbar Load	Regression Equations x : Required Force [N] y : Lumbar Load [N]/[-]	Determination Coefficient
Average of Compression Force of L4-L5 [N]	$y = 12.2 x + 1581.4$	0.995
Maximum Value of Compression Force of L4-L5 [N]	$y = 13.8 x + 1760.6$	0.997
Minimum Value of Compression Force of L4-L5 [N]	$y = 10.936 x + 1455.8$	0.992
Average of Anterior / Posterior Shear Force of L4-L5 [N]	$y = 2.2437 x + 389.11$	0.998
Maximum of Anterior / Posterior Shear Force of L4-L5 [N]	$y = 2.854 x + 329.3$	0.999
Minimum of Anterior / Posterior Shear Force of L4-L5 [N]	$y = 1.7248 x + 263.56$	0.996
Average of Medial / Lateral Shear Force of L4-L5 [N]	$y = 0.913 x + 115.64$	0.997
Maximum of Medial / Lateral Shear Force of L4-L5 [N]	$y = 1.0837 x + 149.97$	0.999

Table 4 *(Continued)*

Parameters Related to Lumbar Load	Regression Equations x : Required Force [N] y : Lumbar Load [N]/[-]	Determination Coefficient
Minimum of Medial / Lateral Shear Force of L4-L5 [N]	y = 0.6221 x + 52.694	0.990
Average of Muscle Activity in Left Sinae Eector Muscle [-]	y = 0.0027 x + 0.3016	0.995
Average of Muscle Activity in Right Sinae Eector Muscle [-]	y = 0.0008 x + 0.1375	0.989

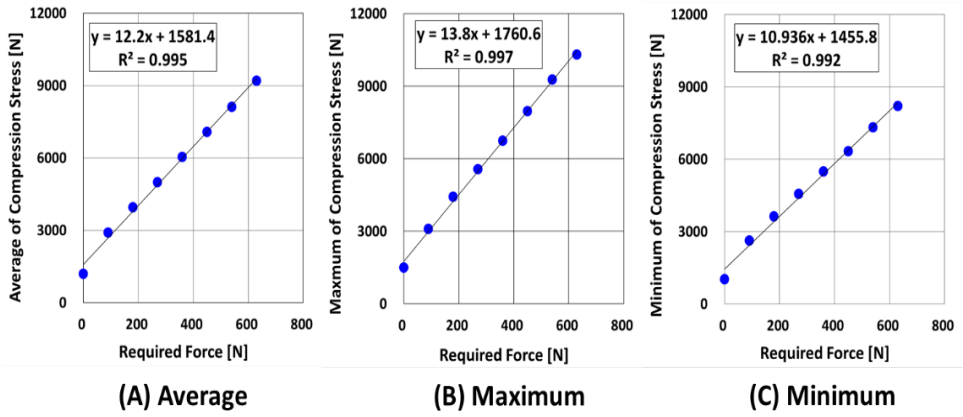

Figure 3. The scatter plot between the required force and compression stress of L4–L5

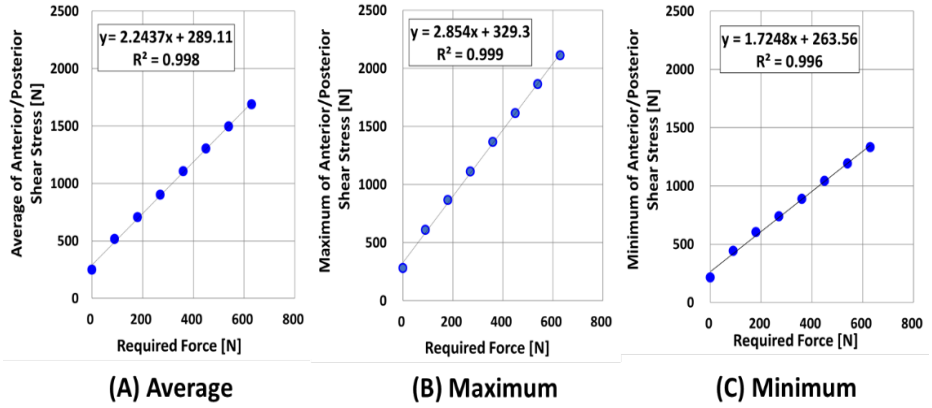

Figure 4. The scatter plot between the required force and anterior/posterior shear stress of L4–L5

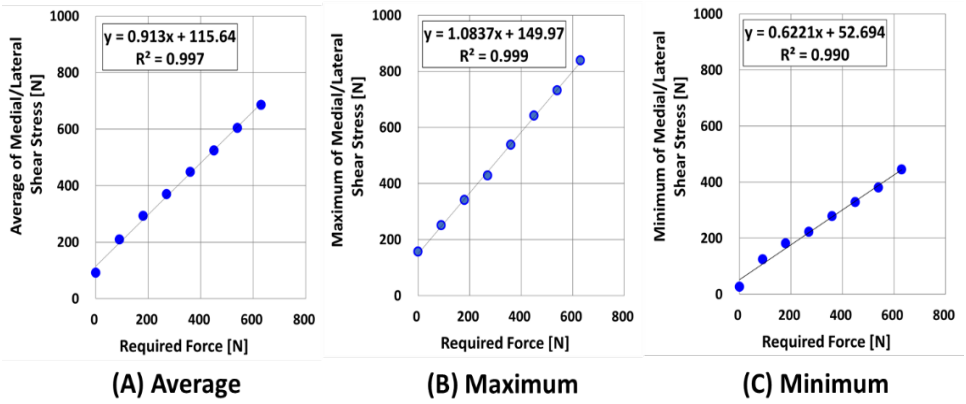

Figure 5. The scatter plot between the required force and medial/lateral shear stress of L4–L5

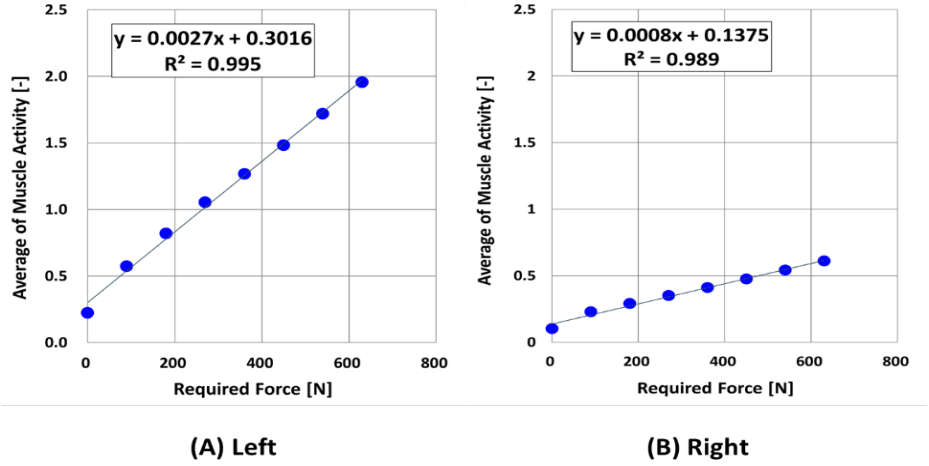

Figure 6. The scatter plot between the required force and activity of spinae erector muscle (average value)

In this paper, we consider about the relationship between compression stress of the L4-L5 joint and the required force as an example of using regression equations. The regression equation for the maximum value of compression stress of L4–L5 joint suggests the possibility that when the required force is more than 120 N, the compression stress exceeds 3400 N, which was defined as injury threshold by NIOSH (Waters et al., 1993). Based on these results, caregivers should be careful with the required force while supporting standing-up based on the weight and remained ability of each patient for preventing low back pain. Furthermore, these results suggest that when the required force is more than 120 N during supporting standing-up motion, a caregiver should reduce the lumbar loads by posture modification, working with multiple caregivers, or using assistive devices.

However, it is considered that using multiple caregivers or assistive devices are limited for time, efficiency, cost, and workspace. Therefore, a caregiver should practice a suitable posture and movement for preventing low back pain during patient handling such as supporting standing-up. For example, pulling instead of lifting procedures (Schibye et al., 2003) and the body mechanics theory (Ibrahim & Elsaay, 2015; Itami et al., 2010; Karahan & Bayraktar, 2004) may be applied to reduce lumbar load. Moreover, our previous study found that the opening stance length and width of caregiver was possibly useful for reducing the L4–L5 joint stress (Kitagawa et al., 2019). The findings of this study may be used for quantitative prevention of low back pain among caregivers based on the relationship between the required force and compression stress of the L4–L5 joint with injury threshold of NIOSH. Then, we also consider the relationship between activities of erector spinae muscle and the required force. *Figure 6* showed that when required force was more than 260 N, activity of left erector spinae muscle exceeded 1.0 as limit of the musculoskeletal model. Therefore, it is considered that the required force more than 260 N causes of fatigue or pain for erector spinae muscle in supporting standing-up. Thus, our regression equations obtained from the musculoskeletal simulation contributes to quantitatively consider lumbar loads of caregiver during patient handling based on injury thresholds and the required force.

A potential limitation is that there are differences between this simulation and the actual patient handling motions because of some factors such as the patient weights and trajectory of center of gravity are limited. This study is unable to investigate and correlate the patient and the caregiver, because we could not build a patient model. Thus, further study using new simulation environment includes patient model is necessary. This study could not simulate other patient handlings besides supporting standing-up. Future studies must investigate the other patient handlings that lead to low back pain, such as patient transfer and repositioning on the bed (Schibye et al., 2003). Our musculoskeletal simulation could not change several parameters, such as body height, body weight, and motion time because we validated this model for one setup of body parameters (body height 1.8 m, body weight 75 kg) (Kitagawa et al., 2019). In this paper, lumbar loads were not underestimated because we focused on a tall or chubby person who caused larger lumbar loads. However, future study should build model that could change parameters via further validations. The relationships between required force and lumbar loads obtained from this study are limited to only linear relationships. There is possibility that actual relationships are not only linear. Therefore, we will consider new simulation model that includes actual characteristics of muscle obtained from electromyography (EMG) in future works. Accordingly, we will build and verify new musculoskeletal model that is improved these limitations. Subsequently, we will investigate the relationship between the required force and lumbar loads in various parameters and several types of patient handling.

CONCLUSION

In this study, we investigated the quantitatively relationships between the required force and lumbar load such as vertebral stress and muscle activity in supporting standing-up by computational musculoskeletal simulation. The results showed that there were high significant correlations between the required force and all lumbar loads ($r > 0.9$, $p < 0.01$). In addition, regression equations with high determination coefficients ($R^2 > 0.9$) were obtained for each lumbar load. These regression equations contribute to quantitatively consider lumbar loads of caregiver during patient handling based on injury thresholds and the required force.

ACKNOWLEDGMENTS

The first author is supported by a scholarship from the "Nakatani Foundation for Advancement of Measuring Technologies in Biomedical Engineering".

REFERENCES

Chaffin, D. B. (2005). Primary prevention of low back pain through the application of biomechanics in manual materials handling tasks. *Giornale Italiano di Medicina del Lavoro ed Ergonomia*, *27*(1), 40-50.

Damsgaard, M., Rasmussen, J., Christensen, S. T., Surma, E., & De Zee, M. (2006). Analysis of musculoskeletal systems in the AnyBody Modeling System. *Simulation Modelling Practice and Theory*, *14*(8), 1100-1111. doi: 10.1016/j.simpat.2006.09.001

Daynard, D., Yassi, A., Cooper, J. E., Tate, R., Norman, R., & Wells, R. (2001). Biomechanical analysis of peak and cumulative spinal loads during simulated patient-handling activities: A substudy of a randomized controlled trial to prevent lift and transfer injury of health care workers. *Applied Ergonomics, 32*(3), 199-214. doi: 10.1016/s0003-6870(00)00070-3

De Zee, M., Hansen, L., Wong, C., Rasmussen, J., & Simonsen, E. B. (2007). A generic detailed rigid-body lumbar spine model. *Journal of Biomechanics*, *40*(6), 1219-1227. doi: 10.1016/j.jbiomech.2006.05.030

Doss, R., Robathan, J., Abdel-Malek, D., & Holmes, M. W. (2018). Posture coaching and feedback during patient handling in a student nurse population. *IISE Transactions on Occupational Ergonomics and Human Factors, 6*(3-4), 116-127. doi: 10.1080/24725838.2018.1428838

Holtermann, A., Clausen, T., Jørgensen, M. B., Burdorf, A., & Andersen, L. L. (2013). Patient handling and risk for developing persistent low-back pain among female healthcare workers. *Scandinavian Journal of Work*, *Environment & Health, 39*(2), 164-169. doi: 10.5271/sjweh.3329

Ibrahim, R. A. E., & Elsaay, O. E. A. E. (2015) The effect of body mechanics training program for intensive care nurses in reducing low back pain. *IOSR Journal of Nursing and Health Science*, *4*(5), 81–96. doi: 10.9790/1959-04548196

Itami, K., Yasuda, T., Otsuki, Y., Ishibashi, M., & Maesako, T. (2010). Development of a checking system for body mechanics focusing on the angle of forward leaning during bedmaking. *Educational Technology Research*, *33*(1-2), 63-71. doi: 10.15077/etr.KJ00006713267

Iwakiri, K., Takahashi, M., Sotoyama, M., Liu, X., & Koda, S. (2016). Low back pain among workers in care facilities for the elderly after introducing welfare equipment. *Sangyo Eiseigaku Zasshi = Journal of Occupational Health*, *58*(4), 130-142. doi: 10.1539/sangyoeisei.b15023

Kanda, Y. (2013) Investigation of the freely available easy-to-use software 'EZR' for medical statistics. *Bone Marrow Transplant*, *48*(3), 452-458. doi: 10.1038/bmt.2012.244

Karahan, A. & Bayraktar, N. (2004) Determination of the usage of body mechanics in clinical settings and the occurrence of low back pain in nurses. *International Journal of Nursing Studies*, *41*(1), 67-75. doi: 10.1016/s0020-7489(03)00083-x

Kitagawa, K., Nishisako, Y., Nagasaki, T., Nakano, S., & Wada, C. (2019). Musculoskeletal simulation of the relationship between foot position and stress of the l4–l5 joint in supporting standing-up motion to prevent low back pain among caregivers. *Journal of Mechanics in Medicine and Biology*, *19*(02), 1940016. doi: 10.1142/s0219519419400165

McGill, S. M., & Norman, R. W. (1985). Dynamically and statically determined low back moments during lifting. *Journal of Biomechanics*, *18*(12), 877-885. doi: 10.1016/0021-9290(85)90032-6

McGill, S. M., Norman, R. W., Yingling, V. R., Wells, R. P., & Neumann, P. (1998, October, 19-22). Shear happens! Suggested guidelines for ergonomists to reduce the risk of low back injury from shear loading. In *Proceedings of the 30th Annual Conference of the Human Factors Association of Canada* (pp. 157-161). Mississauga, Canada.

Merryweather, A. S., Loertscher, M. C., & Bloswick, D. S. (2009). A revised back compressive force estimation model for ergonomic evaluation of lifting tasks. *Work*, *34*(3), 263-272. doi: 10.3233/wor-2009-0924

Nakano, S., Okada, H., Higo, S., Nakamura, K., Kitagawa, K., & Wada, C. (2019). Usefulness of simulation method to improve efficiency of chair-to-wheelchair transfer of patients performed by caregivers. *Journal of Physical Therapy Science*, *31*(10), 802-806. doi: 10.1589/jpts.31.802

Ning, X. (2017). An EMG-assisted modeling approach to assess passive lumbar tissue loading in vivo during trunk bending. *Journal of Electromyography and Kinesiology, 36*, 1-7. doi: 10.1016/j.jelekin.2017.06.004

Rajaee, M. A., Arjmand, N., Shirazi-Adl, A., Plamondon, A., & Schmidt, H. (2015). Comparative evaluation of six quantitative lifting tools to estimate spine loads during static activities. *Applied Ergonomics*, *48,* 22-32. doi.org/10.1016/j.apergo.2014.11.002

Waters, T. R., Putz-Anderson, V., Garg, A., & Fine, L. J. (1993). Revised NIOSH equation for the design and evaluation of manual lifting tasks. *Ergonomics*, *36*(7), 749-776. doi: 10.1080/00140139308967940

Weames, G. G., Stothart, P., & Robertson, D. G. E. (1994). Comparison of the 1991 NIOSH lifting equation and M. erector spinae EMG. *Proceeding of the 8th Annual Canadian Society for Biomechanics Biennial Conference and Symposium, 8,* 152-153.

Pertanika J. Sci. & Technol. 28 (S2): 71 - 81 (2020)

PERTANIKA JOURNALS

SCIENCE & TECHNOLOGY

Journal homepage: http://www.pertanika.upm.edu.my/

Linear Regression Technique for Improvement of Feet Position Estimation during Standing Balance Using a Cane with Millimeter Wave Radar

Ibai Gorordo Fernandez[1]*, Kodai Kitagawa[1], Kawthar Abdul Rahman[2], Azura Che Soh[3], Alpha Agape Gopalai[4], Siti Anom Ahmad[2] and Chikamune Wada[1]

[1]Deparment of Life Science and Systems Engineering, Kyushu Institute of Technology, 2-4 Hibikino, Wakamatsu-ku, Kitakyushu-shi, Fukuoka 808-0196, Japan
[2]Malaysian Research Institute on Ageing (MyAgeing), Universiti Putra Malaysia 43400 Serdang, Selangor, Malaysia
[3]Department of Electrical and Electronic Engineering, Faculty of Engineering, Universiti Putra Malaysia 43400 Serdang, Selangor, Malaysia
[4]School of Engineering, Monash University of Malaysia, Bandar Sunway 46150 Selangor, Malaysia

ABSTRACT

It is estimated that one in three seniors fall at least once a year. Falls are a global problem for the elderly that affects their quality of life and poses a great risk. In our research, we are trying to develop a system that could prevent falls by estimating the fall risk in real time. The system would measure the balance of the user by measuring the position of the Center of Gravity inside the Base of Support. In our previous research, we presented a system with a millimeter wave radar attached to a cane to measure the area of the Base of Support. However, the obtained results for the foot position estimation error were significantly worse than similar studies. One of the reasons was that the sensor was not really estimating the position of the feet but the position of the lower legs. Therefore, in this research we present a correction model to improve the feet position estimation. The proposed model was able to reduce the foot position estimation RMSE from 54

ARTICLE INFO

Article history:
Received: 10 February 2020
Accepted: 13 November 2020
Published: 31 December 2020

DOI: https://doi.org/10.47836/pjst.28.S2.06

E-mail addresses:
ibai.gorordo@hotmail.com (Ibai Gorordo Fernandez)
kitagawakitagawa156@gmail.com (Kodai Kitagawa)
kawthar.ar@gmail.com (Kawthar Abdul Rahman)
azuracs@upm.edu.my (Azura Che Soh)
alpha.agape@monash.edu (Alpha Agape Gopalai)
sanom@upm.edu.my (Siti Anom Ahmad)
wada@brain.kyutech.ac.jp (Chikamune Wada)
*Corresponding author

ISSN: 0128-7680
e-ISSN: 2231-8526

© Universiti Putra Malaysia Press

mm down to 34 mm, which is closer to the results of other similar studies measuring the position of the feet.

Keywords: Balance analysis, falls, feet position estimation, millimeter wave radar

INTRODUCTION

Falls are a major health risk for the elderly. It is estimated that about one in three seniors falls at least once a year (Rubenstein & Josephson, 2002). Moreover, according to the same study, more than half of these seniors suffered multiple falls each year. Even though elderly fall rates vary depending on the country, e.g. 20% in Japan (Sakita et al., 2015) or 32.8% in Malaysia (Kioh & Rashid, 2018), falls pose a great risk for the elderly. It is estimated that falls are the cause of over 400,000 deaths worldwide every year and over 50% of those fallers were aged 60 years or older (Jagnoor et al., 2013).

Furthermore, falls also affect severely to the quality of life of the elderly. Falls in the elderly often result in injuries that lead to mobility impairments. For this reason, assistive devices such as cane or walker are commonly prescribed to the elderly population. It is estimated that there are over 4 million cane users only in the United States (Bateni & Maki, 2005). The use of these assistive devices helps mobility impairment patients to recover some mobility by improving the stability of the user. This is achieved by increasing the area of the Base of Support (BoS), which refers to the area between the contact points of the body with the ground. As long as the Center of Gravity (CoG) is kept inside the BoS, stable balance is maintained. That is why by increasing the area of the BoS, for example using assistive devices, it increases the stable range of movement of the CoG inside the BoS. However, as recent studies show, assistive device users have a higher injury fall risk compared to non-users (West et al., 2015).

Due to the terrible consequences of falls, many studies have tried to develop a system to detect falls. The use of these devices can reduce the adverse consequences of falls by providing rapid treatment as soon as a fall is detected (Igual et al., 2013). Most of the developed fall detection systems used one inertial sensor (Pierleoni et al., 2015) or multiple inertial sensors (Nyan et al., 2008) attached to the body to detect falls. Similarly, Lan et al. (2010) attached a wireless inertial sensor to a single tip cane to detect fall events using a multi-stage thresholding algorithm.

Recently, a higher number of studies have developed ambient sensor-based fall detection systems. These systems use sensors fixed in different parts of a room to detect falls inside the field of view of the sensors. Different types of sensors have been used in these kinds of systems. For example, Amin et al. (2016) used a doppler radar to detect different types of falls, while Yang et al. (2016) used a depth camera to detect any fall

that happened inside the camera's field of view. Similarly, De Miguel et al. (2017) also developed a fall detection system using a low cost camera.

On the other hand, multiple studies have developed balance assessment systems to predict the risk of falls over the long term. These types of systems mostly use force platforms to estimate the movement of the CoG or the Center of Pressure (CoP) during standing balance to assess the balance of the patients (Clark et al., 2010). Another common method is the use of an inertial sensor attached to the body to estimate the postural sway during stance as an indicator of stability (Mancini & Horak, 2010). The limitation of these systems is that even though they can accurately estimate the fall risk in the future, due to the unpredictability of falls, these systems cannot be used to measure the fall risk in real time.

However, a few studies have tried to develop real time fall risk assessment systems. The objective of our research is to develop a real time fall risk assessment system by measuring the position of the CoG inside the BoS in daily life. Measuring the fall risk in real time could help to prevent falls by alerting the user when the risk of fall is high. Van Meulen et al. (2016) developed a similar system for balance analysis by placing multiple sensors underneath a pair of sandals. However, due to the high number of sensors, each shoe had two 3D force/moment sensors, two inertial sensors and an ultrasonic sensor; the shoes were heavy (1 kg) and could be dangerous for the elderly due the extra sole height. For this reason, in our previous study (Fernandez & Wada, 2019), we developed a system to estimate the area of the BoS by using a millimeter wave radar attached to a cane. By attaching the sensor to normal cane, the system could be used without the need to wear any special shoes or clothes. However, the obtained results were worse than other similar studies.

For this reason, in this research we present a correction model to improve the feet position estimation. The proposed correction model takes the estimated lower leg position obtained from our previous system and outputs a corrected feet position.

MATERIALS AND METHODS

Previous Study

The data used in this research was obtained in our previous study (Fernandez & Wada, 2019). In that study, 3 young male subjects (age 24.67 ± 2.08) with no previous balance or gait impairments participated in the experiment. The subjects were asked to stand for 3 seconds while placing the right foot in 9 different locations based on the results from previous studies (Kuan et al., 1999). The 9 different foot locations corresponded with three different stance lengths and three different stance width combinations as shown in Table 1.

In our previous study, we attached a millimeter wave radar (AWR1642, Texas Instruments) to a single tip cane at a height of 10 cm and pointing towards the feet. The radar was used to measure the 2D horizontal position of the reflected points inside its

110 deg. field of view (FoV) at 20 Hz. Then, our developed algorithm was used on the reflected point cloud to extract the 2D position of the centroids for the left and right feet as shown in Figure 1.

Table 1

Stance length and width values for the 9 different foot locations in the experiment

Pattern Number	Stance Length (cm)	Stance Width (cm)
1	18.8	23.5
2	18.8	19.6
3	18.8	15.7
4	28.6	23.5
5	28.6	19.6
6	28.6	15.7
7	38.4	23.5
8	38.4	19.6
9	38.4	15.7

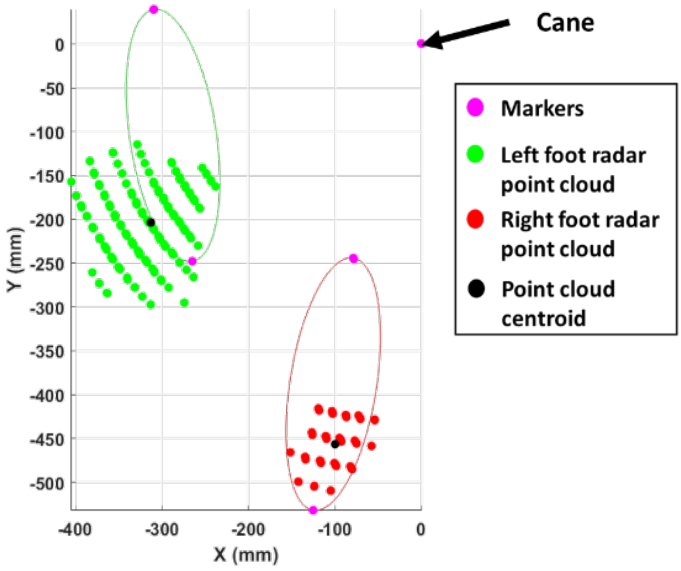

Figure 1. Example of the point cloud data and centroids obtained from the radar as well as the position of the reflected markers

On the other hand, in order to validate the results from the radar, we used an optical motion capture system with 8 infrared cameras (FLEX 13, Oprtitrack). The motion capture system tracked the 3D position of 5 reflective markers placed in the shoes and the cane. As shown in Figure 1, two markers were placed in each shoe, one at the front and one at the rear, and another marker was placed on the tip of the cane. The motion capture system captured the position of the markers at 100 Hz, but then the captured 3D position was downsampled to 20 Hz to match with the sampling frequency of the radar. As a result, a total of 3851 samples were obtained both from the motion capture system as well as from the millimeter wave radar.

As a result, our previous system was able to calculate the area of the Base of Support with a RMSE value of 92.04 cm^2, corresponding with the 7% of the total Base of the Support area. Also, the foot distance error was of 5.4 cm, it was significantly worse than the error of 2.26 cm obtained in a similar study that used a shoe type measurement device (Widodo & Wada, 2017).

One of the reasons for these worse results was that the reflected points were not representing the position of the feet, but the position of the lower leg as shown in Figure 2 with the reflected points in blue. This happened because the lower leg had a larger surface area than the shoes, therefore more points were reflected on the lower leg compared to the points reflected on the shoes. However, since the objective of our research was to estimate the fall risk using the position of the feet, we needed to develop a model to obtain the correct position of the feet.

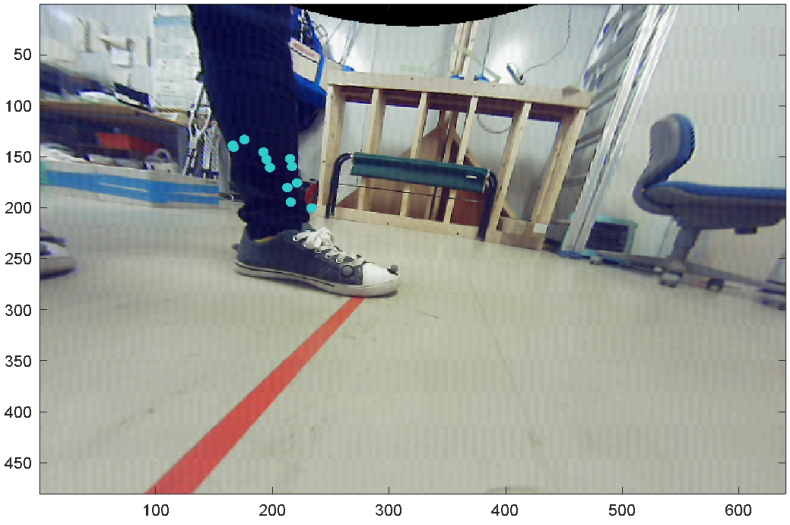

Figure 2. Example of the position of the points obtained from the radar (blue) that reflected on the lower leg

Correction Model

For that purpose, in this research we developed a correction model that took the centroids (red points in Figure 3), that represented the 2D position of the lower legs, and estimated the correction distances. The correction ($horDist_L$, $verDist_L$, $horDist_R$ and $verDist_R$) represented the horizontal and vertical distances from the centroid to the heel marker as shown in Figure 3.

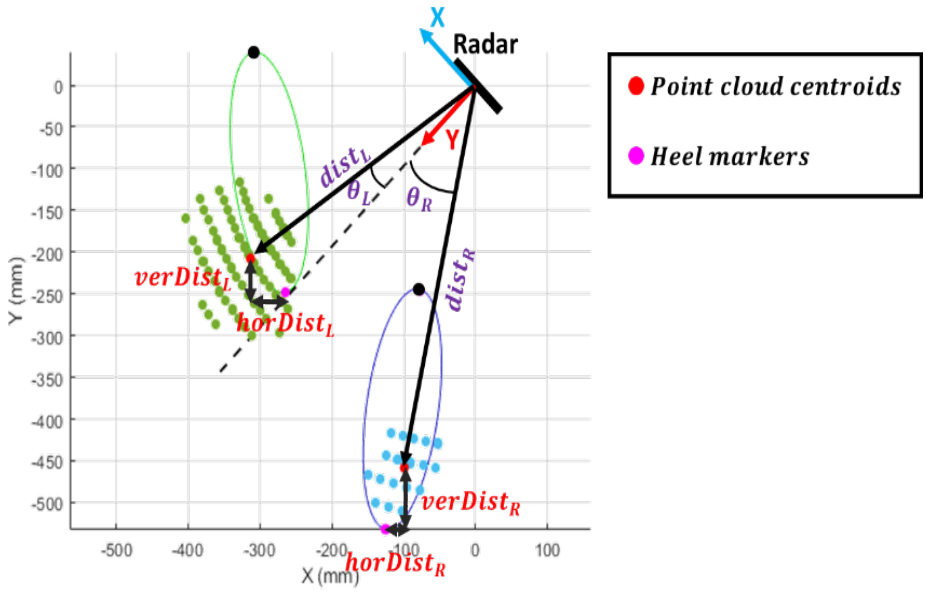

Figure 3. Diagram describing the input (θ_L, θ_R, $dist_L$, and $dist_R$) and output ($horDist_L$, $verDist_L$, $horDist_R$ and $verDist_R$) of the correction model

On the other hand, the position of the centroids was represented in polar coordinates where θ_L and θ_R were the angles from the Y axis of the radar for the left and right centroids respectively; and similarly, $dist_L$ and $dist_R$ were the distances from the radar to the centroids as shown in Figure 3. Also, for simplicity, instead of creating one model for the 4 correction distances, we generated 4 different models, one for each correction distance.

Parameter Selection

In order to create each of the 4 correction models, it was necessary to decide which parameter was going to be selected as input for each model. For that purpose, instead of only trying to use the position of the centroids (θ_L, θ_R, $dist_L$, and $dist_R$), another 56 different parameters were extracted from those 4 parameters. Then, in order to select the best

parameter for each model, the Pearson correlation between each of the extracted parameters and each of the correction distances was calculated.

Once all the correlation values were extracted, the parameter with the highest absolute Pearson correlation was selected for each correction model. The Pearson correlation represents the linear correlation between the two variables. Therefore, the parameter with the highest Pearson correlation could provide more information about the desired correction distance than the rest of the parameters.

Linear Regression Model

Finally, in order to obtain each of the correction models, a linear regression model was used to estimate each correction distance based on the values from its corresponding selected parameter. Figure 4 depicts the linear fits for each of the 4 correction distances as well as the 95 % confidence interval regions.

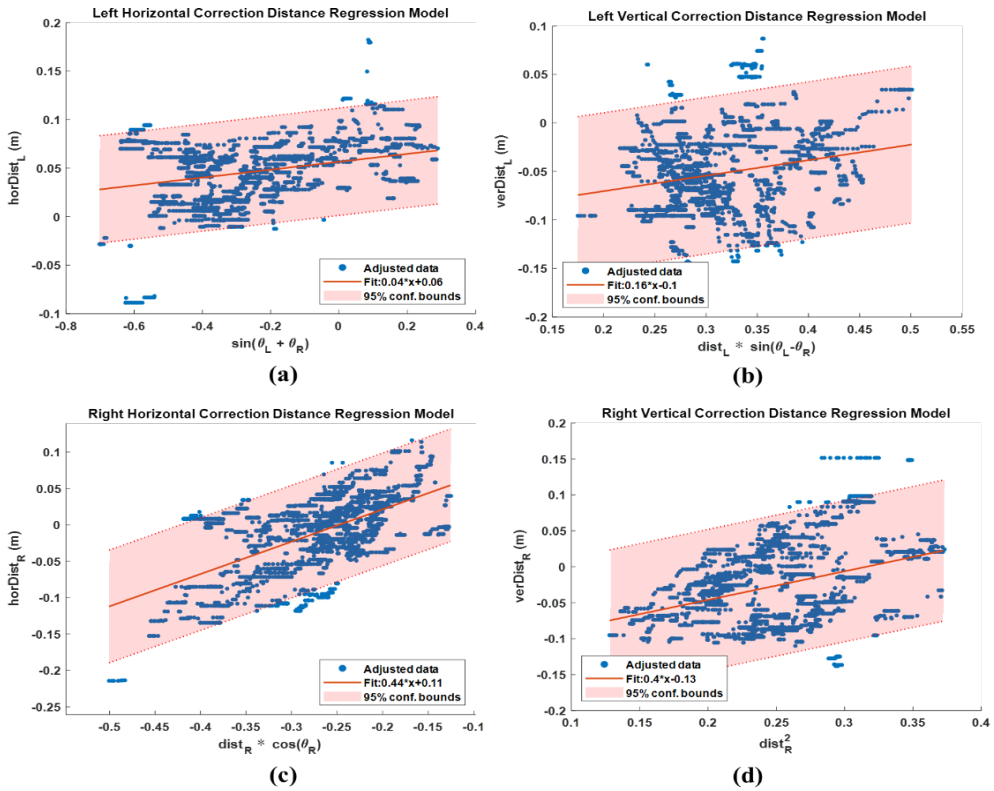

Figure 4. Linear regression models for each of the 4 correction distances: (a) $horDist_L$, (b) $verDist_L$, (c) $horDist_R$, (d) $verDist_R$.

RESULTS AND DISCUSSIONS

Table 2 summarizes the results for the correction models. The table shows the Pearson correlation between each correction distance and its selected parameter, the linear fit function, as well as the RMSE value for the linear fit. As it can be observed, the correction model for the $verDist_R$ had the highest RMSE fit. A higher RMSE fit indicates that when using the correction model to correct the feet position, a higher error can be expected. One of the reasons why the results for the right foot were worse than those for the left foot, was that while the left foot was in front of the radar, the right foot was near the limit of the field of view of the radar. Because of this, in some cases, the number of reflected points on the right lower leg were scarce and the noise was higher than for the left side.

Next, once the 4 linear correction models were generated, these models were used to estimate the correction distances for each of the measurements. Then, the correction distances were used to update the previous estimated centroid positions in order to estimate the position of the heels. As a result, we were able to reduce the foot position estimation from 62.66 cm to 35.31 mm for the left foot (43.65 % error reduction) and from 54.76 to 45.6 mm for the right foot (16.73 % error reduction). The reason why the error reduction for the left foot position estimation was worse than for the right foot both in absolute and in relative terms was because regression fit error was also worse for the correction models of the right foot than of the left foot as shown in Table 2.

Table 2

Summary of the results for the correction models generation

Correction Distance	Selected Parameter	Pearson Corr.	Fit Function	Fit RMSE (mm)
$horDist_L$	$\sin(\theta_L+\theta_R)$	0.31	y = 0.04*x+0.06	28.2
$verDist_L$	$dist_L*\sin(\theta_L-\theta_R)$	0.2	y = 0.16*x-0.1	41.1
$horDist_R$	$dist_L*\cos(\theta_R)$	0.6	y = 0.44*x+0.11	39.5
$verDist_R$	$(dist_R)^2$	0.35	y = 0.4*x-0.13	49.9

Similarly, Table 3 summarizes the stance length and stance width RMSE values before and after applying the correction model. As it can be observed, even though the error reduction for the stance length estimation was smaller than 1 cm, the RMSE value for the stance width was reduced to almost half after applying the correction model.

Overall, the RMSE value for the distance between the feet (Foot Distance RMSE in Table 3) was reduced from 54.39 mm down to 34.19 mm after applying the correction models, representing a 37.14 % error reduction. The obtained foot distance RMSE was

closer to the error of 22.6 mm obtained by Widodo and Wada (2017). Even though the current results are still worse than those of previous studies, our current system can estimate the feet position without the need to wear special heavy shoes, as the weight of our sensor system is only 38 g.

Table 3

Summary of the stance length and stance width RMSE values before and after applying the correction models

	Stance Width RMSE (mm)	Stance Length RMSE (mm)	Foot Distance RMSE (mm)
Before Correction	63.46	43.47	54.39
Corrected	33.44	34.93	34.19

CONCLUSIONS

In this paper, a correction model for foot position estimation is presented. The proposed model takes the raw centroids of the radar point cloud data and using a linear regression model estimates the correct heel position. The proposed model was evaluated using the data from our previous study and the obtained results showed that the model was able to reduce the feet position estimation almost down to half.

However, the proposed model was only tested on data during standing balance. Also, one of the limitations of this study is the reduced number of participants. In the future, we will test our sensor with a higher number of participants as well as using data taken also during gait experiments in order to observe how the system works also during dynamic movements. For that purpose, it is necessary to know the orientation of the radar in order to transform the radar point cloud data from the local axes of the radar to the world coordinates. That is why we will also add an inertial sensor to our system in order to estimate the orientation and movement of the cane during gait.

ACKNOWLEDGEMENT

This research was partly funded by the Collaboration Program between Kyushu Institute of Technology and Universiti Putra Malaysia.

REFERENCES

Amin, M. G., Zhang, Y. D., Ahmad, F., & Ho, K. C. D. (2016). Radar signal processing for elderly fall detection: The future for in-home monitoring. *IEEE Signal Processing Magazine*, *33*(2), 71-80. doi:10.1109/msp.2015.2502784

Bateni, H., & Maki, B. E. (2005). Assistive devices for balance and mobility: Benefits, demands, and adverse consequences. *Archives of Physical Medicine and Rehabilitation*, *86*(1), 134-145. doi:10.1016/j.apmr.2004.04.023

Clark, R. A., Bryant, A. L., Pua, Y., McCrory, P., Bennell, K., & Hunt, M. (2010). Validity and reliability of the Nintendo Wii Balance Board for assessment of standing balance. *Gait and Posture*, *31*(3), 307-310. doi:10.1016/j.gaitpost.2009.11.012

De Miguel, K., Brunete, A., Hernando, M., & Gambao, E. (2017). Home camera-based fall detection system for the elderly. *Sensor, 17*(12), 1-21. doi:10.3390/s17122864

Fernandez, I. G., & Wada, C. (2019, March 12-14). Cane with millimeter wave radar for base of support measurement. In *2019 IEEE 1st Global Conference on Life Sciences and Technologies, LifeTech* (pp. 133-136). Osaka, Japan.

Igual, R., Medrano, C., & Plaza, I. (2013). Challenges, issues and trends in fall detection systems. *BioMedical Engineering Online*, *12*(1), 2-24. doi:10.1186/1475-925x-12-66

Jagnoor, J., Keay, L., & Ivers, R. (2013). A slip and a trip? Falls in older people in Asia. *Injury*, *44*(6), 701-702. doi: 10.1016/j.injury.2013.03.009

Kioh, S. H., & Rashid, A. (2018). The prevalence and the risk of falls among institutionalised elderly in Penang, Malaysia. *Medical Journal of Malaysia*, *73*(4), 212-219.

Kuan, T. S., Tsou, J. Y., & Su, F. C. (1999). Hemiplegic gait of stroke patients: The effect of using a cane. *Archives of Physical Medicine and Rehabilitation, 80*(7), 777-784. doi:10.1016/s0003-9993(99)90227-7

Lan, M., Nahapetian, A., Vahdatpour, A., Au, L., Kaiser, W., & Sarrafzadeh, M. (2010, September 10-12). SmartFall: An automatic fall detection system based on subsequence matching for the smartcane. In *Conference on Body Area Networks* (pp. 1-8). Los Angeles, California.

Mancini, M., & Horak, F. B. (2010). The relevance of clinical balance assessment tools to differentiate balance deficits. *European Journal of Physical and Rehabilitation Medicine, 46*(2), 239-248.

Nyan, M. N., Tay, F. E. H., & Murugasu, E. (2008). A wearable system for pre-impact fall detection. *Journal of Biomechanics, 41*(16), 3475-3481. doi:10.1016/j.jbiomech.2008.08.009

Pierleoni, P., Belli, A., Palma, L., Pellegrini, M., Pernini, L., & Valenti, S. (2015). A high reliability wearable device for elderly fall detection. *IEEE Sensors Journal, 15*(8), 4544-4553. doi:10.1109/JSEN.2015.2423562

Rubenstein, L. Z., & Josephson, K. R. (2002). The epidemiology of falls and syncope. *Clinics in Geriatric Medicine, 18*(2), 141-158. doi:10.1016/s0749-0690(02)00002-2

Sakita, M., Murakami, S., Saito, T., & Kumagai, S. (2015). Falls and fall prevention in elderly people: Summary of recent reviews. *Japanese Journal of Health Promotion and Physical Therapy, 4*(4), 161-169. doi:10.9759/hppt.4.161

Van Meulen, F. B., Weenk, D., Buurke, J. H., Van Beijnum, B. J. F., & Veltink, P. H. (2016). Ambulatory assessment of walking balance after stroke using instrumented shoes. *Journal of Neuroengineering and Rehabilitation, 13*(1), 1-10. doi:10.1186/s12984-016-0146-5

West, B. A., Bhat, G., Stevens, J., & Bergen, G. (2015). Assistive device use and mobility-related factors among adults aged ≥ 65 years. *Journal of Safety Research, 55,* 147-150. doi:10.1016/j.jsr.2015.08.010

Widodo, R. B., & Wada, C. (2017). Artificial neural network based step-length prediction using ultrasonic sensors from simulation to implementation in shoe-type measurement device. *Journal of Advanced Computational Intelligence and Intelligent Informatics, 21*(2), 321-329. doi:10.20965/jaciii.2017.p0321

Yang, L., Ren, Y., & Zhang, W. (2016). 3D depth image analysis for indoor fall detection of elderly people. *Digital Communications and Networks, 2*(1), 24-34. doi:10.1016/j.dcan.2015.12.001

Pertanika J. Sci. & Technol. 28 (S2): 83 - 94 (2020)

SCIENCE & TECHNOLOGY

Journal homepage: http://www.pertanika.upm.edu.my/

Acetylcholine Receptor-based Biosensor Derived from Asian Swamp Eel, *Monopterus Albus* for Heavy Metals Biomonitoring

Siti Aishah Muhammad Khalidi[1,2], Mohd Khalizan Sabullah[1,2]*, Suraya Abdul Sani[1], Mohd Yunus Abd Shukor[2], Ain Aqilah Basirun[2], A'aishah Abd Gafar[2], 'Izazy Nur Mohd Jaafar[2] and Noreen Nordin[1]

[1]Faculty of Science and Natural Resources, Universiti Malaysia Sabah, Jalan UMS, 88400 Kota Kinabalu, Sabah, Malaysia
[2]Department of Biochemistry, Faculty of Biotechnology and Biomolecular Sciences, Universiti Putra Malaysia, UPM 43400 Serdang, Selangor, Malaysia

ABSTRACT

Cholinesterase-based biosensor well known as a sensitive method to detect the existence of harmful dissolved compounds in any type of water source, especially the river. This alternative biosensor can be used to determine the level of pollution of the water in a short period of time as well as to evaluate the low cost and simple service. The aim of this study was to exceed the effectiveness of acetylcholinesterase source extracted from the brain tissue of Asian swamp eel; *Monopterus albus* as a potential environmental biosensor. Purified acetylcholinesterase exposed to a different type of metal ions and mercury showed the highest percentage of inhibition at 62.9% followed by chromium at 59.22% while silver, arsenic, cadmium, cobalt, copper, nickel, zinc and lead at not more than 50% (approximately 37-50%). Metal ions such as mercury, zinc, chromium and copper showed exponential decay type inhibition curves with calculated half maximal inhibitory concentration; IC_{50} in the ascending sensitivity order 0.005, 0.595, 0.687 and 1.329 mgL^{-1}, respectively. Field trial works exhibited that the acetylcholinesterase was applicable in sensing heavy metals pollution from the river which closed to the industrial and agricultural sites at near real-time and verified using ICP-OES. This study proves

ARTICLE INFO

Article history:
Received: 10 February 2020
Accepted: 13 November 2020
Published: 31 December 2020

DOI: https://doi.org/10.47836/pjst.28.S2.07

E-mail addresses:
asyaaishah@yahoo.com (Siti Aishah Muhammad Khalidi)
khalizan@ums.edu.my (Mohd Khalizan Sabullah)
yunus.upm@gmail.com (Mohd Yunus Abd Shukor)
suraya.abdulsani@ums.edu.my (Suraya Abdul Sani)
shazin563@gmail.com (Ain Aqilah Basirun)
aishababa93@gmail.com (A'aishah Abd Gafar)
izazynur@gmail.com ('Izazy Nur Mohd Jaafar)
ryeennordin@yahoo.com (Noreen Nordin)
* Corresponding author

ISSN: 0128-7680
e-ISSN: 2231-8526

© Universiti Putra Malaysia Press

the potential use of acetylcholinesterase sourced from *M. albus* as a biomonitoring tool to assess the contamination level of the river.

Keywords: Acetylcholinesterase, biosensor, heavy metal, IC_{50}, *Monopterus albus*

INTRODUCTION

The main enzyme found in the neuromuscular junction and cholinergic nervous system, brain cholinesterase, specifically acetylcholinesterase (AChE), is triggered to suppress synaptic transmission. The function of AChE is to hydrolyse of acetate and choline neurotransmitter acetylcholine (ACh) (Colovic et al., 2013). Anticholinesterase can block the activity of AChE and causes synaptic aggregation of Ach, including insecticides and toxic substances, (Sussman et al., 1991). Throughout aquatic organisms such as fish, ubiquitous cholinesterase (ChE) was also found. Fish can thus be a high potential biomarker for controlling pollution in terms of analysing their developmental and behavioural modifications as well as the evaluation of ChE activity for heavy metal treatments.

Biomarkers are considered as one of the methods most capable of ecotoxicological implementations, able to provide early recognition of toxic water disclosure and the main indication of potential effects at advanced levels of biological organisation, such as workforce and environmental effects (Quintaneiro et al., 2016). Previous studies showed that several freshwater systems in Malaysia, including the Klang river, the Langat Basin river and also the Mamut river in eastern Malaysia, have become a concern about their heavy metal toxicity levels, such as copper (Cu), cadmium (Cd), zinc (Zn), and lead (Pb) (Alam et al., 2015 & Naji et al., 2014).

In this research, AChE was commonly used for insecticide biomonitoring and is also useful for heavy metal detection (Bocquene et al., 1990; Frasco et al., 2008; Olson & Christensen, 1980). The AChE assay's rate and versatility make it desirable to use a portable spectrophotometer in the field. We realized in this work that *Monopterus albus,* AChE was sensitive to pollutants such as mercury, copper, silver and chromium. Therefore, we used this enzyme to trap heavy metals from a variety of aquatic bodies in the several river samples in Malaysia.

MATERIALS AND METHODS

Chemicals

Significantly, MERCK had imported the products for the processing of heavy metals from atomic absorption spectrometry standard solutions like; chromium (Cr^{6+}), nickel (Ni^{2+}), zinc (Zn^{2+}), silver (Ag^{2+}), arsenic (As^{5+}), cadmium (Cd^{2+}), cobalt (Co^{2+}), copper (Cu^{2+}), mercury (Hg^{2+}) and lead (Pb^{2+}) while acetylthiocholine iodide (ATC) and 5, 5-dithiobis (2-nitrobenzoic acid) (DTNB) were purchased from Sigma-Aldrich. These solutions were freshly prepared, before being used.

Preparation of Brain AChE Extractions

M. albus were brought from supplier at Selangor, Malaysia. The fish were delivered to the laboratory alive and picked for the experiment (according to apparent health conditions). The fish were starved a day before the experiment to reduce the potential dietary factors on the fish's organic metabolite status. The fish was slaughtered in an ice-filled box, called as freeze-killed followed by the dissection of the fish brain. The brain samples extracted from the eel were then homogenized using an Ultra-Turrax T25 Homogenizer with a buffer proportion of 1:4(brain(w): Buffer(v) of a 0.1 M sodium phosphate buffer pH 7.5 comprising 1mM of phenylmethylsulfonyl fluoride. The sample supernatant was collected and stored at-20°C for the purification method process after a centrifugation cycle at 10,000 x *g* at 4°C for 10 minutes. The thawing process of the sample took place after it was left at ambient temperature.

Preparation of Affinity Purified AChE

The AChE was purified using procainamide chromatography (Sabullah et al., 2014) with a slight-modification using a different matrix which was procainamide-Sepharose CL-6B. Chromatography of the procainamide affinity was used to partially purify the AChE after precipitation from the selected fraction. The matrix was packed to a bed height of 4 cm in a column syringe, 1 mL of the supernatant was loaded into the column of affinity containing procainamide-sepharose CL-6B and washed with 6 ml of buffer containing 20 mM of pH 7.0 sodium phosphate buffer into the column with gravity flow rate. This stage is essential for removing the unbounded protein from the column to the matrix. For eluting buffer, 20 mM sodium phosphate buffer pH 7.0 containing 1M NaCl was then loaded to elute the ChE from *M. albus,* which was bounded to the affinity matrix. A 1 mL of fractions was obtained and examined for the determination of enzyme activity and protein concentration. The maximum enzyme activity fraction was taken and deposited at -25°C.

ChE Activity and Protein Content Determination

The activity of *M. albus* ChE was determined using a slight modification of Ellman et al. (1961) method and read at the wavelength of 405 nm using 96-well microplate. A 200 µL sodium phosphate buffer (0.1 M, pH 7.0), 20 µL DTNB (0.1 mM) and 10 µL ChE sample were inserted into the wells of the microplate and incubated for 15 minutes, and initial reading was obtained. Subsequently, 20 µL of a substrate (5.0 mM ATC) was applied to the mixture and incubated for 10 min. ChE activity was determined as the amount of substrate (µM) broken down by ChE per minute (U) with an extinction coefficient of 13.6 mM^{-1} cm^{-1} while the specific activity was expressed as µmole/min/mg of protein or U mg-1 of protein. The determination of the protein content has been evaluated, as stated by Bradford, 1976. The standard quantitative value of the protein was Bovine serum albumin (BSA). The

assay were conducted in the dark area, and all the triplicates were done. For the non-linear regression analysis software available on the Internet (www.graphpad.com), IC_{50} of heavy metals was calculated using a one-phase exponential decline model on Graphpad PRISM 5.

Field Trials

During good and hot weather, sampling was done but stopped at the rainy season to prevent dilution of the sample. Water samples (Table 1) were immediately checked using the inhibitive assay, as mentioned above, with the spectrophotometer for the present of

Table 1
Sampling location was conducted at nine rivers from six different state

Location	Classification	SAMPLE Code	SAMPLING COORDINATE	Remark
Penang	Class IV	SJP1	N 5°14'45.81", E 100°28'20.3"	Dark in colour and smelly
		SJP2	N 5°14'22.23", E 100°28'30.2"	
		SJP3	N 5°14'28.13", E 100°28'57.4"	
Melaka	Class III	SMM1	N 2°13'32.55", E 102°15'16.5"	Yellowish brown colour and smelly
		SMM2	N 2°13'37.17", E 102°15'39.7"	
		SMM3	N 2°13'48.27", E 102°15'33.2"	
Selangor	Class IV	SKS1	N 3°00'57.87", E 101°42'36.0"	Yellowish brown colour and smelly
		SKS2	N 3°01'31.52", E 101°42'31.3"	
		SKS3	N 3°01'58.69", E 101°42'08.4"	
Pahang	Class II	SBP1	N 3°31'17.22", E 101°54'37.1"	Yellow color but sometime clear
		SBP2	N 3°31'16.75", E 101°54'27.9"	
		SBP3	N 3°31'34.68", E 101°54'13.8"	
Terangganu	Class II	STT1	N 5°21'05.66", E 103°03'56.5"	Yellow-green color
		STT2	N 5°18'21.41", E 103°05'23.1"	
		STT3	N 5°18'53.47", E 103°05'37.4"	
Sabah	Class II	SIS1	N 5°58'58.16", E 116°07'6.84"	Yellowish color
		SIS2	N 6°00'14.43", E 116°07'6.02"	
		SIS3	N 6°00'43.52", E 116°6'51.53"	
	Class III	SSS1	N 5°58'08.72", E 116°04'13.9"	Yellowish brown colour and smelly
		SSS2	N 5°57'59.59", E 116°04'14.3"	
		SSS3	N 5°57'54.04", E 116°04'10.7"	
	Class II	STS1	N 6°05'25.84", E 116°12'12.7"	Yellowish color with strong smell
		STS2	N 6°04'55.97", E 116°12'34.3"	
		STS3	N 6°05'07.56", E 116°12'21.8"	
	Not Recorded	SKT1	N 5°41'05.82", E 116°22'45.8"	Clean and clear. Considered as Class I river.
		SKT2	N 5°40'49.95", E 116°22'35.5"	
		SKT3	N 5°40'46.78", E 116°22'29.1"	

Note. River classification is based on Water Quality Index reported by DOE, 2018
Sample code abbreviation: SJP = Sungai Jawi, Penang; SMM = Sungai Melaka, Melaka; SKS = Sungai Kuyuh, Selangor; SIS = Sungai Inanam, Sabah; SSS = Sungai Sembulan, Sabah; STE = Sungai Telipok, Sabah; STA = Sungai Keinop-Tambunan, Sabah.

bioavailable heavy metals. Atomic emission spectrometry (ICP-OES, Optima 3700DV, Perkin-Elmer, USA) had been used to measure the determination of heavy metal content in our samples. Distilled water had been used as a study control. Using 90 mm Whatman filter paper, 50 mL of each sample was initially filtered, followed by ultrafiltration using 0.45-micron nylon syringe filters. The sample was treated with a few drops of 70% nitric acid analytical grade to prevent the metal ion from reacting and sticking to the sample tube wall. ICP-OES has been tested using a standard multi-element solution containing; Cr^{6+}, Ni^{2+}, Zn^{2+}, Ag^{2+}, As^{5+}, Cd^{2+}, Co^{2+}, Cu^{2+}, Hg^{2+} and Pb^{2+} (excluded in this study) and optimized standardization according to the recommendation of the manufacturer. All the experiments were carried out in triplicate.

Data and Statistical Analysis

The percent of inhibition level was calculated according to the formula:

$$\%\text{Inhibition} = \frac{\text{Activity of control} - \text{Activity of sample} \times 100}{\text{Activity of control}}$$

The values shown are means ± standard deviation. Graphpad Prism version 5.0 was used to analyse all data. A comparison between groups was obtained by one-way analysis of variance (ANOVA) with post hoc analysis by Tukey's test or by using a student's t-test. $P<0.005$ was regarded to be statistically significant.

RESULTS AND DISCUSSIONS

Sample Extraction and Purification

Table 2 shows that ChE was purified with a yield of 38.73% at 20.53-fold. The yield decreased due to the loss of enzyme activity caused by such an external temperature factor that was higher than the optimal enzyme temperature (Robinson, 2015). The total protein amount decreased while the activity of the enzyme increased throughout this phase of purification. The purification is required to reduce any inference from other proteins

Table 2
Purification table for purification of ChE from M. albus

Procedure	Total protein (µg)	Total ChE activity (U)	Specific activity (U/µg)	Purification folds	Yield (%)
Crude homogenate	0.53	47.68	89.96	1	100
Procainamide-Sepharose CL-6B	0.01	18.47	1847	20.53	38.73

Note. The specific activity from each step of purification is displayed in (U/µg), which means µmole/min/mg of protein.

to ensure that the desired purified protein can achieve maximum performance (Forget et al., 2002; Gao & Zhu 2001; Talesa et al., 2001). The purification process does not affect the activity of the enzyme because it appears the molecular structure and the activity of the enzyme can only be affected by the enzyme and substratum temperature, pH and concentration (Bisswanger, 2014). In this study, the enzyme's specific activity increased at the end of the experiment throughout the purification process.

Metal Ion Inhibition Study

Figure 1 shows that Cr and Hg showed the highest inhibition, decreasing ChE activity to less than 50% and showing a sense of value ($P<0.005$) between them. ChE also inhibited *in vitro* by silver (Ag^{2+}), arsenic (As^{5+}), cadmium (Cd^{2+}), chromium (Cr^{6+}), cobalt (Co^{2+}), copper (Cu^{2+}), mercury (Hg^{2+}), nickel (Ni^{2+}), zinc (Zn^{2+}) and lead (Pb^{2+}) by lowering activity to 52.88%, 52.22%, 57.35%, 40.78%, 56.54%, 51.73%, 37.10%, 62.59%, 50.47% and 57.79% respectively when ATC was used as the substrate at the concentration of 10 ppm. Other than that, Hg and Cu were rated as the highest rank of heavy metal toxicity, and this assertion (Alam & Maughan, 1992; Apartin & Ranco, 2001; Bellas et al., 2001; Martin et al., 1981; Ramakritinan et al., 2012; Strubelt et al., 1996) has been confirmed by other previous studies. Besides, the high inhibition of Hg on ChE activity was in line with studies using fishes such as *Puntius javanicus, Anabas testudineus* and *Clarias gariepinus* (Ahmad et al., 2016; Padrillah et al., 2017; Sabullah et al., 2014). Various heavy metals normally

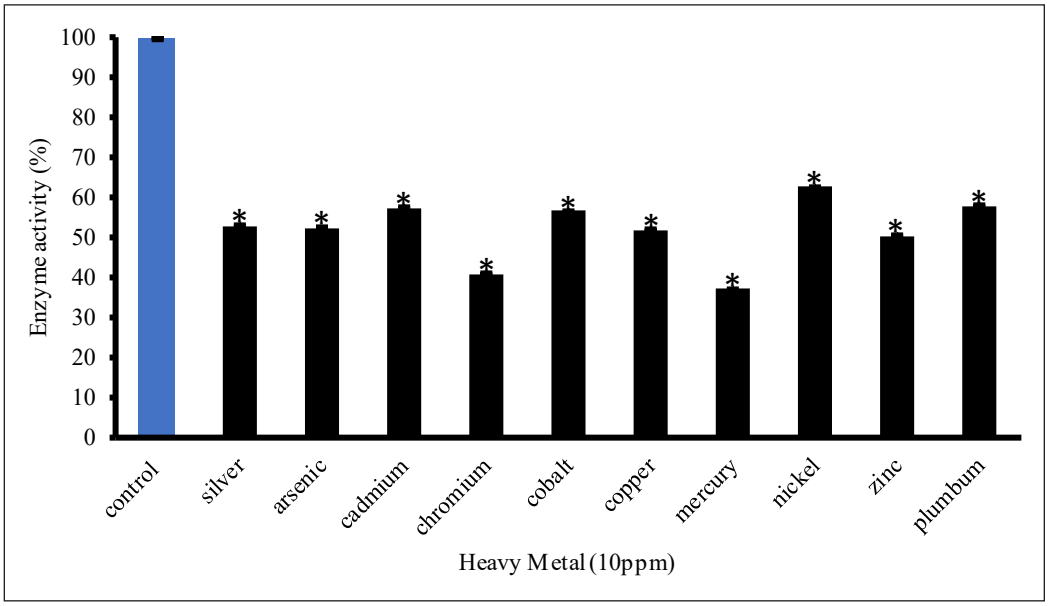

Figure 1. Effect of different types of heavy metals on the enzymatic activity of purified ChE from *M. albus* brain after inhibition at 10ppm. Error bars represent mean ± standard error (n=3). Statistical significance of different from control: *P <0.005.

offered different inhibition or vulnerability to purified ChE activity (Gbaye et al., 2012; Kuca et al., 2005; Santarpia et al., 2013). Past investigations studies had found heavy metal had blocked the use of substrates either specifically binding to the active enzyme site or binding to the allosteric site, leading in the conformation change and the failure of substrates to shape the complex of compound substrates (Ahmad et al., 2016; Basirun et al., 2018; Giedroc et al., 2007; Glusker et al., 1999; Mathonet et al., 2006; Padrillah et al., 2017).

Selected metal ion; Hg^{2+}, Zn^{2+}, Cr^{6+} and Cu^{2+}, showed exponential decay type inhibition curves with calculated half maximal inhibitory concentration; IC_{50} in the ascending sensitivity order of 0.005, 0.595, 0.687 and 1.329 mgL^{-1}, respectively in Table 3. The lower IC_{50} value will give a higher potency of the antagonist, and the lower the concentration of toxicant is required to inhibit the maximum biological response.

Table 3
The IC_{50} value using GraphPad Prism 5 with a type analysis of nonlinear regression by equation of one phase exponential decay

Metal ions	IC_{50} (95% confidence interval) mg L^{-1}	R^2
Cr^{6+}	0.687 (0.4440 to 0.9031)	0.9604
Cu^{2+}	1.329 (1.1460 to 1.5830)	0.9801
Hg^{2+}	0.005 (0.0020 to 0.0120)	0.9916
Zn^{2+}	0.595 (0.3387 to 0.9444)	0.9254

Field Trial

The purpose of this project was to test the ability of *M. albus* AChE to detect anti-AChE in various river samples (Figure 2) identified by DOE (2018) as polluted (Class IV and V), slightly polluted (Class II and III) and WQI-based clean river (Class I). *Ex-situ* testing was performed, and Table 4 shows the percentage of the remaining activity of purified AChE after exposure to tap water and river samples, while the red dotted line shows a percentage below 80%; or inhibition more than 20%, considered as contaminated as stated by Sabullah et al. (2015) which this idea supported by Ahmad et al., 2016 and Hayat et al., 2016. The result shows that 13 samples were considered unpolluted, where SEM 1 and SA 3 were not statistically significantly different ($p > 0.05$) with control. In contrast, the others showed less than 20% of AChE inhibition (about 10% to 20% of inhibition) such as SEM 3 and SA 1. Some samples showed slight contamination as the percentage of SA 4, SA 2 and SEM 4 to the unpolluted range was less than 3% to 10%. Shukor et al. (2013) reported that any sample inhibiting AChE activity by more than 50% was was classified as toxic and harmful to aquatic habitat. In this analysis, no toxic sample was detected. Meanwhile, according to Sabullah et al. (2015), the cholinesterase inhibition of more than 20% the sample was considered polluted. In this analysis, the polluted sample could be SEM 2 at 24.17% corresponding to the number of variables and the highest concentration of metal

Table 4
Quantification of metal ions concentration in river samples from Peninsular area and Sabah area using ICP-OES

Sample	Inhibition (%)	Metal ion concentration (ppb)								
		Ag	As	Cd	Cr	Cu	Hg	Pb	Ni	Zn
Tap Water	0	*nd	*nd	*nd	*nd	*nd	*nd	*nd	*nd	0.01 ± 0.001
SEM 1	0	0.632 ± 0.043	*nd	*nd	0.287 ± 0.075	*nd	*nd	*nd	*nd	*nd
SEM 2	24.17± 2.22	0.679 ± 0.021	*nd	*nd	1.317 ± 0.027	16.69 ± 1.190	*nd	42.125 ± 2.999	25.540 ± 0.978	579.81± 25.479
SEM 3	16.67± 3.14	0.704± 0.068	1.14± 0.02	*nd	0.077 ± 0.001	0.283± 0.007	*nd	*nd	*nd	3.760± 0.184
SEM 4	8.33 ± 1.55	0.349± 0.090	*nd	*nd	2.759 ± 0.006	4.970± 0.356	*nd	*nd	*nd	4.575± 0.677
SA 1	20.70± 2.47	0.821± 0.064	*nd	*nd	*nd	8.055 ± 0.003	*nd	0.191± 0.004	*nd	15.01± 3.511
SA 2	4.12 ± 0.112	0.459± 0.079	*nd	*nd	*nd	*nd	*nd	*nd	*nd	5.383± 0.649
SA 3	0	0.393± 0.025	*nd	*nd	*nd	*nd	*nd	0.034± 0.001	*nd	4.176± 0.615
SA 4	2.43± 0.287	0.935± 0.180	*nd	*nd	*nd	*nd	*nd	*nd	*nd	*nd

*Note. *nd = not detected*

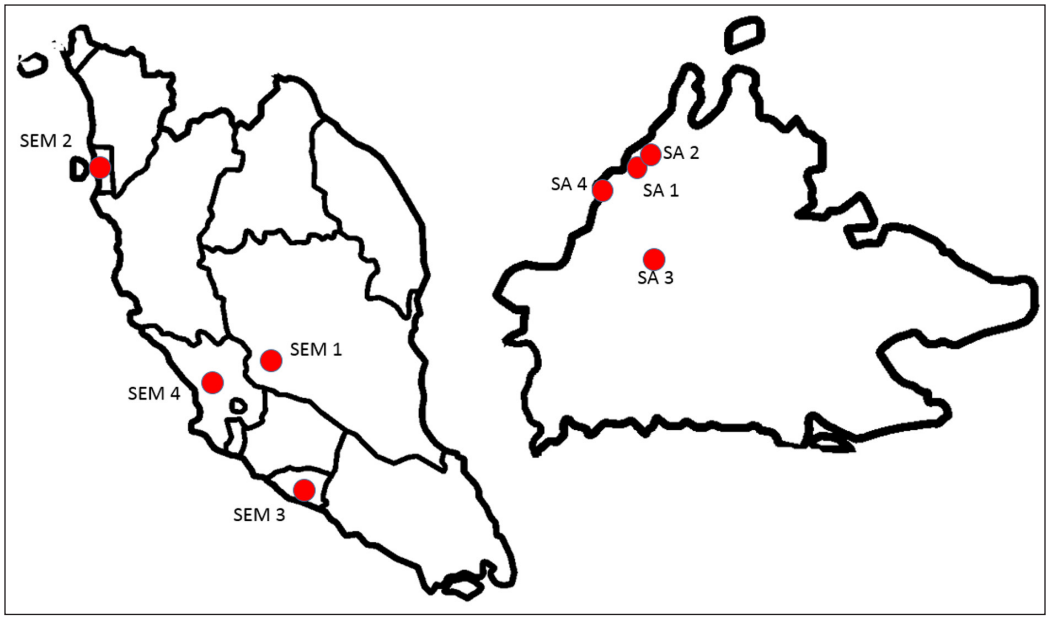

Figure 2. The map of sampling locations from six different states; SEM 1,2,3 and 4 denoted River Bentong, River Jawi, Penang, River Melaka and River Kuyuh river while SA 1,2,3 and 4 marked as River Telipok, River Sembulan, River Keinop and River Tuaran

ions, especially zinc at 579.8 ppb and lead 42.125 ppb. The results obtained in this study show the potential applicability of the biomonitoring assay. Biomonitoring allows only a positive sample, indicating inhibition of enzyme activity to be sent for instrumental testing. The cost of control will, therefore, be reduced dramatically.

CONCLUSION

In this study, purified *M. albus* brain ChE demonstrates activity inhibition after exposure to heavy metals that can later be extended and evolved into an alternative biosensing approach based on these findings. Furthermore this study shows significant inhibition of heavy metals, particularly mercury and chromium. This study, therefore, indicates that *M. albus* may be a potential new source of ChE to replace the existing commercial ChE. This work may add new data and information that are useful for future biomonitoring studies using this enzyme.

ACKNOWLEDGMENT

The project was supported by fund from Universiti Malaysia Sabah (UMS) under UMSGreat Grant No. GUG0293-2/2018.

REFERENCES

Ahmad, S. A., Wong, Y. F., Shukor, M. Y., Sabullah, M. K., Yasid, N. A., Hayat, N. M., … & Syed, M. A. (2016). An alternative bioassay using *Anabas testudineus* (Climbing perch) cholinesterase for metal ions detection. *International Food Research Journal*, *23*(4), 1446-1452.

Alam, P., Siddiqui, N. Q., Basudan, O. A., Al-Rehaily, A., Alqasoumi, S. I., Abdel-Kader, M. S., … & Shakeel, F. (2015). Comparative profiling of biomarker psoralen in antioxidant active extracts of different species of genus finus by validated HPTLC method. *African Journal of Traditional, Complementary and Alternative Medicines, 12*(1), 57-67. doi:10.4314/ajtcam.v12i1.9

Alam, M. K. & Maughan, O. E. (1992). The effect of malathion, diazinon, and various concentrations of zinc, copper, nickel, lead, iron, and mercury on fish. *Biological Trace Element Research, 34*(3), 225-236. doi:10.1007/bf02783678

Apartin, C. & Ronco, A. (2001). Development of a free beta-galactosidase in vitro test for the assessment of heavy metal toxicity. *Environmental Toxicology: An International Journal, 16*(2), 117-120. doi:10.1002/tox.1014

Bellas, J., Vázquez, E. & Beiras, R. (2001). Toxicity of Hg, Cu, Cd, and Cr on early developmental stages of *Ciona intestinalis* (Chordata, Ascidiacea) with potential application in marine water quality assessment. *Water Research, 35*(12), 2905-2912. doi:10.1016/s0043-1354(01)00004-5

Bisswanger, H. (2014). Enzyme assays. *Perspectives in Science, 1*(1-6), 41-55. doi: 10.1016/j.pisc.2014.02.005

Bocquené, G., Galgani, F. and Truquet, P. (1990). Characterization and assay conditions for use of AChE activity from several marine species in pollution monitoring. *Marine Environmental Research, 30*(2), 75-89. doi:10.1016/0141-1136(90)90012-d

Bradford, M. M. (1976). A rapid and sensitive method for the quantitation of microgram quantities o f protein utilizing the principle of protein-dye binding. *Analytical Biochemistry, 72*(1-2), 248-254. doi:10.1016/0003-2697(76)90527-3

Colovic, M. B., Krstic, D. Z., Lazerevic-Pasti, T. D., Bondzic, A. M. & Vasic, V. M. (2013). Acetylcholinesterase inhibitors: Pharmacology and toxicology. *Current Neuropharmacology, 11*(3), 315-335. doi: 10.2174/1570159X11311030006

Ellman, G. L., Courtney, K. D., Andres, J. V. & Featherstone, R. M. (1961). A new and rapid colorimetric determination of acetylcholinesterase activity. *Biochemical Pharmacology*, *7*(2), 88-95. doi:10.1016/0006-2952(61)90145-9

Forget, J., Livet, S. & Leboulenger, F. (2002). Partial purification and characterization of acetylcholinesterase (AChE) from the estuarine copepod *Eurytemora affinis* (Poppe). *Comparative Biochemistry and Physiology C: Toxicology and Pharmacology, 132*(1), 85-92. doi:10.1016/s1532-0456(02)00050-9

Frasco, M. F., Fournier, D., Carvalho, F. and Guilhermino L. (2008). Does mercury interact with the inhibitory effect of dichlorvos on *Palaemon serratus* (Crustacea: Decapoda) cholinesterase? *Science of the Total Environment, 404*(1), 88-93. doi:10.1016/j.scitotenv.2008.06.012

Gao, J. & Zhu, K. Y. (2001). An acetylcholinesterase purified from the greenbug (*Schizaphis graminum*) with some unique enzymological and pharmacological characteristics. *Insect Biochemistry and Molecular Biology, 31*(11), 1095-1104. doi:10.1016/s0965-1748(01)00057-1

Gbaye, O. A., Holloway, G. J. & Callaghan, A. (2012). Variation in the sensitivity of Callosobruchus (Coleoptera: Bruchidae) acetylcholinesterase to the organophosphate insecticide malaoxon: Effect of species, geographical strain and food type. *Pest Management Science, 68*(9), 1265-1271. doi:10.1002/ps.3293

Giedroc, D. P. & Arunkumara, A. I. (2007). Metal sensor proteins: Nature's metalloregulated allosteric switches. *Dalton Transactions,* (29), 3107-3120. doi: 10.1039/b706769k

Glusker, J. P., Katz, A. K., & Bock, C. W. (1999). Metal ions in biological systems. *The Rigaku Journal, 16,* 8-16. doi: 10.1201/9781482289893

Hayat, N. M., Shamaan, N. A., Sabullah, M. K., Shukor, M. Y., Syed, M. A., Khalid, A. & Ahmad, S. A. (2016). The use of lates calcarifer as a biomarker for heavy metals detection. *Rendiconti Lincei 27*(3), 463–472. doi:10.1007/s12210-015-0501-7

Kuca, K., Cabal, J. & Kassa, J. (2005). In vitro reactivation of sarininhibited brain acetylcholinesterase from different species by various oximes. *Journal of Enzyme Inhibition and Medicinal Chemistry, 20*(3), 227-232. doi:10.1080/14756360500043208

Mathonet, P., Barrios, H., Soumillion P. & Fastrez, J. (2006). Selection of allosteric β-lactamase mutants featuring an activity regulation by transition metal ions. *Protein Science, 15*(10), 2335-2343. doi:10.1110/ps.062304406

Martin, M., Osborn, K. E., Billig, P. & Glickstein, N. (1981). Toxicities of ten metals to *Crassostrea gigas* and *Mytilus edulis* embryos and cancer magister larvae. *Marine Pollution Bulletin, 12*(9), 305-308. doi:10.1016/0025-326x(81)90081-3

Naji, P., Griffin, B. P., Asfahan, F., Barr, T., Rodriguez, L. L., Grimm, R. & Desai, M. Y. (2014). Predictors of long-term outcomes in patients with significant myxomatous mitral regurgitation undergoing exercise echocardiography. *Circulation, 129*(12), 1310–1319. doi:10.1161/circulationaha.113.005287

Olson, D. L. & Christensen, G. M. (1980). Effects of water pollutants and other chemicals on fish acetylcholinesterase *in-vitro*. *Environmental Research, 21*(2), 327-335. doi:10.1016/0013-9351(80)90034-1

Padrillah, S. N., Ahmad, S. A., Yasid, N. A., Sabullah, M. K., Daud, H. M., Khalid, A. & Shukor, M. Y. (2017). Toxic effect of copper on liver and cholinesterase of *Clarias gariepinus*. *Environmental Science and Pollution Research, 24*(28), 22510-22523. doi:10.1007/s11356-017-9923-3

Quintaneiro, C., Ranville, J. F. & Nogueira, A. J. A. (2016). Physiological effects of essential metals on two detritivores*: Atyaephyra desmarestii* (Millet) and *Echinogammarus meridionalis* (Pinkster). *Environmental Toxicology and Chemistry, 35*(6), 1442–1448. doi:10.1002/etc.3284

Ramakritinan, C. M., Chandurvelan R. & Kumaraguru, A. K. (2012). Acute toxicity of metal: Cu, Pb, Cd, Hg and Zn on marine molluscs, *Cerithedia cingulate* G., and *Modiolus philippinarum* H. *Indian Journal Geomarine Science, 41*(2), 141-145.

Robinson, P. K. (2015). Enzyme: Principles and biotechnological applications. *Essays in Biochemistry, 15*(59), 1-41. doi: 10.1042/bse0590001

Sabullah, M. K., Sulaiman, M. R., Shukor, M.Y.A., Syed, M. A., Shamaan N. A., Khalid, A. & Ahmad, S. A. (2014). The assessment of cholinesterase from the liver of *Puntius javanicus* as detection of metal ions. *The Scientific World Journal 2014*, 1-9. doi: 10.1155/2014/571094

Sabullah, M. K., Sulaiman, M. R., Shukor, M. S., Yusof, M. T., Johari, W. L. W., Shukor, M. Y., & Syahir, A. (2015). Heavy metals biomonitoring via inhibitive assay of acetylcholinesterase from *Periophthalmodon schlosseri*. *Rendiconti Lincei, 26*(2), 151–158.doi:10.1007/s12210-014-0359-0

Santarpia, L., Grandone, I. & Contaldo, F. (2ull013). Butyrylcholinesterase as a prognostic marker: A review of the literature. *Journal of Cachexia, Sarcopenia and Muscle, 4*(1), 31-39. doi:10.1007/s13539-012-0083-5

Shukor, M. Y., Abo-Shakeer, L. K. A., Ahmad, S. A., Shamaan, N. A. & Syed, M. A. (2013). Isolation and characterization of a molybdenum-reducing *Bacillus pumilus* strain ibna. *Journal of Environmental Microbiology and Toxicology 1*(1), 9-14. doi: 10.21315/tlsr2017.28.1.5

Strubelt, O. (1996). Comparative studies on the toxicity of mercury, cadmium, and copper toward the isolated perfused rat liver. *Journal of Toxicology and Environmental Health Part A, 47*(3), 267-283. doi:10.1080/009841096161780

Sussman, J. L., Harel, M., Frolow, F., Oefner, C., Goldman, A., Toker, L. & Silman, I. (1991). Atomic structure of acetylcholinesterase from *Torpedo californica*: A prototypic acetylcholine-binding protein. *Science, 253*(5022), 872-879. doi:10.1126/science.1678899

Talesa, V., Romani, R., Antognelli, C., Giovannini E. & Rosi, G. (2001). Soluble and membrane-bound acetylcholinesterases in *Mytilus galloprovincialis* (Pelecypoda: Filibranchia) from the northern adriatic Sea. *Chemico-Biological Interactions, 134*(2), 151–166. doi:10.1016/s0009-2797(01)00152-1

Pertanika J. Sci. & Technol. 28 (S2): 95 - 106 (2020)

PERTANIKA JOURNALS

SCIENCE & TECHNOLOGY

Journal homepage: http://www.pertanika.upm.edu.my/

Profiling of Cholinesterase Extracted from The Brain Tissue of *Diodon hystrix* and Its Inhibition Reaction Towards Carbamates

Akid Haris[1], Noreen Nordin[1], Nur Azizah Mustapa[1], Suraya Abd. Sani[1], Mohd Yunus Shukor[2] and Mohd Khalizan Sabullah[1]*

[1]Faculty of Science and Natural Resources, University Malaysia Sabah, Jalan UMS, 88400 Kota Kinabalu, Sabah, Malaysia
[2]Faculty of Biotechnology and Biomolecular Sciences, Universiti Putra Malaysia, 43400 UPM Serdang, Selangor Darul Ehsan, Malaysia

ABSTRACT

Diodon hystrix, commonly known as spot-fin porcupine fish is a salt-water fish belonging to the *Diodontidae* family. It is widely distributed in Sabah wet market due to its commercial value. This study exploits the effectiveness of Cholinesterase (ChE) obtained from the brain tissue of *D. hystrix* in detecting carbamates inhibitory activities. Carbamate pesticides known to inhibit ChE and toxic towards living organisms can contaminate the water bodies. By using diethylaminoethanol (DEAE) Sepharose ion exchange chromatography, a total of 40% recovery yield of ChE was obtained with a 165.77 purification fold. Furthermore, the ChE showed a high affinity towards acetylthiocholine iodide (ATC) with an optimum activity at pH 7.45 and temperature ranging from 20 to 40°C. Among five different types of carbamates, methomyl was found to have the highest percentage of inhibition analyzed using ChE inhibitory assay, followed by carbofuran, bendiocarb, carbaryl and propoxur with >85% inhibition rate. The results concluded that ChEs extracted from the *brain* tissue of *D. hystrix* are applicable to be used as a bioindicator in detecting the presence of carbamates.

Keywords: Carbamates, cholinesterase, *diodon hystrix*ion, exchange chromatography, inhibitory activities, water pollution

ARTICLE INFO

Article history:
Received: 10 February 2020
Accepted: 13 November 2020
Published: 31 December 2020

DOI: https://doi.org/10.47836/pjst.28.S2.08

E-mail addresses:
akidharis96@gmail.com (Akid Haris)
ryeennordin@yahoo.com (Noreen Nordin)
izzah0506@yahoo.com (Nur Azizah Mustapa)
suraya.abdulsani@ums.edu.my (Suraya Abd. Sani)
yunus.upm@gmail.com (Mohd Yunus Shukor)
khalizan@ums.edu.my (Mohd Khalizan Sabullah)
* Corresponding author

INTRODUCTION

Almost all of today's applications require water such as in agriculture, industrial, animal husbandry, tourism, fishery and even simple individual tasks. However, unethical use of water resources is becoming worse

ISSN: 0128-7680
e-ISSN: 2231-8526

© Universiti Putra Malaysia Press

and this threatens the quality of water which will slowly and surely get more polluted with time (Gonzalez et al., 2009). The pollution of water bodies from direct and indirect use of natural or artificial compounds, such as carbamates can be toxic to the human body due to its ability to inhibit cholinesterase enzyme (ChE) (Hayat et al., 2015). In order to curb this issue, water monitoring and rehabilitation are needed. A fast, cost-effective and reliable way of contamination screening before using high-performance technology such as High Pressure Liquid Chromatography (HPLC) can help ease this process.

ChE is an enzyme responsible for lysing choline base esters which serve as neurotransmitters found in animals. This enzyme can be subdivided into acetylcholinesterase (AChE), butyrylcholinesterase (BChE) and propionyl cholinesterase (PChE) with PChE being closely related to BChE (Ahmad et al., 2016). The most apparent difference between AChE and BChE is their ligand-binding specificity due to the difference in the number of aromatic residues in their gorge (Rosenberry et al., 2017). Nonetheless, all three sub-types of ChE are susceptible towards carbamate inhibitory activities which disable them from hydrolyzing choline-based esters.

Carbamate pesticides are widely used to control the development of pests through inhibition of cholinesterase activities, with high acute toxicity similar to the organophosphates (OP). Carbamates and OP differ in their mode of action during the formation of the ChE-inhibitor complex. OP are irreversible inhibitors where after being phosphorylated in ChE, cannot be reversed. Carbamates, on the other hand, are temporary or reversible inhibitors where decarbamylation via spontaneous hydrolysis would shorten the inhibition time (Darvesh et al., 2008). When AChE is inhibited in the body, acetylcholine will accumulate in synapses which can cause severe central nervous system disorder (Berman et al., 2017).

The bioaccumulation of toxicants in marine organisms causes severe effects to the fish, handlers and also humankind (Almroth, 2008). Multiple past studies had proven the sensitivity of fish towards toxicants (Monserrat et al., 2002; Sturm et al., 2000), making them a suitable biomarker. This study used *D. hystrix* mostly due to its availability and increasing commercial value in Sabah. It can be found at prices as low as RM 5 per kilogram but their commercial value in Sabah has been increasing in recent years, mostly as a delicacy for both tourists and locals. Other than that, *D. hystrix* interesting characteristics such its ability to host multiple endo and ectoparasites (Quilichini et al., 2010) with high survival endurance were also considered during the selection process. Observing the inhibition of ChE by pesticide *in vitro* helps to bypass detoxification defenses and bioactivation of compounds in non-target tissues (Assis et al., 2012). ChE based early-warning biomarker that was thoroughly researched and recently applied for pollution assessment showed tissue-specific variations in AChE responses towards inhibitors (Hayat et al., 2015). This can also be true for different species of fish. Hence, this study focused on the profiling of

ChE extracted from the brain tissue of *D. hystrix* where AChE was concentrated to test its ability to detect carbamate inhibitory activities.

MATERIALS AND METHODS

Chemicals

The materials used in the study include Acetylthiocholine iodide (ATC), butyrylthiocholine iodide (BTC), propionyl thiocholine iodide (PTC), 5,5-dithio-bis-(2-nitrobenzoic acid) (DTNB), diethylaminoethanol-Sepharose (DEAE-Sepharose), Bradford solution and bovine serum albumin (BSA) were obtained from Sigma-Aldrich, Germany.

Preparation of Crude Homogenate

A total of three *D. hystrix* was obtained from the Kota Kinabalu Wet Market. Each fish was approximately 500-800g in weight with 30-40 cm in length. After being killed, the brain was extracted and weighed. The crude brain sample was homogenized in 0.1 M sodium phosphate buffer pH 7.5 along with 2 mM phenylmethylsulfonyl fluoride (PMSF) with the ratio of brain and buffer; 1:4 (w/v). The homogenate was centrifuged at 10, 000 rpm (11200 × *g*) for 13 minutes at 4°C. The supernatant was stored in a clean microcentrifuge tube at -20°C after separating it from the pallet prior to further analysis (Ahmad et al., 2016).

Partial Purification (Ion Exchange Chromatography)

DEAE-Sepharose was loaded into a disposable desalting column with a 0.9 cm diameter and was allowed to settle giving a 3 cm bed height. The column was then washed with a five-batch volume of washing buffer (20 mM sodium phosphate buffer, pH 7.5), cleaning the matrix and calibrating the flow rate. A total of 300 µL of crude supernatant was loaded into the column before running another three-batch volumes of washing buffer into the column. Next, five batch volumes of elution buffer (20 mM sodium phosphate buffer containing increasing NaCl concentration from 0.2 M to 1 M) was loaded into the column while simultaneously collecting 1 mL fractions until the end of the elution stage (Acikara, 2013). According to Ellman et al. (1961) and Bradford et al. (1976), enzyme activity and protein content determination are applied on all of the fractions collected with fractions showing high ChE activity combined (Sabullah et al., 2015).

Enzyme Activity Determination

The activity of ChE was determined using a 96 microplate well assay according to the method of Ellman et al. (1961) with a slight modification. This study used acetylthiocholine iodide (ATC) as a substrate for both pH and temperature profiling. A total of 20 µL DTNB (0.067 mM), 200 µL of 0.1 M sodium phosphate buffer at pH 7.45 and 10 µL extracted ChE

were loaded into the microplate wells and incubated at room temperature for 15 minutes. After that, 20 µL of 0.5 mM ATC was added, followed with another 10 minutes incubation at room temperature. The changes in colour of solution from colourless to yellow indicates a reaction. The enzyme activity was determined by calculating the quantity of substrate (µmol) hydrolyzed by ChE per minute and per protein (U or $\mu molmin^{-1}mg^{-1}$) with 13.6 $mM^{-1}cm^{-1}$ as extinction coefficient. Specific enzyme activity was indicated as µmole min^{-1} mg^{-1} of protein or Umg^{-1} of protein. The assays were performed in the dark with each test done in triplicates.

Substrate Specificity

Acetylthiocholine iodide (ATC), butyrylthiocholine iodide (BTC) and propionyl thiocholine iodide (PTC) were the three synthetic substrates used in determining ChE specificity. The concentration of each substrate was set from 0.5 to 2.5 mM. The assay reaction mixture was incubated for 10 minutes at room temperature before the absorbance reading at 405nm was taken (Sabullah et al., 2014). Biomolecular constant (K_m) and maximum velocity (V_m) was determined using Michaelis-Menten curves; plotted using GraphPad Prism Software version 5.

pH and Temperature Profiling

The overlapping buffering system was applied to test *D. hystrix* optimum pH. The buffers were comprised of acetate buffer (0.1 M; pH 3.0, 4.0 and 5.0), sodium phosphate buffer (0.1 M; pH 5.0, 6.0, 7.5 and 8.0) and Tris-HCl buffer (0.1 M; pH 7.5, 8.0 and 9.0). With reference to Ahmad et al. (2016), optimum temperature was deduced by incubating the reaction mixture at a selected temperature of 20, 25, 30, 40, 50 and 60 °C.

ChE Inhibitory Assay

The inhibitory effect of five types of carbamates, namely methomyl, carbofuran, bendiocarb, carbaryl and propoxur was tested by incubating them with D. hystrix ChE. Carbamates were selected due to its widespread use in agriculture to control pests and it could be toxic when they were discharged into the water bodies without proper treatment. The test mixture comprised 150 µL sodium phosphate buffer (0.1 M, pH 7.5), 50 µL of carbamates with 10 ppm final concentration, 20 µL DTNB (0.067 mM) and 10 µL of extracted ChE. For control, carbamates were replaced with sodium phosphate buffer. The mixture was incubated for 15 minutes at room temperature before the addition of 20 µL of substrate. It was then incubated again for 10 minutes at room temperature. Reading of absorbance was taken at 405 nm following 10 minutes incubation (Sabullah et al., 2015). ChE inhibition rates for each pesticide were then calculated using Equation 1.

$$Inhibition(\%) = \frac{Uc - Ui}{Uc}(100)$$

Equation 1: Carbamates inhibition rate towards ChE (%)

Uc = Control enzyme activity

Ui = Enzyme activity with carbamates inhibition

RESULTS AND DISCUSSIONS

Cholinesterase (ChE) Purification Profile

Figure 1 shows the purification profile of ChE by comparing the enzyme activity and the protein fractions obtained from ion exchange chromatography. A total of 37 fractions were obtained, each with a total volume of 1 mL. Fraction 14 displayed the highest ChE activity followed by fraction 12 and 13, while the highest protein concentration was observed in fraction 13. The low protein concentration with high enzyme activity on fraction 14 suggests that it has the highest amount of ChE. Fractions 12 to 16 were selected and combined for enzyme profiling due to their high enzyme activity and protein concentration. Table 1 shows the ChE specific activity and final yield of protein for each stage in the sample purification process from crude homogenate until the sample had gone through ion exchange chromatography.

Following the principle of anion-exchange gel chromatography of DEAE-Sepharose, it is understood that the positive charge matrix will exhibit ionic interaction towards a negative charge sample that passes through the column. Due to proteins having different

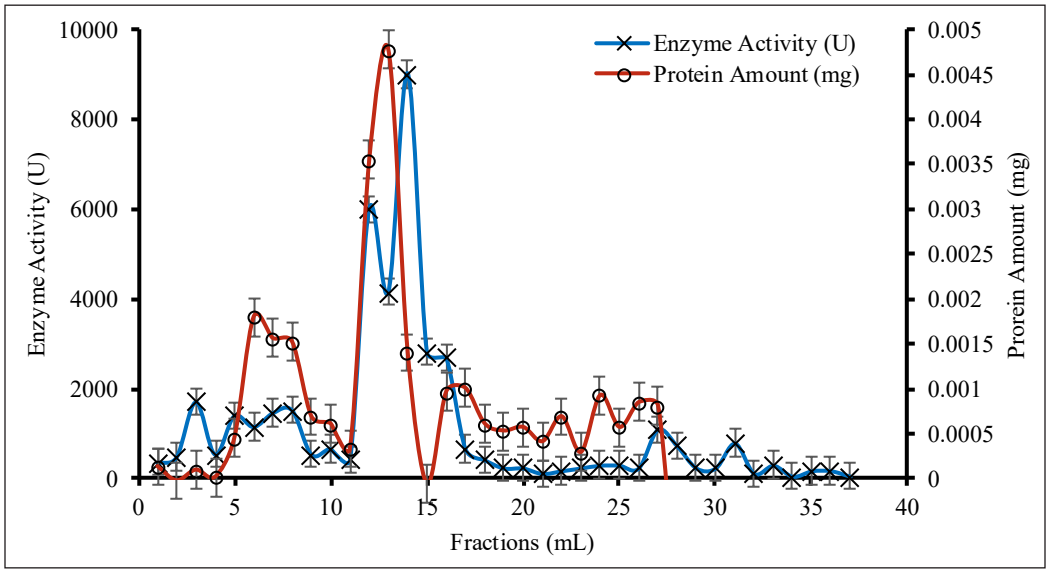

Figure 1. DEAE-Sepharose ion exchange chromatography profile on ChE purification from brain tissue of *D. hystrix* with error bars represented by mean ± standard error (n=3)

Table 1
ChE purification table of D. hystrix. *Specific activity displayed in(U mg^{-1}) indicates µmole/min/mg protein*

Sample	Total protein (mg)	Total ChE activity (U)	Specific activity (Umg^{-1})	Purification fold	Yield (%)
Crude homogenate	7.54	32720.59	4339.60	1.00	100
Supernatant (centrifuged;11200g, 13 minutes, 4°C)	3.66	32169.12	8789.38	2.03	98.31
DEAE Sepharose sample extract	0.009	13112.75	1456972.68	165.77	40.07

total charge and ionic strength, separation of other proteins from the targeted ChE can be achieved. It is important to know the isoelectric point of the targeted enzyme in order to make sure the ChE is negatively charged. Thus, the sample solution needs to have pH higher than the isoelectric point of ChE, which is approximately ±5.35 (Bon and Rieger, 1975). Different concentrations of NaCl helps in eluting ChE by displacement of bound proteins through ions in the buffer competing for the binding site where further increase in ionic strength displaces proteins based on their charge strength (Acikara, 2013). Figure 1 shows the abundance of protein amounts in fraction 13, although low enzyme activity was observed opposite to that of fraction 14. This displayed the principle of ion-exchange chromatography very clearly. This study can be further proven in Table 1, which shows the drastic decrease in protein amount due to foreign proteins being filtered from ChE at different NaCl concentrations. Purification is important in enzyme profiling which helps in increasing the ChE reactivity towards targeted toxicants. Further tests in the future using Native polyacrylamide gel electrophoresis (Native-PAGE) would better support the results obtained from ion-exchange chromatography (Hayat et al., 2015).

Substrate Specificity Profiling

Figure 2 shows hydrolyzation of three synthetic substrates (ATC, BTC, PTC) each with increasing concentration from 1 mM to 5 mM obeying Michaelis-Menten plot. All three substrates displayed similar increases in hydrolytic activity along with the increase in concentration. However, it can be observed that ChE activity starts to reach plateau nearing the 5 mM concentration. There is a clear significant difference to which substrate ChE from the D. hystrix brain reacts to. The curve indicated that ATC had the highest ChE activity, followed by PTC and lastly BTC. Following further analysis in Table 2, ATC displayed the lowest K_m value, thus having the highest affinity towards ChE from *D. hystrix* brain compared to BTC and PTC. Although PTC indicated a high V_{max} value, its catalytic efficiencies (V_{max}/K_m) still fall short in comparison to ATC. Both data indicated that ATC is the most favored substrate of ChE from *D. hystrix* brain, followed by PTC and BTC. This also suggests that the ChE obtained in the brain was mostly AChE.

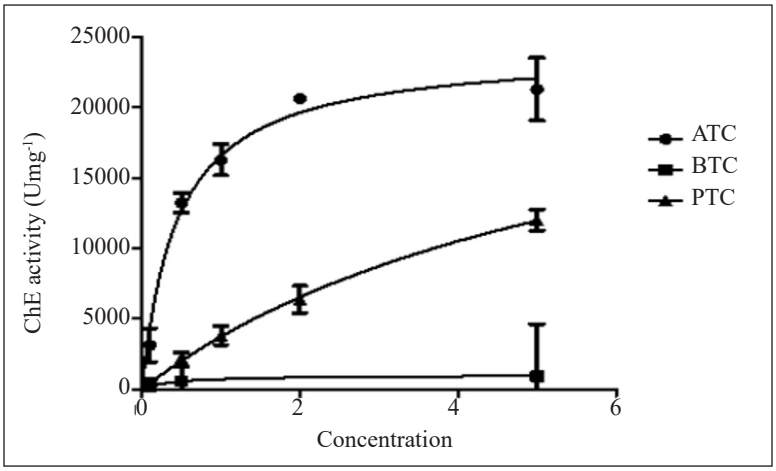

*Figure 2***.** ChE profile on substrate specificity using three synthetic substrates (ATC, BTC, PTC). Error bar represented by mean ± standard error (n=3).

Table 2
Table of comparison of ATC, BTC and PTC on their maximum velocity (V_{max}), biomolecular constant (K_m) and catalytic efficiencies (V_{max}/K_m) with ChE from the brain tissue of D. hystrix

	Mean point (95% confidence intervals)		
Substrate	**ATC**	**BTC**	**PTC**
V_{max} (µmol/min/mg)	981.10	1547.00	3633.00
K_m (mM)	0.07	2.33	1.33
Catalytic efficiencies (V_{max}/K_m)	14015.71	663.95	2731.58

To further discuss, in the study done by Sabullah et al., (2014) on *P. javanicus* liver tissue, ChE was found to be specific towards BTC with (V_{max}/K_m) higher than ATC and PTC. However, a study on *M. albus* brain tissue by Khalidi et al. (2019) found that ATC had the highest (V_{max}/K_m), similar to the result obtained in this study. These results proved that different parts of organs and different species of fish incorporated ChE with different substrate specificity of either ATC, BTC or PTC.

Profiling of Optimum pH and Temperature

Figure 3 shows the pH profile of ChE in overlapping buffer system of acetate buffer, sodium phosphate buffer and Tris-HCl buffer. The highest ChE activity was indicated at pH ±(7.45-7.50) for both sodium phosphate buffer and Tris-HCl buffer with no significant difference between the two values. Similarly, both buffers showed a decline in enzyme activity, starting from pH 8.0 to 9.0. The pattern in Figure 3 indicates that ChE from *D. hystrix* is optimum and can be regulated in both sodium phosphate buffer and Tris-HCl buffer at pH 7.45 to 7.50. However, due to Tris-HCl high sensitivity towards temperature (AppliChem, 2008), sodium phosphate buffer is more suitable to be used for enzyme profiling. These

attributes are also dependent on the pK_a value of the buffer, which determines the range in which the buffer is considered adequate. Sodium phosphate buffer thus fits perfectly to optimize ChE from *D.hystrix* brain tissue with its pK_a value falls in the range of 5.8 to 8.0.

In Figure 4, ChE enzyme activity with different temperatures was displayed. Optimum temperature was at 40°C where a steady increase in enzyme activity could be observed from 20 to 40°C but no significant difference was observed ($p>0.05$). Similar to other enzymes, kinetic energy increases as temperature increases, thus resulting in higher enzyme activity. However, a sharp decline of enzyme activity was shown at higher temperature presumably due to denaturation of the biological shape of ChE resulting in a bell-shaped curve. The ChE starts to denature when the temperature is higher than its optimum temperature (Ahmad et al., 2016) which in this study was at temperature >40°C.

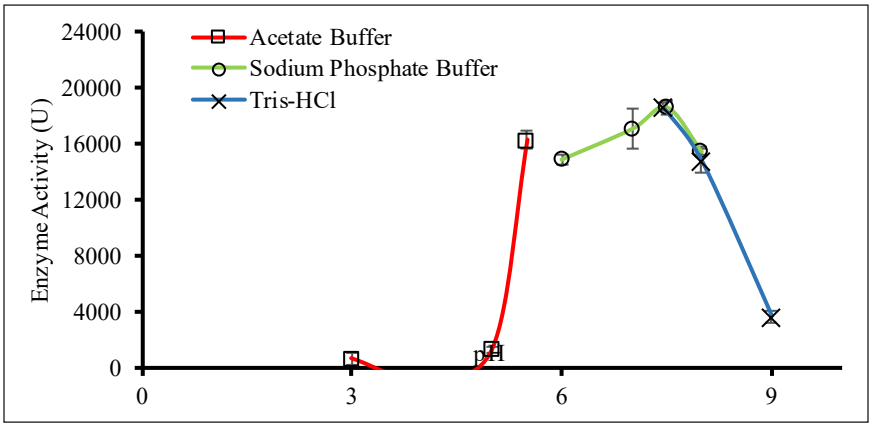

Figure 3. pH profile of ChE from *D. hystrix* brain tissues through overlapping buffer system of three different buffers (acetate buffer, sodium phosphate buffer and Tris-HCl buffer) with error bar represented by mean ± standard deviation (n=3)

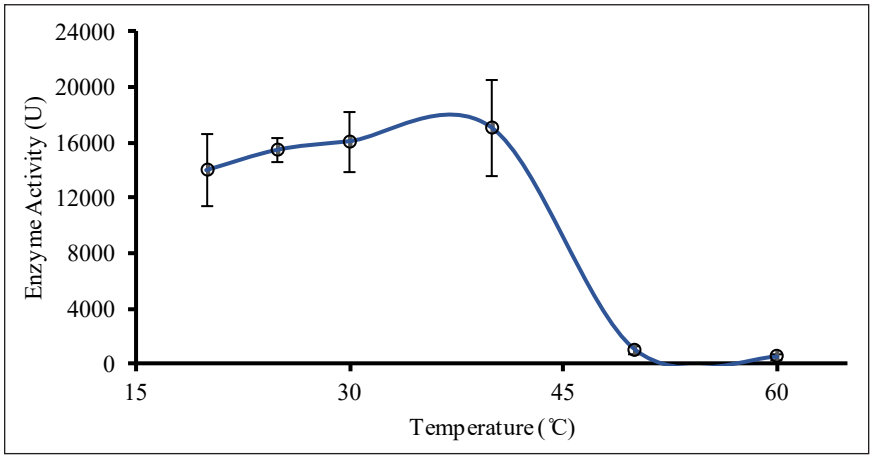

Figure 4. Temperature profile of ChE from *D. hystrix* brain tissues with error bar represented by mean ± standard deviation (n=3)

Similar to its substrate specificity, ChE extracted from different sources may or may not exhibit similar optimum pH and temperature. In this case, two studies by Ahmad et al. (2016) that evaluated the brain tissue of *Tor tambroides*[b] and liver tissue of *Anabas testudineus*[a] showcased that AChE optimum temperature was in the range of 25 to 35°C for *T. tambroides*, falling into the same temperature range in this study. *A. testudineus* AChE showed an optimum temperature of 40°C, similar to the result obtained in this study despite using different organs and species, thus further solidifying the point made.

ChE Inhibitory Assay

Figure 5 shows the reactivity of ChE enzyme from *D. hystrix* brain tissue towards the inhibitory effect of bendiocarb, propoxur, methomyl, carbofuran and carbaryl at 10 ppm concentration. All of the carbamates elicit inhibitory activities higher than 85% with highest in methomyl at 98%. The strength of carbamate inhibitory activities are as follows; met homyl>carbofuran>bendiocarb>carbaryl>propoxur. According to Sabullah et al. (2015), in comparison to organophosphate, which can also inhibit ChE, carbamates bind to AChE esoteric sites without the need of any bioconversion. This study implied that carbamates-based pesticide could bind to AChE more easily than organophosphate. All of the tested carbamates are applied as a broad-spectrum insecticide that could kill more than one species of insects. In concurrent to their applications, methomyl and carbofuran are mainly used in fields and crops whereas bendiocarb, carbaryl and propoxur were also found in household pest control. It was stated by Gupta et al. (2011) that methomyl and carbofuran were highly dangerous towards any living system and this statement was further supported by Dorko et al. (2011) indicating that insecticides applied as household pest control had lower toxicity towards vertebrates. A study carried out by Mahboob et al. (2014) on *Labeo rohita* found

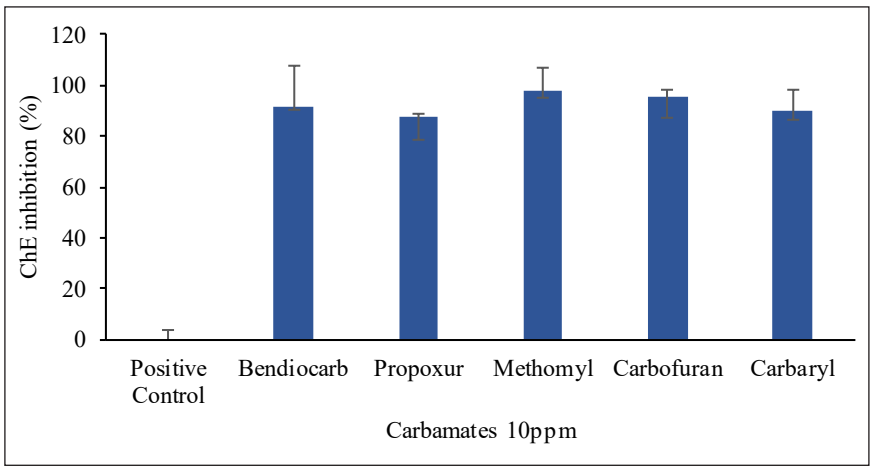

Figure 5. Inhibition test profile of five different types of carbamates at 10ppm concentration on ChE from *D. hystrix* brain tissues with error bar represented by mean ± standard deviation (n=3)

that carbofuran exposure disrupted the functions of organs that included the brain, gills, muscle, kidney, liver and even non-organs such as blood. These multiple findings thus solidified the result and present a logical explanation to why methomyl and carbofuran have the highest inhibitory activities in comparison to the other carbamates.

CONCLUSION

The extraction of cholinesterase (ChE) enzyme from the brain tissues of *D. hystrix* was achieved using DEAE-Sepharose ion-exchange chromatography. Through substrate specificity test, it was observed that the partially purified ChE enzyme was proned towards ATC with lowest K_m value (0.07011 mM) and highest catalytic efficiency value of 13993.72 ($V_{max}K_m^{-1}$). The optimum pH was in the range of pH ±7.45 and 7.5 with an optimum temperature at 20 to 40°C. ChE inhibitory assay showed all pesticides were able to inhibit ChE of *D. hystrix* with methomyl having the highest inhibiting ability at 98%, while propoxur with the lowest inhibition rate. This study proved that the extraction and partial purification of ChE from the brain tissues of *D. hystrix* were efficient and were able to show high reactivity towards carbamates inhibitory activities without applying higher cost consuming methods such as the HPLC. This also implies that ChE from *D. hystrix* brain tissues can be applied as a biomarker tool due to its ability in detecting carbamates inhibitory activities with the change in color following the Ellman assay principles. Further analysis regarding this enzyme on the wider variety of toxicants can help determine the efficacy of it as a biomarker.

ACKNOWLEDGEMENT

Acknowledgment towards University Malaysia Sabah for Skim Dana NIC, SDN0020-2019.

REFERENCES

Acikara, O. B. (2013). Ion-exchange chromatography and its applications. In Martin, D. F., & Martin, B. B. (Ed.), *Column chromatography* (pp. 31-58). Rijeka, Croatia: InTech .

Ahmad, S. A., Sabullah, M. K., Yasid, N. A., Shamaan, N. A., Abd Shukor, M.Y., Jirangon, H., … & Syed, M.A. (2016). Evaluation of acetylcholinesterase source from fish, for detection of carbamate. *Journal of Environmental Biology*, *37*(4), 479-484.

Ahmad, S. A., Wong, Y. F., Shukor, M. Y., Sabullah, M. K., Yasid, N. A., Hayat, N. M., ... & Syed, M. A. (2016). An alternative bioassay using *Anabas testudineus* (Climbing perch) colinesterase for metal ions detection. *International Food Research Journal, 23*(4), 1446-1452

Almroth C., Sturve, B., Stephensen, J., Fredrik Holth, E., & Forlin, L. (2008). Protein carbonyls and antioxidative defenses in corkwing wrasse (*Symphodus melops*) from a heavy metal-polluted and PAH-polluted site. *Marine Environment Research*, *66*, 271–277. doi:10.1016/j.marenvres.2008.04.002

AppliChem. (2008). *Biological buffers*. Darmstadt, Germany: PanReac AppliChem ITW Reagents.

Assis, C. R., Linhares, A. G., Oliveira, V. M., Franca, R. C., Carvalho, E. V., Bezerra, R. S., & de Carvalho Jr, L. B. (2012). Comparative effect of pesticides on brain acetylcholinesterase in tropical fish. *Science of the Environment*, *441*, 141-150. doi:10.1016/j.scitotenv.2012.09.058

Berman, T. T., Goen, T., Novack, L., Beacher, L., Grinshpan, L., Segev, D., & Tordjman, K. (2017). Corrigendum to urinary concentrations of organophosphate and carbamate pesticides in residents of a vegetarian community. *Environment International*, *96*(2016), 34-40. doi: 10.1016/j.envint.2017.06.017

Bon, S., and Rieger, F. (1975). Interactions between lectins and electric eel acetylcholinesterase. *FEBS Letters, 53*(3), 282-286. doi:10.1016/0014-5793(75)80037-8

Bradford M. M. (1976). A rapid and sensitive method for the quantitation of microgram quantities of protein utilizing the principle of protein dye binding. *Analytical Biochemistry*, *72*(1-2), 248–254. doi:10.1016/0003-2697(76)90527-3

Darvesh, S., Darvesh, K. V., McDonald, R. S., Mataija, D., Walsh, R., Mothana, S., ... & Martin, E. (2008). Carbamates with differential mechanism of inhibition toward acetylcholinesterase and butyrylcholinesterase. *Journal of Medicinal Chemistry, 51*(14), 4200-4212. doi:10.1021/jm8002075

Dorko, F., Danko, J., Flešárová, S., Boroš, E., & Sobeková, A. (2011). Effect of pesticide bendiocarbamate on distribution of acetylcholine- and butyrylcholine-positive nerves in rabbit's thymus. *European Journal of Histochemistry, 55*(4), 1-4. doi:10.4081/ejh.2011.e37

Ellman, G. L., Courtney, K. D., Andres, V. J., & Featherstone, R. M. (1961). A new and rapid calometric determination of acetylcholinesterase activity. *Biochemical Pharmacology*, *7*(2), 88-95. doi:10.1016/0006-2952(61)90145-9

Gonzalez, C., Greenwood, R., & Quevauviller, P. (2009). Rapid chemical and biological techniques for water monitoring. In Gonzalez, C., Greenwood, R., & Quevauviller, P. (Ed.), *Rapid chemical and biological techniques for water monitoring* (pp. 1–419). United Kingdom: Wiley Blackwell.

Gupta, R. C., Malik, J. K., & Milatovic, D. (2011). Organophosphate and carbamate pesticides. In Gupta, R. C. (Ed.), *Reproductive and developmental toxicology* (pp. 471–486). Georgia, USM: Elsevier.

Hayat, N. M., Shamaan, N. A., Shukor, M. Y., Sabullah, M. K., Syed, M. A., Khalid, A., ... & Ahmad, S. A. (2015). Cholinesterase-based biosensor using *Lates calcarifer* (Asian Seabass) brain for detection of heavy metals. *Journal of Chemical and Pharmaceutical Sciences*, *8*(2), 376–381.

Khalidi, S. A. M., Sabullah, M. K., Sani, S. A., Ahmad, S. A., Shukor, M. Y., Jaafar, I. N. M., & Gunasekaran, B. (2019). Acetylcholinesterase from the brain of *Monopterus albus* as detection of metal ions. *Journal of Physics: Conference Series*, *1358*, 1-11. doi:10.1088/1742-6596/1358/1/012028

Mahboob, S., Ahmad, L., Sultana, S., AlGhanim, K., Al-Misned, F., & Ahmad, Z. (2014), Fish cholinesterases as biomarkers of sublethal effects of organophosphorus and carbamates in tissues of *Labeo rohita*. *Journal of Biochemical and Molecular Toxicology*, *28*(3), 137-142. doi:10.1002/jbt.21545

Monserrat, J. M, Bianchini, A., & Bainy, A. C. D. (2002). Kinetic and toxicological characteristic of acetylcholinesterase from the gills of oyster (*Crassostrea rhizophorea*) and other aquatic species. *Marine Environment Research*, *54*(3-5), 781-785. doi:10.1016/s0141-1136(02)00136-8

Quilichini, Y., J. Foata, J. Justine, R. Bray, B. Marchand. (2010). Ultrastructural study of the spermatozoon of *Heterolebes maculosus* (Digenea, Opistholebetidae), a parasite of the porcupinefish *Diodon hystrix* (Pisces, Teleostei). *Parasitology International, 59(*3), 427-434. doi:10.1016/j.parint.2010.06.002

Rosenberry, T. L., Brazzolotto, X., Macdonald, I. R., Wandhammer, M., Trovaslet-leroy, M., Darvesh, S., & Nachon, F. (2017). Comparison of the binding of reversible inhibitors to human butyrylcholinesterase and acetylcholinesterase: A crystallographic, kinetic and calorimetric study. *Molecules, 22*(12), 1–21. doi:10.3390/molecules22122098

Sabullah, M. K., Ahmad, S. A., Shukor, M. Y., Shamaan, N. A., Khalid, A., Gansau, A. J., ... & Sulaiman, M. R. (2015). Acetylcholinesterase from *Puntius javanicus* for the detection of carbamates and organophosphates. *Journal of Chemical and Pharmaceutical Sciences*, *8*(2), 348–353.

Sabullah, M. K., Sulaiman, M. R., Shukor, M. Y. A., Syed, M. A., Shamaan, N. A., Khalid, A., & Ahmad, S. A. (2014). The assessment of cholinesterase from the liver of *Puntius javanicus* as detection of metal ions. *Scientific World Journal*, *2014*, 1-9. doi:10.1155/2014/571094

Sturm, A., Wogram, J., & Segner, H. (2000). Different sensitivity to organophosphates of acetylcholinesterase and butyrylcholinesterase from three-spined stickleback (*Gasterosteus aculeatus*): Application in biomonitoring. *Environmental Toxicology and Chemistry: An International Journal, 19*(6), 1607-1615. doi:10.1002/etc.5620190618

Pertanika J. Sci. & Technol. 28 (S2): 107 - 119 (2020)

SCIENCE & TECHNOLOGY

Journal homepage: http://www.pertanika.upm.edu.my/

Cholinesterase from the Liver of *Diodon hystrix* for Detection of Metal Ions

Noreen Nordin, Ronaldo Ron Cletus, Mohd Khalizan Sabullah*, Siti Aishah Muhammad Khalidi, Rahmath Abdulla and Siti Aqlima Ahmad

Faculty Science and Natural Resources, Universiti Malaysia Sabah, 88400, Kota Kinabalu, Sabah, Malaysia
Department of Biochemistry, Faculty of Biotechnology and Biomolecular Sciences, Universiti Putra Malaysia, 43400 Serdang, Selangor, Malaysia

ABSTRACT

The discharge of industrial effluents into nearby water bodies affects the inhabitants including living organisms. The presence of foreign materials such as heavy metals can be a threat to the ecosystem as they are enormously carcinogenic even though in minute concentration. Hence, an economical and time-efficient preliminary screening test is crucial to be developed for the detection of heavy metals, prior to employment of high technology instruments. In this study, cholinesterase (ChE) from Sabah porcupine fish, *Diodon hystrix* was purified to test for its potential as an alternative biosensor in detecting metal ions. Few enzymatic parameters including specificity of substrate, temperature and pH were applied to determine its optimal enzymatic activity. ChE enzyme was found to be more sensitive towards the presence of substrate, butyrylthiocholine iodide (BTC), in contrast to acetylthiocholine iodide (ATC) and propionylthiocholine iodide (PTC) with the effective coefficient at 7193, 3680.15 and 2965.26 V_{max}/K_m, respectively. Moreover, the extracted ChE enzyme showed the optimum activity at pH 9 of 0.1 M Tris-HCl and at 25°C to 30°C range of temperature. When subjected to heavy metals, ChE enzyme was significantly inhibited as the enzyme activity was reduced in the sequence of Hg > Ag > Cr > Cu > Cd > Pb ≥ Zn > As. As a conclusion, the partially purified ChE enzyme proved its sensitivity towards metal ion exposure and can be used as an alternative method in screening the level of contamination in the environment.

Keywords: Cholinesterase, diodon hystrix, heavy metals, pH, substrates, temperature

ARTICLE INFO

Article history:
Received: 10 February 2020
Accepted: 13 November 2020
Published: 31 December 2020

DOI: https://doi.org/10.47836/pjst.28.S2.09

E-mail addresses:
ryeennordin@yahoo.com (Noreen Nordin)
ronronaldo96@gmail.com (Ronaldo Ron Cletus)
khalizan@ums.edu.my (Mohd Khalizan Sabullah)
asyaaishah@yahoo.com (Siti Aishah Muhammad Khalidi)
rahmathabdulla@ums.edu.my (Rahmath Abdulla)
aqlima@upm.edu.my (Siti Aqlima Ahmad)
* Corresponding author

ISSN: 0128-7680
e-ISSN: 2231-8526

© Universiti Putra Malaysia Press

INTRODUCTION

Water covers around 71% of the Earth surface. Water is being utilised by all life forms in various industries including food manufacturing and leisure industries. Yet, the accessibility of excellent water sources is gradually worsened as it is becoming polluted over time (Ahmad et al., 2016a; Gonzalez et al., 2009). The incorporation of noxious wastes such as heavy metals and pesticides into the ecosystem, deriving from multiple agrarian and industrial activities can produce alarming effects (Fatima et al., 2014; Sabullah et al., 2014).

The heavy metals are naturally prevailed elements and no less fivefold larger relative to water molecules. Their toxicity corresponds to exposure level, types of chemical and dosage. Mercury, lead, arsenic and cadmium are among the pre-eminent important materials that could affect the community health (Gupta et al., 2015). Based on the United States Environmental Protection Agency (USEPA), toxicity of heavy metals is discerned as carcinogenic to humans.

A series of observations is implemented as precautionary steps in controlling and reducing contamination level (Wang et al., 2018). The presence of toxicants may cause negative health effects and death. Hence, the preliminary evaluation of water quality is crucial for utilisation in everyday life. Equipped with contemporary automation such as High-Performance Liquid Chromatography (HPLC) and Inductively Coupled Plasma (ICP) in quantifying toxicants level, these inventions are costly, time-consuming and require expertise for handling (Sabullah et al., 2015). Therefore, alternatively, biosensor using enzyme can be used as a preliminary screening to detect contaminants level semi-quantitatively.

Cholinesterase (ChE) is an esterase responsible for lyses of choline esters, most of which act as neurotransmitters in the nervous system. ChE involves in hydrolysing acetylcholine (Ach) into its constituents, acetic acid and choline (Ch) (Čolović et al., 2013). Certain compounds such as carbamates and organophosphates possess high affinity in inhibiting ChE activity (Fukuto, 1990; Johnson & Moore, 2012). Other than that, the metal ions are competent in binding at either ChE active or allosteric sites, impeding its activity.

The inhibition of ChE activity permits the detection of toxicants. From the observation, this scenario can be exploited in detecting metal ions at varying concentrations. Moreover, the process can be minimised as no involvement of the experts is needed. The screening time could also be reduced in which only samples showing enzymatic inhibition are selected for the secondary screening. Thus, numerous researchers are opting in addressing future biosensor advancement in order to satisfy the needs of the emergent world despite many issues arisen in the development of biosensor.

The porcupine fish, *Diodon hystrix* which holds hundred spines on its body is selected in this project. *D. hystrix* exhibits a distinct defence mechanism when it senses athreat, this fish will inflate its body by taking water inside and deflating when it is no longer threatened.

This fish' through its skin can produce toxic or poisonous substances. It is interesting as *D. hystrix* uses many ChE enzymes to properly function for its unique expertise. The objective of the present project was to extract and partially purify the ChE enzyme from the liver tissue of *D. hystrix*. Then, the substrate specificity, optimum temperature and pH of purified ChE were determined and the inhibitor effects on the ChE enzymatic activity were assessed.

MATERIALS AND METHODS

Materials

Five adult porcupine fish, *Diodon hystrix* sized 30-33.5 cm and weighing 800-1000g were obtained from the local Sabah wet market at Kota Kinabalu, Sabah.

Sample Preparation

The liver of *Diodon hystrix* was dissected out and weighed immediately. Using mortar and pestle for extraction, liver tissue was squeezed and subsequently transferred into a beaker containing sodium phosphate buffer (0.1 M, pH 7) in a ratio of 1:4 (w/v) in cold condition. The homogenisation was performed using Ultra-Turrax T-25 homogeniser in which 500 µL homogenate was stored at -20°C for enzyme and protein assay. The centrifugation of homogenate was taken place at 10,000 $\times g$ for 10 minutes at 4°C to eliminate the presence of cell debris. The supernatant was collected and stored at -20°C for further purification.

Ion Exchange Chromatography Purification

The purification of ChE was performed using diethylaminoethanol (DEAE) matrix linked to Sepharose (Peterson & Sober, 1956). A syringe (0.9 cm diameter, 6 cm height) was packed with matrix and let to settle until 3 cm bed height was obtained. The flow rate was calibrated at 0.2 mL/min. The column was washed with 5 batch volumes of washing buffer (25 mM sodium phosphate buffer, pH 7.5) and then eluted with eluting buffer (25 mM sodium phosphate buffer, pH 7.5 at various concentrations of 0.2 M, 0.4 M, 0.6 M, 0.8 M and 1.0 M NaCl). The fractions were collected with a volume of 1 mL from washing to eluting stages. The column then washed with five batch volumes of washing buffer and stored in 20% ethanol at 4°C.

Cholinesterase Enzyme and Protein Assay

The enzyme activity of ChE was assayed using modified Ellman method (Ellman et al., 1961). The reaction mixture was prepared containing 200 µL of 0.1 M sodium phosphate buffer, pH 7.5, 20 µL of 0.067 mM 5.5'-dithiobis-2-nitrobenzoic acid (DTNB) and 10 µL of ChE sample. The mixture was loaded into 96 microplates well. The mixture was incubated

for 15 minutes at room temperature before the addition of 20 µL acetylthiocholine iodide (ATC) into the mixture. It was then incubated for additional 10 minutes before absorbance reading was recorded at 405 nm using multimode detector. The ChE sample was substituted with 0.1 M sodium phosphate buffer, pH 7.5 for the control test. The production of yellow colour signified ChE activity with extinction coefficient of 0.0136 $\mu M^{-1}cm^{-1}$. A unit of activity is defined as amount of substrate (µmole) hydrolysed by AChE per minute (U) with 0.0136 $\mu M^{-1}cm^{-1}$ extinction coefficient.

The protein assay was performed using Bradford method (Bradford, 1976). The determination of protein content was quantified using bovine serum albumin as a standard. The reaction mixture containing 200 µL Bradford reagent and 20 µL ChE sample was loaded into the well and absorbance was recorded at 595 nm after 10 minutes incubation at room temperature.

Optimal pH, Temperature and Substrate Specificity

The determination of optimum pH was carried out using an overlapping buffer system; 0.1 M acetic acid (pH ranged 3.0 to 5.5), sodium phosphate (pH ranged 6.0 to 8.0) and Tris-HCl buffers (pH ranged 7.0 to 9.0). The optimal temperature was determined by incubation at 6 different temperature ranged from 15°C to 45°C, followed by addition of substrate.

The substrate specificity test was performed using three substrates, acetylthiocholine iodide (ATC), butyrylthiocholine iodide (BTC) and propionylthiocholine iodide (PTC). The assay was performed separately for each substrate with concentration from 0 mM, 0.1 mM, 0.5 mM, 1.0 mM, 1,5 mM, 2.0 mM and 2.5 mM. The determination of preferred substrate was calculated using Michaelis-Menten kinetics (maximal velocity, V_{max} and biomolecular constant, K_m) using GraphPad PRISM version 5 software.

Metal Ions Inhibition Study

The eight types of heavy metals were used which were copper (Cu^{2+}), silver (Ag^{2+}), cadmium (Cd^{2+}), arsenic (As^{5+}), chromium (Cr^{5+}), mercury (Hg^{2+}), lead (Pb^{2+}) and zinc (Zn^{2+}) at concentration of 5 mg/L . The assay was prepared containing 150 µL 0.1 M Tris-HCl buffer, pH 9, 50 µL 5 mg/L metal ions, 20 µL 0.067 mM DTNB and 10 µL ChE enzyme. The reaction mixture was loaded into the well and incubated for 15 minutes at room temperature. BTC with a volume of 20 µL was added into the reaction mixture and incubated for 10 minutes at room temperature. The absorbance was recorded at 405 nm and the control test was conducted by replacing heavy metals with distilled water.

Statistical Analysis

All data obtained were in the form of means ± standard deviation (SE) and analysed using GraphP ad Prism version 5.0. The one-way analysis of variance (ANOVA) with post hoc

analysis by Tukey's test was employed to calculate the comparison between two or more groups of data.

RESULTS AND DISCUSSION

Purification Profile

The purification of ChE from *Diodon hystrix* was successfully performed using DEAE-Sepharose matrix with total of 26 fractions. The highest ChE activity was in fraction of 19 to 26. The fractions 1 to 16 showed low ChE activity indicated no overloading of enzyme inside the column with fraction 27 as a control. Figure 1 shows ChE from liver tissue of *D. hystrix* was purified at 3.65-fold with 45.3% recovery. The low recovery may be due to ligand leakage, absorption of non-specific protein and interaction on the surfaces such as unsuitable temperature and pH (Efremova et al., 2001). Besides, low total ChE recovery may be due to the existence of thermal energy in the system.

The partial purification procedure was summarised in Table 1. The fold was denoted as specific activity after fractionation divides with crude homogenate and applied to estimate

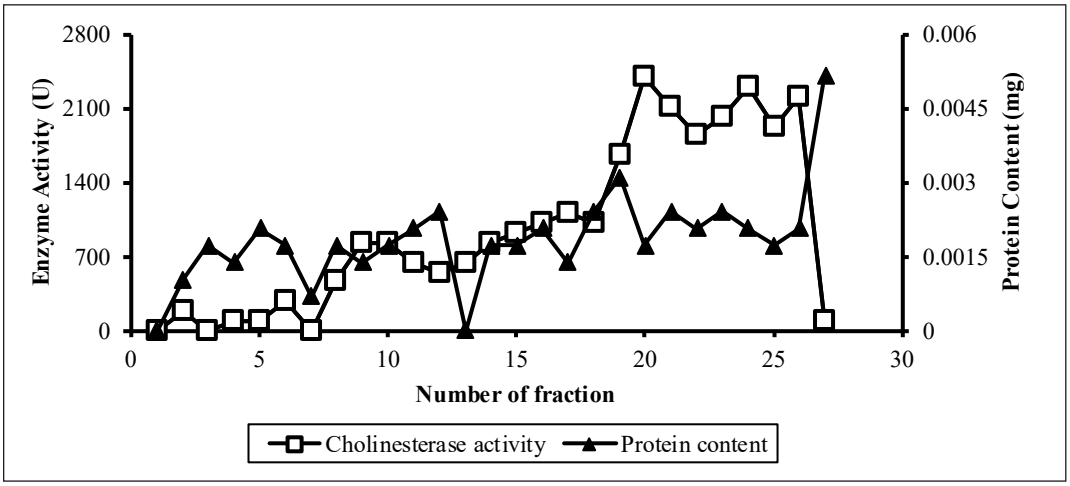

Figure 1. The purification profile of ChE from liver extract of *D. hystrix* using DEAE matrix

Table 1
The comparison of extraction and purification methods of D. hystrix *ChE, in which total ChE activity was expressed in U for each purification step*

	Total recovery		Specific activity (U/mg)	Purification folds (x)	Yield (%)
	Total protein (mg)	Total ChE activity (U)			
Crude homogenate	8.76	7659.375	871.91	1	100
Supernatant	3.97	5269.669	1326.70	1.52	68.8
Purified	0.75	2389.71	3186.28	3.65	45.34

the times of enzyme has purified. Meanwhile, yield was determined using the homogenate as a reference point with 100 % retained enzymatic activity during purification process. From Table 1, it can be noted that the decrement of the number of protein and ChE activity through each step. The removal of unwanted protein such as insoluble fats and inorganic during the elution stage has increased the specific activity of the desired protein.

The low yield percentage indicated the denaturation of purified enzyme during purification process. The partially purified enzyme may denature due to inappropriate surrounding temperature and pH used along the process. Temperature can cause the enzyme to be more active and produce high kinetic energy to facilitate more collision which can alter the structure of enzyme. For pH, the enzyme reacts with hydrogen ion that binds to the active site, hence changing the shape of the enzyme (Efremova et al., 2001; Robinson, 2015).

Substrate Specificity

The cholinesterase (ChE) works in hydrolysis of the predominant choline ester, acetylcholine, Ach. However, Ach was not being utilised as a substrate in this study as the liver could contain acetylcholinesterase (AChE), butyrylcholinesterase (BuChE) and propionylcholinesterase (PuChE) (Askar et al., 2011; Garcia-Aylion et al., 2012). Lockridge (2015) stated that BuChE and PuChE were abundant in livers but differed in their functions.

As can be seen in Figure 2, the prompt increase on the steepness of the BTC line was noted, indicating the sensitivity of the purified enzyme towards BTC as compared to the other substrates. However, PTC showed high enzymatic activity indicating the affinity of both synthetic substrates towards the purified ChE enzyme. To double confirm, the kinetic parameters of purified enzyme on substrates were determined using GraphPad Prism software.

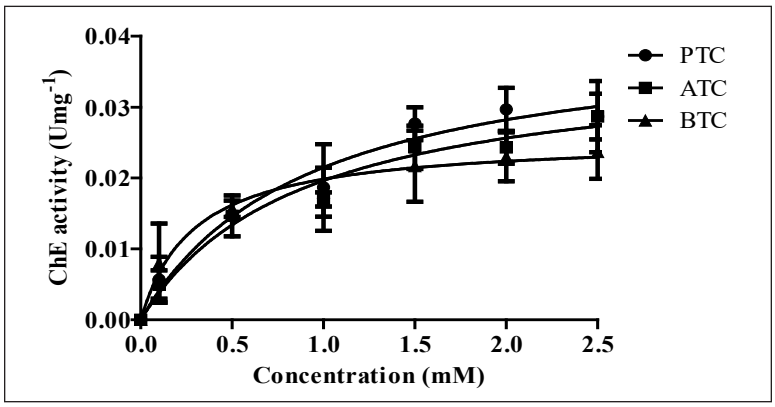

Figure 2. Michaelis-Menten plot of *D. hystrix* ChE incubated in three different synthetic substrates; Acetylthiocholine iodide (ATC), butyrylthiocholine iodide (BTC) and propionylthiocholine iodide (PTC) at concentration of 0 to 2.5 M

Based on Table 2, the value of K_m for BTC, 0.2909 mM was lower than ATC and PTC. The highest V_{max} value was noted by PTC which was 3355.56 Umg^{-1}, followed by ATC (3054.22 Umg^{-1}) and BTC (2092.44 Umg^{-1}). The data obtained was in line with Figure 2. The preferable synthetic substrate of the enzyme was determined based on the catalytic efficiency (V_{max}/K_m). The BTC was demonstrated as the preferable synthetic substrate with the highest ratio of 7193 U mg^{-1} mM^{-1} as compared to the other two substrates. The result obtained was in line with the previous studies conducted using BTC as a specific substrate for the purified ChE from liver tissue of *Puntius javanicus, Anabas testudineus* and *Clarias gariepinus* (Ahmad et al., 2016b; Padrillah et al., 2017; Sabullah et al., 2014).

Table 2
The comparison of K_m and V_{max} of synthetic substrates; acetylthiocholine iodide (ATC), butyrylthiocholine iodide (BTC) and propionylthiocholine iodide (PTC) using GraphPad Prism software

	Mean point (95 % confidence intervals)		
	ATC	**BTC**	**PTC**
V_{max} (U/mg)	3054.22	2092.44	3355.56
K_m (mM)	1.030	0.2909	0.9118
Catalytic efficiencies (V_{max}/ K_m)	2965.26	7193	3680.15

pH Profile

The pH profile of the purified enzyme was assessed using three buffer types; acetic acid, sodium phosphate and Tris-HCl buffer. An overlapping buffer system was utilized to cancel the effects of other buffers on the enzymatic activity.

Figure 3 presents the highest pH condition of ChE activity was at pH 9 (the highest studied) in 0.1 M Tris-HCl buffer. The pH can alter the hydrogen and ionic bonding of

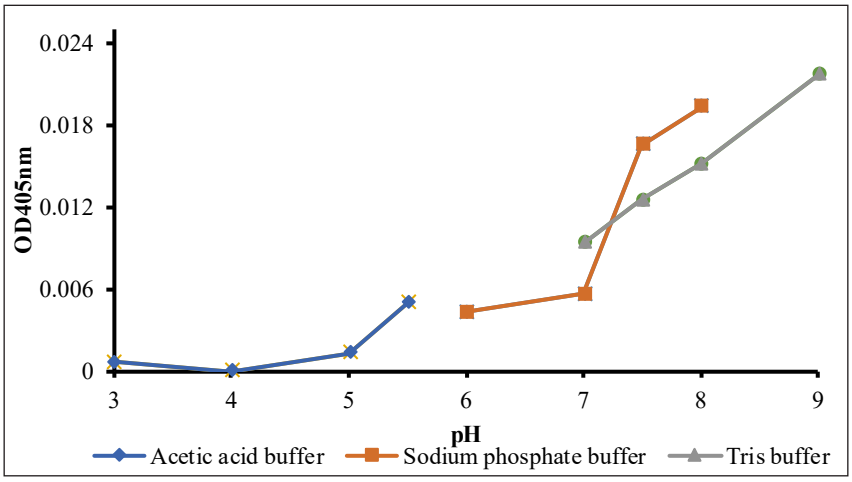

Figure 3. Optimization of pH for *D.hystrix* ChE activity. Data presented in absorbance value at wavelength of 405 nm (Final reading – initial reading)

enzyme and stop the enzyme-substrate complex formation (Reece et al., 2011). At low pH, the presence of excessive hydrogen ion leads to protonation of the imidazole group of histidine at catalytic triad of enzyme, and thus resulting in the loss of catalytic properties of enzyme (Masson et al., 2002; Masson & Lockridge, 2010). At high pH, the alteration of charge of substrate binds to the enzyme causes no enzyme-substrate complex formation. The previous studies on the ChE activity of *Lates calcarifer, Clarias gariepinus* and *Monopterus albus* were also conducted using Tris-HCl buffer system which signified that ChE enzyme could work efficiently in the alkaline environment (Fadzil et al., 2018; Hayat et al., 2015, 2017; Khalidi et al., 2019; Sabullah et al., 2019).

Temperature Profile

The optimisation of the purified enzyme was conducted in different incubation temperatures as shown in Figure 4. The bell-shaped curve showed the optimum temperature of *D. hystrix* ChE at the range of 25°C to 30°C. At optimal temperature, more enzyme-substrate complexes are formed which lead to an elevated number of products produces. Basically, the activity of the purified ChE was retarded at the temperature lower than 25°C, as it did not have sufficient kinetic energy to facilitate the number of effective collisions between enzyme and substrate per unit time. High temperature may denature the enzyme and inactivates the active site. At extreme temperature, the thermal energy can cause more vibration until high enough to alter the bonds supporting the three-dimensions (3D) configuration of the enzyme and lowered the enzymatic activity (Bernabei et al., 1993; Fairbrother et al., 1991; Reece et al., 2011).

Fish was categorised as cold-blooded organisms, hence warmer temperature, beyond 30°C may denature or inactivate ChE (Sabullah et al., 2014). Almost all published studies on bioassay using liver ChE source from various animal types were carried out at temperature

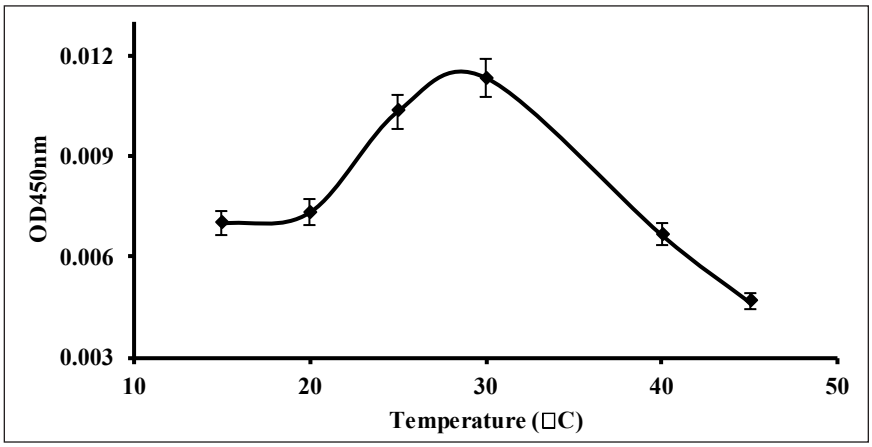

Figure 4. Optimization of temperature profile for *D. hystrix* ChE activity. Data presented in absorbance value at wavelength of 405 nm (Final reading – initial reading)

range of 25 to 30°C (Askar et al., 2011; Sabullah et al., 2014; Sanchez-Hernandez et al., 2011).

Inhibition Study

The effectiveness of bioassay for purified ChE was determined by inhibition study of toxicants. The purified ChE was exposed with incubation of eight metal ions with final concentration of 5 mg/L. From Figure 5, all metal ions were significantly inhibited the purified ChE by lowering the activity to 63.42, 92.68, 80.56, 70.73, 75.37, 2.44, 85.36 and 87.05 % for $Ag^{(2+)}$, $As^{(5+)}$, $Cd^{(2+)}$, $Cr^{(6+)}$, $Cu^{(2+)}$, $Hg^{(2+)}$, $Pb^{(2+)}$ an $Zn^{(2+)}$, respectively. Mercury (Hg^{2+}) showed the highest inhibition of ChE activity, followed by other four metal ions, but the inhibition did not exceed 50% activity. The toxicity level was assigned in decreasing order from $Hg^{2+} > Ag^{2+} > Cr^{6+} > Cu^{2+} > Cd^{2+} > Pb^{2+} \geq Zn^{2+} > As^{5+}$.

Heavy metals involved in the formation of enzyme-substrate complex, although they can bind to enzyme active or allosteric sites and disrupt the formation. The binding of metal ions initiated reaction with functional hydroxyl and sulfhydryl groups, which eventually changes the shape and stops the substrates binding (Frasco et al., 2007; Glusker et al., 1999). The amino acids produce protein attraction on the presence of metal ions. The cation pull from imidazole group of histidine relates to attraction of free heavy metals and nitrogenous substrates (Dvir et al., 2010; Ma & Dougherty, 1997; Sussman & Silman, 1992).

The researches done by Frasco et al. (2007) and Wang et al. (2009) stated that among all metal ions, mercury and copper were the potent inhibitors for ChE, which coincided

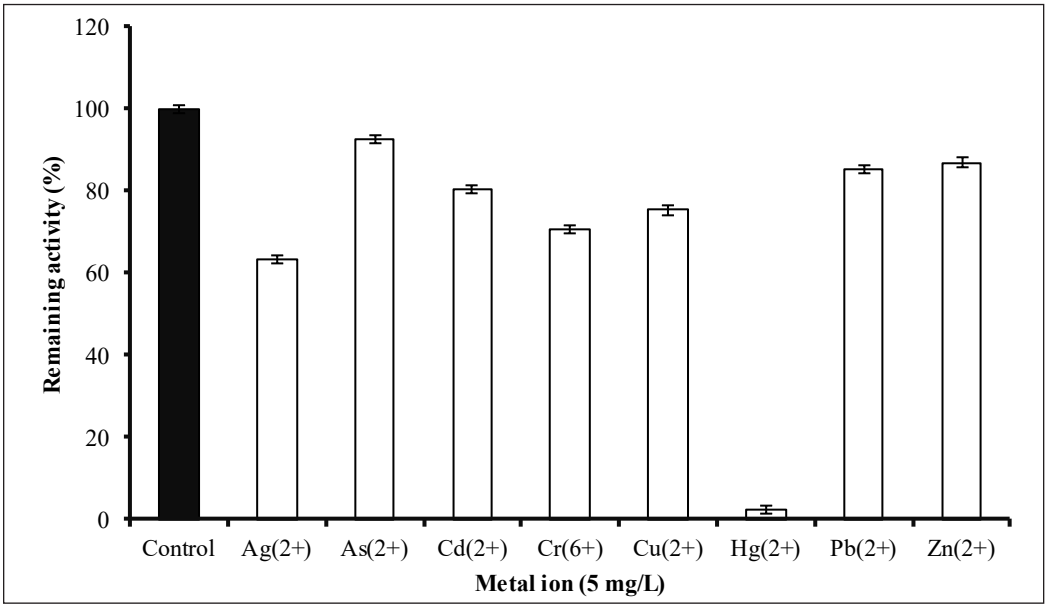

Figure 5. The percentage remaining activity of *D. hystrix* ChE after incubated in 5 mg/L of eight heavy metals. The alphabet denotes as statistically significant differences between each metal ion ($p<0.05$)

with the finding in this study. Ariöz & Wittung-Stafshede (2018) specified that the classic structural of transition metals like Cu permitted illustration on the binding potency of metal ions in inhibiting the ChE activity. Numerous studies conducted using fishes, for example *Lates calcarifer, Puntius javanicus, Anabas testudineus* and *Clarias gariepinus* displayed high Hg inhibition towards ChE activity (Ahmad et al., 2016b; Hayat et al., 2017; Padrillah et al., 2017; Sabullah et al., 2014). Study by Aidil et al. (2013) demonstrated the sensitivity of AChE of *Pangasius hypophthalmus* towards metal ions exposure such as Ag, Hg, Cd, Cu, Zn, Cr and Pb. The inhibition of these metal ions displayed the exponential decay type curve and its IC_{50} values were equal and lower in comparison to the existing biosensor assays like papain, immobilised urease, bromelain, Microtox™, *Daphnia magna* and rainbow trout. This study provides insight on the capability of ChE of *D. hystrix* in the detection of contaminants.

CONCLUSION

The cholinesterase (ChE) enzyme from liver tissue of *D. hystrix* was successfully purified using ion-exchange chromatography using DEAE-Sepharose as the matrix. The enzymatic parameters of ChE were determined, in which the enzyme worked at optimal rate in condition of pH 9, 0.1 M Tris-HCl buffer at temperature range of 25°C to 30°C, alongside with the presence of BTC as the synthetic substrate. The inhibition study concluded that *D. hystrix C*hE was sensitive towards a few metal ions, especially towards Hg^{2+}. Therefore, ChE of *D. hystrix* provides a promising alternative source for biorceptor to substitute the current ChE source in the market. It is recommended to explore the potential of purified *D. hystrix* ChE in detecting other pollutants like detergents, drug, dyes or pesticides.

ACKNOWLEDGEMENTS

The project was supported by Universiti Malaysia Sabah (UMS) under UMSGreat Grant No. GUG-0376-1/2019.

REFERENCES

Ahmad, S. A., Sabullah, M. K., Shamaan, N. A., Shukor, M. Y., Jirangon, H., Khalid, A. & Syed, M. A. (2016a). Evaluation of acetylcholinesterase source from fish, for detection of carbamate. *Journal of Environmental Biology, 37*(4), 479–484.

Ahmad, S. A., Wong, Y. F., Shukor, M. Y., Sabullah, M. K., Yasid, N. A., Hayat, N. M., … & Syed, M. A. (2016b). An alternative bioassay using *Anabas testudineus* (Climbing perch) cholinesterase for metal ions detection. *International Food Research Journal, 23*(4), 1446-1452.

Aidil, M. S., Sabullah, M. K., Halmi, M. I. E., Sulaiman, R., Shukor, M. S., Shukor, M. Y., ... & Syahir, A. (2013). Assay for heavy metals using an inhibitive assay based on the acetylcholinesterase from *Pangasius hypophthalmus* (Sauvage, 1878). *Fresenius Environmental Bulletin, 22*(12)*,* 3572-3576.

Ariöz, C. & Wittung-Stafshede, P. (2018). Folding of copper proteins: Role of the metal?. *Quarterly Reviews of Biophysics, 51,* 1-39. doi:10.1017/s0033583518000021

Askar, K. A., Kudi, A. C. & Moody, A. J. (2011). Comparative analysis of cholinesterase activities in food animals using modified Ellman and Michel assays. *Canadian Journal of Veterinary Research*, *75*(4), 261–270.

Bernabei, M., Chiavarini, S., Cremisini, C. & Palleschi, G. (1993). Anticholinesterase activity measurement by a choline biosensor: Application in water analysis. *Biosensors and Bioelectronics*, *8*(5), 265–271. doi:10.1016/0956-5663(93)80014-g

Bradford, M. M. (1976). Rapid and sensitive method for the quantitation of microgram quantities of protein utilizing the principle of protein-dye binding. *Analytical Biochemistry, 72*(1-2)*,* 248-254. doi:10.1016/0003-2697(76)90527-3

Čolović, M. B., Krstić, D. Z., Lazarević-Pašti, T. D., Bondžić, A. M. & Vasić, V. M. (2013). Acetylcholinesterase inhibitors: Pharmacology and toxicology. *Current Neuropharmacol, 11*(3), 315-335. doi:10.2174/1570159X11311030006

Dvir, H., Silman, I., Harel, M., Rosenberry, T. L. & Sussman, J. L. (2010). Acetylcholinesterase: From 3D structure to function. *Chemico-Biological Interactions, 187*(1-3), 10-22. doi:10.1016/j.cbi.2010.01.042

Efremova, N. V., Sheth, S. R. & Leckband, D. E. (2001). Protein-induced changes in poly (ethylene glycol) brushes: Molecular weight and temperature dependence. *Langmuir, 17*(24), 7628-7636. doi:10.1021/la010405c

Ellman, G. L., Courtney, K. D., Andres, J. V. & Featherstone, R. M. (1961). A new and rapid colorimetric determination of acetylcholinesterase activity. *Biochemical Pharmacology, 7*(2), 88- 95. doi:10.1016/0006-2952(61)90145-9

Fadzil, N. I., Ahmad, S. A., Yasid, N. A., Sabullah, M. K., Daud, H. M., Khalid, A., … & Shukor, M. Y. (2017). Characterisation of cholinesterase and histopathological features of brain of *Clarias gariepinus* following exposure to cadmium. *Journal of Environmental Biology, 40*(2), 133-142. doi: 10.22438/jeb/40/2/MRN-815

Fairbrother, A., Marden, B. T., Bennett, J. K. & Hopper, M. J. (1991). Cholinesterase-inhibiting insecticides: Their impact on wildlife and the environment. In P. Mineau (Ed.), *Methods used in determination of cholinesterase activity* (pp. 35-710). New York: Elsevier. doi:10.1016/0300-483X(92)90129-3

Fatima, M., Usmani, N., Mobarak, Hossain, M., Siddiqui, M. F., Zafeer, M. F., Firdaus, F. & Ahmad, S. (2014). Assessment of genotoxic induction and deterioration of fish quality I commercial species due to heavy-metal exposure in an urban reservoir. *Archives of Environmental Contamination and Toxicology, 67*(2), 203-213. doi:10.1007/s00244-014-0024-8

Frasco, M. F. Colletier, J. P. & Weik, M. (2007). Mechanisms of cholinesterase inhibition by inorganic mercury. *The FEBS Journal*, *274*(7), 1849–1861. doi:10.1111/j.1742-4658.2007.05732.x

Fukuto, T. R. (1990). Mechanism of action of organophosphorus and carbamate insecticides. *Environmental Health Perspectives, 87,* 245-254. doi: 10.1289/ehp.9087245

García-Ayllón, M. S., Small, D. H., Avila, J. & Sáezvalero, J. (2011). Revisiting the role of acetylcholinesterase in Alzheimer's disease: Cross-talk with P-tau and B-amyloid. *Frontiers in Molecular Neuroscience, 4*(22), 1-9. doi: 10.3389/fnmol.2011.00022

Glusker, J. P., Katz, A. K. & Bock, C. W. (1999). Metal ions in biological systems. *The Rigaku Journal, 16*(2), 381-412. doi:10.1201/9781482289893

Gonzalez, C., Greenwood, R. & Quevauviller, P. (2009). *Rapid chemical and biological techniques for water monitoring*. Chichester, England: Wiley. doi:10.1002/9780470745427

Gupta, V. K., Singh, S., Agrawal, A. Siddiqi, N. J. & Sharma, B. (2015). Phytochemicals mediated remediation of neurotoxicity induced by heavy metals. *Biochemistry Research International, 2015,* 1-9. doi:10.1155/2015/534769

Hayat, N. M., Ahmad, S. A., Shamaan, N. A., Sabullah, M. K., Shukor, M. Y., Syed, M. A., … & Dahalan, F. A. (2017). Characterisation of cholinesterase from kidney tissue of Asian Seabass (*Lates calcarifer*) and its inhibition in presence of metal ions. *Journal of Environmental Biology, 38*(3), 383-388. doi:10.22438/jeb/38/3/MRN-987

Hayat, N. M., Shamaan, N. A., Shukor, M. Y., Sabullah, M. K., Syed, M. A., Khalid, A., … & Ahmad, S. A. (2015). Cholinesterase-based biosensor using *Lates calcarifer* (Asian seabrass) brain for detection of heavy metals. *Journal of Chemical and Pharmaceutical Sciences, 8*(2), 376-381.

Johnson, G. & Moore, S. W. (2012). The carboxylesterase/cholinesterase gene family in invertebrate deuterostomes. *Comparative Biochemistry and Physiology Part D: Genomics and Proteomics*, *7*(2), 83–93. doi:10.1016/j.cbd.2011.11.003

Khalidi, M. S. A., Sabullah, M. K., Sani, S. A., Ahmad, S. A., Shukor, M. Y., Jaafar, I. N. M. & Gunasekaran, B. (2019). Acetylcholinesterase from the brain of *Monopterus albus* as detection of metal ions. *Journal of Physics: Conference Series, 1358,* 1-11. doi:10.1088/1742-6596/1358/1/012028

Lockridge, O. (2015). Review of human butyrylcholinesterase structure, function, genetic variants, history of use in the clinic, and potential therapeutic uses. *Pharmacology and Therapeutics, 148,* 34-46. doi:10.1016/j.pharmthera.2014.11.011

Ma, J. C., & Dougherty, D. A. (1997). The cation− π interaction. *Chemical Reviews, 97*(5), 1303-1324. doi:10.1021/cr9603744

Masson, P. & Lockridge, O. (2010). Butyrylcholinesterase for protection from organophosphorus poisons; catalytic complexities and hysteretic behaviours. *Archives of Biochemistry and Biophysics, 494*(2), 107-120. doi:10.1016/j.abb.2009.12.005

Masson, P., Schopfer, L. M., Bartels, C. F., Froment, M. T., Ribes, F., Nachon, F., & Lockridge, O. (2002). Substrate activation in acetylcholinesterase induced by low pH or mutation in the π-cation subsite. *Biochimica et Biophysica Acta (BBA)-Protein Structure and Molecular Enzymology, 1594(*2), 313-324. doi:10.1016/s0167-4838(01)00323-5

Padrillah, S. N., Ahmad, S. A., Yasid, N. A., Sabullah, M. K., Daud, H. M., Khalid, A. & Shukor, M. Y. (2017). Toxic effects of copper on liver and cholinesterase of *Clarias gariepinus. Environmental Science and Pollution Research*, *24*(28), 22510–22523. doi:10.1007/s11356-017-9923-3

Peterson, E. A. & Sober, H. A. (1956). Chromatography of Proteins. I. Cellulose ion exchange adsorbents. *Journal of the American Chemical Society, 78*(4)*,* 751-755. doi:10.1021/ja01585a016

Reece, J. B., Urry, L. A., Cain, M. L., Wasserman, S. A., Minorsky, P. V. & Jackson, R. B. (2011). *Campbell biology ninth edition (Book 9)*. California, USA: Benjamin Cummings.

Robinson, P. K. (2015). Enzymes: Principles and biotechnological applications. *Essays in Biochemistry, 59*(November), 1-41. doi:10.1042/bse0590001

Sabullah, M. K., Shukor, M. Y., Shamaan, N. A., Khalid, A., Gansau, A. J., Sulaiman, M. R., … & Ahmad, S. A. (2015). Purification and anticholinesterase sensitivity of cholinesterase extracted from liver tissue of *Puntius javanicus*. *International Journal of Agriculture & Biology, 17*(5)*,* 1025-1030. doi:10.17957/ijab/15.0012

Sabullah, M. K., Khalidi, M. S. A., Wahid, A. D. N., Sani, A. S., Abdulla, R., Faik, M. A. A., … & Shukor, M. Y. (2019). Assessment of *Monopterus albus* liver as a source of cholinesterase for the detection of heavy metals. *Journal of Physics: Conference Series, 1358,* 1-9. doi:10.1088/1742-6596/1358/1/012029

Sabullah, M. K., Sulaiman, M. R., Shukor, M. Y. A., Syed, M. A., Shamaan, N. A., Khalid, A. & Ahmad, S. A. (2014). The assessment of cholinesterase from the liver of *Puntius javanicus* as detection of metal ions. *The Scientific World Journal*, *2014,* 1-9. doi:10.1155/2014/571094

Sussman, J. L. & Silman, I. (1992) Acetylcholinesterase: Structure and use as a model for specific cation-protein interaction. *Current Opinion in Structural Biology, 2*(5), 721-729. doi:10.1016/0959-440x(92)90207-n

Wang, L., Zhang, F. Y., Pilot, E., Yu, J., Nie, C. J., Holdaway, J., … & Krafft, T. (2018). Taking action on air pollution control in the Beijing-Tianjin-Hebei (BTH) region: Progress, challenges and opportunities. *International Journal of Environmental Research and Public Health, 15*(2), 2-27. doi:10.3390/ijerph15020306

Wang, Z., Zhao, J., Li, F., Gao, D. & Xing, B. (2009). Adsorption and inhibition of acetylcholinesterase by different nanoparticles. *Chemosphere, 77*(1), 66-73. doi:10.1016/j.chemosphere.2009.05.015

Pertanika J. Sci. & Technol. 28 (S2): 121 - 134 (2020)

SCIENCE & TECHNOLOGY

Journal homepage: http://www.pertanika.upm.edu.my/

Isolation and Characterisation of Thermophilic *Bacillus licheniformis* SUNGC2 as Producer of *α*-Amylase from Malaysian Hot Spring

Marwan Jawad Msarah[1,2], Ayesha Firdose[1], Izyanti Ibrahim[1] and Wan Syaidatul Aqma[1]*

[1]Department of Biological Sciences & Biotechnology, Faculty of Science and Technology, Universiti Kebangsaan Malaysia, 43600, Bangi, Selangor
[2]Department of Radiology Technologies, Al-Hadi University, 10022, Baghdad, Iraq

ABSTRACT

Screening of new source of novel and industrially useful enzymes is a key research pursuit in enzyme biotechnology. The study aims to report the characteristics of novel thermophilic microorganisms isolated from Sungai Klah (SK) Hot Spring, Perak, Malaysia, that can produce α-amylase. The morphological and biochemical properties were examined for SUNGC2 sample. The isolate was further screened for amylase, followed by 16S rRNA and analytical profile index (API) test. This isolate was further subjected to pH optimisation for *α*-amylase production. It was found that SUNGC2 was an *α*-amylase producer and was identified as *Bacillus licheniformis* SUNGC2 with NCBI accession numbers MH062901. The enzyme was found to exhibit an optimum temperature of 50°C and a pH of 7.0. The relative activity of the enzyme was obtained based on the improvement of the culture conditions. The highest amount of amylase production was 24.65 U/mL at pH 7.0, consecutively the growth was also highest at pH 7.0 with a 9.45-fold increase in specific activity by ammonium phosphate precipitation of 80% (w/v). The results showed that the bacteria isolated from the hot spring are a significant source of thermophilic enzymes that are highly promising in biotechnology.

Keywords: Alpha amylase, *bacillus licheniformis*, thermophilic, hot spring

ARTICLE INFO

Article history:
Received: 10 February 2020
Accepted: 13 November 2020
Published: 31 December 2020

DOI: https://doi.org/10.47836/pjst.28.S2.10

E-mail addresses:
marwan_masar21@yahoo.com (Marwan Jawad Msarah)
ayeshafirdose27@gmail.com (Ayesha Firdose)
izzy@ukm.edu.my (Izyanti Ibrahim)
syaidatul@ukm.edu.my (Wan Syaidatul Aqma)
* Corresponding author

INTRODUCTION

The thermophilic *Bacillus* can be isolated from different extreme environments including thermal hot-springs, shallow vents and deep sea hydrothermal with optimum growth temperatures range between 45°C

ISSN: 0128-7680
e-ISSN: 2231-8526

© Universiti Putra Malaysia Press

and 70°C (Adiguzel et al., 2009). Thermophilic bacilli enzymes can be produced in enormous quantities employing a comparatively less complicated purifying method that is highly beneficial compared to those from mesophilic or psychrophilic bacteria (Burgess et al., 2010). Currently, the screening for a new source of novel and beneficial enzymes for biotech industries is in great demand. Novel enzymes ought to have the benefit of being stable at high temperatures, wide pH range, different concentrations of salts, solvents and also possess a variety of uses in industrial processes. The advantages of using thermophilic enzymes are well documented as industrial catalysts with the potential revenue reflected on the rapid growth of the enzymes market (Burgess et al., 2010; Van Der Maarel et al., 2002). Generally, the extracellular enzymes are more stable at various ranges of temperature and pH, and easier to be isolated and purified compared to the intracellular enzymes (Teodoro & Martins 2000).

The operation of biotechnological techniques at high thermal levels offers several benefits, and one example is temperature increase has a considerable effect on the solubility and bioavailability of organic compounds (Ameri et al., 2015). Consequently, several thermo-active amylases have been isolated and characterised, such as from *Bacillus* sp. (Ardhi et al., 2020), and *Bacillus licheniformis* ATCC 9945a (Božić et al., 2011). Amylase enzymes (*α*-amylase, β-amylase, and γ-amylase) are essential enzymes in current biotechnology and makeup approximately 30% of the global production of enzymes alternating from the process of converting starch to sugar syrups, to producing cyclo-dextrins specifically for pharmaceutics (Van Der Maarel et al., 2002). *α*-amylases are universally allocated all through animals, flora and microbial kingdoms. The production of amylases is economically viable due to the microbial enzyme's ability to be manipulated to obtain enzymes of desired characteristics (Teodoro & Martins 2000). *α*-Amylases cleave α-1,4-glycosidic bonds of carbohydrates and oligosaccharides. Therefore, they are used for industrial starch liquefaction and saccharification (Chai et al., 2016). The amylase family of enzymes is very important because of its versatility as potential industrial applications and among bacteria, *B. licheniformis, B. subtilis, B. stearothermophilus* and *B. amyloliquefaciens* have been extensively commercialised and applied for the production of the enzymes for different uses (Deljou & Arezi 2016; Vidyalakshmi et al., 2009). Their applications in biotechnology include starch processing, biofuel, food, paper, textile and detergent industries, bioremediation of environmental pollutants and in clinical and medical applications. Industrial production of enzymes requires high productivity and in certain condition, the application of wild-type strains are not suitable for enzyme production (Jujjavarapu & Dhagat 2019). The properties of α-amylases such as thermostability and pH profile should match its application. Therefore, the diversity of the applications creates the need to search for novel *α*- amylases with advanced and enriched properties (Panosyan et al., 2020). The raw starch degrading amylases ideal for use in industry as well as for their attractive production cost-effectiveness (Mohammad et al., 2017).

Hot springs are promising environments for thermophilic microorganisms and in the past few decades, hot springs globally have proven to be significant targets to isolate new thermotolerant or thermophilic microorganisms as a source for the production of thermozymes that offer significant stability (Verma et al., 2014). Malaysia has a significant number of hot springs, especially along the edge of the Banjaran Titiwangsa mountain range (Samsudin et al., 1997). The Sungai Klah (SK) Hot Spring, Perak ranks as the second hottest geothermal spring in the country. It has increased in attractiveness as it is considered a natural biomass degrading bioreactor because of the existence of an underwater vegetation bed (Chan et al., 2015; Lee et al., 2018). Biological studies of the Malaysian hot springs are limited due to the lack of complete information on their microbial communities (Chan et al., 2017). Nonetheless, (SK) Hot Spring has an abundant and varied phylogenetic population of thermophiles and a source with potential to isolate bacteria capable of producing amylase. This is due to its natural environment, high total organic carbon (TOC), plant litter shallow stream and geochemical parameters and a wide range of temperature and pH (Chan et al., 2017; Msarah et al., 2018). Nevertheless, no persistent research has focused on further utilisation of these thermophiles. The current study aims at amylolytic screening, isolation and characterisation of new thermophilic microorganisms isolated from Sungai Klah Hot Spring, that can possess high biotechnological and environmental potential, and as a continuous line of research for thermophilic bacteria acquired from hot springs in Malaysia.

MATERIALS AND METHODS

Isolation, Cultivation and Qualitative Screening of *α*- Amylase Producer Bacteria

The strains used in this study have been isolated from Sungai Klah Hot Spring, Perak, Malaysia. The 23 samples isolated were then serially diluted from 10^{-1} to 10^{-6} with sterile distilled water and spread on nutrient agar (NA) plates. The inoculated plates were incubated at 50°C for three days with morphological observation of the culture. The shape, size, colour, elevation and margin of the colonies were identified and the pure colonies were streaked on a NA containing 1% starch (Starch NA), incubated and observed for 36 hours at 50°C. Single colonies confirm as amylase production by forming clear hydrolysis zones after a 0.5% (w/v) iodine solution was dispensed over the isolates.

Identification, DNA Sequencing and Phylogenetic Analysis

Bacterial isolates were investigated for its physiological, cultural, morphological and biochemical characteristics (Harley & Prescott 2005). Biochemical tests for the identification of thermophilic isolates including the production of indole, catalase, citrate and oxidase, urease test, and nitrate reduction were carried out. Colony grown on NA was used for the determination of colony morphologies. The growth temperature range was confirmed through incubation of the isolate at 30, 40, 50, 60 and 70°C. Bacterial growth

on NaCl (1% to 7% (w/v)) and on blood agar were also observed. Further, isolates were identified using Analytical Profiling Index (API) strip tests according to the manufacturer's instructions for API 50 CHB and API20E strips (bioMérieux, SA, Marcy-l'Etoile, France). Bacterial suspension (100 µL) was inoculated into the strips and incubated in a temperature ranged from 50-55°C for 48 hours. The pattern of the reactions obtained was coded into a numerical profile.

16S rRNA gene sequence analysis was conducted to confirm the identification of bacterial isolates. Amplification of the 16S rRNA gene was carried out by polymerase chain reaction (PCR) with Prime Thermal Cycler (Techne®/Bibby Scientific, UK), using forward primer, 8-27 F, 5'-AGAGTTTGATCCTGGCTCAG-3' and reverse primer, 1492 R, 5'- GGTTACCTTGTTACGACT T-3'.

The bacterial genomic DNA of the isolates was subjected to purification employing the TE boil extraction method which is the modified protocol for bacterial DNA extraction (Li et al., 2003). Bacterial culture was grown in nutrient broth at 50°C for 18 hours. An appropriate number of bacterial cells was transferred to 1.5 mL micro-centrifuge tube and it was centrifuged for 1 min at 11200 x g. The pellet was suspended in 200 µL TE buffer [10 mmol/L Tris-HCl (pH 8.0), 1 mmol/L EDTA], and the mixture was briefly vortexed. The suspension was then put in a boiling water bath at 100°C for 1 min, then freezed at -70°C for 3 min. The next step involved heating in boiling water bath at 100°C for 2 min, freezing at -70°C for 3 min (repeating for two times), then finally subjecting to centrifugation for 5 min at 11200 x g. The supernatant (100 µL) was placed into a sterile tube and kept at -20°C for PCR. PCR was conducted using PROMEGA Go Taq®/USA Green Mix, 2X. PCR protocol was subjected to heating up to the temperature of 94°C for 5 min for the initial DNA denaturation, and then by 30 cycles with the following cycling profile: 94°C for 1 min, 54°C for 1 min, and 1.5 min at 72°C for annealing. A final extension step was conducted following the amplifying reaction for 5 min at a temperature of 72°C. The range of identity for identifying bacteria employing the 16S rRNA gene analysis is ≤ 99% and ≥ 97% to the GenBank database and according to Drancourt et al. (2000) it permits distinguishing the strain at the genus level.

Bacterial Isolate *α*- Amylase Production Medium

Bacterial isolate was investigated for α-amylase production on a medium (g/L): NaCl (0.1), soluble starch (10), magnesium sulphate $MgSO_4.7H_2O$ (1.0), disodium phosphate Na_2HPO_4 (3.0), peptone (2.0) and ferrous sulphate $FeSO_4$ (0.03). Erlenmeyer flask (250 mL) consisted of 1 mL inoculum ($1x10^8$ cells/mL) mixed with 99 mL cultivation medium was incubated in an orbital shaker at 50°C/48 hours and agitated at 100 rpm. Filtration of the medium was done by using Whatman No.1 filter paper every 6 hours intervals. The cell free filtrate was employed for the *α*-amylase assay and the bacterial growth was measured at 600 nm (Kumar & Raja, 2019). The protein level was decided based on the approach

described by Bradford (1976) at 595 nm. The total protein was expressed as mg/mL. All experiments were carried out in triplicates in at least three different occasions.

Amylase Assay

The *α*-amylase activity was carried out by using a modification of the di-nitro-salicylic acid (DNS) technique on the basis of the reducing sugars freed from the soluble starch and were determined by glucose standard curve (Miller, 1959). The standard curve was prepared by dissolving 100 mg of glucose in 100 mL of distilled water and working standard was prepared by diluting 10 mL of stock solution to 100 mL with distilled water. The standard curve was prepared by taking 0, 0.2, 0.4, 0.6, 0.8 and 1 mL of the working standard glucose solution and the final volume was made up to 1 mL by adding distilled water. One mL of glucose oxidase peroxidase reagent was added and the mixture was incubated at 35 ºC for 40 min. The reaction was terminated by the addition of 2 mL of 6N-HCl, and the absorbance was recorded at a wavelength of 540 nm using Spectrophotometer. One mL soluble starch (1% soluble starch (w/v) in sodium citrate buffer (0.05 M/ pH 5.9) was heated in a water bath at 50°C for 10 min. Then, 0.1 mL of crude enzyme was added to the substrate, followed by incubation at 50°C for 10 min through mild shaken. The reaction was halted by adding 2.0 mL of DNS reagent. The reaction mixture was then subjected to heat for 10 min at 100°C, then allowed to cool to 27°C before dilution with distilled water (16.9 mL). Then the mixture measured by using UV-Visible spectrophotometer at 540 nm absorbance and the specific activity was then calculated and and reported in units per millilitre (U/mL). The enzyme acitivity is calculated by measuring umole of product formed (glucose) in 10 minutes assay by 0.1 mL enzyme sample (which will give umole/ min/mL) (Ibrahim et al., 2013).

Optimisation of pH

The optimisation of culture conditions was evaluated with a variation of pH (ranging between 3.0, 7.0 and 9.0). The incubation temperature was set at 50°C, the agitation speeds of 200 rpm, and the inoculum size of 0.5 McFarland to increase amylase production by *B. licheniformis* SUNGC2. The medium was filtered using Whatman No.1 filter paper after 18 hours of cultivation and then the cell free filtrate used for the amylase assay. The mixture's absorbance was verified at 540 nm and bacterial growth was measured at 600 nm absorbance. All experiments were carried out in triplicates for at least three different occasions (Ardh et al., 2020).

RESULTS AND DISCUSSION

Isolation of *α*-Amylase Producing Bacteria

The knowledge about thermophilic bacteria and the enzymes they produce from hot springs in Malaysia is significant and still moving forward in comparison with additional

hot springs located worldwide (Chan et al., 2015, 2017; Msarah et al., 2018, 2020). In this study thermophilic α-amylase producing bacteria were positively isolated from Sungai Klah Hot Spring in Perak, Malaysia. α-Amylase activity was confirmed by the appearance of a clear surrounding (halo) of the colonies after staining with Lugol's iodine (Figure 1b). The qualitative screening of 23 isolates showed that isolate SUNGC2 produced the largest hydrolysis zone and therefore was selected for further optimisation process.

Enzyme production primarily linked to the growth of the microorganisms is called growth associated-enzymes, and according to Niu et al. (2009) and Asoodeh et al. (2010) some starch degrading enzymes such as α-amylases are produced according to this mechanism. The results displayed that enzyme production was related to the growth of the isolate SUNGC2 (0.261 mg/mL) at 18 hours (Figure 2). SUNGC2 showed a decline

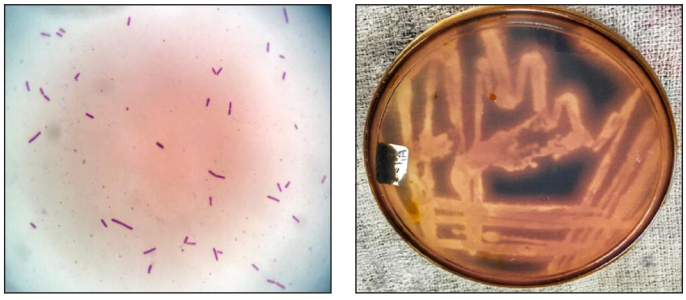

(a) (b)

Figure 1. Microscope (a) and amylase qualitative screening (b) of *B. licheniformis* SUNGC2

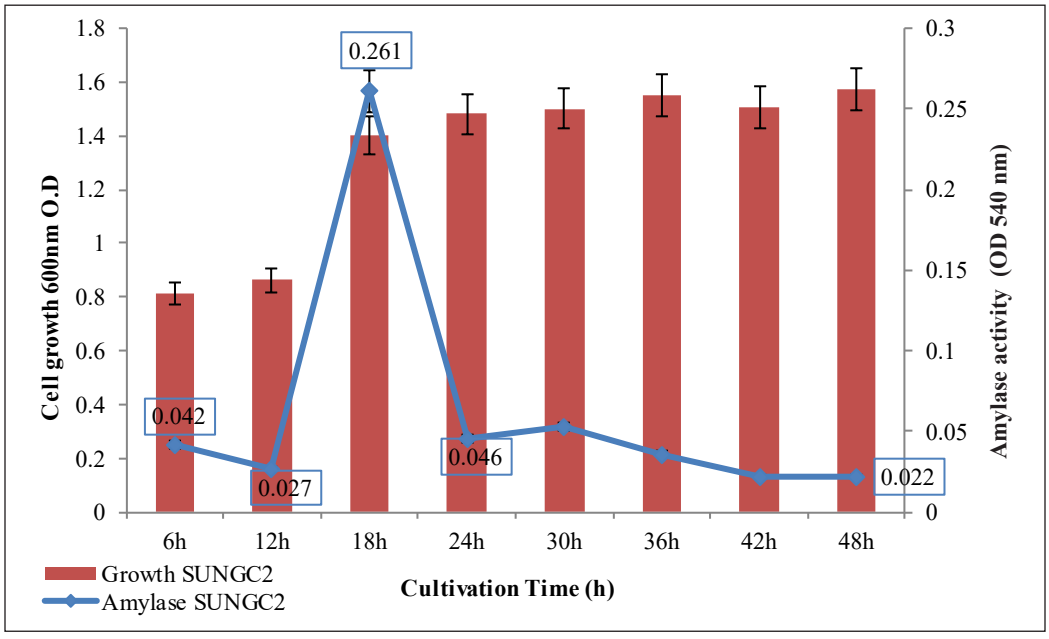

Figure 2. Amylase production and growth profile of *B. licheniformis* SUNGC2

in amylase production after 18 hours until it reached 0.022 mg/mL at 48 hours, while the growth of SUNGC2 was increasing in log phase.

Identification of *α*-Amylase Producer Isolate SUNGC2

SUNGC2 was identified based on its biochemical tests and microscopic characteristics. SUNGC2 was a Gram positive, rod-shaped bacterium, a pale colony in colour, flat elevation with irregular margins and producing distinctive scent. Additionally, the biochemical and cultural characteristics were also observed for further identification (Table 1). SUNGC2 showed positive results for the catalase production, nitrate reduction, citrate tests, grew well in 7% sodium chloride medium and positive beta hemolytic on blood agar. However, urease utilisation and indole tests showed negative results. It was observed that SUNGC2 grew at temperature of 55°C. SUNGC2 was identified as a *Bacillus* sp. based on 16S rRNA identification. The *Bacillus* sp. together with the thermophilic bacilli in general require uncomplicated nutritional requirements; hence, they have no requirement for any particular amino acids for growth and are able grow on enriched media like tryptone soya agar (TSA) or nutrient agar (NA) (Haki & Rakshit 2003). Thermophilic *Bacillus* sp. possess an optimum growth temperature typically ranging from 50 to 70°C but differ among species and strains. They can be readily cultured and sub-cultured in the laboratory and utilised to extract useful compounds (Burgess et al., 2010).

Table 1
Microscopic, morphology and biochemical characteristics of B. licheniformis *SUNGC2*

Characteristics	SUNGC2	Biochemical tests	SUNGC2
Colony	Irregular	Indole production	Negative
Margin	Irregular	Catalase production	Positive
Elevation	Flat	Citrate production	Positive
Surface	Shiny and moist	Oxidase production	Negative
Color	Pale	Urease test	Negative
Odor	Yes	Nitrate reduction test	Positive
Growth	Aerobic and facultative anaerobic growth	Growth at 55°C	Positive
Gram staining	Positive	Hemolysis on the blood agar plate	β-hemolytic
The shape of vegetative cells	Rod-shaped	Growth in 7% sodium chloride	Positive

Gene analysis was achieved by using 16S rRNA amplification and 301 bases nucleotide sequence was obtained. Sequence then was analysed using Basic Local Alignment Search Tool (BLAST). The results showed 98% similarity with *Bacillus licheniformis*. The sequences of SUNGC2 were stored in the GenBank database according to accession numbers of MH062901. The phylogenetic tree was built based on 16S rDNA sequence

alignment employing Neighbor-Joining technique for the SUNGC2 strain (Figure 3). A total of 235 positions can be found in the final dataset. Evolutionary analyses were carried out via MEGA7 software (Kumar et al., 2016). Therefore, it was recommended that isolate SUNGC2 identified as *B. licheniformis* with the strain name of SUNGC2. Additional identification was then performed by API CHB50. SUNGC2 was identified by the API 50 CHB identification kit to provide additional details of the isolate's metabolic abilities.

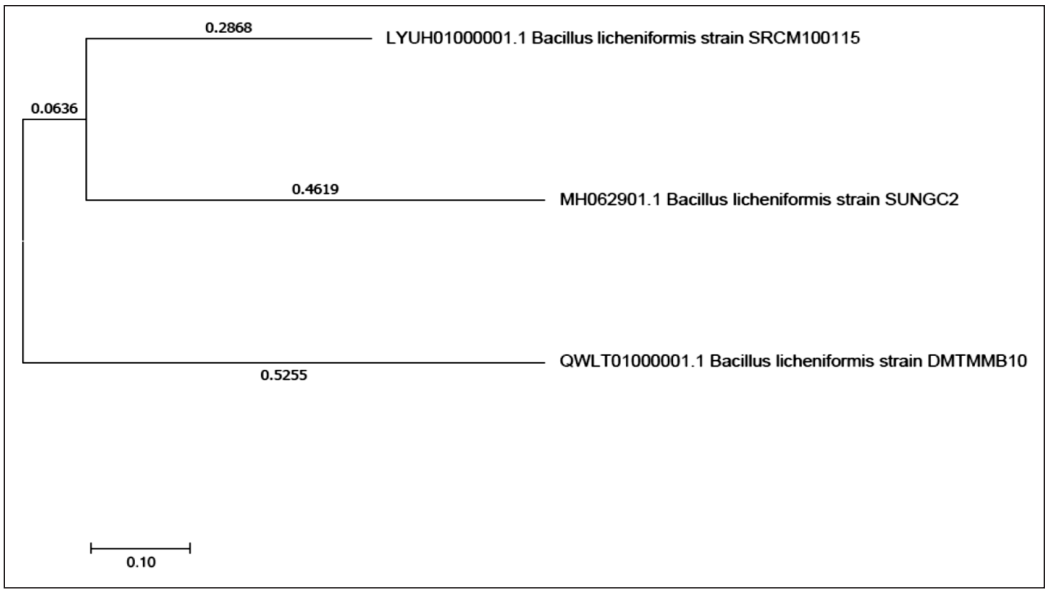

Figure 3. Evolutionary relationships of taxa for *B. licheniformis* SUNGC2

The outcomes are presented in Table 2 and Table 3. The isolate was identified as *B. licheniformis* according to the combination of partial 16S sequencing analysis and API 50CHB.

The API 50 CHB and API 20E result using apiweb™, showed a very good agreement with the previous results, that strain SUNGC2 is *Bacillus licheniformis* with % ID of 99.3 homology.

Table 2
API50CH profile of B. licheniformis *SUNGC2*

Test No.	Substrate	SUNGC2	Test No.	Substrate	SUNGC2
0	Control	-	26	Salicin	+
1	Glycerol	+	27	D-Cellobiose	+
2	Erythritol	+	28	D-Maltose	+
3	D-arabinose	+	28	D-Lactose	+
4	L-arabinose	+	29	D-Sucrose	-
5	Ribose	+	30	Trehalose	-

Table 2 *(continue)*

Test No.	Substrate	SUNGC2	Test No.	Substrate	SUNGC2
6	D-xylose	+	31	Gentiobiose	+
7	L-xylose	-	32	Melibiose	+
8	Adonitol	-	33	Raffinose	+
9	ß methyl-D-Xyloside	-	34	Melezitose	-
10	Galactose	+	35	Starch	+
11	Glucose	+	36	Glycogen	+
12	Fructose	+	37	Inulin	+
13	Mannose	+	38	D-Turanose	-
14	L-Sorbose	-	39	D-Tagatose	+
15	Rhamnose	+	40	D-Fucose	+
16	Dulcitol	-	41	L-fucose	-
17	Inositol	+	42	D-Lyxose	+
18	Sorbitol	+	43	D-Arabitol	-
19	Mannitol	+	44	L-Arabitol	-
20	L-Methyl-D-mannoside	-	45	L-Sorbose	-
21	D-Methyl-D-glucoside	+	46	Xylitol	-
22	N-Acetylglucosamine	+	47	Gluconate	+
23	Amygdalin	+	48	2-Ketogluconate	-
24	Arbutin	+	49	5-Ketogluconate	-
25	Aesculin	+			
Significant taxa	*Bacillus licheniformis*	% ID 99.3	T		

+, positive reaction; - negative reaction; ? non conclusive

Table 3
API 20E profile of B. licheniformis *SUNGC2*

Strains code	API 20E														
SUNGC2	**ONPG**	**ADH**	**LDC**	**ODC**	**Citrate**	**H_2S**	**Urease**	**TDA**	**Indole**	**VP**	**Gelatin GEL**	**Nitrate NIT**	**Temperature**	**Incubation**
	+	-	-	-	+	-	-	-	-	+	+	+	45h	24
		1			2			0			7			h

pH Optimisation for *α*-Amylase Production

In our study, an additional rise in the pH level led to a reduction in the activity of α-amylase as observed by Teodoro and Martins (2000). Figure 4, the amylase production was maximum at pH 7.0 (24.65 U/mL) and minimum at pH 9.0 (7.65 U/mL). The highest specific activity

obtained by ammonium phosphate precipitation 80% (w/v) was 3.79 U/µg for SUNGC2 (9.45-fold increase). Various researches have mentioned that the optimisation of amylase production by *Bacillus* spp. is due to the specific enzyme conditions for each application (Hmidet et al., 2009). Commonly, the enhancement of the microbial production of enzymes involves the optimisation of environmental parameters such as temperature, pH, and nutrients. Amylase stability is beneficial for various applications and the characterisation of enzymes is significantly important for industrial applications. In this study, the pH effects on amylase activity in a range of 3.0-9.0 and are represented in Figure 4.

Enzymes from thermophilic microorganisms have special characteristics such as high stability to changes in wide range of pH (Alrumman et al., 2018). Elkhalil and Gaffar (2011) reported that the pH activity profile of α-amylase produced from *B. acidocaldarius* had an activity optimum at pH 6.0. Several researchers studied the production of α-amylase from *Bacillus* sp. and found its maximum activity at pH between 5.0 and 6.5 (Ardhi et al., 2020; Deljou & Arezi 2016; Teodoro & Martins 2000). However, Thippeswamy et al. (2006) reported a pH of 6.5 as an optimum for *α*-amylase activity. It was detected that the highest amylase activity occurred at pH 6.0. However, the highest bacterial growth occurred at pH 8.0, suggesting that the bacteria need an alkaline environment to synthesise the enzymes and that synthesis was not growth dependent.

Similarly, the growth was highest at pH 7.0 and had a proportional relationship to the amylase production. The amylase extracted from *B. licheniformis* SUNGC2 has wide-

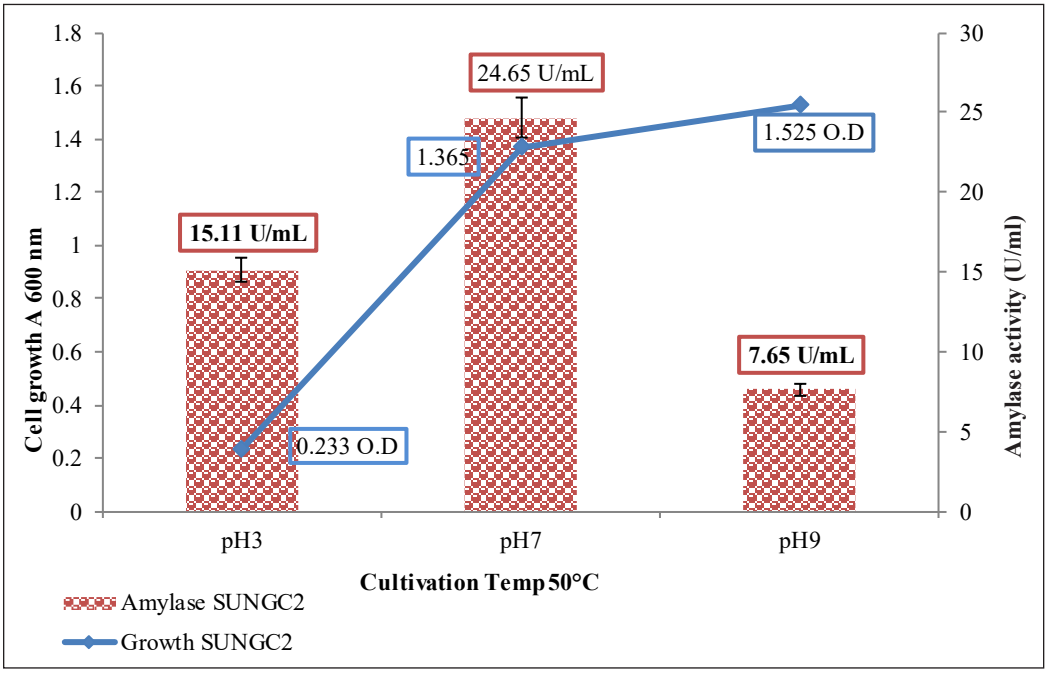

Figure 4. Effect of growth and pH on the enzyme activity of *B. licheniformis* SUNGC2

ranging pH activity (pH 3.0-9.0) with optimal pH at 7.0 which is close by to the optimum pH value of most *Bacillus* sp. amylase (Divakaran et al., 2011). The enzyme had about 30% relative activity at pH 9.0 and about 50% at pH 3.0. At pH 7.0, the enzyme expressed 100% relative activity. According to the results, the amylase activity of *B. licheniformis* SUNGC2 was observed to be maximum at pH 7.0 which in agreement to the findings by Oyeleke and Oduwole (2009) and Vidyalakshmi et al., (2009). Nevertheless, other research on amylase activity of *B. licheniformis* MIR 29 was found to be optimum at pH 9.0 (Ferrero et al., 2009).

CONCLUSIONS

The thermophilic *B. licheniformis* SUNGC2 was isolated and characterised from a Sungai Klah Hot Spring water samples from Perak, Malaysia. SUNGC2 was able to produce *α*-amylase at 50°C and the growth and enzyme activity were showed to be optimum at pH 7.0. At 18 hours of cultivation at pH 7.0, the *α*-amylase activity was shown to be increased by 9.45-fold compared to control. The results showed promising thermophilic microorganism *B. licheniformis* SUNGC2 capable of producing thermostable *α*-amylase, with stability over wide-ranging pH which makes SUNGC2 a good candidate for various applications in biotechnology.

ACKNOWLEDGEMENTS

The authors acknowledge Universiti Kebangsaan Malaysia for financially supporting the project under Geran Universiti Penyelidikan (GUP-2018-112) and for the research facilities.

REFERENCES

Adiguzel, A., Ozkan, H., Baris, O., Inan, K., Gulluce, M., & Sahin, F. (2009). Identification and characterisation of thermophilic bacteria isolated from hot springs in Turkey. *Journal of Microbiological Methods*, 79(3), 321-328. doi: 10.1016/j.mimet.2009.09.026

Alrumman, S., Mostafa, Y. S. M., Al-Qahtani, S., & Taha, T. H. T. (2018). Hydrolytic enzyme production by thermophilic bacteria isolated from Saudi Hot Springs. *Open Life Sciences 13*(1), 470-480. doi: 10.1515/biol-2018-0056

Ameri, A., Shakibaie, M., Amirpour-Rostami, S., Ameri, A., Adeli-Sardou, M., Khazaeli, P., … & Farootanfar, H. (2015). Partial purification and characterisation of a thermoalkalophilic lipase originated from *Bacillus atrophaeus* FSHM2 and its application for ester synthesis. *Biotechnology*, *14*(4), 154-164. doi:10.3923/biotech.2015.154.164

Ardhi, A., Sidauruk, A. N., Suraya, N., Pratiwi, N. W., & Pato, U. (2020). Molecular identification of amylase-producing thermophilic bacteria isolated from Bukit Gadang Hot Spring, West Sumatra, Indonesia. *Biodiversitas Journal of Biological Diversity, 21*(3), 994-1000. doi:10.13057/biodiv/d210319

Asoodeh, A., Chamani, J., & Lagzian, M. (2010). A novel thermostable, acidophilic α-amylase from a new thermophilic "Bacillus sp. Ferdowsicous" isolated from Ferdows hot mineral spring in Iran: Purification and biochemical characterisation. *International Journal of Biological Macromolecules*, *46*(3), 289-297. doi:10.1016/j.ijbiomac.2010.01.013

Božić, N., Ruiz, J., López-Santín, J., & Vujčić, Z. (2011). Production and properties of the highly efficient raw starch digesting α-amylase from a *Bacillus licheniformis* ATCC 9945a. *Biochemical Engineering Journal*, *53*(2), 203-209. doi:10.1016/j.bej.2010.10.014

Bradford, M. M. (1976). A rapid and sensitive method for the quantitation of microgram quantities of protein utilising the principle of protein-dye binding. *Analytical Biochemistry*, *72*(1-2), 248-254. doi:10.1016/0003-2697(76)90527-3

Burgess, S. A., Lindsay, D., & Flint, S. H. (2010). Thermophilic Bacilli and their importance in dairy processing. *International Journal of Food Microbiology*, *144*(2), 215-225. doi:10.1016/j.ijfoodmicro.2010.09.027

Chan, C. S., Chan, K. G., Ee, R., Hong, K. W., Urbieta, M. S., Donati, E. R., … & Goh, K. M. (2017). Effects of physiochemical factors on prokaryotic biodiversity in Malaysian circumneutral hot springs. *Frontiers in Microbiology*, *8*, 1-14. doi:10.3389/fmicb.2017.01252

Chan, C. S., Chan, K. G., Tay, Y. L., Chua, Y. H., & Goh, K. M. (2015). Diversity of thermophiles in a Malaysian hot spring determined using 16S rRNA and shotgun metagenome sequencing. *Frontiers in Microbiology*, *6*, 1-15. doi:10.3389/fmicb.2015.00177

Deljou, A., & Arezi, I. (2016). Production of thermostable extracellular α-amylase by a moderate thermophilic *Bacillus licheniformis* isolated from Qinarje Hot Spring (Ardebil prov. of Iran). *Periodicum Biologorum*, *118*(4), 405-416. doi:10.18054/pb.v118i4.3737

Divakaran, D., Chandran, A., & Pratap Chandran, R. (2011). Comparative study on production of α-amylase from *Bacillus licheniformis* strains. *Brazilian Journal of Microbiology*, *42*(4), 1397-1404. doi:10.1590/s1517-83822011000400022

Drancourt, M., Bollet, C., Carlioz, A., Martelin, R., Gayral, J. P., & Raoult, D. (2000). 16S ribosomal DNA sequence analysis of a large collection of environmental and clinical unidentifiable bacterial isolates. *Journal of Clinical Microbiology*, *38*(10), 3623-3630. doi:10.1128/jcm.38.10.3623-3630.2000

Elkhalil, E. A., & Gaffar, F. Y. (2011). Biochemical characterisation of thermophilic amylase enzyme isolated from Bacillus strains. *International Journals of Science and Nature 2*(3), 616-620.

Ferrero, M. A., Castro, G. R., Abate, C. M., Baigori, M. D., & Sineriz, F. (1996). Thermostable alkaline proteases of *Bacillus licheniformis* MIR 29: Isolation, production and characterisation. *Applied Microbiology and Biotechnology*, *45*(3), 327-332. doi:10.1007/s002530050691

Haki, G. D., & Rakshit, S. K. (2003). Developments in industrially important thermostable enzymes: A review. *Bioresource Technology*, *89*(1), 17-34. doi:10.1016/s0960-8524(03)00033-6

Harley, J. P., & Prescott, L. M. (2005). *Laboratory exercises in microbiology.* New York: McGraw-Hill.

Hmidet, N., Ali, N. E. H., Haddar, A., Kanoun, S., Alya, S. K., & Nasri, M. (2009). Alkaline proteases and thermostable α-amylase co-produced by *Bacillus licheniformis* NH1: Characterisation and potential

application as detergent additive. *Biochemical Engineering Journal*, *47*(1-3), 71-79. doi:10.1016/j.bej.2009.07.005

Ibrahim, D., Zhu, H. L., & Yusof, N. (2013). *Bacillus licheniformis* BT5. 9 isolated from Changar Hot spring, Malang, Indonesia, as a potential producer of thermostable α-amylase. *Tropical Life Sciences Research*, *24*(1), 71-84.

Jujjavarapu, S. E., & Dhagat, S. (2019). Evolutionary trends in industrial production of α-amylase. *Recent Patents on Biotechnology*, *13*(1), 4-18. doi:10.2174/2211550107666180816093436

Kumar, R. M., & Raja, S. S. (2019). Isolation, screening and identification of potential thermo stable bacterial enzyme producers in Sangameshwar, Tural Hot Spring. *Journal of Drug Delivery and Therapeutics*, *9*(4), 510-517. doi:10.22270/jddt.v9i4.3094

Kumar, S., Stecher, G., & Tamura, K. (2016). MEGA7: Molecular evolutionary genetics analysis version 7.0 for bigger datasets. *Molecular Biology and Evolution*, *33*(7), 1870-1874. doi:10.1093/molbev/msw054

Lee, L. S., Goh, K. M., Chan, C. S., Annie Tan, G. Y., Yin, W. F., Chong, C. S., & Chan, K. G. (2018). Microbial diversity of thermophiles with biomass deconstruction potential in a foliage rich hot spring. *Microbiology Open*, *7*(6), 1-13. doi:10.1002/mbo3.615

Li, M., Gong, J., Cottrill, M., Yu, H., de Lange, C., Burton, J., & Topp, E. (2003). Evaluation of QIAamp® DNA Stool Mini Kit for ecological studies of gut microbiota. *Journal of Microbiological Methods*, *54*(1), 13-20. doi:10.1016/s0167-7012(02)00260-9

Miller, G. L. (1959). Use of dinitrosalicylic acid reagent for determination of reducing sugar. *Analytical Chemistry*, *31*(3), 426-428. doi:10.1021/ac60147a030

Mohammad, B. T., Al Daghistani, H. I., Jaouani, A., Abdel-Latif, S., & Kennes, C. (2017). Isolation and characterization of thermophilic bacteria from Jordanian hot springs: *Bacillus licheniformis* and *Thermomonas hydrothermalis* isolates as potential producers of thermostable enzymes. *International Journal of Microbiology*, *2017*, 1-12. doi:10.1155/2017/6943952

Msarah, M. J., Ibrahim, I., Hamid, A. A., & Aqma, W. S. (2020). Optimisation and production of alpha amylase from thermophilic Bacillus spp. and its application in food waste biodegradation. *Heliyon*, *6*(6), e04183. doi:10.1016/j.heliyon.2020.e04183

Msarah, M., Ibrahim, I. & Aqma, W.S. (2018). Enzyme activity screening of thermophilic bacteria isolated from Dusun Tua Hot Spring. *AIP Conference Proceedings 1940*(1), 020070-1–020070-5. doi:10.1063/1.5027985

Msarah, M., Ibrahim, I., & Aqma, W.S. (2018). Isolation of thermophilic bacteria producing extracellular enzyme from Sungai Klah Hot Spring, Malaysia. *Malaysian Applied Biology*, *47*(5), 269-275.

Niu, D., Zuo, Z., Shi, G. Y., & Wang, Z. X. (2009). High yield recombinant thermostable α-amylase production using an improved *Bacillus licheniformis* system. *Microbial Cell Factories*, *8*(1), 4-7. doi:10.1186/1475-2859-8-58

Oyeleke, S. B., & Oduwole, A. A. (2009). Production of amylase by bacteria isolated from a cassava waste dumpsite. *African Journal Microbiology, 3*(4), 143-146.

Panosyan, H., Margaryan, A., & Birkeland, N. K. (2020). Geothermal springs in Armenia and Nagorno-Karabakh: potential sources of hydrolase-producing thermophilic bacilli. *Extremophiles*, *24*, 519–536. doi:10.1007/s00792-020-01173-1

Samsudin A. R, Hamzah, U, Rahman, R. A, Siwar, C, Jani, M. F. M., & Othman, R. (1997). Thermal springs of Malaysia and their potential development. *Journal of Asian Earth Sciences*, *15*(2-3), 275-284. doi:10.1016/s1367-9120(97)00012-6

Teodoro, C. E. D. S., & Martins, M. L. L. (2000). Culture conditions for the production of thermostable amylase by Bacillus sp. *Brazilian Journal of Microbiology*, *31*(4), 298-302. doi:10.1590/s1517-83822000000400011

Thippeswamy, S., Girigowda, K., & Mulimani, V. H. (2006). Isolation and identification of alpha amylase producing Bacillus sp. from dhal industry waste. *Indian Journal of Biochemistry and Biophysics 43*(5), 295-298.

Van Der Maarel, M. J., Van der Veen, B., Uitdehaag, J. C., Leemhuis, H., & Dijkhuizen, L. (2002). Properties and applications of starch converting enzymes of the α-amylase family. *Journal of Biotechnology*, *94*(2), 137-155. doi:10.1016/s0168-1656(01)00407-2

Verma, A., Gupta, M. & Shirkot, P. (2014). Isolation and characterisation of thermophilic bacteria in natural hot water springs of Himachal Pradesh (India). *Bioscan, 9*(3), 947-952.

Vidyalakshmi, R., Paranthaman, R. & Indhumathi, J. (2009). Amylase production on submerged fermentation by Bacillus spp. *World Journal of Chemistry*, *4*(1), 89-91.

Pertanika J. Sci. & Technol. 28 (S2): 135 - 148 (2020)

PERTANIKA JOURNALS

SCIENCE & TECHNOLOGY

Journal homepage: http://www.pertanika.upm.edu.my/

Effect of Steam and Bleaching Treatment on the Characteristics of Pineapple Leaves Fibre Derived Cellulose

Surenthiran Gnanasekaran, Siti Nur Najihah Muslih, Jun Haslinda Shariffuddin, and Noor Ida Amalina Ahamad Nordin*

Faculty of Chemical and Process Engineering Technology, Universiti Malaysia Pahang, Lebuhraya Tun Razak, 26300 Gambang, Pahang, Malaysia

ABSTRACT

Pineapple leaf fibres (PALF) is one of the abundant residues generated from pineapple plantation. The residues are left on the plantation for nutrient cycling or burning, and this circumstance leads to environmental issues. PALF has high cellulose content among other natural fibres. Cellulose is a reinforcing element that exists as whisker-like microfibrils and has a long-chain structure. In this study, cellulose produced from PALF was treated by steam and chemical treatment. The fibre was treated with steam at 121°C, a pressure of 21 psi for 30 or 60 min. Next, the steam-treated fibre was treated with 5 wt% sodium chlorite ($NaClO_2$) solution with pH adjusted between 4 and 5 for 90 min. The condition was varied with three different temperatures, which were room temperature, 50, and 70°C. Then, the bleached fibre was treated with 5 wt% sodium hydroxide (NaOH) at room temperature for 3 h. After the treatments, the fibre was analysed for its thermal stability, morphology, and chemical composition. Cellulose obtained from the treatment condition of steam for 60 min, bleaching at 70°C, and alkali treatment at room temperature expressed the highest degradation temperature of 276°C at 20% weight loss, percentage of cellulose of 86% and lowest moisture content (8%) compared to others sample. It also had an excellent surface morphology with finest fibril disintegration. It showed longer steam treatment (60 min) degrading more hemicellulose; and bleaching treatment at high temperature (70°C), increasing the rate of oxidative delignification. In conclusion, the suggested treatment provides a simple but efficient method to isolate cellulose that can be used for various types of applications.

Keywords: Cellulose, chemical treatment, pineapple leaf fibre (PALF), steam treatment, thermal degradation

ARTICLE INFO

Article history:
Received: 10 February 2020
Accepted: 13 November 2020
Published: 31 December 2020

DOI: https://doi.org/10.47836/pjst.28.S2.11

E-mail addresses:
surenthirangnanasekaran@gmail.com (Surenthiran Gnanasekaran)
snnajihah95@gmail.com (Siti Nur Najihah Muslih)
junhaslinda@ump.edu.my (Jun Haslinda Shariffuddin)
idamalina@ump.edu.my (Noor Ida Amalina Ahamad Nordin)
* Corresponding author

ISSN: 0128-7680
e-ISSN: 2231-8526

© Universiti Putra Malaysia Press

INTRODUCTION

Pineapple is a perennial herbaceous plant with 0.75 – 1.5 m height and 0.9 – 1.2 m spread. It has a short stem with dark green colour. This tropical plant originated from Southeast America and was cultivated in Tanah Melayu in 1922 (Najeeb et al., 2020). In 2015, pineapple plantation grown in Malaysia covered an area of 10 847 hectares with an estimated fruit production of 272 570 metric tons (Abd-Halim, 2016). Several agencies are responsible for the success of this industry such as the Federal Agricultural Marketing Authority (FAMA), Malaysian Pineapple Industry Board (MPIB), and some local universities (MPIB, 2010).

While Malaysia is known as one of the largest pineapple producers in Asia, at the same time, it creates a large quantity of waste from this industry (Najeeb et al., 2020; Shafie et al., 2012). Pineapple waste is not fully utilised and usually burnt, and this circumstance may lead to air pollution. Pineapples are mostly consumed for nutritional purposes either as a fresh product or processed fruit. Only 20% of the pineapple is canned for nutrition usage and the rest, which includes leaves, peeled skin, core, base, and crown, is discarded as waste (Shafie et al., 2012).

Pineapple leaf fibre (PALF) is one of the abundantly available waste materials generated from the pineapple industry (Sena Neto et al., 2013; Wan Nadirah et al., 2012). Usually, PALF is left on the plantation for nutrient cycling (Ahmed et al., 2000). Attempts have been made to utilise PALF for feedstock and energy production (Asim et al., 2015). Besides, the use of natural fibres for composites, as alternatives to traditional reinforcement materials offers numerous advantages such as low cost, high specific properties, low energy consumption, low density, biodegradability, flexibility and availability of a wide variety of fibres around the globe (Benyahia et al., 2014). Components of natural fibre consist of cellulose, hemicellulose and lignin (Satha et al., 2020). Cellulose has relatively high strength, high stiffness, low density and good thermal stability (Mahardika et al., 2018). Higher content of cellulose (80%) in PALF compared to other natural fibres makes it promising candidate for reinforcing biocomposite (Cherian et al., 2010; Huda et al., 2008). The application of cellulose includes household items (Lavanya et al., 2011), wall insulation (Ashik et al., 2015), packaging (Sena Neto et al., 2013) and others. Numerous studies have shown the potential of PALF as reinforced material in a polymer matrix (Garcia et al., 2016).

The objective of this study was to produce cellulose from PALF using steam and chemical treatment. Recently much work has been done on pre-treatment to extract the cellulose. Nevertheless, little has been done about the physiochemical treatment. These may increase the accessibility of cellulose using the mild treatment. Therefore, in this study, PALF was treated with the different retention time of steam treatment and followed by the different temperature of bleaching treatment to maximize the removal of hemicellulose and lignin with less degradation of cellulose.

MATERIAL AND METHODS

Materials

Pineapple leaves were collected from Pekan Pina Sdn. Bhd., Pekan, Pahang, Malaysia. Sodium hydroxide, sodium chlorite and sulphuric acid were obtained from Sigma Aldrich Malaysia.

Methods

Fibre Preparation. Pineapple leaves were washed with tap water to remove dirt. Cleaned leaves were cut into 1 to 2 cm for storage purposes. The fibre was dried in oven at 70°C for 24 h to prevent fungal growth and contamination. Samples were stored in sealed plastic bags at room temperature until further use (Prado & Spinacé, 2019).

Steam Treatment of Fibre. PALF was treated with steam at 121°C and 21 psi for 30 or 60 min using Hirayama HVE-50 Autoclave Sterilizer (Cherian et al., 2010). After steam treatment, the fibre was washed with distilled water and dried overnight at 70°C (Santos et al., 2013).

Fibre Bleaching. Steam-treated fibre (1 g fibre:50 mL solution) was bleached using 5 wt% sodium chlorite solution with pH adjusted between 4 and 5 using sulphuric acid for 90 min under three different conditions: room temperature, 50, and 70°C in Jeio Tech BS-06 Water Bath. After bleaching, the treated fibre was washed with distilled water and dried overnight at 70°C (Santos et al., 2013).

Alkaline Treatment of Fibre. Bleached fibre (1g fibre:50 mL solution) was treated using 5 wt% sodium hydroxide (NaOH) solution at room temperature for 3h (Prado & Spinacé, 2019). After that, the treated fibre was washed with distilled water and dried overnight at 70°C (Santos et al., 2013). The dried samples were ground using Retsch Ultra Centrifugal Mill ZM 200 for analysis purposes.

Overall treatment process was summarized in Figure 1.

Thermal Stability Analysis. The samples were tested using Hitachi STA7200 Thermal Analysis System for thermogravimetric analysis (TGA). The measurements were conducted in a nitrogen atmosphere at a rate of 100 mL/min by constant heating at 10°C/min with ramping temperature ranging from 30 to 600°C. About 4–7 mg of the sample was placed in a ceramic crucible and tested (Abraham et al., 2011). The moisture content of the sample was obtained from TG analysis at temperature of 150°C.

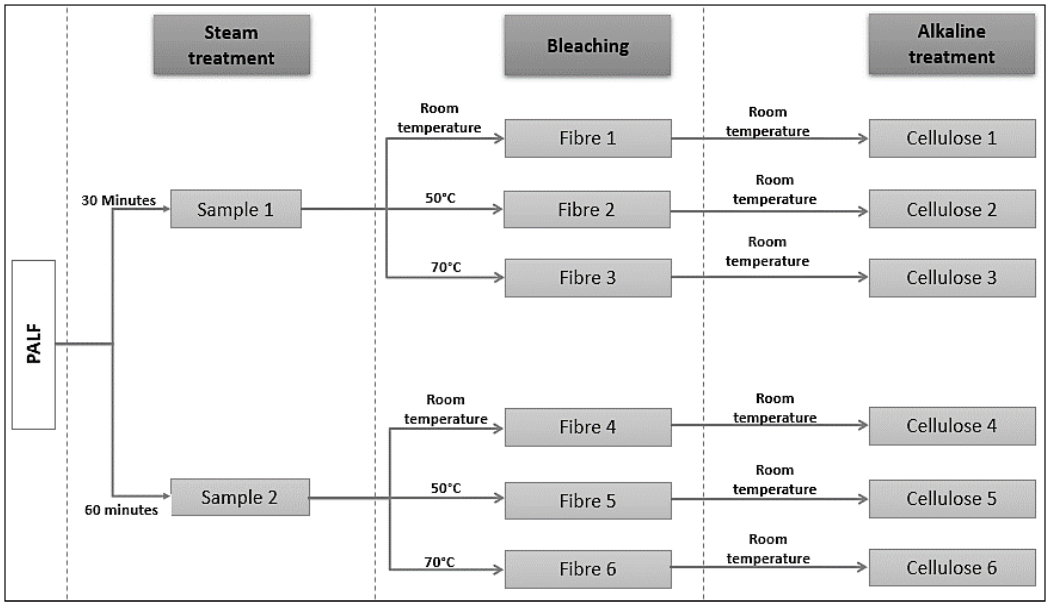

Figure 1. Summarized treatment on PALF by steam, bleaching and alkaline treatment to isolate cellulose

Morphology Analysis. Hitachi TM3030 Plus Tabletop Microscope was used for scanning electron microscopy (SEM) to obtain the surface morphology of cellulose. Prior to SEM analysis, samples were coated with platinum using sputtering techniques (Cherian et al., 2010).

Chemical Composition of Cellulose. Cellulose samples were analysed for its chemical composition. The isolated cellulose was bleached using 5 wt% sodium chlorite solution with pH adjusted to 4–5 using sulphuric acid at 70°C to obtain the percentage of lignin. The bleached fibre was washed with distilled water and dried overnight at temperature of 70°C. Next, the bleached sample was immersed in 5 wt% sodium hydroxide solutions at room temperature for 24 h to obtain the percentage of hemicellulose. After that, the treated fibre was washed with distilled water and dried overnight at 70°C. The residue left contained only cellulose (Nordin et al., 2017). Equations 1 to 3 were used to calculate the percentage of chemical composition in the samples.

$$Lignin\,\% = \frac{Initial\,weight\,(g)_{dry} - \,Weight\,after\,extraction,\,NaClO_2\,(g)_{dry}}{Initial\,weight\,(g)_{dry}} \times 100\%$$

[Eq. 1]

$$Hemicellulose\,\% = \frac{Weight\,after\,extraction,NaClO_2\,(g)_{dry} - Weight\,after\,extraction,NaOH\,(g)_{dry}}{Initial\,weight\,(g)_{dry}} \times 100\%$$

[Eq. 2]

$$Cellulose\,\% = \frac{The\ residue\ of\ NaOH\ extraction\ (g)_{dry}}{Initial\ weight\ (g)_{dry}} \times 100\% \qquad \textbf{[Eq. 3]}$$

RESULTS AND DISCUSSION

Physical Appearance of Treated Fibre

Physical Appearance of Steam-treated PALF. Figure 2 shows the physical appearances of the steam-treated fibre where (a) was 30 min and (b) was 60 min of steam treatment. As portrayed in Figure 2, PALF treated with steam for 60 min (sample b) had a darker brown colour compared to 30 min sample (sample a). Hemicellulose has low thermal degradation, which makes it degrade easier than cellulose and lignin.

Hydrolysis of hemicellulose takes place during steam treatment, by breaking down into monosugar which consists of numerous amounts of hydroxyl group. However, under the high temperature of steam treatment, the total number of hydroxyl groups consisting of O and H decreases due to degradation of monosugar. This mechanism also known as caramelization of monosugar (Stelte, 2013). Hence, PALF that undergoes steam treatment for 60 min is darker than 30 min treated PALF, due to longer residence time of steam treatment causes high degradation of hemicellulose by eliminating hydroxyl group and increasing of carbon content.

(a) (b)

Figure 2. Physical appearance of fibre after steam treatment for (a) 30 min and (b) 60 min

Physical Appearance of Steamed_Bleached PALF. Figure 3 shows the physical appearance of fibre after steam treatment followed by bleaching treatment. Bleaching temperature was varied at room temperature (sample 1 and 4), 50°C (sample 2 and 5) and 70°C (sample 3 and sample 6). As seen in Figure 3, fibre with bleaching temperature of 70°C has the lightest colour compared to other samples either the samples were treated with steam for 30 or 60 min. $NaClO_2$ act as an oxidative agent in delignification process

by oxidizing aromatic ring or benzoquinone structure of lignin and hemicellulose to change its solubility (Wu et al., 2019). It also may react with the side chain carbon–carbon double bond and carbonyl bond of lignin for further oxidative degradation, leading to lignin removal (Hubbell & Ragauskas, 2010; Lee et al., 2014). According to Listiyani et al. (2012) temperature of bleaching treatment gives an significant impact on oxidative delignification of PALF. When the temperature of bleaching treatment is increased, the rate of oxidative delignification will increase which causes more lignin and hemicellulose to solubilize (Hefti, 1960). Hence, the lighter colour of fibre demonstrates that more lignin and hemicellulose were oxidized and removed during the treatment. The fibre surface was still rough after undergoing the treatments, indicating that in order to produce cellulose, further treatment is needed to improve the fibre surface and size.

(a) (b)

Figure 3. Physical appearance of fibre after steam and bleaching treatment; **(a)** steam treatment 30 min with bleaching treatment at (1) room temperature; (2) 50°C; (3) 70°C **(b)** steam treatment 60 min with bleaching treatment at (4) room temperature; (5) 50°C; (6) 70°C

Physical Appearance of Cellulose (Steamed, bleached, and alkaline-treated PALF). Figure 4 shows the physical appearance of cellulose isolated from PALF. The cellulose was obtained after steam, bleached and finally was alkali treated at room temperature for

(a) (b)

Figure 4. Physical appearance of cellulose after steamed; bleached; and alkaline treated: (a) steam 30 min: bleached (Cellulose 1) room temperature; (Cellulose 2) 50°C; (Cellulose 3) 70°C, then alkaline treated at room temperature, 3 h and (b) steam 60 min: bleached at (Cellulose 4) room temperature; (Cellulose 5) 50 °C; (Cellulose 6) 70°C, then alkaline treated at room temperature, 3 h

3h as detailed in Figure 1. The sample portrays the difference in the colour gradient of the cellulose. A lighter colour of cellulose indicates that more components have been removed during the treatment (Kouadri & Satha, 2018; Sharma et al., 2018). The cellulose surface was also smoother and appeared cottony after the treatment, compared to that from the previous treatment. Moreover, the major effect of these alkaline treatment is to de-lignify the biomass, disrupt the connection between cellulose and alter the structure of treated biomass to increase the accessibility of cellulose (Sindhu et al, 2014). Since cellulose is moderately resistant to alkali treatment, it is an effective way to remove lignin and hemicellulose with less degradation of the cellulose component (Mishra et al., 2004).

Thermal Stability of Cellulose. Figure 5 shows the thermal degradation temperature of cellulose, while Figure 6 illustrates the differential thermal gravimetry of cellulose.

All samples had a one-step degradation between 200 and 400°C except for Cellulose 1. Cellulose 1 demonstrated two-step degradation, at temperature of 200 to 300°C and at temperature of 300 to 400°C. The first weight loss transition occurred between 50 and 150°C due to the evaporation of water molecules in the cellulose (Satha et al., 2020). The second transition, which occurred from 180 to 350°C, is mainly contributed to the degradation of the cellulose component, and low molecular weight lignin components (Najeeb et al., 2020; Paluvai et al., 2015). The third transition occurred between 350 to 500°C due to the degradation of lignin, which has a higher molecular weight.

Cellulose 1 may content more percentage of lignin, due to bleaching treatment conducted at room temperature. It seems that room temperature is not an effective condition for bleaching of lignin. That may explain the trend of thermal degradation of Cellulose 1. Cellulose 4, Cellulose 5, and Cellulose 6 experienced more weight loss at temperature

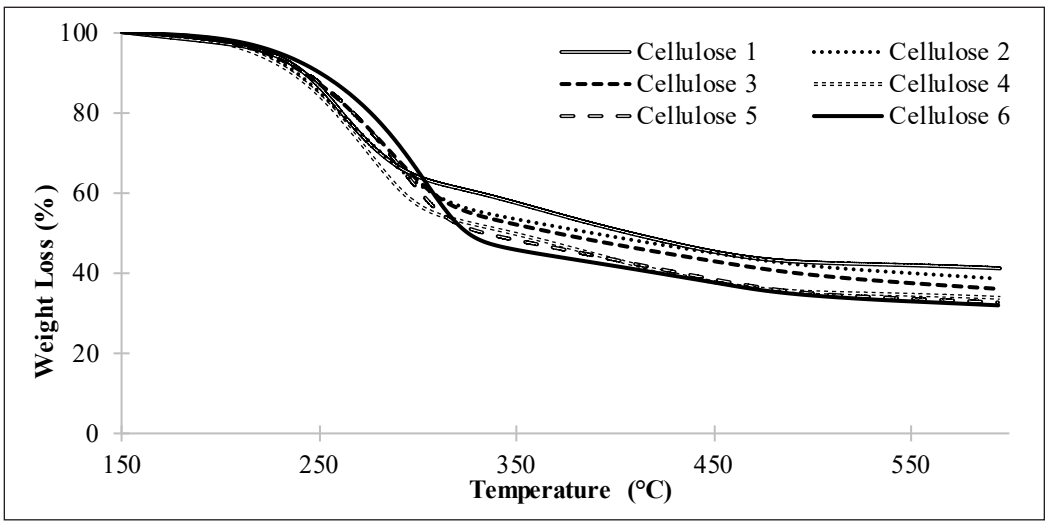

Figure 5. Weight loss of cellulose

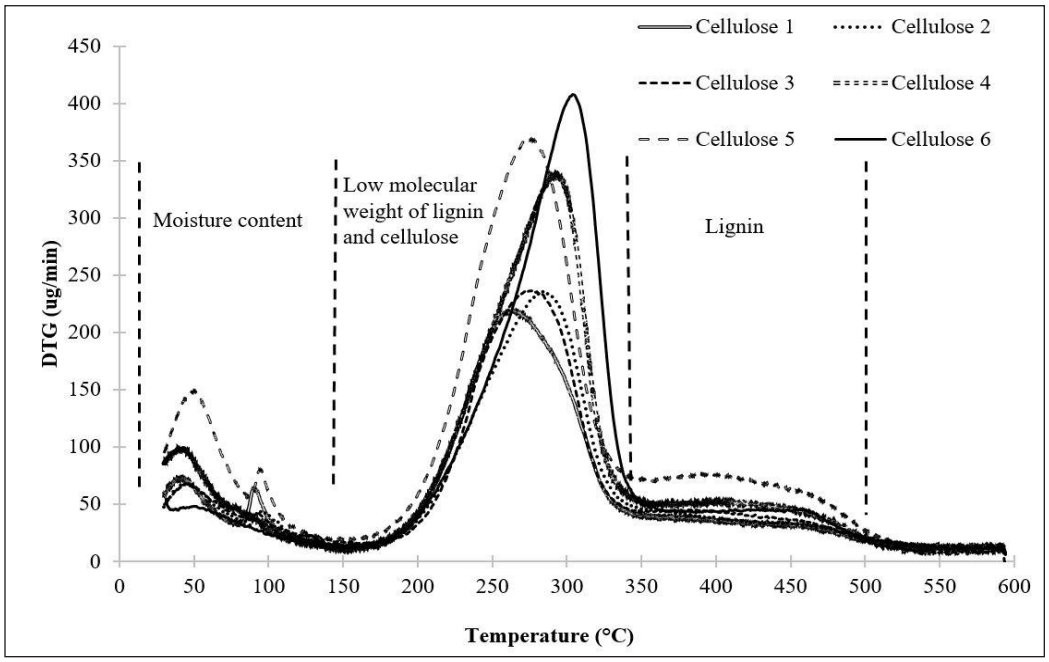

Figure 6. DTG of cellulose

range of 180 to 350°C compared to Cellulose 1, 2, and 3. It could also be observed that the residue at 600°C, is mainly lignin, for Cellulose 4 to 6 was lower compared to Cellulose 1 to 3. Thus, it can be concluded that the percentage of cellulose was higher in samples 4 to 6, and contained less hemicellulose and lignin due to more percentage of these components being removed by the treatment (Lee et al., 2020). But among Cellulose 4 to 6, Cellulose 6 recorded the highest cellulose content. It may be because bleaching at high temperature makes the lignin decomposition by chloride higher (Hefti, 1960). It was also reported by Wan Nadirah et al. (2012) that an increase in the amount of cellulose would increase the percentage of crystallinity of the fibre. Increasing the percentage of crystallinity may also improve its thermal stability (Djafari Petroudy, 2017).

Table 1 summarises the degradation of cellulose at 5%, 20%, and 50% weight loss. As mentioned, temperature around 200°C will degrade low molecular weight of lignin, thus Cellulose 1 had the lowest temperature for 5% weight loss. The same trend occurred at 20% of weight loss. However, at the temperature above 350°C, the lignin component with high molecular weight would start to degrade. Therefore, at this range of temperature, it was observed Cellulose 6 had the lowest degradation temperature due to less lignin composition and more cellulose. This results were in agreement with physical appearance of light brown colour of Cellulose 6 compared to Cellulose 1 (Kouadri & Satha, 2018). Cellulose 6 also had the lowest percentage of residue at 600°C, which was 32.02%, showing the low percentage of lignin. (Lee et al., 2020; Rambabu et al., 2016).

Table 1
Summary of thermal degradation of cellulose

Cellulose	Temperature for 5% weight loss (°C)	Temperature for 20% weight loss (°C)	Temperature for 50% weight loss (°C)	Residue at 600°C (%)
Cellulose 1	216.16	261.22	406.59	41.25
Cellulose 2	220.13	258.22	387.60	38.68
Cellulose 3	221.47	260.48	369.30	36.15
Cellulose 4	222.74	266.82	347.30	33.40
Cellulose 5	223.39	266.93	333.15	32.73
Cellulose 6	228.19	275.80	325.16	32.02

Moisture content of the samples were obtained from the TG analysis at temperature of 150°C, as presented in Table 2. The moisture content of Cellulose 1 to 6 was reduced and Cellulose 6 had the lowest moisture content (8.22%). This may be due to closer packing of the cellulose molecules and the increase in PALF crystallinity (Mohamed et al., 2014). Low moisture content may help to delay early damage of composite reinforced with cellulose due to swelling effect. Swelling may cause structural modification of the cellulose fibre leading to reduced mechanical properties of biocomposite (Célino et al., 2014).

Table 2
Moisture content of cellulose at 150°C

Cellulose	Moisture content at 150°C (%) (dry basis)
Cellulose 1	14.15
Cellulose 2	12.72
Cellulose 3	12.52
Cellulose 4	12.07
Cellulose 5	12.03
Cellulose 6	8.22

Cellulose Morphology. Figure 7 shows the SEM image of untreated PALF. Untreated PALF is glued with lignin and hemicellulose which causes all the fibrils associated with bundles. Impurities could be seen deposited on the fibre surface.

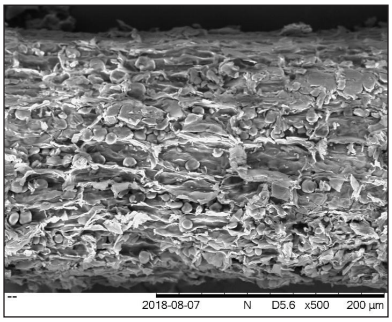

Figure 7. Impurities is deposited on the surface of untreated PALF

Figures 8 depicts the SEM images of the samples. As illustrated in the figure, the loose structure of the fibres is noticeable. Due to the treatments performed to the PALF, the fibril surface is exposed, making hemicellulose and lignin accessible to steam or chemical treatment, and also surface impurities were removed. The treatments aided in breaking down the lignocellulosic components and solubilised the lignin and hemicellulose

to expose the hidden cellulose. In addition, the treatments also assisted in further fibril disintegration.

As shown in Figure 8 (f), the Cellulose 6 is more exposed and has a looser structure, as more protective layers have been removed due to the longer duration of steam treatment and a higher temperature of bleaching (Rambabu et al., 2016). Moreover, due to the alkaline treatment, the fibril surface is smoother than other samples.

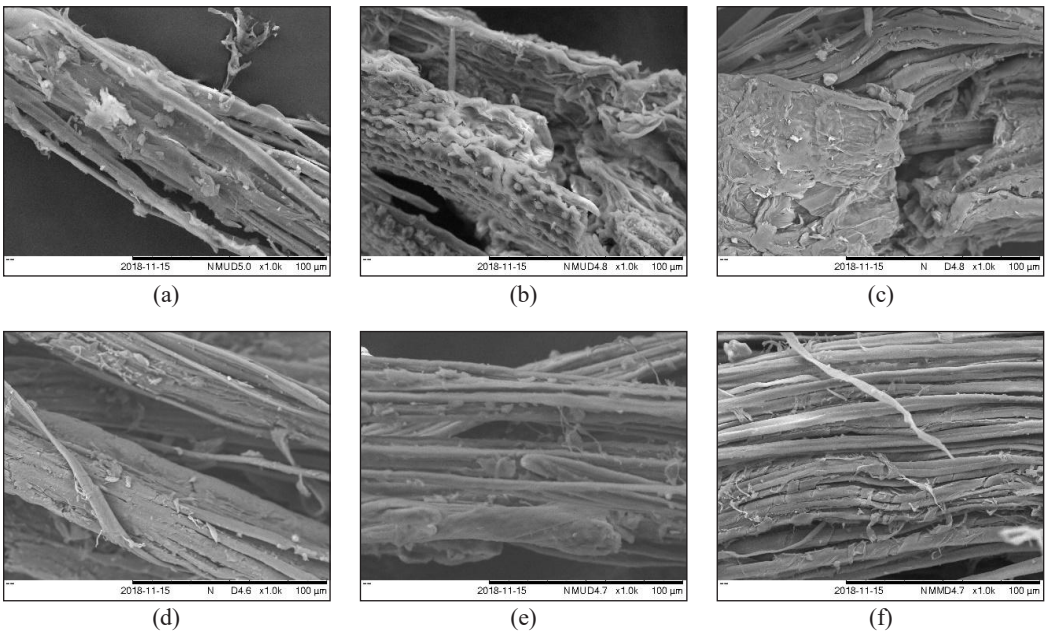

(a) (b) (c)

(d) (e) (f)

Figure 8. SEM images of (a) Cellulose 1, (b) Cellulose 2, (c) Cellulose 3, (d) Cellulose 4, (e) Cellulose 5 and (f) Cellulose 6

Chemical Composition of Cellulose. The chemical compositions of Cellulose 1–6 are listed in Table 3. Cellulose 6 has the highest percentage of cellulose content and lowest hemicellulose and lignin, which are 85.90%, 3.74%, and 10.36%, respectively, compared to the others sample.

Table 3
Chemical composition of the samples

Cellulose	Chemical composition (wt %)		
	Cellulose	**Hemicellulose**	**Lignin**
Cellulose 1	48.91	12.42	38.68
Cellulose 2	54.59	10.17	35.25
Cellulose 3	60.85	7.40	31.76
Cellulose 4	67.99	6.64	25.36
Cellulose 5	74.84	5.64	19.52
Cellulose 6	85.90	3.74	10.36

Steam treatment and alkali treatment did remove some percentage of hemicellulose and lignin as reported by others (Cherian et al., 2010; Rambabu et al., 2016). Longer steam treatment could help in removing hemicellulose content. It can be observed in Cellulose 1 and Cellulose 4, where percentage of hemicellulose was 50% lower in Cellulose 4 when steam treated was 30 min longer. Steam treatment may also contribute in reducing lignin component as Cellulose 4 had 30% lower of lignin composition compared to Cellulose 1.

Bleaching treatment is known to be able to reduce the percentage of lignin (Sena Neto et al., 2013; Garcia et al., 2016; Wu et al., 2019). However, bleaching at room temperature was not efficient to remove lignin content. This result was in agreement with the physical appearance and TG analysis. Cellulose 1 had a darker colour compared to other samples and had higher residue, showing the percentage of lignin was higher.

It can be concluded that 60 min of steam treatment, bleaching at moderate to high temperature and alkali treatment had better efficiency in modifying fibre composition. The treatments significantly removed more hemicellulose component and solubilised lignin giving more purified cellulose.

CONCLUSIONS

The physical appearance, thermal stability, morphology, and chemical composition of cellulose produced from PALF were studied. For physical appearance, a lighter colour indicates that more components have been removed during the treatment especially lignin. All cellulose samples showed the same trend of weight loss, with a one-step degradation that occurred between 200 and 350°C, except for Cellulose 1. The improved degradation temperature indicates that the Cellulose 6 can withstand moderate to high temperature and contains less moisture compared to the other samples. For the morphological analysis of cellulose, the loose structure of the fibres can be clearly noticed. Due to the treatments performed to the PALF, the fibril surface is exposed as most of the components inside the fibre, such as hemicellulose and lignin, and surface impurities have been removed. Cellulose 6 shows the best result among all samples, where it has the highest cellulose content of 85.90%. It also has the highest degradation temperature of 275.8°C at 20% weight loss and the lowest moisture content of 8.22%. Cellulose 6 exhibits excellent surface morphology, where the fibril is more exposed and has a looser structure. In conclusion, the combination of steam treatment for a longer period and bleaching treatment at a high temperature can remove hemicellulose and lignin significantly and increase the accessibility of cellulose with good thermal stability and morphology.

ACKNOWLEDGEMENT

We would like to thank Universiti Malaysia Pahang for the financial assistance through the research grant RDU1703177.

REFERENCES

Abd-Halim, N. (2016). Policy intervention for the development of the pineapple industry in Malaysia. *Food and Fertilizer Technology Center for the Asian and Pacific Region*, *65*, 79-83.

Abraham, E., Deepa, B., Pothan, L., Jacob, M., Thomas, S., Cvelbar, U., & Anandjiwala, R. (2011). Extraction of nanocellulose fibrils from lignocellulosic fibres: A novel approach. *Carbohydrate Polymers*, *86*(4), 1468-1475. doi:10.1016/j.carbpol.2011.06.034

Ahmed, O. H., Husni, M. H., Hanafi, M. M., Syed Omar, S. R., & Anuar, A. R. (2000). Macronutrients distribution and cycling of pineapple planted on tropical peat. *Pertanika Journal of Tropical Agricultural Science, 23*(2), 89 - 95.

Ashik, K. P., & Sharma, R. S. (2015). A Review on mechanical properties of natural fiber reinforced hybrid polymer composites. *Journal of Minerals and Materials Characterization and Engineering*, *3*(05), 420–426. doi:10.4236/jmmce.2015.35044

Asim, M., Abdan, K., Jawaid, M., Nasir, M., Dashtizateh, Z., Ishak, M., & Hoque, M. E. (2015). A review on pineapple leaves fibre and its composites. *International Journal of Polymer Science*, *2015,* 1 - 16. doi:10.1155/2015/950567

Benyahia, A., Merrouche, A., Rahmouni, Z. E. A., Rokbi, M., Serge, W., & Kouadri, Z. (2014). Study of the alkali treatment effect on the mechanical behavior of the composite unsaturated polyester-Alfa fibers. *Mechanics & Industry*, *15*(1), 69 – 73. doi:10.1051/meca/2013082

Célino, A., Fréour, S., Jacquemin, F., & Casari, P. (2014). The hygroscopic behavior of plant fibers: A review. *Frontiers in Chemistry*, *2014*(1), 1–12. doi:10.3389/fchem.2013.00043

Cherian, B. M., Leão, A. L., De Souza, S. F., Thomas, S., Pothan, L. A., & Kottaisamy, M. (2010). Isolation of nanocellulose from pineapple leaf fibres by steam explosion. *Carbohydrate Polymers, 81*(3), 720-725. doi:10.1016/j.carbpol.2010.03.046

Djafari Petroudy, S. R. (2017). Physical and mechanical properties of natural fibers. In Mizi, F., & Feng, F. (Ed.), *Advanced high strength natural fibre composites in construction* (pp. 59 – 83). Cambridge, England: Woodhead Publishing. doi: 10.1016/B978-0-08-100411-1.00003-0

García, A., Gandini, A., Labidi, J., Belgacem, N., & Bras, J. (2016). Industrial and crop wastes: A new source for nanocellulose biorefinery. *Industrial Crops and Products*, *93*, 26–38. doi:10.1016/j.indcrop.2016.06.004

Hefti, H. (1960). Sodium chlorite bleaching. *Textile Research Journal*, *30*(11), 861–867. doi:10.1177/004051756003001108

Hubbell, C. A., & Ragauskas, A. J. (2010). Effect of acid-chlorite delignification on cellulose degree of polymerization. *Bioresource Technology*, *101*(19), 7410–7415. doi:10.1016/j.biortech.2010.04.029

Huda, M. S., Drzal, L. T., Mohanty, A. K., & Misra, M. (2008). Effect of chemical modifications of the pineapple leaf fiber surfaces on the interfacial and mechanical properties of laminated biocomposites. *Composite Interfaces*, *15*(2–3), 169–191. doi:10.1163/156855408783810920

Kouadri, I., & Satha, H. (2018). Extraction and characterization of cellulose and cellulose nanofibers from citrullus colocynthis seeds. *Industrial Crops & Products*, *124*, 787 – 796. doi:10.1016/j.indcrop.2018.08.051

Lavanya, D., Kulkarni, P., Dixit, M., Raavi, P. K., Krishna, L., & Vamsi, N. (2011). Sources of cellulose and their applications - A review. *International Journal of Drug Formation and Research*, *2*(6), 19-38.

Lee, C. H., Khalina, A., Lee, S. H., Padzil, F. N. M., & Ainun, Z. M. A. (2020). Physical, morphological, structural, thermal and mechanical properties of pineapple leaf fibers. In Jawaid, M., Asim, M., Md. Tahir, P., & Nasir, M. (Ed.), *Green energy and technology* (pp. 91 – 121). Singapore: Springer. doi:10.1007/978-981-15-1416-6_6

Lee, H. V., Hamid, S. B. A., & Zain, S. K. (2014). Conversion of lignocellulosic biomass to nanocellulose: Structure and chemical process. *Scientific World Journal*, *2014*, 1 – 20. doi:10.1155/2014/631013

Listiyani, M. A. D., Campbell, R. E., Miracle, R. E., Barbano, D. M., Gerard, P. D., & Drake, M. A. (2012). Effect of temperature and bleaching agent on bleaching of liquid Cheddar whey. *Journal of Dairy Science*, *95*(1), 36–49. doi:10.3168/jds.2011-4557

Mahardika, M., Abral, H., Kasim, A., Arief, S., & Asrofi, M. (2018). Production of nanocellulose from pineapple leaf fibers via high-shear homogenization and ultrasonication. *Fibers*, *6*(2), 1–12. doi:10.3390/fib6020028

Mishra, S., Mohanty, A. K., Drzal, L. T., Misra, M., & Hinrichsen, G. (2004). A review on pineapple leaf fibers, sisal fibers and their biocomposites. *Macromolecular Materials and Engineering*, *289*(11), 955–974. doi:10.1002/mame.200400132

MPIB. (2010). *Peneraju industri nanas negara*. Johor Bahru, Malaysia: Malaysian Pineapple Industry Board.

Mohamed, A. R., Sapuan, S. M., & Khalina, A. (2014). Mechanical and thermal properties of josapine pineapple leaf fiber (PALF) and PALF-reinforced vinyl ester composites. *Fibers and Polymers*, *15*(5), 1035–1041. doi:10.1007/s12221-014-1035-9

Najeeb, M. I., Sultan, M. T. H., Yoshito Andou, Shah, A. U. M., Kubra Eksiler, Jawaid, M., & Ariffin, A. H. (2020). Characterization of silane treated Malaysian yankee pineapple AC6 leaf fiber (PALF) towards industrial applications. *Journal of Materials Research and Technology,* Article in press, 1-12. doi:10.1016/j.jmrt.2020.01.058

Nordin, N. I. A. A., Ariffin, H., Hassan, M. A., Shirai, Y., Ando, Y., Ibrahim, N. A., & Yunus, W. M. Z. W. (2017). Superheated steam treatment of oil palm mesocarp fiber improved the properties of fiber-polypropylene biocomposite. *BioResources*, *12*(1), 68-81. doi:10.15376/biores.12.1.68-81

Paluvai, N. R., Mohanty, S., & Nayak, S. K. (2015). Studies on thermal degradation and flame retardant behavior of the sisal fiber reinforced unsaturated polyester toughened epoxy nanocomposites. *Journal of Applied Polymer Science*, *132*(24), 15–17. doi:10.1002/app.42068

Prado, K. S., & Spinacé, M. A. S. (2019). Isolation and characterization of cellulose nanocrystals from pineapple crown waste and their potential uses. *International Journal of Biological Macromolecules*, *122*, 410–416. doi:10.1016/j.ijbiomac.2018.10.187

Rambabu, N., Panthapulakkal, S., Sain, M., & Dalai, A. K. (2016). Production of nanocellulose fibers from pinecone biomass: Evaluation and optimization of chemical and mechanical treatment conditions on mechanical properties of nanocellulose films. *Industrial Crops and Products*, *83*, 746–754. doi:10.1016/j.indcrop.2015.11.083

Santos, R. M. dos, Flauzino Neto, W. P., Silvério, H. A., Martins, D. F., Dantas, N. O., & Pasquini, D. (2013). Cellulose nanocrystals from pineapple leaf, a new approach for the reuse of this agro-waste. *Industrial Crops and Products*, *50*, 707–714. doi:10.1016/j.indcrop.2013.08.049

Satha, H., Kouadri, I., & Benachour, D. (2020). Thermal, structural and morphological studies of cellulose and cellulose nanofibers extracted from bitter watermelon of the Cucurbitaceae family. *Journal of Polymers and the Environment*, *28*(7), 1914-1920. doi:10.1007/s10924-020-01735-6

Sena Neto, A. R., Araujo, M. A., Souza, F. V., Mattoso, L. H., & Marconcini, J. M. (2013). Characterization and comparative evaluation of thermal, structural, chemical, mechanical and morphological properties of six pineapple leaf fibre varieties for use in composites. *Industrial Crops and Products, 43*, 529 - 537. doi:10.1016/j.indcrop.2012.08.001

Sindhu, R., Pandey, A., & Binod, P. (2014). Alkaline treatment. In Pandey, A., Negi, S., Binod, P. & Larroche, C. (Ed.), *Pretreatment of biomass: Processes and technologies* (pp. 51–60). Amsterdam, Netherlands: Elsevier. doi:10.1016/B978-0-12-800080-9.00004-9

Shafie, S. M., Mahlia, T. M. I., Masjuki, H. H., & Ahmad-Yazid, A. (2012). A review on electricity generation based on biomass residue in Malaysia. *Renewable and Sustainable Energy Reviews, 16*(8), 5879-5889. doi:10.1016/j.rser.2012.06.031

Sharma, A., Thakur, M., Bhattacharya, M., Mandal, T., & Goswami, S. (2018). Commercial application of cellulose nano-composites – A review. *Biotechnology Reports*, *21*, 1-15. doi:10.1016/j.btre.2019.e00316

Stelte, W. (2013). *Steam explosion for biomass pre-treatment*. Gregersensvej, Denmark: Danish Technological Institute.

Wan Nadirah, W. O., Jawaid, M., Al Masri, A. A., Abdul Khalil, H. P. S., Suhaily, S. S., & Mohamed, A. R. (2012). Cell wall morphology, chemical and thermal analysis of cultivated pineapple leaf fibres for industrial applications. *Journal of Polymers and the Environment*, *20*(2), 404–411. doi:10.1007/s10924-011-0380-7

Wu, Y., Wu, J., Yang, F., Tang, C., & Huang, Q. (2019). Effect of H_2O_2 bleaching treatment on the properties of finished transparent wood. *Polymers*, *11*(5), 1–13. doi:10.3390/polym11050776

Pertanika J. Sci. & Technol. 28 (S2): 149 - 160 (2020)

SCIENCE & TECHNOLOGY

Journal homepage: http://www.pertanika.upm.edu.my/

Physical and Mechanical Study of Palm Oil Fuel Ash (POFA) based Geopolymer as a Stabilizer for Soft Soil

Isam Adnan Khasib[1] and Nik Norsyahariati Nik Daud[1,2]*

[1]Department of Civil Engineering, Faculty of Engineering, Universiti Putra Malaysia, 43400, Serdang, Selangor, Malaysia
[2]Housing Research Center (HRC), Faculty of Engineering, Universiti Putra Malaysia, 43400, Serdang, Selangor, Malaysia

ABSTRACT

Construction of structures on soft soil is a challenging task and considered as one of the biggest concerns in geotechnical engineering. Binders that are environmentally friendly such as fly ash based geopolymer have been explored widely. In this study, the agro-waste material, Palm Oil Fuel Ash (POFA) was used to produce an environmentally friendly geopolymer binder to be used in soft soil stabilization. POFA was used in three ratios; 10%, 20% and 30% of dry weight of soil to produce geopolymer. Sodium hydroxide (NaOH) was used as an alkali activator at 12 molarity along with sodium silicate (Na_2SiO_3). Physical properties of soil (Atterberg Limits, Plasticity Index, and Linear Shrinkage Limit) and compaction assessment; before and after mixing with the geopolymer binder were investigated. The studied soil was classified as an inorganic high plasticity silt (MH), according to the Unified Soil Classification System (USCS). From compaction results; optimum moisture content (OMC) values showed a decreased pattern from 24.7% to 17.5%; and maximum dry density (MDD) increased from 1.37 Mg/m^3 to 1.73 Mg/m^3 for geopolymer with POFA ranging from 0% to 30% of the dry weight of soil, respectively. The optimum dosage of POFA based geopolymer was found to be 30% according to all tests mentioned. These properties suggest the potential use of the agro-waste based geopolymer binder to stabilize the soft soil.

ARTICLE INFO

Article history:
Received: 10 February 2020
Accepted: 13 November 2020
Published: 31 December 2020

DOI: https://doi.org/10.47836/pjst.28.S2.12

E-mail addresses:
essamkasseeb@gmail.com (Isam Adnan Khasib)
niknor@upm.edu.my (Nik Norsyahariati Nik Daud)
* Corresponding author

Keywords: Agro-waste, geopolymer, geotechnical properties, palm oil fuel ash, soft soil, stabilization

INTRODUCTION

Population growth and space limitations make soil improvement necessary to provide a strong underground layer to assist in

ISSN: 0128-7680
e-ISSN: 2231-8526

© Universiti Putra Malaysia Press

infrastructure construction. Expansive and plastic soils are considered a destruction that damages the foundations, roads and water networks, so this is considered a huge challenge to geotechnical engineers.

Stabilization of soil has been widely investigated by many studies using traditional binders such as lime, cement or a combination of both (Asgari et al., 2015; Wang et al., 2018). Although they have shown their effectiveness in soil stabilization, they have some deficiencies. Too much consumption of energy and natural resources for the production process make these binders unsuitable for stabilization as well as their financial and environmental issues. Cement manufacture produces a lot of CO_2 emissions, and CO_2 has been proven to be one of the main causes of global warming and high temperature associated (Gartner, 2004; Matthews et al., 2009). It was indicated that for producing 1 ton of cement, nearly 1 ton of CO_2 was emitted (Du et al., 2016). Moreover, CO_2 emitted due to cement production forms around 7% of the total greenhouse gases in the atmosphere (Criado et al., 2007).

Other cementitious materials used in stabilization include aluminosilicate materials such as fly ash. The intent of using fly ash in soil stabilization is for industrial wastes disposal and the good strength associated when applied to the soil. Kolias et al. (2005) studied the effectiveness of using high calcium fly ash along with cement in high and low plastic clay soils stabilization and the results showed that tensile, compressive and flexural strength, modulus of elasticity was enhanced. The main types of fly ash are class C and class F fly ash. Nalbantoğlu (2004) used class C fly ash to stabilize expansive soil and after laboratory testing, the results indicated that class C fly ash reduced clay size particles, plasticity index and the swell potential which led to texture and plasticity improvement of soil. In addition to that, class F fly ash has been investigated to stabilize sandy soil to be used as base layers in highways when combined with cement since it cannot be used alone due to low reactivity with soil (Arora & Aydilek, 2005). By-products agricultural wastes such as palm oil fuel ash (POFA) has shown its capability as good binder in soil stabilization. POFA has proven it's possibility to replace the use of cement in stabilization of peat soil based on unconfined compression tests since it has shown high strength comparing to cement stabilized soil (Ahmad et al., 2011). Moreover, Nik Daud et al. (2018) investigated both agricultural wastes, palm oil fuel ash and rice husk ash and they had shown their effectiveness in stabilization in terms of physical properties and optimum conditions of soil.

However; in recent years, researchers started looking for binders that could provide better strength, replacing the disadvantages of traditional binders and be environmental friendly at the same time. They came up with the idea of what was called geopolymer to be considered as the next generation. Geopolymer can be defined as an inorganic polymer mainly from Al and Si with 3D cross-linked polysialate chains structure with an empirical formula of M_n [-(SiO_2) z-AlO_2] H_2O, where M is an alkali cation, z is the Si/Al molar ratio, n is the polymerization degree (Duxson et al., 2007).

Alkali activation process happens when adding an alkali activator such as NaOH, KOH, Na_2SiO_3, K_2SiO_3 or a combination of them to the fly ash and the result is called alkali activated material or geopolymer. The need of a liquid alkali activator is to dissolve the aluminum (Al) and silicon (Si) found in fly ash to help in the geopolymerization process by forming aluminosilicate gels (Pourakbar et al., 2016). Factors affecting geopolymer characteristics and strength include type and chemical composition of aluminosilicate material used, type and molarity of alkali activator, alkali activator to aluminosilicate material ratio, curing time and curing temperature. Preparation and physical structure of different types of fly ash based geopolymer corresponding to their expected compressive strength as well as their applications have been reported (Zhuang et al., 2016). In recent years, many researches started investigating the feasibility of using aluminosilicate materials in producing geopolymer to be used to stabilize the soft soil (Phetchuay et al., 2016; Phummiphan et al., 2016). Rivera et al. (2020) studied clay soil stabilization using alkali activated fly ash (two types of fly ash) mixed with granulated blast-furnace slag (GBFS) and lime; and tested for unconfined compressive strength (UCS), flexural strength (FS) and durability where NaOH and Na_2SiO_3 were used as alkaline activator. Moreover, Teing et al. (2019) investigated the efficiency of using alkali activated fly ash at high percentages in stabilization of residual soil using unconfined compressive strength, scanning electron microscope (SEM) and energy dispersive X-ray spectroscopy (EDX) tests. Furthermore, fly ash along with coir fibers in an alkaline environment have been used to stabilize soft soil for subgrade applications (Tan et al., 2019). A comparative study made using fly ash in stabilizing soil with and without alkali activator found that strength of alkali activated fly ash was increased from 0.3 to 2.8 MPa at 28 days (Rios et al., 2016).

In very limited trials, agricultural wastes based geopolymer such as Palm oil fuel ash (POFA) based geopolymer have been employed in stabilization of clayey soil. Pourakbar et al. (2015) used alkali activated palm oil fuel ash to stabilize high plasticity clay and it was concluded that alkali activated agricultural waste was an efficient binder that could extinguish the use of cement and be environmentally friendly at the same time. Also, Sukmak et al. (2017) studied strength and microstructural properties of soil stabilized with POFA based geopolymer to find the optimum ratios of alkali activator and POFA. However, most research efforts focused on the microstructural properties of POFA based geopolymer stabilized soil such as scanning electron microscope (SEM), fourier transform infrared (FTIR) and X-ray diffraction tests; and mechanical properties such as unconfined compressive strength. For a better understanding of stabilization with POFA based geopolymer, identification of physical properties (liquid limit, plastic limit and shrinkage limit); and pH of soft soil stabilized with POFA based geopolymer is required. Plasticity is known to have a huge influence on soil stabilized performance (Little & Nair, 2009). Therefore, such agricultural waste geopolymer binder should be clearly studied to understand its impact on the properties of soft soil.

The primary aim of this researh was to investigate the effectiveness of using POFA as an agro-waste based geopolymer binder to stabilize soft soil. Due to that matter, physical and chemical properties of soft soil before and after treatment with POFA based geopolymer had been investigated to identify the feasibility of using such binder in soil stabilization. Furthermore, optimum conditions of soil; optimum moisture content (OMC) and maximum dry density (MDD) of treated and untreated soil with POFA based geopolymer would be determined by compaction behavior.

MATERIALS AND METHODS

The materials used to produce POFA based geopolymer in this research were: Palm oil fuel ash (POFA) and alkali activators; sodium silicate (Na_2SiO_3) and sodium hydroxide (NaOH). POFA was obtained from Tenaga Sulpom Sdn Bhd, Selangor, Malaysia; and it was a residue after the burning of palm oil fibers and bunches in furnace to generate electricity and the waste generated named as POFA. Alkali activators were provided by a chemical supplier in Kuala Lumpur, Malaysia; NaOH was provided in pellets while Na_2SiO_3 was in liquid phase.

Soil Sample

The soil sample used in this study was categorized as a residual soil. Residual soil is a soil in which parent material has decomposed in situ. The soil was naturally dried and an oven was used to remove any moisture content before the testing process was carried out. After drying, the soil was separated manually using a small hammer and mechanically with a soil grinder to be ready for physical properties, pH and compaction tests.

Palm Oil Fuel Ash (POFA)

POFA was dried in the oven at 110 ± 5°C inside the laboratory. After drying, POFA was sieved using 300 µm sieve to remove large and not fully combusted materials. Since particles size of POFA highly affects the strength of POFA based geopolymer, a smaller size of particles should be obtained (Sharma et al., 2019). Therefore, after sieving the dried POFA, it was pulverized using Los Angeles abrasion machine by rotating the drum 30,000 cycles as shown in Figure 1 (Ranjbar et al., 2014). The prepared POFA was kept sealed in order not to get any moisture content from the surrounding that may affect stabilization process.

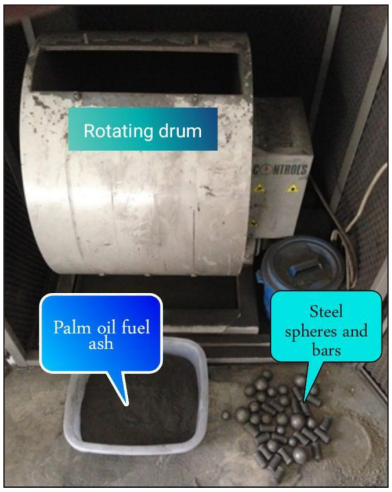

Figure 1. Los Angeles abrasion machine used in the study

Alkaline Activators

In this study, sodium silicate (Na_2SiO_3) and sodium hydroxide (NaOH) were used as alkali activators (L). Sodium hydroxide (NaOH) was dissolved in distilled water to prepare a 12-molarity sodium hydroxide (NaOH) solution. The solution was kept for 24 hours before it was mixed with sodium silicate (Na_2SiO_3). Since the molarity of the alkali solution was very high, the preparation was handled with gloves and mask.

POFA Based Geopolymer

Palm oil fuel ash was mixed with sodium silicate (Na_2SiO_3) and sodium hydroxide (NaOH). Ratio of sodium silicate to sodium hydroxide used was 2.5 and ratio of POFA to liquid alkali activator (L) which is combined between Na_2SiO_3 and NaOH was 1.32. These ratios were kept invariables during testing to investigate the feasibility of increasing geopolymer dosage and its effect on soil properties. After preparation of POFA and L in the proper weights, they were mixed inside a mixer for 10 minutes at a slow mode to produce a homogenous geopolymer. POFA based geopolymer before application to soil is shown in Figure 2.

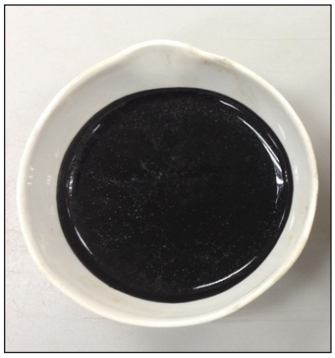

Figure 2. POFA based geopolymer using 10% POFA material

Sample Preparation and Characterization Tests

Three POFA based geopolymer mixes were prepared and poured into soil. These mixes were prepared using POFA to be 10%, 20% and 30% of the dry weight of soil and then calculating the required quantities of NaOH and Na_2SiO_3 to produce the geopolymer before the application to soil. Table 1 illustrates the calculated weights of alkali activators (L); NaOH, Na_2SiO_3 and POFA used for 1 kilogram of dry soil. After geopolymer preparation, the soil was added to the geopolymer and mixed for another 10 minutes to ensure that the mixture is homogenous and then tested immediately. For testing methods, Physical properties of soil including Atterberg limits (liquid limit; LL and plastic limit; PL) and linear shrinkage limit were tested in accordance to British standard (British Standard Institution, 1990) before and after application of POFA based geopolymer to soil. Optimum moisture content (OMC) and maximum dry density (MDD) were investigated according to British Standard (British Standard Institution, 1990) by standard proctor compaction test. Moreover, pH of natural soil and treated samples had been studied using pH meter after curing for 8 hours to know the effect of alkali activator on soil's acidity and alkalinity before and after treatment.

Table 1
Geopolymer ingredients for each 1 kg of soil

# of geopolymer mixture	POFA (%)	POFA (g)	L (g)	NaOH (g)	Na_2SiO_3 (g)
1	10	100	76.9	22	54.9
2	20	200	153.8	44	109.8
3	30	300	230.8	66	164.8

Note. POFA – palm oil fuel ash; L – Liquid alkali activator, NaOH – sodium hydroxide, Na_2SiO_3 – sodium silicate

RESULTS AND DISSCUSION

Physical and Chemical Properties of POFA Based Geopolymer Stabilized Soil

The basic characteristics of soil before any treatment are illustrated in Table 2. According to Unified Soil Classification System (USCS), the soil was classified as inorganic high plasticity silt (MH) with liquid and plastic limits values are 50.8% and 31.5%, respectively. Figure 3 shows the particle size distribution of the soil examined with percent of passing sieve no. 200 is 52.2%. Although this type is not the most critical type of soil, it is still one of the challenges to geotechnical engineers. The chemical composition of POFA using XRF test is illustrated in Table 3**.** pH of untreated soil was 4.01 (as shown in Table 2) which indicates a strong acidic behavior, and this is due to the agricultural activities accompanying with the heavy use of fertilizers at the sample's location. According to the results shown in Table 4, liquid limit and plastic limit for the treated soil have shown a consistent behavior. Liquid limit and plastic limit increased almost steadily when increasing the dosage of POFA based geopolymer comparing to the untreated soil. This refers to the small particles' size of POFA mixed with the soil which results in high specific surface area of the particles. Therefore, increasing the surface area will increase the required water to cover the particles, resulting in liquid and plastic limit's increase (Taha, 2009).

Table 2
Physical properties of studied soil

Soil property	Unit	Standard	Value
pH	-	BS 1377: Part 3	4.01
Initial moisture content	%	BS 1377: Part 2	30.8
Specific gravity	-	BS 1377: Part 2	2.62
Plastic limit	%	BS 1377: Part 2	31.5
Liquid limit	%	BS 1377: Part 2	50.8
Shrinkage limit	%	BS 1377: Part 2	5.4
Optimum moisture content	%	BS 1377: Part 4	24.7
Maximum dry density	Mg/m^3	BS 1377: Part 4	1.37

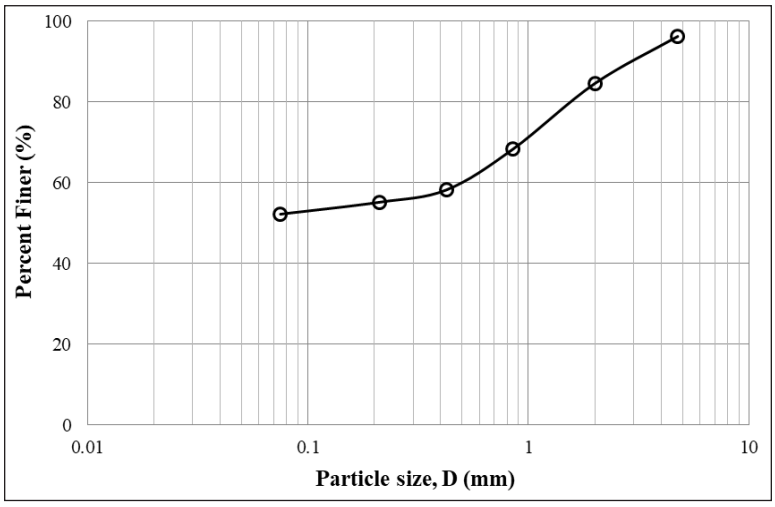

Figure 3. Particle size distribution curve of studied soil

Table 3
Chemical composition of POFA using XRF test

Component	%
Silicon dioxide (SiO_2)	42.23
Aluminum oxide (Al_2O_3)	16.88
Calcium oxide (CaO)	12.1
Potassium oxide (K_2O)	9.56
Sodium oxide (Na_2O)	5.83
Iron oxide (Fe_2O_3)	2.76
Magnesium oxide (MgO)	1.31

Table 4
Physical and chemical properties of soil treated with POFA – based geopolymer

Properties	Unit	Geopolymer in soil (%)			
		0	10	20	30
Plastic limit	%	31.5	34.6	38.3	40.1
Liquid limit	%	50.8	53.4	57.5	59.2
Shrinkage limit	%	5.4	5.2	4.7	4.5
Plasticity index	%	19.3	18.8	19.2	19.1
pH	-	4.01	12.8	13.92	14.0

However, some variations were exhibited regarding the plasticity index values. The highest value of plasticity index, which is the difference between, and liquid and plastic limits appeared in untreated soil and the lowest value was found to be at 10% POFA mixture.

The linear shrinkage limit decreased while increasing the percentage of geopolymer in the soil. The shrinkage value of untreated soil was 5.4% and then started to decrease

by adding POFA based geopolymer. In particular, this reduction in shrinkage was mainly contributed by the strong bonding – geopolymer cementitious bonds combine soil particles together- and well arrangement of POFA within the soil particles in the existence of an alkali activator which works as a lubricant to facilitate the integration of geopolymer with soil resulting in low shrinkage limit.

Mixing soil with POFA based geopolymer produced a strong increase in pH, ranging from 12.8 until 14.0 for geopolymer-soil mixture with POFA ranging from 10% to 30% of soil dry weight. Clearly, this increase in pH reflects the ability of hydroxide ions (OH-) found in the alkali activator to generate the hydrolysis of alumina-silicate bonds in the geopolymer by increasing the value of pH to assist in the condensation reactions (Abdullah et al., 2020). The minimum pH value needed to sustain the geopolymerization process is 11 (Garcia-Lodeiro et al., 2015); in this study all values of pH were above 11, this indicates that geopolymerization process is effective and takes a place.

Liquid limit and plasticity index values for all samples tested were plotted on plasticity index chart as indicated in Figure 4. It shows that there was no considerable effect on the class of the original soil sample since all samples lie under A-line (soil was MH and remained MH before and after treatment). Also, it can be clearly observed that there was no noticeable change in plasticity index value.

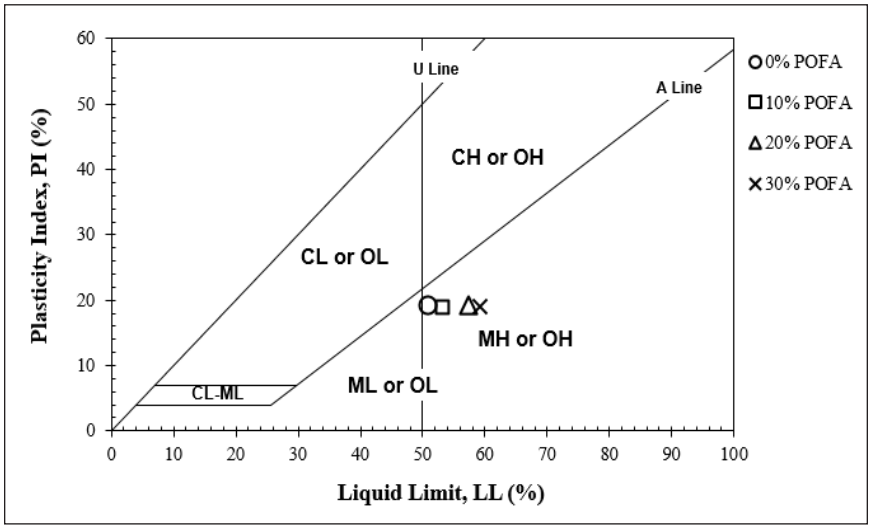

Figure 4. Plasticity index chart

Compaction Behavior

Figure 5 shows the moisture content and dry density relationship for untreated soil and treated samples. According to the curves, optimum moisture content (OMC) shows a decreasing pattern while maximum dry density (MDD) reveals an increment when

increasing the geopolymer dosage. When POFA in the geopolymer mix increased from 0% to 30% of dry weight of soil, MDD increased from 1.37 Mg/m^3 to 1.73 Mg/m^3 and OMC decreased from 24.7% reaching to 17.5%. Undoubtedly, this is due to the effects of alkali activators used to produce the geopolymer mix since they performed as a lubricant that reduced the friction and repulsion forces; and improved sliding between soil particles which increased the dry density. Also, lubrication effect reduced the amount of free water required to obtain the optimum conditions, resulting in lower optimum moisture content.

Geopolymer with 30% POFA of the dry weight of soil showed the optimum conditions regarding maximum dry density and optimum moisture content between all treated samples with values 1.73 Mg/m^3 and 17.5%, respectively. This outcome was expected since the maximum quantity of alkaline activators were added in this mixture and could dissolve most of silicon and aluminum present in the POFA and soil compared to other dosages, leading to better OMC and MDD (Cristelo et al., 2011). Table 5 depicts the exact values of optimum moisture content and maximum dry density of the treated and untreated samples.

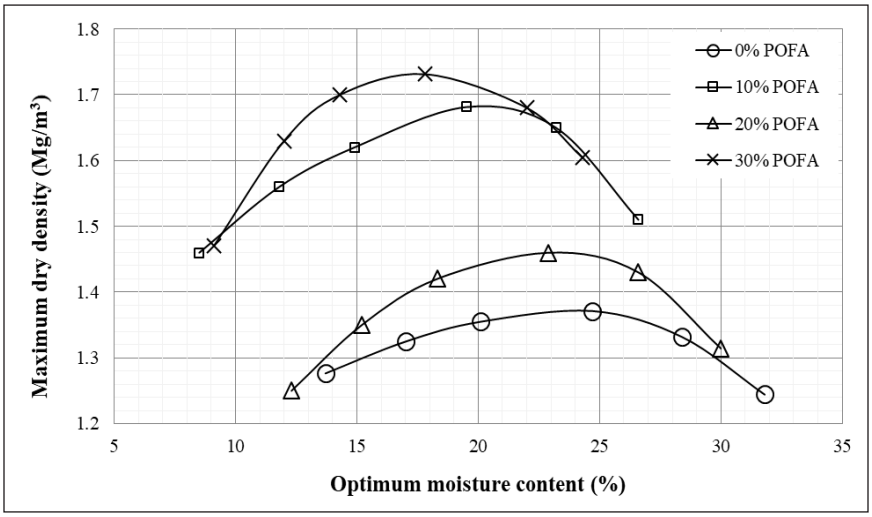

Figure 5. Maximum dry density and optimum moisture content curves of untreated and treated soil

Table 5
Compaction properties of treated and untreated soil

Parameter	Unit	Geopolymer (%)			
		0	10	20	30
OMC	%	24.7	23.0	20.3	17.5
MDD	Mg/m^3	1.37	1.48	1.68	1.73

Note: OMC – optimum moisture content, MDD – maximum dry density

CONCLUSION

This paper has described the effectiveness of using POFA as an agro-waste based geopolymer binder to stabilize soft soil. It can be concluded that POFA based geopolymer can be considered a potential binder to be used in soil stabilization. Treated soil has shown to have better plasticity behavior after mixed with geopolymer. Palm oil fuel ash based geopolymer has improved physical properties of soil including Atterberg limits, optimum moisture content and maximum dry density. It was realized that there were some changes in values of each property studied especially in the determination of optimum conditions of the treated soil. Finally, this study suggested the applicability of using agro-waste based geopolymer binder to stabilize the soft soil.

ACKNOWLEDGEMENT

The authors would like to express deep gratitude for the technical and financial support offered by the Civil Engineering Department, Engineering Faculty, Universiti Putra Malaysia.

REFERENCES

Abdullah, H. H., Shahin, M. A., Walske, M. L., & Karrech, A. (2020). Systematic approach to assessing the applicability of fly-ash based geopolymer for clay stabilization. *Canadian Geotechnical Journal*, *57*(9), 1356-1368. doi:10.1139/cgj-2019-0215

Ahmad, J., Abdul Rahman, A. S., Mohd Ali, M. R., & Khif, K. F. (2011, December 5-6). Peat soil treatment using POFA. In *2011 IEEE Colloquium on Humanities, Science and Engineering Research* (pp. 66–70). Penang, Malaysia. doi:10.1109/CHUSER.2011.6163816

Arora, S., & Aydilek, A. H. (2005). Class F fly-ash-amended soils as highway base materials. *Journal of Materials in Civil Engineering*, *17*(6), 640–649. doi:10.1061/(asce)0899-1561(2005)17:6(640)

Asgari, M. R., Baghebanzadeh Dezfuli, A., & Bayat, M. (2015). Experimental study on stabilization of a low plasticity clayey soil with cement/lime. *Arabian Journal of Geosciences*, *8*(3), 1439–1452. doi:10.1007/s12517-013-1173-1

British Standard Institution (1990). *BS 1377: 1990. Method of test for soils for civil engineering purposes. Part 5: Compressibility, permeability and durability test*. London, United Kingdom: British Standards Institute.

Criado, M., Fernández-Jiménez, A., de la Torre, A. G., Aranda, M. A. G., & Palomo, A. (2007). An XRD study of the effect of the SiO2/Na2O ratio on the alkali activation of fly ash. *Cement and Concrete Research*, *37*(5), 671–679. doi:10.1016/j.cemconres.2007.01.013

Cristelo, N., Glendinning, S., & Teixeira Pinto, A. (2011). Deep soft soil improvement by alkaline activation. *Proceedings of the Institution of Civil Engineers: Ground Improvement*, *164*(2), 73–82. doi:10.1680/grim.900032

Du, Y. J., Bo, Y. L., Jin, F., & Liu, C. Y. (2016). Durability of reactive magnesia-activated slag-stabilized low plasticity clay subjected to drying-wetting cycle. *European Journal of Environmental and Civil Engineering*, *20*(2), 215–230. doi:10.1080/19648189.2015.1030088

Duxson, P., Fernández-Jiménez, A., Provis, J. L., Lukey, G. C., Palomo, A., & Van Deventer, J. S. J. (2007). Geopolymer technology: The current state of the art. *Journal of Materials Science*, *42*(9), 2917–2933. doi:10.1007/s10853-006-0637-z

Garcia-Lodeiro, I., Palomo, A., & Ernandez-Jimenez, A. F. (2015). Crucial insights on the mix design of alkali-activated cement-based binders. In Pacheco-Torgal, F., Labrincha, J., Leonelli, C., Paloma, A. and Chindaprasit, P. (Ed.), *Handbook of alkali-activated cements, mortars and concretes* (pp. 49-74). Cambridge, United Kingdom: Woodhead Publishing. doi:10.1533/9781782422884.1.49

Gartner, E. (2004). Industrially interesting approaches to "low-CO_2" cements. *Cement and Concrete Research*, *34*(9), 1489–1498. doi:10.1016/j.cemconres.2004.01.021

Kolias, S., Kasselouri-Rigopoulou, V., & Karahalios, A. (2005). Stabilisation of clayey soils with high calcium fly ash and cement. *Cement and Concrete Composites*, *27*(2), 301–313. doi:10.1016/j.cemconcomp.2004.02.019

Little, D., & Nair, S. (2009). *Recommended practice for stabilization of subgrade soils and base materials.* Texas, USA: National Cooperative Highway Research Program, Transportation Research Board of the National Academies. doi:10.17226/22999

Matthews, H. D., Gillett, N. P., Stott, P. A., & Zickfeld, K. (2009). The proportionality of global warming to cumulative carbon emissions. *Nature*, *459*(7248), 829–832. doi:10.1038/nature08047

Nalbantoğlu, Z. (2004). Effectiveness of class C fly ash as an expansive soil stabilizer. *Construction and Building Materials*, *18*(6), 377–381. doi:10.1016/j.conbuildmat.2004.03.011

Nik Daud, N. N., Sadan, N. A., Adesiji, R., & Anijiofor, S. C. (2018, November 7-9). Soil properties of residual soil mixed with agricultural waste ashes. In *Proceeding of 1st International Civil Engineering Conference* (pp. 165-169). Minna, Nigeria

Phetchuay, C., Horpibulsuk, S., Arulrajah, A., Suksiripattanapong, C., & Udomchai, A. (2016). Strength development in soft marine clay stabilized by fly ash and calcium carbide residue based geopolymer. *Applied Clay Science, 127-128,* 134-142. doi:10.1016/j.clay.2016.04.005

Phummiphan, I., Horpibulsuk, S., Sukmak, P., Chinkulkijniwat, A., Arulrajah, A., & Shen, S. L. (2016). Stabilisation of marginal lateritic soil using high calcium fly ash-based geopolymer. *Road Materials and Pavement Design*, *17*(4), 877–891. doi:10.1080/14680629.2015.1132632

Pourakbar, S., Asadi, A., Huat, B. B. K., & Fasihnikoutalab, M. H. (2015). Soil stabilisation with alkali-activated agro-waste. *Environmental Geotechnics*, *2*(6), 359–370. doi:10.1680/envgeo.15.00009

Pourakbar, S., Huat, B. B. K., Asadi, A., & Fasihnikoutalab, M. H. (2016). Model study of alkali-activated waste binder for soil stabilization. *International Journal of Geosynthetics and Ground Engineering*, *2*(4), 1-12. doi:10.1007/s40891-016-0075-1

Ranjbar, N., Mehrali, M., Behnia, A., Alengaram, U. J., & Jumaat, M. Z. (2014). Compressive strength and microstructural analysis of fly ash/palm oil fuel ash based geopolymer mortar. *Materials and Design*, *59*, 532–539. doi:10.1016/j.matdes.2014.03.037

Rios, S., Cristelo, N., da Fonseca, A. V., & Ferreira, C. (2016). Structural performance of alkali-activated soil ash versus soil cement. *Journal of Materials in Civil Engineering*, *28*(2), 1–11. doi:10.1061/(asce)mt.1943-5533.0001398

Rivera, J. F., Orobio, A., Mejía de Gutiérrez, R., & Cristelo, N. (2020). Clayey soil stabilization using alkali-activated cementitious materials. *Materiales de Construcción*, *70*(337), 1-12. doi:10.3989/mc.2020.07519

Sharma, P. K., Singh, J. P., & Kumar, A. (2019). Effect of particle size on physical and mechanical properties of fly ash based geopolymers. *Transactions of the Indian Institute of Metals*, *72*(5), 1323–1337. doi:10.1007/s12666-019-01628-w

Sukmak, P., Sukmak, G., Horpibulsuk, S., Setkit, M., Kassawat, S., & Arulrajah, A. (2017). Palm oil fuel ash-soft soil geopolymer for subgrade applications: Strength and microstructural evaluation. *Road Materials and Pavement Design*, *20*(1), 110–131. doi:10.1080/14680629.2017.1375967

Taha, M. R. (2009). Geotechnical properties of soil-ball milled soil mixtures. In Bittnar, Z., Bartos, P. J. M., Nemecek, J., Smilauer, V., & Zeman, J. (Ed.), *Nanotechnology in Construction 3* (pp. 377-382). Berlin, Germany: Springer. doi:10.1007/978-3-642-00980-8_51

Tan, T., Huat, B. B. K., Anggraini, V., Shukla, S. K., Tan, T., Huat, B. B. K., ... & Nahazanan, H. (2019). Strength behavior of fly ash-stabilized soil reinforced with coir fibers in alkaline environment. *Journal of Natural Fibers*, 1–14. doi:10.1080/15440478.2019.1691701

Teing, T. T., Huat, B. B. K., Shukla, S. K., Anggraini, V., & Nahazanan, H. (2019). Effects of alkali-activated waste binder in soil. *International Journal of GEOMATE, 17*(59), 82–89. doi:10.21660/2019.59.8161

Wang, D., Zentar, R., & Abriak, N. E. (2018). Durability and swelling of solidified/stabilized dredged marine soils with class-F fly ash, cement, and lime. *Journal of Materials in Civil Engineering*, *30*(3), 1–12. doi:10.1061/(asce)mt.1943-5533.0002187

Zhuang, X. Y., Chen, L., Komarneni, S., Zhou, C. H., Tong, D. S., Yang, H. M., ... & Wang, H. (2016). Fly ash-based geopolymer: Clean production, properties and applications. *Journal of Cleaner Production*, *125,* 253–267. doi:10.1016/j.jclepro.2016.03.019

Pertanika J. Sci. & Technol. 28 (S2): 161 - 172 (2020)

SCIENCE & TECHNOLOGY

Journal homepage: http://www.pertanika.upm.edu.my/

Deep Learning Object Detector Using a Combination of Convolutional Neural Network (CNN) Architecture (MiniVGGNet) and Classic Object Detection Algorithm

Asmida Ismail[1, 3]*, Siti Anom Ahmad[1,4]*, Azura Che Soh[1], Mohd Khair Hassan[1] and Hazreen Haizi Harith[2]

[1]Department of Electrical and Electronic Engineering, Faculty of Engineering, Universiti Putra Malaysia, 43400, Serdang, Malaysia
[2]Department of Biological and Agricultural Engineering, Faculty of Engineering, Universiti Putra Malaysia, 43400, Serdang, Malaysia
[3]Department of Engineering Technology, Faculty of Technical and Vocational, Universiti Pendidikan Sultan Idris, 35900, Tanjung Malim, Malaysia
[4]Malaysia Research Institute on Ageing (MyAgeing™), Universiti Putra Malaysia, 43400, Serdang, Malaysia

ABSTRACT

The object detection system is a computer technology related to image processing and computer vision that detects instances of semantic objects of a certain class in digital images and videos. The system consists of two main processes, which are classification and detection. Once an object instance has been classified and detected, it is possible to obtain further information, including recognizes the specific instance, track the object over an image sequence and extract further information about the object and the scene. This paper presented an analysis performance of deep learning object detector by combining a deep learning Convolutional Neural Network (CNN) for object classification and applies classic object detection algorithms to devise our own deep learning object detector. MiniVGGNet is an architecture network used to train an object classification, and the data used for this purpose was collected from specific indoor environment building. For object detection, sliding windows and image pyramids were used to localize and detect objects at different locations, and non-maxima suppression (NMS) was used to obtain the final bounding box to localize the object location. Based on the experiment result, the percentage of classification accuracy of the network is 80% to 90% and the time

ARTICLE INFO

Article history:
Received: 10 February 2020
Accepted: 13 November 2020
Published: 31 December 2020

DOI: https://doi.org/10.47836/pjst.28.S2.13

E-mail addresses:
asmida@ftv.upsi.edu.my (Asmida Ismail)
sanom@upm.edu.my (Siti Anom Ahmad)
azuracs@upm.edu.my (Azura Che Soh)
khair@upm.edu.my (Mohd Khair Hassan)
hazreen@upm.edu.my (Hazreen Haizi Harith)
* Corresponding author

ISSN: 0128-7680
e-ISSN: 2231-8526

© Universiti Putra Malaysia Press

for the system to detect the object is less than 15sec/frame. Experimental results show that there are reasonable and efficient to combine classic object detection method with a deep learning classification approach. The performance of this method can work in some specific use cases and effectively solving the problem of the inaccurate classification and detection of typical features.

Keywords: Classification, convolutional neural network, deep learning, detection, miniVGGNet

INTRODUCTION

In any task, such as image recognition, object detection and neural language processing, deep learning has recently achieved superior performance (Zhao et al., 2017). The object detection system is used to detect and locate particular substances or things by determining the type or class of the object. It is a computer technology related to computer vision and image processing that recognizes instances of semantic objects in digital images and videos. Typically, there are two steps included in an object detector system framework, which is object classification component and object detection component. Object classification and detection are applied in many computer vision fields, including image retrieval, surveillance, security, machine inspection, and automated vehicle systems (Subhi & Ali, 2019, 2018; Subhi et al., 2018, 2019a, 2019b; Vahab et al., 2019).

Classification is a method of separating a target object from all the other categories and making representations more hierarchical, semantic, and informative for visual recognition. In conventional classification methods, the image characteristics are typically carefully hand-crafted to optimise the distinction capability. A variety of hand-crafted designed features have been explored beforehand such as SIFT (Lowe, 2004), the histogram of gradient oriented, HOG (Dalal et al., 2005) and Haar-like (Lienhart & Maydt, 2002). These hand-designed features, however, are not learnt from the essence of data and are subjective to designer interpretation. Due to the variety of appearances, lighting conditions and backgrounds, it is difficult to construct a comprehensive feature descriptor manually in order to define all kinds of objects perfectly. Usually, there is a classifier used to classify an object in an image such as Supported Vector Machine (SVM) (Lewes, 2015), Deformable Part-based Model (DPM) (Felzenszwalb et al., 2010) and AdaBoost (Freund & Schapire, 1997).

Object detection is one of the computer vision's fundamental problems. It classifies each object in an image and uses 2D rectangular bounding box to label the position of the object. There are some classical algorithm for object detection used to detect an object such as Viola-Jones object detection (Wang, 2014), SVM classification with HOG features (Sugiarto et al., 2017), image segmentation and blob analysis (Patil et al., 2015) and image segmentation using background subtraction algorithms (Shaikh et al., 2014). Most of these approaches, however, are standardised and not robust for the various data varieties. By

extracting feature descriptors using the traditional vision algorithm, the system needs to process an object in the camera feed for about 30 seconds to 1 minute and just allowing not more than 70% classification accuracy (Lee, 2015). With the advent of deep learning technology, algorithms for image-based object detection such as Faster R-CNN (Ren et al., 2016), SSD (Liu et al., 2016), YOLO (Redmon & Farhadi, 2017), and Mask R-CNN (He et al., 2018) were used to achieve extremely high accuracy in an object detection system. However, this end-to-end object detection algorithm is computational complex and required a powerful GPU for training the data.

This paper will combine a deep learning algorithm for image classification and classic object detection algorithm to devise our own deep learning object detector. CNN architecture was used to train a network for object classification and a combination of sliding windows, image pyramids and NMS was used for object detection purposes.

The paper is structured as follows: the next section will explain the materials and overall methods followed by results analysis and discussions, and the paper will be concluded in the final section.

MATERIALS AND METHODS

Overall System

Figure 1 shows the overall object detector system using a combination of the convolutional neural network (CNN) architecture (miniVGGNet) and classical object detection algorithm. The processes consist of multiple steps, which are the combination of the building image dataset, followed by an object classification algorithm and ended with an object detection method.

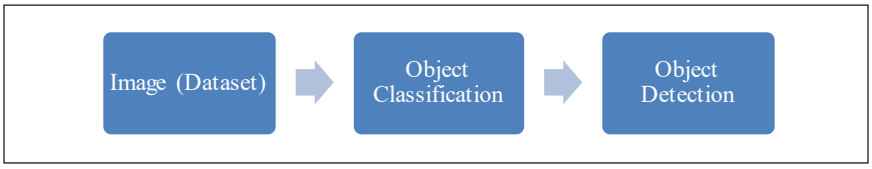

Figure 1. Overall System of an object detector

Building Dataset

Gathering an initial dataset is the first step to creating a deep learning network. The images must be labeled and connected to each others in the same classes. The number of images should be roughly standardised for each class. In this research, data were collected from the real environment field for classification purposes. The data was collected in the fully furnished student residence and was named as an INDOOR dataset.

Figure 2 indicates the random images of INDOOR datasets. The INDOOR dataset consists of 840 images, 32 x 32 x 3 (RGB) in size, resulting in 3072 elements of vector

dimensionality. It consists of 14 classes, including bed, chair, cupboard, door, fan, kitchen cabinet, microwave, rack, refrigerator, shower, sink, table study, toilet bowl and washing machine. The dataset contains of 630 training images and 210 test images. From each class, the train and test images are randomly selected.

Figure 2. INDOOR dataset

Object Classification

Figure 3 displays the process of building an image classification model using deep learning CNN. The processes are made up of several phases which are pre-processing of images, dataset splitting, network training and tuning hyperparameter value.

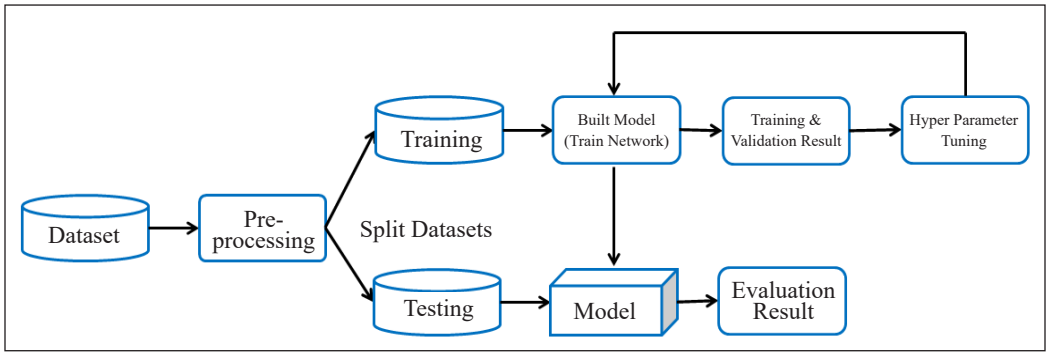

Figure 3. Object classification algorithm – method for building object classification model using deep learning CNN

Pre-processing

Some pre-processing steps could be performed before the model of deep learning is equipped. The images must be scaled to 32 x 32 pixels to ensure the dimensions and aspect ratio is the same. The images provided to the input layer should be square before the model construction. The next step, after the image has been resized is to apply channel ordering. The depth is the number of channels on the image or the number of filters in the layers of CNN architecture. The ordering of dimensions defined the form of the input and used it in the image to learn multi-level features.

Dataset Splitting

The dataset must be divided into two parts: a training set, and a test set. The classifier uses a training set to "learn" what each class looks likes by predicting the input data, and then correcting the data on its own when predictions are incorrect. Once the classifier model has been trained, a test set is used to assess the classifier performance. It is important to ensure that the training set and test set are separate and not overlap with each other.

Network Training

The network will be trained from the images training dataset. The network must learn how to classify each of the classes in the labeled data from the training process. When the network makes an error it learns from the mistakes and improves itself. A simple CNN that accepts an input uses a convolution layer, then an activation layer, followed by fully connected layer, and finally a softmax classifier to obtain classification probabilities. The CNN network architecture used in this paper to create a classification model is miniVGGNet. MiniVGGNet generally consists of two sets of CONV => ACT => CONV => ACT => POOL layers, followed by a set of FC => ACT => FC => SOFTMAX layers. Of these layer types, the only layers containing parameters that are learned during the course of training are CONV and FC. ACT layers are also used in the network to make the architecture explicit. POOL layers are important as CONV and FC because they have a major impact on the spatial dimensions of the image as it passes through CNN.

The detailed architecture of the network is shown in Table 1, where the size of the initial input image is 32 x 32 x 3 and will be training on INDOOR dataset.

Based on Table 1, 32 filters with each of size 3 x 3 will learn on the first two CONV layers. The following layers of CONV will learn 64 filters, with each 3 x 3 in size. Over a 2 x 2 window with a 2 x 2 stage, POOL layers perform max pooling. RELU is an activation element (ACT) used in this architecture.

Table 1
MiniVGGNet architecture design review

Layer Type	Output Size	Filter Size/ Stride
INPUT IMAGE	32 × 32 × 3	
CONV	32 × 32 × 32	3 × 3, K=32
ACT	32 × 32 × 32	
CONV	32 × 32 × 32	3 × 3, K=32
ACT	32 × 32 × 32	
POOL	16 × 16 × 32	2 × 2
DROPOUT	16 × 16 × 32	
CONV	16 × 16 × 64	3 × 3, K=64
ACT	16 × 16 × 64	

Table 1 (*continue*)

Layer Type	Output Size	Filter Size/ Stride
CONV	16 × 16 × 64	3 × 3, K=64
ACT	16 × 16 × 64	
POOL	8 × 8 × 64	2 × 2
DROPOUT	8 × 8 × 64	
FC	512	
ACT	512	
DROPOUT	512	
FC	10	
SOFTMAX	10	

Note. Sizes of output volume are included for each layer, together with convolutional filter size/pool size.

Hyperparameter Tuning

To extrapolate different data patterns, the machine learning model may require different constraints, weights, or learning rates. These measures are called hyperparameters, and these parameters need to be tuned to enhance the model's accuracy and solve the machine learning problem optimally. Hyperparameter tuning uses an ordered list of hyperparameter components - optimal model, which reduces the predefined loss function of independent data. In this paper, the different value of learning rate decay was modified, and batch normalization layers were applied to the networks to compare the network performance.

Based on Figure 4, the coloured boxes indicate the final value that had been choosing for the classification model. The value of 07.5 was chosen as a learning rate decay factor value because it was based on the highest classification accuracy of training and validation results.

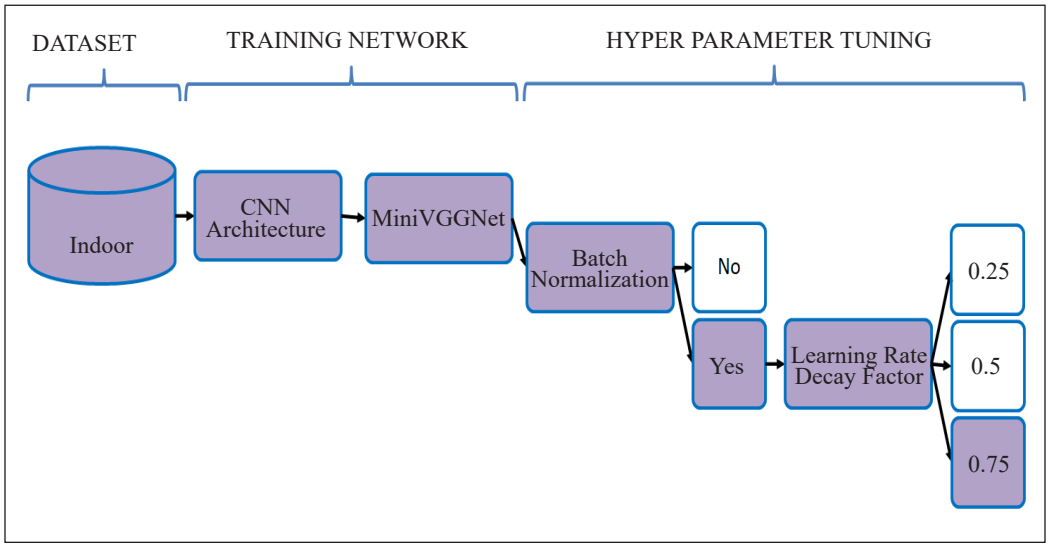

Figure 4. Object classification pipeline

Object Detection

There are four fundamental steps needed when building a deep learning object detector using classic object detection, as shown in Figure 5. The first step is scanning an image at all scales and locations using an image pyramid. An image pyramid is used to reduce (or in some cases, increases) the size of the input image. It is called as an image pyramid because the image was stack from largest to smallest and it looks like a pyramid. The second step is to extract image features by using sliding windows. A sliding window that sits on top of the image will slides from left-to-right and top-to-bottom, classifying each region of interest (ROI) along the way. The sliding window will enable the system to detect precisely where an object is located in the image. The sliding window will runs on each scale of the image pyramid and enabling the system to detect objects that are both closer and farther away from the image. At each stop of the sliding window and image pyramid, the ROI will be extracted and fed into a CNN classification model. That is in the third step where CNN trained model will be used to classify extracted features from each window. When using a sliding window and image pyramid implies to trained classification model, it will report multiple bounding boxes for the same object. By applying non-maxima suppression (NMS) in step 4, the problem of overlapping bounding boxes can be solved, where NMS will keep only the largest confident prediction and obtain only one final bounding box for the object detection.

Figure 6 shows the object detection pipeline of the system. This method of object detection is a better approach, as it uses a combination of a deep learning model for object classification and classical object detection algorithm, which avoids the need to train end to end deep learning object detection frameworks. However, this method has some drawbacks such as slower response and tedious process.

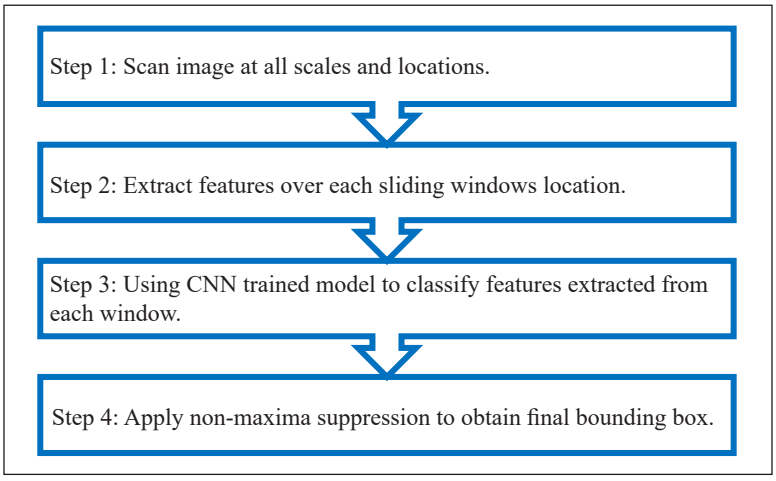

Figure 5. The four fundamental steps of traditional object detection

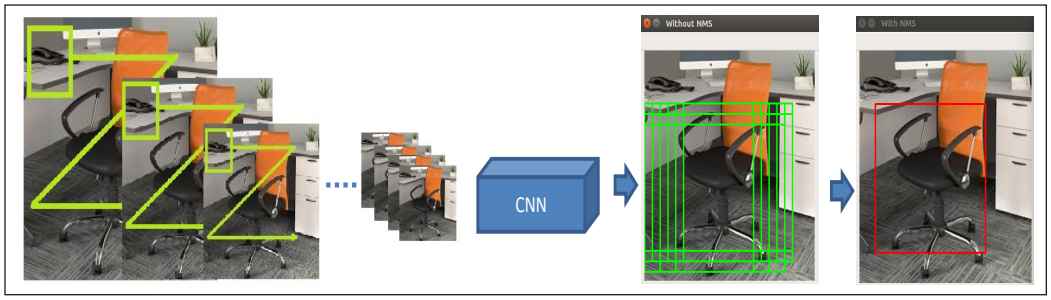

Figure 6. Object detection pipeline

RESULTS AND DISCUSSION

Classification Result

Training results and validation results will be shown in the training loss and accuracy and validation loss and accuracy graph. The python terminal will show the percentage of evaluation accuracy. The network has been trained on INDOOR dataset using miniVGGNet architecture, and the result is shown in the Figure 7.

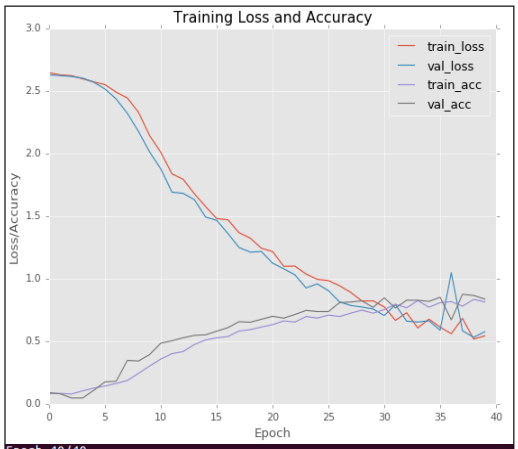


```
Epoch 40/40
630/630 [==============================] - 1s 2ms/step - loss: 0.5437
159 - val_loss: 0.5769 - val_acc: 0.8381
[INFO] serializing network...
[INFO] evaluating network...
                precision    recall  f1-score   support

           bed       1.00      0.54      0.70        13
         chair       0.83      1.00      0.90        19
     cupboard       0.64      0.88      0.74         8
          door       0.63      0.71      0.67        17
           fan       0.72      1.00      0.84        13
kitchen_cabinet       0.83      0.79      0.81        19
     microwave       1.00      0.88      0.93        16
          rack       0.83      0.71      0.77        21
  refrigerator       1.00      1.00      1.00        11
        shower       0.92      0.79      0.85        14
          sink       1.00      1.00      1.00        14
   table_study       0.65      0.79      0.71        14
   toilet_bowl       0.94      0.94      0.94        17
washing_machine       1.00      0.79      0.88        14

     micro avg       0.84      0.84      0.84       210
```

(a)

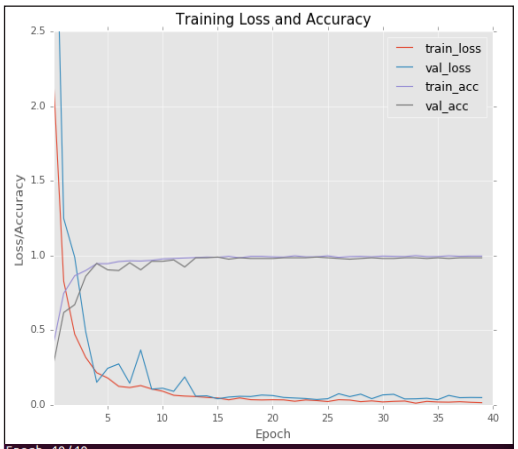


```
Epoch 40/40
630/630 [==============================] - 2s 3ms/step - loss: 0.017
loss: 0.0427 - val_acc: 0.9810
[INFO] serializing network...
[INFO] evaluating network...
                precision    recall  f1-score   support

           bed       1.00      1.00      1.00        13
         chair       1.00      1.00      1.00        19
     cupboard       1.00      1.00      1.00         8
          door       0.94      1.00      0.97        17
           fan       1.00      1.00      1.00        13
kitchen_cabinet       1.00      0.89      0.94        19
     microwave       0.94      1.00      0.97        16
          rack       1.00      0.95      0.98        21
  refrigerator       1.00      1.00      1.00        11
        shower       1.00      1.00      1.00        14
          sink       0.93      1.00      0.97        14
   table_study       1.00      1.00      1.00        14
   toilet_bowl       1.00      0.94      0.97        17
washing_machine       0.93      1.00      0.97        14

     micro avg       0.98      0.98      0.98       210
```

(b)

Figure 7. Object classification result: (a) model trained without batch normalization; (b) model trained with batch normalization

Figure 7 shows the comparison of the object classification result when adding batch normalization layer to the network. The result is shown in Figure 7(a) is the model train without batch normalization, while Figure 7(b) shows the result while the model trained with batch normalization. From the graph plot, there is a positive affect batch normalization has on the training process. The model that implements with batch normalization shows more reliable and the classification accuracy improved by 14% from 84% to 98%. Applying batch normalization helps to reduce overfitting and allows the network to achieve greater classification accuracy because the batch normalization layer are used to normalize the activations of the given input volume before transferring it to the next layer of the network.

Conveniently, the Keras library provides a LearningRateScheduler class that allows us to define a custom learning rate function and then apply it automatically during the training process. By adjusting the learning rate decay factor value, it will help to mitigate the effects of overfitting during the training process. Through epoch-to-epoch modification of the learning rate value, the loss will decrease, the accuracy will increase, and the overall amount of time takes to train a network will decrease. Based on the result shown in Figure 8(a) and Figure 8(b), adding the learning rate decay factor to the network can increase

```
Epoch 40/40
630/630 [==============================] - 2s 3ms/step - loss: 0.017
loss: 0.0427 - val_acc: 0.9810
[INFO] serializing network...
[INFO] evaluating network...
                precision    recall  f1-score   support

           bed       1.00      1.00      1.00        13
         chair       1.00      1.00      1.00        19
       cupboard      1.00      1.00      1.00         8
          door       0.94      1.00      0.97        17
           fan       1.00      1.00      1.00        13
kitchen_cabinet      1.00      0.89      0.94        19
     microwave       0.94      1.00      0.97        16
          rack       1.00      0.95      0.98        21
  refrigerator       1.00      1.00      1.00        11
        shower       1.00      1.00      1.00        14
          sink       0.93      1.00      0.97        14
   table_study       1.00      1.00      1.00        14
   toilet_bowl       1.00      0.94      0.97        17
washing_machine      0.93      1.00      0.97        14

     micro avg       0.98      0.98      0.98       210
```

(a)

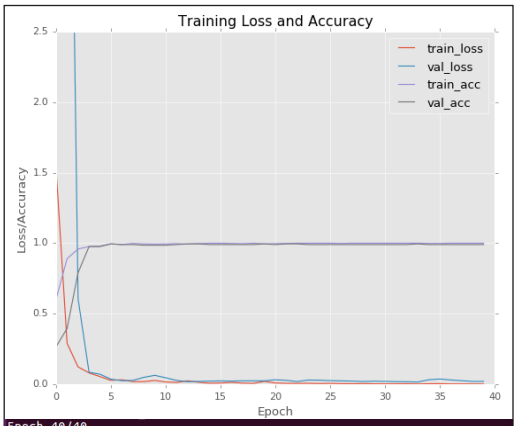


```
Epoch 40/40
630/630 [==============================] - 2s 3ms/step - loss: 0.0014
loss: 0.0198 - val_acc: 0.9905
[INFO] serializing network...
[INFO] evaluating network...
                precision    recall  f1-score   support

           bed       0.93      1.00      0.96        13
         chair       1.00      1.00      1.00        19
       cupboard      1.00      1.00      1.00         8
          door       0.94      1.00      0.97        17
           fan       1.00      1.00      1.00        13
kitchen_cabinet      1.00      0.95      0.97        19
     microwave       1.00      1.00      1.00        16
          rack       1.00      0.95      0.98        21
  refrigerator       1.00      1.00      1.00        11
        shower       1.00      1.00      1.00        14
          sink       1.00      1.00      1.00        14
   table_study       1.00      1.00      1.00        14
   toilet_bowl       1.00      1.00      1.00        17
washing_machine      1.00      1.00      1.00        14

     micro avg       0.99      0.99      0.99       210
```

(b)

Figure 8. Object classification result: (a) model trained without learning rate decay factor; (b) model trained on learning rate decay factor (f=0.75)

the classification accuracy of the model and at the same time can reduce overfitting on the graph plot. By adjusting the value of the learning rate decay factor by 0.75 in Figure 8(b), the classification accuracy of the model increase by 1% from 98% to 99%. Adding the learning rate factor value will control the rate in learning rate drops that affect the classification accuracy.

Detection Result

Figure 9 shows the object detection result by applying our deep learning object detector. The figure shows the comparison of object detection by applying NMS and without applying NMS. Results in Figure 9 (a) and (b) show object detector without NMS yields multiple bounding boxes in the image and applying non-maxima suppression (NMS), to remove overlapping bounding boxes, and keeping only the one with the largest probability/ confidence. The information of the detecting objects about time detection and object classes

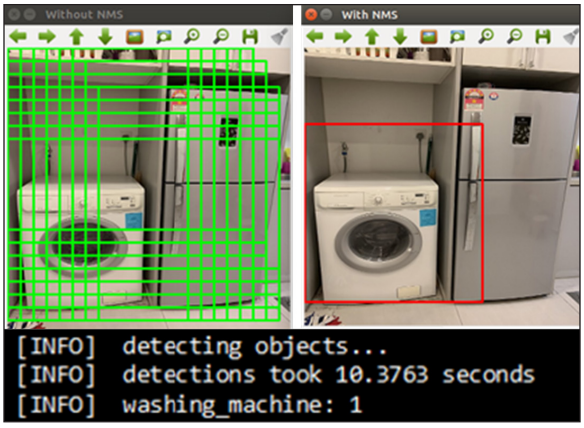

(a)

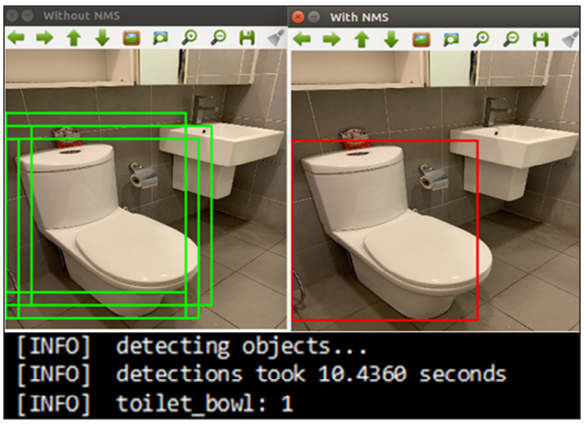

(b)

Figure 9. Object detection result, comparison between applying NMS and without NMS: (a) Applying our object detector to detect the washing machine in the image; (b) Applying our object detector to detect toilet bowl in the image.

was shown in the python terminal. Based on the result, the time taken for object detection is more than 10 seconds, which means that this object detector system is incredibly slow but this is an acceptable trade-off between accuracy and detection time. This system can detect only one object that has a larger probability and cannot detect multiple objects in one image.

CONCLUSION

This paper presents an analysis performance of deep learning object detector by combining a deep learning Convolutional Neural Network (CNN) for object classifying and applies some of the classic object detection algorithms to devise our own deep learning object detector. MiniVGGNet architecture was used as a classification model and a combination of the image pyramid, sliding window and NMS was used as an object detection algorithm. These approaches have a benefit, where they can treat any deep learning model trained for classification as an object detector.

ACKNOWLEDGEMENTS

The authors wish to express their sincere gratitude to the Control and Signal Processing community Faculty of Engineering, Universiti Putra Malaysia for their support and encouragement during this research. This research was funded through a Putra Graduate Initiative (IPS) UPM grant project code GP-IPS/2018/9606100.

REFERENCES

Dalal, N., Triggs, B., & Europe, D. (2005, June 20-25). Histograms of oriented gradients for human detection. In *IEEE Computer Society Conference on Computer Vision and Pattern Recognition* (pp. 886-893). San Diego, California. doi:10.1109/CVPR.2005.177

Felzenszwalb, P. F., Society, I. C., Girshick, R. B., Member, S., Mcallester, D., & Ramanan, D. (2010). Object detection with discriminatively trained part-based models. *IEEE Transactions on Pattern Analysis and Machine Intelligence*, *32*(9), 1627–1645. doi: 10.1109/tpami.2009.167

Freund, Y., & Schapire, R. E. (1997). A decision-theoretic generalization of on-line learning and an application to boosting. *Journal of Computer and System Sciences, 55*(1), 119-139. doi:10.1006/jcss.1997.1504

He, K., Gkioxari, G., Dollar, P., & Girshick, R. (2018). Mask R-CNN. *IEEE Transactions on Pattern Analysis and Machine Intelligence*, *42*(2), 386-397. doi:10.1109/TPAMI.2018.2844175

Lee, A. (2015). *Comparing deep neural networks and traditional vision algorithms in mobile robotics*. Retrieved September 16, 2020, from https://www.cs.swarthmore.edu/~meeden/cs81/f15/papers/Andy.pdf

Lewes, G. H. (2015). Efficient learning machines. In Awad, M., & Khanna, R. (Ed.), *Support vector machines for classification* (pp. 39-66). Berkeley, California: Apress. doi:10.1007/978-1-4302-5990-9_3

Lienhart, R., & Maydt, J. (2002, September 22-25). An extended set of Haar-like features for rapid object detection. In *IEEE International Conference on Image Processing* (pp. 900–903). Rochester, New York. doi:10.1109/ICIP.2002.1038171

Liu, W., Anguelov, D., Erhan, D., Szegedy, C., Reed, S., Fu, C. Y., & Berg, A. C. (2016). Computer vision - ECCV. In (Ed.), *SSD : Single shot multibox detector* (pp. 21-37). Dordrecht, Netherlands: Springer. doi:10.1007/978-3-319-46448-0_2

Lowe, D. G. (2004). Distinctive image features from scale-invariant keypoints. *International Journal of Computer Vision, 60*(2), 91–110. doi: 10.1023/b:visi.0000029664.99615.94

Patil, A., Student, M. E., & Dhanvijay, M. (2015). Blob detection technique using image processing for identification of machine printed characters. *Journal of Innovations in Engineering Research and Technology [IJIERT]2*(10), 1–8. doi:10.5281/zenodo.1467487

Redmon, J., & Farhadi, A. (2017, July 21-26). YOLO9000: Better, faster, stronger. In *IEEE Conference on Computer Vision and Pattern Recognition (CVPR)* (pp. 7263-7271). Honolulu, Hawaii. doi:10.1109/CVPR.2017.690

Ren, S., He, K., Girshick, R., & Sun, J. (2016). Faster r-cnn: Towards real-time object detection with region proposal networks. *IEEE Transaction on Pattern Analysis and Machine, 39*(6), 1137-1149. doi:10.1109/tpami.2016.2577031

Shaikh, S. H., Saeed, K., & Chaki, N. (2014). SpringerBriefs in computer science. In Zdonik, S., Shekhar, S., Wu, X., Jain, L. C., Padua, D., Shen, X. S., ... & Lee, N. (Ed.), *Moving object detection using background subtraction* (pp. 15-23). Cham, Switzerland: Springer. doi:10.1007/978-3-319-07386-6

Subhi, M. A., Md Ali, S. H., Ismail, A. G., & Othman, M. (2018). Food volume estimation based on stereo image analysis. *IEEE Instrumentation & Measurement Magazine, 21*(6), 36-43. doi:10.1109/mim.2018.8573592

Subhi, M. A., & Ali, S. M. (2018, December 3-6). A deep convolutional neural network for food detection and recognition. In *IEEE-EMBS Conference on Biomedical Engineering and Sciences (IECBES)* (pp. 284-287). Sarawak, Malaysia. doi:10.1109/IECBES.2018.8626720

Subhi, M. A., Ali, S. H., & Mohammed, M. A. (2019a). Vision-based approaches for automatic food recognition and dietary assessment: A survey. *IEEE Access, 7*, 35370-35381. doi:10.1109/access.2019.2904519

Subhi, M. A., Ali, S. H., & Abdulameer, M. (2019b). Deep convolutional networks for food detection and classification. *Journal of Computational and Theoretical Nanoscience, 16*(5-6), 2433-2438. doi:10.1166/jctn.2019.7913

Sugiarto, B., Prakasa, E., Wardoyo, R., Damayanti, R., Krisdianto, Dewi, L. M, ... & Rianto, Y. (2017, November 1-2). Wood identification based on histogram of oriented gradient (HOG) feature and support vector machine (SVM) classifier. In *2017 2nd International Conferences on Information Technology, Information Systems and Electrical Engineering (ICITISEE)* (pp. 337-341). Yogyakarta, Indonesia. doi:10.1109/ICITISEE.2017.8285523

Vahab, A., Naik, M. S., Raikar, P. G., & Prasad, S. R. (2019). Applications of object detection system. *International Research Journal of Engineering and Technology*, *6*(4), 4186–4192.

Wang, Y. (2014). An analysis of the Viola-Jones face detection algorithm. *Image Processing On Line, 4*, 128-148. doi:10.5201/ipol.2014.104

Zhao, B., B., Feng, J., Wu, X., & Yan, S. (2017). A survey on deep learning-based fine-grained object classification and semantic segmentation. *International Journal of Automation and Computing, 14*(2), 119-135. doi:10.1007/s11633-017-1053-3

Pertanika J. Sci. & Technol. 28 (S2): 173 - 182 (2020)

SCIENCE & TECHNOLOGY

Journal homepage: http://www.pertanika.upm.edu.my/

Integrated Braking Force Distribution for Electric Vehicle Regenerative Braking System

Anith Khairunnisa Ghazali[1], Mohd Khair Hassan[1]*, Mohd Amran Mohd Radzi[1] and Azizan As'arry[2]

[1]Department of Electrical and Electronic, Faculty of Engineering, Universiti Putra Malaysia, 43400 Serdang, Selangor, Malaysia
[2]Department of Mechanical and Manufacturing, Faculty of Engineering, Universiti Putra Malaysia, 43400 Serdang, Selangor, Malaysia

ABSTRACT

The automotive industry has made a significant contribution to everyday life by fulfilling society's mobility needs. Traditionally, electric vehicles (EV) were introduced as an alternative to the traditional internal combustion engine (ICE) to reduce the emission, which improves air quality. The regenerative braking system (RBS) technology is increasing rapidly as an alternative energy-saving solution instead of using the conventional fossil fuel process. In addition, conventional braking creates energy loss because it produces unnecessary heat during braking. Therefore, (RBS) was deliberately designed to solve these drawbacks. Several researchers have found an efficient way to recover regenerative energy, but do not pay enough attention to state-of-the-art (SOC), motor performance and overall performance. This paper designs a new braking force distribution that introduces integrated braking by combining the default ADVISOR and the new parallel braking distribution to improve the SOC battery for three driving cycles. The design of the braking part was based on the braking force distribution of vehicle speed, consisting mainly of friction and regenerative braking ratio allocation in parallel form. The suggested delivery method is evaluated by simulation and shows that the overall performance and battery life are increased. The proposed method was experimentally evaluated using ADVISOR Matlab for the efficiency and final state of the battery.

Keywords: Braking force distribution, electric vehicles, regenerative braking

ARTICLE INFO

Article history:
Received: 10 February 2020
Accepted: 13 November 2020
Published: 31 December 2020

DOI: https://doi.org/10.47836/pjst.28.S2.14

E-mail addresses:
akg_anith@yahoo.com (Anith Khairunnisa Ghazali)
khair@upm.edu.my (Mohd Khair Hassan)
amranmr@upm.edu.my (Mohd Amran Mohd Radzi)
zizan@upm.edu.my (Azizan As'arry)
* Corresponding author

ISSN: 0128-7680
e-ISSN: 2231-8526

© Universiti Putra Malaysia Press

INTRODUCTION

One of the most vital features of electricity based vehicle is their ability to recuperate the braking energy. Recovering and reusing the process of braking energy able to improve the fuel economy which is focused on frequent braking events such as urban driving. Due to the shortage of fossil fuel sources and environmental pollution issues, alternative fuels and hybrid technology has received vast attention (Zhang et al., 2013). Nowadays, many automotive industries produce electric vehicles as a solution. However, limited driving mileage becomes a critical issue. During the charging process, the time taken for the battery to reach full charge is high. Due to this factor, electric vehicle technology are still not at the satisfied level (Kiyakli & Solmaz, 2019). The main consideration during braking system design must be the braking performance that braking system design should be able to stop or slow down the vehicle as fast as possible and keep the vehicle in stable condition as well. (Goodarzi et al., 2008). In order to produce better braking performance and improve regenerative braking efficiency, an integrated braking strategy has been proposed in this research. The performance of the battery state of charge is analyzed and verified through simulation results.

One of the most vital features of electricity based vehicle is their capability to recuperate the braking energy. The recovering process of braking energy able to improve the fuel economy which is focused on frequent braking events such as urban driving. Consequently, cooperation between regenerative and frictional braking systems of electrified vehicles is important for vehicle control in safety driving manoeuvres (Lv et al., 2015).

In general, the electric motor in electric vehicle (EV) works as an alternator to transform mechanical energy into electrical energy. The captured energy will store in energy storage for future usage (Lv et al., 2015). To slow down the vehicle, the braking torque required must be larger than torque produced by the electric motor. To improve regenerative efficiency, braking torque has to be designed. The vehicle speed based of braking distribution is considered in this research. Most of EV used a combination of frictional braking and regenerative braking. Therefore, the appropriate design of good braking distribution is a major attention. The main issue designing the braking distribution is to consider the safety and ensure the battery condition without overcharging. The crucial topic in constructing the regenerative braking system is the method to allocate the overall braking forces required between the regenerative and frictional brake in order to capture and convert optimum kinetic energy into electrical energy. During deceleration, the braking force should distribute the highest ratio to the front axle to improve braking energy recovery. At lower speed, the energy recovered is minimal and it is difficult to reach the demands of the pedal drivers (Yeo & Kim, 2002). In general, the proposed method of regulating energy savings and its impact is clear and apparent.

METHODS

Figure 1 below illustrates the electric vehicle driving process model. This model is used to evaluate the state of charge battery and braking performance in this research. The major component consists of driver block, brake strategy, battery, motor and vehicle model.

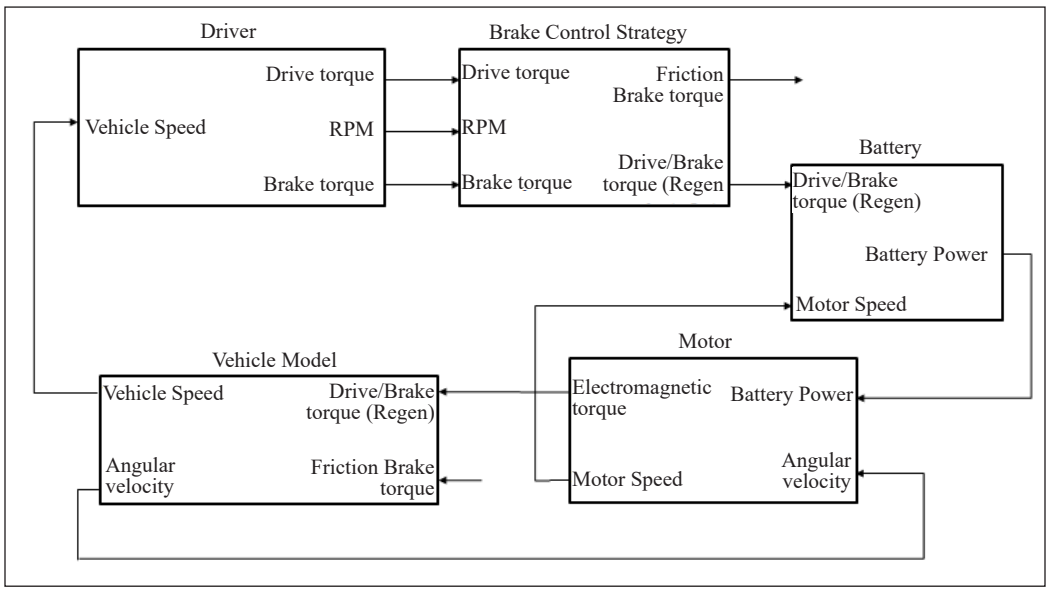

Figure 1. Electric vehicle block diagram

Vehicle Dynamics

The longitudinal dynamics of the vehicle during the deceleration process can be modeled by considering aerodynamic resistance, rolling resistance, and gradient resistance (Mehrdad et al., 2005).

Aerodynamic resistance is a force which the oncoming air applies on a moving body. The equation expresses as:

$$F_a = 0.5\rho C_d A_f (\Delta V)^2 \quad (1)$$

Where, C_d is the coefficient of air resistance, A_f is windward are, ρ is the air density and ΔV is the differential speed between vehicle and air. The rolling resistance is the energy that vehicles pass through tires to maintain movement at a regular speed over a surface. The tire rolling resistance is calculated with this equality:

$$F_r = mgC_r cos\alpha \quad (2)$$

Where C_r is the coefficient of rolling resistance, m is the total weight and α is the angle. Next, the gradient resistance appears due to the component of gravity. When a vehicle

goes up or down a slope, the weight component always directed a downward direction. The equation for gradient resistance formulated as:

$$F_g = mg\ sin\alpha \tag{3}$$

Braking Distribution Strategy

The parallel strategy distributes the regenerative and friction based on vehicle speed. Furthermore, vehicle speed high influence in ensuring the braking safety. Therefore during the design process of regenerative braking distribution, considering the vehicle speed is vital. Figure 2 describes the motor efficiency map during operation. At low speed of the vehicle the regenerative should be minimal due to the smallest kinetic energy. Next, when the speed is increasing at the middle range, the regenerative braking should increase to a certain range. During accelerating at high speed, the regenerative braking should be high due to great kinetic energy of motor (Gang & Zhi, 2018).

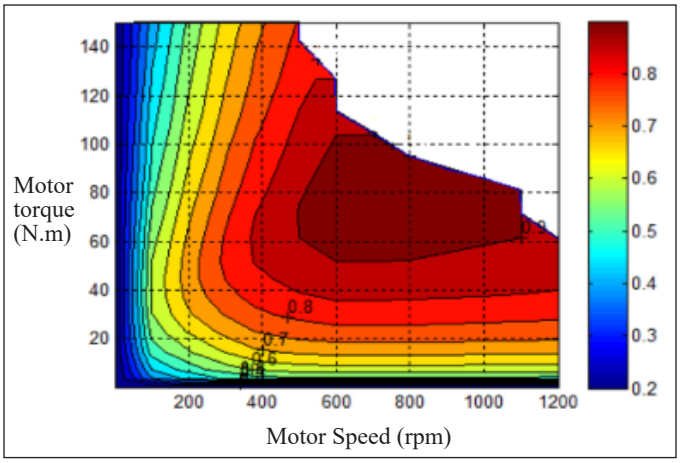

Figure 2. Motor map efficiency

Figure 3 shows the new parallel braking control strategy based on vehicle speed. This technique operates regenerative and friction at the same time during the braking process. A standard look-up table for the distribution of the brake forces provided by the regenerative and frictional brakes is shown in Figure 3. The rationale behind this approach is that the recovery energy decrease at lower speed and increase at higher speed (Zhou et al., 2011). The regenerative braking coefficient is the ratio of regenerative braking torque and total braking torque in between the range 0 to 1. The balance of braking is carried out by certain vehicle resistances such as aerodynamic resistance, initial losses, rolling resistance, etc. (Panagiotidis et al., 2018). The regenerative ratio is higher during high acceleration and during the lower speed of vehicle, regenerative does not work and friction brake takes place (Zhang et al., 2019).

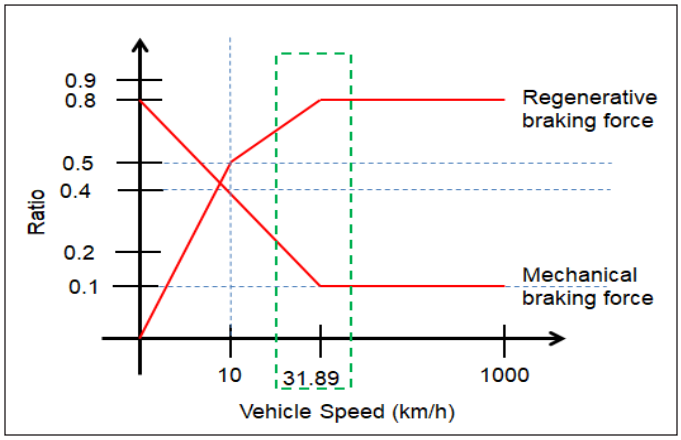

Figure 3. New parallel braking force distribution

In this research, the new proposed braking strategy introduces average speed due to the most frequent speed implement during urban driving as the highest ratio of regenerative braking instead of using the ADVISOR default technique design that introduces the highest ratio of regenerative braking at standard speed which is 60 km/h. According to Mahayadin et al.'s (2018) findings, urban driving Malaysia's average speed is 31.89 km/h.

Figure 4 shows the integrated braking strategy proposed in this paper. The integrated braking is a combination of default braking system and parallel braking that uses Malaysia's average speed for high regenerative braking ratio. The merits of applying such strategy are to improve as well as to enhance the performance of regenerative braking by determining appropriate braking ratio coefficient that should be implemented during deceleration. The new parallel braking force distribution will act as tuning component in order to optimize recovered energy to optimum output.

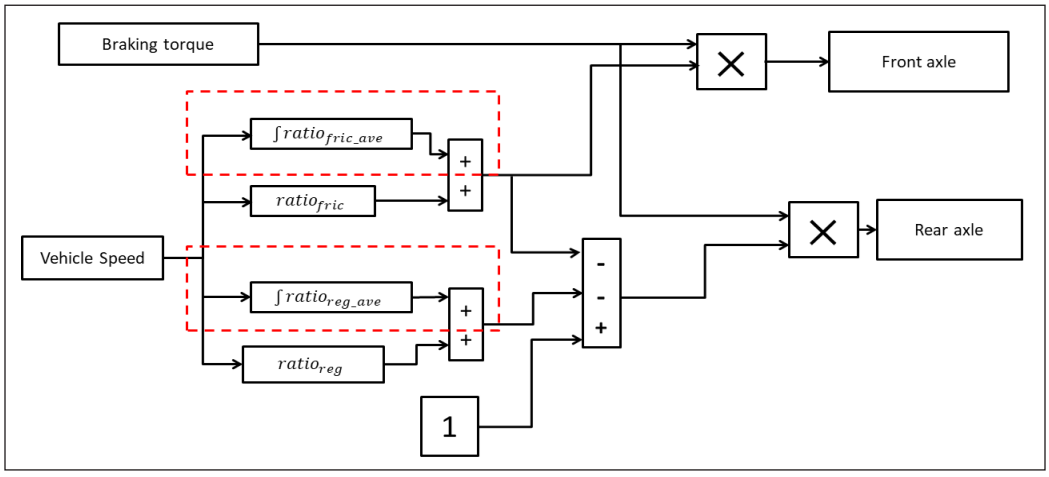

Figure 4. Integrated braking strategy

$$T_{tot} = T_{fric} + T_{reg} \quad (4)$$

T_{tot} = Total braking torque request

T_{fric} is the friction braking of front and rear axle, T_{reg} is the regenerative braking of rear axle.

The distribution for friction and regenerative distribution at rear axle express as:

$$T_r = T_{r_fric} + T_{r_reg} \quad (5)$$

$$T_{r_gen} = T_r \cdot (ratio_{reg} + ratio_{reg_ave}) \quad (6)$$

$$T_{r_fric} = T_r \cdot \left(1 - (ratio_{fric} + ratio_{fric_ave}) - (ratio_{reg} + ratio_{reg_ave})\right) \quad (7)$$

T_{r_fric} and T_{r_reg} represent the friction braking torque request for friction and regenerative of rear axle. The $ratio_{fric}$, $ratio_{fric_ave}$, $ratio_{reg}$ and $ratio_{reg_ave}$ denotes as brake distribution coefficient for friction and regenerative braking.

RESULTS

Simulation Result

To determine the performance of the proposed braking strategy, vehicle driving simulation had been completed using NEDC and US06 drive cycle. Drive cycle is driving pattern that represents actual driving behavior for experimental purpose. The aim of a drive cycle is to decrease the time and cost of an expensive on-road test. This research used NEDC for urban driving and US06 for high acceleration driving behavior (Mcdonald et al., 2012). The driving behavior of NEDC and US06 are shown in Figures 5 and 6.

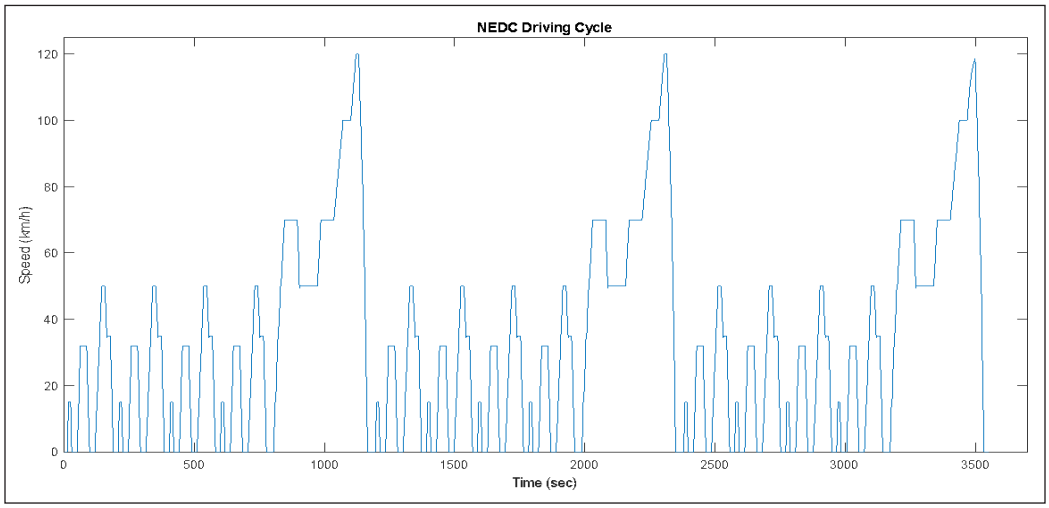

Figure 5. NEDC driving cycle

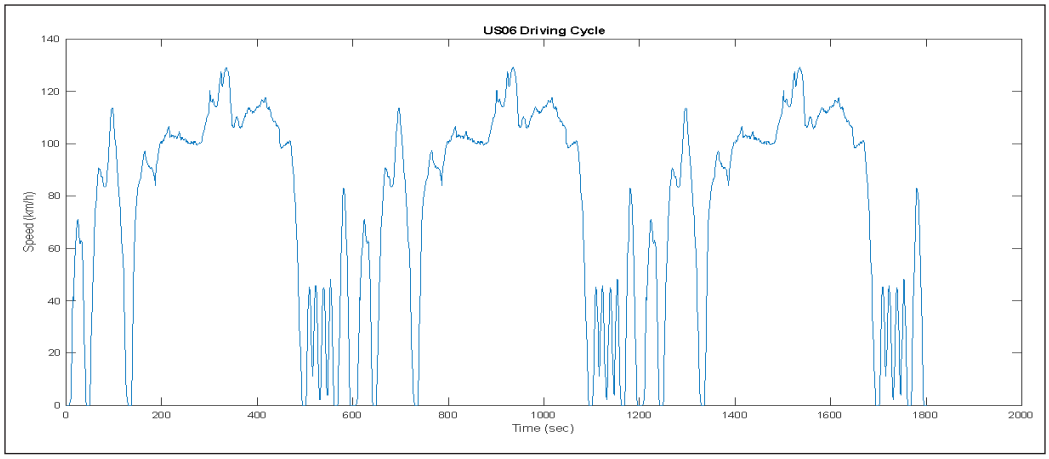

Figure 6. US06 driving cycle

Simulation results of NEDC state of charge is presented in Figure 7. Based on this, the output, the first cycle of NEDC for integrated strategy did not recover much energy to avoid overcharging at 90% of the battery level. The consequences of integrated braking could be seen from the second cycle where the ratio SOC dropped about 0.98 and at the third cycle, the SOC increased to about 0.023. This is due to the tuning components that purposely optimize the SOC to the optimum value. The final value of SOC for the default strategy was 0.3375, while the SOC value for the integrated strategy was 0.7329 higher than default. Table 1 summarizes the brake loss, energy transmitted, motor efficiency and overall efficiency. Comparing to the default strategy, the brake loss for integrated strategy was 43485 higher than the default strategy. However, the energy transmitted regenerative purpose improved to 3031, motor efficiency improved to 0.85 and overall efficiency was 0.601.

The driving performance of US06 obtained is recorded in Table 2. It is clearly visible that the brake loss using integrated braking strategy was reduced to 30 kJ, while the energy transmitted improved to 231530 kJ. Next, the motor efficiency was reduced to 0.76 but still was in high motor efficiency range and the overall efficiency increased to 0.952. The state of charge for US06 improved from 0.024 to 0.3657 as illustrated in Figure 8.

Table 1
NEDC driving performance

	Default	Integrated	Improvement
Brake loss (kJ)	2555	45775	43485
Energy transmitted (kJ)	4599	88734	3031
Motor efficiency	0.67	0.85	0.18
Overall efficiency	0.434	1.758	0.601

Table 2
US06 driving performance

	Default	Integrated	Improvement
Brake loss (kJ)	3500	162680	-30
Energy transmitted (kJ)	6299	231530	206440
Motor efficiency	0.81	0.76	0.02
Overall efficiency	0.529	0.952	0.21

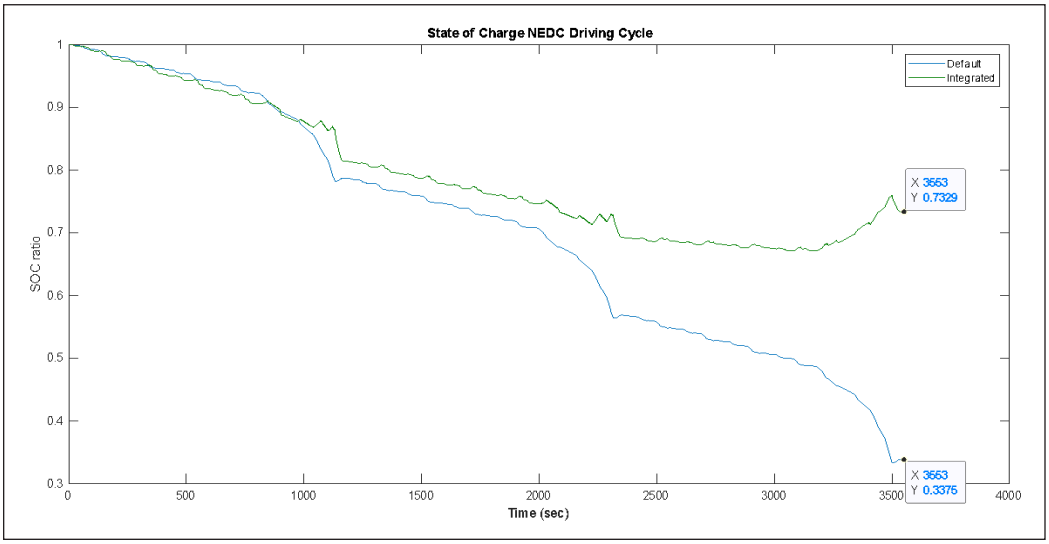

Figure 7. NEDC state of charge

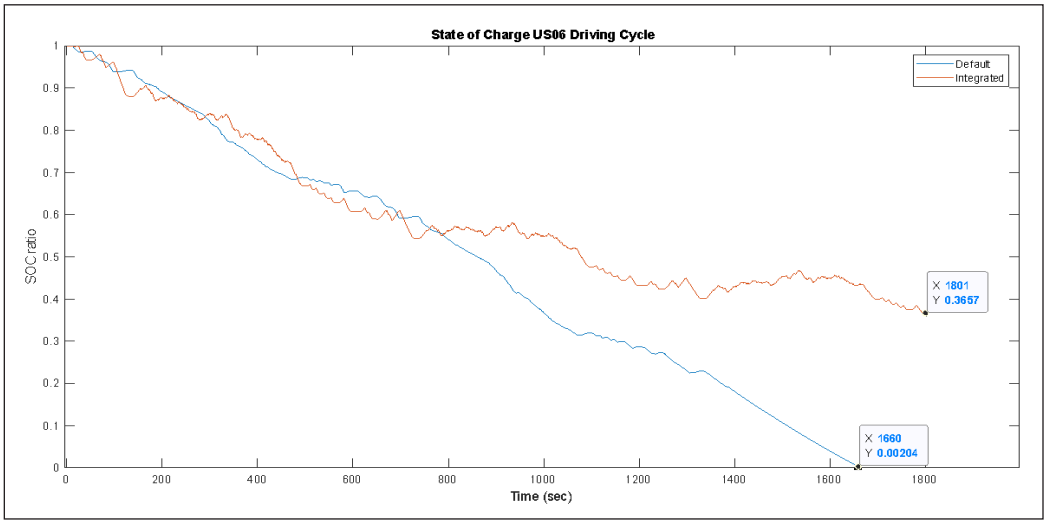

Figure 8. US06 state of charge

CONCLUSION

This research proposed the regenerative braking system using integrated braking force distribution. In order to improve the energy efficiency of the electric vehicle, several parameters such as overall efficiency, energy transmitted, energy loss during driving and SOC battery had been taken in consideration. The simulation results show that the proposed braking strategy was able to improve the energy efficiency of the electric vehicle.

ACKNOWLEDGEMENT

The authors would like to thank Universiti Putra Malaysia for funding this project under Putra Grant with grant number GP/2018/9591900.

REFERENCES

Gang, L., & Zhi, Y. (2018). Energy saving control based on motor efficiency map for electric vehicles with four-wheel independently driven in-wheel motors. *Advances in Mechanical Engineering, 10*(8), 1–18. doi:10.1177/1687814018793064

Goodarzi, A., Behmadi, M., & Esmailzadeh, E. (2008). An optimised braking force distribution strategy for articulated vehicles. *International Journal of Vehicle Mechanics and Mobility, 46*(1), 849-856. doi:10.1080/00423110802037107

Kiyakli, A. O., & Solmaz, H. (2019). Modeling of an electric vehicle with MATLAB/simulink. *International Journal of Automotive Science and Technology, 2*(4), 9-15. doi:10.30939/ijastech..475477

Lv, C., Zhang, J., Li, Y., & Yuan, Y. (2015). Novel control algorithm of braking energy regeneration system for an electric vehicle during safety-critical driving maneuvers. *Energy Conversion and Management*, *106*, 520–529. doi:10.1016/j.enconman.2015.09.062

Mahayadin, A. R., Ibrahim, I., Zunaidi, I., Shahriman, A. B., Faizi, M. K., Sahari, M., ... & Nagaya, Y. (2018, August 16-17). Development of driving cycle construction methodology in Malaysia ' s urban road system. In *2018 International Conference on Computational Approach in Smart Systems Design and Applications* (pp. 1-5). Kuching, Malaysia.

Mcdonald, D., Sault, L., & Marie, S. (2012, March 23-24). Electric vehicle drive simulation with MATLAB / simulink. In *Proceedings of the 2012 North-Central Section Conference* (pp. 1-24). Ohio, USA.

Mehrdad, E., Yimin, G., Sebastian, E. G., & Ali, E. (2005). *Modern electric, hybrid electric, and fuel cell vehicles*. Ohio, USA: CRC PRESS.

Panagiotidis, M., Delagrammatikas, G., & Assanis, D. (2018). Development and use of a regenerative braking model for a parallel hybrid electric vehicle. *SAE Transactions, 109,* 1180-1191.

Yeo, H., & Kim, H. (2002). Hardware-in-the-loop simulation of regenerative braking for a hybrid electric vehicle. *Journal of Automobile Engineering, 216*(11), 855-864. doi:10.1243/095440702321031405

Zhang, J., Lv, C., Qiu, M., Li, Y., & Sun, D. (2013). Braking energy regeneration control of a fuel cell hybrid electric bus. *Energy Conversion and Management*, *76*, 1117–1124. doi:10.1016/j.enconman.2013.09.003

Zhang, W., Yang, J., Zhang, W., & Ma, F. (2019). Research on regenerative braking of pure electric mining dump truck. *World Electric Vehicle Journal, 10*(2), 1–17. doi:10.3390/wevj10020039

Zhou, M., Gao, Z., & Zhang, H. (2011). Research on regenerative braking control strategy of hybrid electric vehicle. *Proceedings of 2011 6th International Forum on Strateguc Technology*, *1*, 300-303. doi: 10.1109/ifost.2011.6021027

Pertanika J. Sci. & Technol. 28 (S2): 183 - 196 (2020)

SCIENCE & TECHNOLOGY

Journal homepage: http://www.pertanika.upm.edu.my/

Design and Synthesis of a New Amphipathic Cyclic Decapeptide with Rapid, Stable, and Continuous Antibacterial Effects

Hisham N. Farrag, Khaled Metwally, Shinya Ikeno and Tamaki Kato*

Department of Biological Functions Engineering, Graduate School of Life Science and Systems Engineering. Kyushu Institute of Technology, Wakamatsu Campus, Fukuoka Prefecture, 808-0196 Japan

ABSTRACT

Pathogens can acquire high resistance against even the most powerful antibiotics because of the long periods of treatment and high usage of antimicrobial agents. In addition, the severe side effects of commonly used antibiotics can initiate secondary diseases or may lead to death. Antimicrobial peptides (AMPs) have been reported to exhibit prokaryotic selectivity and low microbial resistance. Furthermore, AMPs show a good ability to penetrate the cell walls of microorganisms. In this study, a cyclic decapeptide and its linear counterpart were synthesized by a standard solid phase peptide synthesis method (SPPS) in a quantitative yield of the linear decapeptide (97%) and a good yield of the cyclic form (45%). Antibacterial studies were performed using *Escherichia coli* (a widespread Gram-negative pathogen) and *Bacillus thuringiensis* as a representative Gram-positive pathogen. The minimal inhibitory concentration (MIC) values were evaluated by the broth microdilution method. The cyclic peptide and its linear counterpart exhibited MIC values of 0.16 and 0.3 mg/mL, respectively, against *Escherichia coli*. Against *Bacillus thuringiensis*, the peptides had the same MIC value of 0.24 mg/mL. Time-kill studies were performed using *E. coli*, which indicated a fast killing effect of both peptides (≥ 99% of the bacterial cells) after 1 h of incubation using a concentration of two times the MIC value for each peptide. Moreover, bacterial cell viability studies against *E. coli* carried out using a high bacterial concentration showed that both peptides have a maximum killing effect of more than 80% of the tested bacterial cells.

Keywords: Antibiotics, antimicrobial peptides, cyclic decapeptides, *Escherichia coli*, SPPS

ARTICLE INFO

Article history:
Received: 10 February 2020
Accepted: 13 November 2020
Published: 31 December 2020

DOI: https://doi.org/10.47836/pjst.28.S2.15

E-mail addresses:
farrag.hisham320@mail.kyutech.jp (Hisham N. Farrag)
metwally.khaled-abdelfatteh735@mail.kyutech.jp (Khaled Metwally)
ikeno@life.kyutech.ac.jp (Shinya Ikeno)
tmkato@life.kyutech.ac.jp (Tamaki Kato)
* Corresponding author

ISSN: 0128-7680
e-ISSN: 2231-8526

© Universiti Putra Malaysia Press

INTRODUCTION

Antimicrobial agents can act as double-edged swords, as they can affect the targeted microorganisms but also have harmful effects on the host cells (Brummett & Fox, 1989; Khaliq & Zhanel, 2003; Mingeot-Leclercq & Tulkens, 1999). The most effective antimicrobial agents exhibit high selectivity toward a microorganism's cells without affecting the mammalian cells. In addition, the microorganisms should show no resistance toward the antimicrobial agent during the treatment. Recently, antimicrobial peptides (AMPs) produced by some types of fungi have been reported to have rapid and strong effects on microorganisms *via* destruction of the cell membranes (Stengel et al., 2001). The degradation end products of such peptides are amino acids, which indicates their potential safety. Thus, many researchers have investigated this type of peptide antibiotic, especially the natural antimicrobial decapeptides, for example, streptocidins and tyrocidins. There are two types of natural peptides, cyclic and linear peptides. Some examples of cyclic AMPs include the streptocidins (Gebhardt et al., 2001), the tyrocidins (Chalovich & Eisenberg, 2013), gramicidin S (Swierstra et al., 2016), and the loloatins (Gerard et al., 1999). Examples of linear AMPs include the gramicidins A, B, and C (Kessler et al., 2004). The overall charge of the bacterial cell membrane plays an important role in the biological efficacy. It has been shown that most bacterial cell membranes carry negative charges because of the presence of lipoteichoic acid moieties linked to either peptidoglycan or the plasma membrane. The lipoteichoic acid moieties are negatively charged because of the presence of phosphate ions in their chemical structure (Silhavy et al., 2010). Therefore, bacterial cell walls prefer adhesion to positively charged surfaces rather than negatively charged surfaces. In addition, it has been found that there is no bacterial growth after the adhesion to positively charged surfaces (Gottenbos et al., 2001).

The hydrophobic residues of peptides are important for the penetration of AMPs into the bacterial cell wall. These hydrophobic residues can construct a nonlamellar phase *via* a self-assembly process inside the lipid bilayer of the bacterial cell wall (Chen et al., 2010). In addition, alanine, valine, and leucine have been investigated for their importance as aliphatic amino acids, to facilitate the formation of secondary structures in the bacterial cell membrane and to increase the solubility of peptides (Narayanan & Dias, 2013).

Herein, a new anti-bacterial cyclic decapeptide and its linear counterpart were designed and investigated in terms of antibacterial behavior against standard and high concentrations of bacteria. Positively charged moieties incorporated in peptides encourage adherence with the negatively charged bacterial cell wall. For that purpose, four lysine amino acid residues were incorporated into the decapeptides to serve as the source of a positive charge. In addition, increasing the hydrophobicity of the whole molecule was achieved by incorporating leucine, valine, tryptophan, tyrosine, and phenylalanine into the decapeptide structure to increase the penetration of the whole peptide inside the bacterial cell membrane. The antibacterial effect was studied against the Gram-positive *Bacillus*

thuringiensis and Gram-negative bacterial strain *Escherichia coli*. The minimal inhibitory concentration (MIC) values were determined. Time-kill studies were conducted for both forms of decapeptides against *E. coli*. Cell viability assays were performed using a high concentration of *E. coli* to study the ability of the antibacterial peptides to overcome and control a source of infection by investigating the maximum killing effect of their secondary structures.

MATERIALS AND METHODS

Synthetic Protocol

As shown in Figure 1, the linear decapeptide H-KVYKFKWLKA-OH (peptide 1) was designed to contain cationic residues (four lysine residues) to interact with the negatively charged bacterial membrane. Hydrophobic residues were added to the structure (tyrosine, tryptophan, and phenylalanine) to interact with the membrane lipids. In addition, aliphatic residues were incorporated to improve the interaction with the bacterial membrane receptors and to increase the solubility of the peptide. The cyclic decapeptide KVYKFKWLKA (peptide 2) was synthesized to study the difference in the antibacterial effect of the rigid cyclic structure compared with the linear peptide. Peptide 1 [molecular weight (MW) ~1310] was prepared *via* the standard solid phase peptide synthesis method using 9-fluorenylmethoxycarbonyl (Fmoc) chemistry (as shown in Scheme 1) and 2-chlorotrityl

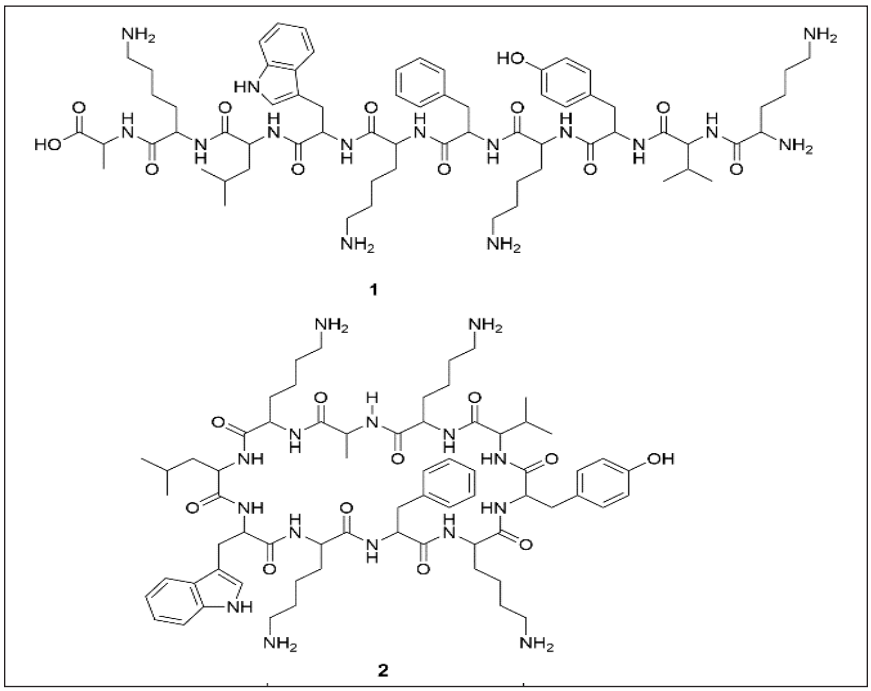

Figure 1. Design of the linear (1) and cyclic (2) antimicrobial decapeptides (KVYKFKWLKA)

resin as the solid support (Kreutzer et al., 2018). All Fmoc-protected amino acids, resin, piperidine, *O*-benzotriazole-*N*, *N*, *N*', *N*'-tetramethyl-uronium-hexafluorophosphate (HBTU), 1-hydroxy-benzotriazole hydrate (HOBt·H_2O), *N*, *N*-diisopropylethylamine (DIPEA), and 2, 2, 2-trifluoroacetic acid (TFA) were purchased from Watanabe Chemical Industries, Ltd, Japan. Other reagents and solvents were purchased from Wako Pure Chemical Industries, Ltd, Japan.

As shown in Scheme 1, the synthesis was started by loading an alanine amino acid onto 2-chlorotrityl chloride resin. Fmoc-L-amino acid residues were then coupled to the loaded alanine residue using HBTU, DIEA, and HOBT in *N*, *N*-dimethylformamide (DMF) as the solvent for the coupling process. The Fmoc protecting groups were removed using 20% (v/v) piperidine in DMF. The cleavage of the side-chain protected linear decapeptide from the resin was performed using a mixture of 2, 2, 2-trifluoroethanol/ acetic acid/dichloromethane at a ratio of 3:1:1 (v/v/v) (Amblard et al., 2006). Purification was performed using a semi-preparative RP-HPLC Hitachi L-7100 instrument equipped with an XTerra Prep MS C18 OBD 10 µm column (19 × 150 mm; Waters). The mobile phases were acetonitrile containing 0.1% TFA, and H_2O containing 0.1% TFA, and the peak intensity was determined at a wavelength of 220 nm(Huber & Majors, 2007).

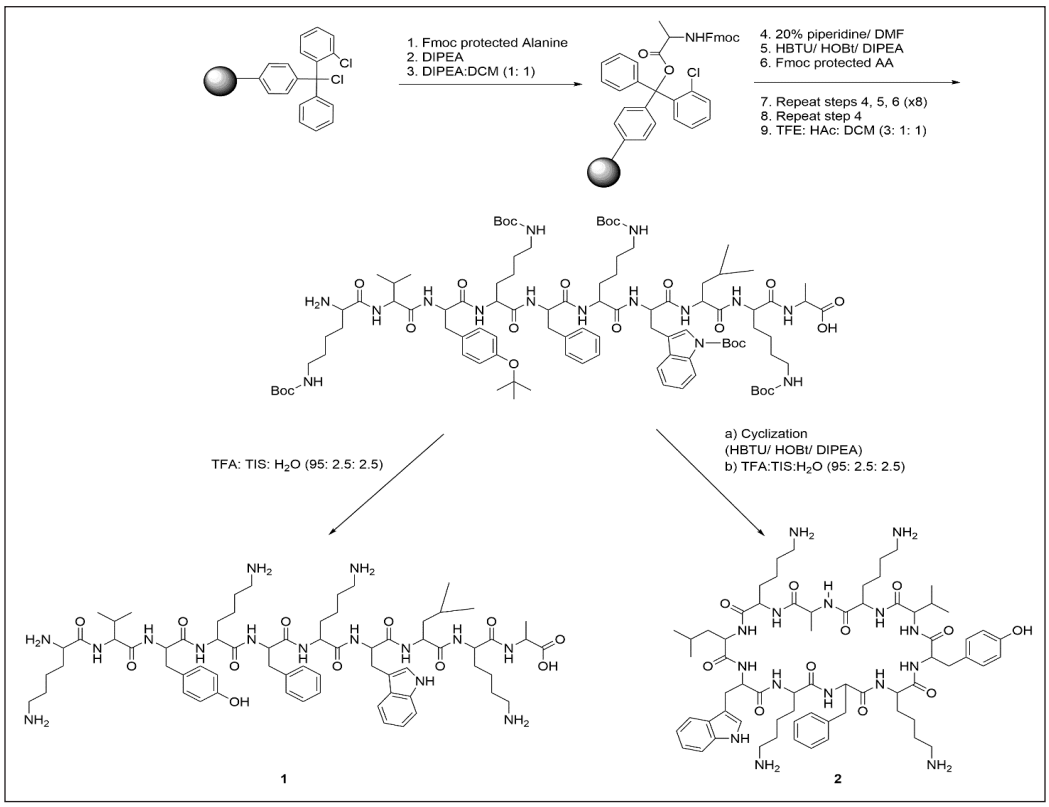

Scheme 1. Synthetic protocol of the linear and cyclic decapeptides (KVYKFKWLKA)

The removal of the side-chain protecting groups was achieved using a mixture of TFA/trisisopropylsilane (TIS)/H_2O at a ratio of 95:2.5:2.5 (v/v/v). Lyophilization was carried out in a VD-800F freeze dryer (TAITEC) to obtain the linear decapeptide 1. The cyclization reaction was achieved using a concentration of 0.5 mM of the linear decapeptide 1 to avoid dimer formation. Two equivalents (equiv.) of HBTU and 5 equiv. of DIPEA were used for the cyclization process. The removal of the protecting groups of the cyclic decapeptide was carried out using TFA/TIS/H_2O at a ratio of 95:2.5:2.5 (v/v/v). Purification was achieved using semi-preparative RP-HPLC followed by Lyophilization to yield the target cyclic decapeptide 2 (Tapeinou et al., 2015).

Antibacterial Assays

MIC Evaluation. MIC values were determined by the broth microdilution method using 96-well microplates (Standards & Testing, 2018). *E. coli* and *B. Thuringiensis* bacterial strains were chosen to determine the broad-spectrum effect of the cyclic decapeptide and the linear counterpart against both Gram-positive and Gram-negative bacterial strains. The bacterial strains were inoculated in a freshly prepared Luria Bertani (LB) broth medium at a temperature of 37°C (for *E.coli*), and in a freshly prepared tryptic soy broth at a temperature of 27°C (*B. thuringiensis*). Both bacterial strains were shaken at 160 rpm overnight. The cultures were diluted up to 5×10^5 CFU/mL ($OD_{600} = 0.05$). The cyclic and linear decapeptide solutions were prepared by dissolving each peptide separately in distilled water at a concentration of 1 mg/mL. The stock solutions were diluted across 96-well microplates by 2-fold serial dilution using the growth media to reach a total volume of 200 µL. Negative controls were used to ensure the adequate growth of the bacteria. Kanamycin and ampicillin, 0.25 and 0.5 mg/mL solutions, respectively, were used as positive controls. The bacterial cultures were inoculated with the test and control compounds and incubated for 24 h at the designated temperatures for each bacteria. MIC values were determined as the minimal concentration where no visible bacterial growth was detected. All experiments were carried out in triplicate.

Time-kill Assays. Time-kill assays were performed using *E. coli* and 96-well microplates with clear bottoms (Nunclon™ Surface, Denmark). The bacterial culture was prepared as previously described. The killing effect was measured *via* a colorimetric assay using dimethyl sulfoxide (DMSO), and water-soluble tetrazolium salt (WST-8) reagent (Microbial Viability Assay Kit-WST, Dojindo, Japan). The Kit-WST can detect viable bacterial cells by a colorimetric assay. DMSO acts as an electron carrier, it carries electrons from the viable cells to WST causing a change in color from yellow to orange because of the formation of WST-8 formazan. The color change can be detected by a microplate reader at a wavelength of 460 nm. A blank was made by the media, tested peptide, and the Kit-WST. Peptides

1 and 2 were tested at two times the MIC values. Runs without the antimicrobial agents were performed to confirm the adequate growth of the bacteria (negative controls). The bacterial culture was added to the tested peptides and incubated in a shaking incubator at 37°C for 24 h. The absorbance values were measured using a microplate reader (Perkin Elmer, USA) at 460 nm at different time intervals, 1, 6, and 24 h, to determine the surviving bacterial cells. The readings were subtracted from the reagent blank and compared with the negative control to determine the %viability. From the %viability data, the %killing can be determined for the tested peptides. Time-kill assays were conducted in triplicate.

Bacterial Cell Viability Assays. Measuring cell viability was achieved by two methods. The first method was carried out by counting colony forming units (CFUs) on freshly prepared agar plates, while the other method used a colorimetric assay in 96-well microplates with clear, flat bottoms (Nunclon™ Surface, Denmark) using Kit-WST reagent. The *E. coli* bacterial strain was used at a high concentration (OD_{600} = 1.6), equal to 32 times the concentration used in the previously described assays (OD_{600} = 0.05). Peptides 1 and 2 were used at the following concentrations: 0.5, 0.25, 0.14, and 0.04 mg/mL. The bacterial cells were cultured in LB broth, then harvested at 4000 rpm for 10 min. The precipitated pellets were re-suspended in phosphate-buffered saline (PBS at a pH of 6.8) and divided into equal volumes, one for each peptide concentration. The treated bacterial solutions were incubated at 37°C for 12 h, then diluted serially by 2-fold up to three times. Portions (180 µL) of the diluted bacterial suspension were expanded using freshly prepared agar plates incubated for 24 h at 37°C. Another set of 180-µL portions was added to a 96-well microplate and mixed with 20 µL of Kit-WST reagent and incubated for 1 h. The absorbance was measured on a microplate reader (Perkin Elmer, USA) at 460 nm. Runs without the antimicrobial agents were carried out for both experiments. All the experiments were performed in triplicate

RESULTS AND DISCUSSIONS

Synthetic Protocol

The linear decapeptide 1 was synthesized using a standard Fmoc/ SPPS method as described above. The %yield of the obtained peptide 1 was approximately 97%, which was calculated by dividing the real obtained yield by the theoretical yield (calculated based on the loading rate equation of the first loaded amino acid) multiplied by 100. The structure and the purity were confirmed by mass spectrometry with a sharp peak at 1309.791 m/z, as shown in Figure 2 (a). Peptide 2 was obtained by cyclization of peptide 1 using HBTU and DIPEA as described above and the %yield was approximately 45% after the purification step. The structure and purity were confirmed by mass spectrometry with a sharp peak at 1291.7825 m/z, as shown in Figure 2 (b).

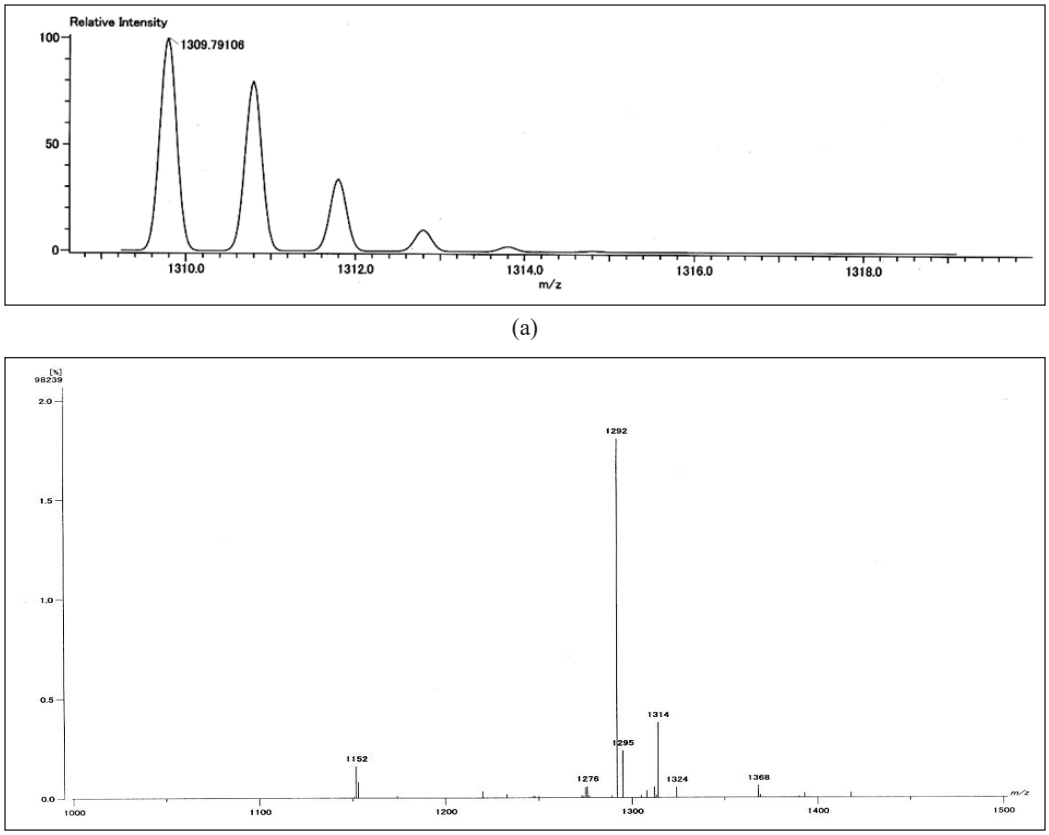

Figure 2. Mass spectra of peptide 1 (a) and peptide 2 (b)

Antibacterial assays

MIC Evaluation. The MIC values against *E. coli* and *B. thuringiensis* were evaluated for both peptides as the minimum concentration of the peptides showing no visible growth of the bacteria. Peptide 2 was more effective against the Gram-negative bacteria than the Gram-positive bacteria with MIC values of 0.16 and 0.24 mg/mL, respectively. Peptide 1 and 2 showed similar efficacy against Gram-positive bacteria with a MIC value of 0.24 mg/mL. Peptide 1 was more effective against the Gram-positive bacteria than the Gram-negative bacteria with MIC values of 0.24 and 0.3 mg/mL, respectively. Ampicillin was used as a standard positive control for the Gram-positive bacteria and kanamycin was used as the positive control for the Gram-negative bacteria. The MIC value of ampicillin was 0.03 mg/mL and the MIC value of kanamycin was 0.015 mg/mL.

The positive controls, kanamycin sulfate and ampicillin, were used in the MIC assay and the MIC values are given above. The antibacterial effects of the positive controls were higher than those of the tested peptides. One of the most important issues with antibiotic

agents is the resistance acquired by bacteria against those antibiotics, which may be solved by the use of AMPs. In addition, severe side effects can be caused by kanamycin, for example, kidney toxicity, loss of hearing, and allergic reactions (Sharma et al., 2016). Side effects observed with ampicillin include hypersensitivity, nausea, vomiting, and other gastrointestinal disorders (Raynor, 1997). Although the use of AMPs is still under investigation, they are considered to be safe as they are short peptides made of unmodified amino acids. In addition, bacteria rarely show resistance toward AMPs.

In general, cationic AMPs act by attacking the bacterial cell membranes resulting in the degeneration of the lipid bilayer leading to cell death (Zhang et al., 2001). The amphipathic structures of both the synthesized peptides gave them the ability to penetrate the bacterial cell wall (Jenssen, 2006). The cationic residues initiate electrostatic interaction forces toward the negatively charged bacterial cell membrane, while the hydrophobic moieties facilitate the penetration of the peptide (Madani et al., 2011). In addition, this amphipathic structure encourages the peptides to act in a micellar fashion by covering small parts of the cell membrane before the diffusion through the lipid bilayer, which leaves holes across the cell membrane (Bolintineanu & Kaznessis, 2011).

Time-kill Assays. *E. coli* is a major pathogen initiating numerous types of bacterial infections, which has developed multidrug resistance because of the chronic usage of antimicrobial agents. For these reasons, *E. coli* was chosen to perform the time-kill assay. The kit-WST reagent was used in this assay to detect the viable bacterial cells *via* a colorimetric technique using 96-well microplates. The reagent undergoes a reduction to WST-8 formazan by the action of NADPH from the viable bacterial cells. The resulting WST-8 formazan dye (orange color) can be determined by measuring the color intensity using a microplate reader at 460 nm.

The time-kill assay was used to determine the time needed for the peptides to exert the maximum antimicrobial effect against *E. coli* over 24 h (Figure 3). The time-kill assay can detect whether the bacteria show any resistance against tested compounds. Peptides 1 and 2 showed a very rapid maximal bactericidal effect against *E. coli* ($\geq$ 99%) over 1 h of incubation at a concentration of two times the MIC value. *E. coli* exhibited a minimal regrowth after 24 h of approximately 9% for peptide 1. The obtained data illustrated the rapid effect of both peptides 1 and 2 against the *E. coli* strain, and the highly stable bactericidal activity of peptide 2 over peptide 1. In addition, the bacterial resistance against peptide 2 (the cyclic form) was negligible, while for peptide 1, the bacteria showed a low level of resistance.

Bacterial Cell Viability Assays. The *E .coli* strain was used at a high concentration to detect the efficiency and the continued action of peptides 1 and 2. As shown in Figure 4,

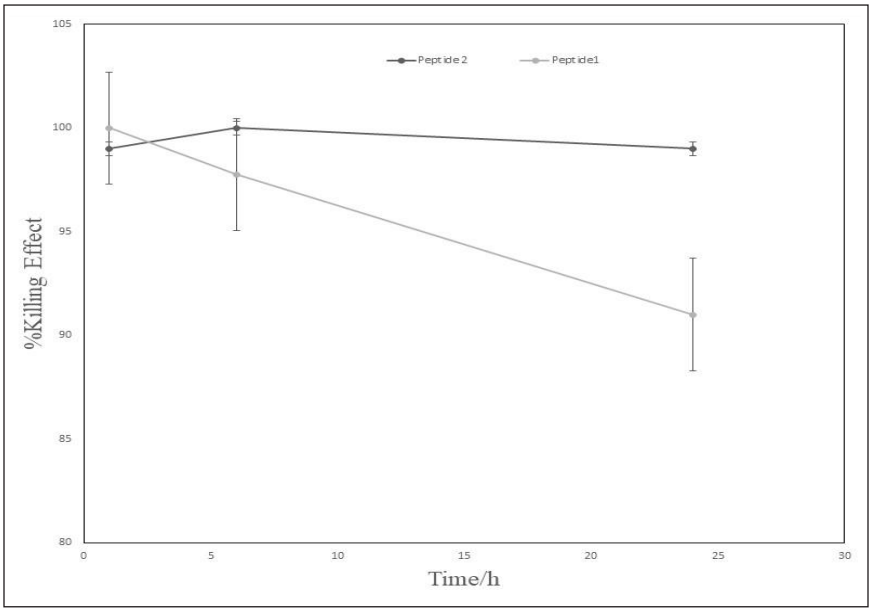

Figure 3. Time-kill assay of peptide 1 and peptide 2 using *E-coli*, the killing effect was measured at different time intervals (1, 6, and 24 h), at a peptide concentration of two times the MIC values during incubation at 37°C for 24 h

both assays gave nearly the same results. For the CFU counting method, peptides 1 and 2 at a concentration of 0.5 mg/mL showed a maximum killing effect of 83% and 86%, respectively. While at a concentration of 0.25 mg/mL, the peptides showed killing effects of 64% and 76%, respectively. At a concentration of 0.14 mg/mL, which is lower than the MIC values of both peptides, the killing effects were 58% and 65%, respectively. The lowest concentration of 0.04 mg/mL killed 21% and 30% of the bacterial cells, respectively.

The colorimetric assay confirmed the results obtained by the CFU counting method showing killing effects for peptide 1 of 71%, 56%, 24%, and 4% at concentrations of 0.5. 0.25, 0.14, and 0.04 mg/mL, respectively. Peptide 2 showed killing effects of 77%, 58%, 35%, and 16%, respectively. These data indicate that both peptides can form highly stable secondary structures at relatively high concentration levels. These structures had a maximum bactericidal effect, killing more than 80% of the total tested bacteria, after 12 h of incubation.

AMPs are oligopeptides having a different number of amino acid residues arranged in varying sequences. Generally, AMPs can be classified as cationic AMPs, cationic amphipathic peptides, cationic host defense peptides, host defense peptides, anionic antimicrobial peptides/proteins, and α-helical antimicrobial peptides (Park et al., 2017). AMPs can attack a wide range of organisms from viruses to parasites. However, particular AMPs can have a selective effect on one type of microbes (e.g. antiviral, antibacterial, or

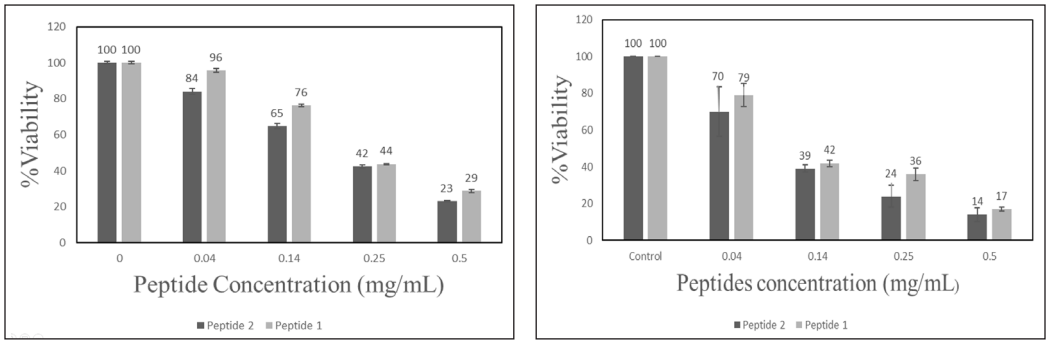

(a) (b)

Figure 4. (a) Bacterial cell viability assay using Kit-WST reagent and (b) CFU counting method for the antibacterial screening of both cyclic (peptide 2) and linear (peptide 1) forms against *E.coli*

antifungal peptides) (Hancock & Scott, 2000). Nevertheless, there are some AMPs that can have an effect on a wide range of microbs, for example, indolicidin can kill HIV, bacteria, and fungi (Robinson et al., 1998).

AMPs kill microorganisms *via* numerous mechanisms of action (Dutta et al., 2017; Yeung et al., 2011). However, antibacterial peptides act mainly by two mechanisms of action. The first method involves interaction with the bacterial cell membrane. Peptides need to possess an amphipathic character to achieve a proper interaction with the cell membrane. To have amphipathic character, the peptides need to include cationic and hydrophobic residues in the main structure of the designed peptide. These residues allow the peptide to interact with the bacterial cell membrane by electrostatic and hydrophobic forces. These interaction forces allow penetration of the peptide into the cell membrane resulting in cell death (Madani et al., 2011). The other mechanism of antibacterial peptides is by affecting some essential cell components, such as DNA or other vital intracellular components (Hsu et al., 2005).

Herein, an amphipathic linear decapeptide was synthesized by a standard Fmoc/ SPPS method. The reaction was continued as a one-pot synthesis from the loading of the first amino acid residue until the cleavage of the whole peptide. The purpose of this method was to increase the yield of the reaction and reduce the exposure to atmospheric humidity and oxygen, which have undesirable effects on the synthetic procedures. Both peptides were investigated for preliminary antibacterial action against Gram-positive and Gram-negative bacterial strains.

The MIC values were determined and the obtained results showed that peptides 1 and 2 had similar effects toward Gram-positive bacteria, while peptide 2 showed a higher effect against Gram-negative bacteria than peptide 1. This is because of the difference in the bacterial cell wall structure between the two strains. As shown in Figure 5 (a) and (b), the Gram-negative bacterial cell wall mainly consists of a thin, negatively charged,

peptidoglycan layer covered with an outer envelope of lipopolysaccharide. While, Gram-positive bacteria (c) have a thicker peptidoglycan layer but lack the outer hydrophobic lipopolysaccharide envelope (Silhavy et al., 2010). Thus, the more hydrophobic peptide 2 could penetrate the outer lipopolysaccharide layer in Gram-negative bacteria better than peptide 1, while both peptides act in the same manner toward Gram-positive bacteria, which lack the lipopolysaccharide envelope.

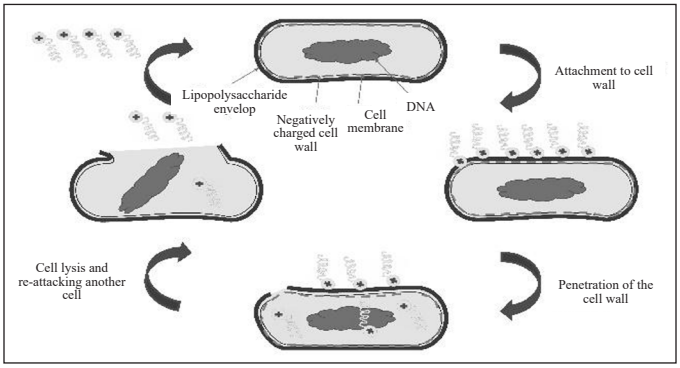

(a)

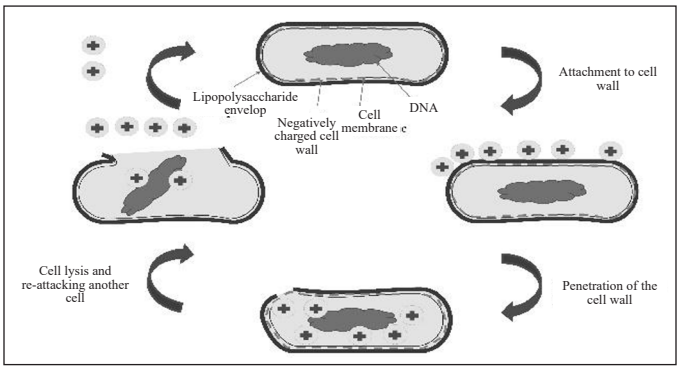

(b)

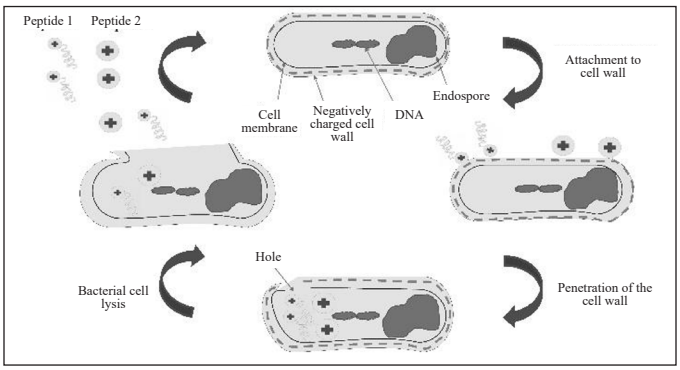

(c)

Figure 5. Suggested mode of action of peptides 1 and 2 against Gram-negative bacteria [(a) & (b)] and Gram-positive bacteria (c)

A time-kill assay was carried out to determine the time needed for the peptides to initiate their antibacterial effect. This assay showed that both peptides 1 and 2 had a rapid killing effect of approximately ≥ 99% over 1 h against *E. coli*. Bacterial cell viability was measured by the CFU counting method and the results were confirmed with a colorimetric assay. These assays were carried out to determine the effect of peptides 1 and 2 on a high concentration of the tested bacteria of approximately 32 times the concentration used in the earlier experiments. The results showed that a concentration of 0.5 mg/mL of either peptide showed a lethal effect on more than 80% of the total bacterial count over incubation for 12 h. In addition, a concentration of 0.25 mg/mL of either peptide was sufficient to kill more than 50% of the highly concentrated bacterial culture over incubation for 12 h. At a low concentration of 0.04 mg/mL, peptide 1 showed a very low killing effect because of the lack of the rigid structure, and the lower hydrophobicity, compared with peptide 2. Furthermore, at a low concentration, neither peptide could form the secondary structures that are important for the killing effect. We suggest that both peptides 1 and 2 can exert their action without being affected, or used by, the tested bacterial cells, and after bacterial cell lysis, the peptides can continue to attack more bacterial cells.

CONCLUSION

The newly designed cyclic decapeptide (peptide 2) and its linear counterpart (peptide 1) were synthesized using a standard Fmoc/SPPS method with yields of 97% and 45%, respectively. Both peptides showed antibacterial activity against the Gram-negative and Gram-positive bacterial strains, *E. coli*, and *B. thuringiensis,* respectively. However, peptide 2 showed a relatively higher potency against Gram-negative bacteria at lower concentration levels because of a superior ability to penetrate the bacterial cell wall compared with the linear counterpart. The MIC value for peptide 2 had a relatively lower value of 0.16 mg/mL compared with peptide 1, which had a MIC value of 0.3 mg/mL, against Gram-negative bacteria. While both peptide forms showed a similar MIC value of 0.24 mg/mL against Gram-positive bacteria. A time-kill assay indicated a rapid killing effect of both peptide forms, as the peptides could kill ≥ 99% of the tested bacterial strain (*E. coli*) after 1 h of incubation. The bacterial cell viability assay illustrated the maximum efficacy of peptides 1 and 2 enabling the death of more than 80% of cells at a high concentration of the tested bacterial cells.

ACKNOWLEDGEMENT

I would like to express my deep gratitude to Associate Professor Tamaki Kato and Associate Professor Shinya Ikeno, my research supervisors, for their patient guidance, enthusiastic encouragement, and useful critiques of this research work.

REFERENCES

Amblard, M., Fehrentz, J., Martinez, J., & Subra, G. (2006). Methods and protocols of modern solid phase peptide synthesis. *Molecular Biotechnology, 33*(3), 239-254. doi:10.1385/mb:33:3:239

Bolintineanu, D. S., & Kaznessis, Y. N. (2011). Computational studies of protegrin antimicrobial peptides: A review. *Peptides*, *32*(1), 188–201. doi:10.1016/j.peptides.2010.10.006

Brummett, R. E., & Fox, K. E. (1989). Aminoglycoside-induced hearing loss in humans. *Antimicrobial Agents and Chemotherapy*, *33*(6), 797–800. doi:10.1128/aac.33.6.797

Chalovich, J. M., & Eisenberg, E. (2013). NIH public access. *Magnetic Resonance Imaging*, *31*(3), 477–479. doi:10.1016/j.immuni.2010.12.017

Chen, J., Zhang, B., Xie, C., Lu, Y., & Wu, W. (2010). Synthesis of a highly hydrophobic cyclic decapeptide by solid-phase synthesis of linear peptide and cyclization in solution. *Chinese Chemical Letters*, *21*(4), 391–394. doi:10.1016/j.cclet.2009.11.026

Clinical and Laboratory Standard Institute (2018). *M100 performance standards for antimicrobial*. Wayne, New Jersey: Clinical and Laboratory Standards Institute.

Dutta, S. R., Gauri, S. S., Ghosh, T., Halder, S. K., DasMohapatra, P. K., Mondal, K. C., & Ghosh, A. K. (2017). Elucidation of structural and functional integration of a novel antimicrobial peptide from *Antheraea mylitta*. *Bioorganic and Medicinal Chemistry Letters*, *27*(8), 1686–1692. doi:10.1016/j.bmcl.2017.03.003

Gebhardt, K., Pukall, R., & Fiedler, H. P. (2001). Streptocidins A-D, novel cyclic decapeptide antibiotics produced by Streptomyces sp. Tü 6071. I. Taxonomy, fermentation, isolation and biological activities. *The Journal of Antibiotics*, *54*(5), 428–433. doi:10.7164/antibiotics.54.428

Gerard, J. M., Haden, P., Kelly, M. T., & Andersen, R. J. (1999). Loloatins A-D, cyclic decapeptide antibiotics produced in culture by a tropical marine bacterium. *Journal of Natural Products*, *62*(1), 80–85. doi:10.1021/np980219f

Gottenbos, B., Grijpma, D. W., van der Mei, H. C., Feijen, J., & Busscher, H. J. (2001). Antimicrobial effects of positively charged surfaces on adhering Gram-positive and Gram-negative bacteria. *Journal of Antimicrobial Chemotherapy*, *48*(1), 7–13. doi:10.1093/jac/48.1.7

Hancock, R. E. W., & Scott, M. G. (2000). The role of antimicrobial peptides in animal defenses. *Proceedings of the National Academy of Sciences, 97*(16), 8856-8861. doi:10.1073/pnas.97.16.8856

Hsu, C. H., Chen, C., Jou, M. L., Lee, A. Y. L., Lin, Y. C., Yu, Y. P., ... & Wu, S. H. (2005). Structural and DNA-binding studies on the bovine antimicrobial peptide, indolicidin: Evidence for multiple conformations involved in binding to membranes and DNA. *Nucleic Acids Research, 33*(13), 4053–4064. doi:10.1093/nar/gki725

Huber, U., & Majors, R. E. (2007). Principles in preparative HPLC. *Agilent Technologies Inc., Germany, 2,* 60-71.

Jenssen, H., Hamill, P., & Hancock, R. E. (2006). Peptide antimicrobial agents. *Clinical Microbiology Reviews*, *19*(3), 491–511. doi:10.1128/CMR.00056-05

Kessler, N., Schuhmann, H., Morneweg, S., Linne, U., & Marahiel, M. A. (2004). The linear pentadecapeptide gramicidin is assembled by four multimodular nonribosomal peptide synthetases that comprise 16

modules with 56 catalytic domains. *Journal of Biological Chemistry, 279*(9), 7413-7419. doi:10.1074/jbc.m309658200

Khaliq, Y., & Zhanel, G. G. (2003). Fluoroquinolone-associated tendinopathy: A critical review of the literature. *Clinical Infectious Diseases, 36*(11), 1404-1410. doi:10.1086/375078

Kreutzer, A. G., Salveson, P. J., Yang, H., & Supports, S. (2018.). *Standard practices for Fmoc-based Solid-Phase Peptide Synthesis in The Nowick laboratory, (Version 1.6.3), 1–14*. Retrieved September 19, 2018, from https://www.chem.uci.edu/~jsnowick/groupweb/files/Standard_practices_for_Fmoc_based_solid_phase_peptide_synthesis_in_the_Nowick_Laboratory_V_1point6.pdf

Madani, F., Lindberg, S., Langel, Ü., Futaki, S., & Gräslund, A. (2011). Mechanisms of cellular uptake of cell-penetrating peptides. *Journal of Biophysics, 2011*, 1-10. doi:10.1155/2011/414729

Mingeot-Leclercq, M. P., & Tulkens, P. M. (1999). Aminoglycosides: Nephrotoxicity. *Antimicrobial Agents and Chemotherapy 43*(5), 1003–1012. doi:10.1128/AAC.43.5.1003

Narayanan, C., & Dias, C. L. (2013). Hydrophobic interactions and hydrogen bonds in β-sheet formation. *The Journal of Chemical Physics, 139*(11), 115103. doi:10.1063/1.4821596

Park, A. J., Okhovat, J. P., & Kim, J. (2017). Antimicrobial peptides. In Gaspari A., Tyring S., Kaplan D. (Ed.) *Clinical and basic immunodermatology* (pp. 81-95). Cham, Switzerland: Springer. doi: 10.1007/978-3-319-29785-9_6

Raynor, B. D. (1997). Penicillin and ampicillin. *Primary Care Update for OB/GYNS, 4*(4), 147-152. doi:10.1016/S1068-607X(97)00012-7

Robinson, W. E., Mcdougall, B., Tran, D., & Selsted, M. E. (1998). Anti-HIV-1 activity of indolicidin, an antimicrobial peptide from neutrophils. *Journal of Leukocyte Biology, 63*(1), 94-100. doi:10.1002/jlb.63.1.94

Sharma, V., Bhagat, S., Verma, B., Singh, R., & Singh, S. (2016). Audiological evaluation of patients taking kanamycin for multidrug resistant tuberculosis. *Iranian Journal of Otorhinolaryngology, 28*(86), 203–208.

Silhavy, T., Kahne, D., & Walker, S. (2010). The bacterial cell envelope. *Cold Spring Harbor Perspectives in Biology*, *2*(5), 1–16. doi:10.1101/cshperspect.a000414

Stengel, D., Bauwens, K., Sehouli, J., Ekkernkamp, A., & Porzsolt, F. (2001). Systematic review and meta-analysis of antibiotic therapy for bone and joint infections. *The Lancet Infectious Diseases*, *1*(3), 175–188. doi:10.1016/s1473-3099(01)00094-9

Swierstra, J., Kapoerchan, V., Knijnenburg, A., van Belkum, A., & Overhand, M. (2016). Structure, toxicity and antibiotic activity of gramicidin S and derivatives. *European Journal of Clinical Microbiology and Infectious Diseases*, *35*(5), 763–769. doi:10.1007/s10096-016-2595-y

Tapeinou, A., Matsoukas, M. T., Simal, C., & Tselios, T. (2015). Review cyclic peptides on a merry-go-round; towards drug design. *Biopolymers*, *104*(5), 453–461. doi:10.1002/bip.22669

Yeung, A. T. Y., Gellatly, S. L., & Hancock, R. E. W. (2011). Multifunctional cationic host defence peptides and their clinical applications. *Cellular and Molecular Life Sciences*, *68*(13), 2161–2176. doi:10.1007/s00018-011-0710-x

Zhang, L., Rozek, A., & Hancock, R. E. W. (2001). Interaction of cationic antimicrobial peptides with model membranes. *Journal of Biological Chemistry*, *276*(38), 35714–35722. doi:10.1074/jbc.m104925200

Pertanika J. Sci. & Technol. 28 (S2): 197 - 216 (2020)

PERTANIKA JOURNALS

SCIENCE & TECHNOLOGY

Journal homepage: http://www.pertanika.upm.edu.my/

Enzyme Kinetics Study for Heterogeneous System of Pretreated Kenaf Hydrolysis

Nur Izyan Wan Azelee[1,2,3]*, Norhafiza Nordin[1], Rosli Md Illias[1,2], Nor Hasmaliana Abdul Manas[1] and Mohd Nazlee Faisal Md Ghazali[1]

[1]Department of Bioprocess and Polymer Engineering, School of Chemical and Energy Engineering, Faculty of Engineering, Universiti Teknologi Malaysia (UTM), 81300 Skudai, Johor, Malaysia
[2]Institue of Bioproduct Development (IBD), Universiti Teknologi Malaysia (UTM), 81310 Skudai, Johor, Malaysia
[3]Centre of Lipids Engineering and Applied Research (CLEAR), Ibnu Sina Institute for Scientific and Industrial Research, Universiti Teknologi Malaysia, 81310 UTM Skudai, Johor, Malaysia

ABSTRACT

The peculiarity of spatially restricted diffusion and molecular collision processes results in considerable contrast in a reaction between the reactant and catalyst in the heterogeneous system from its corresponding homogeneous structure. The identification of the enzymatic hydrolysis process of pre-treated kenaf and to convert it into simple sugars employing a systematic kinetic investigation is the aims of this study. The influence of substrate concentration on xylanase hydrolysis was performed in water bath shakers. In-house recombinant xylanase expressed in *Pichia pastoris* was used for the hydrolysis at pH 4.0 in 50 mM sodium citrate buffer with 200 rpm agitation. Modified Prout-Tompkins equation was used for the heterogeneous substrate hydrolysis. The results obtained show that temperature simultaneously influenced the time dependency of the reducing sugar yield. Dependence of the enzymatic rate of reaction can be calculated effectively on the conversion of substrates over different temperatures. The activation energy needed for pretreated kenaf hydrolysis was among the least compared to other lignocelluloses, which was only 25.15 kJ/mol. In conclusion, the exponential kinetic equation by the Modified Prout-Tompkins equation offers a solid understanding of xylanase hydrolysis on the pretreated kenaf. Thus, the prediction

ARTICLE INFO

Article history:
Received: 10 February 2020
Accepted: 13 November 2020
Published: 31 December 2020

DOI: https://doi.org/10.47836/pjst.28.S2.16

E-mail addresses:
nur.izyan@utm.my (Nur Izyan Wan Azelee)
norhafizanordin224@gmail.com (Norhafiza Nordin)
r-rosli@utm.my (Rosli Md. Illias)
hasmaliana@utm.my (Nor Hasmaliana Abdul Manas)
nazlee@utm.my (Mohd Nazlee Faisal Md Ghazali)
* Corresponding author

ISSN: 0128-7680
e-ISSN: 2231-8526

© Universiti Putra Malaysia Press

of the degree of hydrolysis required at the predetermined temperature and time values used can be quickly and precisely determined.

Keywords: Enzymatic hydrolysis, hemicellulose, heterogeneous system, kenaf, kinetic study

INTRODUCTION

Kenaf (*Hibiscus cannabinus L.*) is lignocellulosic biomass capable of generating bioenergy, xylooligosaccharides (XOS), and other value-added biomolecules. In the long term considering lignocellulosic biomass is another option for crop source, the economical, substantial, and renewable raw material (Mandelli et al., 2014). Despite cellulose, lignin, and a low number of extractives, it is a rapidly growing biomass and rich in hemicelluloses (Azelee et al., 2014). The hemicellulose is arbitrary and does not have a defined form that can be promptly hydrolyzed by dilute acid or base along with other various hemicellulolytic enzymes (De Menezes et al., 2009). The employment of enzyme technology in bioconversion processes provides advantages over conventional chemical technology in reducing the complexity of the carbohydrate–lignin complex.

Current research has raised huge concerns about the development of XOS from lignocellulose (rather than xylose) for the prebiotics, nutraceuticals, and food industries in particular. Attributable to this goal, the enzyme complex ratio developed needs to be wisely optimized, and its efficiencies tested. Enzymatic hydrolysis generally associates a buffer solution with complicated interfaces between the enzyme(s), substrate, and reaction environment. The reciprocal interaction between various enzyme activities is profiting a heterogeneous reaction of xylan or xylooligomer enzymatic hydrolysis. Plus, the kinetic view of reactions has become more complicated due to the existence of a broad range of xylooligomer chain lengths. Xylan, which degrades in the enzymatic media, is similar to other hydro-associated cleavages of heterocyclic ether bonds by the hydronium-catalyzed approach (Garrote et al., 2002). Xylan's enzymatic hydrolysis obeys the kinetic principles of insoluble substrates, where the assessment of the activation energy is vital to acquiring effective hydrolysis.

Enzyme kinetic is a catalyst analysis of quantitative enzyme which gives data regarding reaction rates. The understanding of the way of the enzyme acts and the actions of enzymes during the reaction are the fundamental grounds in the enzyme kinetics research. Enzyme kinetics studies calculate the enzyme affinity to substrate inhibitors and provide details on mechanisms of the reaction (Cinar et al., 2020; Valchev et al., 1998). The kinetic parameters also indicate the substrate's affinity to the enzyme. Enzyme kinetics generally involves the assessment of the enzyme-mobilized response rates at a varying concentration of substrates and enzymes.

The explanation on the kinetic process needs to consider most heterogeneous equations relating to other activity of heterogeneous catalytic, topochemical and diffusion (Valcheva

et al., 2000), and most heterogeneous conditions kinetic research applied the first method of hydrolysis velocity as the parameter of the primary concentration of enzymes (Chrastil, 1988; Nill et al., 2018). Due to its significant correlation variable ($R^2 = 0.9974$), the revised Prout-Tompkins equation, notably, best described the heterogeneous enzyme hydrolysis kinetics (Valtcheva et al., 2003)

Towards this end, this study aims to understand the hydrolysis mechanism on the pretreated kenaf by xylanase (the main hemicellulosic xylan degrading enzyme) by a systematic kinetic study into simple reducing sugars. It is of practical significance as it can predict the reaction rate, enzyme concentration, and the hydrolysis intensity needed at a certain temperature that has been determined beforehand. Figure 1 shows the general hydrolysis mechanism of xylanase on the pretreated kenaf.

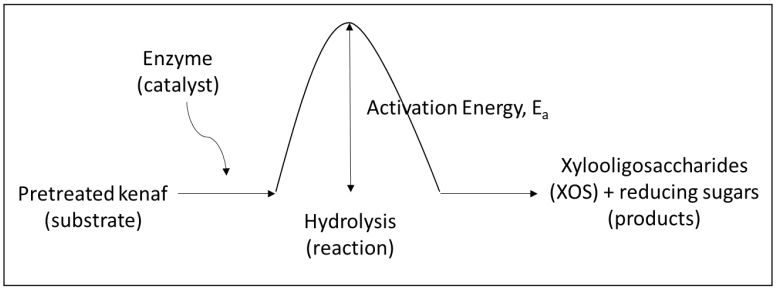

Figure 1. Hydrolysis mechanism of xylanase on the pretreated kenaf

MATERIALS AND METHODS

Preparation of the Raw Substrate

A company that is involved with kenaf processing in Bachok, Kelantan (North-East, Peninsular Malaysia) had generously provided the fresh whole kenaf stems including the core and the bast which were aged 3 to 4 months old. The constant weight of the kenaf stems was achieved by oven-dried for 24 h (105°C). The kenaf stem's moisture content was about 10 % (w/w). To acquire 40–60 mesh particle size, the dried kenaf stem was then hand-cut into tiny chunks and grounded using a mechanical grinder (Model RT-20, China). Eventually, before proceeding with the pretreatment procedures outlined below, the dried-ground kenaf stem was stored in a sealed container.

Pretreatment of Kenaf

The kenaf underwent 2-stages pretreatment with 7% $Ca(OH)_2$ for 1.5 hour, followed by 20% peracetic acid (PPA) for subsequent 2 h (Azelee et al., 2014)

Kinetic Study

The system of hemicellulose hydrolysis is never constructed precisely for the sake of its complicated nature and varying reaction conditions. Following the experimental result, a batch kinetic system was modelled and carried out for the hydrolysis of enzymatic hemicellulose. Based on the heterogeneous equation of the modified Prout-Tompkins equation as presented in (Equation 1), the kinetic model for the reaction of xylanase to the insoluble kenaf substrate was constructed in this analysis. The enzymatic hydrolysis of hardwood pulp (Valchev et al., 1998) and the steam-exploded wheat straw had widely employed the model previously (Radeva et al., 2012).

In this kinetic study of the enzyme, three different temperatures (30, 40, and 50°C) were used. Temperature variance was examined using the Arrhenius equation in the apparent rate constant, k. The equation of Arrhenius (Equation 2) provides the reliance of the rate constant, k of a chemical reaction on the absolute temperature T (in Kelvin), where A is the pre-exponential factor (or merely the *prefactor*), E_a is the activation energy, and R is the Universal gas constant (8.31446 $\frac{J}{mol.K}$). The rate, v was measured in (Equation 3) as a function of the degree of substrate conversion, ∝ at varying temperatures, and the graph was eventually constructed.

$$\frac{\propto}{(1-\propto)} = (k\ t)^{x} \qquad \text{(Equation 1)}$$

$$k = Ae^{\frac{-E_a}{RT}} \qquad \text{(Equation 2)}$$

$$v = x\ k \left[\frac{\propto}{(1-\propto)}\right]^{\frac{(x-1)}{x}} (1-\propto)^{2} \qquad \text{(Equation 3)}$$

Enzyme Kinetic by Prediction and Experimental Values

Given this test, the kinetic variable was dimensional quantity α, the amount of reduced sugar which moved across the solution at a particular moment (Rs) and the overall saturated quantity, Rs_{max} $\propto = \frac{Rs}{Rs_{max}}$. Rs is the present value of reduced sugars, whereas Rs_{max} is the utmost amount of reduced sugars produced during the treatment of enzymes. The Rs_{max} values for various temperatures are therefore calculated by the equation derived (as in Equation 4). The detailed mathematical derivation of the formula is shown in the supplementary data.

$$R\ s_{max} = \frac{2\ R\ s_1 \left[\left(\frac{t_1}{t_2}\right)^{x} - 1\right]}{\left[2\left(\frac{t_1}{t_2}\right)^{x} - 1\right]} \qquad \text{(Equation 4)}$$

However, another set of kinetic calculation (for the E_a and A values) was performed based on the experimental values obtained directly from the graph of reducing sugars (RS) versus time. Moreover, a comparison was made to determine the most suitable method (by prediction or experimental) for the calculation of the kinetic study of xylanase hydrolysis on the pretreated kenaf stem.

RESULTS AND DISCUSSION

Comprehending the hydrolysis process on the pretreated kenaf by xylanase (the main hemicellulosic xylan degrading enzyme) into simple reducing sugars by a structured kinetic investigation was the purpose of this kinetics analysis of enzymatic hydrolysis. It was of significance as it might predict the degree of hydrolysis needed at specified temperature levels, the concentration of the enzyme, and the time required to accomplish the reaction.

Figure 2 demonstrates the experimental results about the variation of reducing sugars (Rs) with the time (t) in the temperature range studied. After the first exponential increase, the mechanisms decelerate throughout every temperature from the kinetic curves. Consequently, a test with a prolonged period of incubation is usually required to determine the maximum amount of sugar reduction (Rs_{max}). Furthermore, the measurement of substrate concentration in terms of its molecular weight is hard to achieve in the study, attributable to the laborious and unmeasurable method to determine the concentration of the insoluble substrate required in the heterogeneous reaction. Within the sense of the prominent Michaelis-Menten equation, which is widely applied for homogeneous reactions and is not restricted to a time constraint, these descriptions and the configuration of the kinetic curves do not imply the likelihood of their mathematical explanations (Radeva et al., 2012).

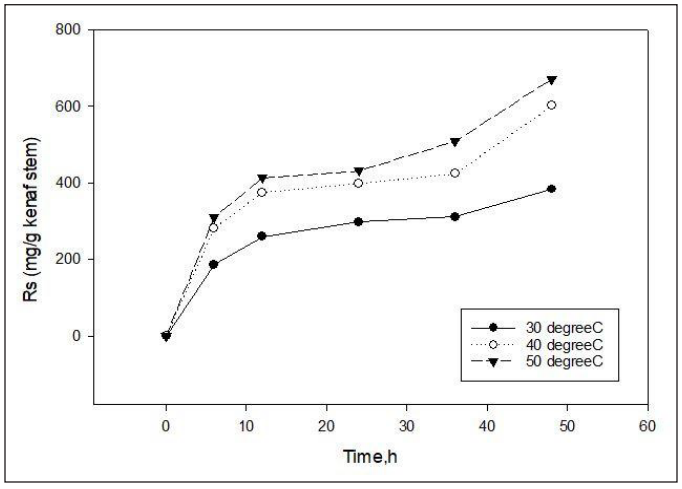

Figure 2. Kinetic curves (at the exponential phase) of the enzymatic xylanase hydrolysis of the pretreated kenaf stem at different temperatures from 0 h until 48 h. Other operating conditions were set at the optimum value of the xylanase hydrolysis (T = 40°C, pH 4.0, substrate loading = 2% and xylanase loading = 400 U).

Although the xylanase kinetic behaviour matches the Michaelis–Menten framework on clearly identified soluble oligosaccharides but this traditional Michaelis–Menten method is insufficient to explain xylanase activity on insoluble hemicellulose (xylan) (Fialho & Carmona, 2004). The renowned Michaelis-Menten principle is not fit to be generalized for heterogeneous structures that have an uncertain amount of substrates. Thus, derivations of kinetic formula relating to dispersion, topochemical and alternative forms of heterogeneous processes were investigated by prior researchers for a kinetic description (Valchev et al., 1998; Valtcheva et al., 2003)

The ability of the components to move within the system is part of the significant dissimilarities between homogeneous and heterogeneous kinetics. Although reactant molecules inhomogeneous environments are typically accessible to each other, solid-state reactions also take place within crystal lattices or with molecules that have to pass through lattices where mobility is limited and possibly rely on lattice deformities. If the rate of the process is regulated by the reaction interface movement of the reactants or products, a product layer can increase (Khawam & Flanagan, 2006; Welch, 1955).

Therefore in this analysis, the enzyme kinetics study utilizing xylanase (the key xylan backbone degrading enzyme) was analyzed based on the modified Prout-Tompkins formula for the processing of simple reducing sugars. Similar findings for the xylanase activity on kraft pulp have also been documented (Valcheva et al., 2000).

Thermogravimetry is often used to study reaction kinetics in the solid-state, although other appropriate analytical approaches are applicable for the assessment of kinetic reactions (Cai et al., 2018). The determined parameter must be converted into a fraction of conversion ($\propto$) that can be employed for every single analytical process in kinetic equations. A dimensionless quantity ($\propto$) is recognized as a kinetics variable used in (Equation 1), which is the proportion of the amount of sugar reduction that has been transferred at a particular point in time (Rs) and its maximum values beneath the saturation level, (Rs_{max} $\propto = \frac{Rs}{Rs_{max}}$). Besides, $\propto$ also feasible to facilitate the degree of conversion of the substrate or also to explain the degree of hydrolysis, where x is an unvarying constant features of the model or power factor, and k is a constant rate of reaction calculated in reciprocal time units (Valchev et al., 1998). The activity of xylanase on pretreated kenaf can be defined as a topochemical process, meaning that the reaction occurs at the interphase limit. The rate of reaction also relies on the size and shape of the shifting interaction surface result from the substrate's heterogeneous structure (Valchev et al., 1998). Owing to this complex heterogeneous composition of the pretreated kenaf matrix, it specifies the reaction zones and their topochemical mechanism. It is well established that the following Equation 1 can be implemented efficiently to topochemical chain mechanism reactions and diffusion regulated heterogeneous processes.

Temperature Dependence of the Hydrolysis Process

In the current study, the kinetics of kenaf stem hemicellulose hydrolysis was studied at temperatures of 30ºC, 40ºC, and 50ºC, under optimized xylanase hydrolysis conditions (2% substrate concentration, 400 U of xylanase activity, and in a pH 4.0 system of sodium acetate buffer). Experimental results on the total value of reducing sugar, Rs, produced after enzymatic hydrolysis was recorded to acquire the kinetic curves, as demonstrated in Figure 2. They are reducing sugar yield that can be observed increasing with time when the temperature rises from 30°C to 40°C but is not preferred at 50°C. The thermal inactivation of the enzyme may contribute to the decrease of the reducing sugars at 50°C at a longer hydrolysis time. (Valcheva et al., 2000).

At the start of the process, it was presumed that at low concentrations of reducing substances ($\propto$<<1), Equation 1) was reduced to Equation 5:

$$\propto = (k\ t)^{\chi} \qquad \text{(Equation 5)}$$

Therefore,

$$\frac{R\ s}{R\ s_{\ max}} = (k\ t)^{\chi} \qquad \text{(Equation 6)}$$

The logarithmic form of (Equation 6), is presented as in (Equation 7)

$$ln\ R\ s\ =\ ln\ (\ Rs_{\ max}) + \chi\ .\ lnk + \chi\ .\ lnt \qquad \text{(Equation 7)}$$

Dependence of reducing sugars over time at different temperatures in logarithmic coordinates is presented in Figure 3. By utilizing the experimental kinetic information, $Rs=f(t)$, at the initial stage of the process it facilitates the determination of the coefficient χ at a specified temperature. The data in Figure 3 shows that the coefficient χ is temperature independent and the average result is 0.2746.

It is also possible that from Equation 7, a maximal value of the reducing substances can be measured with a value for χ from Equation 8. It may assist to provide an accurate and better regression for Rs_{max}. Thus, the Rs_{max} values are estimated for various temperature adopting the Equation 8

$$Rs_{\ max} = \frac{2\ Rs_1\ \left[\ \left(\frac{t_1}{t_2}\right)^{x}\ -\ 1\ \right]}{\left[\ 2\ \left(\frac{t_1}{t_2}\right)^{x}\ -\ 1\ \right]} \qquad \text{(Equation 8)}$$

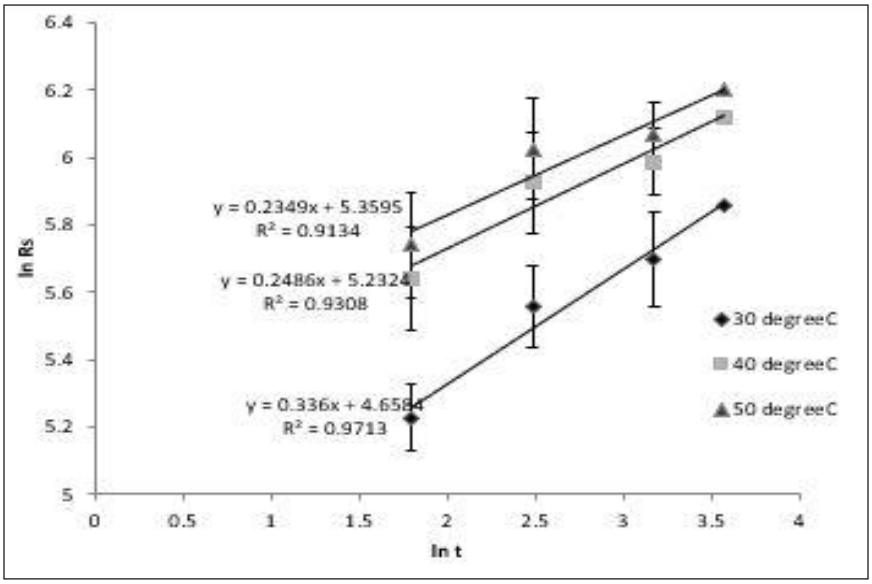

Figure 3. The dependences of the amount of reducing sugars on time in logarithmic coordinates at various temperatures (30°C, 40°C and 50°C)

The predicted Rs_{max} values for three temperatures are briefed in Table 1 below. The detailed calculation for each temperature is shown in the supplementary data.

Table 1
Rs_{max} values at different temperatures

Temperature, ºC	Rs_{max}
30	650.173
40	980.036
50	1084.04

Significantly higher Rs_{max} was obtained from the study compared to the one achieved by Valcheva et al. (2000) where only 37.5 mg/g of sugar was obtained from kraft pulp xylanase hydrolysis. The high yield of the Rs_{max} achieved in the study showed the high efficiency of xylanase hydrolysis on the pretreated kenaf stem. This method and the equation were developed for Rs_{max} substantial contributions to related process kinetics being studied. Further analysis of the kinetic data was performed on the basis of the modified Prout-Tompkins (Equation 1).

From the logarithmic form of Equation 1, the apparent rate constant, k was found and is presented in Equation 9.

$$ln \frac{\propto}{1 - \propto} = \chi \ . ln \frac{\propto}{1 - \propto} = \chi \ . ln \qquad \text{(Equation 9)}$$

In addition, linear relations for three temperatures following Equation 9 are shown in Figure 6. The calculated constants k and χ were proofs that the values of χ from Equation 7 and Equation 9 are in strong compromise to one another (90 % confidence level). In this study, the pre-treated kenaf stem used is categorised as the harder to degrade material (hardwood) due to the crystalline structure of the lignocellulose (Rowell & Rowell, 1996). A prior study by Zhang et al. (1999) reported that the degree of hydrolysis (α) of the harder-to-degrade material was more susceptible temperature than the rate for the easier-to-degrade material. On that account, the temperature rises from 30°C to 40°C is, therefore, necessary to achieve the optimum hydrolysis of xylanase for the pretreated kenaf stem. On the contrary, a rise in temperature from 40°C to 50°C is required for steam-exploded wheat straw as it is categorized as easier to degrade material (Radeva et al., 2012).

In Figure 4, the inhomogeneity coefficient, $\propto$ is predicted from the gradient of the straight lines. For temperature readings of 30ºC, 40ºC and 50ºC, it was discovered to be equal to 0.229. In instances where it is independent of temperature, just entropy inhomogeneity is accounted for by the coefficient of $\propto$ (Radeva et al., 2012).

In Figure 5, linear relations are presented in accordance with Equation 9 for three varying temperatures. The linear relationship is significant for the calculations of the kinetic constant of χ and k (Table 2). Valcheva et al. (2000) had also performed a similar study with four different temperatures (20 to 50°C) on kraft pulp and all of them showed a straight line with high correlation coefficient. In this analysis, the correlation coefficient, R, and standard deviation calculated by the Revised Prout-Tompkins equation is 0.9097 and 0.119, respectively. The values of χ and k for each temperature (Table 2) are acquired from the plot of $ln\frac{[\propto}{(1-\propto)]}$ versus $ln\ t$ in Figure 5.

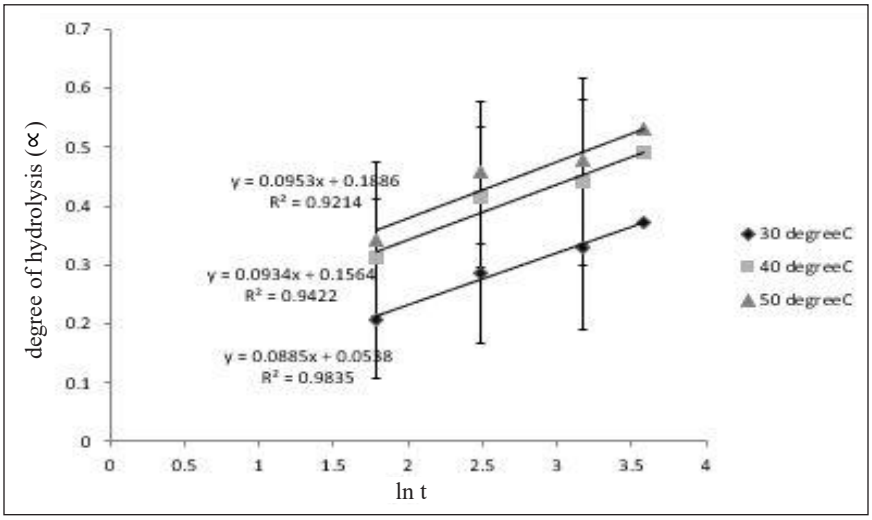

Figure 4. The linear dependences of the kinetic variables (degree of hydrolysis ($\propto$) against different time (t) in logarithmic coordinates) at given temperatures for 2% of pretreated kenaf stem

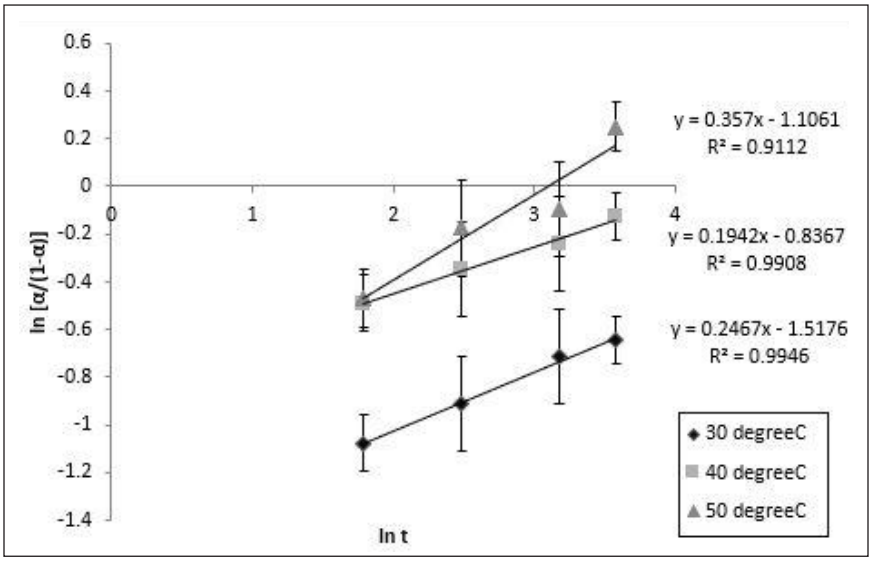

Figure 5. The linear form of Prout-Tompkins equation for different temperatures

Table 2
The values of χ and k at different temperatures

Temperature, ˚C	*x*	*k*
30	0.2467	0.00737
40	0.1943	0.00969
50	0.3570	0.00915

Research on hardwood pulp by Valchev et al. (1998) offers a different value of χ and k for temperature 20 to 40°C. The values to other substrates would be slightly different. These values are crucial for investigating variations in temperature using the Arrhenius equation (Valcheva et al., 2000).

The Determination of Activation Energy from the Enzymatic Hydrolysis of the Pretreated Kenaf using the Predicted Values of Rs_{max}

To attain the kinetic parameters (model, E_a, A), the temperature variation of the apparent rate constant, k was studied using the Arrhenius equation (Khawam & Flanagan, 2006). The Arrhenius equation gives dependence on the rate constant, k of a chemical reaction on the absolute temperature T (in Kelvin), where A is the pre-exponential factor (or simply the *prefactor*), E_a is the activation energy, and R is the Universal gas constant (8.31446 $\frac{J}{mol.K}$). The Arrhenius equation and its derivation are shown in Equations 10 and 11.

$$k = A\ e^{\frac{-E}{RT}} \quad \text{(Equation 10)}$$

$$ln\ k = \frac{-E_a}{RT} + ln\ A \quad \text{(Equation 11)}$$

As shown in Figure 6 at the grounds of the statistically significant correlation between $ln\ k$ and $\frac{1}{T}$, the activation energy, E_a and the pre-exponential factor A was revealed to be: E_a = 8.95 $\frac{J}{mol.K}$ and A = 0.271. The pre-exponential factor units, A, are analogous to the rate constant units and should differ according to reaction order. Supposing that the reaction is first order, then the unit is s^{-1}. Since the concentration of the reactant in this study is constant (because the concentration of enzymes does not rise or drop with time, the concentration of one of the reactants remains constant because it is distributed in vast quantities and its concentration can be absorbed within the constant rate), the order of this reaction is known as a pseudo-first-order reaction. This pseudo-first-order reaction is very beneficial, as it significantly simplifies the quantification of the kinetics of the reaction. It can be complicated to observe a second-order reaction mostly because the two reactants associated must be calculated concurrently. Other complications may occur because it requires a certain amount of each reactant to calculate the reaction rate, for example, which can make one's experiment uneconomical if one or both of the reactants required are costly. The majority of kinetic findings recognize the restricted parts of the kinetic curves generally apply pseudo-first or second-order equations (Valtcheva et al., 2003).

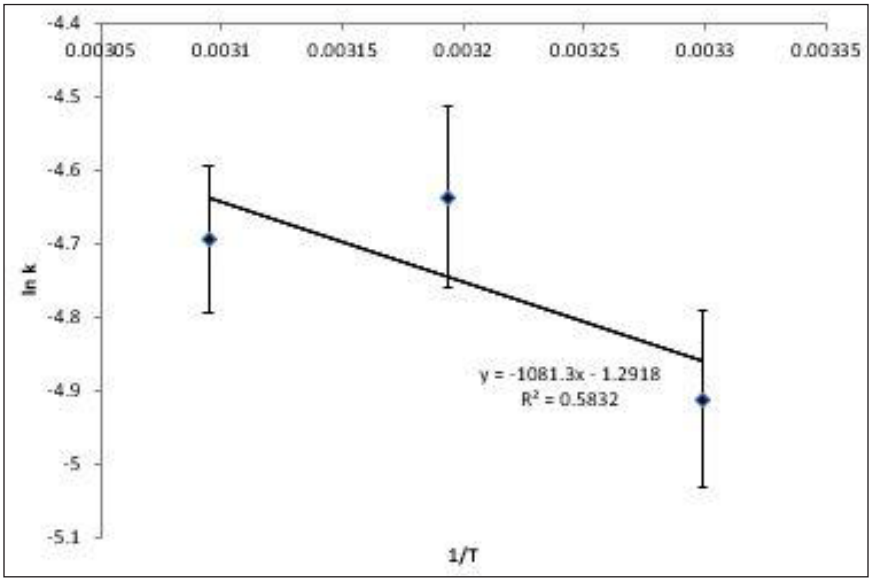

Figure 6. Linear relation between $ln\ k$ and $\frac{1}{T}$ from the Arrhenius equation. The activation energy was calculated to be 8.95 kJ/mol

By using the above equation with identified values of k and χ, the rate v can be determined for other $\propto$. The rate v is shown in Figure 7 as a function of the degree of substrate conversion, $\propto$ at different temperatures. At temperature 40ºC, absolute values of the rate and their variations with $\propto$ in the entire process are the highest while the lowest rate is at 30ºC. The pre-exponential factor, A, which decreases when $\propto$ increases contribute to the rate decreases with time. The measurements of the reaction area and its availability may be related to the pre-exponential component A,which is developed during the process on the basis of xylan-enzyme complexes and modifications. The application of the topochemical kinetic model to the evaluation of the reaction may also be taken into consideration. The process initially occurs on the kenaf's most accessible outer surface and eventually permeates into the kenaf fibre matrix. The consistent activation energy indicates that on the surface and within the capillary system, the energy properties of the xylan-enzyme complex are the same, i.e. the enzyme has a chemical interaction with the same xylan only.

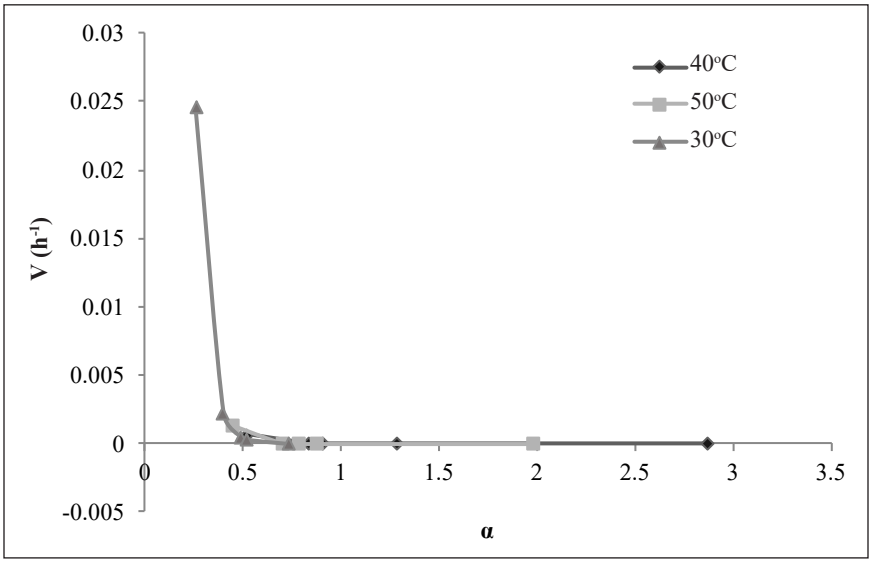

Figure 7. The present rate of hydrolysis in enzymes, v reliance on the degree of substrate conversion, $\propto$ for different temperatures

The Determination of Activation Energy from the Enzymatic Hydrolysis of the Pretreated Kenaf using the Actual Values of Rs_{max} Obtained from the Experiment

As the rate of hydrolysis, v decreased dramatically to 0 when $\propto > 0.5$, the temperature variation of hydrolysis rate, v which at the given degree of substrate conversion, $\propto$ did not satisfy the Arrhenius equation. To obtain an excellent v profile, the values of Rs_{max} from the experimental result were used to rectify the previously projected values of the Rs_{max}. Therefore, an amended assessment of $\propto$ was conducted by using the Rs_{max} from

experimental data. The values of Rs_{max} for respective temperature were gained from the graph in Figure 8 and are shown in Table 3.

In Figure 8, the reaction is labelled as a burst phase at around 40 hours when the graph grows exponentially for all three temperatures. This type of graph obtained in the study can be called as pre-steady-state kinetics or may be appealed as Burst kinetics. Burst kinetics is a form of enzyme kinetics which pertains to the initial high enzyme turnover velocity when the enzyme is introduced to the substrate. This initial phase of product development at high velocity is termed the "Burst Period". This duration is examined as the enzymes become saturated with substrates up to saturation of all enzymes. After the saturation of all enzymes, the Burst Phase leads to a linear velocity of reaction (Praestgaard et al., 2011). The Burst kinetics accounts well for the experimental data that have successfully used the Burst kinetics model for the hydrolysis of Cellobiohydrolases (exo-cellulases) on cellulose. Before reaching the steady-state kinetics interests in the development and utilization of intermediate enzyme-substrate up till their steady-state concentrations are attained. The rate subsequently decreases as it enters a steady state. A single enzyme turnover was analyzed during the rapid burst period of the process.

This nonlinearity of the heterogeneous reaction kinetics could be clarified either one or more among this considerations: inactivation of the enzyme, inhibition of the product, or heterogeneity of the substrate (Zhang et al., 1999). The restriction of the mass transfer suggests that the rate of reaction is not entirely determined by the catalytic capacity of the enzyme. The mass-transfer rates of the substrate(s) from the bulk reaction medium to the

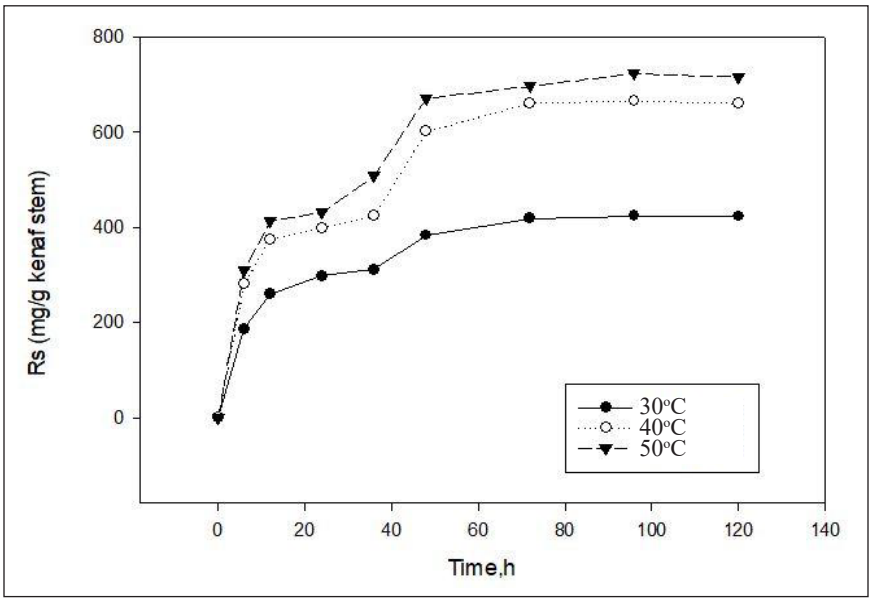

Figure 8. Overall kinetic curves of enzyme action for different temperatures.

enzyme site as well as the mass-transfer rates of the product(s) from that channel back to the reaction medium need to be taken into consideration (Illanes et al., 2013). Due to the virtue of the structural changes inside the substrate, kinetic action will not intrinsically be similar to the free enzyme.

Based on the graph obtained by the experiment, the Rs_{max} values for each temperature (30°C, 40°C and 50°C) are shown in Table 3 below.

Table 3
Rs_{max} values for respective temperature (based on the experimental research)

Temperature, ˚C	Rs_{max}
30	550
40	680
50	723

Figure 9 describes the linear dependencies derived using the experimental result. To obtain the inhomogeneity coefficient, $\propto$ each value of Rs is divided at each time with the median value of Rs_{max} gained from the respective temperature. The determination of $\propto$ is essential to be used in the next step of determining the kinetic values of χ and k. The linear form of Prout-Tompkins equation using the value of $\propto$ (initially determined) for vary temperatures are also presented in Figure 10.

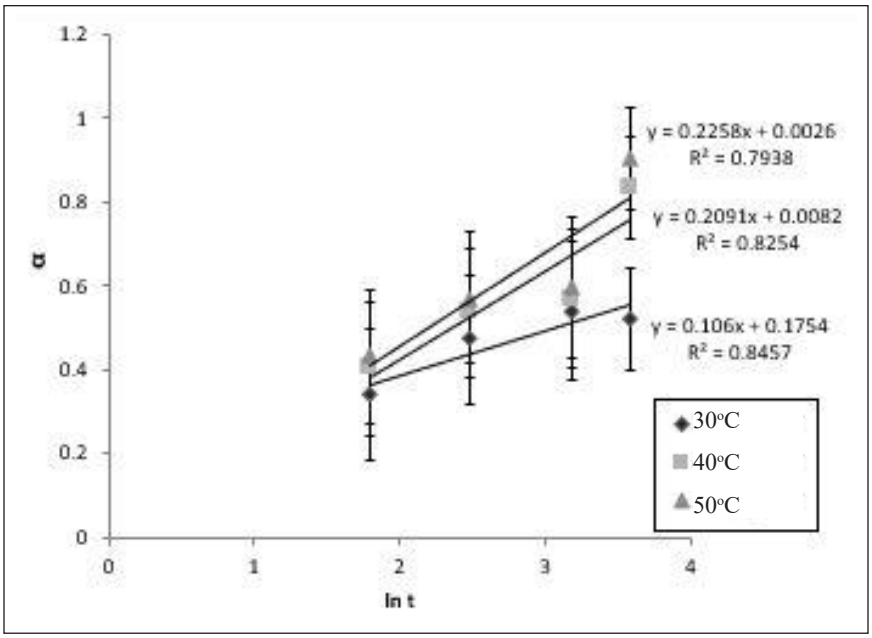

Figure 9. Linear dependences of the kinetic variable, $\propto$ vs. $ln\ t$ (experimental work)

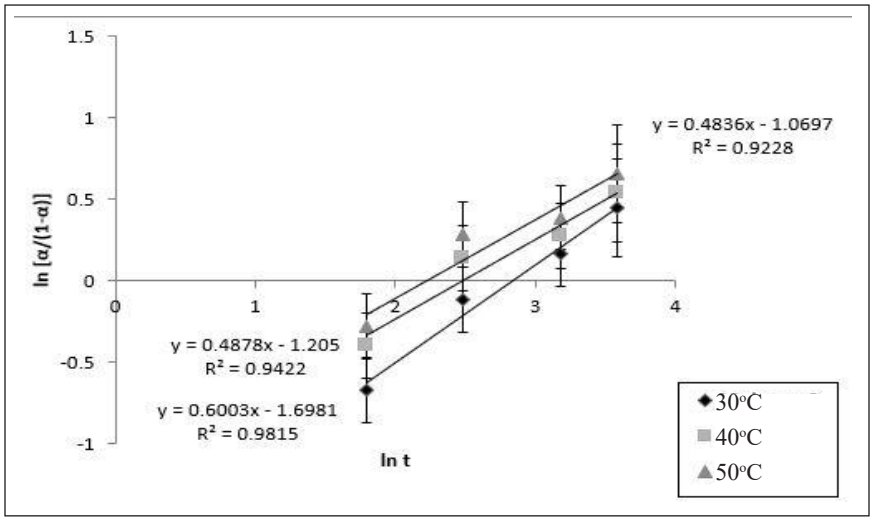

Figure 10. The linear form of Prout-Tompkins equation for vary temperatures (experimental work)

In the analysis, the correlation coefficient R and standard deviation for using the Revised Prout-Tompkins equation are respectively 0.9064 and 0.0532. The values of χ and *k* acquired for respective temperature from the plot of $ln\frac{\propto}{1-\propto}$ versus $ln\ t$ are recorded in Table 4.

Table 4
The values of χ and k at different temperatures (gained from the experimental values)

Temperature, ˚C	χ	*k*
30	0.6005	0.0590
40	0.4878	0.0846
50	0.4836	0.1090

The values of activation energy, E_a and pre-exponential factor, A are determined by plotting the values of $ln\ k$ against $\frac{1}{T}$ with T in Kelvin (Figure 10).

The applicability of the logarithmic form of Equation 4 approved by the linear behaviour. Based on the linear relation between $ln\ k$ and $\frac{1}{T}$ (shown in Figure 11), the activation energy, E_a and the pre-exponential factor, A in the analysis it was identified that: E_a = 25.15 $\frac{J}{mol.K}$ and A = 1290.648 respectively. The R^2 value is above 0.90, which is 0.9945 proving that the obtained result is reliable.

For comparison, Leszczynski and Shukla (2012) had reported that the energy needed for the activation of glycosidic C-O bond in the absence of a catalyst was estimated to be 41.83 $\frac{J}{mol.K}$ which was relatively higher than what had been obtained in the study. Hence, with the addition of xylanase enzyme as the bio-catalyst to hydrolyse the pretreated kenaf stem has managed to reduce the amount of activation energy required successfully. Smaller

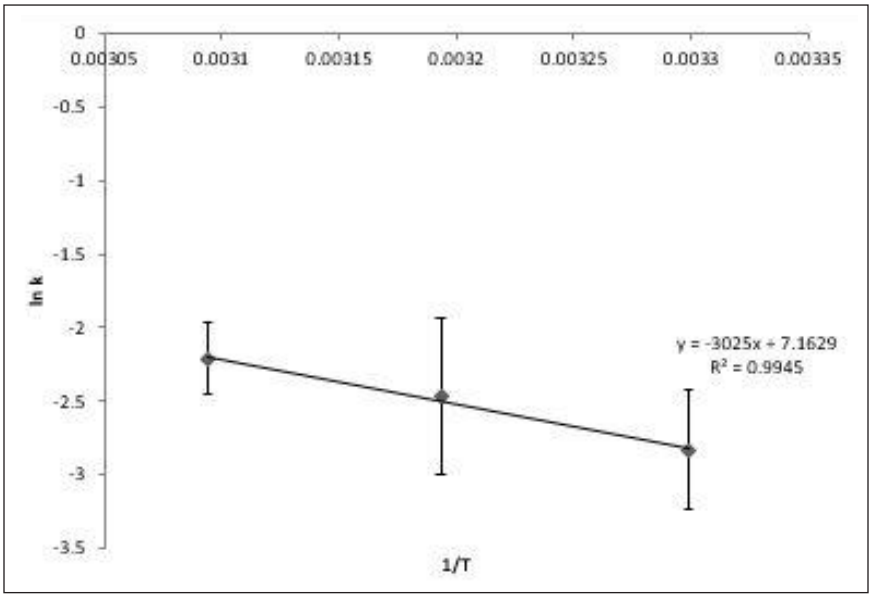

Figure 11. Linear relation between $ln\ k$ and $\frac{1}{T}$ (from the experimental values)

activation energy is preferred as a more effective way to bring about a substrate's reaction or hydrolysis. The presence of xylanase enables a more significant percentage of reactant molecules to gain sufficient power for transit through the state of transition and become products.

The breakdown of this C-O glycosidic bond demanded less energy to activate than the C-N glycosidic bond where the breakdown of the C-N bond was expected to be 100.79 $\frac{J}{mol.K}$ (Leszczynski & Shukla, 2012). Besides, hydrothermal treatment has measured the activation energy usually required for the cleavage of hardwood xylan (*Eucalyptus saligna*) glycosidic bonds is 125.6 $\frac{J}{mol.K}$. Model studies proposed that the degradation rate differs subjected to classification of the structure for the lignocellulosic bonds even though they are chemically labile in acid (Christopher, 2012). The energy of 129.2 $\frac{J}{mol.K}$ is required for activation as well as the frequency variables within 2.56 x 10^{15} to 2.57 x 10^{14} for acid hydrolysis of Beechwood hemicellulose from *Fagus crenata*. Whereas, multiple reports have demonstrated a broad range of activating energy for the hydrolysis of acid (106.2–159.7 $\frac{J}{mol.K}$). Xylobiose which is the analog from the acid hydrolysis of Cellobiose reveals an activating energy of 137 $\frac{J}{mol.K}$. This outcome is approximately similar to the glucans cleavage energy (other lignocellulose conformation) (Dumitriu, 1998). Conversely, hardly any kinetic reaction constants are identified in alkaline hydrolysis literature (Dumitriu, 1998).

The present predicted rate of the hydrolysis process is at varying values. The temperature outcome is graphed in Figure 12. The process rate is seen to be the highest at $\propto$ values below 0.4. It then declines substantially, most likely due to the exertion of the active site available on the substrate region (Radeva et al., 2012; Valtcheva et al., 2003). Earlier research reported that standard hydrolysis cellulose process began with proportionately steady momentum, then the rate of hydrolysis declined, and usually concluded with incomplete hydrolysis of the substrate later when enormous doses of the enzyme were introduced. This circumstance can arise with the disappearance of enzyme stability or activity, the consequence from the hindrance of the reaction output, a possible elevation in the recalcitrance of the substrate from the hydrolysis process, or rivalry amidst various enzyme elements on the substrate's active sites (Chandra et al., 2011). The difficulty in comparing the speed and degree of hemicellulose hydrolysis by different xylanases is the result of the non-linear system. This non-linearity also affects the process of hemicellulose hydrolysis as the rate declines and usually halts before all substrate is metabolized. The finding supports the theory which, over time, a decline in the rate of xylanase activity of kenaf hemicellulose is because of a reduction in the simple degradable substrate. The absent of β-xylosidase stimulation for xylanase activity dismisses the idea of inhibition of substances being the reason for the reported non-linearity.

Table 5 below demonstrates a table of contrast on the activation energy required for hydrolysis of varying substrate. Particularly in comparison with some of the other substrates, the xylanase hydrolysis on the pretreated kenaf stem has shown to have a rather low activation energy. This means that with a slow step with less energy barrier, the xylanase

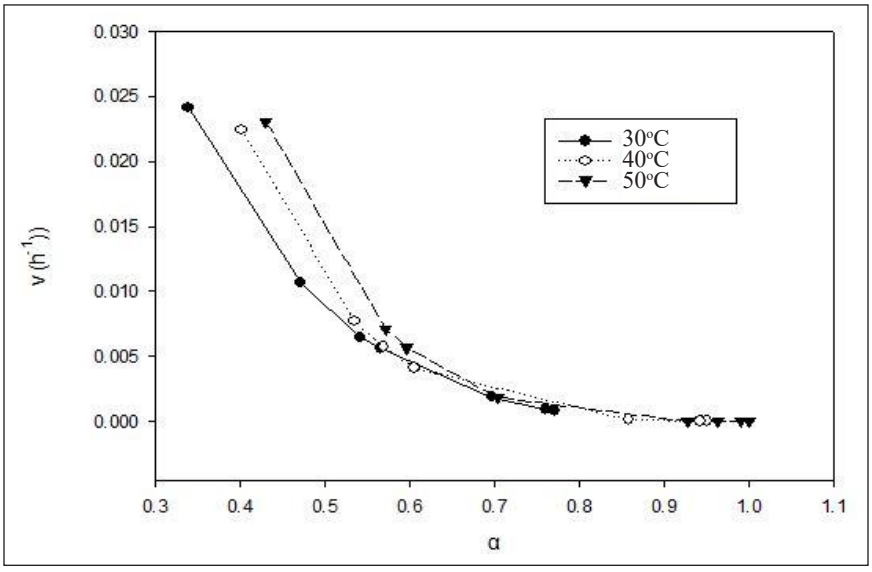

Figure 12. Dependence of the enzymatic hydrolysis current rate, *v* on the degree of substrate conversion, ∝ at various temperature values (30°C, 40°C and 50°C).

enzyme was able to shift the reaction pathway to another. The value of activation energy obtained in the study is within the common range used by other hydrolysis enzymes.

Table 5
Comparison between various substrate hydrolysis and the activation energy required for the process

Substrate	Activation energy, $E_a(\frac{J}{mol.K})$	Reference
Kenaf	25.15	This study
Hardwood kraft pulp	34.1	(Valchev et al., 1998)
Kraft pulp	34.6	(Valcheva et al., 2000)
Pulp	22.2	(Valtcheva et al., 2003)
Wheat straw	20	(G. Radeva, 2011)
Wheat straw	46.7	(Radeva et al., 2012)

CONCLUSION

The xylanase hydrolysis kinetics of the pretreated kenaf was evaluated after pretreatment with alkali-acid (Ca_2(OH)–PPA). It has been discovered that the exponential kinetic equation offers an excellent clarification on the behaviour of xylanase, and the activation energy needed for hydrolysis is lower than some lignocellulose. Temperature influences the time dependence of the reduced sugar yield. It is of practical significance since it gives prediction on the degree of hydrolysis demanded at predetermined temperature values and the time spent. Moreover, the reaction rate depends on the conversion of the substrate and the value can be estimated at different temperature levels.

ACKNOWLEDGMENT

This work was supported by UTM Transdisciplinary Research Grant (References Grant Q.J130000.3551.05G64) and Institute of Bioproduct Development (IBD), Universiti Teknologi Malaysia. We thank the Everise Crimson (M) Sdn. Bhd. for providing us with the kenaf sample and Genencor Danisco for the free enzyme samples.

REFERENCES

Azelee, N. I. W., Jahim, J. M., Rabu, A., Murad, A. M. A., Bakar, F. D. A., & Illias, R. M. (2014). Efficient removal of lignin with the maintenance of hemicellulose from kenaf by two-stage pretreatment process. *Carbohydrate Polymers, 99*, 447-453. doi:10.1016/j.carbpol.2013.08.043

Cai, J., Xu, D., Dong, Z., Yu, X., Yang, Y., Banks, S. W., & Bridgwater, A. V. (2018). Processing thermogravimetric analysis data for isoconversional kinetic analysis of lignocellulosic biomass pyrolysis: Case study of corn stalk. *Renewable and Sustainable Energy Reviews, 82*, 2705-2715. doi:10.1016/j.rser.2017.09.113

Chandra, R. P., Au-Yeung, K., Chanis, C., Roos, A. A., Mabee, W., Chung, P. A., ... & Saddler, J. N. (2011). The influence of pretreatment and enzyme loading on the effectiveness of batch and fed-batch hydrolysis of corn stover. *Biotechnology Progress, 27*(1), 77-85. doi:10.1002/btpr.508

Chrastil, J. (1988). Determination of the first order consecutive reaction rate constants from final product. *Computers & Chemistry, 12*(4), 289-292. doi:10.1016/0097-8485(88)80002-0

Christopher, L. (Ed.) (2012). *Integrated forest biorefineries: Challenges and opportunities*. Cambridge, United Kingdom: Royal Society of Chemistry. doi: 10.1039/9781849735063

Cinar, K., Gunes, G., & Gulec, H. A. (2020). Enzymatic synthesis of prebiotic carbohydrates from lactose: Kinetics and optimization of transgalactosylation activity of β-galactosidase from Aspergillus oryzae. *Journal of Food Process Engineering*, *43*(8) e13435. doi:10.1111/jfpe.13435

De Menezes, A. J., Siqueira, G., Curvelo, A. A., & Dufresne, A. (2009). Extrusion and characterization of functionalized cellulose whiskers reinforced polyethylene nanocomposites. *Polymer, 50*(19), 4552-4563. doi:10.1016/j.polymer.2009.07.038

Dumitriu, S. (Ed.) (1998). *Polysaccharides: Structural diversity and functional versatility*. Boca Raton, Florida: CRC Press. doi: 10.1021/ja0410486

Fialho, M. B., & Carmona, E. C. (2004). Purification and characterization of xylanases from *Aspergillus giganteus*. *Folia Microbiol (Praha), 49*(1), 13-18. doi:10.1007/bf02931639

Garrote, G., Domínguez, H., & Parajó, J. C. (2002). Autohydrolysis of corncob: Study of non-isothermal operation for xylooligosaccharide production. *Journal of Food Engineering, 52*(3), 211-218. doi:10.1016/s0260-8774(01)00108-x

Illanes, A., Wilson, L., & Vera, C (2013). Enzyme kinetics in a heterogeneous system. In Illanes, A., Wilson, L., & Vera, C. (Ed.), *Problem solving in enzyme biocatalysis* (pp. 87-140). New Jersey, USA: John Wiley and Sons Ltd. doi: 10.1002/9781118341742.ch03

Khawam, A., & Flanagan, D. R. (2006). Solid-state kinetic models: Basics and mathematical fundamentals. *The Journal of Physical Chemistry B, 110*(35), 17315-17328. doi:10.1021/jp062746a

Leszczynski, J., & Shukla, M. (Eds.) (2012). *Practical aspects of computational chemistry II: An overview of the last two decades and current trends*. New York, London: Springer. doi: 10.1007/978-94-007-0923-2

Mandelli, F., Brenelli, L., Almeida, R., Goldbeck, R., Wolf, L., Hoffmam, Z., ... & Squina, F. (2014). Simultaneous production of xylooligosaccharides and antioxidant compounds from sugarcane bagasse via enzymatic hydrolysis. *Industrial Crops and Products, 52*, 770-775. doi:10.1016/j.indcrop.2013.12.005

Nill, J., Karuna, N., & Jeoh, T. (2018). The impact of kinetic parameters on cellulose hydrolysis rates. *Process Biochemistry, 74*, 108-117. doi:10.1016/j.procbio.2018.07.006

Praestgaard, E., Elmerdahl, J., Murphy, L., Nymand, S., McFarland, K. C., Borch, K., & Westh, P. (2011). A kinetic model for the burst phase of processive cellulases. *The FEBS Journal, 278*(9), 1547-1560. doi:10.1111/j.1742-4658.2011.08078.x

Radeva, G., Valchev, I., Petrin, S., Valcheva, E., & Tsekova, P. (2012). Kinetic model of enzymatic hydrolysis of steam-exploded wheat straw. *Carbohydrate Polymers, 87*(2), 1280-1285. doi:10.1016/j.carbpol.2011.09.012

Radeva, G., Valchev, I., Petrin, S., Valcmeva, E., & Tsekova, P. (2011). Comparative kinetic analysis of enzyme hydrolysis of steam-exploded wheat straw. *Cellulose Chemistry and Technology, 46*(1-2), 61-67.

Rowell, R. M., & Rowell, J. (1996). Chemical composition of fibers. In J. Stein (Ed.), *Paper and composites from agro-based resources* (pp. 83-134). Massachusetts, USA: CRC Press.

Valchev, I., Yotova, L., & Valcheva, E. (1998). Kinetics of xylanase treatment of hardwood pulp. *Bioresource Technology, 65*(1–2), 57-60. doi:10.1016/s0960-8524(98)00020-0

Valcheva, E., Veleva, S., Valchev, I., & Dimitrov, I. (2000). Kinetic model of xylanase action on kraft pulp. *Reaction Kinetics and Catalysis Letters, 71*(2), 231-238. doi:10.1023/A:1010310706612

Valtcheva, E., Veleva, S., Radeva, G., & Valtchev, I. (2003). Enzyme action of the laccase-mediator system in the pulp delignification process. *Reaction Kinetics and Catalysis Letters, 78*(1), 183-191. doi:10.1023/A:1022538621950

Welch, A. J. E. (1955). *Solid-solid reactions*. New York, NY: Academic Press

Zhang, S., Wolfgang, D. E., & Wilson, D. B. (1999). Enzyme action of the laccase-mediator system in the pulp delignification process. *Biotechnology Bioengineering, 66*(1), 35-41. doi: 10.1023/A:1022538621950

Pertanika J. Sci. & Technol. 28 (S2): 217 - 230 (2020)

PERTANIKA JOURNALS

SCIENCE & TECHNOLOGY

Journal homepage: http://www.pertanika.upm.edu.my/

Effect of Reaction Temperature on the Growth of Carbon Nanotubes from Waste Natural Rubber Glove

Mohammad Adib Hazan[1], Syazwani Mohamad[2], Mohamad Amin Hamid[1], Shahira Liza[2], Md Shuhazlly Mamat[1], Kar Fei Chan[1] and Yazid Yaakob[1,3]*

[1]Department of Physics, Faculty of Science, Universiti Putra Malaysia, 43400 UPM Serdang, Selangor, Malaysia
[2]TriPrem i-Kohza, Malaysia-Japan International Institute Technology, Universiti Teknologi Malaysia, 54100 Kuala Lumpur, Malaysia
[3]Microscopy Unit, Institute of Bioscience, Universiti Putra Malaysia, 43400 UPM Serdang, Selangor, Malaysia

ABSTRACT

Natural rubber (NR) glove disposal is not environmentally appropriate and a range of approaches have been suggested to overcome the problem. Herein we indicate a simple method for producing high-value nanotubes from waste NR glove as a partial solution to the environmental problem. The laboratory-based waste NR glove was selected as a carbon precursor. Carbon nanotubes (CNTs) were synthesized using chemical vapor deposition (CVD) method comprising ferrocene over SiO_2 substrate, which acted as a catalyst and surface for the carbon conversion process. The growth temperature was varied using 500, 600 and 700°C. The carbon precursor was analyzed using thermogravimetric analysis (TGA) to determine the optimum thermal decomposition of the waste. The CNTs collected after CVD process were analyzed using Raman spectroscopy, field emission scanning electron microscopy (FESEM), transmission electron microscopy (TEM). Optimization studies to determine the effect of temperature showed that the highest yield of CNTs was produced under a reaction temperature of 700°C (yield % = 5.47%, Raman I_D/I_G ratio = 0.82). The nanomaterials formed confirmed as CNTs and amorphous carbon under TEM images of the tubular structure of the products with a diameter range of 13 – 16 nm.

Keywords: Carbon nanotubes, chemical vapor deposition, waste natural rubber

ARTICLE INFO

Article history:
Received: 10 February 2020
Accepted: 13 November 2020
Published: 31 December 2020

DOI: https://doi.org/10.47836/pjst.28.S2.17

E-mail addresses:
adib.hazan@gmail.com (Mohammad Adib Hazan)
syazwani.mohamad@graduate.utm.my (Syazwani Mohamad)
helangphy95@gmail.com (Mohamad Amin Hamid)
shahiraliza@utm.my (Shahira Liza)
shuhazlly@upm.edu.my (Md Shuhazlly Mamat)
kfeichan08@gmail.com (Kar Fei Chan)
yazidakob@upm.edu.my (Yazid Yaakob)
* Corresponding author

ISSN: 0128-7680
e-ISSN: 2231-8526

© Universiti Putra Malaysia Press

INTRODUCTION

The research of carbon nanotubes (CNTs) keeps on increasing since its first discovery by Iijima in 1991 (Golnabi, 2012; Iijima, 1991). From that CNTs have been taken into account in many applications due to their robust properties such as high electrical conductivity, as well as thermal conductivity and mechanical strength (Okolo et al., 2019; Prasek et al., 2011). Due to their properties, the demand of the CNTs is increasing each year in a large scale as they have been using in wide field of technologies such as electronics, optics and composite materials.

Therefore, several methods to synthesize CNTs have been developed. The most common methods are arc discharge, laser ablation and chemical vapor deposition (CVD) (Paul & Samdarshi, 2011). Among these methods, CVD was reported to be a versatile method in which it can easily control the parameter of CNTs growth by modulating the temperature, the gas flow rate, the reaction time, the catalyst materials and the state of the carbon precursor. Furthermore, CVD is capable of high scale mass production of CNTs at low cost (Azam et al., 2013a; Liu et al., 2011a).

Carbon precursors used in CVD usually from the well-known carbon sources that have been commercially used in industries such as ethane, benzene and acetylene (Faizah et al., 2008; Louis et al., 2005; Sobri et al., 2016). However, these carbon precursors are classified as fossil-based carbon source and it is a non-renewable source which produces heavy pollution and expensive. Thus, researchers are trying to find a new candidate for carbon precursor that is renewable and sustainable. Nowadays, carbon precursor from natural sources and waste materials have picked the researcher's interest as they can replace the fossil-based carbon sources. Well studied natural carbon sources include turpentine oil, eucalyptus, palm oil, and camphor (Ghosh et al., 2007, 2008; Kumar & Ando, 2005; Suriani et al., 2012). Other waste materials carbon source includes sugarcane bagasse waste, plastic waste, printed circuit board and waste latex (Alves et al., 2012; Hazan et al., 2019; Quan et al., 2010; Yao et al., 2017). These carbon precursors have been simplified in Table 1. Furthermore, using waste materials to form high-value products such as CNT helps in reducing the amount of waste and pollution, especially from non-biodegradable waste.

World rubber production keeps increasing each year including the natural rubber (NR) and synthetic rubber production. The world rubber consumption is also increasing year by year due to the production of rubber materials such as vehicle tire, children toys, shoe hills and soles and massively used in the production of natural rubber glove. According to Malaysian Investment Development Authority (MIDA) Malaysia is the main stakeholder, holding 60% of the global output for rubber glove and which is exported to more than 195 countries (Bernama, 2019) A variety of gloves produced is non-reusable such as surgical glove. Thus, the waste produced from the use of surgical rubber gloves around the world is high, especially with the Covid-19 pandemic looming all around the world. In recent

Table 1
Precursor for the synthesis of CNTs from different class of hydrocarbon

Hydrocarbon source	Temperature (°C)	Diameter of CNTs	References
Fossil based			
Ethane	720	30 nm	(Louis et al., 2005)
Benzene	900	8-30 nm	(Sobri et al., 2016)
Acetylene	750-850	~44 nm	(Faizah et al., 2008)
Natural source			
Turpentine oil	850		(Ghosh et al., 2008)
Eucalyptus	850	0.79-1.71 nm	(Ghosh et al., 2007)
Palm oil	750	23-26 nm	(Azmina et al., 2012)
Camphor	800-1050	1.2-40 nm	(Kumar & Ando, 2005)
Waste materials			
Sugarcane bagasse	600 & 1000	20-50 nm	(Alves et al., 2012)
Plastics waste	700-900	20-40 nm	(Yao et al., 2017)
Printed circuit board	900	~338 nm	(Quan et al., 2010)
Waste latex	700	5-20 nm	(Hazan et al., 2019)

years, many researches have been geared to use waste with a high percentage of carbon content as a precursor for CNT growth. The waste NR glove contains a very high amount of hydrocarbon chain as it was made up of the monomer of polyisoprene (C_5H_8) (Yip & Cacioli, 2002). Hence, we find it interesting to study the feasibility of waste NR glove as a green precursor for high-quality CNT growth using CVD methods.

To optimize the production of CNTs, different parameters of the CVD method can be varied. One of the crucial parameters in the CVD method to grow CNT is the growth temperature and it affects the growth rate of the CNT (Acomb et al., 2015; Alves et al., 2011). Lee et al. (2001) varied the growth temperature in between 750°C and 950°C using iron catalyst. Increasing the growth temperature will increase the yield of CNT as the carbon diffuses faster, and in turn increases the carbon reaction rates during deposition through the catalyst particles (Lee et al., 2001; Liu et al., 2011b).

In this work, we studied the synthesis of CNTs by utilizing the waste NR glove as carbon precursor source. Our aim was to inspect and identify the effect of growth temperature on the production of CNTs. This could be achieved by varying the growth temperature at 500°C, 600°C and 700°C while the other parameters were set constant in CVD method.

MATERIALS AND METHODS

The waste NR glove was obtained from the Unigloves Sdn Bhd, Negeri Sembilan and used as carbon precursor for the synthesis of CNTs via CVD method. The waste NR glove was characterized using thermogravimetric analysis (TGA, Mettler Toledo TGA/ SDTA 851) to identify the thermal decomposition and to determine the optimal temperature for pyrolysis

of the carbon precursor. Pyrolysis was needed to vaporize the waste NR glove, which was solid at room temperature into gas state rich in hydrocarbon chain. The vaporized waste NR glove was then pushed into the reactor chamber in the furnace by argon gas.

The process for carbon nanotubes growth via CVD was done by using waste NR glove as shown in Figure 1 as a carbon precursor and setup as the schematic diagram in Figure 2. The catalyst utilized was ferrocene mix with ethanol and dripped over SiO_2 coated glass slide and put at the center of the furnace. The gas flow for argon and hydrogen was fixed at 60 cc/min and 5 cc/min, respectively. The reaction temperature was set at 500°C with a heating rate of 10°C/min and the pyrolysis of carbon precursor was set to 450°C. The reaction time for carbon growth was fixed at 15 min and then the furnace being cooled. This method was then repeated for growth temperature 600°C and 700°C. The samples were collected afterward and characterized using Raman spectroscopy (URaman-M, Technospex Pte Ltd), field emission electron microscopy (FESEM, NOVA NANOSEM 230, Fei) and transmission electron microscopy (TEM, JEM2100F, JEOL).

Figure 1. Photographic image of waste NR glove

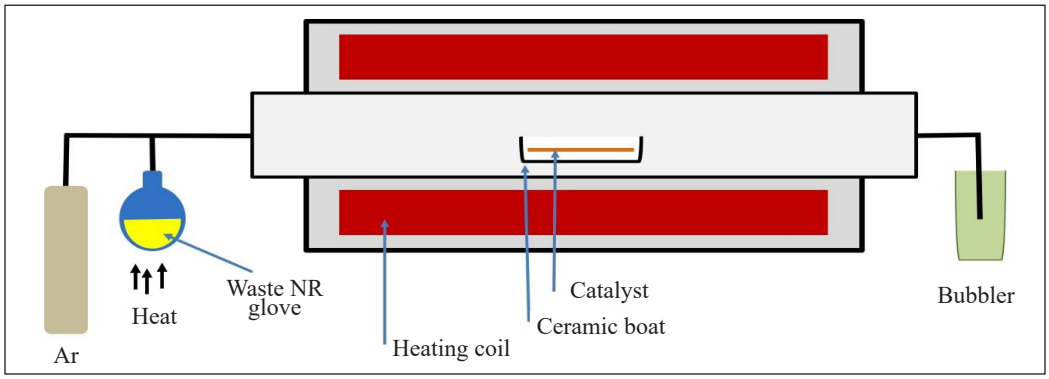

Figure 2. Schematic diagram of the CVD system

RESULTS AND DISCUSSION

Precursor Analysis

The thermal decomposition of NR glove waste was studied using thermal gravimetric analysis (TGA) under nitrogen atmosphere in the range from 25-600°C. This was to predict the optimal temperature of waste NR glove at which the pyrolysis process would be acted upon. Figure 3 shows that the main degradation region lies between 320°C and 450°C, the degradation region referring to the liberation of gaseous products that will be used in the production of CNTs via CVD (Essawy et al., 2017). Approximately at 460°C, the decomposition process was complete with 25% of the residual weight from the actual weight of NR glove waste were collected at the end of the process. As such, 450°C was selected as the temperature at which the pyrolysis would be undertaken to ensure a high amount of gaseous product to be utilized in the synthesis of CNTs.

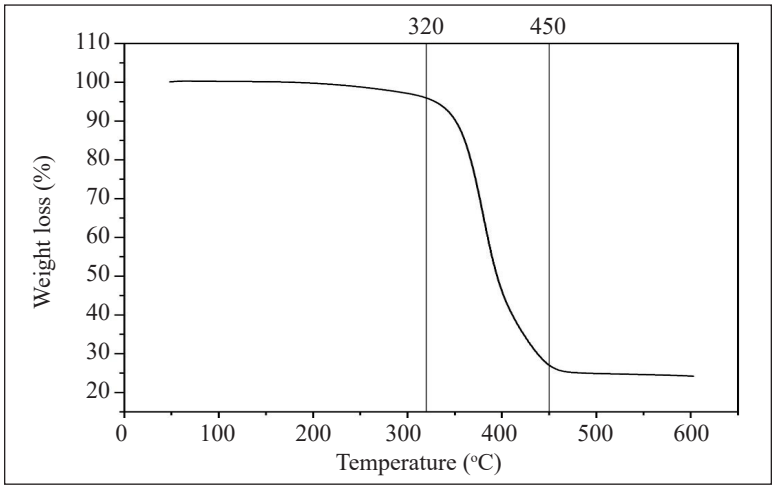

Figure 3. TGA profile of NR glove waste.

Raman Spectra Analysis

Raman spectroscopy measurement was performed to characterize the CNTs present in the samples as presented in Figure 4. Two prominent Raman peaks centered at around 1350 and 1550 cm^{-1} (Ferrari & Robertson, 2000) could be easily observed for the CNTS samples at 600°C and 700°C while at 500°C there was no peak formed in a range of D peak and G peak indicating there were no formation of nanotubes inside the sample. However, there were broad spectra with no clear peak was observed at 500°C which indicated the formation of amorphous carbon. The amorphous carbon is a mixture of sp^2 and sp^3 hybridized bonds without crystalline structure (Judai et al., 2016) which is different from the graphitic structure such as CNTs, graphite and graphene that have a well-defined crystalline structure with carbon atoms having sp^2 bonding (Aqel et al., 2012; Azam et al.,

2013a). Amorphous carbon is found to be harmful to the growth of CNTs due to its role in inhibiting the catalyst by attaching itself on the surface of the catalyst, since there are no peak observed (Marton et al., 2013). This inhibits the diffusion of carbon through the catalyst particle, halting the growth of CNT. From Figure 5c, the FESEM image of the sample at 500°C growth temperature depicts more amorphous carbon deposited on the catalyst-substrate surface after the CVD process.

In the production of CNT, two major peaks were associated with the quality of the CNT formed which were the defect peak (D band) and graphitic peak (G band). The peak at 1315 cm^{-1} corresponded to the D band which indicated the lattice defects and disorders of sp^2 carbons that were introduced during growth in the CVD process and the peak at 1550 cm^{-1} (G band) was the tangential C-C stretching modes (Dresselhaus et al. 2002, 2005; Mamedov et al., 2002; Suriani et al., 2012). The intensity ratio of I_D/I_G can be used to estimate the amount of defect and disorder in carbon materials (Chen et al., 2013). The increasing I_D/I_G ratio for CNTs formation implies that there are more defects in the samples. The height intensity of the peaks also indicates the quality of the nanotubes formed. The I_D/I_G ratio at 600°C and 700°C were 0.83 and 0.82 respectively. From Figure 4 the D peak and G peak for the sample at 600°C and 700°C have the slightly same height. Thus, we know that the sample after CVD had a defect and graphitic structure in a fair amount. A well-defined crystalline structure CNTs would have a very sharp G peak with low intensity of D peak. At 500°C, the amorphous spectra had shown that there was no formation of CNTs at this temperature and at 600°C the defined peak D and G shown with I_D/I_G ratio of 0.83. At 700°C growth temperature, the I_D/I_G ratio was reduced by 0.01, indicating the quality of CNTs formed was increasing.

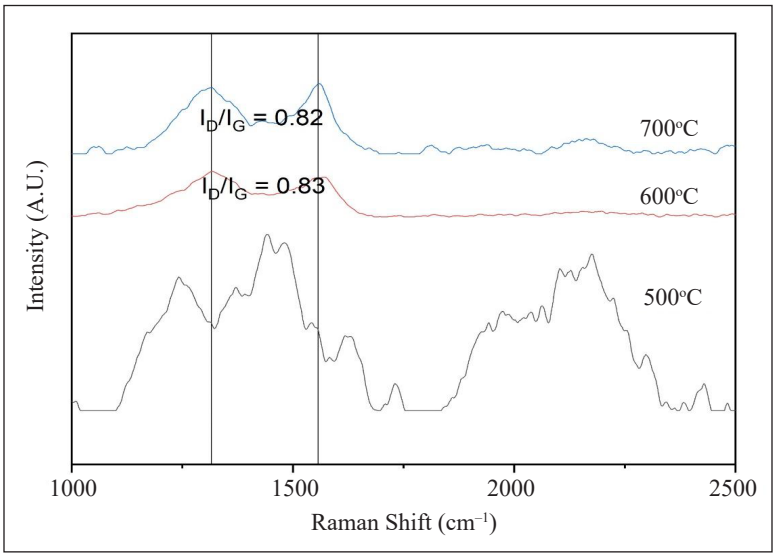

Figure 4. Raman spectrum of CNTs at 500°C (grey), 600°C (red) and 70°C (blue)

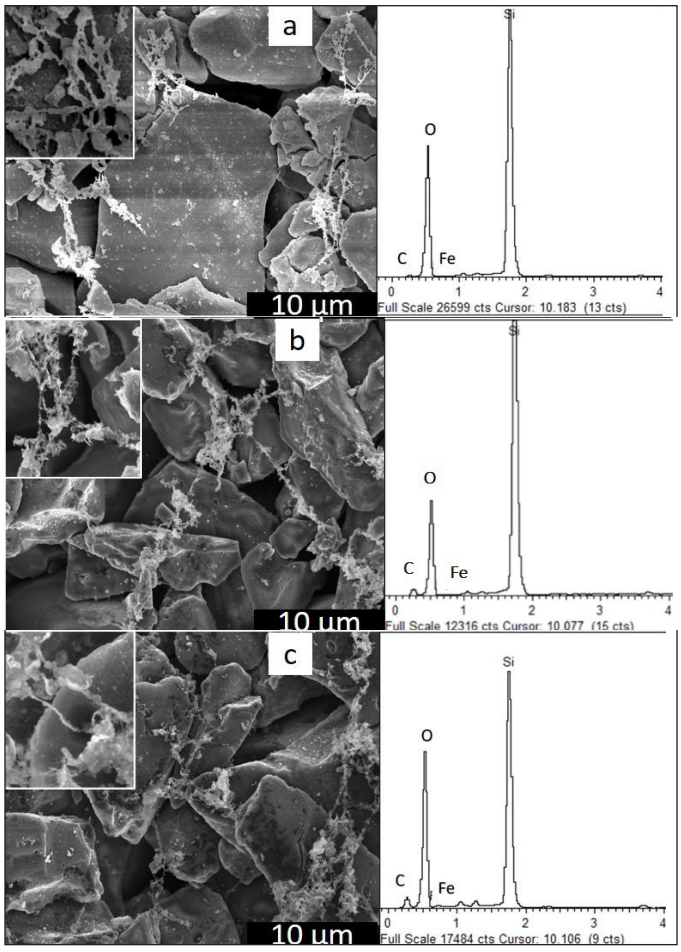

Figure 5. SEM images and corresponding EDX spectrum of CNTs grown using waste NR glove as precursor at 10k magnification a) 500°C b) 600°C and c) 700°C

Morphology of the Synthesized CNTs

The images were taken by FESEM (Figure 5) for the growth temperature at 500 – 700°C shows the morphologies of carbon nanostructure depending mainly on the CVD reaction temperature, under the parameters stated previously. It was observed that the fibrous structure formed with some amorphous carbon attached. The fibrous structure ranging from 15 – 40 nm can be classified as CNTs (Adams et al., 2012; Kumar et al., 2016). This result was confirmed using EDX and it shows the presence of carbon element inside the sample after the CVD process. The intensity of the carbon element was low compared to other elements indicating that the carbon element was low at the selected area during the characterized. Both silica and iron elements had the highest intensity since SiO_2 and ferrocene had been used as substrate and catalyst in this experiment, respectively. However, the yield percentage of carbon deposition increased with the temperature from 500 – 700°C.

The diameter of the CNTs formed was in the range of 15 – 40 nm. The CNTs formed were not clean as there was an attachment of amorphous carbon along the nanotubes. The nanotubes were likely to link from one to another nanotube. The yield of the CNMs produced was increasing with the reaction temperature. Figure 6 (b) is in agreement with a study by Liu et al. (2011b) where the higher the reaction temperature the higher the yield of carbon products produced. At 700°C, the CNMs yield recovered was 5.37% while at 500 and 600°C, the CNMs yield recovered was 1.72% and 3.42%, respectively. EDX spectrum and atomic percentage from Figure 5 and Table 2 further support our finding where the carbon percentage increased as the temperature increased.

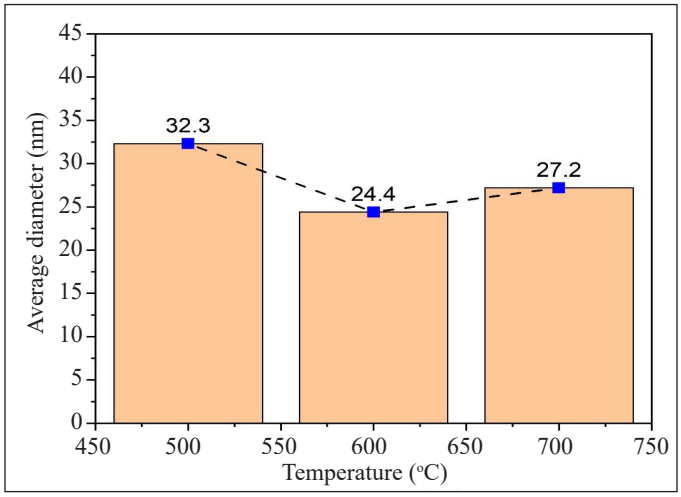

(a)

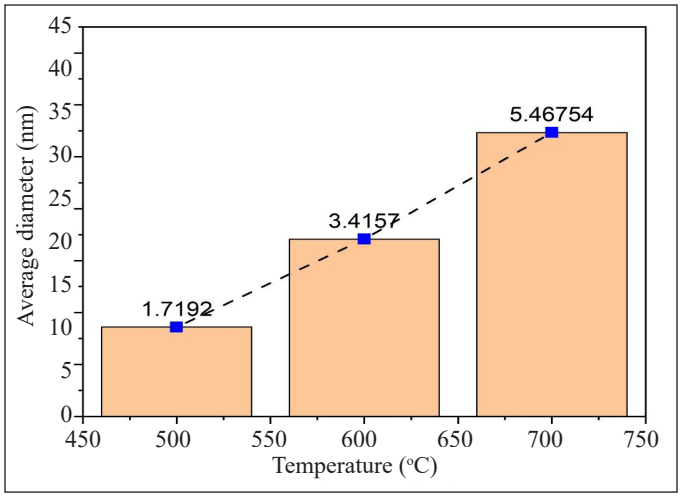

(b)

Figure 6. (a) average diameter of the CNTs and (b) the percentage yield of the CNMs at 500 – 700°C

Table 2
Atomic percentage of element

Element	500°C		600°C		700°C	
	Weight%	Atomic%	Weight%	Atomic%	Weight%	Atomic%
C	2.99	4.87	11.19	18.04	12.33	18.43
O	52.40	64.17	40.07	48.52	53.56	60.11
Si	44.12	30.78	48.23	33.26	33.02	21.22
Fe	0.49	0.17	0.52	0.18	1.09	0.35
Totals	100.00		100.00		100.00	

The CNTs formation can be explained by the solubility-diffusion-precipitation mechanism as it was accepted by Baker (1989) and Kumar and Ando (2010) where the hydrocarbon released the carbon particle and diffused onto the metal catalyst surface and the carbon started to precipitate at the surface of the metal catalyst. The SiO_2 substrate acts as catalyst-supporting materials for nanotubes growth and provides place for catalyst to attach (Jourdain & Bichara, 2013). When heat is applied, the carbon atoms vibrate more quickly and collide more often to increase the rate of diffusion resulting in increasing the diffusion rate of carbon atoms onto the catalyst surface. Thus, the higher the rate of carbon diffusion the higher the yield of carbonaceous materials produced. In return, the growth rate of CNTs and the carbon deposit-increases with the increase of reaction temperature as the carbon diffuses onto the catalyst particle faster, producing a mixture of CNTs and amorphous carbon (Tripathi et al., 2017). The result is supported by other studies on the effect of reaction temperature (Acomb et al., 2015; Cui et al., 2011; Shirazi et al., 2011).

Transmission electron microscopy (TEM) was used for detailed structural analysis of the nanomaterial's formation. Figure 7 shows the structure of the nanomaterials formation at 500°C, 600°C and 700°C. Figure 7 (b) shows the formation of CNTs can be seen clearly at 600°C compared at 500 and 700°C synthesis temperature (Figure 7 (a) and (c). The graphitic layer started to form at 500°C but there was no formation of CNTs. This tells us, the production of CNTs needs higher temperature to form. At 600°C the CNTs was successfully formed. Figure 8 shows the TEM image of the successful CNTs grows at 100 nm and 50 nm magnification. The CNTs formed was agglomerated with the iron nanoparticles attached to it. The graphitic plane or structure was forming from the cracked gas from the pyrolysis of waste NR glove. The CNTs were confirmed to form based on the tubular structure seen at the inset of the TEM image in Figure 8 with diameter of CNTs of 13 nm and 16.67 nm. The CNTs growth was nonuniform size having a rough surface of the nanotube. There also amorphous carbon attached to it due to the deposition of carbon and iron particles as it was used for nucleation sites for CNTs growth.

Figure 7 (c) shows the nanomaterial forms without defined shape. This may be due to the increasing rate of carbon diffusion onto the catalyst. As the rate increasing the

carbon atom are not well arrange themselves to for tube structure. The other solid reason as mentioned by Ming et al. (2016), is the formation of CNTs having its own range of temperature peak depending on the hydrocarbon sources. A higher temperature than the peak temperature, would lead to the agglomeration of metal catalyst and resulting in deactivation of metal catalyst. The inactive metal catalyst tends to form amorphous carbon rather than CNTs. The yield percentage of carbon attachment increases as the temperature increases indicating the rate of carbon diffusion increases. The diameter of the CNTs formed is biggest at 700°C as the agglomeration of metal catalyst leads to a bigger size of catalyst. Hence the diameter of nanotube form will increase along with mixture of amorphous carbon as the metal catalyst starts to be inactive.

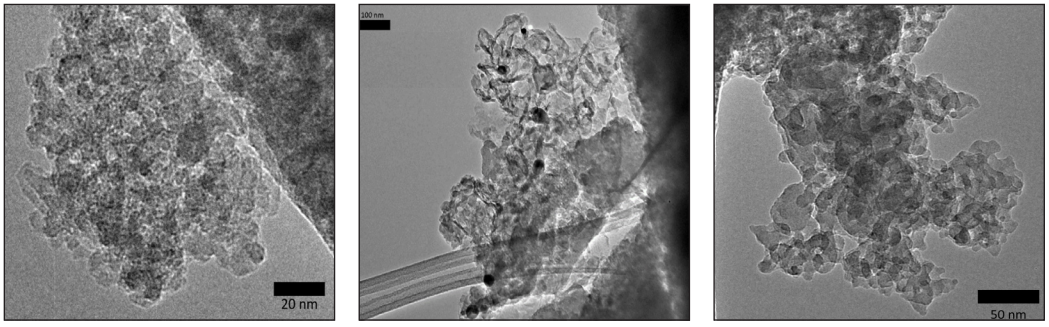

(a) (b) (c)

Figure 7. TEM images of CNTs formed after CVD at a) 500°C, b) 600°C and c) 700°C

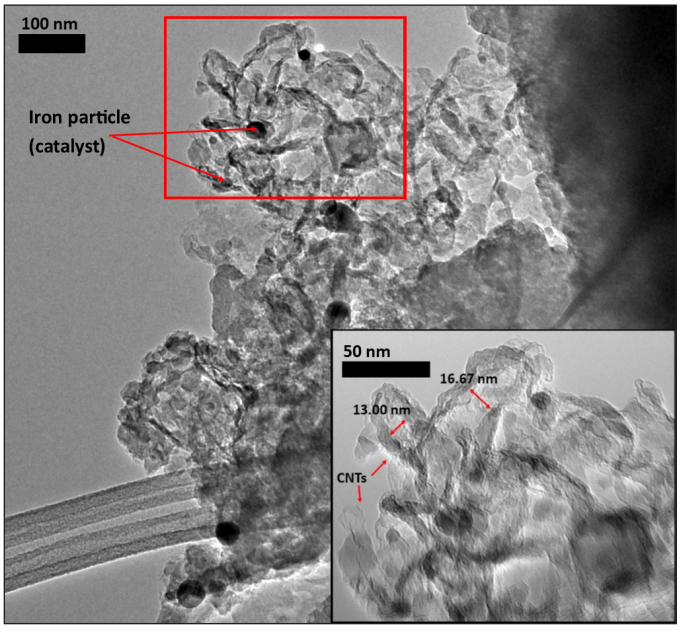

Figure 8. TEM images of CNTs formed after CVD at 600°C

CONCLUSION

Waste NR glove contains a high amount of hydrocarbon chain which was successfully synthesized to CNTs using CVD technique over SiO_2 substrate. CNTs were formed from the cracked hydrocarbon derived from the pyrolysis of the waste NR glove which produced solid carbon that could diffuse on a catalyst surface. The optimum CNTs were produced at 700°C with an average diameter of nanotubes 27.2 nm and the highest yield of deposited carbon was 5.47%. This project offers a potential precursor for synthesizing CNTs from rubber-based materials. Further study is needed to increase the yield of the CNTs and improve the purity of the CNTs synthesized from waste NR glove to be equaled to conventional precursor. Through this, we can change the conventional precursor with waste NR glove precursor. This can be done by changing the parameters such as catalyst and also catalyst support for CVD reaction.

ACKNOWLEDGMENT

This project received funding from Universiti Putra Malaysia through the Geran Putra-Inisiatif Putra Muda (GP-IPM/2017/9543800), and supported by Ministry of Higher Education (MoHE) under the Fundamental Research Grant Scheme (FRGS/1/2018/STG07/UPM/02/3).

REFERENCES

Acomb, J. C., Wu, C., & Williams, P. T. (2015). Effect of growth temperature and feedstock:catalyst ratio on the production of carbon nanotubes and hydrogen from the pyrolysis of waste plastics. *Journal of Analytical and Applied Pyrolysis*, *113*, 231–238. doi:10.1016/j.jaap.2015.01.012

Adams, T., Duong, B., & Seraphin, S. (2012). Effects of catalyst components on carbon nanotubes grown by chemical vapor deposition. *Journal of Undergrauduate Research in Physics*, (January), 1–8.

Alves, Joner O., Zhuo, C., Levendis, Y. A., & Tenório, J. A. S. (2011). Catalytic conversion of wastes from the bioethanol production into carbon nanomaterials. *Applied Catalysis B: Environmental*, *106*(3–4), 433–444. doi:10.1016/j.apcatb.2011.06.001

Alves, Joner Oliveira, Soares Tenório, J. A., Zhuo, C., & Levendis, Y. A. (2012). Characterization of nanomaterials produced from sugarcane bagasse. *Journal of Materials Research and Technology*, *1*(1), 31–34. doi:10.1016/s2238-7854(12)70007-8

Aqel, A., El-Nour, K. M. M. A., Ammar, R. A. A., & Al-Warthan, A. (2012). Carbon nanotubes, science and technology part (I) structure, synthesis and characterisation. *Arabian Journal of Chemistry*, *5*(1), 1–23. doi:10.1016/j.arabjc.2010.08.022

Azam, M. A., Izamshah, R., Mohamad, N., Isomura, K., & Shimoda, T. (2013a). Nanostructuring ultra-thin co films to active catalyst particles for vertically aligned single-walled CNT growth. *Procedia Engineering*, *68*, 566–571. doi:10.1016/j.proeng.2013.12.222

Azam, M. A., Manaf, N. S. A., Talib, E., & Bistamam, M. S. A. (2013b). Aligned carbon nanotube from catalytic chemical vapor deposition technique for energy storage device: A review. *Ionics*, *19*(11), 1455–1476. doi:10.1007/s11581-013-0979-x

Azmina, M. S., Suriani, A. B., Salina, M., Azira, A. A., Dalila, A. R., Asli, N. A., ... & Rusop, M. (2012). Variety of bio-hydrocarbon precursors for the synthesis of carbon nanotubes. *Nano Hybrids*, *2*, 43–63. doi:10.4028/www.scientific.net/nh.2.43

Baker, R. T. K. (1989). Catalytic growth of carbon filaments. *Carbon*, *27*(3), 315–323. doi:10.1016/0008-6223(89)90062-6

Chen, S., Bao, P., & Wang, G. (2013). Synthesis of Fe2O3-CNT-graphene hybrid materials with an open three-dimensional nanostructure for high capacity lithium storage. *Nano Energy*, *2*(3), 425–434. doi:10.1016/j.nanoen.2012.11.012

Cui, T., Lv, R., Huang, Z. H., Wang, M., Kang, F., Wang, K., & Wu, D. (2011). Temperature effect on synthesis of different carbon nanostructures by sulfur-assisted chemical vapor deposition. *Materials Letters*, *65*(3), 587–590. doi:10.1016/j.matlet.2010.10.073

Dresselhaus, M. S., Dresselhaus, G., Jorio, A., Souza Filho, A. G., & Saito, R. (2002). Raman spectroscopy on isolated single wall carbon nanotubes. *Carbon*, *40*(12), 2043–2061. doi:10.1016/s0008-6223(02)00066-0

Dresselhaus, M. S., Dresselhaus, G., Saito, R., & Jorio, A. (2005). Raman spectroscopy of carbon nanotubes. *Physics Reports*, *409*(2), 47–99. doi:10.1016/j.physrep.2004.10.006

Essawy, H., Fathy, N., Tawfik, M., El-Sabbagh, S., Ismail, N., & Youssef, H. (2017). Fabrication of single-walled carbon nanotubes from vulcanized scrap rubber via thermal chemical vapor deposition. *RSC Advances*, *7*(21), 12938–12944. doi:10.1039/c7ra00349h

Faizah, M. Y., Sidek, R. M., & Naim, M. M. R. (2008). Synthesis of carbon nanotubes for acetylene detection. *Journal of Engineering Science and Technology*, *3*(1), 71–78.

Ferrari, A. C. & Robertson, J. (2000). Interpretation of *Raman Spectra* of disordered and amorphous carbon. *Physical Review B, 61*(20), 14095-14107. doi:10.1103/physrevb.61.14095

Ghosh, P., Afre, R. A., Soga, T., & Jimbo, T. (2007). A simple method of producing single-walled carbon nanotubes from a natural precursor: Eucalyptus oil. *Materials Letters*, *61*(17), 3768–3770. doi:10.1016/j.matlet.2006.12.030

Ghosh, P., Soga, T., Afre, R. A., & Jimbo, T. (2008). Simplified synthesis of single-walled carbon nanotubes from a botanical hydrocarbon: Turpentine oil. *Journal of Alloys and Compounds*, *462*(1–2), 289–293. doi:10.1016/j.jallcom.2007.08.027

Golnabi, H. (2012). Carbon nanotube research developments in terms of published papers and patents, synthesis and production. *Scientia Iranica*, *19*(6), 2012–2022. doi:10.1016/j.scient.2012.10.036

Hazan, M. A., Mamat, M. S., Haroun, R. Z., Kamis, S. L., Ismail, I., Hussein, M. Z., ... & Yaakob, Y. (2019). Carbon nanostructures grown from waste latex via chemical vapor deposition. *Malaysian Journal of Microscopy*, *15*(1), 1–9.

Iijima, S. (1991). Helical microtubules of graphitic carbon. *Nature*, *354*(6348), 56–58. doi:10.1038/354056a0

Jourdain, V., & Bichara, C. (2013). Current understanding of the growth of carbon nanotubes in catalytic chemical vapour deposition. *Carbon*, *58*, 2–39. doi:10.1016/j.carbon.2013.02.046

Judai, K., Iguchi, N., & Hatakeyama, Y. (2016). Low-temperature production of genuinely amorphous carbon from highly reactive nanoacetylide precursors. *Journal of Chemistry*, *2016,* 1-6. doi:10.1155/2016/7840687

Kumar, M., & Ando, Y. (2005). Controlling the diameter distribution of carbon nanotubes grown from camphor on a zeolite support. *Carbon*, *43*(3), 533–540. doi:10.1016/j.carbon.2004.10.014

Kumar, M., & Ando, Y. (2010). Chemical vapor deposition of carbon nanotubes: A review on growth mechanism and mass production. *Journal of Nanoscience and Nanotechnology*, *10*(6), 3739–3758. doi:10.1166/jnn.2010.2939

Kumar, R., Singh, R. K., & Tiwari, R. S. (2016). Growth analysis and high-yield synthesis of aligned-stacked branched nitrogen-doped carbon nanotubes using sesame oil as a natural botanical hydrocarbon precursor. *Materials and Design*, *94*, 166–175. doi:10.1016/j.matdes.2016.01.025

Lee, C. J., Park, J., Huh, Y., & Yong Lee, J. (2001). Temperature effect on the growth of carbon nanotubes using thermal chemical vapor deposition. *Chemical Physics Letters*, *343*(1–2), 33–38. doi:10.1016/s0009-2614(01)00680-7

Liu, J., Jiang, Z., Yu, H., & Tang, T. (2011a). Catalytic pyrolysis of polypropylene to synthesize carbon nanotubes and hydrogen through a two-stage process. *Polymer Degradation and Stability*, *96*(10), 1711–1719. doi:10.1016/j.polymdegradstab.2011.08.008

Liu, W. W., Aziz, A., Chai, S. P., Mohamed, A. R., & Tye, C. T. (2011b). The effect of carbon precursors (methane, benzene and camphor) on the quality of carbon nanotubes synthesised by the chemical vapour decomposition. *Physica E: Low-Dimensional Systems and Nanostructures*, *43*(8), 1535–1542. doi:10.1016/j.physe.2011.05.012

Louis, B., Gulino, G., Vieira, R., Amadou, J., Dintzer, T., Galvagno, S., … & Pham-Huu, C. (2005). High yield synthesis of multi-walled carbon nanotubes by catalytic decomposition of ethane over iron supported on alumina catalyst. *Catalysis Today*, *102–103*, 23–28. doi:10.1016/j.cattod.2005.02.031

Mamedov, A. A., Kotov, N. A., Prato, M., Guldi, D. M., Wicksted, J. P., & Hirsch, A. (2002). Molecular design of strong single-wall carbon nanotube/polyelectrolyte multilayer composites. *Nature Materials*, *1*(3), 190–194. doi:10.1038/nmat747

Marton, M., Vojs, M., Zdravecká, E., Himmerlich, M., Haensel, T., Krischok, S., … & Redhammer, R. (2013). Raman spectroscopy of amorphous carbon prepared by pulsed arc discharge in various gas mixtures. *Journal of Spectroscopy*, *2013*, 1-6. doi:10.1155/2013/467079

Ming, H., Peiling, D., Yunlong, Z., Jing, G., & Xiaoxue, R. (2016). Effect of reaction temperature on carbon yield and morphology of CNTs on copper loaded nickel nanoparticles. *Journal of Nanomaterials*, *2016,* 1-5. doi:10.1155/2016/8106845

Okolo, C., Rafique, R., Iqbal, S. S., Subhani, T., Saharudin, M. S., Bhat, B. R., & Inam, F. (2019). Customizable ceramic nanocomposites using carbon nanotubes. *Molecules*, *24*(17), 1–10. doi:10.3390/molecules24173176

Paul, S., & Samdarshi, S. K. (2011). A green precursor for carbon nanotube synthesis. *Xinxing Tan Cailiao/ New Carbon Materials*, *26*(2), 85–88. doi:10.1016/s1872-5805(11)60068-1

Prasek, J., Drbohlavova, J., Chomoucka, J., Hubalek, J., Jasek, O., Adam, V., & Kizek, R. (2011). Methods for carbon nanotubes synthesis—review. *Journal of Materials Chemistry*, *21*(40), 15872-15884. doi:10.1039/ C1JM12254A

Quan, C., Li, A., Gao, N., & Dan, Z. (2010). Characterization of products recycling from PCB waste pyrolysis. *Journal of Analytical and Applied Pyrolysis*, *89*(1), 102–106. doi:10.1016/j.jaap.2010.06.002

Shirazi, Y., Tofighy, M. A., Mohammadi, T., & Pak, A. (2011). Effects of different carbon precursors on synthesis of multiwall carbon nanotubes: Purification and functionalization. *Applied Surface Science*, *257*(16), 7359–7367. doi:10.1016/j.apsusc.2011.03.146

Sobri, S., Jasni, J., Yasin, F. M., Jamal, S. H., Janudin, N., & Kasim, N. A. M. (2016). Synthesis of carbon nanotubes and volatile organic compounds detection. *MATEC Web of Conferences*, *39*, 3–6. doi:10.1051/ matecconf/20163901006

Suriani, A. B., Azmina, M. S., Salina, M., Dalila, A. R., Falina, A. N., Rosly, J., & Rusop, M. (2012, November 5-6). Effect of synthesis time on carbon nanotubes growth from palm oil as carbon source by thermal chemical vapor deposition method. In *International Conference on Electronic Devices, Systems, and Applications* (pp. 18–21). Kuala Lumpur, Malaysia.

Tripathi, P. K., Durbach, S., & Coville, N. J. (2017). Synthesis of multi-walled carbon nanotubes from plastic waste using a stainless-steel CVD reactor as catalyst. *Nanomaterials, 7*(10), 1-17. doi:10.3390/ nano7100284

Yao, D., Wu, C., Yang, H., Zhang, Y., Nahil, M. A., Chen, Y., … & Chen, H. (2017). Co-production of hydrogen and carbon nanotubes from catalytic pyrolysis of waste plastics on Ni-Fe bimetallic catalyst. *Energy Conversion and Management*, *148*, 692–700. doi:10.1016/j.enconman.2017.06.012

Yip, E., & Cacioli, P. (2002). The manufacture of gloves from natural rubber latex. *Journal of Allergy and Clinical Immunology*, *110*(2), S3–S14. doi:10.1067/mai.2002.124499

Pertanika J. Sci. & Technol. 28 (S2): 231 - 242 (2020)

SCIENCE & TECHNOLOGY

Journal homepage: http://www.pertanika.upm.edu.my/

Secured Electrocardiograph (ECG) Signal Using Partially Homomorphic Encryption Technique–RSA Algorithm

Muhammad Umair Shaikh[1], Wan Azizun Wan Adnan[3] and Siti Anom Ahmad[1, 2]*

[1]Department of Electrical and Electronic Engineering, Faculty of Engineering, Universiti Putra Malaysia, 43400 UPM, Serdang, Selangor, Malaysia
[2]Malaysian Research Institute on Ageing (MyAgeing™), Universiti Putra Malaysia, 43400 Serdang, Selangor, Malaysia
[3]Department of Computer and Communication System Engineering, Faculty of Engineering, Universiti Putra Malaysia 43400 UPM, Serdang, Selangor, Malaysia

ABSTRACT

ECG signal differs from individual to individual, making it hard to be emulated and copied. In recent times ECG is being used for identifying the person. Hence, there is a requirement for a system that involves digital signal processing and signal security so that the saved data are secured at one place and an authentic person can see and use the ECG signal for further diagnosis. The study presents a set of security solutions that can be deployed in a connected healthcare territory, which includes the partially homomorphic encryption (PHE) techniques used to secure the electrocardiogram (ECG) signals. This is to record confidentially and prevent the information from meddling, imitating and replicating. First, Pan and Tompkins's algorithm was applied to perform the ECG signal processing. Then, partially homomorphic encryption (PHE) technique - Rivest-Shamir-Adleman (RSA) algorithm was used to encrypt the ECG signal by using the public key. The PHE constitutes a gathering of semantically secure encryption works that permits certain arithmetical tasks on the plaintext to be performed straightforwardly on the ciphertext. The study shows a faster and 90% accurate result before and after encryption that indicates the lightweight and accuracy of the RSA algorithm. Secure ECG signal provides innovation in multiple healthcare sectors such as medical research, patient care and hospital database.

Keywords: ECG signal, arrhythmias detection, PHE technique–RSA algorithm

ARTICLE INFO

Article history:
Received: 10 February 2020
Accepted: 13 November 2020
Published: 31 December 2020

DOI: https://doi.org/10.47836/pjst.28.S2.18

E-mail addresses:
mushaikh1986@gmail.com (Muhammad Umair Shaikh)
wawa@upm.edu.my (Wan Azizun Wan Adnan)
sanom@upm.edu.my (Siti Anom Ahmad)
* Corresponding author

ISSN: 0128-7680
e-ISSN: 2231-8526

© Universiti Putra Malaysia Press

INTRODUCTION

Cardiovascular disease (CVD) generally refers to conditions that involve narrowed or blocked blood vessels that can lead to a heart attack, chest pain (angina) or stroke. CVD, especially coronary artery disease (CAD) is a leading cause of human morbidity and mortality. According to the world health organization (WHO), one in every four death is caused because of CVD [WHO, 2017]. The ECG is the wave representation of the heart activity. There are many widespread applications for ECG signals such as clinical diagnosis, understanding of the physiology of cardiac arrhythmias, interpretation for medical researcher and human-machine interface.

Similarly, sharing the patient's information through the internet of thing (IoT) for faster diagnosis has security and privacy issues. The patient's health database security is one of the greatest dangers looked by the providers. Ensuring and verifying this information has never been progressively basic. According to Civil Rights reports 2015, above 0.112 billion healthcare data were undermined ("Modifications to the HIPAA Privacy, Security, Enforcement, and Breach Notification Rules under the Health Information Technology for Economic and Clinical Health Act and the Genetic Information Nondiscrimination Act; other modifications to the HIPAA rules.," 2013). From that point forward, cybercriminals have turned out to be much progressively mindful of the estimation of healthcare records. The present situation demands extremely secured details of patients. Consequently, to secure the patient's information, the development of the secured ECG signal is the main challenge in the healthcare industry because it is very essential to record confidentially and to prevent mistreatment. This issue will be tackled by encrypting the ECG signals, utilizing the proposed PHE technique. The study contributes the natural algorithm -RSA-calculation and signal processing steps. In RSA, the sender will encode the ECG information by utilizing the public key and the receiver will unscramble the information by utilizing private keys for providing high security. According to the various applications of ECG, the secured ECG signal helps the healthcare providers and researchers for further studies of arrhythmia detection.

The Pan and Tompkins, QRS complex method used in this study to process the acquired ECG signal. The QRS complex is a method for determining the statistical self-affinity of a signal. This method has been used for the detection and analysis of cardiovascular abnormalities or ECG analysis (Shaikh, Ahmad, & Wan Adnan, 2019). The security features of the study protect the authenticity and confidentiality of the patient's information.

This paper is organized as follows: Section 2 discusses briefly previous related work on secured ECG signal and healthcare data security. Section 3 introduces our proposed methodology consisting of QRS complex detection and the encryption of ECG using PHE. Simulations results are presented and discussed in section 4 and finally, section 5 presents the conclusion.

A brief introduction of the Pan and Tompkins method is studied first then the ECG recording techniques and security techniques- RSA- technique are reviewed subsequently. This study focuses on improving the security of the ECG signal.

RELATED WORK

The secured and self-diagnostic ability of the ECG signal plays a vital role in the detection of ECG arrhythmias and transmits the signal. PHE schemes are used in certain applications like e-casting or Private Information Retrieval (PIR). However, these applications were confined as far as the sorts of homomorphic assessment tasks. In other words, PHE plans must be utilized for specific applications, whose algorithms include only addition or multiplication operation.

Lin, et al. (2016) proposed a Community-Based ECG Monitoring System for Patients with Cardiovascular Diseases. They aimed to develop a community-based electrocardiogram (ECG) monitoring system for cardiac outpatients to wirelessly detect heart rate, provide personalized healthcare, and enhance interactive social contact because of the prevalence of deaths from cardiovascular disease and the growing problem of aging in the world. The system not only strengthens the performance of the ECG monitoring system but also emphasizes the ergonomic design of wearable devices and user interfaces. Besides, it enables medical professionals to diagnose cardiac symptoms remotely and electronically manage medical reports and suggestions. The downsides are this system does not have any selfdiagnostic capability and there is no assurance that patients' data are authenticated at the server-side.

Motwani and Chaudhari (2014) proposed a Chaos encryption method for data Encrypted concealment in the ECG signal. The chaos encryption scheme is used to encrypt the text before hiding into the signal. The scheme is suitable for data protection in hospitals. The drawback of this scheme is that it does not directly encrypt the signal whereas our proposed method encrypts the ECG signal and authenticates the information at the server-side.

Qin et al. (2017) proposed an adaptive and time effective R-peak detection algorithm for ECG processing. The algorithm performance, including accuracy and time consumption, is better than the Pan and Tompkins method. Qin's algorithm is a stand-alone that is capable of only acquiring the ECG signals and visualizing the signals. It does not have any connection to the database at the health care provider for further analysis and diagnosis. The ECG signal is not secure at the server-side.

Park and Lee (2018) proposed a medical diagnosis system using e-health cloud servers in a privacy-preserving manner when medical datasets were owned by multiple data owners. The proposed system is the first one that achieves the privacy of the medical dataset, symptoms, and diagnosis results and hides the data access pattern even from the

e-health cloud servers system. However, to the best of our knowledge, none of the ECG systems discussed so far has incorporated security techniques relating to the authentication and secure ECG signal using partially HE technique

This study covers a greater scope than Lin, et al. (2016), Motwani and Chaudhari (2014), Qin et al. (2017) and Park and Lee (2018) research. Firstly, Pan and Tompkins algorithm was performed on ECG signal for the detection of the QRS complex. Secondly, the ECG signal was encrypted by using the PHE- RSA- algorithm. Lastly, heart rate was calculated and arrhythmia detected. PHE technique is one of the block ciphers with lightweight properties for enhancing confidentiality, integrity and authentication in ECG signal transmission in comparison to Gentry (Li, et al., 2013) AES (Hameed, et al., 2019) algorithm and ECG steganography (Sivaranjani, 2017).

METHODS

The research was divided into two parts. The first part was QRS complex detection using Pan and Tompkins algorithm and the second part was the encryption of ECG signal using the PHE technique to make the signal more secure and difficult for a hacker to hack the information. The methodology flowchart of this study began by applying two stages following the steps of the Pan and Tompkins algorithm. The first stage was the preprocessing stage in which the signal was prepared for later detection, removing noise, smoothing the signal and amplifying the QRS slope and width. The second stage was the decision stage, in this stage thresholds were applied to the signal to remove noise peaks and consider only signal peaks. Indeed, it necessitates making the data ready for feature extraction in the ECG signal preprocessing stage. In this way, a suitable feature space is provided and the accuracy of the system is increased. Subsequently, in the next step, the method of encryption was studied.

In the feature extraction phase, the functionality of all features, namely, signal to noise ratio, use of threshold, signal peaks defined as those of the QRS complex and R-R interval were studied. Additionally, for the security of the ECG signal PHE was considered. After the moving window coordinates output (x6), the encryption-decryption calculation had been utilized. By encrypting the signal, the signal would be changed. The final result after the decryption was in the form of a normal or abnormal heart rate (HR). It offers assistance to the therapeutic professional for encouraging the conclusion and restorative analyst for advance considers. Ultimately, the performances of the algorithm are evaluated by calculating the classification error and accuracy using some statistical analysis. Likewise, the methodology flow chart of this research is demonstrated in Figure 1 involving the whole procedure step by step.

The MIT-BIH Arrhythmia database from the physio net website was used to test the proposed method of this study (Moody & Mark, 2001). The database was the primary for

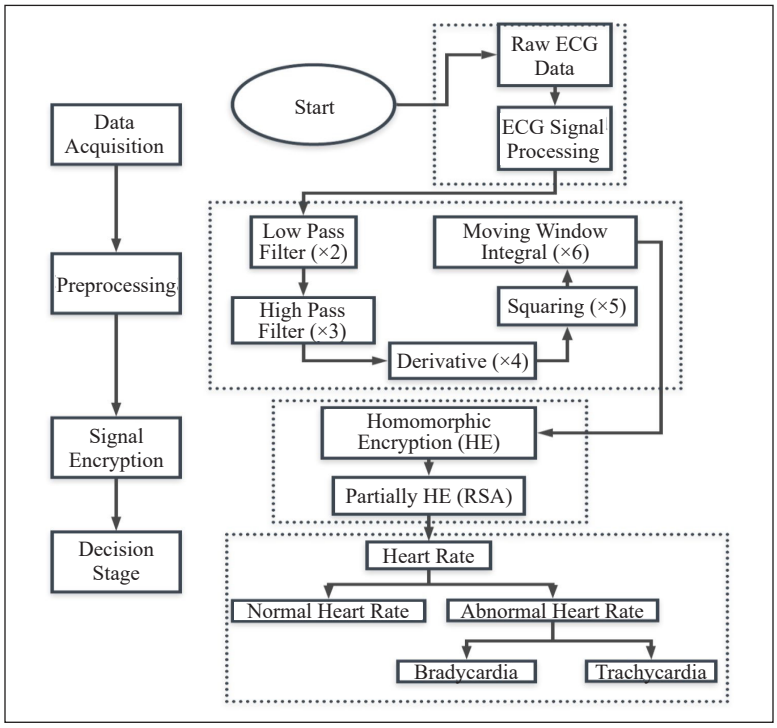

Figure 1. Methodology flow chart of the study in detail

the most part accessible set of standard test fabric for assessment of arrhythmia finders and had been utilized for that reason as well as for fundamental investigations into the cardiac flow at more than 500 destinations around the world.

The designed algorithm was performed using MATLAB (R2019a) with an Intel Core (TM) i5 3.10 GHz processor, 8 GB RAM, and 500 GB hard disk running on a windows 10. The simple and fast proposed algorithm was applied to 20 random different ECG signals from the MIT-BIH arrhythmia database. The signal length was 21,600 samples. For example, a one- minute waveform with a sample rate of 360 samples per second requires 21,600 rows of data for each column with a sampling rate of 360 Hz for each ECG recording (Michalek, 2006).

ECG Signal Processing

The methodology followed Pan and Tompkins algorithm. The raw ECG signal was passed through the bandpass filter for the QRS detection reduced noise by matching the spectrum of the average QRS complex. Then the filtered signal was passed through derivative, squaring and window integration phases. The signal-to-noise ratio increase, after the ECG signal, had passed through the bandpass filter stage x(3). This permits the use of thresholds that are just above the noise peak levels. Thus, the overall sensitivity of the detector improves.

Whereas, signal peaks are defined as those of the QRS complex, while noise peaks are those of the T waves, muscle noise, etc. After the determination of the QRS complex the point which showed the location of R points were determined. The cardiac cycle (RR) interval was obtained and heart rate was calculated.

ECG Signal Encryption

The methodology followed Pan and Tompkins algorithm (Afonso et al., 1999). The raw ECG signal was passed through the bandpass filter for the QRS detection reduced noise by matching the spectrum of the average QRS complex. Then the filtered signal was passed through derivative, squaring and window integration phases. The signal-to-noise ratio increase, after the ECG signal, had passed through the bandpass filter stage x(3). This permits the use of thresholds that are just above the noise peak levels. Thus, the overall sensitivity of the detector improves. Whereas, signal peaks are defined as those of the QRS complex, while noise peaks are those of the T waves, and muscle noise. After the determination of the QRS complex the point which showed the location of R points was determined. The cardiac cycle (RR) interval was obtained and heart rate was calculated. The complete process is shown in Figure 2.

Partially Homomorphic Encryption (PHE)

For encrypting the signal RSA algorithm was used. The RSA is an asymmetric cryptography algorithm. It is also known as public-key cryptography with two different keys, because

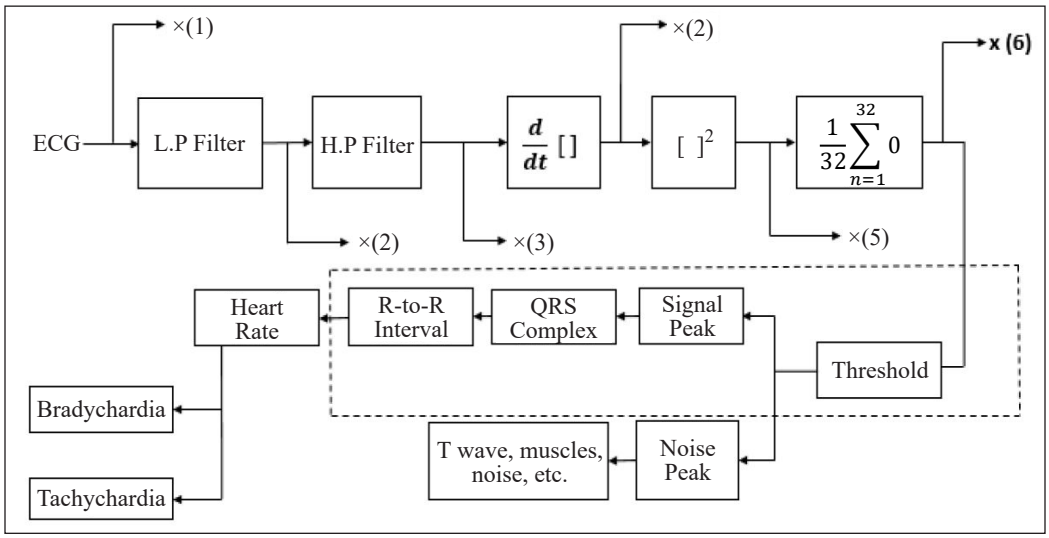

Figure 2. Various stages of high-speed QRS detection. x(1) is the input ECG signal. x(2) is the low passed ECG, x(3) is the band passed ECG, x(4) is the differentiated ECG, x(5) is the squaring output, x(6) is the window integrated output (Shaikh et al., 2019).

one of the keys is a public key and the other key must be kept private. The result obtained from RSA is in the form of normal and abnormal heart rate.

Where,

pk is public-key = (n,e), m1 is plaintexts. m1 is ECG signals after window integrated output (x6).

RSA is a public-key encryption technique used to encrypt and decrypt the signal by using two keys. RSA is used to encrypt the ECG information by using public and private keys.

RSA Algorithm Design.

Input: ECG signal after moving window integrated output (x6)

Output: Normal or abnormal heartbeat.

Step1: Get ECG signal (x6)

Step2: Convert (x6) to integer representation Ims Step3: Generate key pair

1. Choose two random primes p and q
2. Perform n = p*q
3. By using Euler's totient function calculate Phi
4. Calculate e that is relatively prime to Phi
5. Compute the private exponent d from e, p and q.
6. Output (n, e) as the public key and (n, d) as the private key.

Step4: Encrypt the (x6) with a public key (n,e).

Step5: The ciphertext (C) is computed.

Step6: Decrypt the signal using the private key.

Encryption Process. The public key *(n, e)* is used to encrypt the signal (x6) at the transmitter to produce the cipher message *C* by using the formula:

$$C = M^e \bmod n$$

Then, this ciphered or encrypted message *C* is transmitted to the intended receiver.

Decryption Process

The private key *(n, d)* is used to decrypt the ciphered message *C* at the receiver to produce the plain message *M* by using the following formula:

$$M = C^d \bmod n$$

Decision Stage. After the encryption of the ECG signal, the next stage was the decision stage. By encrypting the signal the signal values will change. After the decryption, the system would show the same result without compromising the signal efficiency meant the RSA algorithm would not affect the signal value and showed the same results. The decrypted

result displays regular or irregular heartbeat. The heartbeat is irregular if its value is below 60bpm (bradycardia) and above 100bpm (tachycardia). This result will help further analysis.

RESULTS AND DISCUSSION

The database was downloaded from the MIT-BIH website for arrhythmia detection. Pan and Tompkins's algorithm was used to do signal processing before applying the RSA algorithm for Signal encryption. The length of the signal was 21,600 samples having a sampling rate of 360 Hz for 20 random ECG recording. Figure 3. shows an input of record 100 ECG from the database.

Figure 4 shows the processing steps for record 100. In the preprocessing stage, low and high pass filters were used to remove the noise and any existing artifacts. The next step was differentiation use to find the high slope use to distinguish the QRS complexes from other ECG waves. The next step consisted of step to step squaring of the sample used to make all data positive and accentuated the higher frequencies in the signal. After that squared waveform passed through the moving window integrator.

Figure 5 shows the encryption of the ECG signal using the RSA algorithm. After the encryption of the signal (x6) system would request the private key. If the user entered the wrong private key the signal would not decrypt and request for the correct private key as shown in Figure 6. By providing the correct private key the system would display the result in the form of normal and abnormal heartbeat. If the heartbeat was abnormal it would display two types of arrhythmias i.e. bradycardia (heartbeat below 60BPM) and tachycardia (heartbeat above 100BPM).

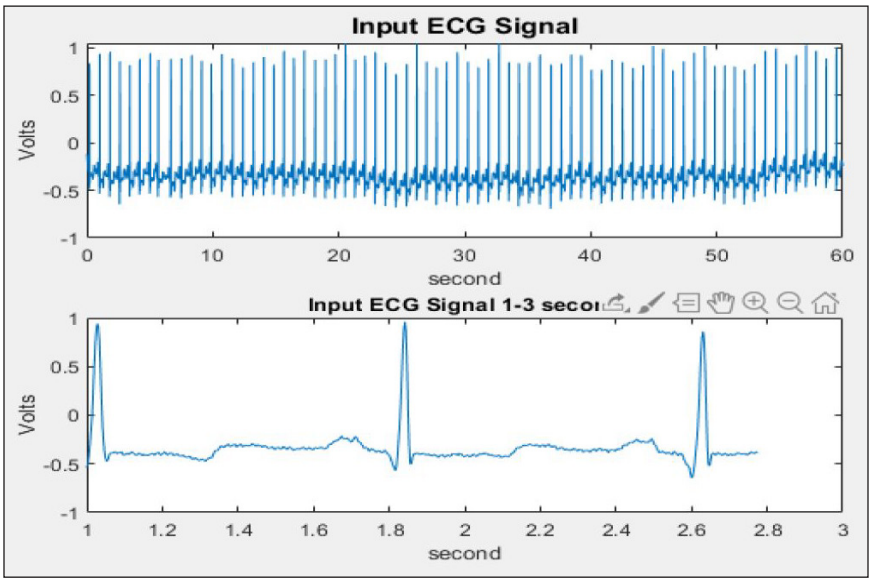

Figure 3. Input ECG signal from the MIT-BIH database

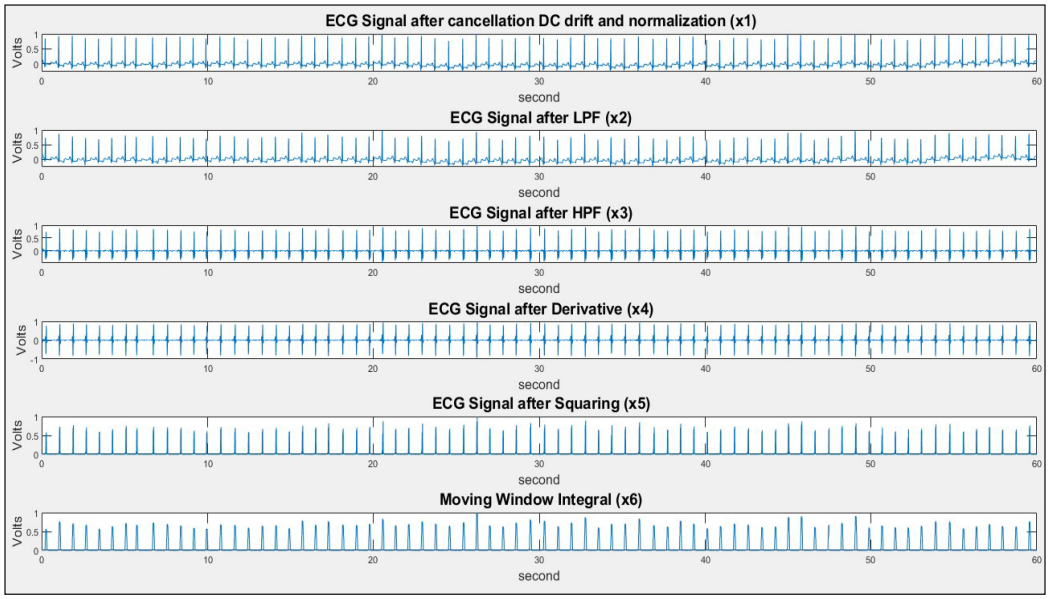

Figure 4. Signal processing steps of ECG 100 record

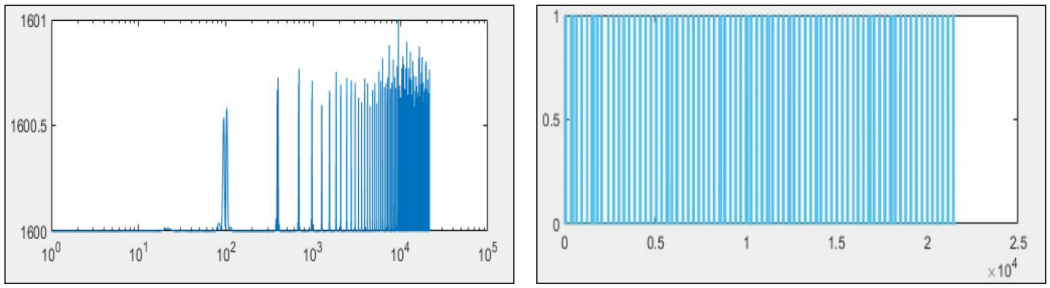

(a) (b)

Figure 5. Shows ECG signal encryption using the RSA algorithm (a) Encryption of signal (x6) (b) Cipher of a signal.

```
end.
end
Enter tifie Private E<ey65 P =
65
Wrong key enter
Enter tifie Private KeylQ2
P =
102
Wrong key enter
Enter tifie Private KeylOO
P =
lOO
Heart beat is normal
fx »
```

Figure 6. System request for the correct private key to display the result

Figure 7 shows the result in the form of a heartbeat after entering the correct private key. The obtained results are summarized in Table 1. The 20 records were considered from the MIT-BIH database arrhythmia database. The MIT-BIH database was used to compare the result with our design PHE techniques and decryption. Out of 20 records, 18 records showed the same result after the decryption of the ECG signal.

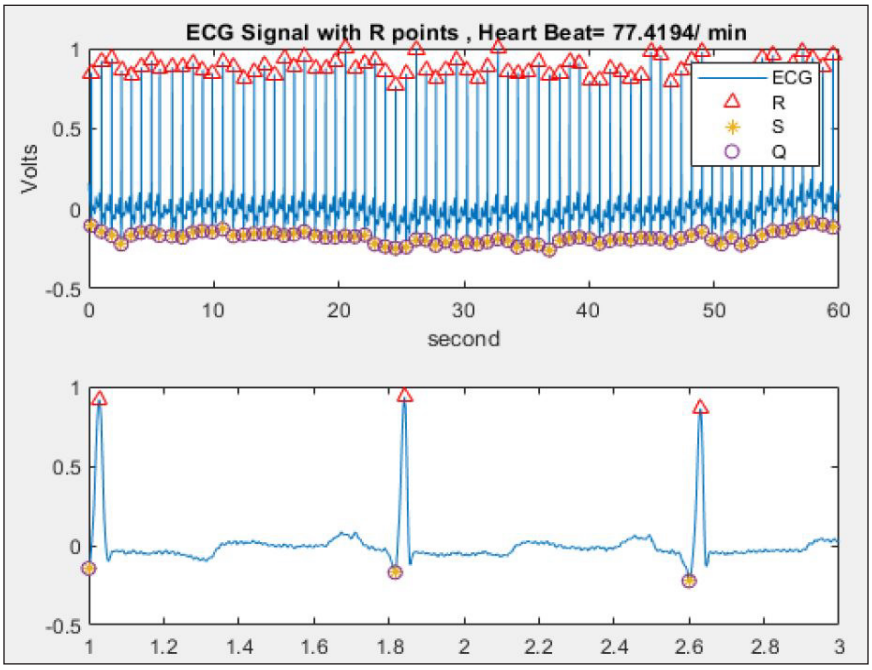

Figure 7. R-R interval and heartbeat detection

Table 1
Comparison of result with MIT-BIH data and result after RSA algorithm

Record No.	**MIT-BIH Arrhythmia Database**	**Proposed methodology mean HR**	**Result**
Record 100	70-89 bpm	73.5 bpm	Normal (Same output)
Record 101	55-79 bpm	64.86 bpm	Normal (Same output)
Record 102	72-78 bpm	80 bpm	Normal (Same output)
Record 105	78-102bpm	58 bpm	Abnormal (Bradycardia, Not same output)
Record 106	49-87 bpm	72 bpm	Normal (Same output)
Record 113	48-87 bpm	59 bpm	Abnormal (Bradycardia, Same output)
Record 114	51-82 bpm	57 bpm	Abnormal (Bradycardia, Same output)
Record 115	50-84 bpm	69 bpm	Normal (Same output)
Record 116	74-86 bpm	78 bpm	Normal (Same output)

Table 1 (*continue*)

Record No.	MIT-BIH Arrhythmia Database	Proposed methodology mean HR	Result
Record 117	48-66 bpm	49 bpm	Abnormal (Bradycardia, Same output)
Record 118	54-91 bpm	72 bpm	Normal (Same output)
Record 121	55-83 bpm	58 bpm	Abnormal (Bradycardia, Same output)
Record 122	67-97 bpm	84 bpm	Normal (Same output)
Record 123	41-65 bpm	55 bpm	Abnormal (Bradycardia, Same output)
Record 124	47-64 bpm	48 bpm	Abnormal (Bradycardia, Same output)
Record 201	31-61 bpm	140 bpm	Abnormal (Tachycardia. Not same output)
Record 210	63-158 bpm	109 bpm	Abnormal Tachycardia , Same output)
Record 213	101-113bpm	110 bpm	Abnormal (Tachycardia, Same output)
Record 215	81-215 bpm	122 bpm	Abnormal (Tachycardia, Same output)
Record 232	24-28 bpm	50 bpm	Abnormal (Bradycardia, Same output)

CONCLUSION

Accessibility, reliability, confidentially and secrecy of data are the main aspects that should be maintained in ECG signal security. Protecting ECG signal from modification, disruption, extermination as well as the illegal access are the main goal of signal security. A secure and efficient communication system for the ECG signal based on the PHE algorithm is designed in this work. The presented cryptosystem was implemented and its performance was evaluated using different signals from the MIT-BIH arrhythmia database. The results obtained demonstrated that the accuracy of signal was at a satisfying level which confirmed the suitability, reliability, high security and effectiveness of the introduced scheme to be applied in practical applications like signal data encryption/decryption. After comparing the signal before and after encryption the proposed RSA algorithm provided 90% accuracy compared to the unencrypted database result. The output shows the result in the form of the normal and abnormal heartbeat which helps to diagnose the different arrhythmias like bradycardia and tachycardia. The idea from this study can be used to secure other medical signals. The security parameter in this investigation will verify the restorative information with the goal that the information is not lost and to keep patient's data in a single place.

ACKNOWLEDGEMENTS

The authors are grateful for the financial support provided by the Ministry of Education of Malaysia through Universiti Putra Malaysia under Grant Putra [GP/2018/9667300].

REFERENCES

Afonso, V. X., Tompkins, W. J., Nguyen, T. Q., & Luo, S. (1999). ECG beat detection using filter banks. *IEEE Transactions on Biomedical Engineering, 46*(2), 192-201. doi: 10.1109/10.740882

Hameed, M. E., Ibrahim, M. M., Manap, N. A., & Attiah, M. L. (2019). Comparative study of several operation modes of AES algorithm for encryption ECG biomedical signal. *International Journal of Electrical and Computer Engineering, 9*(6), 4850-4859. doi:10.11591/ijece.v9i6.pp4850-4859

Jati, G., Rachmasari, A. R., Jatmiko, W., Mursanto, P., & Sediono, W. (2018, September 23-24). An efficient secure ECG compression based on 2D-SPIHT and SIT algorithm. In *2017 International Workshop on Big Data and Information Security (IWBIS)* (pp. 155–160). Jakarta, Indonesia.

Li, J., Song, D., Chen, S., & Lu, X. (2013, October 30 – November 1). A simple fully homomorphic encryption scheme available in cloud computing. In *IEEE 2nd International Conference on Cloud Computing and Intelligence Systems (*pp. 214-217). Hangzhou, China.

Lin, B. S., Wong, A. M., & Tseng, K. C. (2016). Community-based ECG monitoring system for patients with cardiovascular diseases. *Journal of Medical Systems, 40*(4), 1-12. doi:10.1007/s10916-016-0442-4

Michalek, P. J. (2006). *An authentic ECG simulator*. (Master thesis). University of Central Florida, Florida.

Moody, G. B., & Mark, R. G. (2001). The impact of the MIT-BIH arrhythmia database. *IEEE Engineering in Medicine and Biology Magazine, 20*(3), 45-50. doi:10.1109/51.932724

Motwani, P., & Chaudhari, D. (2014). Encrypted data concealment in electrocardiogram signal using chaos encryption method. *International Journal for Research in Emerging Science and Technology, 1*(5), 60–63.

Pan, J. & Tompkins, W. J. (1985). A real-time QRS detection algorithm. *IEEE Trans Biomed Eng. 32*(3), 230-236. doi: 10.1109/TBME.1985.325532.

Park, J., & Lee, D. H. (2018). Privacy preserving k -nearest neighbor for medical diagnosis in e-health cloud. *Journal of Healthcare Engineering 2018,* 1-11. doi:10.1155/2018/4073103

Qin, Q., Li, J., Yue, Y., & Liu, C. (2017). An adaptive and time-efficient ECG R-peak detection algorithm. *Journal of Healthcare Engineering, 2017,*1-14. doi:10.1155/2017/5980541

Shaikh, M. U., Ahmad, S. A., & Wan Adnan, W. A. (2019, December 3-6). Investigation of data encryption algorithm for secured transmission of electrocardiograph (ECG) signal. In *2018 IEEE EMBS Conference on Biomedical Engineering and Sciences* (pp. 274-278). Sarawak, Malaysia

Sivaranjani, B. & Radha, N. (2017, October 19-20). Securing patient's confidential information using ECG steganography. In *2017 2nd International Conference on Communication and Electronics Systems* (pp. 540-544). Coimbatore, India.

US Department of Health and Human Services. (2013). Modifications to the HIPAA privacy, security, enforcement, and breach notification rules under the health information technology for economic and clinical health act and the genetic information nondiscrimination act; other modifications to the HIPAA rules. *Federal Register, 78*(17), 5566-5702.

Pertanika J. Sci. & Technol. 28 (S2): 243 - 258 (2020)

SCIENCE & TECHNOLOGY

Journal homepage: http://www.pertanika.upm.edu.my/

Dark Fermentative Biohydrogen Production from Palm oil Mill Effluent: Operation Factors and Future Progress of Biohydrogen Energy

Fatin Sakinah Rosman[1], Mohd Zulkhairi Mohd Yusoff[1,2]*, Mohd Rafein Zakaria[1,3], Toshinari Maeda[4] and Mohd Ali Hassan[1]

[1]Department of Bioprocess Technology, Faculty of Biotechnology and Biomolecular Sciences, Universiti Putra Malaysia, 43400 Serdang, Selangor, Malaysia
[2]Laboratory of Biopolymer and Derivatives, Institute of Tropical Forestry and Forest Products (INTROP), Universiti Putra Malaysia, 43400 UPM Serdang, Selangor, Malaysia
[3]Laboratory of Processing and Product Development, Institute of Plantation Studies, Universiti Putra Malaysia, 43400, UPM Serdang, Selangor, Malaysia
[4]Department of Biological Functions and Engineering, Graduate School of Life Science and Systems Engineering, Kyushu Institute of Technology, 2-4 Hibikino, Wakamatsu-ku, Kitakyushu, Fukuoka 808-0196, Japan

ABSTRACT

Malaysia is one of the largest producers and exporters of palm oil, thus, a large amount of palm oil mill effluent (POME) is generated through this process. POME contributes to environmental pollution if it is not properly treated. This complex effluent consists of colloidal matters and mainly organic components with more than 90% water. Thus, it is useful to be used as a substrate for fermentative processes, including biohydrogen production. Biohydrogen from POME is a renewable source that can potentially serve as an alternative to substitute fossil fuels. The abundance of POME and the rising price of fossil fuels in the global market create a demand for this source of energy. However, the complexity of the substituents in POME makes the optimisation of this effluent as a substrate in dark fermentation a challenge. This review article explores the important parameters that need to be considered for optimal biohydrogen production, such as the bioreactor operational parameters and the microbial consortium. Besides, the potential of metabolic engineering as a tool to overcome the limitations of the microbial strains to metabolise POME for increased

ARTICLE INFO

Article history:
Received: 10 February 2020
Accepted: 13 November 2020
Published: 31 December 2020

DOI: https://doi.org/10.47836/pjst.28.S2.19

E-mail addresses:
sakinah_fatin@yahoo.com (Fatin Sakinah Rosman)
mzulkhairi@upm.edu.my (Mohd Zulkhairi Mohd Yusoff)
mohdrafein@upm.edu.my (Mohd Rafein Zakaria)
toshi.maeda@life.kyutech.ac.jp (Toshinari Maeda)
alihas@upm.edu.my (Mohd Ali Hassan)
* Corresponding author

ISSN: 0128-7680
e-ISSN: 2231-8526

© Universiti Putra Malaysia Press

biohydrogen production was also reviewed. However, further research and development are needed to increase the biohydrogen yield on par with commercial demand.

Keywords: Biohydrogen, dark fermentation, hydrogen-producing microorganisms, palm oil mill effluent

INTRODUCTION

As the availability of fossil fuels is steadily decreasing over the years, a renewable alternative source of energy needs to be considered. Biohydrogen is one of the potential replacements of fossil fuels. Biohydrogen refers to hydrogen that has been generated through biological processes (Kapdan & Kargi, 2006). Biohydrogen is a clean energy source and considered renewable since it can be produced continuously from various renewable sources such as oil palm biomass and food waste (Mohd Yasin et al., 2013). This gas is odourless, colourless, combustible, and nontoxic. Unlike hydrocarbon fuels, hydrogen gas burns cleanly without emitting any environmental pollutants. This is because hydrogen combustion only produces water vapour (H_2O) (Mokhtar et al., 2019).

Table 1 shows the comparison between gasoline, ethanol, methane, and hydrogen, respectively as energy carriers. Biohydrogen is also an interesting biofuel since it is scale-independent and has a high conversion rate to electricity via fuel cells compared to other gaseous fuels (Groot, 2003). According to the International Energy Agency (IEA), in 2018, the cost of hydrogen gas production from renewable sources is approximately USD 3.0-7.5/kg, while the cost of using coal as a feedstock is about USD 1.2-2.2/kg of hydrogen (IEA, 2020). In 2020, it can be seen that the prices of alternative fuels (biodiesel B20 USD 2.36/gallon, biodiesel B99-B100 USD 3.51/gallon) are comparative to hydrocarbon fuels (diesel USD 2.61/gallon and gasoline USD 1.91/gallon) (Energy, 2020).

In order to make the production of biohydrogen more sustainable and cost-effective, the use of renewable resources as the feedstock is more ideal compared to the conventional simple sugars. Thus, in conjunction with a sustainable and environmentally friendly strategy, many researchers have preferred to utilise organic biomass as alternative substrates for biohydrogen production.

The POME generated will be utilised by anaerobic microorganisms in a bioreactor as a substrate to generate biohydrogen through a process called dark fermentation. Thus, to take full advantage of this inexhaustible resource, the efficiency of the dark fermentation process by the microbes needs to be optimised. Therefore, this review also covers the crucial factors that may contribute to the efficiency of biohydrogen production through dark fermentation. This includes microbial limitation, environmental limitation, operational condition, and the application of metabolic engineered microorganisms. The current development and future projection of biohydrogen production from the renewable substrate were discussed thoroughly.

Table 1
Properties of energy carriers; H_2, CH_4, ethanol, and gasoline

Energy Carrier Properties	Hydrogen	Methane	Ethanol	Gasoline
Density, gas (NTP) (kg m^{3-1})	0.0899	0.651	N.A.	N.A.
Density, liquid (kg m^{3-1})	70.8	422.6	789.3	720 -780
Melting point (°C)	-259.1	-182.3	-114.15	-40
Boiling point (°C)	-252.76	-161.15	78.29	N.A.
Lower heating value (MJ kg^{-1})	119.9	50.0	N.A.	44.6
Energy per unit mass (MJ kg^{-1})*	141.9	55.5	29.9	47.4
Energy per unit volume (GJ m^{3-1})	0.013	0.651	23.6	34.85
Flame temperature (°C)	2045	1875	N.A.	2200
Self-ignition temperature (°C)	585	540	423	228-501
Minimal ignition energy (mJ)	0.2	0.29	N.A.	0.24
Ignition limits in air (vol %)	4 – 75	5.3 – 15	4.3 -19	1.0 – 7.6
Flame propagation in air (m s^{-1})	2.65	0.4	N.A.	0.4
Diffusion coefficient in air (cm^2 s^{-1})	0.61	0.16	N.A.	0.05
Toxicity	No	No	No	Yes
N.A. = not available				

Sources: (Najafpour et al., 2015: Xu et al., 2009)

Substrate for Biohydrogen Production via Dark Fermentation

The increasing trend in palm oil production gains the concern of environmental activist groups. This is because palm oil plantation expansion leads to deforestation, causing loss of biodiversity. An increase in palm oil production also reflected the increase in crude palm oil (CPO) production. CPO production becomes an environmental issue due to the massive generation of POME from the process of CPO extraction where a tonne of CPO produces approximately 3.05 tonnes of POME (Singh et al., 2010). POME is the largest wastewater produced and the most problematic environmental pollutant in the palm oil industry (Singh et al., 2010). This complex effluent is viscous, brownish in colour, and consists of colloidal matters, with more than 90% of water. The solids content of POME comprises more than 5% total solids and around 4% suspended solids (Taifor et al., 2017). The POME also has a discharge temperature of 80–90°C.

The pre-treatment of POME is vital before its utilisation, not only as a substrate for biohydrogen production through microbial fermentation but also for the production of various products such as biosolvents (Hipolito et al., 2008), bioacids (Mumtaz et al., 2008) and polyhydroxyalkanoates (PHA) (Hassan et al., 1997). The alkaline-heat supernatant pre-treatment was shown to produce the highest biohydrogen production (2.18 mol H_2/mol total carbohydrate) by POME compared to other pre-treatment like acid (Kamal et al., 2012).

MATERIALS AND METHODS

General Factors that Influence Biohydrogen Productivity: Nutrients

Macronutrients and micronutrients are essential in dark fermentation which includes: carbon and nitrogen sources (Lin & Lay, 2004a), ammonium, phosphate (Lin & Lay, 2004b), sulphur, sulphate (Cheng et al., 2011), iron (Yang & Shen, 2006), and elemental traces (Lin & Lay, 2005). The concentration of these nutrients also influences the growth of microbes and hydrogen production. The ranges of nitrogen concentration around 0.1-2.0 g N/L with a C/N ratio of 3.3 to 130 were found to result in optimal growth.

Besides microbial growth, the efficiency of biohydrogen production also relies on the microbial hydrogenases that are involved in hydrogen metabolism. The most important element that influences the action of hydrogenases is ferredoxin (Chou et al., 2007). This is because iron is important for hydrogenase activity and may deviate the fermentation pathways away from biohydrogen production (Yang & Shen, 2006). Reported that magnesium, sodium, and zinc were reported as the most significant elements for biohydrogen production. The optimum concentrations of elements were (mg/L) 0.25 Zn^{2+}, 4.8 Mg^{2+}, 1 Fe^{2+} and 393 Na^{+}. The maximum biohydrogen yield was 233 mL H_2/g/hexose from sucrose-containing wastewater (Lin & Lay, 2005).

Buffer. Organic acids are by-products produced from the dark fermentation of biohydrogen production. The accumulation of these acids will reduce the pH of the growth medium of the microbes, resulting in a decrease in biohydrogen production or stunting the microbial growth. Therefore, a strong buffer in the medium is required to oppose the pH change caused by organic acids produced. Carbonate buffers ($NaHCO_3$ and NH_4CO_3) are widely used in biohydrogen dark fermentation studies. However, the use of these buffers may result in the formation of additional CO_2 due to the interaction of HCO_3^- with acidic metabolites (Lin & Lay, 2005). This situation should be avoided as the gas build-up will induce toxicity of the microbial environment. Hence, the use of phosphate buffer is preferable to alleviate this concern. This is because some studies have found that the use of phosphate buffers like K_2HPO_4 and Na_2HPO_4 could maintain the pH values of the medium and promote hydrogen production (Lin et al., 2011).

Hydrogen Partial Pressure. The theory predicts that by reducing the partial pressure of hydrogen may increase the biohydrogen yields from glycerol. High dissolved H_2 concentration in the culture medium inhibits H_2 production and favour the hydrogen consumption pathway instead (Mandal et al., 2006). Immediate removal of H_2 from the culture medium is recommended to facilitate maximum H_2 yields that showed hydrogen yield was doubled to 3.9 mol H_2/mol glucose (Chong et al., 2009). Another method that can be employed is by adding chemicals like KOH and NaOH, to absorb carbon dioxide

from the headspace and by removing the dissolved gases (Saady, 2013). The addition of the chemicals will create a vacuum environment. However, the addition of the chemicals will increase the pH of the medium, thus, affecting the optimal pH needed to maintain bacterial growth. Agitation served to remove dissolved gases such as CO_2 and H_2 from the fermentation medium. Ferchichi et al. (2005) revealed the agitation up to 100 rev/min yielded 1.66 mol-H_2/mol.

Limitation of Dark Fermentation for Biohydrogen Production

Physicochemical Conditions. Table 2 depicts the advantages, disadvantages, and mechanisms of biohydrogen production through dark fermentation. The metabolism of bacteria for biohydrogen production through dark fermentation is highly dependent on the physicochemical factors. Among the crucial factors are the pH, hydraulic retention time, partial pressure of hydrogen, temperature, fermentation products, by-products inhabitation and growth media.

Table 2
Microbial biohydrogen production mechanisms by dark fermentation: advantages and disadvantages

Mechanism	$C_6H_{12}O_6 + 2H_2O \rightarrow 2CH_3COOH + 4H_2 + 2CO_2$
Advantages	• H_2 production from various carbohydrates and organic wastes • High H_2 production rates • No light required • Simpler process for engineering than the others • H_2 can be produced along with the high-value compounds (e.g.: glucogenic acid and 1,3-propanediol)
Disadvantages	• CO_2 present in the product gas • Incomplete oxidisation of organic materials to H_2, low H_2 yields • Effluent treatment required • Impurity of product gas, traces of H_2S, methane and carbon dioxide.

Sources: Mohd Yasin et al. 2011; Vignais & Billoud 2007

Substrate Inhibition. The mechanisms of biohydrogen production involving microbes are catalysed by mainly hydrogenase and nitrogenase enzymes (Vignais et al., 2006). Both mechanisms utilise the presence of protons as the electron sink during the metabolism of organic substrates that act as electron donors. The nitrogenase enzyme catalyses the reduction of nitrogen gas to ammonia (Tamagnini et al., 2002). The absence of N_2 will, therefore, shift the total electron flux to biohydrogen production instead. This reaction is irreversible and can produce biohydrogen even at saturated biohydrogen concentration in the medium and this reaction is energy-intensive (Vignais et al., 2006).

The hydrogenases can be distinguished based on the types of electron donors and acceptors used in hydrogen metabolisms such as NAD, cytochrome, coenzyme, and ferredoxins. The enzymes can also be classed based on the metallic cofactors and

sequence similarity of the hydrogenases. There are currently three known classes: [NiFe]-hydrogenases (Forzi & Sawers, 2007), [FeFe]-hydrogenases and [Fe]-hydrogenases (Fang et al., 2017). Interestingly, it was found that the functionality of the different Hyd enzymes largely depending on the pH (Sanchez-Torres et al., 2013). The majority of studies on biohydrogen production involves the metabolism of simple sugars. POME is a complex substance which could not be readily available for microbes to metabolise. It leads to long adaptive phases and low conversion rates into the product. However, the components of the complex substrates will be transformed into simple compounds through the degradation process. The stoichiometric reactions involved in the dark fermentation were explicated in Table 3.

Table 3
Stoichiometries reaction of dark fermentation of glucose for biohydrogen production

Reaction	Stoichiometry	ΔG0' (kJ reaction)	Reference
Oxidation of glucose	$C_6H_{12}O_6 + 12H_2O \rightarrow 12H_2 + 6HCO_3^- + 6H^+$	+ 3.2	(Chou et al., 2008)
Acetate production	$C_6H_{12}O_6 + 4H_2O \rightarrow 2CH_3COO^- + 4H_2 + 2HCO_3^- + 4H^+$	- 206.3	
Butyrate production	$C_6H_{12}O_6 + 2H_2O \rightarrow CH_3CH_2CH_2COO^- + 2H_2 + 2HCO_3^- + 3H^+$	- 254.8	
Ethanol production	$C_6H_{12}O_6 + 2H_2O \rightarrow 2CH_3CH_2OH + 2HCO_3^- + 2H^+$	- 235.0	
Acetate and ethanol Production	$C_6H_{12}O_6 + 3H_2O \rightarrow CH_3CH_2OH + CH_3COO^- + 2H_2 + 2HCO_3^- + 3H^+$	- 215.716	(Hwang et al., 2004)
Lactate production	$C_6H_{12}O_6 \rightarrow 2CH_3CHOHCOO^- + 2H^+$	- 198.1	(Kim et al., 2009)
Butanol production	$C_6H_{12}O_6 + H_2O \rightarrow CH_3CH_2CH_2OH + 2HCO_3^- + 2H^+$	- 280.5	(Chin et al., 2003)
Propionate production	$C_6H_{12}O_6 + 2H_2 \rightarrow 2CH_3CH_2COO^- + 2H_2O + 2H^+$	- 359.0	(Morimoto et al., 2005)
Valerate production	$C_6H_{12}O_6 + H_2 \rightarrow CH_3CH_2CH_2CH_2COO^- + HCO_3^- + H_2O + 2H^+$	- 330.9	(Chou et al., 2008)
Acetogenesis	$4H_2 + 2HCO_3^- + H^+ \rightarrow CH_3COO^- + 4H_2O$	- 104.6	
Acidogenesis	$C_6H_{12}O_6 \rightarrow 3CH_3COO^- + 3H^+$	- 310.6	(Kim et al., 2009)

Temperature. The temperature influences the microbial growth and consequently increases enzymatic reactions and the rate of chemical synthesis (Dasgupta et al., 2010). Dark fermentation metabolism can occur within a wide range of temperatures 15-45°C (mesophilic), hyper-thermophilic (more than 80°C). Previous studies on the production of biohydrogen under thermophilic conditions were compared in Table 4.

The effects of temperature from mesophilic to thermophilic (25 - 55°C) during the fermentation were investigated by Yossan et al. (2012) and the results showed that the

Table 4
Advantages and disadvantages of biohydrogen dark fermentation in thermophilic condition

Advantages	Disadvantages
• Increase in the rates of chemical and enzymatic reactions • Increase in thermodynamic favourability of H_2-production. H_2 production becomes less affected by the partial pressure of H_2. • The solubility of H_2 and CO_2 to water decreases • Reactors are less prone to contamination by H_2-consuming organisms • Decreased diversity of side products • Some thermophiles excrete exoenzymes, which can hydrolyze biopolymers • Suitable for direct processing high-temperature wastewaters • Destruction of pathogens in the reactor effluent	• Low cell densities achieved • Energy need for heating

Source: (Hallenbeck, 2005; Hawkes et al., 2002)

biohydrogen yield was optimum at 37°C. The highest yield of biohydrogen was obtained using 55°C reactor temperature with 985.3 mL/L POME. O-thong et al. (2011) optimised three different temperatures between 35-75°C, which produced the biohydrogen production at 1104 mL H_2/L POME (35°C), and maximum at 4750 mL H_2/L POME (55°C), respectively. Based on the statistical analysis, the optimal condition for biohydrogen production was at 60°C, with a maximum production of biohydrogen at 4820 mL H_2/L POME. These studies have clearly shown that high temperature is the most ideal fermentation temperature to achieve the highest biohydrogen yield using POME.

pH. The optimal growth pH is microbial dependent and an important factor in suppressing the behaviour of the hydrogen-consuming methanogens. Studies showed different initial pH yielded different biohydrogen value, 2584 mL H_2/ L POME (pH 4.5), 4750 mL H_2/L POME (pH 5.5) and 4300 mL H_2/ L POME (pH 6.5), respectively (O-thong et al., 2011). The optimal initial pH for biohydrogen production was found at 5.5, where the reaction achieved the maximum production of biohydrogen at 4820 mL H_2 L/POME. RSM analyses from different studies showed the optimum production of biohydrogen was found at 272 mL H_2/g substrate with an initial pH around 5.70. Another experiment using microflora in POME sludge also showed that the maximum biohydrogen production rate was 98 mL H_2/h with initial pH at 5.98 (Rasdi et al., 2009).

Under slightly acidic conditions, the bacteria growth of methanogens will be suppressed. The ability of biohydrogen-producing bacteria to develop will be increased. Moreover, controlling the pH in dark fermentation is important because organic acids generated as by-products tend to reduce the pH of the culture medium (Li & Chen, 2007).

Products Inhibition. Biohydrogen is typically produced from the metabolism of glucose or sucrose that also produces secondary products such as acetate and butyrate. The organic

acids can reduce the rate of cell growth at lower concentrations and cause changes in cell metabolic process (Kyazze et al., 2006). The organic acids (undissociated) may pass through the cell membrane and dissociate within the cell of bacteria. This occurs when the pH inside the cell is higher than its surroundings. Therefore, high organic acid concentrations can disrupt the proton motive force (pH gradient) across the cell membrane, resulting in metabolic inhibition (Van Ginkel & Logan, 2005). Thus, biohydrogen production is typically more influenced by the disassociated butyric acid than by acetic acid, due to butyric acid having lower pK_a value than acetic acid at 4.7 (Hawkes et al., 2007).

Another end-product which could suppress the biohydrogen production is ethanol. Lack of bacteria tolerance against ethanol. Thermophilic bacteria are less ethanol-tolerant than mesophilic bacteria (Burdette et al., 2002). The most ethanol-tolerant strains are the *Thermoanaerobacter* sp. strain A10 (Georgieva et al., 2007) and *Clostridium thermocellum* sp. strain SS22 (5% (v/v) (Rani & Seenayya, 1999).

Inoculum. Most of the microbes that are studied for biohydrogen production are obligate anaerobes (i.e *Clostridia*). However, the combination of facultative anaerobes with obligate anaerobes in the biohydrogen production may create more advantageous (Chong et al., 2009). Several bacteria can metabolise the complex material such as POME into simple sugars or organic acids, while others utilise these intermediate products to produce biohydrogen. The highest yield of biohydrogen was reported to be at 2.15 mol H_2/mol-hexose from 3.2 L anaerobic batch sequencing reactor (ASBR) (O-Thong et al., 2007). In another study, the highest biohydrogen yield was 1773 N mL H_2/L POME using continuous batch. The studies evidenced that mixed cultures are more advantageous compared to pure cultures.

Single culture also plays a significant role particularly its metabolism and the optimal growth conditions during biohydrogen production. O-Thong et al. (2009) showed that the *Thermoanaerobacterium* had produced 25.9 mmol H_2/d from POME. Chong and colleagues found that the *Clostridium butyricum* EB6 generated 948 mL H_2/mL glucose from POME (Chong et al., 2009). Besides, it is also important to reduce the presence of bacteria that may inhibit the production of biohydrogen like methanogens and sulphate reducers. Methanogens may be depleted using shorter hydraulic retention time (HRT), provided that the HRT is not exceeding the crucial value where biohydrogen producing bacteria may be washed out (Ismail et al., 2010).

Metabolic Engineering Approaches

Metabolic engineering is one of the available strategies to address the limitations presented by dark fermentation in the production of biohydrogen. The theoretical biohydrogen yield from dark fermentation using glucose as a carbon source is 12 mol H_2 and 6 mol CO_2 per

mole glucose, but there are no reported natural bacteria that possess the metabolism that is capable to generate this value (Chaudhary et al., 2012). However, based on several known fermentation reactions, the theoretical maximum H_2 yield is only 4 mol H_2/ mol glucose produced by strictly anaerobic bacteria. Meanwhile, facultative bacteria can only produce biohydrogen yield of 2 mol H_2/mol glucose (Mohd Yasin et al., 2013). Therefore, the theoretical maximum yield represents only 25% of substrate conversion into biohydrogen, signalling the inefficiency of the system. This is because other metabolic by-products of dark fermentation like butyrate, propionate, ethanol, lactate, including biomass, are also generated in significant amounts (Table 3).

E.coli has been employed as a robust model strain for metabolic engineering and protein engineering to improve the productivity of hydrogen-producing bacteria (Sanchez-Torres et al., 2013). Even though obligate anaerobes like *Clostridia* spp. showed higher hydrogen production compared to *E. coli* (Table 5), they require more sophisticated cultivation set-up because they are obligate anaerobes.

Table 5
Types of microorganism, bioreactor types and scales and biohydrogen production from POME through the dark fermentation process

Microorganism	Hydrogen Yield	Hydrogen Production Rate	Reactor Type	References
C. butyricum EB6	298 mL H_2/g carbohydrate	849.5 mL H_2/h	3L Reactor	(Chong, Sabaratnam, et al., 2009)
Thermoanaerobacterium-	6.5 L H_2/L-POME	25.9 mmol H_2/L/d	150 mL bottle	(O-Thong et al., 2007)
Thermosaccharolyticum	4.6 L H_2/L-POME	-	1L ASBR	
Mixed culture	199 mmol H_2/L-POME	-	1L Reactor	(O-Thong et al., 2007)
Mixed culture	0.27 L H_2/g-COD	9.1 L H_2 /L/ POME/d	3.2L ASBR	(Prasertsan et al., 2009)
Mixed culture	840 NmL H_2/L-POME	35 N mL/H_2/L/ POME/h	50L CSTR	(Yusoff et al., 2009)
Suspended Mixed culture	145.9cm^3H_2/g-COD	240.5 cm^3 H_2/g-VSS/d	122 cm^3 vials	(Ismail et al., 2010)
Mixed culture	1054 NmL H_2/L-POME	44 N mL H_2/L/ POME/h	50L CSTR	(Yusoff et al., 2009)

Maeda and his colleagues designed the robust engineered *E. coli* strains for enhanced biohydrogen production (Maeda et al., 2008). To date, the framework for metabolic engineering is restricted to the well-described microorganism, limiting the window of opportunity to discover novel genes that may increase the production of biohydrogen.

Future Progress of Dark Fermentation for Biohydrogen Production

The largest obstacle to biohydrogen production using POME was low biohydrogen molar yield, which only reached 10-20% of the total energy the substrate can provide (Angenent et al., 2004). In addition, estimation of the use of POME to produce biohydrogen is determined using simple sugars such as glucose, since it is impossible to measure the moles of complex substrates like POME. Many studies have shown that the lower yield of biohydrogen production through dark fermentation is due to the bioconversion of POME into multiple by-products (Hipolito et al., 2008). The presence of multiple by-products will not only increase the pH of the culture medium but also cause the purification of products more difficult.

Technologies and systems for biohydrogen production are well known, but currently imperfect for complex substrates. Most of the technical issues are related to the use of stand-alone technology, such as exclusive use of dark fermentation (Levin, 2004). The integrated biohydrogen and methane production system is currently the best solution to these issues. The advantages of the two-stage system include the efficiency of the process, higher yield of biogas and high total energy recovery (Hawkes et al., 2002). Figure 1 shows the emerging POME biohydrogen manufacturing approach using hybrid systems. In the first stage, POME will be transformed into organic acids and biohydrogen using dark fermentation, followed by the conversion of the organic acids into biohydrogen via photo fermentation. By implementing this hybrid system, biohydrogen production efficiency increased from the first stage at 50% to 70% in the second stage (Cheng et al., 2011). However, the main problem in the hybrid system is the implementation of the second stage

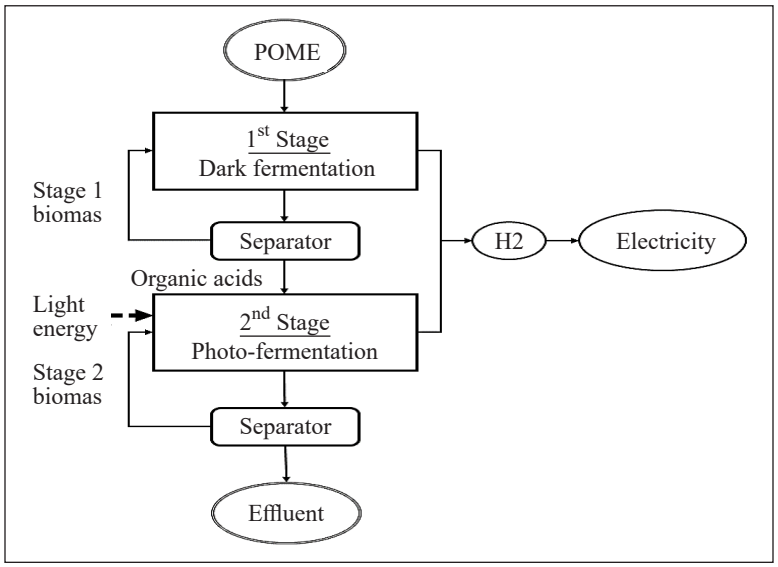

Figure 1. The proposed strategy of an integrated system by combining dark and photo fermentation to produce biohydrogen from POME as a carbon source

(photo fermentation), where it requires high cost and complex infrastructure to set up the photobioreactor (Cheng et al., 2011).

Another method to improve the fermentation flux is through the integration of metabolic engineering of the microbial strains with optimal fermentation parameters. For example, integrating the metabolic engineering and low partial pressure during fermentation process was found to significantly enhance the hydrogen production (Mandal et al., 2006). However, not many kinds of research have been conducted in pairing metabolic engineering and bioprocessing technology. Most efforts in influencing the metabolic pathway of POME fermentation for biohydrogen production are centred on editing the Fe and Ni hydrogenases pathways as mentioned in another section.

The modification of existing pathways using metabolic engineering approaches will also lead to the creation of a new robust strain with higher hydrogen yield and better productivity. In addition, through metabolic engineering, genetic modification can be made to fully exploit the abundant substrate availability of POME and its derivatives (Taifor et al., 2017). These strategies can also be applied for other applications to construct recombinant strains to produce a wide range of chemicals and bioproducts. Therefore, the application of the metabolic engineering methods in industrial-scale bioprocessing is a promising study to improve the production of biohydrogen.

CONCLUSION

Dark fermentation is one of the anaerobic fermentation processes applied for biohydrogen production. The performance can be recovered by manipulating the factors that have tremendous influences on biohydrogen production, including pH, temperature, medium formulation, and the application of genetic engineering. Bench studies provide basic essential information to know and understand the microbial limitation, environmental limitation, and operational condition for biohydrogen production. The production strains can be manipulated by genetic engineering to obtain the strains that can utilise POME for biohydrogen production with minimal intermediate products, such as organic acids, solvents, or amino acids. Another important step is to shift the biohydrogen production from bench to pilot scale-mostly operated by continuous systems, without compromising the ability of microorganisms to convert complex substrate into biohydrogen. Nevertheless, further investigation from the bench studies and the industry are needed to enhance the efficient utilisation of wastewater, like POME, towards maximal biohydrogen production through dark fermentation.

ACKNOWLEDGEMENTS

The authors would like to acknowledge and thank Universiti Putra Malaysia for the Grant Putra (UPM/700-2/1/GP-IPM/2017/9559800) and the provision of Graduate Research Fund to the first author, Fatin Sakinah Rosman.

REFERENCES

Angenent, L. T., Karim, K., Al-Dahhan, M. H., Wrenn, B. A., & Domiguez-Espinosa, R. (2004). Production of bioenergy and biochemicals from industrial and agricultural wastewater. *Trends in Biotechnology, 22*(9), 477-485. doi:10.1016/j.tibtech.2004.07.001

Burdette, D. S., Jung, S. H., Shen, G. J., Hollingsworth, R. I., & Zeikus, J. G. (2002). Physiological function of alcohol dehydrogenases and long-chain (C30) fatty acids in alcohol tolerance of *Thermoanaerobacter ethanolicus*. *Applied and Environmental Microbiology, 68*(4), 1914-1918. doi:10.1128/aem.68.4.1914-1918.2002

Chaudhary, N., Ngadi, M. O., & Simpson, B. (2012). Comparison of glucose, glycerol and crude glycerol fermentation by *Escherichia Coli* K12. *Journal of Bioprocessing & Biotechniques, S*(01), 1-5. doi:10.4172/2155-9821.s1-001

Cheng, C. L., Lo, Y. C., Lee, K. S., Lee, D. J., Lin, C. Y., & Chang, J. S. (2011). Biohydrogen production from lignocellulosic feedstock. *Bioresource Technology, 102*(18), 8514-8523. doi:10.1016/j.biortech.2011.04.059

Cheng, J., Su, H., Zhou, J., Song, W., & Cen, K. (2011). Hydrogen production by mixed bacteria through dark and photo fermentation. *International Journal of Hydrogen Energy, 36*(1), 450-457. doi:10.1016/j.ijhydene.2010.10.007

Chin, H. L., Chen, Z. S., & Chou, C. P. (2003). Fedbatch operation using *Clostridium acetobutylicum* suspension culture as biocatalyst for enhancing hydrogen production. *Biotechnology Progress, 19*(2), 383-388. doi:10.1021/bp0200604

Chong, M. L., Rahim, R. A., Shirai, Y., & Hassan, M. A. (2009). Biohydrogen production by *Clostridium butyricum* EB6 from palm oil mill effluent. *International Journal of Hydrogen Energy, 34*(2), 764-771. doi:10.1016/j.ijhydene.2008.10.095

Chong, M. L., Sabaratnam, V., Shirai, Y., & Hassan, M. A. (2009). Biohydrogen production from biomass and industrial wastes by dark fermentation. *International Journal of Hydrogen Energy, 34*(8), 3277-3287. doi:10.1016/j.ijhydene.2009.02.010

Chou, C. J., Jenney, F. E., Jr., Adams, M. W., & Kelly, R. M. (2008). Hydrogenesis in hyperthermophilic microorganisms: Implications for biofuels. *Metabolic Engineering, 10*(6), 394-404. doi:10.1016/j.ymben.2008.06.007

Chou, C. J., Shockley, K. R., Conners, S. B., Lewis, D. L., Comfort, D. A., Adams, M. W., & Kelly, R. M. (2007). Impact of substrate glycoside linkage and elemental sulfur on bioenergetics of and hydrogen production by the hyperthermophilic archaeon *Pyrococcus furiosus*. *Applied and Environmental Microbiology, 73*(21), 6842-6853. doi:10.1128/aem.00597-07

Fang, X., Sastry, A., Mih, N., Kim, D., Tan, J., Yurkovich, J. T., . . . Palsson, B. O. (2017). Global transcriptional regulatory network for *Escherichia coli* robustly connects gene expression to transcription factor activities. *Proceedings of the National Academy of Sciences, 114*(38), 10286-10291. doi:10.1073/pnas.1702581114

Ferchichi, M., Crabbe, E., Hintz, W., Gil, G. H., & Almadidy, A. (2005). Influence of culture parameters on biological hydrogen production by *Clostridium saccharoperbutylacetonicum* ATCC 27021. *World Journal of Microbiology and Biotechnology, 21*(6-7), 855-862. doi:10.1007/s11274-004-5972-0

Forzi, L., & Sawers, R. G. (2007). Maturation of [NiFe]-hydrogenases in *Escherichia coli. BioMetals, 20*(3-4), 565-578. doi:10.1007/s10534-006-9048-5

Georgieva, T. I., Skiadas, I. V., & Ahring, B. K. (2007). Effect of temperature on ethanol tolerance of a thermophilic anaerobic ethanol producer Thermoanaerobacter A10: Modeling and simulation. *Biotechnology and Bioengineering, 98*(6), 1161-1170. doi:10.1002/bit.21536

Hallenbeck, P. C. (2005). Fundamentals of the fermentative production of hydrogen. *Water Science Technology, 52*(1-2), 21-29. doi:10.2166/wst.2005.0494

Hassan, M. A., Shirai, Y., Kusubayashi, N., Karim, M. I. A., Nakanishi, K., & Hasimoto, K. (1997). The production of polyhydroxyalkanoate from anaerobically treated palm oil mill effluent by *Rhodobacter sphaeroides. Journal of Fermentation and Bioengineering, 83*(5), 485-488. doi:10.1016/s0922-338x(97)83007-3

Hawkes, F., Hussy, I., Kyazze, G., Dinsdale, R., & Hawkes, D. (2007). Continuous dark fermentative hydrogen production by mesophilic microflora: Principles and progress. *International Journal of Hydrogen Energy, 32*(2), 172-184. doi:10.1016/j.ijhydene.2006.08.014

Hawkes, F. R., Dinsdale, R., Hawkes, D. L., & Hussy, I. (2002). Sustainable fermentative hydrogen production: Challenges for process optimisation. *International Journal of Hydrogen Energy, 27*(11-12), 1339-1347. doi:10.1016/s0360-3199(02)00090-3

Hipolito, C. N., Crabbe, E., Badillo, C. M., Zarrabal, O. C., Morales Mora, M. A., Flores, G. P., ... & Ishizaki, A. (2008). Bioconversion of industrial wastewater from palm oil processing to butanol by *Clostridium saccharoperbutylacetonicum* N1-4 (ATCC 13564). *Journal of Cleaner Production, 16*(5), 632-638. doi:10.1016/j.jclepro.2007.02.005

Hwang, M. H., Jang, N. J., Hyun, S. H., & Kim, I. S. (2004). Anaerobic bio-hydrogen production from ethanol fermentation: the role of pH. *Journal of Biotechnology, 111*(3), 297-309. doi:10.1016/j.jbiotec.2004.04.024

IEA. (2020). *World energy prices 2020*. International Energy Agency. Retrieved October 5, 2020, from https://www.iea.org/reports/energy-prices-2020

Ismail, I., Hassan, M. A., Abdul Rahman, N. A., & Soon, C. S. (2010). Thermophilic biohydrogen production from palm oil mill effluent (POME) using suspended mixed culture. *Biomass and Bioenergy, 34*(1), 42-47. doi:10.1016/j.biombioe.2009.09.009

Kamal, S. A., Jahim, J. M., Anuar, N., Hassan, O., Daud, W. R. W., Mansor, M. F., & Rashid, S. S. (2012). Pre-treatment effect of Palm Oil Mill Effluent (POME) during hydrogen production by a local isolate *Clostridium butyricum*. *International Journal on Advanced Science, Engineering and Information Technology, 2*(4), 325-331. doi:10.18517/ijaseit.2.4.214

Kapdan, I. K., & Kargi, F. (2006). Bio-hydrogen production from waste materials. *Enzyme and Microbial Technology, 38*(5), 569-582. doi:10.1016/j.enzmictec.2005.09.015

Kim, S., Seol, E., Oh, Y. K., Wang, G. Y., & Park, S. (2009). Hydrogen production and metabolic flux analysis of metabolically engineered *Escherichia coli* strains. *International Journal of Hydrogen Energy, 34*(17), 7417-7427. doi:10.1016/j.ijhydene.2009.05.053

Kyazze, G., Martinez-Perez, N., Dinsdale, R., Premier, G. C., Hawkes, F. R., Guwy, A. J., & Hawkes, D. L. (2006). Influence of substrate concentration on the stability and yield of continuous biohydrogen production. *Biotechnology Bioengineering, 93*(5), 971-979. doi:10.1002/bit.20802

Lee, D. H., Lee, D. J., & Chiu, L. H. (2011). Biohydrogen development in United States and in China: An input–output model study. *International Journal of Hydrogen Energy, 36*(21), 14238-14244. doi:10.1016/j.ijhydene.2011.05.084

Levin, D. (2004). Biohydrogen production: Prospects and limitations to practical application. *International Journal of Hydrogen Energy, 29*(2), 173-185. doi:10.1016/s0360-3199(03)00094-6

Li, D., & Chen, H. (2007). Biological hydrogen production from steam-exploded straw by simultaneous saccharification and fermentation. *International Journal of Hydrogen Energy, 32*(12), 1742-1748. doi:10.1016/j.ijhydene.2006.12.011

Lin, C. Y., & Lay, C. H. (2004a). Carbon/nitrogen-ratio effect on fermentative hydrogen production by mixed microflora. *International Journal of Hydrogen Energy, 29*(1), 41-45. doi:10.1016/s0360-3199(03)00083-1

Lin, C. Y., & Lay, C. H. (2004b). Effects of carbonate and phosphate concentrations on hydrogen production using anaerobic sewage sludge microflora. *International Journal of Hydrogen Energy, 29*(3), 275-281. doi:10.1016/j.ijhydene.2003.07.002

Lin, C., & Lay, C. (2005). A nutrient formulation for fermentative hydrogen production using anaerobic sewage sludge microflora. *International Journal of Hydrogen Energy, 30*(3), 285-292. doi:10.1016/j.ijhydene.2004.03.002

Lin, Y. B., Chen, H., & Yue, L. R. (2011). Effects of K_2HPO_4 on fermentative biohydrogen production of biohydrogenbacterium R3 Sp.nov. *Advanced Materials Research, 280*, 1-4. doi:10.4028/www.scientific.net/amr.280.1

Mandal, B., Nath, K., & Das, D. (2006). Improvement of biohydrogen production under decreased partial pressure of H2 by *Enterobacter cloacae. Biotechnology Letters, 28*(11), 831-835. doi:10.1007/s10529-006-9008-8

Mohd Yasin, N. H., Fukuzaki, M., Maeda, T., Miyazaki, T., Hakiman Che Maail, C. M., Ariffin, H., & Wood, T. K. (2013). Biohydrogen production from oil palm frond juice and sewage sludge by a metabolically engineered *Escherichia coli* strain. *International Journal of Hydrogen Energy, 38*(25), 10277-10283. doi:10.1016/j.ijhydene.2013.06.065

Mohd Yasin, N. H., Rahman, N. A. A., Man, H. C., Mohd Yusoff, M. Z., & Hassan, M. A. (2011). Microbial characterization of hydrogen-producing bacteria in fermented food waste at different pH values. *International Journal of Hydrogen Energy, 36*(16), 9571-9580. doi:10.1016/j.ijhydene.2011.05.048

Mokhtar, M., Mohd Yusoff, M. Z., Mohamad Ali, M. S., Mustapha, N. A., Wood, T. K., & Maeda, T. (2019). Pseudogene YdfW in *Escherichia Coli* decreases hydrogen production through nitrate respiration pathways. *International Journal of Hydrogen Energy, 44*(31), 16212-16223. doi:10.1016/j.ijhydene.2019.04.228

Morimoto, K., Kimura, T., Sakka, K., & Ohmiya, K. (2005). Overexpression of a hydrogenase gene in *Clostridium paraputrificum* to enhance hydrogen gas production. *FEMS Microbiology Letters, 246*(2), 229-234. doi:10.1016/j.femsle.2005.04.014

Mumtaz, T., Abd-Aziz, S., Rahman, A. A., Yee, P. L., & Hassan, M. A. (2008). Pilot-scale recovery of low molecular weight organic acids from anaerobically treated palm oil mill effluent (POME) with energy integrated system. *African Journal of Biotechnology, 7*, 3900-3905. doi:10.5897/AJB08.640

Najafpour, G. D., Shahavi, M. H., & Neshat, S. A. (2015). Assessment of biological hydrogen production processes: A review. In *International Conference on Chemical and Bioprocess Engineering* (pp. 1-10). Kota Kinabalu, Malaysia. doi:10.3303/CET1865042

O-thong, S., Mamimin, C., & Prasertsan, P. (2011). Effect of temperature and initial pH on biohydrogen production from palm oil mill effluent: Long-term evaluation and microbial community analysis. *Electronic Journal of Biotechnology, 14*(5), 1-12. doi:10.2225/vol14-issue5-fulltext-9

O-Thong, S., Prasertsan, P., Intrasungkha, N., Dhamwichukorn, S., & Birkeland, N. K. (2007). Improvement of biohydrogen production and treatment efficiency on palm oil mill effluent with nutrient supplementation at thermophilic condition using an anaerobic sequencing batch reactor. *Enzyme and Microbial Technology, 41*(5), 583-590. doi:10.1016/j.enzmictec.2007.05.002

Prasertsan, P., O-Thong, S., & Birkeland, N. K. (2009). Optimization and microbial community analysis for production of biohydrogen from palm oil mill effluent by thermophilic fermentative process. *International Journal of Hydrogen Energy, 34*(17), 7448-7459. doi:10.1016/j.ijhydene.2009.04.075

Rani, K. S., & Seenayya, G. (1999). High ethanol tolerance of new isolates of *Clostridium thermocellum* strains SS21 and SS22. *World Journal of Microbiology and Biotechnology, 15*(2), 173-178. doi:10.1023/A:1008863410460

Rasdi, Z., Nor`Aini, A. R., Abd-Aziz, S., Phang, L.-Y., Mohd Yusoff, M. Z., Chong, M. L., & Hassan, M. A. (2009). Statistical optimization of biohydrogen production from palm oil mill effluent by natural microflora. *The Open Biotechnology Journal, 3*(1), 79-86. doi:10.2174/1874070700903010079

Saady, N. M. C. (2013). Homoacetogenesis during hydrogen production by mixed cultures dark fermentation: Unresolved challenge. *International Journal of Hydrogen Energy, 38*(30), 13172-13191. doi:10.1016/j.ijhydene.2013.07.122

Sanchez-Torres, V., Mohd Yusoff, M. Z., Nakano, C., Maeda, T., Ogawa, H. I., & Wood, T. K. (2013). Influence of *Escherichia coli* hydrogenases on hydrogen fermentation from glycerol. *International Journal of Hydrogen Energy, 38*(10), 3905-3912. doi:10.1016/j.ijhydene.2013.01.031

Singh, R. P., Ibrahim, M. H., Esa, N., & Iliyana, M. S. (2010). Composting of waste from palm oil mill: A sustainable waste management practice. *Reviews in Environmental Science and Bio/Technology, 9*(4), 331-344. doi:10.1007/s11157-010-9199-2

Taifor, A. F., Zakaria, M. R., Mohd Yusoff, M. Z., Toshinari, M., Hassan, M. A., & Shirai, Y. (2017). Elucidating substrate utilization in biohydrogen production from palm oil mill effluent by *Escherichia coli*. *International Journal of Hydrogen Energy, 42*(9), 5812-5819. doi:10.1016/j.ijhydene.2016.11.188

US Department of Energy (2020). *Clean cities alternative fuel price report*. Retrieved October 5, 2020, from https://afdc.energy.gov/fuels/prices.html

Van Ginkel, S., & Logan, B. E. (2005). Inhibition of biohydrogen production by undissociated acetic and butyric acids. *Environmental Science & Technology, 39*(23), 9351-9356. doi:10.1021/es0510515

Vignais, P., Magnin, J., & Willison, J. (2006). Increasing biohydrogen production by metabolic engineering. *International Journal of Hydrogen Energy, 31*(11), 1478-1483. doi:10.1016/j.ijhydene.2006.06.013

Vignais, P. M., & Billoud, B. (2007). Occurrence, classification, and biological function of hydrogenases: An overview. *Chemical Reviews 107*(10), 4206-4272. doi:10.1021/cr050196r

Xu, Q., Singh, A., & Himmel, M. E. (2009). Perspectives and new directions for the production of bioethanol using consolidated bioprocessing of lignocellulose. *Current Opinion in Biotechnology, 20*(3), 364-371. doi:10.1016/j.copbio.2009.05.006

Yang, H., & Shen, J. (2006). Effect of ferrous iron concentration on anaerobic bio-hydrogen production from soluble starch. *International Journal of Hydrogen Energy, 31*(15), 2137-2146. doi:10.1016/j.ijhydene.2006.02.009

Yossan, S., O-Thong, S., & Prasertsan, P. (2012). Effect of initial pH, nutrients and temperature on hydrogen production from palm oil mill effluent using thermotolerant consortia and corresponding microbial communities. *International Journal of Hydrogen Energy, 37*(18), 13806-13814. doi:10.1016/j.ijhydene.2012.03.151

Yusoff, M. Z. M., Hassan, M. A., Abd-Aziz, S., & Nor Aini, A. R. (2009). Start-up of biohydrogen production from palm oil mill effluent under non-sterile condition in 50 L continuous stirred tank reactor. *International Journal of Agricultural Research, 4*(4), 163-168. doi:10.3923/ijar.2009.163.168

Pertanika J. Sci. & Technol. 28 (S2): 259 - 271 (2020)

SCIENCE & TECHNOLOGY

Journal homepage: http://www.pertanika.upm.edu.my/

Cellulose Nanofibers from Waste Paper and their Utilization as Reinforcement Materials in Poly((*R*)-3-Hydroxybutyrate-*co*-(*R*)-3-Hydroxyhexanoate Bionanocomposite

Tengku Arisyah Tengku Yasim-Anuar[1]*, Nur Sharmila Sharip[2], Liana Noor Megashah[1], Hidayah Ariffin[1,2] and Nor Azlin Muhamad Nor[1]

[1]Faculty of Biotechnology and Biomolecular Sciences, Universiti Putra Malaysia, 43400, UPM Serdang, Selangor, Malaysia
[2]Laboratory of Biopolymer and Derivatives, Institute of Tropical Forestry and Forest Products, Universiti Putra Malaysia, 43400, UPM Serdang, Selangor, Malaysia

ABSTRACT

Waste paper is the second-highest municipal solid waste collected in Malaysia and as current practice, it is recycled for further use in the manufacturing of low-grade products. Instead of continuously utilizing waste paper for low-grade products manufacturing, it can be used as a feedstock to produce high bioproducts such as cellulose nanofiber (CNF). Hence, this study explored the potential of waste paper as a feedstock for CNF production. The waste paper was subjected to a different number of cycles of wet disk milling (WDM): 0, 5, 10, 15 and 20 cycles. The presence of nano-sized cellulose was confirmed by FE-SEM micrographs, where CNF with diameter size 20 – 40 nm was formed after 10 cycles of milling. It was also revealed that the obtained CNF possessed appropriate properties as a reinforcement material. The tensile strength and Young's modulus of poly((R)-3-hydroxybutyrate-*co*-(*R*)-3-hydroxyhexanoate (PHBHHx) increased by 19 and 12%, respectively after the reinforcement of 1% CNF. Overall, this study portrays that waste paper could be utilized as a raw material for CNF production, without the need for chemical pretreatment.

ARTICLE INFO

Article history:
Received: 10 February 2020
Accepted: 13 November 2020
Published: 31 December 2020

DOI: https://doi.org/10.47836/pjst.28.S2.20

E-mail addresses:
tengkuarisyah@gmail.com (Tengku Arisyah Tengku Yasim-Anuar)
nursharmilasharip@gmail.com (Nur Sharmila Sharip)
lianamegashah@gmail.com (Liana Noor Megashah)
hidayah@upm.edu.my (Hidayah Ariffin)
alin.azlinnor@yahoo.com (Nor Azlin Muhamad Nor)
* Corresponding author

Keywords: Bionanocomposite, cellulose nanofiber, mechanical properties, P\poly((*R*)-3-hydroxybutyrate-*co*-(*R*)-3-hydroxyhexanoate, waste paper

INTRODUCTION

Over the years, the demands of cellulose increases because of its strength, biodegradability, renewability, and biocompatibility especially in paper, board

ISSN: 0128-7680
e-ISSN: 2231-8526

© Universiti Putra Malaysia Press

and composite industries (Arévalo & Peijs, 2016; Gao et al., 2013; Sreekala et al., 1997; Wang et al., 2010). Despite of its excellent properties, cellulose production however causes environmental issues mainly because of the harmful chemical usage and inefficient effluents discharge to extract it from the raw material (Abraham et al., 2013; Prakash et al., 2017). In order to minimize the environmental pollution, wastes comprising cellulose such as waste paper can be reprocessed to produce high value-added bioproducts.

Waste paper is a combustible and post-consumer waste that is usually disposed in a trash bin before being piled up on land. Currently, waste paper is the second-highest municipal solid waste collected in Malaysia behind organic waste (47%), which is around 15% (Jereme et al., 2015). As a current practice, waste paper is recycled for further use in the manufacturing of new fibrous products such as low-grade paper and board (Hietala et al., 2018). Nevertheless, the recycling process may shorten the fibers and results in strength reduction. Hence, instead of utilizing waste paper for low-grade products, it can be used as a feedstock to produce value-added bioproducts such as cellulose nanofiber (CNF). Indirectly, the use of secondary raw material like waste paper will result in higher resource efficiency, thus may avoid resource depletion and unnecessary disposal of wastes (Hietala et al., 2018).

CNF is now mainly derived from various plant fibers that have been refined to nanoscale. Due to the fibrillation process, the hydrogen bonds (H-bonds) are broken down, hence forming nano-sized fibers in diameter called CNF. In general, CNF consists of alternating crystalline and amorphous domains (Chang et al., 2012). It also has long and flexible linked fibers around 20 to 100 nm in diameter, and several micrometers in length (Tibolla et al., 2014).

It is worth noting that CNF nowadays has received much attention from various fields due to its superior physical properties, which mainly derived from its nano-size structure as well as its chemical, biological and mechanical characteristics such as having high specific surface area, high crystallinity, thermally, chemically and rheologically stable, biodegradable, biocompatible and lack of toxicity (Lin & Dufresne, 2014). Many studies have been conducted to determine CNF potentials in various fields ranging from household materials to high-tech industrial applications. CNF is expected to be a promising renewable nanomaterial that can replace uses of non-renewable materials in various products manufacturing including as a reinforcement material to produce bionanocomposites.

Besides the use of degradable reinforcement materials, an attempt has also been widely conducted to replace synthetic polymers as one of the environmentally friendly solutions to minimize environmental pollution. Poly((*R*)-3-hydroxybutyrate-*co-(R)*-3-hydroxyhexanoate (PHBHHx) has been highlighted as one of the potential bio-polymer for various polymer-based products manufacturing. Despite of its biodegradability, the shortcoming of PHBHHx lies on its low thermal, crystallinity and mechanical properties

compared to synthetic plastics (Jing, 2012). Hence, this limits its usage for only certain applications. In fact, the low crystallization rate of the polymer serves as an obstacle during the industrial processing of the material (Buntinx et al., 2017). In order to tackle this obstacle, researchers have looked into techniques such as adding nucleating fillers, microfillers or nanofillers and the incorporation of CNF is expected to help overcome this matter (Xu et al., 2017). Improved property of PHBHHx will widen its usage in various applications, range from household to high-end applications, and indirectly will widen the utilization of PHBHHx as single-use plastics, and ultimately contributes to the less accumulation of single-use plastics.

Hence, this study explored the feasibility of WDM to produce CNF from waste paper. The potential of waste paper-CNF as a reinforcement material for PHBHHx bionanocomposite was also evaluated by analyzing the morphological, thermal and mechanical properties.

MATERIALS AND METHODS

Materials

Waste papers were collected from Administrator Office, Universiti Putra Malaysia. The papers were cut to approximately 3 cm using a milling cutter and stored in a plastic bag at room temperature prior to further processing. Poly((*R*)-3-hydroxybutyrate-*co*-*(R)*-3-hydroxyhexanoate (P(HB-*co*-11%-HHx)) (Mn 126,000, Mw 352,000 Da after purification) was supplied by Kaneka Corporation Japan and used as received.

Production of Cellulose Nanofiber by Wet Disk Milling

Waste papers were soaked in distilled water at a concentration of 2 wt% for 72 hours prior to wet disk milling (WDM). The suspension was then subjected to wet disk mill grinder (Multi mill, Grow Engineering Co. Ltd., Adachi-ku, Tokyo, Japan) for 5 - 20 cycles at 1800 rpm to produce CNF. The CNF slurry was then stored in a sealed bottle at 2°C prior to usage and an approximate 10 mL of slurry suspension was freeze-dried for characterization.

Production of Bionanocomposite

Bionanocomposites made up of 95 – 99 wt% PHBHHx and 1 – 5 wt% CNF were melt blended using a Brabender Plastograph EC internal mixer (Brabender GmbH & Co. KG, Germany) with a mixing speed 60 rpm for 20 min at 150°C. Water molecules from the CNF suspension were evaporated from the hopper, resulted in the formation of PHBHHx/CNF bionanocomposite lump. The PHBHHx/CNF bionanocomposites were then hot-pressed at 150°C for 5 min under 10 atm of pressure to obtain bionanocomposite sheets.

Morphological Analysis

The morphology of CNF was analyzed by field-emission scanning electron microscopy (FE-SEM) (Sirion 200, FEI, Eindhoven, Netherlands) (Yasim-Anuar et al., 2017). The CNF was silver-coated for 50s using vacuum sputter-coated prior to FE-SEM analysis.

X-ray Diffraction Analysis

The crystallinity index (*Crl)* of CNF from the waste paper was analyzed using X-ray diffraction (Shimadzu XRD-6000, Kyoto, Japan). The data was generated with a scan range from 5° to 50°. The *Crl* was determined using the following equation:

$$Crl = \frac{I_{002} - I_{am}}{I_{002}} \times 100\%$$

It is to note that I_{002} at an angle of 2θ=23 and I_{am} at an angle of 2θ=18 correspond to the cellulose and amorphous region respectively (Yasim-Anuar et al., 2018).

Thermogravimetric Analysis

Thermal stability and decomposition temperature of CNF obtained from waste papers and PHBHHx/CNF bionanocomposites were determined by the thermogravimetric analyzer (TGA) (TG 400, Perkin Elmer, Waltham, MA, USA). Samples weighing in a range of 9 – 10 mg were analyzed at a heating rate of 10°C/min under a nitrogen flow of 20 mL/min, from 50 to 550°C (Yasim-Anuar et al., 2019).

Mechanical Analysis

The tensile properties of PHBHHx/CNF bionanocomposites were measured based on ASTM D638 and ASTM D790, using Intron Universal Testing Machine (P5567, 30kN, INTROP Universiti Putra Malaysia, Malaysia). The reported values were the average value of five measurements of each sample.

RESULTS AND DISCUSSION

Characterization of Cellulose Nanofiber from Waste Paper

Morphological Observation. The morphology of waste paper and CNF was observed by FE-SEM as shown in Figure 1. From the FE-SEM micrograph, an irregular structure and presence of bundles of fibers with a size larger than 1000 nm can be observed for waste paper prior to WDM (Figure 1a). Reduction in diameter size could be observed after WDM, and this could be seen as early as 10 cycles. The diameter size of waste paper was reduced from approximately 100 – 900 nm for 5 cycles, to 20 – 40 nm after 10 cycles, 10 – 25 nm

after 15 cycles and 5 – 25 nm after 20 cycles of WDM. This might be attributed to shear and frictional force at the surface layer of cellulose fibers caused by milling stones during WDM processing. During WDM, cellulose fibers were grounded by two counteracting grinding disks at extremely high speed, impact forces and friction. This physical damage then causes fibrillation by breaking down the hydrogen bonds of cellulose fibers, which leads to the transverse cleavage of them along the longitudinal axis (Dubey et al. 2018). Hence, the large bundles of fibers can be disintegrated into individual nanosize fibers with the network structure.

From the morphologies of CNF after WDM as shown in Figure 1 (a-e), the single fibril obviously reduced to nanoscale size by increasing the milling cycles, suggesting that CNF was successfully extracted from cellulose fibers by using the present method. In fact, it was also revealed that no obvious difference could be observed by increasing the WDM cycles up to 20 cycles. This was in contrast with other nanofibrillation methods like ultrasonication. Our previous research on ultrasonication revealed that by prolonging the ultrasonication to more than 9 hours might lead to re-agglomeration of CNF, and eventually increased the diameter size of CNF (Yasim-Anuar et al., 2018). This might be attributed to the reformation of H-bonds between CNF as well as due to the attraction of van der Walls forces, which mainly occurred due to stress on the CNF surface. This phenomenon occurred mainly due to the longer processing time and adhesion of CNF to one another (Yasim-Anuar et al.,

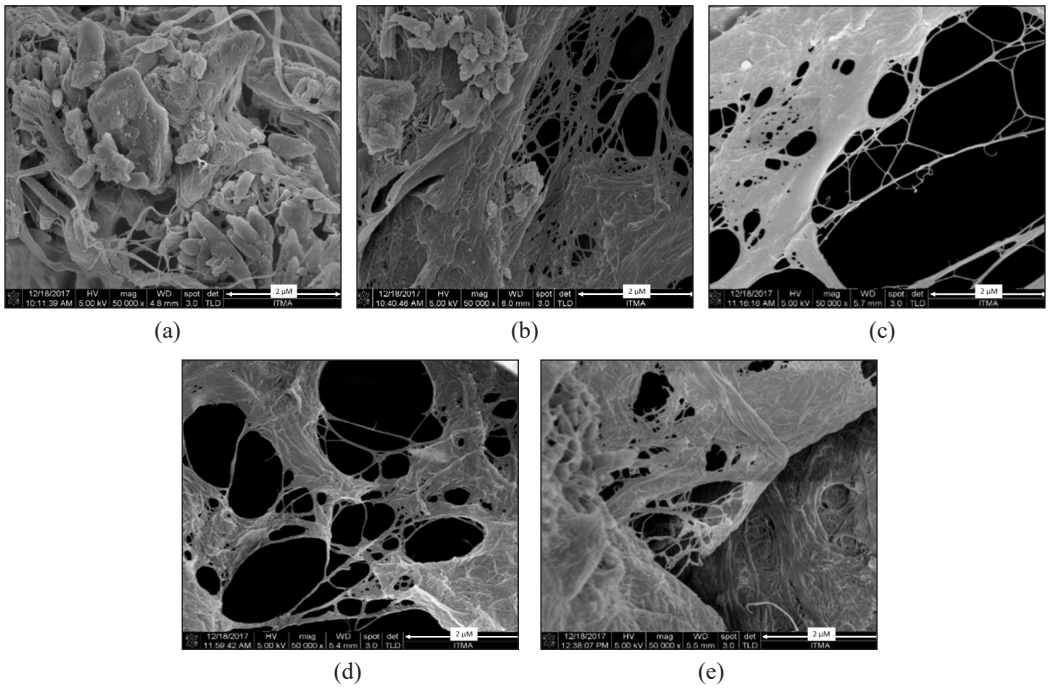

Figure 1. FE-SEM micrographs of (a) cellulose from waste paper and CNF after (b) 5, (c) 10, (d) 15 and (e) 20 cycles. The magnifications for (a) and (b-e) were 10,000x and 50,000x, respectively.

2018). This, however, did not occur to CNF produced by WDM and this proved that this method was more efficient in nanofibrillating CNF into smaller diameter sizes.

Thermal stability and Crystallinity Index of Cellulose Nanofiber

Thermogravimetric analysis was carried out to investigate the thermal stability of CNF. The obtained TG and DTG thermograms of cellulose from waste paper and CNF were plotted as shown in Figure 2. A small weight loss was observed around 50 – 170 ºC mainly due to the evaporation of water from CNF (Yasim-Anuar et al., 2019). The dramatic weight losses were found in a temperature range between 200 – 350 ºC for all samples, which corresponds to the decomposition of cellulose. This finding indicates that cellulose decomposes rapidly at a higher temperature. It was identified that the temperature degradation ($Td_{50\%}$) reduced by prolonged the WDM process. The $Td_{50\%}$ reduced from 340 ºC to approximately 328 – 336 ºC after milling. The reduction was highly attributed to the exposure of CNF to high shear and frictional forces, caused by grinding stones during WDM. In addition, thermal degradation might occur early due to the reduction in diameter size and increment of surface area (Abraham et al. 2013).

This result also corresponded to the *Crl* which was analyzed by XRD. Figure 3 shows that all samples exhibited similar diffraction peaks at around 2θ=21.5 – 23.5. The *Crl* of cellulose fiber was approximately 85% prior to milling, and the value reduced to 80 – 82% after milling. Mechanical forces from high shear and frictional force during WDM could damage the crystalline structure of CNF, hence reduce the *Crl* values. This was supported by reports from Jang et al. (2015), Norrrahim (2018) and Zakaria et al. (2015). Hence, it can be noted that by prolonging the milling process, the crystalline structure of CNF might be disrupted, thus reducing the *Crl* value.

Based on the morphology and average diameter, it was revealed that by WDM the waste paper up to 10 cycles was able to produce CNF with size less than 100 nm, which

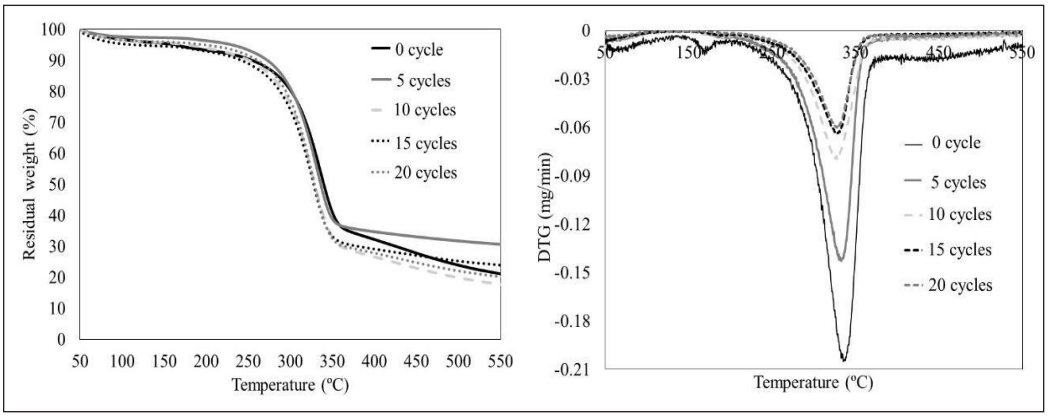

Figure 2. The TG and DTG thermograms of CNF produced by different milling cycles

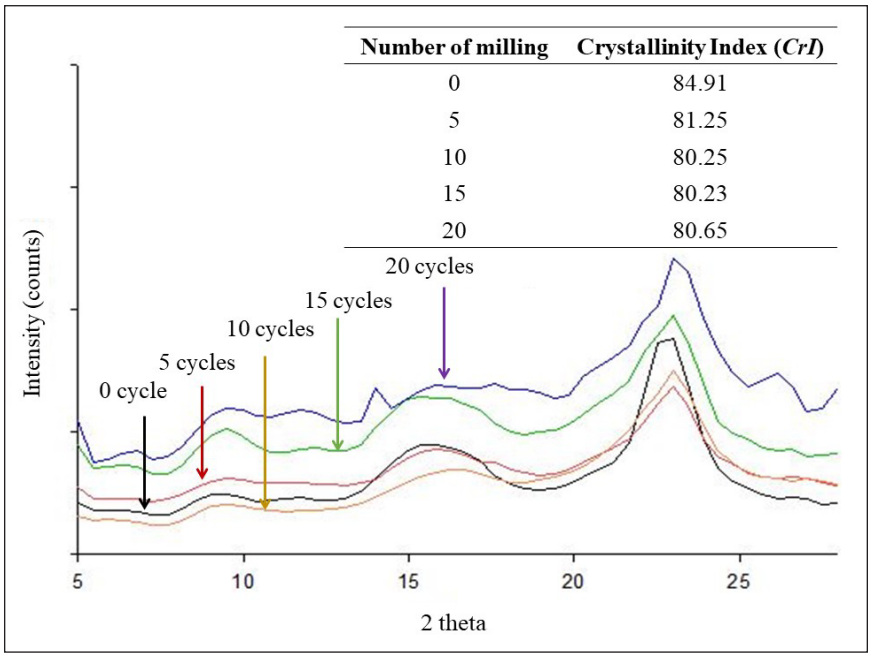

Figure 3. The XRD diffraction patterns of CNF produced by different milling cycles

fulfilled the standard of Malaysian NanoVerify. In fact, by taking into consideration the crystallinity and thermal stability, the results only showed a slight reduction of about 3.2 and 5.5%, respectively after 10 cycles of milling, in comparison to the cellulose before being nanofibrillated. It was also revealed that the CNF produced using this nanofibrillation method was having comparable properties with CNF produced from other nanofibrillation methods as shown in Table 1. This indirectly proves that WDM exhibited excellent CNF formability as compared to other fibrillation methods.

Evaluation of CNF Production from Waste Paper by Wet Disk Milling

Conventionally, CNF is mainly produced from lignocellulosic biomass, agricultural waste, softwood and hardwood. In order to produce CNF from these sources, pretreatment is needed to extract only cellulose and remove other impurities (Yasim-Anuar et al., 2019). In contrast to other sources as shown in Tables 1 and 2, pretreatment is unnecessary and can be skipped for waste paper as they are mainly composed of cellulose. Concerns regarding the ink contained in the waste paper may rise, however, the deinking process can be skipped if the targeted application does not involve direct contact with foods and humans, such as for the manufacturing of automotive compartment, building and construction materials. Regardless of having impurities, which mostly comes from ink, the CNF produced from waste paper is having similar characteristics with CNF produced from other sources and this was highly due to the effectiveness of WDM.

Table 1
Properties of CNF produced from different sources and nanofibrillation methods

Source of cellulose	Fibrillation methods and conditions	Findings	Ref.
OPMF-cellulose	*Method:* Electrospinning *Condition:* Voltage: 15kV - Concentration: 6% (w/v) - Solvent: ([EMIM]Cl), ([C10MIM][Cl]) and DMF	Diameter: 200 – 500 nm *Crl*: 56% $T_{d50\%}$: 254°C	Yasim-Anuar et al. (2017)
Sisal fibers *(Agave sisalana)*	*Method:* Ultrasonication Condition: Time: 2 h Power: 750 W Solution: Ethanol	Size: 50 nm *Crl*: 78.9% $T_{d50\%}$: -	Sosiati et al. (2017)
Tunicate, unbleached hardwood *(Eucalyptus grandis×E. ur ophylla)* and softwood *(Picea abies)*	*Pre-fibrillation:* Cellulose suspension was subjected to enzyme hydrolysis and TEMPO-oxidation *Method:* High-pressure homogenization: *Condition:* Pressure: 925 bar (1st pass) and 1600 (subsequent passes) Passes: 5	Diameter size: 10 – 70 nm *Crl*: - $T_{d50\%}$: 313.8°C	Zhao et al. (2017)
Oil palm empty fruit bunch (OPEFB)	*Method*: Wet grounded using Fritsch Pulverisette 7 nano-grinder *Condition*: Time: 30 min Speed: 722 rpm Concentration: 5% (w/v)	Diameter size: 10 – 100 nm *Crl*: 85.09% T_{max}: 350°C	Supian et al. (2020)
Waste paper	*Method:* Wet disk milling *Condition:* Cycles: 10 cycles Speed: 1800 rpm Concentration: 2% (w/v)	Diameter size: 20 – 40 nm *Crl*: 80 – 82% $T_{d50\%}$: 328 – 336ºC	This study

The utilization of waste paper and chemical-free nanofibrillation method (WDM) for CNF production was to promote the idea of using renewable and sustainable reinforcement material for polymer composites. The implication of the processing method on CNF production was evaluated according to the Principles of Green Chemistry (Anastas & Warner, 1998; Cinelli et al., 2017). Based on the overall evaluation, it was observed that by nanofibrillating waste paper using wet disk milling method was able to fulfill six criteria of the green chemistry principle. Among the criteria are, no waste generation, hazardless

Table 2
Pretreatment for extracting cellulose prior to nanofibrillation

Sources	Pretreatment	Nanofibrillation	Findings	Ref.
Henequen *(Agave fourcryodes)*	Dewaxed with a (3:1, v/v, toluene and ethanol) for 72h at 45°C, followed by KOH solution at room temperature for 8 h. Then, the fibers were treated with 3M HCl, followed by acid hydrolysis and bleaching with a mixture of $NaClO_2$ and glacial acetic acid (5:1) for 4 h at 50°C.	Homogenizing at 15,000 rpm for 4 h.	Diameter size: 51 – 103 nm *Crl* (%): - T_{max}: -	Fazeli et al. (2018)
Balsa tree	Bleached with a mixture of $NaClO_3$ and CH_3COOH solution at 70°C for 1 h. The process was repeated 3 times.	Grinding using ultra-fine friction grinder for 30 passes at 1500 rpm.	Diameter size: 1-100 nm *Crl* (%): - T_{max}: -	Kumode et al. (2017)
Oil palm mesocarp fiber	Treated with 5% (w/v) $NaClO_3$ solution at 70 °C for 90 min, followed by 6% (w/v) KOH solution at room temperature for 24 h.	Extruded at 100 rpm for 1h.	Diameter size: Less than 100 nm *Crl* (%): - T_{max}: -	Yasim-Anuar et al. (2019)
Waste paper	No pretreatment was carried out.	Wet disk milling at 1800 rpm for 10 cycles.	Diameter size: 20 – 40 nm *Crl* (%): 80 – 82% $T_{d50\%}$: 328 – 336ºC	This study

processing, chemicals and solvents-free process, use of renewable feedstocks as well as process effectiveness and safety level (Cinelli et al., 2017).

The 1st principle highlights on waste management. Under this principle, waste generation should be prevented as it may lead to costly waste treatment and environmental issues. Considering a continuous nanofibrillation process of cellulose suspension by WDM to produce CNF, waste generation can be prevented using this method. Principle number 3, 4 and 5 highlight on the hazardless, chemicals as well as the solvent-free process. The WDM is hazardless as it does not involve the use of chemicals along with the treatment. Hence, it is relatively safer for the operator and environment to adapt this technology to produce CNF. Other than that, this study also fulfills the requirement of the 7th principle. As one of the post-consumer wastes, waste paper has not been fully utilized for valuable bioproducts manufacturing despite made up of cellulose. The use of waste paper as a feedstock for this study proves that the high-value-added CNF can be produced from discarded materials. This study also meets the requirement of principle number 12, which stress on accident prevention. WDM is conducted at atmospheric pressure and involves no corrosive chemicals, hence it is safe to be operated. Based on the overall evaluation, WDM

can be considered as an alternative, safe and environmentally-friendly nanofibrillation treatment that can produce CNF effectively.

Characterization of Bionanocomposites Reinforced CNF

To evaluate the reinforcement effect of CNF produced in this study, the CNF was incorporated in PHBHHx by liquid assisted melt-blending method. The mechanical analysis revealed that CNF was able to improve the tensile strength and Young's modulus of PHBHHx/CNF bionanocomposites as shown in Table 3.

Table 3
Mechanical properties of PHBHHx reinforced CNF

	Tensile strength (MPa)	Young's modulus (MPa)
Neat PHBHHx	28.05 ± 1.27	2320.1 ± 97.81
PHBHHx/1% CNF	34.67 ± 1.68	2636.28 ± 93.18
PHBHHx/3% CNF	33.66 ± 1.68	2537.72 ± 87.06
PHBHHx/5% CNF	33.43 ± 1.30	2613.87 ± 93.03

It was observed that both tensile strength and Young's modulus increased up to 19 and 12%, respectively after 1 wt% CNF was incorporated in the PHBHHx. Thus, this proved that the incorporation of CNF significantly improved the mechanical properties as compared to the neat PHBHHx. In fact, it could be reached at a low reinforcement level. This proved that CNF and PHBHHx had good interfacial adhesion mainly due to their hydrophilicity properties. The adhesion of CNF and PHBHHx was influenced by hydrogen bond formed between CNF-matrix chain and eventually created a strong fiber-matrix adhesion, thus able to enhance the mechanical properties of biocomposites (Kargarzadeh et al., 2017). This was in accordance with other studies that also incorporated a low amount of CNF in polymers such as thermoplastic starch (Fazeli et al., 2018), polyethylene (Yano et al., 2018) and polyether block amide (Ziaei-tabari et al., 2017).

However, it was also noticeable that the values were slightly reduced when 3 and 5 wt% CNF were incorporated in the PHBHHx, but these were still higher than those of neat PHBHHx as a reference. This might be because of the agglomeration of CNF in the polymer matrix. According to Herrera et al. (2016), CNF tends to agglomerate during melt-processing, and as the filler content increased, the size of the agglomerates increases, thus broaden their distribution. This indirectly leads to poor mechanical properties of the composites. In fact, according to Mittal et al. (2018), reduction in mechanical properties starts to occur after reaching a threshold limit and this is mainly due to poor mechanical interlocking, which may degrade load transfer between fibers and matrix. Indirectly, this explains the reduction in mechanical properties for PHBHHx bionanocomposites composed of 3 and 5 wt% CNF.

CONCLUSION

The environmentally friendly WDM process was found to be able to nanofibrillate waste paper from micrometer range to 20 – 40 nm after 10 cycles of milling. It was also revealed that the obtained CNF was able to improve the tensile strength and Young's modulus of PHBHHx by 19 and 12%, respectively higher than the neat polymer. Overall, the utilization of waste paper-CNF as a reinforcement material for PHBHHx bionanocomposite is possible as evidenced in this study, without compromising the mechanical performance of the bionanocomposites produced. The CNF produced by WDM was also found to have low environmental impacts, thus able to promote sustainable and safe nanofibrillation processing.

ACKNOWLEDGEMENT

The authors would like to thank Kaneka Corporation Japan for supplying Poly((R)-3-hydroxybutyrate-co-(R)-3-hydroxyhexanoate (P(HB-co-11%-HHx)), and the Ministry of Higher Education (MOHE), Malaysia through Fundamental Research Grant Scheme (Grant Number: FRGS/1/2019/TK05/UPM/02/1) for the research funding.

REFERENCES

Abraham, E., Deepa, B., Pothen, L. A., Cintil, J., Thomas, S., John, M. J., … & Narine, S. S. (2013). Environmental friendly method for the extraction of coir fibre and isolation of nanofibre. *Carbohydrate Polymers*, *92*(2), 1477–1483. doi:10.1016/j.carbpol.2012.10.056

Anastas, P. T., & Warner, J. C. (1998). *Green chemistry: Theory and practice*. New York, USA: Oxford University Press.

Arévalo, R., & Peijs, T. (2016). Binderless all-cellulose fibreboard from microfibrillated lignocellulosic natural fibres. *Composites Part A: Applied Science and Manufacturing*, *83*, 38–46. doi:10.1016/j.compositesa.2015.11.027

Buntinx, M., Vandewijngaarden, J., Peeters, R., Yperman, J., & Carleer, R. (2017, May 9-12). Modified poly(3-hydroxybutyrate-co-3-hydroxyhexanoate) with interesting properties for food packaging applications. In *28th IAPRI World Symposium on Packaging 2017* (pp. 20-21). Lausanne, Switzerland.

Cinelli, M., Coles, S. R., Nadagouda, M. N., Błaszczyński, J., Słowiński, R., Varma, R. S., & Kirwan, K. (2017). Robustness analysis of a green chemistry-based model for the classification of silver nanoparticles synthesis processes. *Journal of Cleaner Production*, *162*, 938–948. doi:10.1016/j.jclepro.2017.06.113

Dubey, R., Toh, Y., & Yeh, A. (2018). Enhancing cellulose functionalities by size reduction using media-mill. *Scientific Reports*, *8*(1), 1–11. doi:10.1038/s41598-018-29777-w

Fazeli, M., Keley, M., & Biazar, E. (2018). Preparation and characterization of starch-based composite films reinforced by cellulose nanofibers. *International Journal of Biological Macromolecules*, *116*, 272–280. doi:10.1016/j.ijbiomac.2018.04.186

Gao, K., Shao, Z., Wu, X., Wang, X., Li, J., Zhang, Y., … & Wang, F. (2013). Cellulose nanofibers/reduced graphene oxide flexible transparent conductive paper. *Carbohydrate Polymers*, *97*(1), 243–251. doi:10.1016/j.carbpol.2013.03.067

Herrera, N., Salaberria, A. M., Mathew, A. P., & Oksman, K. (2016). Plasticized polylactic acid nanocomposite films with cellulose and chitin nanocrystals prepared using extrusion and compression molding with two cooling rates: Effects on mechanical, thermal and optical properties. *Composites Part A: Applied Science and Manufacturing*, *83*, 89–97. doi:10.1016/j.compositesa.2015.05.024

Hietala, M., Varrio, K., Berglund, L., Soini, J., & Oksman, K. (2018). Potential of municipal solid waste paper as raw material for production of cellulose nanofibres. *Waste Management*, *80*, 319–326. doi:10.1016/j.wasman.2018.09.033

Jang, J.-H., Lee, S.-H., Endo, T., & Kim, N.-H. (2015). Dimension change in microfibrillated cellulose from different cellulose sources by wet disk milling and its effect on the properties of PVA nanocomposite. *Wood Science and Technology*, *49*(3), 495–506. doi:10.1007/s00226-015-0703-2

Jereme, I. A., Siwar, C., Begum, R. A., Talib, B. A., & Alam, M. M. (2015). Assesing problems and prospects of solid waste management in Malaysia. *Journal of Social Sciences and Humanities*, *10*(2), 70–87. doi:10.31235/osf.io/2csqj

Jing, L. (2012). *Development of poly(3-hydroxybutyrate-co-3-hydroxyhexanoate)/polycaprolactone blend*. (Unpublished master thesis). National University of Singapore, Singapore.

Kargarzadeh, H., Mariano, M., Huang, J., Lin, N., Ahmad, I., Dufresne, A., & Thomas, S. (2017). Recent developments on nanocellulose reinforced polymer nanocomposites: A review. *Polymer, 132*, 368–393. doi:10.1016/j.polymer.2017.09.043

Kumode, M. M. N., Bolzon, G. I. M., Magalhães, W. L. E., & Kestur, S. G. (2017). Microfibrillated nanocellulose from balsa tree as potential reinforcement in the preparation of 'green' composites with castor seed cake. *Journal of Cleaner Production*, *149*, 1157–1163. doi:10.1016/j.jclepro.2017.02.083

Lin, N., & Dufresne, A. (2014). Nanocellulose in biomedicine: Current status and future prospect. *European Polymer Journal*, *59*, 302–325. doi:10.1016/j.eurpolymj.2014.07.025

Mittal, G., Rhee, K. Y., Mišković-Stanković, V., & Hui, D. (2018). Reinforcements in multi-scale polymer composites: Processing, properties, and applications. *Composites Part B: Engineering*, *138*(October), 122–139. doi:10.1016/j.compositesb.2017.11.028

Norrrahim, M. N. F. (2018). *Superheated steam pretreatment of oil palm biomass for improving nanofibrillation of cellulose and performance of polypropylene / cellulose nanofiber composites*. (Unpublished Doctoral thesis). Universiti Putra Malaysia, Selangor.

Norrrahim, M. N. F., Ariffin, H., Yasim-Anuar, T. A. T., Ghaemi, F., Hassan, M. A., Ibrahim, N. A., … & Yunus, W. M. Z. W. (2018). Superheated steam pretreatment of cellulose affects its electrospinnability for microfibrillated cellulose production. *Cellulose*, *25*(7), 3853-3859. doi:10.1007/s10570-018-1859-3

Prakash Menon, M., Selvakumar, R., Suresh kumar, P., & Ramakrishna, S. (2017). Extraction and modification of cellulose nanofibers derived from biomass for environmental application. *RSC Advances, 7*(68), 42750–42773. doi:10.1039/c7ra06713e

Sosiati, H., Wijayanti, D. A., Triyana, K., & Kamiel, B. (2017). Morphology and crystallinity of sisal nanocellulose after sonication. *AIP Conference Proceedings*, *1877*, 1-7. doi:10.1063/1.4999859

Sreekala, M. S., Kumaran, M. G., & Thomas, S. (1997). Oil palm fibers: Morphology, chemical composition, surface modification, and mechanical properties. *Journal of Applied Polymer Science*, *66*(5), 821–835. doi:10.1002/(sici)1097-4628(19971031)66:5<821::aid-app2>3.0.co;2-x

Supian, M. A. F., Amin, K. N. M., Jamari, S. S., & Mohamad, S. (2020). Production of cellulose nanofiber (CNF) from empty fruit bunch (EFB) via mechanical method. *Journal of Environmental Chemical Engineering*, *8*(1), 1-5. doi:10.1016/j.jece.2019.103024

Tibolla, H., Pelissari, F. M., & Menegalli, F. C. (2014). Cellulose nanofibers produced from banana peel by chemical and enzymatic treatment. *LWT - Food Science and Technology*, *59*(2), 1311–1318. doi:10.1016/j.lwt.2014.04.011

Wang Y., Wang G., Cheng H., Tian G., Liu Z., Xiao Q. F., … Gao X. (2010). Structures of bamboo fiber for textiles. *Textile Research Journal, 80*(4), 334–343. doi:10.1177/0040517509337633

Xu, P., Feng, Y., Ma, P., Chen, Y., Dong, W., & Chen, M. (2017). Crystallization behaviours of bacterially synthesized poly(hydroxyalkanoate)s in the presence of oxalamide compounds with different configurations. *International Journal of Biological Macromolecules, 104*, 624–630. doi:10.1016/j.ijbiomac.2017.06.001

Yano, H., Omura, H., Honma, Y., Okumura, H., Sano, H., & Nakatsubo, F. (2018). Designing cellulose nanofiber surface for high density polyethylene reinforcement. *Cellulose*, *25*(6), 3351–3362. doi:10.1007/s10570-018-1787-2

Yasim-Anuar, T. A. T., Ariffin, H., & Hassan, M. A. (2018). Characterization of cellulose nanofiber from oil palm mesocarp fiber produced by ultrasonication. *Material Science and Engineering*, *368*(1), 1–11. doi:10.1088/1757-899x/368/1/012033

Yasim-Anuar, Tengku Arisyah Tengku, Ariffin, H., Norrrahim, M. N. F., & Hassan, M. A. (2017). Factors affecting spinnability of oil palm mesocarp fiber cellulose solution for the production of microfiber. *BioResources*, *12*(1), 715–734. doi:10.15376/biores.12.1.715-734

Yasim-Anuar, Tengku Arisyah Tengku, Ariffin, H., Norrrahim, M. N. F., Hassan, M. A., Tsukegi, T., & Nishida, H. (2019). Sustainable one-pot process for the production of cellulose nanofiber and polyethylene / cellulose nanofiber composites. *Journal of Cleaner Production*, *207*, 590–599. doi:10.1016/j.jclepro.2018.09.266

Zakaria, M. R., Norrrahim, M. N. F., Hirata, S., & Hassan, M. A. (2015). Hydrothermal and wet disk milling pretreatment for high conversion of biosugars from oil palm mesocarp fiber. *Bioresource Technology*, *181*, 263–269. doi:10.1016/j.biortech.2015.01.072

Zhao, Y., Moser, C., Lindström, M. E., Henriksson, G., & Li, J. (2017). Cellulose nanofibers from softwood, hardwood, and tunicate: Preparation-structure-film performance interrelation. *ACS Applied Materials and Interfaces*, *9*(15), 13508–13519. doi:10.1021/acsami.7b01738

Ziaei-tabari, H., Khademieslam, H., Bazyar, B., Nourbakhsh, A., & Hemmasi, A. H. (2017). Preparation of cellulose nanofibers reinforced polyether-b-amide nanocomposite. *BioResources, 12*(3), 4972–4985. doi:10.15376/biores.12.3.4972-4985

Pertanika J. Sci. & Technol. 28 (S2): 273 - 286 (2020)

PERTANIKA JOURNALS

SCIENCE & TECHNOLOGY

Journal homepage: http://www.pertanika.upm.edu.my/

Nutritional Characteristics of Biochar from Pineapple Leaf Residue and Sago Waste

Norshidawatie Bohari[1,2], Hasmah Mohidin[1,2]*, Juferi Idris[3,4], Yoshito Andou[5], Sulaiman Man[1,2], Hushairy Saidan[3] and Suraiya Mahdian[1,6]

[1]Faculty of Plantation and Agrotechnology, Universiti Teknologi MARA (UiTM), Melaka Branch, Jasin Campus, 77300 Merlimau, Melaka, Malaysia
[2]Faculty of Plantation and Agrotechnology, Universiti Teknologi MARA (UiTM), Sarawak Branch, Samarahan Campus, 94300 Kota Samarahan, Sarawak, Malaysia
[3]Faculty of Chemical Engineering, Universiti Teknologi MARA (UiTM), Sarawak Branch, Samarahan Campus, 94300 Kota Samarahan, Sarawak, Malaysia
[4]Faculty of Chemical Engineering, Universiti Teknologi MARA (UiTM), 40450 Shah Alam, Selangor, Malaysia
[5]Graduate School of Life Science and System Engineering, Kyushu Institute of Technology, Kitakyushu, Fukuoka, Japan
[6]Faculty of Plantation and Agrotechnology, Universiti Teknologi MARA (UiTM), Sarawak Branch, Mukah Campus, 77300 Mukah, Sarawak, Malaysia

ABSTRACT

Biochar produced from biomass with high nutrient content is essential for improving the quality of agricultural soils. An abundance of biomass is converted into biochar with high nutrient content, but studies on the conversion of pineapple and sago waste into biochar are still limited. This research aimed to produce biochar from pineapple leaf (PLB), sago bark (SBB), and sago pith (SPB) through the carbonization process with low temperature. The samples were carbonized using a laboratory electric oven at a low temperature of 350°C. The raw biomass and biochar produced were then subjected to elemental analysis and characterization. The mineral contents of carbonized biochar such as K, N, S, Mg, and Ca increased from those of the feedstock concentrations. For PLP, K element increased 24-fold from 2.44 ± 0.73% to 48.32 ± 9.92%, while N element increased from 6.13 ± 2.39% to 8.33 ± 5.34%. However, for both SBB and SPB, N and K nutrients increased by 2-fold. The

ARTICLE INFO

Article history:
Received: 10 February 2020
Accepted: 13 November 2020
Published: 31 December 2020

DOI: https://doi.org/10.47836/pjst.28.S2.21

E-mail addresses:
norshidawatie1994@gmail.com (Norshidawatie Bohari)
hasmah@uitm.edu.my (Hasmah Mohidin)
juferi@uitm.edu.my (Juferi Idris)
yando@life.kyutech.ac.jp (Yoshito Andou)
sman@uitm.edu.my (Sulaiman Man)
hushairy@uitm.edu.my (Hushairy Saidan)
suraiya6551@uitm.edu.my (Suraiya Mahdian)
* Corresponding author

ISSN: 0128-7680
e-ISSN: 2231-8526

© Universiti Putra Malaysia Press

study reveals that pineapple leaf biochar has the potentials to be used as an alternative soil amendment to elevate soil nutrient and quality.

Keywords: Biochar, low carbonization, pineapple leaf, sago bark, sago pith residue

INTRODUCTION

With the growing in agriculture sector, the amount of agro-waste generated annually has also been increasing. Agamuthu (2009) stated that about 998 million tons of crop residues, including biomass wastes and crop fibre residues, were produced yearly, and Asia is the main contributor. Malaysia recorded more than 70 million tons of crop residues annually (Chong et al., 2014). Agricultural wastes fibers such as sago wastes and pineapple residues have contributed to a massive landfill problem and solid pollutants to the environment after harvesting. In Sarawak, sago palm (*Metroxylon sagu.* Rottb.) is a new emerging plantation crop, with about 43,326 hectares of sago crop are grown in large scale in Mukah (Naim et al., 2016). Their findings indicated that the highest contributor of sago wastes were residues from sago pith residues (SPW) and sago bark wastes (SBW). According to another study conducted by Chong et al. (2014), approximately 90% of the sago starch is produced in Sarawak, and sago bark is an abundant waste product from sago starch extraction.

Pineapple (*Ananas comosus)* is a highly nutritive, non-seasonal tropic fruit with a fine flavor. In Malaysia, pineapple is the top five fruits with the most promising demand in the local and export markets (Nazri & Pebrian, 2017). In Sarawak, pineapple production has increased by 70% from 17 metric tonnes per hectare in 2014 to 29 metric tonnes per hectare (Edward, 2016). Sarawak is targeting 2,500 hectares by 2020, with an average production of 45 metric tons per hectare. Pineapple leaf fibre (PLF) is one of the abundantly available waste materials in Malaysia and has not been studied as required. According to Asim et al. (2015), PLF is one of the waste materials in the agriculture sector, which is widely grown in Malaysia as well as Asia. Commercially pineapple fruits are very important and leaves are considered as organic waste materials that are left behind after fruit harvesting, which is being used for producing natural fibres. The chemical composition of PLF constitutes holocellulose (70%–82%), lignin (5%–12%), and ash (1.1%). In Malaysia, waste management of these leaves is improving time to time, whereby the leaves are collected and consigned for research and industry utilization (Padzil et al., 2020).

Pineapple residues can be categorized as a contributor to wastes because they consist of pulp, peels, stem, and leaves (Nunes et al., 2009). If these crop residues are not handled with proper disposal, it may result in bad environmental effect where the residues might inhibit the drainage system after disposal. In addition, the cost of disposal is expensive due to high transportation cost and restricted landfill for disposal activity (Upadhyay et al., 2010).

Biochar is a carbon-rich product produced from the slow thermochemical pyrolysis of biomass materials from organic wastes such as crop residues, livestock manure, sewage sludge, and composts and then applied to soils as an amendment. Interest in biochars has recently been driven by two major global issues: climate change and the realization of the need for sustainable soil management. Biochar can be described as carbonized product after pyrolysis process which can be obtained from residues or plant biomass which highly improves soil properties and increases crop growth and soil fertility. Fu et al. (2016) indicated that the increase of pyrolysis temperature increased pH, electrical conductivity (EC), and carbon (C) content of pineapple biochar. This proves that biochar has the potential as an additive agent to increase nutrient content and enhance its properties. Lehmann (2007) stated that all organic material added to the soil would give significant effect in increasing soil functions variety, including retention (ability to reserve nutrients) for plant growth. However, biochar holds nutrients more effectively, so there are more available nutrients compared to leaf, compost, and manure fertilizer. Biochar application into soil has the potential of increasing the C content, water and nutrient retention in soil (Mawardiana et al., 2013).

Due to high cellulose and lignin contents in sago bark and pineapple waste but with low commercial values, their disposal is a problem to the mills due to their large quantity. However, a few research work has been done on the conversion of these underutilized agrowastes such as pineapple waste and sago waste into biochar as an alternative soil amendment. Thus, the aim of this study is to evaluate the potential of nutrients produced by biochar from pineapple leaf, sago bark and sago pith as organic feedstocks under controlled carbonization to elevate soil nutritional status and soil quality.

MATERIALS AND METHODS

Sample Preparation

Raw PL biomass was obtained from pineapple smallholders in Kampung Melayu, Samarahan meanwhile SB and SP biomass were purchased from Sago Mill in Mukah, Sarawak. The raw biomass was washed and oven dried at 105°C until constant weight. Then it was crushed into fine powder and ground into a size of about 2 mm using a heavy-duty grinder (Claoston et al., 2014).

Carbonization Preparation

Biochar production was performed according to Leng et al. (2011). Samples were placed into ceramic crucibles with fitting lids and carbonized at 350°C for 2 h in a large chamber muffle furnace (Type 62700; Thermo Scientific Barnstead/Thermolyne, USA). All biochars were then ground to pass a 1-mm sieve and kept at room temperature prior to analysis. The yield of biochar was calculated as follows:

$$\text{Biochar yield (\%)} = \frac{Mass\ of\ biochar\ (g)}{Mass\ of\ raw\ material\ after\ oven\ dry\ (g)} \times 100\%$$

Analytical Methods

Elemental analysis was carried out based on Idris et al. (2014). The main elements obtained from raw PL, SB and SP biomass, and PL, SB, and SP biochar samples were analyzed using an inductive coupled plasma–optical effluent spectrophotometer (ICP–AES, model: Perkin Elmer 2100). Approximately 1–2 g of sample was first placed in the furnace and the temperature was gradually increased to 300°C until smoke ceased and was subsequently raised to 500°C. The process continued at this temperature until white or greyish-white ash was obtained. The sample was then digested using concentrated hydrochloric acid (37% v/v) and nitric acid (20% v/v). pH analysis was measured using an Oakton pH 700 Benchtop Meter (Barwant et al., 2018). For Electrical Conductivity (EC) measurement, the samples was soaked with deionized water. The ratio used was 1:5 of solid/water and agitated for 24 h. The EC was measured and recorded using a CON 700 EC meter (Eutech Instruments, USA). For the FTIR (Fourier-transform Infrared Spectroscopy) analyses, 10 mg of the biochar was mixed with 190 mg of spectroscopic-grade KBr; the mixture was first hand ground and then ground in a Wig-L-bug using a stainless steel vial with a stainless steel ball pestle for 30 s. The FTIR measurements were performed with an ATR-ThermoFisher Nicolet iS5 FTIR spectrometer. The scans were carried out in the range from 4000 to 650 cm^{-1} with a resolution of 4 cm^{-1} and 64 scans per sample. Thermogravimetric analysis (TGA) was performed using a thermogravimetric analyzer (Mettler Toledo) under air atmosphere at a heating rate of 10°C/min from ambient temperature to 600°C. A sample mass of 3.5 ± 0.5 mg was used for each analysis and the mean values were used provided that the deviations were within 5 %. The mass loss (TG) of the samples was represented as a function of temperature. Surface morphologies of raw and biochar of SB, SP, and PL were identified by SEM (JCM-6000, JEOL, Japan). The samples were prepared by coating with carbon at the outer layer of the sample, and then elemental components were observed under microscopy detection. X-ray diffraction (WAXD) analysis was performed using an X-ray diffractometer (MiniFlex 600, Rigaku Co., Japan) at 40 kV and 15 mA at room temperature. The X-ray initiator used was Cu Kα radiation (λ = 1.54 Å). The diffraction angle was examined from 5° to 60° at a rate of 10°/min.

RESULTS AND DISCUSSION

Characteristic of Biomass

The results for the elemental analysis of pineapple leaf, sago bark, and sago pith for raw biomass are shown in Table 1. The basic elements, namely, primary macronutrients (N, P,

and K) and the secondary micronutrients (Ca, Mg, and S) of the raw incinerated pineapple leaves were adequate and can support the initiation of any plant growth.

Table 1
Elemental compositions of raw biomass

Element	Composition (%)		
	Pineapple leaf	Sago bark	Sago pith residue
C	48.4 ± 0.27	49.73 ± 5.31	49.67 ± 6.58
N	6.13 ± 2.39	4.43 ± 3.65	3.38 ± 1.62
O	41.77 ± 2.29	41.96 ± 6.19	45.92 ± 7.63
Mg	0.56 ± 0.18	0.23 ± 0.23	0.24 ± 0.13
P	0.44 ± 0.22	0.11 ± 0.24	0.14 ± 0.08
S	0.14 ± 0.03	0.24 ± 0.11	0.03 ± 0.04
K	2.44 ± 0.73	2.27 ± 1.21	0.20 ± 0.16
Ca	0.12 ± 0.14	1.03 ± 0.23	0.42 ± 0.28

N no of repetition 30

It was observed that the raw PL and SB had high K content compared to SP. This result might be due to the naturally high K in pineapple leaves.

Pineapple waste is one type of organic material containing a high C/N ratio (50%–70%). Materials that have high C/N give a greater influence to change the soil physical properties (Ridwan et al., 2018). According to Hunt et al. (2010), by converting biomass into biochar, many of its carbon content would become fixed into a more stable form. The exothermic process during the biochar production via pyrolysis precipitated carbon dioxide onto the biochar surfaces (Lehmann, 2007).

Comparing the results in Tables 1 and 2, for PLP, K element increased of 24-fold from 2.44 ± 0.73% to 48.32 ± 9.92%, while N element increased from 6.13 ± 2.39% to 8.33 ± 5.34%. However, for both SBB and SPB, N and K elements increased 2-fold. The highest yield of biochar was 52.00% (SBB), followed by 51.43% (PLB), and 46.48% (SPB). After carbonization at 350°C, the differences in yield between all of them were small and insignificant comparatively. This indicates that although with low energy consumption through the oven-drying electrical source, the overall yield values were still acceptable.

It was observed that the C content in SBB and SPB increased but otherwise for PLB (Table 2) after carbonization. As pyrolysis occurred, the oxygen content of all the biomass decreased. However, the elements of K, Mg, and S increased in PLB and SPB compared to those in SBB. Due to the carbonization at 350°C, the weight loss and volatile content disappeared. Hence, the nutrient content in biochar accumulated and increased after carbonization. This result is supported by Idris et al. (2014) where the utilization of biochar improved the soil fertility and reduced the use of chemical fertilizers compared

Table 2
Characteristic of elemental composition on biochar

Properties	Pineapple leaf	Sago bark	Sago pith residue
Yield (%)	51.43	52.00	46.48
pH	8.78	8.59	7.93
EC (mS cm^{-1})	7.38	5.43	4.26
Elemental analysis		**Composition (%)**	
C	19.37 ± 2.03	51.36 ± 3.58	61.66 ± 9.17
N	8.33 ± 5.34	10.65 ± 2.07	6.18 ± 5.41
O	21.95 ± 5.92	33.24 ± 0.63	28.06 ± 7.83
Mg	1.27 ± 0.93	0.16 ± 0.15	0.40 ± 0.29
P	0.39 ± 0.05	0.07 ± 0.07	0.18 ± 0.17
S	0.32 ± 0.14	0.07 ± 0.09	0.05 ± 0.06
K	48.32 ± 9.92	4.01 ± 3.22	0.48 ± 0.11
Ca	0.05 ± 6.33	0.44 ± 0.19	2.99 ± 1.68

to raw biomass for the same purpose with high mineral and low heavy metal contents. In addition, biochar from biomass can be used to prevent erosion and maintain soil moisture while reducing pollution to the environment (Lim & Zaharah, 2000).

Generally, PLB, SBB, and SPB show high pH values. The pH of pineapple leaf biochar was slightly higher (>8) compared to sago bark and sago pith residue biochar (Table 2). The high pH indicates that biochars are good soil liming materials. This finding is in agreement with that of Leng et al. (2017). The property of EC indicates a slightly higher salinity in PLB compared to those in SBB and SPB. Furthermore, higher mineral ash in biochar probably has higher electrical conductivity especially those that have high K^+ ion content as in PLB, due to the mobility of the K^+ ions (Joseph et al., 2007). As PL biochar is rich in minerals, it may be better suited as an alternative organic fertilizer and can acts as a potential soil amendment. Interestingly, among the macronutrients presence, the K content in PL biochar increased tremendously by 20-fold while the K contents in SB and SP biochar increased only 2-fold. High concentrations of potassium (K) and nitrogen (N) could probably be due to the usage of fertilizers which contain potassium nitrate (KNO_3) in the commercial pineapple cultivation. Meanwhile, sago palm is mainly in its natural state condition and often left unfertilized in the mangrove swamp areas. However, there is no clear pattern for the P element in this study. Besides, the concentration of nutrients in the biochar also depends on the process of partial defractionation and/or devolatilization of these nutrients at elevated temperatures (Claoston et al., 2014; Hossain et al., 2011).

Fourier Transform Infrared Spectroscopy (FTIR)

Two weak peaks were observed at 2840–3000 cm^{-1} for PLB due to the C–H stretching from aliphatic groups (Figure 1). The C–H stretching of SBB and SPB between 2840–3000

cm^{-1} reveals the existence of alkane groups and this finding is supported by the findings by Claoston et al. (2014) (Figures 2 and 3). The stretching vibration of the C=C group (1566–1650 cm^{-1}) was identified in the spectrum of PLB which shows the existence of cyclic alkene.

The existence of conjugated aldehyde in SBB and SPB was observed where the peak showed the C=O stretching (1685–1710 cm^{-1}). According to the FTIR spectra analysis, all the biochars exhibited the existence of the C–H stretching, aromatic C=C stretching, and C=O stretching. This observation indicates that biochar began to carbonize as the temperature increased during carbonization, which suggests degradation and depolymerization of cellulose, hemicelluloses and lignin (Cantrell et al., 2012). Table 3 shows the vibration characteristics and compound class for each wavenumber. Overall, based on the FTIR spectra for biochar, carbonization at lower temperatures resulted in dehydration, beginning of bond breakage, and transformational products (Cantrell et al., 2012).

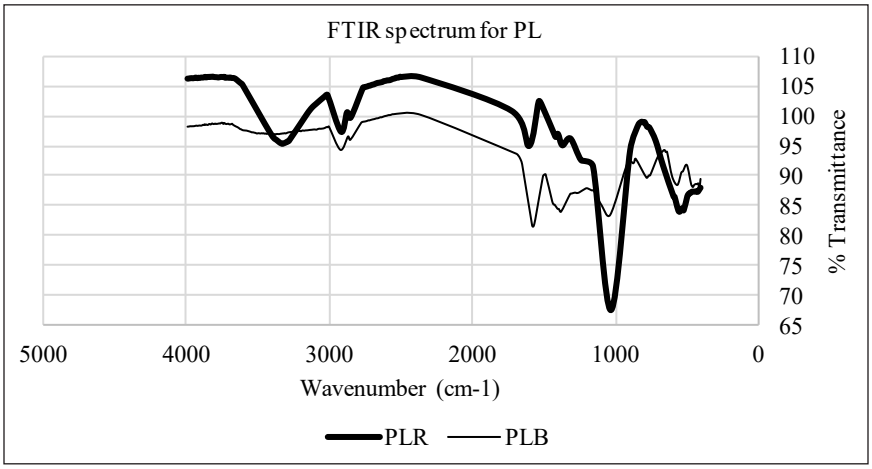

Figure 1. FTIR spectra of raw pineapple leaf (PLR) and biochar (PLB)

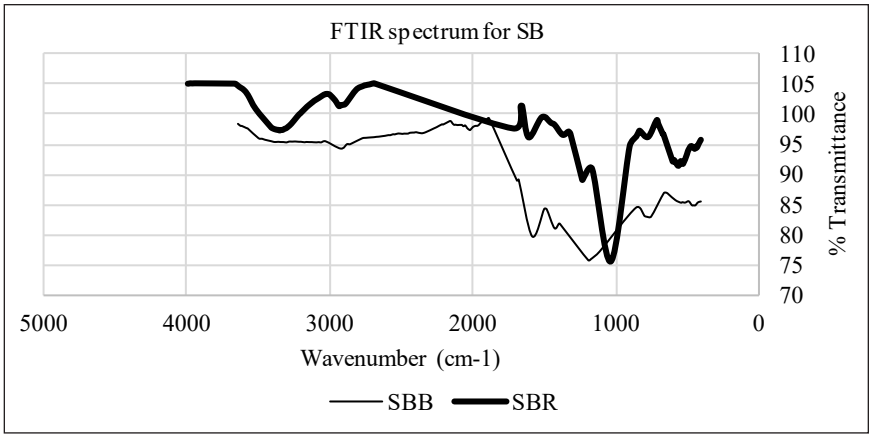

Figure 2. FTIR spectra of raw sago bark (SBR) and biochar (SBB)

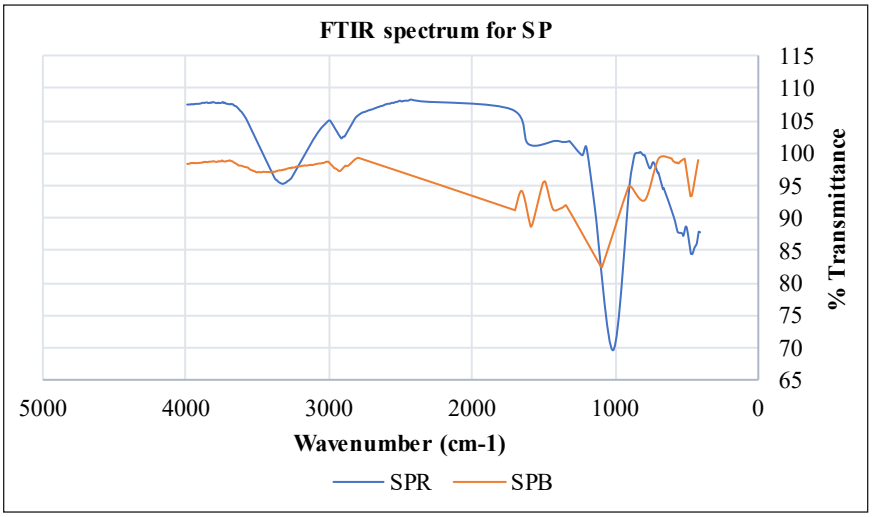

Figure 3. FTIR spectra of raw sago pith (SPR) and biochar (SPB)

Table 3
FTIR spectra of pineapple leaves and sago waste biochar

Wavenumber (cm^{-1})	Pineapple leaf	Sago bark	Sago pith	Vibration characteristics	Compound class
3000–2840	+	+	+	C-H stretching	Alkane
1710–1685	-	+	+	C=O stretching	Conjugated aldehyde
1650–1566	+	-	-	C=C stretching	Cyclic alkene
1450–1390	-	+	+	C–H bending	Methyl group
1385–1380	+	-	-	C–H bending	Gem dimethyl
1250–1020	+	-	-	C–N stretching	Amine
1205–1124	-	+	-	C–O stretching	Tertiary alcohol
1124–1087	-	-	+	C–O stretching	Secondary alcohol

In this analysis, all biochar samples showed a similar thermal degradation where SPB was clearly degraded below PLB and SBB. At 10% degradation, each sample degraded at different temperatures of 374.10, 378.27, and 364.10°C for PLB, SBB, and SPP, respectively (Figure 4). The result shows that SPB was easily degraded due to its characteristics where the samples lost its proportion with the increasing degradation temperature.

Scanning Electron Microscopy/Energy Dispersive X-Ray Analyzer (SEM/EDX)

The result shows that the SEM images have a large amount of pores. The pore structure of PLR was well defined and smaller compared to that of PLB (Figure 5). After carbonization, the biochar produced was observed to have large pores size exposing a variety of pore shapes and became cracked. The structure seemed to be fragile due to its thin walls and

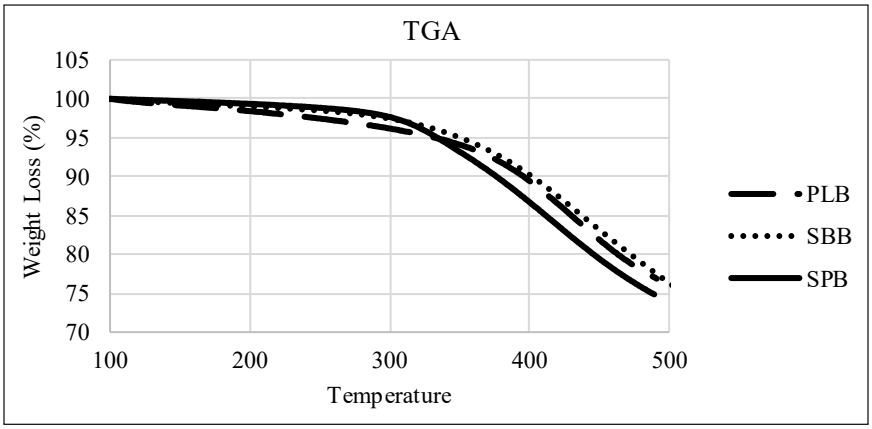

Figure 4. Thermal analysis of the biochars obtained from pineapple leaf (PLB), sago bark (SBB), and sago pith (SPB)

easily broke during pyrolysis. The surface of SBR was rough with smaller pores. After carbonization, many well-defined and softened pores were produced with large pores structure (Figure 6). This might be caused by the evolution of volatile organic compounds. Wahi et al. (2015) stated that devolatilization during pyrolysis might contribute to low denseness, improved pores formation of biochar, and higher porosities. In general, the increase in surface area at a high pyrolysis temperature is due to the removal of volatile material resulting in increased micropore volume (Ahmad et al., 2012).

Based on the outer appearance of SPR (Figure 7), the surface was smooth with many pores. After pyrolysis, biochar produced was observed to have a large pore size. This

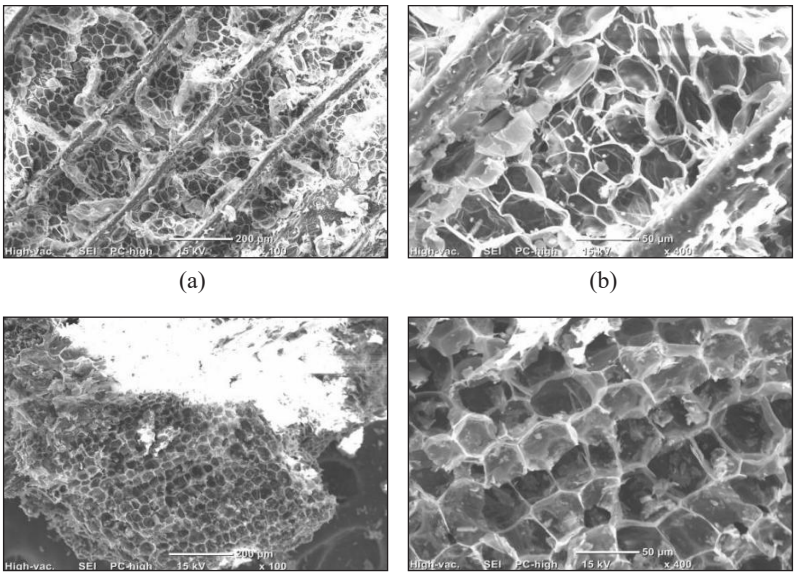

Figure 5. SEM images of raw pineapple leaf, PLR (a–b) and pineapple leaf biochar, PLB (c–d)

indicates that the pyrolysis process was fully utilized to form porous structure of biochar (Claoston et al., 2014). Zakaria et al. (2019) stated that the pores produced could be due to the degradation of organic materials.

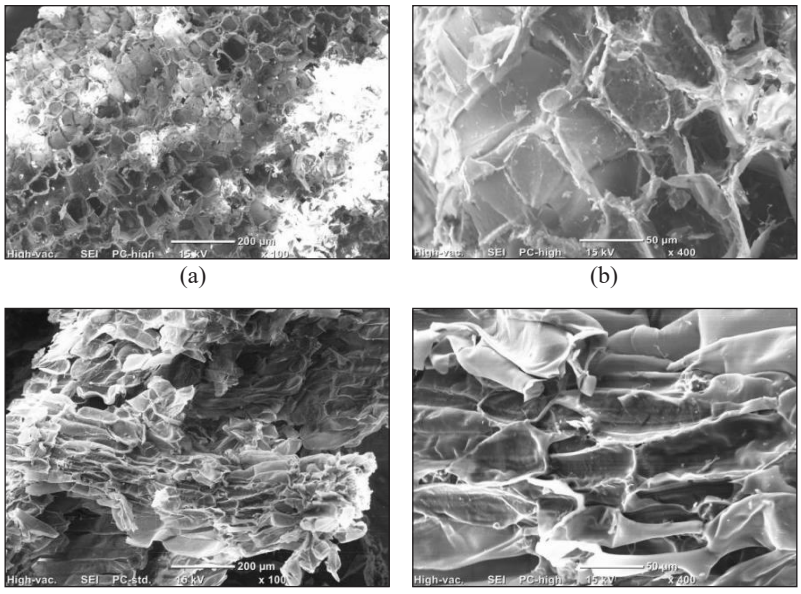

Figure 6. SEM images of raw sago pith, SPR (a–b) and sago pith biochar, SPB (c–d)

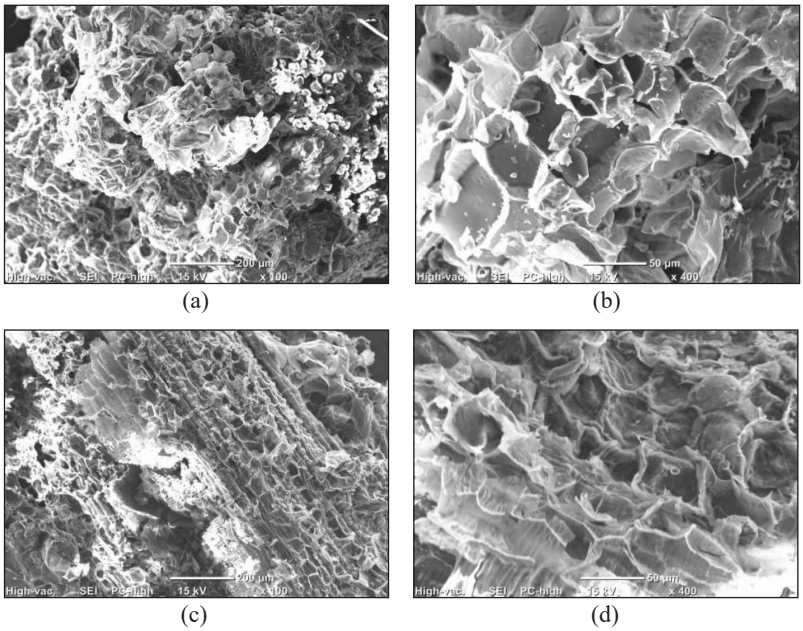

Figure 7. SEM image of raw sago pith, SPR (a-b) and sago pith biochar, SPB (c-d)

X-Ray Diffraction (XRD)

The XRD shape of raw material is demonstrated in Figure 8. The diffractograms of SBR and PLR showed one reflection, corresponding to 2θ values of 22.06° and 22.28°, respectively. Meanwhile, SPR showed two reflections, corresponding to 2θ values of 17.52° and 22.52°. The narrower peaks of raw indicate the presence of cellulose structure (Shaaban et al., 2013).

Decreasing peaks at 2θ values of 21.92°, 21.32°, and 21.54° were observed for SBB, SPB, and PLB, respectively (refer to Figure 9). It might be due to the decomposition of cellulose element. According to Shaaban et al. (2013), the increasing temperature during pyrolysis may cause the peaks of stipulated angles disappear, and cellulose starts to decompose.

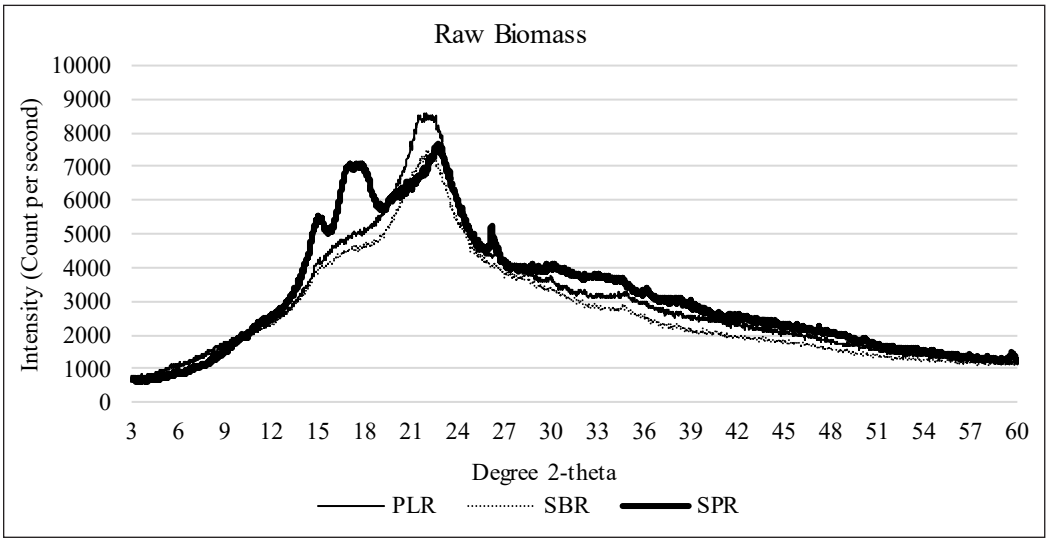

Figure 8. XRD patterns of raw pineapple leaf (PLR), sago bark (SBR), and sago pith (SPR)

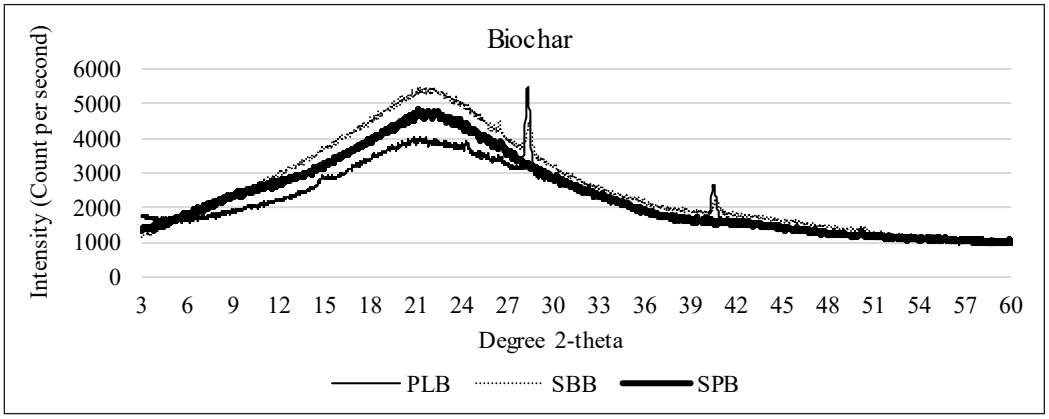

Figure 9. XRD patterns of pineapple leaf (PLB), sago bark (SBB), and sago pith (SPB) biochar

The elemental analysis showed the highest nutrient content in PLB compared to SBB and SPB. PLB has the highest nutrient content of Mg, S, and K. SEM micrographs indicate the best development of pores in PLB compared to those in SBB and SPB, and the results are comparable with other studies. The plant growth in terms of root growth and photosynthesis capacity requires high macronutrients. It can be concluded that the pineapple leaf biochar can be the most suitable additive to be applied to the soil to elevate soil nutritional status and quality.

CONCLUSION

The production of biochar from underutilized pineapple leaf and sago waste was successfully determined using simple carbonization at low temperature. This study showed all minerals (i.e., P, K, Mg, Ca) increased from their initial concentrations in the feedstock. The minerals contents in carbonized biochar such as K, N, S, Mg, and Ca also increased. For PLP, K element increased 24-fold from 2.44 ± 0.73% to 48.32 ± 9.92%, while N element increased from 6.13 ± 2.39% to 8.33 ± 5.34%. However, for SBB and SPB, N and K nutrients only increased 2-fold. SEM micrographs indicate the best development of pores in PLB compared to those in SBB and SPB, and the results are comparable with other studies. The overall results on biochar obtained from pineapple leaves, sago bark, and sago pith residues, indicate the potential of inherent nutrient content in PLB, SBB and SPB to be used as an alternative soil amendment. However, future work needs to be done to quantify the essential nutrients generated to make further recommendations. This study showed that the underutilized pineapple leaf biochar could potentially be used as an alternative to elevate soil nutritional status and to mitigate environmental problems.

ACKNOWLEDGEMENT

The authors are grateful to Universiti Teknologi MARA, Malaysia, UiTM Sarawak Branch, Samarahan Campus, UiTM Melaka Branch, Jasin Campus, and Kyushu Institute of Technology, Japan for the financial and technical support in this study.

REFERENCES

Agamuthu, P., (2009). *Challenges and opportunities in agro-waste management: An Asian perspective.* Retrieved September 20, 2018, from http://www.env.go.jp/recycle/3r/en/forum_asia/results/pdf/20091111/08.pdf

Ahmad, M., Lee, S. S., Dou, X., Mohan, D., Sung, J. K., Yang, J. E., & Ok, Y. S. (2012). Effects of pyrolysis temperature on soybean stover-and peanut shell-derived biochar properties and TCE adsorption in water. *Bioresource Technology, 118*, 536-544. doi:10.1016/j.biortech.2012.05.042

Asim, M., Abdan, K., Jawaid, M., Nasir, M., Dashtizadeh, Z., Ishak, M. R., & Hoque, M. E. (2015). A review on pineapple leaves fibre and its composites. *International Journal of Polymer Science, 2015* 1–16. doi:10.1155/2015/950567

Cantrell, K. B., Hunt, P. G., Uchimiya, M., Novak, J. M., & Ro, K. S. (2012). Impact of pyrolysis temperature and manure source on physicochemical characteristics of biochar. *Bioresource Technology, 107*, 419–428. doi:10.1016/j.biortech.2011.11.084

Chong, K. H., Law, P. L., Rigit, A. R. H., Baini, R., & Shanti, F. S. (2014). Sago bark as renewable energy. *Journal of Civil Engineering, Science and Technology, 5*(2), 29-34. doi:10.33736/jcest.136.2014

Claoston, N., Samsuri, A. W., Ahmad Husni, M. H., & Mohd Amran, M. S., (2014). Effects of pyrolysis temperature on physicochemical properties of empty fruit bunch and rice husk biochars. *Waste Management and Research*, *32*(4), 331-339. doi:10.1177/0734242x14525822

Edward, C. (2016, August 14). Pineapple planters all excited about MD2. *Borneo Post.* Retrieved June 23, 2020, from https://www.theborneopost.com/2016/08/14/pineapple-planters-all-excited-about-md2/

Fu, B., Ge, C, Yue, L., Luo, J., Feng, D., Deng, H., & Yu, H. (2016). Characterization of biochar derived from pineapple peel waste and its application for sorption of oxytetracycline from aqueous solution. *BioResources, 11*(4), 9017–9035. doi:10.15376/biores.11.4.9017-9035

Hossain, M. K., Strezov, V., Chan, K. Y., Ziolkowski, A., & Nelson, P. F. (2011). Influence of pyrolysis temperature on production and nutrient properties of wastewater sludge biochar. *Journal of Environmental Management, 92*(1), 223–228. doi:10.1016/j.jenvman.2010.09.008

Hunt, J., DuPonte, M., Sato, D., & Kawabata, A. (2010). The basics of biochar: A natural soil amendment. *Soil and Crop Management (SCM-30).* Retrieved September 20, 2018, from http://www.ctahr.hawaii.edu/oc/freepubs/pdf/SCM-30.pdf

Idris, J., Shirai, Y., Ando, Y., Ali, A. A. M., Othman, M. R., Ibrahim, I., & Hassan, M. A. (2014). Production of biochar with high mineral content from oil palm biomass. *Malaysian Journal of Analytical Sciences, 18*(3), 700–704.

Joseph, S. D., Downie, A., Munroe, P., Crosky, A., & Lehmann, J. (2007, December 9-11). Biochar for carbon sequestration, reduction of greenhouse gas emissions and enhancement of soil fertility; A review of the materials science. In *Proceedings of the Australian combustion symposium* (pp. 130-133). Sydney, Australia.

Lehmann, J. (2007). Bio-energy in the black. *Frontiers in Ecology and the Environment, 5*(7), 381–387. doi:10.1890/1540-9295(2007)5[381:bitb]2.0.co;2

Leng, L. Y., Husni, M. H. A., & Samsuri, A. W., (2011). Comparison of the carbon-sequestering abilities of pineapple leaf residue chars produced by controlled combustion and by field burning. *Bioresource Technology, 102*(22), 10759–10762. doi:10.1016/j.biortech.2011.08.131

Lim, K. C., & Zaharah, A. R. (2000). Decomposition and N & K release by oil palm empty fruit bunches applied under mature palms. *Journal of Oil Palm Research, 12*(2), 55–62.

Mawardiana, Sufardi., & Husen E. (2013). Pengaruh residu biochar dan pemupukan NPK terhadap sifat kimia tanah dan pertumbuhan serta hasil tanaman padi (*Oryza sativa* L.) musim tanam ketiga [Residual effect of biochar and NPK fertilization toward the dynamics of nitrogen , soil chemical properties and rice crop in third season planting]. *Jurnal Manajemen Sumber Dayalahan, 2*(3), 255–260.

Naim, H. M., Yaakub, A. N., & Hamdan, D. A. A. (2016). Commercialization of sago through estate plantation scheme in Sarawak: The way forward. *International Journal of Agronomy, 2016*, 1–6. doi:10.1155/2016/8319542

Nazri, A. M., & Pebrian, D. E. (2017). Analysis of energy consumption in pineapple cultivation in Malaysia: A case study. *Pertanika Journal of Science & Technology, 25*(1), 17–28.

Nunes, M. C. N., Emond, J. P., Rauth, M., Dea, S., & Chau, K. V., (2009). Environmental conditions encountered during typical consumer retail display affect fruit and vegetable quality and waste. *Postharvest Biology and Technology, 51*(2), 232–241. doi:.1016/j.postharvbio.2008.07.016

Padzil, F. N. M., Ainun, Z. M. A., Kassim, N. A., Lee, S. H., Lee, C. H., Ariffin, H., & Zainudin, E. S. (2020). Chemical, physical and biological treatments of pineapple leaf fibres. In M. Jawaid, M. Asim, P. Tahir & M. Nasir (Eds.), *Pineapple leaf fibers* (pp. 73–90). Singapore: Springer

Ridwan, I., Jaya, A. M., & Mantja, K. (2018). Pengembangan bioindustri kompos limbah pertanian melalui pemberdayaan masyarakat pesisir di Kecamatan Labakkang [Development of Agricultural Waste Compost Bioindustry through Empowerment of Coastal Communities in Labakkang District]. *Jurnal Dinamika Pengabdian (JDP), 3*(2), 165–176. doi:10.20956/jdp.v3i2.4248

Shaaban, A., Se, S., Mitan, N. M. M., & Dimina, M. F. (2013). Characterization of biochar derived from rubber wood sawdust through slow pyrolysis on surface porosities and functional groups. *Procedia Engineering, 68*, 365-371. doi:10.1016/j.proeng.2013.12.193

Upadhyay, A., Lama, J. P., & Tawata, S. (2010). Utilization of pineapple waste. *Journal of Food Science and Technology Nepal, 6,* 10–18. doi:10.3126/jfstn.v6i0.8255

Wahi, R., Aziz, S. M. A., Hamdan, S., & Ngaini, Z. (2015, December 14-16). Biochar production from agricultural wastes via low-temperature microwave carbonization. In *IEEE International RF and Microwave Conference (RFM)* (pp. 244-247). Kuching, Malaysia.

Zakaria, Z. A., Boopathy, R., Dib, J. R. (2019). *Valorisation of agro-industrial residues – volume I: Biological approaches*. Cham, Switzerland: Springer Nature AG.

Pertanika J. Sci. & Technol. 28 (S2): 287 - 298 (2020)

PERTANIKA JOURNALS

SCIENCE & TECHNOLOGY

Journal homepage: http://www.pertanika.upm.edu.my/

Static Mechanical, Thermal Stability, and Interfacial Properties of Superheated Steam Treated Oil Palm Biomass Reinforced Polypropylene Biocomposite

Muhammad Nazmir Mohd Warid[1], Tengku Arisyah Tengku Yasim-Anuar[1], Hidayah Ariffin[1,2]*, Mohd Ali Hassan[1], Yoshito Andou[3] and Yoshihito Shirai[3]

[1]Department of Bioprocess Technology, Faculty of Biotechnology and Biomolecular Sciences, 43400 UPM Serdang, Selangor, Malaysia
[2]Laboratory of Biopolymer and Derivatives (BADs), Institute of Tropical Forestry and Forest Products (INTROP), Universiti Putra Malaysia, 43400 UPM Serdang, Selangor, Malaysia
[3]Department of Biological Functions and Engineering, Graduate School of Life Science and System Engineering, Kyushu Institute of Technology, 2-4 Hibikino, Wakamatsu, Fukuoka 808-0196, Japan

ABSTRACT

In this study, three types of oil palm biomass (OPB) namely, oil palm mesocarp fiber (OPMF), oil palm empty fruit bunch (OPEFB) and oil palm frond (OPF), were studied and compared as the alternative fillers in the biocomposite reinforced polypropylene (PP). The fibers were treated using the optimal condition of superheated steam treatment obtained from previous study. The OPB/PP biocomposites at weight ratio of 30:70 were fabricated by melt blending technique and hot pressed moulding. Results showed that the tensile and flexural properties of optimized-SHS-treated OPB/PP biocomposites were improved by 9 – 30% and 9 – 12%, respectively compared to the untreated OPB/PP biocomposites. The same observation was recorded for thermal stability. Improved surface morphology as shown by the tensile fracture surface indicates better interfacial adhesion between SHS-treated OPB fibers with PP matrix during blending. Overall results showed that OPF/PP biocomposites had better properties compared to biocomposites prepared from OPMF and OPEFB, suggesting that OPF is a better OPB fiber choice as a filler in PP reinforced biocomposite.

Keywords: Biocomposite, oil palm mesocarp fiber (OPMF), oil palm empty fruit bunch (OPEFB), oil palm frond (OPF), superheated steam (SHS) treatment

ARTICLE INFO

Article history:
Received: 10 February 2020
Accepted: 13 November 2020
Published: 31 December 2020

DOI: https://doi.org/10.47836/pjst.28.S2.22

E-mail addresses:
nazmirwarid@gmail.com (Muhammad Nazmir Mohd Warid)
tengkuarisyah@gmail.com (Tengku Arisyah Tengku Yasim-Anuar)
hidayah@upm.edu.my (Hidayah Ariffin)
alihas@upm.edu.my (Mohd Ali Hassan)
yando@life.kyutech.ac.jp (Yoshito Andou)
shirai@life.kyutech.ac.jp (Yoshihito Shirai)
* Corresponding author

ISSN: 0128-7680
e-ISSN: 2231-8526

© Universiti Putra Malaysia Press

INTRODUCTION

Recently, research on the utilization of natural fibers over the synthetic fibers as the reinforcement in biocomposite has been extensively conducted due to the advantages of natural fibers. Natural fibers have low density, high toughness, good specific strength properties, good thermal and insulation properties, low in cost, non-abrasive to the processing equipment, biodegradable and easy to recycle (Acha et al., 2007; Akil et al., 2011; Bogoeva-Gaceva et al., 2007; Raju et al., 2008; Spoljaric et al., 2009). Several natural fibers have been tested for biocomposite fabrication such as kenaf, bamboo, baggase and rice husk. Due to the large amount of oil palm biomass (OPB) in Malaysia, the utilization of OPB to produce valuable products such as biocomposites has been studied (Karuppuchamy et al., 2015; Nordin et al., 2013; Then et al., 2013).

When using natural fiber as filler in polymer composite, surface modification is commonly needed due to incompatibility with the polymer matrix. Natural fiber consists of hydroxyl (OH) group, causes it to be hydrophilic in nature, whereas polymer used in composite application is commonly hydrophobic. Such differences in wetting properties makes them difficult to achieve homogenous dispersion (Yasim-Anuar et al., 2020). Without surface modification, the resulting biocomposites may have poor mechanical properties, mainly due to poor stress transfer between both polymer matrix and fibers (Warid et al., 2016). There have been numerous methods used for surface modification of the natural fibers, including superheated steam (SHS) treatment (Nordin et al., 2013). Optimization study of SHS treatment on the oil palm biomass has been done in order to prepare suitable properties of fibers for biocomposite purpose (Warid et al., 2016). A previous study by Warid et al. (2016) revealed that SHS treatment was able to alter the fiber surface by removing hemicellulose and silica bodies, thus abled to enhance the fiber thermal stability and remove its moisture. This helps in enhancing compatibility with the polymer matrix.

This study aims to compare the use of several types of oil palm biomass, OPMF, OPEFB and OPF as reinforcement material in polypropylene biocomposite. The biocomposites produced were characterized for their mechanical, thermal stability, and surface morphological properties.

MATERIALS AND METHODS

Raw Materials

OPMF and OPEFB were obtained from Seri Ulu Langat Palm Oil Mill, Selangor, Malaysia while OPF was obtained from Taman Pertanian Universiti (TPU), Universiti Putra Malaysia (UPM). OPF was first shredded and pressed to remove the juice as described by Abdullah et al. (2015). The preparation of raw OPMF, OPEFB and OPF were conducted as described by Nordin et al. (2013). The size of each fiber was about 8-10cm in length and no further mechanical treatment was done prior to SHS treatment.

Superheated Steam Treatment

OPB fibers were treated using lab scale superheated steam oven (QF-5200C, Naomoto Corporation, Osaka, Japan) under ambient pressure as described by Nordin et al. (2013). Steam flow rate and heater power of SHS oven were kept constant at maximum value, 4.95 kg/h and 6.6 kW, respectively. OPB fibers were treated using optimized SHS treatment conditions which were obtained from the previous optimization studies (Warid et al., 2016). The optimized SHS treatment temperature and retention time for each OPB fibers are shown in Table 1.

Table 1
Optimized SHS treatment temperature and retention time for OPMF, OPEFB and OPF

Fiber	Temperature (°C)	Retention time (mins)
OPMF	265	5
OPEFB	280	5
OPF	300	9

Biocomposite Production

Untreated and SHS-treated OPB fibers were then subjected to grinding using Wiley-type Mill to obtain the OPB powders. OPB powders which size is less than 150 um was chosen for the biocomposite production. The PP and OPB powders were dried in an oven at 60°C prior to use. The biocomposites were prepared by melt blending PP and fibers in a Brabender internal mixer (Germany) at 170°C with 50 rpm rotor speed for 15 minutes. The weight ratio of OPB/PP was fixed at 30:70. The PP pellet was first loaded in the mixer chamber for about 2 minutes to melt. Next, OPB fibers were added into the mixing chamber and mixing was continued for another 13 minutes. These compounded materials were then compressed into 1-3 mm thickness sheets with length of 150 mm x 150 mm by a hydraulic hot-press at 170°C for 5 minutes, followed by cold pressing at 30°C for 5 minutes.

Chemical Compositional Analysis

Determination of lignin, cellulose and hemicellulose in the OPMF, OPEFB and OPF was done gravimetrically according to the method by (Iwamoto et al., 2008).

Mechanical Test Analysis

For tensile test, the test specimens were cut from 1mm sample sheets using a dumbbell shape cutter of ATM D638 standard. A crosshead speed of 5mm/min was used, and the tests were performed at 25°C. The results were expressed in terms of tensile strength, tensile modulus and elongation at break. The test was performed on five specimens for each formulation and the average values and standard deviations were reported.

For flexural test, a three-point bending test was conducted on the biocomposites according to ASTM D790 standard. The test was conducted at 25°C with a crosshead speed of 1.3 mm/min and a support span length of 48mm. The results were expressed in terms of flexural strength and flexural modulus.

Thermogravimetric Analysis

Thermogravimetric analysis (TGA) was conducted on a TG analyzer model TG4000 in order to confirm the change in the composition of untreated and SHS-treated OPB fibers. The OPB powder sample (6–8 mg) was placed on a ceramic pan. The sample was heated from 50–550°C at a heating rate of 10°C/min under nitrogen flow of 100 mL/min.

Surface Morphology Analysis

The surface morphology of untreated and SHS-treated OPB fibers was observed under a scanning electron microscopy (SEM, LEO 1455 VPSEM Electron Microscopy Ltd., Cambridge, England). For SEM analysis, oven-dried samples were mounted in the stub and gold-coated for 180s prior to the SEM observation. The SEM micrographs were obtained with an acceleration voltage of 5 kV.

RESULTS AND DISCUSSION

Chemical Composition of OPB fibers after SHS Treatment

Based on Table 2, chemical composition analysis showed that the untreated OPMF contained lignin, hemicellulose and cellulose at 24, 35 and 40 wt%, respectively. Lignin composition was higher for all of the OPB fibers after the SHS treatment, while cellulose and hemicellulose composition was reduced. It was reported that SHS treatment is an effective method for hemicellulose removal from lignocellulosic samples (Nordin et al., 2013). Meanwhile, it was demonstrated earlier that SHS treatment affected cellulose content due to thermal degradation of cellulose (Warid et al., 2016). Lignin composition was higher after SHS treatment as the result of cellulose and hemicellulose weight reduction. The

Table 2
Lignocellulose composition of OPB fibers after SHS treatment

	Fiber	Lignin Content (%)	Hemicellulose Content (%)	Cellulose Content (%)
OPMF	Untreated	24.41 ± 3.01	35.20 ± 1.36	40.39 ± 1.74
	265°C / 5 mins	50.40 ± 1.21	9.88 ± 1.01	39.71 ± 0.20
OPEFB	Untreated	14.53 ± 2.23	36.58 ± 2.27	48.89 ± 4.50
	280°C / 5 mins	40.49 ± 3.65	13.17 ± 2.03	46.34 ± 5.67
OPF	Untreated	14.84 ± 1.21	34.14 ± 5.71	51.02 ± 4.72
	300°C / 9 mins	40.49 ± 0.13	9.62 ± 3.29	49.89 ± 3.42

complexity of lignin structure makes it difficult to be degraded, apart from having wide range of thermal degradation temperature which is from 190 to 900°C. This explains the increased in lignin composition after SHS treatment.

Mechanical Properties of OPB Biocomposites

Tensile Properties of Biocomposites. The effectiveness of SHS-treated OPB fibers as reinforcement material in biocomposites can be determined by comparing mechanical properties of SHS-treated OPB/PP biocomposites and untreated OPB/PP biocomposites. Figure 1 shows the tensile strength (TS) and tensile modulus (TM) of both untreated and SHS-treated OPB/PP biocomposites, and PP was used as the control. The TS and TM of PP composites were reported to be about 40 Mpa and 7532 MPa, respectively. In general, the addition of OPB fibers (treated and untreated) into the PP composite reduced the TS. TS is the measurement of the force required to pull material to the point where it breaks. In other words, TS of a material is the maximum amount of stress that it can take before failure, for example in this case, breaking into two. TS of OPB/PP biocomposites reduced

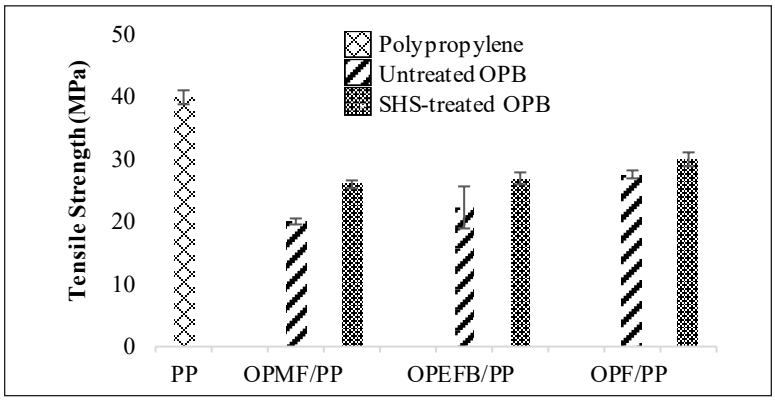

(a)

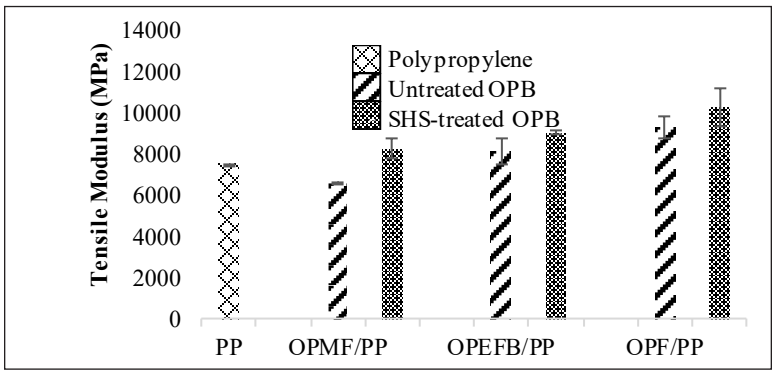

(b)

Figure 1. (a) Tensile strength (MPa) and (b) Tensile modulus (MPa) of OPB biocomposites

as low as 50% compared to TS of PP composite due to poor interfacial adhesion between hydrophobic PP and hydrophilic OPB fibers. This is due to the disruption in structural integrity of PP by the introduction of the fibers (Norrrahim, 2018).

It is interesting to note that TM of the OPB/PP biocomposites were higher compared to that of neat PP, for both untreated and SHS-treated OPB. TM can be explained as the ratio of the pressure on the material (stress) to the strain of the material. In other words, it measures the stiffness of the material. Since fibers are usually stiffer compared to polymer, the addition of OPB fibers into the PP composite caused an increment in TM.

The effect of SHS treatment can be seen in all OPB fiber samples whereby the TS and TM values for all samples were increased when SHS-treated OPB was used as compared to untreated OPB. This can be explained by the improvement in hydrophobicity of the SHS-treated OPB fibers as a result of hemicellulose removal, which contributed to improved compatibility and interfacial adhesion between SHS-treated OPB fibers and PP. Apart from that, SHS treatment improved the adhesive characteristics of OPB fibers by removing impurities covering the surface of the fiber, resulted in fibers with relatively clean and rough surface which are favourable for fibers-polymer interaction (Nordin et al., 2017). All of these reasons contributed to the increase in both TS and TM of SHS-treated OPB/PP biocomposites compared to untreated OPB/PP biocomposites.

OPF/PP biocomposites showed the highest TS and TM at 29.8 MPa and 10303 MPa, respectively. This was followed by OPEFB/PP biocomposites with TS and TM of 26.8 MPa and 9050 MPa, respectively, and finally OPMF/PP biocomposites (TS of 26 MPa and TM of 8273 MPa). The difference in cellulose composition after SHS treatment (Table 1) is expected to be the main reason which contributed to this observation. SHS-treated OPF which contained the highest cellulose showed the best mechanical properties compared to OPEFB and OPF. It is well-known that cellulose contains crystalline portion which provides strength to the biocomposite, and hence the results obtained. Based on this, it can be suggested that OPF is a superior OPB to be used as filler to improve the mechanical properties of PP biocomposite, as compared to OPMF and OPEFB.

Flexural Properties of Biocomposites. Figure 2 shows the flexural strength (FS) and flexural modulus (FM) of both untreated and SHS-treated OPB/PP biocomposites. Neat PP which was used as benchmarked sample had FS and FM of 47 MPa and 1524 MPa, respectively. Overall, all OPB/PP biocomposite samples had lower FS, but higher FM compared to neat PP. In all cases, SHS-treated OPB/PP had higher FS and FM values compared to untreated OPB/PP. This can be explained by better compatibility of SHS-treated OPB with PP as compared to untreated OPB, due to the removal of hemicellulose which caused partial removal of hydrophilic component. This ultimately improved interfacial adhesion between SHS-treated OPB fibers and PP matrix which in turn produced

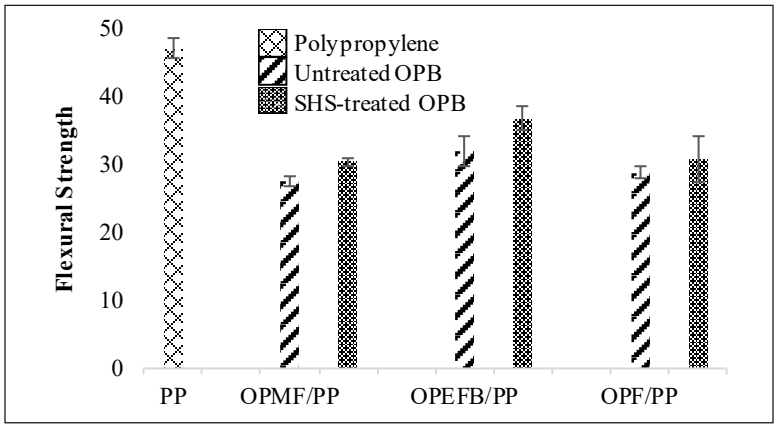

(a)

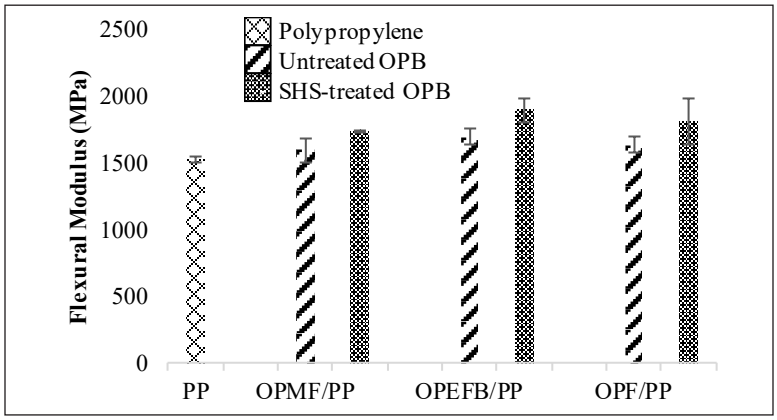

(b)

Figure 2. (a) Flexural strength (MPa) and (b) Flexural modulus (MPa) of OPB biocomposites.

biocomposite with better bending and crack propagation resistance (Nordin et al., 2017). On the other hand, segmental movement of the polymer chains can be hindered when natural fibers are introduced into the polymer matrix and this caused the biocomposites to become stiffer and eventually improved the FM as compared to neat PP.

Thermal Stability of Biocomposites. The thermal stability of biocomposites was evaluated via thermogravimetric (TG) analysis. TG thermograms of PP and OPB/PP biocomposites are illustrated in Figure 3. The information of degradation temperature at 10 and 50% weight loss, temperature at maximum rate degradation, percentage of weight loss and percentage of residual left at 500°C can be interpreted from the thermograms. Detailed interpretations are tabulated in Tables 3.

Degradation temperature at $T_{10\%}$ was used to determine the thermal stability of the biocomposites. It is seen from Figure 3 and Table 3, thermal stability of the SHS-treated OPB/PP biocomposites were higher in comparison with the untreated OPB/PP

biocomposites. The removal of hemicellulose, which possesses the lowest degradation temperature among other lignocellulosic components have increased the thermal stability of the SHS-treated fibers and eventually increased the thermal stability of the biocomposites (Nordin et al., 2017).

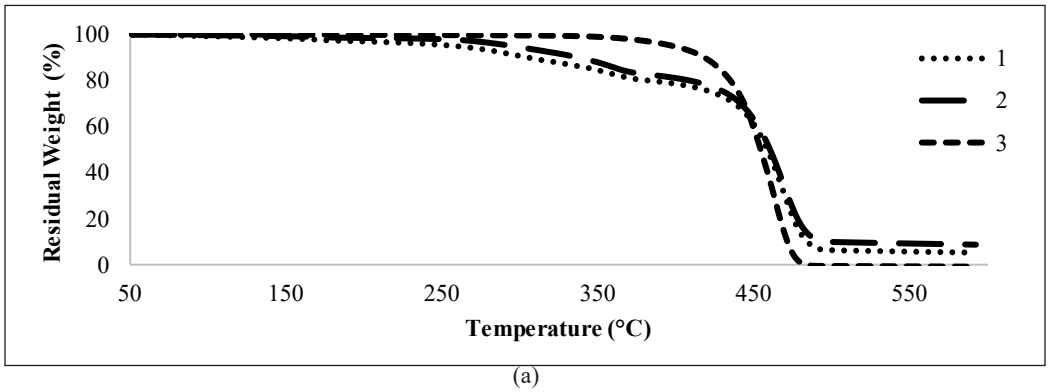

(a)

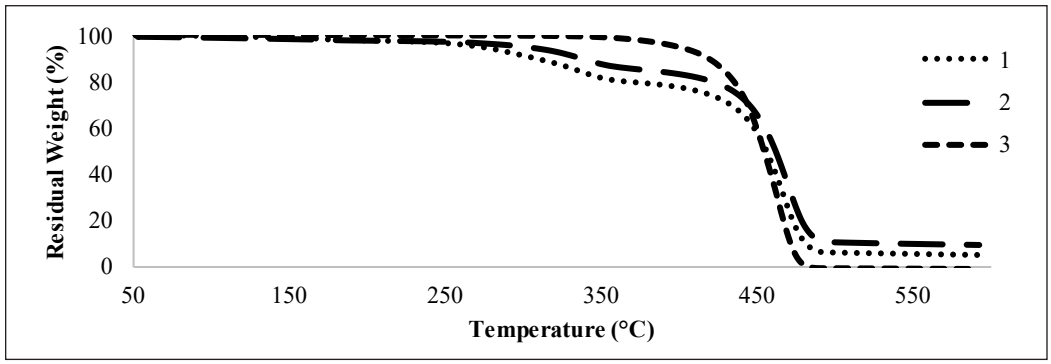

(b)

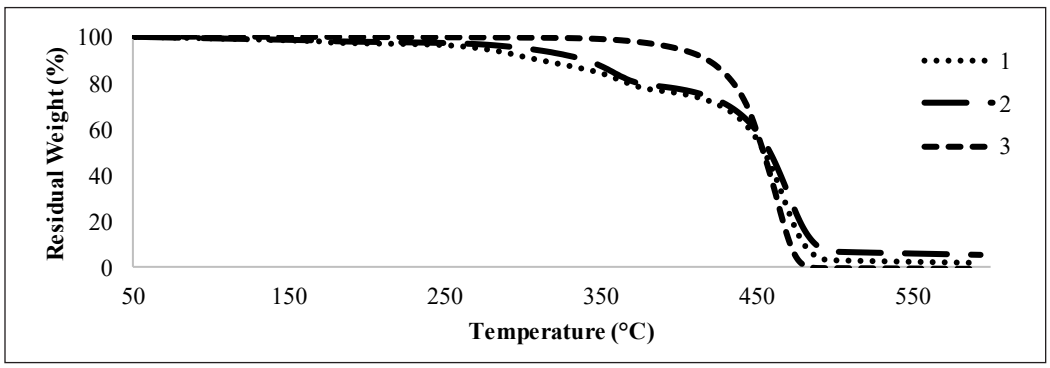

(c)

Figure 3. TG thermogram of (a) OPMF biocomposite, (b) OPEFB biocomposite and (c) OPF biocomposite. Untreated OPB is labelled as (1), SHS-treated OPB (2) and Polypropylene (3)

Table 3
Thermal degradation temperature at 10% fiber degradation as shown by TG thermogram

Biocomposite		Degradation temperature (°C), T_{10}	Residual weight at 500°C (%)
OPMF	Untreated	305	6.1
	Treated	337	9.9
OPEFB	Untreated	307	6.3
	Treated	339	10.3
OPF	Untreated	302	3.5
	Treated	339	6.6

Residual weight at 500°C can be related to the char formation of the biocomposites which is directly correlated to the potency of flame retardation. SHS-treated-OPEFB/PP biocomposite has the highest residue content, which is 10.3%, followed by SHS-treated OPMF/PP biocompsite (9.9%) and SHS-treated OPMF/PP biocompsite (6.6%).

Surface Morphology of Biocomposites. The tensile fractured surface of untreated and SHS-treated OPB/PP biocomposites were analyzed using a scanning electron microscope in order to determine the adhesion behaviour between untreated and SHS-treated OPB fibers with PP matrix. Figure 4 shows the scanning electron micrographs of tensile fractured surfaces of untreated and SHS-treated OPB/PP biocomposites. These tensile fractured surface micrographs can provide useful information regarding the failure mechanism under tensile load for the corresponding biocomposites.

The SEM micrographs of untreated OPB/PP biocomposites clearly show the gaps on the OPB/PP caused by the de-bonding of fibers from polymer matrix during the tensile test. Apart from that, cavities are also observed which can be explained by the fiber pull-out during tensile test. This may be attributed by the poor interfacial adhesion due to incompatibility between hydrophilic OPB fibers and hydrophobic PP matrix. The incompatibility can also be represented by the heterogenous structure where OPB fibers and PP matrix can be easily distinguished in the micrographs. Poor interfacial adhesion eventually resulted in the premature failure as a result of poor stress transfer across the fiber-matrix interface (Nordin et al., 2013b; Warid et al., 2016; Yasim-Anuar et al., 2019). Hence, this explains the decrease in tensile and flexural strength of the biocomposites.

On the other hand, SHS-treated OPB/PP biocomposites exhibited better compatibility as shown by the scarcuty or absence of gaps and cavities on the SHS-treated OPB/PP interface region. The removal of hemicellulose during SHS treatment of OPB fibers had improved the hydrophobicity of the fibers which then enhanced the interaction with the hydrophobic PP matrix. SHS treatment also caused the removal of silica and waxy layers from the surface of OPB fibers (Nordin et al., 2013) which provided rougher surface of fibers which can be exploited by the PP matrix for a better mechanical interlocking during biocomposite fabrication and subsequently reduced the number of fiber pull-out during tensile test.

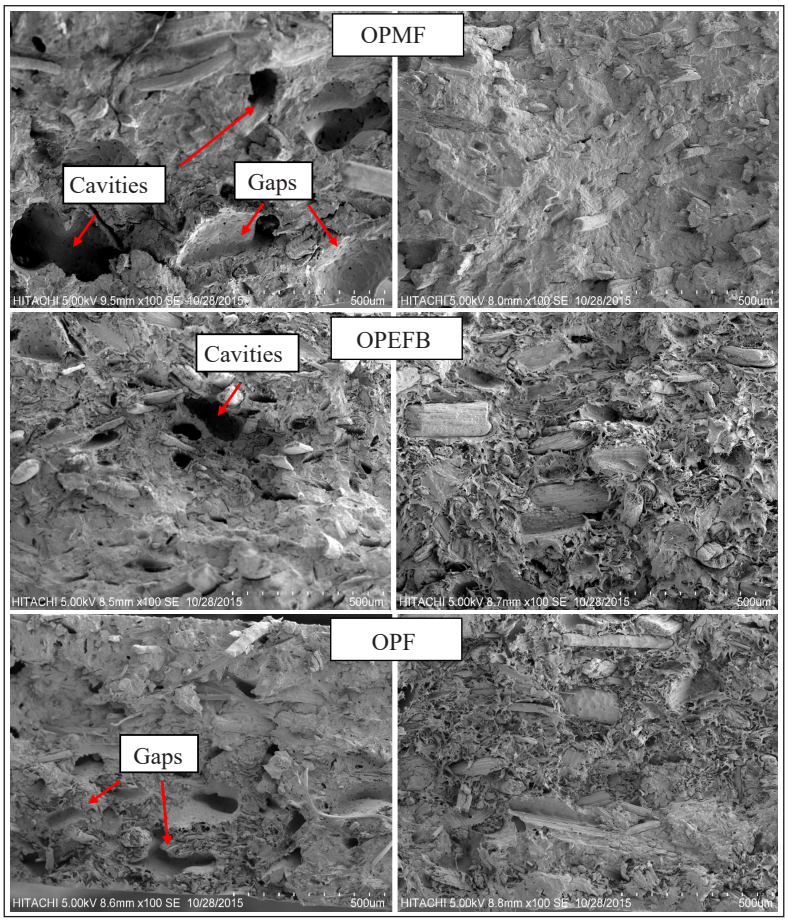

Figure 4. SEM micrographs of tensile fractured surface of untreated (L) and SHS-treated (R) OPB/PP biocomposites

CONCLUSIONS

The properties of the OPB/biocomposites were greatly affected by the types of oil palm biomass used, as well as the treatment of the fiber by SHS. Overall, OPF exhibited better performance in term of mechanical properties. This is contributed by the higher cellulose content in the OPF, the highly crystalline component in lignocellulose which could improve the mechanical properties of the biocomposites prepared using OPF as the filler. On the other hand, SHS treatment greatly affected both the mechanical and thermal properties of the SHS-treated OPB biocomposites as compared to the untreated OPB biocomposites. The removal of hemicellulose during SHS treatment improved the compatibility of the OPB with PP, contributing to better mechanical properties. The removal of hemicellulose also improved the thermal stability of the biocomposites as hemicellulose is the least thermally stable component in lignocellulose.

ACKNOWLEDGEMENT

The authors would like to acknowledge the Ministry of Higher Education, Malaysia, and Universiti Putra Malaysia (UPM), for the financial support. The authors also would like to thank Forest Research Institute Malaysia (FRIM) for the technical support throughout the experiments and to Taman Pertanian Universiti (TPU) UPM and Seri Ulu Langat Palm Oil Mill, Selangor for the raw material supply.

REFERENCES

Abdullah, S. S. S., Shirai, Y., Bahrin, E. K., & Hassan, M. A. (2015). Fresh oil palm frond juice as a renewable, non-food, non-cellulosic and complete medium for direct bioethanol production. *Industrial Crops and Products 63*, 357-361. doi:10.1016/j.indcrop.2014.10.006

Acha, B. A., Reboredo, M. M., & Marcovich, N. E. (2007). Creep and dynamic mechanical behavior of PP–jute composites: Effect of the interfacial adhesion. *Composites Part A: Applied Science and Manufacturing*, *38*(6), 1507–1516. doi:10.1016/j.compositesa.2007.01.003

Akil, H., Omar, M. F., Mazuki, A. A. M., Safiee, S. Z. A. M., Ishak, Z. M., & Bakar, A. A. (2011). Kenaf fiber reinforced composites: A review. *Materials & Design, 32*(8-9), 4107-4121. doi:10.1016/j.matdes.2011.04.008

Bogoeva-Gaceva, G., Avella, M., Malinconico, M., Buzarovska, A., Grozdanov, A., Gentile, G., & Errico, M. E. (2007). Natural fiber eco-composites. *Polymer Composites*, *28*(1), 98 – 107. doi:10.1002/pc.20270

Karuppuchamy, S., Andou, Y., Nishida, H., Nordin, N. I. A. A., Ariffin, H., Hassan, M. A., & Shirai, Y. (2015). Superheated steam treated oil palm frond fibers and their application in plastic composites. *Advanced Science, Engineering and Medicine*, *7*(2), 120–125. doi:10.1166/asem.2015.1659

Nordin, N. I. A. A., Ariffin, H., Hassan, M. A., Shirai, Y., Ando, Y., Ibrahim, N. A., & Yunus, W. M. Z. W. (2017). Superheated steam treatment of oil palm mesocarp fiber improved the properties of fiber-polypropylene biocomposite. *BioResources, 12*(1), 68-81. doi:10.15376/biores.12.1.68-81

Nordin, N. I. A. A., Ariffin, H., Andou, Y., Hassan, M. A., Shirai, Y., Nishida, H., & Ibrahim, N. A. (2013). Modification of oil palm mesocarp fiber characteristics using superheated steam treatment. *Molecules*, *18*(8), 9132–9146. doi:10.3390/molecules18089132

Norrrahim, M. N. F. (2018) *Superheated steam pretreatment of oil palm biomass for improving nanofibrillation of cellulose and performance of polypropylene / cellulose nanofiber composites.* (Doctoral thesis) Universiti Putra Malaysia, Malaysia.

Raju, C., Ratnam, C. T., Ibrahim, N. A., Rahman, M. Z. A., & Yunus, W. M. Z. W. (2008). Enhancement of PVC/ENR blend properties by poly (methyl acrylate) grafted oil palm empty fruit bunch fiber. *Journal of Applied Polymer Science*, *110*(1), 368–375. doi:10.1002/app.28662

Spoljaric, S., Genovese, A., & Shanks, R. A. (2009). Polypropylene–microcrystalline cellulose composites with enhanced compatibility and properties. *Composites Part A: Applied Science and Manufacturing*, *40*(6-7), 791–799. doi:10.1016/j.compositesa.2009.03.011

Then, Y. Y., Ibrahim, N. A., Zainuddin, N., Ariffin, H., & Yunus, W. M. Z. W (2013). Oil palm mesocarp fiber as new lignocellulosic material for fabrication of polymer/fiber biocomposites. *International Journal of Polymer Science*, *2013*, 1–7. doi:10.1155/2013/797452

Warid, M. N. M., Ariffin, H., Hassan, M. A., & Shirai, Y. (2016). Optimization of superheated steam treatment to improve surface modification of oil palm biomass fiber. *BioResources, 11*(3), 5780-5796. doi:10.15376/biores.11.3.5780-5796

Yasim-Anuar, T. A. T., Ariffin, H., Norrrahim, M. N. F., Hassan, M. A., Andou, Y., Tsukegi, T., & Nishida, H. (2020). Well-dispersed cellulose nanofiber in low density polyethylene nanocomposite by liquid-assisted extrusion. *Polymers, 12*(4), 1-17. doi:10.3390/polym12040927

Yasim-Anuar, T. A. T., Ariffin, H., Norrrahim, M. N. F., Hassan, M. A., Tsukegi, T., & Nishida, H. (2019). Sustainable one-pot process for the production of cellulose nanofiber and polyethylene/cellulose nanofiber composites. *Journal of Cleaner Production*, *207*, 590-599. doi:10.1016/j.jclepro.2018.09.266

Pertanika J. Sci. & Technol. 28 (S2): 299 - 316 (2020)

PERTANIKA JOURNALS

SCIENCE & TECHNOLOGY

Journal homepage: http://www.pertanika.upm.edu.my/

Parameters Optimization in Compression Molding of Ultra-high Molecular Weight Polyethylene/Cellulose Nanofiber Bio-nanocomposites by using Response Surface Methodology

Nur Sharmila Sharip[1], Hidayah Ariffin[1,2]*, Yoshito Andou[3], Ezyana Kamal Bahrin[2], Mohammad Jawaid[4], Paridah Md Tahir[5] and Nor Azowa Ibrahim[6]

[1]Laboratory of Biopolymer and Derivatives, Institute of Tropical Forestry and Forest Products (INTROP), Universiti Putra Malaysia, 43400 UPM Serdang, Selangor, Malaysia
[2]Department of Bioprocess Technology, Faculty of Biotechnology and Biomolecular Sciences, Universiti Putra Malaysia, 43400 UPM Serdang, Selangor, Malaysia
[3]Department of Biological Functions and Engineering, Graduate School of Life Science and Systems Engineering, Kyushu Institute of Technology, 2-4 Hibikino, Wakamatsu-ku, Kitakyushu, Fukuoka 808-0196, Japan
[4]Laboratory of Biocomposite Technology, Institute of Tropical Forestry and Forest Products (INTROP), Universiti Putra Malaysia, 43400 UPM Serdang, Selangor, Malaysia
[5]Laboratory of Sustainable Bioresource Management, Institute of Tropical Forestry and Forest Products (INTROP), Universiti Putra Malaysia, 43400 UPM Serdang, Selangor, Malaysia
[6]Department of Chemistry, Faculty of Sciences, Universiti Putra Malaysia, 43400 UPM Serdang, Selangor, Malaysia

ABSTRACT

Conventional UHMWPE molding involves long pressure holding duration, nevertheless in the presence of filler such as cellulose nanofiber (CNF), this may contribute to filler degradation. This study optimized the compression molding parameters of UHMWPE/CNF bio-nanocomposite by using response surface methodology (RSM) in consideration of temperature, pressure and duration as variables. An optimal processing condition of 180°C, 15 MPa, and 20 minutes contributed to more than 80% desirability with tensile strength, yield strength, elongation at break, and Young's modulus values of 22.83 MPa, 23.14 MPa, 487.31%, and 0.391 GPa, accordingly. Mechanical properties of UHMWPE/CNF bio-nanocomposites molded at optimized processing conditions were comparably similar to those prepared at conventional processing condition, and with the advantage of having shorter

ARTICLE INFO

Article history:
Received: 10 February 2020
Accepted: 13 November 2020
Published: 31 December 2020

DOI: https://doi.org/10.47836/pjst.28.S2.23

E-mail addresses:
nursharmilasharip@gmail.com (Nur Sharmila Sharip)
hidayah@upm.edu.my (Hidayah Ariffin)
yando@life.kyutech.ac.jp (Yoshito Andou)
ezyana@upm.edu.my (Ezyana Kamal Bahrin)
jawaid@upm.edu.my (Mohammad Jawaid)
parida.introp@gmail.com (Paridah Md Tahir)
norazowa@upm.edu.my (Nor Azowa Ibrahim)
* Corresponding author

ISSN: 0128-7680
e-ISSN: 2231-8526

© Universiti Putra Malaysia Press

processing time. The results presented herewith provides insight towards a more practical approach for UHMWPE/CNF bio-nanocomposites consolidation process.

Keywords: Bio-nanocomposite, cellulose nanofiber, compression molding, optimization, response surface methodology, ultra-high molecular weight polyethylene

INTRODUCTION

Possessing various excellent properties, ultra-high molecular weight polyethylene (UHMWPE) has been used for various application of aerospace, industrial machineries, microelectronic and medical fields (Li et al., 2017; Raghuvanshi et al., 2012), where it is consolidated into many different products including pipes, panels, gears, body armors, unlubricated bearings and artificial joint component (Khalil et al., 2016; Wang et al., 2018). This engineered thermoplastic is made of a repeating unit of ethylene with molecular weight ranged between 3.5 to 7.5 million g/mol (Kurtz, 2016a). The extremely long and linear structure of UHMWPE enables it to greatly withstand impact and abrasion beside having a very low friction (Chukov et al., 2014; Paxton et al., 2019). Not only that, a lot of studies have been conducted on manufacturing UHMWPE nanocomposites for enhanced properties befitting its applications, including UHMWPE/nanocellulose as artificial joint component (Wang et al., 2016).

While various approaches can be adopted in manufacturing and processing the UHMWPE and/or its composites, the consolidation process is restricted to compression molding and ram extrusion. This is stemmed from very low melt flow index of UHMWPE (0.006 g/min) causing other methods such as injection molding and screw extrusion to be not practical (Kurtz, 2016b; Panin et al., 2017). In comparison to other consolidation method, compression molding is considered more practical and well adapted, especially for molding UHMWPE polymer. Differing from other polymers including conventional polyethylene such as low-density polyethylene or high-density polyethylene, UHMWPE comprises extremely long chains leading to very high melt viscosity and slow diffusion during consolidation (Fu et al., 2010; Gao & Fu, 2019). Hence, UHMWPE molding requires a long pressure holding duration, in order to give adequate time for UHMWPE resin to diffuse with each other and create satisfactory entanglements thus good mechanical properties (Kurtz et al., 1999; Parasnis & Ramani, 1998). Besides, Kurtz (2016b) further described that long duration of hot pressing was necessary due to the relatively low thermal conductivity of UHMWPE.

Nevertheless, long duration molding could be a disadvantage, which may expose polymer to degradation (Campo, 2008), especially in consolidation of UHMWPE containing cellulose nanofiber (CNF) fillers. Appropriate compression molding parameters are essentially needed for polymer diffusion and filler impregnation into the matrix (Xie et al., 2019) while avoiding polymer degradation. Meanwhile, in order to improve its

productivity, the shorter duration is imperative for more effective processing. The effect, conjugated with interaction between the varied parameters, wields an impact towards the quality and mechanical properties of UHMWPE/CNF bio-nanocomposites. Therefore, this study optimized the temperature pressure and duration of compression molding for desirably good mechanical properties. The individual and interaction effects of each variables on UHMWPE/CNF bio-nanocomposites mechanical properties were also investigated.

MATERIALS AND METHODS

Materials

Fine UHMWPE powder (Sigma-Aldrich, USA) with average molecular weight of 3 x 10^6 – 6 x 10^6 g/mol was used in this experiment. Maleic anhydride-*grafted*-polyethylene (MAPE) in pellet form was from the same manufacturer by which it contains approximately 0.5 wt.% maleic anhydride. The melting point and density of UHMWPE and MAPE are 138°C, 0.94 g/mL and 107°C, 0.92 g/mL, respectively. The CNF in slurry form was purchased from ZoepNano Sdn. Bhd., Malaysia with concentration of 2 wt.% solid content and average diameter of 50 nm.

Bio-nanocomposite Fabrication and Molding

UHMWPE/ 3 wt.% CNF/ 3 wt.% MAPE bio-nanocomposite was prepared by using triple screw kneading extruder (Imoto Machinery Co., Ltd., Japan) at temperature 150°C, 60 rpm and 45 minutes melt blending condition. Fabricated bio-nanocomposite was then subjected to compression molding at varied parameters of temperature, pressure and duration.

Mechanical Properties of Bio-nanocomposites

Tensile specimen was prepared from compressed bio-nanocomposite film according to ASTM D638. The test was conducted on compact tensile and compression tester IMC-18E0 (Imoto Machinery Co., Ltd., Japan) at 50 mm/min crosshead speed) (ASTM, 2003). The mechanical properties of bio-nanocomposites after the validation experiment was analyzed using one-way ANOVA and Duncan's multiple range test for statistical analysis.

Experiment Design and Optimization

Compression molding parameters were optimized by using face-centered central composite design (CCD) of response surface methodology (RSM). Varied parameters or variables are molding temperature (X_1), pressure (X_2), and duration (X_3) with a range of 150 to 200°C, 10 to 20 MPa, and 20 to 100 minutes, accordingly. The effect of variables on mechanical properties was investigated through determination of tensile strength (Y_1), yield strength (Y_2), elongation at break (Y_3), and Young's modulus (Y_4) as responses. The coded values

of three operating variables were set at three levels: -1 (minimum), 0 (central), and +1 (maximum) as shown in Table 1. A total of 20 experiments ($2^k + 2k + 6$) inclusive of 8 factorial points, 6 axial points and 6 center points were conducted where the alpha value was set to one.

Data were analyzed by using Design Expert statistical software (Version 7.0, Stat-Ease Inc. Minneapolis, MN, USA) where the significance of each variable and regression coefficients were evaluated by considering more than 95% confidence level ($P<0.05$) of variance analysis (ANOVA). The effect of variable on the responses was expressed in three dimensional (3D) and contour plot response surface in order to locate the optimal level. A second order polynomial equation was used to explain the system behavior as shown in Equation 1 where Y_1, Y_2, Y_3, and Y_4 are the responses and X_1, X_2, and X_3 are the variables influencing Y as response. The β_0 is the constant coefficient; β_1, β_2, β_3 are linear coefficients; β_{12}, β_{13}, β_{23} are interaction coefficients; and β_{11}, β_{22}, β_{33} are quadratic coefficients.

$$Y = \beta_0 + \beta_1X_1 + \beta_2X_2 + \beta_3X_3 + \beta_{12}X_1X_2 + \beta_{13}X_1X_3 + \beta_{23}X_2X_3 + \beta_{11}X_1^2 + \beta_{22}X_2^2 + \beta_{33}X_3^2 \quad \text{(Equation 1)}$$

Table 1
Central composite design matrix of coded and actual level of variables

Run	Temperature (°C), X_1		Pressure (MPa), X_2		Duration (min), X_3	
	Coded	Actual	Coded	Actual	Coded	Actual
1	0	175	0	15	0	60
2	+1	200	-1	10	+1	100
3	0	175	0	15	0	60
4	0	175	+1	20	0	60
5	0	175	0	15	-1	20
6	0	175	0	15	0	60
7	-1	150	-1	10	+1	100
8	0	175	0	15	0	60
9	-1	150	+1	20	+1	100
10	+1	200	+1	20	+1	100
11	+1	200	+1	20	-1	20
12	-1	150	0	15	0	60
13	+1	200	-1	10	-1	20
14	0	175	0	15	+1	100
15	0	175	0	15	0	60
16	+1	200	0	15	0	60
17	0	175	-1	10	0	60
18	-1	150	-1	10	-1	20
19	0	175	0	15	0	60
20	-1	150	+1	20	-1	20

Validation Experiment and Verification

The validity and adequacy of the regression models were proven by comparing the experimental data obtained and the fitted value predicted by the models.

RESULTS AND DISCUSSION

Preliminary Experiment and Range Selection

Selection of range was in accordance to the preliminary experiment of one-variable-at-time (OVAT) for molding duration, while temperature and pressure were selected based on literature. Temperature was ranged between 150°C to 200°C in consideration to melting temperature of UHMWPE which is approximately 140°C (Oral & Muratoglu, 2016) and the degradation temperature of CNF which is around 220°C (Yasim-Anuar et al., 2018). This is because cellulose degradation at high temperature could reduce the stiffness and strength of cellulose composite (Forsgren et al., 2020; Sapieha et al., 1989). Meanwhile, cellulose degradation was negligible at temperature below 200°C (Le Baillif & Oksman, 2009; Gan et al., 2020). Pressure range was set at 10 to 20 MPa as according to Wang & Ge (2007) and the range of duration was selected from 20 to 100 minutes based on the OVAT experiment conducted as shown in Figure 1. High tensile strength and elongation at break of UHMWPE/CNF bio-nanocomposites indicating less voids between UHMWPE granules and sufficient molding time were obtained after 20 minutes molding. Gradual reduction of elongation at break observed through further prolonged duration (60 to 100 minutes) proved appropriate selection of 60 minutes as a center point in between 20 to 100 minutes.

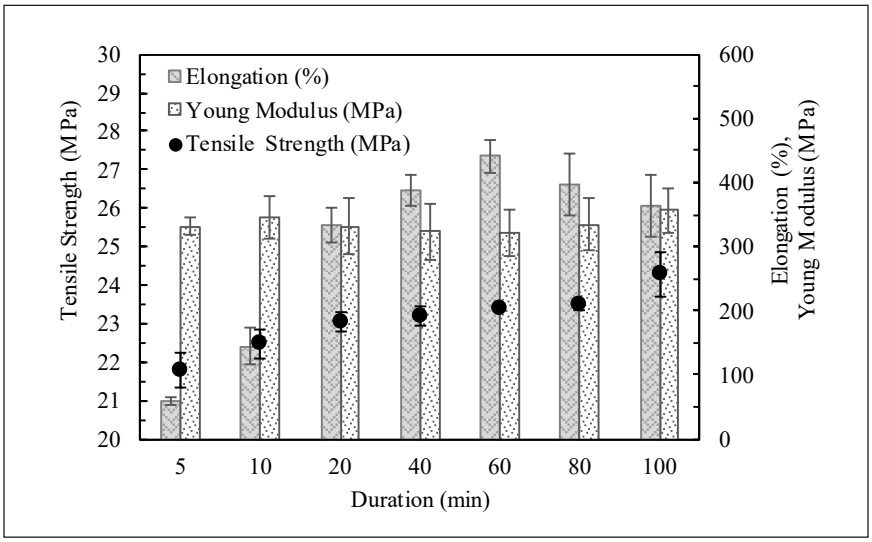

Figure 1. Mechanical properties of UHMWPE/CNF bio-nanocomposites as affected by duration at 175 °C and 15 MPa compression molding

Model Analysis

Table 2 shows the experimental and predicted values of the responses; tensile strength (Y_1), yield strength (Y_2), elongation at break (Y_3) and Young's modulus (Y_4). Natural log transformation was applied on elongation response as the best transformation suggested by the software. This was in consideration to the high maximum to minimum ratio of Y_3, values that were more than three (3.204).

The values obtained from Table 2 were subjected to analysis of variance (ANOVA) in order to select the model for each response, depending on the resulted significant model probability ($P<0.05$), insignificant lack-of-fit probability ($P>0.05$) and more than 80% coefficient of determination (R^2) (Bagheri et al., 2019; Warid et al., 2016). Full quadratic model was adopted as the best-fitted model where the results of ANOVA is tabulated in Table 3.

All models were found significant at the 5% confidence level where the *p*-values were all less than 0.05. The insignificant lack-of fit value ($P>0.05$) of all response models (0.9161,

Table 2
Experimental and predicted values of responses

Run	Tensile strength (MPa), Y_1		Yield strength (MPa)Y_2		Elongation (%), Y_3		Young's modulus (MPa), Y_4	
	*Exp	**Pred	*Exp	**Pred	*Exp	**Pred	*Exp	**Pred
1	25.4	24.8	22.6	22.7	480.3	457.6	0.346	0.343
2	22.8	22.9	23.1	23.1	243.8	238.7	0.361	0.356
3	25.1	24.8	22.7	22.7	473.1	457.6	0.341	0.343
4	24.3	24.3	22.5	22.7	393.9	397.4	0.334	0.337
5	25.0	24.8	22.7	22.7	425.3	436.7	0.347	0.344
6	23.5	24.8	22.9	22.7	455.7	457.6	0.341	0.343
7	25.9	25.9	21.4	21.3	299.0	294.6	0.325	0.333
8	25.0	24.8	22.7	22.7	496.8	457.6	0.333	0.343
9	27.1	27.4	21.3	21.3	371.9	366.8	0.322	0.320
10	22.8	22.5	23.1	23.1	155.1	155.8	0.378	0.378
11	23.6	23.7	23.3	23.2	216.2	215.5	0.366	0.359
12	27.3	26.9	21.4	21.6	385.8	404.7	0.353	0.341
13	23.7	23.5	23.5	23.5	274.4	273.3	0.359	0.362
14	24.8	24.9	22.2	22.4	380.5	398.0	0.339	0.338
15	24.3	24.8	23.3	22.7	468.3	457.6	0.349	0.343
16	23.7	24.0	23.2	23.3	265.9	272.2	0.361	0.369
17	23.5	23.4	22.9	22.9	376.7	401.0	0.351	0.344
18	24.1	24.4	22.0	21.9	262.4	256.5	0.364	0.364
19	25.0	24.8	22.7	22.7	440.0	457.6	0.340	0.343
20	26.6	26.5	21.6	21.6	384.6	385.9	0.321	0.327

*Exp: Experimental; **Pred: Predicted

Table 3
Analysis of variance (ANOVA) for response surface quadratic model

	Tensile strength (MPa), Y_1	Yield strength (MPa), Y_2	Ln Elongation (%), Ln Y_3	Young's Modulus (GPa), Y_4
Model - Quadratic	0.0006*	<0.0001*	<0.0001*	0.0026*
		Linear		
X_1 – Temperature	<0.0001*	<0.0001*	<0.0001*	0.0002*
X_2 – Pressure	0.0357*	0.2392	0.7711	0.1475
X_3 – Duration	0.7930	0.0195*	0.0122*	0.2387
		Interaction		
$X_1 X_2$	0.0407*	0.8171	<0.0001*	0.0102*
$X_1 X_3$	0.0255*	0.6101	0.0025*	0.0416*
$X_2 X_3$	0.4916	0.4619	0.0196*	0.0463*
		Quadratic		
X_1^2	0.0604	0.0548	<0.0001*	0.0339*
X_2^2	0.0212*	0.4529	0.0008*	0.6066
X_3^2	0.8692	0.2564	0.0094*	0.6430
Lack of Fit	0.9161**	0.7571**	0.3047**	0.1337**
R^2	0.9027	0.9463	0.9876	0.8642
Standard deviation	0.56	0.22	0.048	0.0078
Adequate precision	12.183	14.697	31.60	10.550

*statistically significant at $p < 0.05$ for model;
**statistically insignificant at $p > 0.05$ for lack of fit test

0.7571, 0.3047, and 0.1337, accordingly) indicated that each model could successfully predict and represent the data at points that was not included in the regression. This was also supported by high determination coefficients, R^2 by which the obtained values of 0.9027, 0.9463, 0.9876, and 0.8642 implied that 90%, 95%, 99% and 86% variance proportion of tensile strength, yield strength, elongation at break and Young's modulus are predictable by the model. As shown in Figure 2, predictions of all models were in a satisfactory match with the experimental value by which the proximity points were scattered along the fitted line. Additionally, the signal-to-noise ratio (adequate precision) of all response models were of greater than four, implying an adequate signal to navigate the design space including the estimation of the standard error of the predictions (Moradi et al., 2016).

Effect of the Compression Molding Variables on the Mechanical Properties of UHMWPE/CNF Bio-nanocomposites

The estimated regression coefficient explaining the variables effect on responses were expressed in equation follows, where Y_1, Y_2, Y_3, and Y_4 represent tensile strength, yield strength, elongation at break, and Young's modulus, respectively; and X_1, X_2, and X_3 are mixing temperature, pressure and duration, respectively.

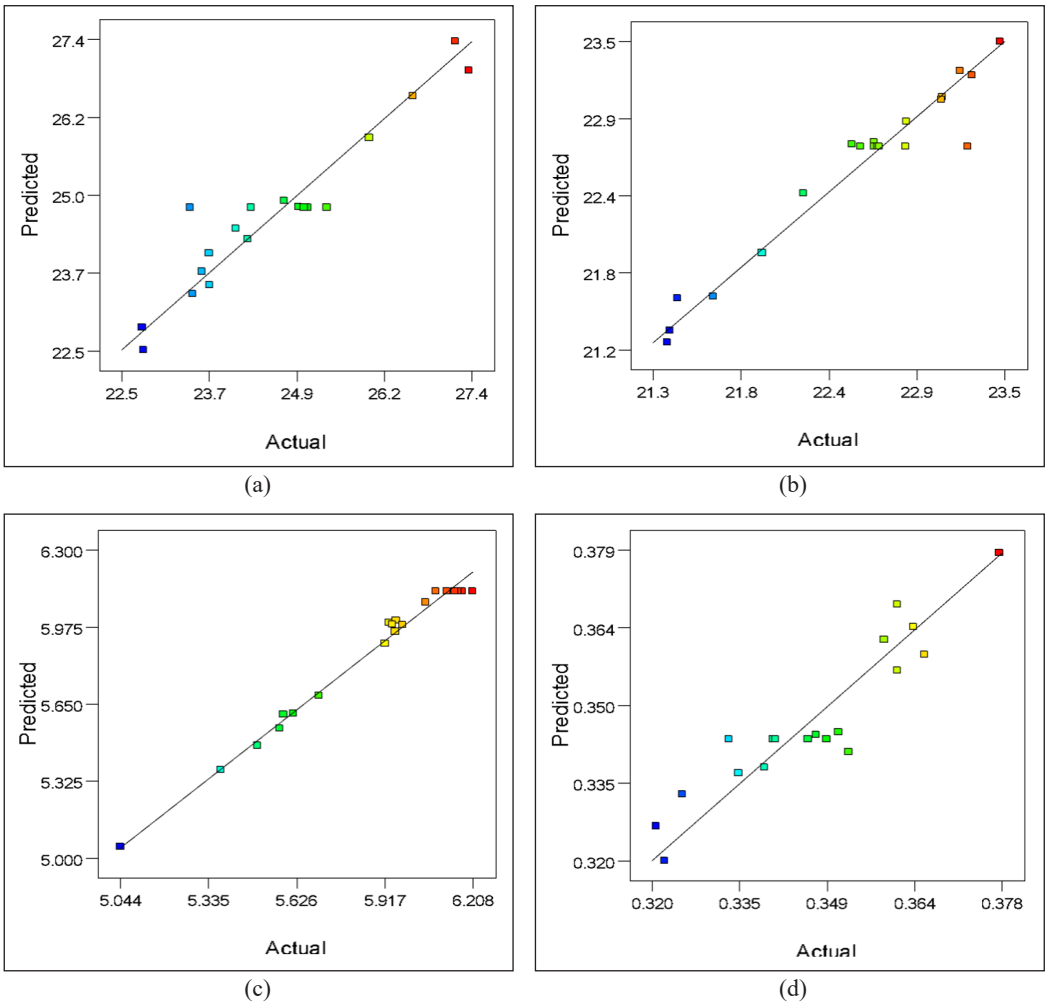

Figure 2. Experimental and predicted values for: (a) tensile strength; (b) yield strength; (c) elongation; and (d) Young's modulus of UHMWPE/CNF bio-nanocomposites

$$Y_1 = 24.76 - 1.44\ X_1 + 0.43\ X_2 + 0.048\ X_3 - 0.47\ X_1X_2 - 0.52\ X_1X_3 - 0.14\ X_2X_3 + 0.72\ X_1^2 - 0.93\ X_2^2 + 0.057\ X_3^2$$

(Equation 2)

$$Y_2 = 22.72 + 0.85\ X_1 - 0.085\ X_2 - 0.19\ X_3 + 0.018\ X_1X_2 + 0.04\ X_1X_3 + 0.058\ X_2X_3 - 0.28\ X_1^2 + 0.1\ X_2^2 - 0.16\ X_3^2$$

(Equation 3)

$$\text{Ln}\ (Y_3) = 6.13 - 0.2\ X_1 - 0.00456\ X_2 - 0.046\ X_3 - 0.16\ X_1X_2 - 0.068\ X_1X_3 - 0.047\ X_2X_3 - 0.32\ X_1^2 - 0.14\ X_2^2 - 0.093\ X_3^2$$

(Equation 4)

$$Y_4 = 0.34 + 0.014\ X_1 - 0.0039\ X_2 - 0.0031\ X_3 + 0.0087\ X_1X_2 + 0.0065\ X_1X_3 + 0.0063\ X_2X_3 + 0.012\ X_1^2 - 0.0025\ X_2^2 - 0.0023X_3^2$$

(Equation 5)

A perturbation plot was used to explain the individual effect of each variables on the responses studied. For instance, the coded units shown in Figure 3 represent the range of variables from -1.0 to +1.0 (*i.e.* 150°C to 200°C for temperature), whereby varied temperature and pressure gave significant linear effect on tensile strength. Increased temperature caused reduction of tensile strength whereby increased pressure up to 0.5 coded unit (17.5 MPa) led to increment of the response before reduced at higher pressure beyond 17.5 MPa.

The three-dimensional and contour plot of response surface showing interaction between variables against tensile strength according to Equation 2 is shown in Figure 4. Significant interaction effect of temperature and pressure was observed in which increased temperature along with pressure remarkably reduced the tensile strength (Figure 4a). In a similar manner, increased temperature along with increased duration of molding reduced the tensile strength despite insignificant linear effect of the later variable (Figure 4b). According to Xie et al. (2019), low temperature of compression molding may lead to insufficient impregnation of fillers and adjacent polymer chains while too high a temperature can lead to degradation. Meanwhile, longer duration could beneficially affected tensile strength due to improved resin flow and better fillers impregnation. Nevertheless, too long exposure to high temperature may also lead to degradation, hence explained the findings in this study by which highest tensile strength was obtained when UHMWPE/CNF bio-nanocomposites was molded at Run 9 (150°C, 15 MPa for 60 minutes) (Table 2). On the other hand, the lowest tensile strength was recorded in Run 2 (200°C, 10 MPa for 100 minutes).

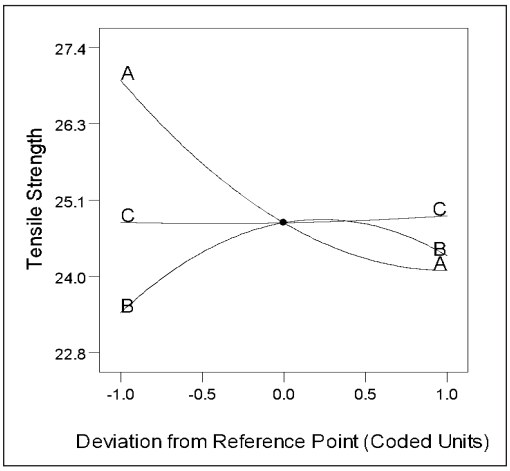

Figure 3. Perturbation plot of tensile strength in response to the changes of (A) temperature, (B) pressure, and (C) duration

In term of yield strength, no significant interaction between all variables was observed despite significant linear effect by temperature and duration (Table 3 and Figure 5a). Increased temperature from 150°C to 200°C (-1.0 to +1.0 coded unit) notably caused increment from approximately 21 MPa to 23 MPa. Prolonged duration from 20 to 60 minutes (-1.0 to 0 coded unit) gave no effect on yield strength but reduced when molded longer up to 100 minutes (+1 coded unit), possibly due to some thermal degradation attributed to long exposure to

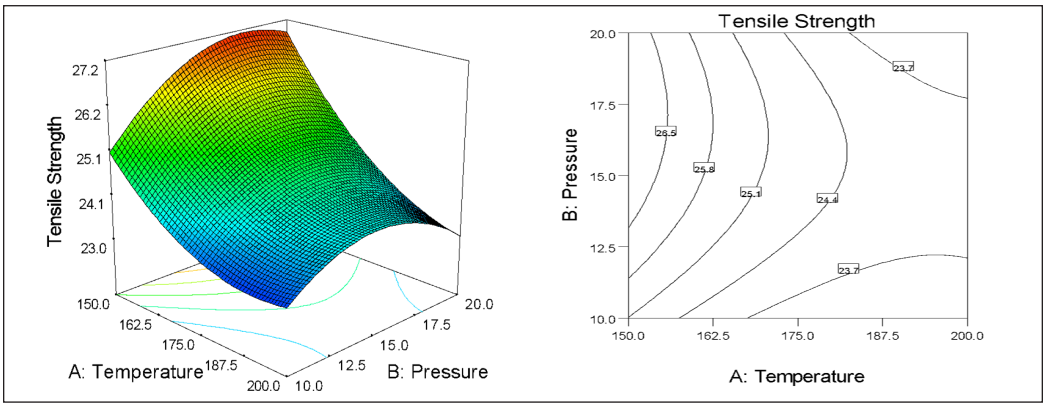

(a)

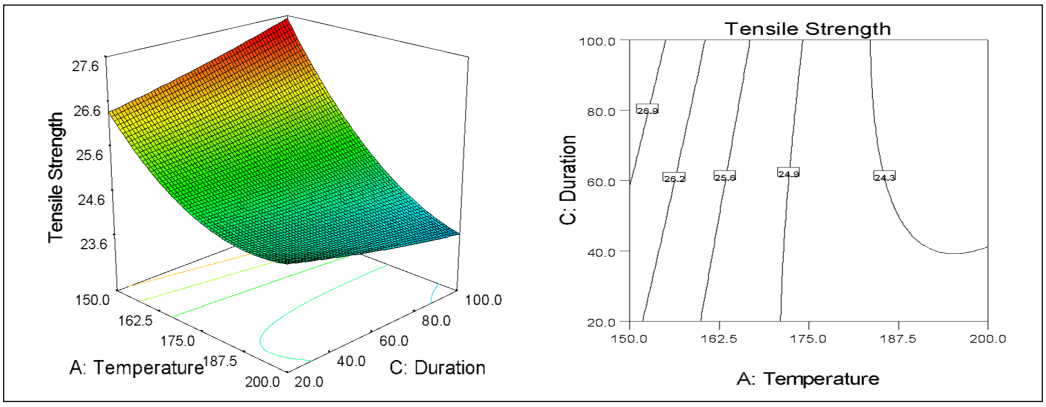

(b)

Figure 4. The 3D and contour plot for the dependence of UHMWPE/CNF bio-nanocomposite tensile strength on: (a) temperature and pressure; and (b) temperature and duration as significant variables

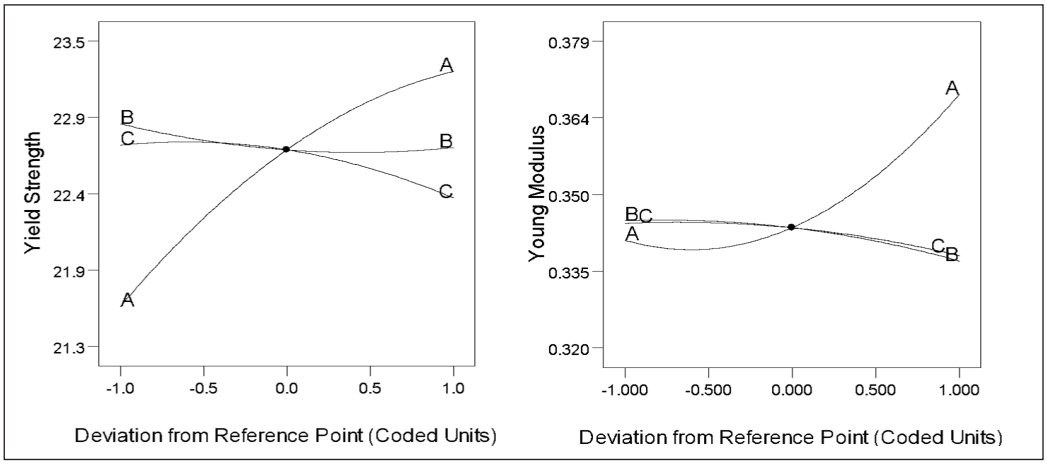

Figure 5. Perturbation plot of yield strength and Young's modulus in response to the changes of (A) temperature, (B) pressure and (C) duration

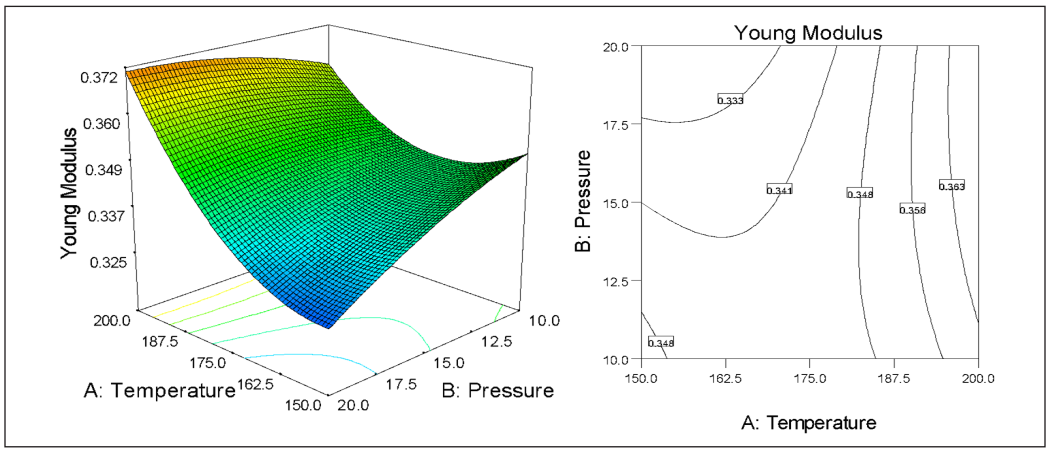

(a)

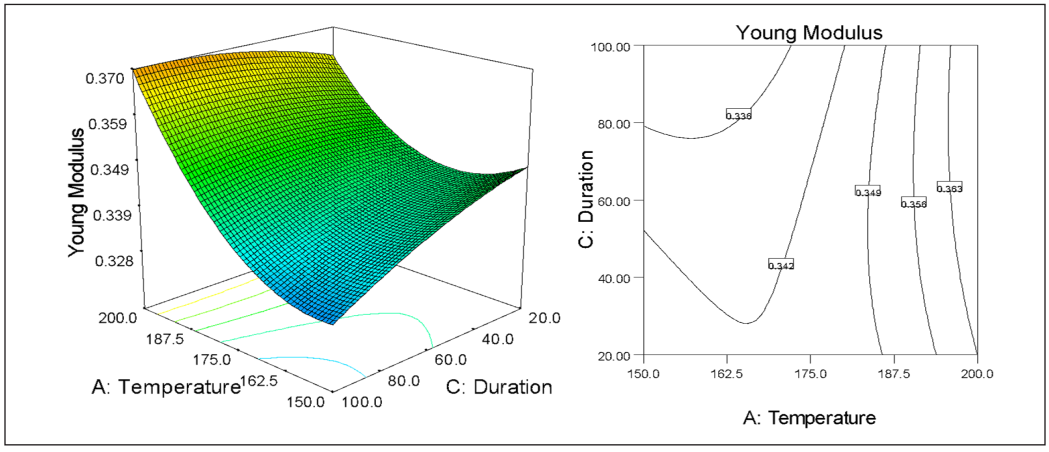

(b)

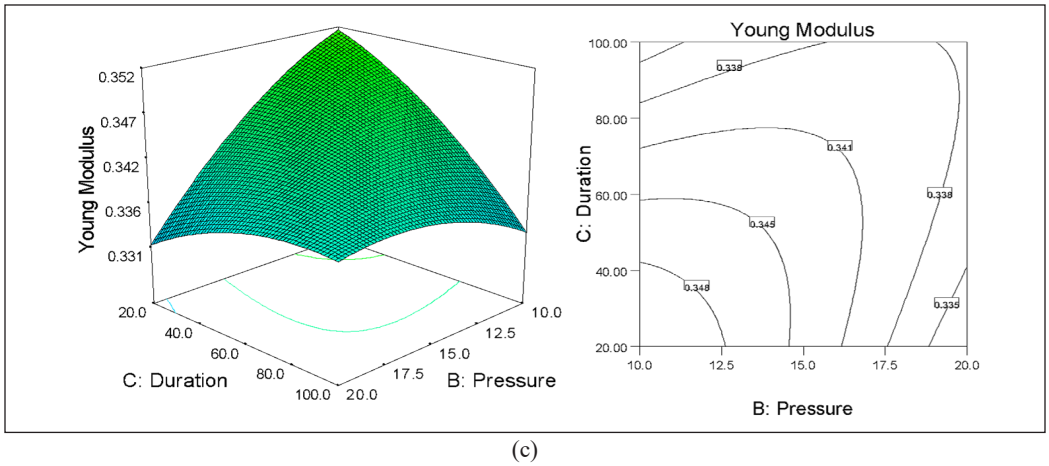

(c)

Figure 6. The 3D and contour plot for the dependence of UHMWPE/CNF bio-nanocomposite Young's modulus on: (a) temperature and pressure; (b) temperature and duration; and (c) pressure and duration as significant variables

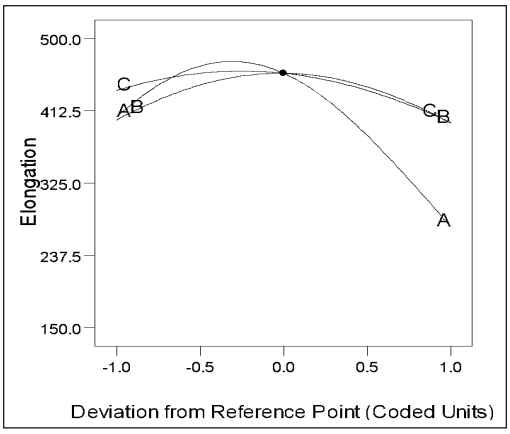

Figure 7. Perturbation plot of elongation at break in response to the changes of (A) temperature, (B) pressure and (C) duration

high temperature and pressure as previously described. In contrary, Young's modulus increased with increases of temperature (Figure 5b) while other variables gave no significant linear effect. Possible UHMWPE degradation was predicted due to exposure to high temperature and pressure. As degradation of polymer leads to formation of shorter chains that enable more packed crystals arrangement (Gleadall, 2015; Riley, 2012), higher crystallinity contributes to increases in Young's modulus (Doyle, 2000; Humbert et al., 2011). The synergistic effect of temperature with pressure, and temperature with duration on Young's modulus can also be seen in Figure 6a and Figure 6b, respectively, where Young's modulus increased along with increase values of the interacted variables. Inversely, the response value decreased by increases of pressure and duration as shown in Figure 6c.

The full quadratic model adopted comprised linear, interaction and quadratic terms indicating effect of variables on the respective response. For elongation at break, all model term listed were found to be significant except for linear pressure effect (Table 3). As shown in Figure 7, increased temperature and duration positively affected this response from -1.0 (lowest range) to -0.5 (162.5°C) and 0 (60 minutes) coded values, respectively. Further increase in both variables caused decrement in elongation at break, whereas interaction between all variables were significant as illustrated in three dimensional and contour plot of elongation break in Figure 8. The responses were in higher values when molded at temperature 162.5 to 175°C, 12.5 to 17.5 MPa and 40 to 60 minutes (Figure 8) suggesting that the optimal temperature for obtaining high elongation at break was within this range.

Response Surface Optimization of the Compression Molding Variables

Mechanical properties of UHMWPE/CNF bio-nanocomposites were notably affected by varied temperature, duration, interaction of other variables with temperature, duration, and pressure in descending order. The impact is however depended on the capability of polymer chains to undergo self diffusion that results in elimination of inter-particle voids beside avoidance of polymer degradation. An incomplete diffused UHMWPE particle/resin and CNF impregnation was expected to cause formation of voids or boundaries hence may act as cracks initiation site that afflicted the mechanical properties including tensile strength and elongation at break. As such, optimized temperature, duration and pressure play role in

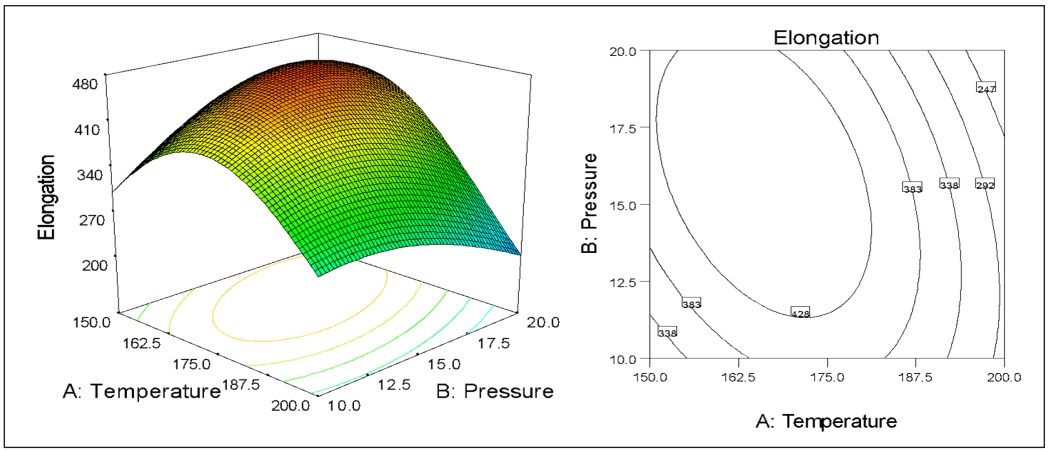

(a)

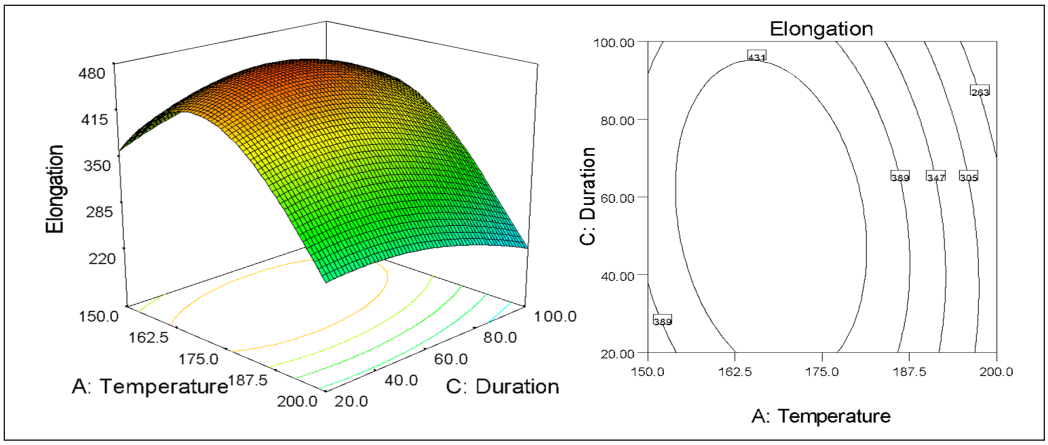

(b)

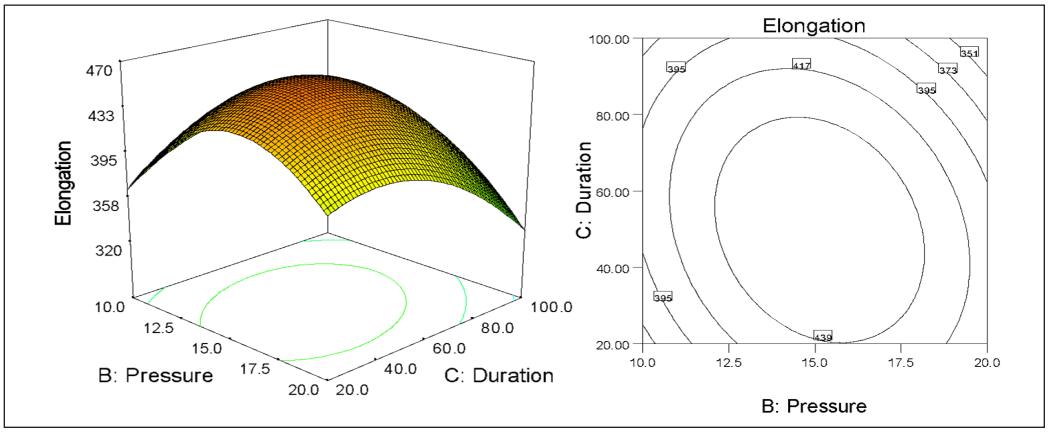

(c)

Figure 8. The 3D and contour plot for the dependence of UHMWPE/CNF bio-nanocomposite elongation at break on: (a) temperature and pressure; (b) temperature and duration; and (c) pressure and duration as significant variables

providing sufficient melt flow and time for UHMWPE polymer chains to allow complete consolidation and eliminates the boundaries through diffused adjacent chains. Additionally, adequate entanglement between adjacent chains could be established and translated into good mechanical properties.

A numerical optimization was conducted based on the design and the criteria of each variables as shown in Table 4. All mechanical properties were set to maximum except yield strength that was set in range. This was due to its small changes affected by varied temperature while other variables were insignificant. Optimum temperature, pressure and duration of compression molding were found to be at 180°C, 15 MPa and 20 minutes, respectively with desirability of 0.811. Verification experiment conducted proved the accuracy of the models where experimental value of all mechanical properties were in agreement with the predicted value by which all percent errors were less than 5% (Table 5).

Table 4
Numerical optimization criterion settings and solutions

Variables constraints								
Name		Goal		Lower limit		Upper limit		
X_1		is in range		150.0		200.0		
X_2		is in range		10.0		20.0		
X_3		minimize		20.0		100.0		
Response constraints								
Y_1		maximize		22.8		27.3		
Y_2		is in range		21.3		23.5		
Y_3		maximize		155.1		496.8		
Y_4		maximize		0.321		0.378		
Optimum Solutions								
No.	X_1	X_2	X_3	Y_1	Y_2	Y_3	Y_4	Desirability
1	180.0	15.0	20.0	24.6	22.9	420.1	0.346	0.811
2	180.5	15.0	20.0	24.6	22.9	417.9	0.346	0.809
3	180.0	17.5	20.0	24.6	22.9	408.1	0.341	0.787
3	180.0	10.0	20.0	23.2	23.1	362.7	0.352	0.681

Table 5
Comparison between predicted and experimental values of UHMWPE/CNF bio-nanocomposites fabricated at optimal conditions

	Predicted	Experimental	Percent error(%)
Tensile strength (MPa), Y_1	24.6	24.1 ± 1.1	1.92
Yield Strength (MPa), Y_2	22.9	23.3 ± 0.5	1.89
Elongation (%), Y_3	420.1	433.5 ± 26.2	3.22
Young Modulus (GPa), Y_4	0.346	0.361 ± 0.026	4.48

In addition, the optimized compression molding parameter obtained in this study was proven to provide comparable mechanical properties to the conventional process which required 45 minutes of molding duration. the duration of optimized condition was only 20 minutes which was less than two times shorter, hence could be favorable for industrial use (Table 6). Specifically, no significant different was observed on elongation and Young's modulus, while yield strength was only 2% higher. The tensile strength was however reduced from 28.0 MPa to 24.1 MPa.

Materials often experienced yielding, inelastic and plastic deformation before rupture. In order, the ability of materials to withstand load and undergo changes is determine through yield strength, Young's modulus and tensile strength. In light of UHMWPE utilization as load bearing materials such as joint arthroplasty component, yield strength is considered more important than tensile strength by which materials yielding under service condition is considered a failure (Fang et al., 2006). Moreover, the mechanical properties obtained from optimized molding conditions surpassed the minimal requirement of standard specification for consolidated UHMWPE for surgical implant (ASTM F648) which are 27 MPa, 19 MPa, and 250 % of tensile strength, yield strength and elongation, respectively (ASTM, 2014).

Table 6
Comparison between conventional and optimized compression molding

	Conventional (Kurtz et al., 1999)	**Optimized** (This study)
Temperature (°C)	175	180
Pressure (MPa)	15	15
Duration (min)	45	20
Tensile strength (MPa)	28.0 ± 1.851^{a}	24.1 ± 1.105^{b}
Yield strength (MPa)	22.8 ± 0.312^{b}	23.3 ± 0.536^{a}
Elongation (%)	461.6 ± 40.304^{a}	433.5 ± 26.242^{a}
Young's modulus (GPa)	0.366 ± 0.018^{a}	0.361 ± 0.026^{a}

CONCLUSIONS

In this paper, optimization of compression molding was conducted in order to reduce the long molding duration of UHMWPE. Optimum condition of molding UHMWPE/CNF bio-nanocomposites was 180°C, 15 MPa, and 20 minutes with more than 80% desirability, resulting in tensile strength, yield strength, elongation at break, and Young's modulus values of 22.83 MPa, 23.14 MPa, 487.31 %, and 0.391 GPa, accordingly. The mechanical properties of UHMWPE/CNF bio-nanocomposites obtained through optimized compression molding showed no significant different with pre-optimized molding whereas the molding time was successfully shortened by half through optimization. The findings suggest a more practical approach for UHMWPE bionanocomposites consolidation process.

ACKNOWLEDGEMENT

This study was funded by Ministry of Higher Education (MOHE, MALAYSIA) through HICoE research grant (Vot No.: 636911). The authors also gratefully acknowledge Universiti Putra Malaysia (UPM, MALAYSIA) and Japan Student Services Organization (JASSO, JAPAN) for provision of scholarship to the first author.

REFERENCES

ASTM. (2003). *Standard test method for tensile properties of plastics (D 638 - 02a)*. American Society for Testing and Materials. Penssylvania, USA. doi:10.1520/D0638-14.1

ASTM. (2014). ASTM F648: *Ultra-high-molecular-weight polyethylene powder and fabricated form for surgical implants, test, 1–9*. American Society for Testing and Materials. Penssylvania, USA. doi:10.1520/F0648-14

Bagheri, V., Ghanbarzadeh, B., Ayaseh, A., Ostadrahimi, A., Ehsani, A., Alizadeh-Sani, M., & Adun, P. A. (2019). The optimization of physico-mechanical properties of bionanocomposite films based on gluten/ carboxymethyl cellulose/ cellulose nanofiber using response surface methodology. *Polymer Testing*, *78*(July), 1-11. doi:10.1016/j.polymertesting.2019.105989

Campo, E. A. (2008). Mechanical properties of polymeric materials. In *Selection of polymeric materials,* (pp. 41–101). William Andrew: Norwich, USA. doi: 10.1016/B978-081551551-7.50004-8

Chukov, D. I., Stepashkin, A. A., Gorshenkov, M. V., Tcherdyntsev, V. V., & Kaloshkin, S. D. (2014). Surface modification of carbon fibers and its effect on the fiber-matrix interaction of UHMWPE based composites. *Journal of Alloys and Compounds*, *586*(SUPPL. 1), S459–S463. doi:10.1016/j.jallcom.2012.11.048

Doyle, M. J. (2000). On the effect of crystallinity on the elastic properties of semicrystalline polyethylene. *Polymer Engineering & Science*, *40*(2), 330–335. doi:10.1002/pen.11166

Fang, L., Leng, Y., & Gao, P. (2006). Processing and mechanical properties of HA/UHMWPE nanocomposites. *Biomaterials*, *27*(20), 3701–3707. doi:10.1016/j.biomaterials.2006.02.023

Forsgren, L., Berglund, J., Thunberg, J., Rigdahl, M., & Boldizar, A. (2020). Injection molding and appearance of cellulose-reinforced composites. *Polymer Engineering & Science*, *60*(1), 5–12. doi:10.1002/pen.25253

Fu, J., Ghali, B. W., Lozynsky, A. J., Oral, E., & Muratoglu, O. K. (2010). Ultra high molecular weight polyethylene with improved plasticity and toughness by high temperature melting. *Polymer*, *51*(12), 2721–2731. doi:10.1016/j.polymer.2010.04.003

Gan, P. G., Sam, S. T., Abdullah, M. F. bin, & Omar, M. F. (2020). Thermal properties of nanocellulose-reinforced composites: A review. *Journal of Applied Polymer Science*, *137*(11), 1-14. doi:10.1002/app.48544

Gao, G., & Fu, J. (2019). Highly crosslinked UHMWPE for joint implants. In Fu, J., Jin, Z.-M., & Wang, J. W. (Ed.), *UHMWPE biomaterials for joint implants: Structures, properties and clinical performance* (pp. 21–68). Singapore: Springer. doi: 10.1007/978-981-13-6924-7_2

Gleadall, A. (2015). Mechanical properties of biodegradable polymers for medical applications. In Pan, J. (Ed.), *Modelling degradation of bioresorbable polymeric medical devices* (pp. 163–199). Manchester, United Kingdom: Woodhead Publishing. doi: 10.1533/9781782420255.2.163

Humbert, S., Lame, O., Séguéla, R., & Vigier, G. (2011). A re-examination of the elastic modulus dependence on crystallinity in semi-crystalline polymers. *Polymer*, *52*(21), 4899–4909. doi:10.1016/j.polymer.2011.07.060

Khalil, Y., Kowalski, A., & Hopkinson, N. (2016). Influence of energy density on flexural properties of laser-sintered UHMWPE. *Additive Manufacturing*, *10*, 67–75. doi:10.1016/j.addma.2016.03.002

Kurtz, S. M. (2016a). A primer on UHMWPE. In *UHMWPE biomaterials handbook: Ultra high molecular weight polyethylene in total joint replacement and medical devices: Third edition* (pp. 1–6). Waltham, USA: William Andrew. doi: 10.1016/B978-0-12-374721-1.00001-8

Kurtz, S. M. (2016b). From ethylene gas to UHMWPE component: The process of producing orthopedic implants. In *UHMWPE biomaterials handbook: Ultra high molecular weight polyethylene in total joint replacement and medical devices: Third edition* (pp. 7-20). Waltham, USA: William Andrew. doi: 10.1016/B978-0-323-35401-1.00002-8

Kurtz, S. M., Muratoglu, O. K., Evans, M., & Edidin, A. A. (1999). Advances in the processing, sterilization, and crosslinking of ultra-high molecular weight polyethylene for total joint arthroplasty. *Biomaterials*, *20*(18), 1659–1688. doi: 10.1016/s0142-9612(99)00053-8

Le Baillif, M., & Oksman, K. (2009). The effect of processing on fiber dispersion, fiber length, and thermal degradation of bleached sulfite cellulose fiber polypropylene composites. *Journal of Temoplastic Composite Materils*, *22(2)*, 115–133. doi:10.1177/0892705708091608

Li, Y., He, H., Huang, B., Zhou, L., Yu, P., & Lv, Z. (2017). In situ fabrication of cellulose nanocrystal-silica hybrids and its application in UHMWPE: Rheological, thermal, and wear resistance properties. *Polymer Composites, 39*(S3), 1–13. doi:10.1002/pc.24690

Moradi, M., Fazlzadehdavil, M., Pirsaheb, M., Mansouri, Y., Khosravi, T., & Sharafi, K. (2016). Response surface methodology (RSM) and its application for optimization of ammonium ions removal from aqueous solutions by pumice as a natural and low cost adsorbent. *Archives of Environmental Protection*, *42*(2), 33–43. doi:10.1515/aep-2016-0018

Oral, E., & Muratoglu, O. K. (2016). Highly cross-linked UHMWPE doped with vitamin E. In Kurtz, S. M. (Ed.) *UHMWPE Biomaterials handbook: Ultra high molecular weight polyethylene in total joint replacement and medical devices: Third edition* (pp. 307–325). Waltham, USA: William Andrew. doi: 10.1016/B978-0-323-35401-1.00018-1

Parasnis, N. C., & Ramani, K. (1998). Analysis of the effect of pressure on compression moulding of UHMWPE. *Journal of Materials Science: Materials in Medicine*, *9*(3), 165–172. doi:10.1023/A:1008871720389

Paxton, N. C., Allenby, M. C., Lewis, P. M., & Woodruff, M. A. (2019). Biomedical applications of polyethylene. *European Polymer Journal*, *118*, 412-428. doi: 10.1016/j.eurpolymj.2019.05.037

Raghuvanshi, S. K., Ahmad, B., Siddhartha, Srivastava, A. K., Krishna, J. B. M., & Wahab, M. A. (2012). Effect of gamma irradiation on the optical properties of UHMWPE (Ultra-high-molecular-weight-polyethylene) polymer. *Nuclear Instruments and Methods in Physics Research, Section B: Beam Interactions with Materials and Atoms*, *271*, 44–47. doi:10.1016/j.nimb.2011.11.001

Riley, A. (2012). Basics of polymer chemistry for packaging materials. In Emblem, A. & Emblem, H. (Ed.), *Packaging technology* (pp. 262–286). Cambridge, England: Woodhead Publishing. doi: 10.1533/9780857095701.2.262

Sapieha, S., Pupo, J. F., & Schreiber, H. P. (1989). Thermal degradation of cellulose-containing composites during processing. *Journal of Applied Polymer Science*, *37*(1), 233–240. doi:10.1002/app.1989.070370118

Wang, J., Cao, C., Yu, D., & Chen, X. (2018). Deformation and stress response of carbon nanotubes/ UHMWPE composites under extensional-shear coupling flow. *Applied Composite Materials*, *25*(1), 35–43. doi:10.1007/s10443-017-9606-8

Wang, S., & Ge, S. (2007). The mechanical property and tribological behavior of UHMWPE: Effect of molding pressure. *Wear*, *263*(7–12), 949–956. doi:10.1016/j.wear.2006.12.070

Wang, S., Feng, Q., Sun, J., Gao, F., Fan, W., Zhang, Z., ... & Jiang, X. (2016). Nanocrystalline cellulose improves the biocompatibility and reduces the wear debris of ultrahigh molecular weight polyethylene via weak binding. *ACS Nano*, *10*(1), 298–306. doi:10.1021/acsnano.5b04393

Warid, M. N. M., Ariffin, H., Hassan, M. A., & Shirai, Y. (2016). Optimization of superheated steam treatment to improve surface modification of oil palm biomass fiber. *BioResources, 11*(3), 5780-5796. doi:10.15376/ biores.11.3.5780-5796

Xie, J., Wang, S., Cui, Z., & Wu, J. (2019). Process optimization for compression molding of carbon fiber–reinforced thermosetting polymer. *Materials*, *12*(15), 2-13. doi:10.3390/ma12152430

Yasim-Anuar, T. A. T., Ariffin, H., & Hassan, M. A. (2018). Characterization of cellulose nanofiber from oil palm mesocarp fiber produced by ultrasonication. *IOP Conference Series: Materials Science and Engineering*, *368*(1), 1-11. doi:10.1088/1757-899x/368/1/012033

Pertanika J. Sci. & Technol. 28 (S2): 317 - 337 (2020)

SCIENCE & TECHNOLOGY

Journal homepage: http://www.pertanika.upm.edu.my/

Reducing Attribute Non-Attendance Risk in Choice Experiment: An application of Design Attribute Relative Importance Index for Waste Management Service Provision in Segmented Markets

Shehu Usman Adam[1], Shaufique F. Sidique[2]* and Mad Nasir Shamsudin[3]

[1]Institute of Agricultural and Food Policy Studies, Putra Infoport, Universiti Putra Malaysia, 43400 UPM Serdang, Selangor Darul Ehsan, Malaysia
[2]School of Business and Economics, Universiti Putra Malaysia, 43400 UPM Serdang, Selangor Darul Ehsan, Malaysia
[3]Faculty of Forestry and Environment, Universiti Putra Malaysia, 43400 UPM Serdang, Selangor Darul Ehsan, Malaysia

ABSTRACT

Attribute non-attendance is an estimation problem that biases welfare estimates in the economic valuation of environmental goods when choice experiment (CE) is used. The potential for observing the problem is increased when segmented markets with dissimilar preferences exist for environmental goods but not captured in the experimental design for CE. The current procedure for avoiding this problem relies on qualitative techniques, which limits applications to large samples and thus prone to bias. To reduce such bias, this study used an alternative technique based on the design-attribute relative importance index (DARII) to determine respondents' prioritization of attributes within and across markets. Our results in solid waste management services demonstrate that all selected attributes were highly ranked across markets. While such finding conforms to expectations based on the interview, we found a statistically significant difference in attributes prioritization across markets. We thus conclude that assuming equal priority for attributes in different market segments may be improper but possibly tangled when the qualitative method is used. As such, the study recommends CE studies to use DARII before the experimental design stage.

Keywords: Attribute non-attendance, choice experiment, DARII, design attributes, heterogeneous market

ARTICLE INFO

Article history:
Received: 10 February 2020
Accepted: 13 November 2020
Published: 31 December 2020

DOI: https://doi.org/10.47836/pjst.28.S2.24

E-mail addresses:
shehusmanadm@unimaid.edu.ng (Shehu Usman Adam)
shaufique@upm.edu.my (Shaufique F. Sidique*)
mns@upm.edu.my (Mad Nasir Shamsudin)
* Corresponding author

ISSN: 0128-7680
e-ISSN: 2231-8526

© Universiti Putra Malaysia Press

INTRODUCTION

Following the first application of choice experiment (CE) to environmental valuation by Adamowicz et al. (1994), growing interest in its use evokes discussions related to methodological improvements. These discussions particularly emphasize pre-modeling issues prior to the experimental design stage (Bliemer & Rose, 2009; Coast & Horrocks, 2007; Kløjgaard et al., 2012; Louviere et al., 2011; Rose & Bliemer, 2009). *Attribute non-attendance* constitutes one of the recent, experimental design-related concerns in CE (Alemu et al., 2013; Hess, 2014, 2012). This problem, which biases welfare estimates, is attributable to the relevant[1] design-attributes selection that constitutes the first step in CE (Alemu et al., 2013; Coast and Horrocks, 2007; Hanley et al., 1998; Hensher et al., 2005).

More importantly, the validity of CE studies depends on a researcher's competence to correctly specify a limited number of design attributes about which the target population holds high preferences (Hess & Hensher, 2010; Mangham et al., 2008). Another related constraint that warrants attribute prioritization prior to experimental design in CE is the model parsimony requirement at the post-design or modeling stage, which does not allow the inclusion of all attributes for the valuation of an environmental resource. Therefore, recent studies have consistently used fewer design attributes (De Bekker-Grob et al., 2012), necessitating prioritization of the attributes' subset for experimental design at the pre-design stage despite the enormous number of attributes possessed by environmental resources.

Surprisingly, despite attribute selection for CE experimental design in economic valuation not being strictly based on economic theory, CE studies explaining how this subset of design-attributes are determined are sparse (Kløjgaard et al., 2012; Mangham et al., 2008). The CE technique is based on Lancaster's theory of value, where utility is conceptualized to depend on the attributes possessed by goods or services (Lancaster, 1966). However, it is implausible to completely describe things via their attributes (Bateman et al., 2002). After selecting the most choice-influencing subset of attributes, the rest are assumed to be captured by the error term specified as a stochastic component in the random utility framework. If the most choice-influencing attributes with the highest preference across respondents are not included, the omission of such important predictors will bias estimated parameters and thus, welfare measures. This could lead to inefficient allocation of resources arising from underestimation or overestimation of welfare values, leading to poor or inappropriate environmental and resource related policies.

It is recently noted that attribute non-attendance arises because some respondents have low preferences for certain attributes among the bundle of alternative choices (Alemu et al., 2013; Hess & Hensher, 2010). This arises as a result of including low preference attributes in the experimental design of a CE. How can the most important subset of

[1] "relevant" as used in this paper denotes the most important choice influencing the sub-set of all attributes about which respondents hold the highest preferences in relative terms.

attributes be determined at the design stage to avoid the inclusion of attributes with low preference based on the current qualitative procedure? This method entails interviewing a sample of stakeholders (Coast and Horrocks, 2007; Hanley et al., 1998; Mangham et al., 2008; Kløjgaard et al., 2012). The problem with interviewing these stakeholders, as it is currently done, arises because the perception of "relative importance" is subjective and allows preferences for attributes to be reached only in small samples. Adam et al. (2013) attempted to address this issue by using an indicator called DARII to determine relative importance in larger samples for a homogeneous market. However, the assumption of a homogenous market, although maintained in most CE studies, is quite inaccurate.

This inaccuracy emerges because the markets for virtually all products are, in reality, imperfect. They contain some homogenous market segments within the bigger markets that are most often heterogeneous (Dibb & Simkin, 2009; Smith, 1956; Wind, 1978;). The markets for environmental resources are prototypes of such heterogeneous markets. This holds for solid waste management service markets where attributes exert unequal relevance across heterogeneous market segments (Naz & Naz, 2005). It also conforms to the expectations of market segmentation advocates (Jones et al., 2005).

Since most solid waste municipalities have different market segments, applying the same attributes would be inappropriate (Adepitan, 2010; Coffey & Coad, 2010). This study aims to address this issue by demonstrating an application of DARII within and across market segments prior to the experimental design stage in CE. This is important to avoid biased estimates that could be induced by attribute non-attendance resulting from imposing the same experimental design on respondents across different markets where preference structure may be dissimilar. We conducted a survey in Lagos, Nigeria on its solid waste management service market, which was characterized by two major segments: affluent and poor neighborhoods. These segments are apparently different in some service attributes (Adepitan, 2010). Lagos State is Nigeria's most populous state, featuring both affluent and poor communities with a population running between 14 million to 21 million people (Leithead, 2017). It has the highest population density in Nigeria and it was chosen because of its remarkably impressive reforms. Once tagged the dirtiest city in the world but now has the most organized solid waste management system in Nigeria with over 300 private sector companies operating in its solid waste management service sector (Adam et al., 2015; Olukanni & Nwafor, 2019).

METHODS

Relative importance index (RII) is usually assessed in cases where variables are perceived important, but perceptions on subjective relative importance varies across respondents. To do that, studies have relied on an average ranking of importance to determine the overall importance rating of each variable. This assessment is common in the literature on project

risk management within the field of construction engineering. Usually the assessment begins with variables[2] identification through a literature review (Andi, 2006; El-Sayegh, 2008; Huwang et al., 2013; Kangari, 1995). The variables are then verified through interviews and expert discussions (Aziz, 2013; Bari et al., 2012; Ramanathan et al., 2012). This entire procedure is consistent with the processes involved in identifying design attributes in CE literature.

Since the first application of this method to attribute selection procedure by Adam et al. (2013), more recent studies have applied it in CE predesign attribute selection. These include an application in solid waste management by Basiru et al. (2017). Other applications were also demonstrated both in transport choice preferences pre-design and job choice determination by Kaffashi et al. (2016) and Alagabi et al. (2017), respectively.

The magnitudes of RII for different attributes are rated either based on perceived mean value and standard deviation or the percentage of respondents assigning a high rating to a factor. Studies relying on mean value and standard deviation as a basis for establishing attributes' relative importance compute the magnitude using the following equation:

$$\text{Relative Importance Index, } RII_{\forall A_i} = \frac{\sum W_{yi} X_i}{n_i}, \quad (0 \leq RII_{\forall A_i} \geq 1) \qquad (1)$$

$$\text{for } A_i = (A_1, A_2, A_3, \ldots, A_n)$$

where A_i denotes the number of attributes ranging from A_1 to A_n. Wy_i denotes the yth weight assigned to responses on the importance of i^{th} attribute as perceived by respondents, Meanwhile, $y = 1, 2, 3, \ldots Y$, where Y is the highest weight W_i can assume. X_i is the frequency of the weight W_y assigned for an i^{th} attribute. n_i denotes the total number of responses to an i^{th} attribute in a sample which may not necessarily be the same for all attributes due to issues such as non-response. Note that the Y for any given W_i is the highest value of the response anchor used while its size depends on the rating scale employed. Generally, authors use response anchors with a five-point or seven-point Likert-type rating scale. In both cases, 1 denotes least effect or influence while 5 or 7 denotes the highest effect.

However, in recent applications, some modifications of RII that incorporate some weighting factors to the denominator in equation (1) are adopted (see Ramanathan et al., 2012 for a review). Authors using these versions noted that mean values and standard deviations of individual attributes are not statistically suitable for computing relative importance. This is because values obtained based on equation (1) would not reflect any relative relationships among attributes of interest to rationalise comparisons (Aziz, 2013; Bari et al., 2012). Thus, this group of authors suggest the use of RII variants that generate values that are easily comparable in relative terms. One of such versions is computed as follows:

[2] Here, the factors or variables referred to in the context of engineering literature is adopted to denote attributes in CE (see Adam et al., 2013)

$$\text{Relative Importance Index, } RII_{\forall A_i} = \frac{\sum W_{yi} X_i}{n_i * Y}, \quad (0 \leq RII_{\forall A_i} \geq 1) \qquad (2)$$

where the magnitude of the computed RII in equation (1) is weighted by the highest value (Y) of the response category based on the adopted rating scale. Therefore, the rating index is expected to range between 0 and 1 regardless of the rating scale used. The closer an attribute's rating index is to 1, the higher is its perceived importance relative to others and vice versa. Therefore, the adjusted RII originally obtained through a Likert scale is transformed into a continuum ranging from 0 to 1 (Adam et al., 2013).

Applicability of RII in Examining Group-Difference in DARII

The procedure and objective involved in the RII coincide with those of design-attribute selection in CE studies. This study's assessment of group-difference in DARII employed the adjusted RII on account of its preference over an unweighted RII (Adam et al., 2013). The application of RII in engineering literature acknowledges the possibility of observing differences in attributes' RII across a distinct group of subjects (respondents), particularly when there are apparent differences across groups. These differences, for example, are distinguishable through demographic characteristics. Such an assessment is deemed important because a composite value of RII reflecting an arbitrary combination of sub-groups may not reflect the specificities of individual groups. Accordingly, a few studies examined these differences. This includes comparing perceived risk factors between two groups (El-Sayegh, 2008) or more (Chan & Kumaraswamy, 1997). Therefore, based on the RII in (2), in cases where heterogeneous groups (markets) are apparent, DARII may be computed as:

$$CDARII_{\forall A_i} = \frac{\sum W_{ci} X_{ci}}{n_{ci} * Y}, \qquad (0 \leq \text{CDARII} \geq 1), \forall\ A_{is} \qquad (3)$$

$$D\ddot{A}RII_{\forall A_i} = \frac{\sum W_{ci} X_{ai}}{n_{1i} * Y}, \qquad (0 \leq D\ddot{A}RII \geq 1), \forall\ A_{is} \qquad (4)$$

$$D\ddot{\dot{A}}\ddot{R}II_{\forall A_i} = \frac{\sum W_{ci} X_{bi}}{n_{2i} * Y}, \qquad (0 \leq D\ddot{\dot{A}}\ddot{R}II \geq 1), \forall\ A_{is} \qquad (5)$$

where n_i, A, W, X and Y are as defined in equation (1) but here, n_1, n_2....,$n_n \in n_i$ while $\text{DÄRII}_{\forall A_i} \neq \text{DÄ}\dot{\text{R}}\text{II}_{\forall A_i}$ and both are distinct from $\text{CDARII}_{\forall A_i}$. The first two represent DARII for the two distinct heterogenous markets within the composite,$\text{CDARII}_{\forall A_i}$.

In CE applications, the combination of the characteristics theory of value (Lancaster, 1966) and the theory of random utility (McFadden, 1973, in Hanley et al., 2001) paves the way for estimating observed respondents' preferences (choices) among different bundles of environmental resources (goods). This is demonstrated in equation (6).

$$U_{ij} = V\left(A_{ij}\left(Z_i\right)\right) + \varepsilon\left(A_{ij}\left(Z_i\right)\right) \quad (6)$$

where each respondent's indirect utility function *(U_i)* depends on preferences made from some choice set *S*, over a finite number of alternative environmental goods (*j*). Besides, *(U_i)* is disaggregated into two components, deterministic (*V*) and stochastic (ε). The utility attainable from various alternatives (*j*), is expected to depend on the set of attributes *(A_i)* of the alternatives. In addition, it is understood that such attributes are viewed differently by different individuals based on the variations in their socioeconomic characteristics denoted by *(Z)* (Hanley et al., 1998). To obtain welfare estimates, cost or price attributes are usually expected to form part of the bundle constituting each alternative (*j*).

Just like the case with DARII, researchers are often interested in estimating differences in welfare across sub-groups (Birol et al., 2009; Naz & Naz, 2005). In similar cases, equation (6) could be taken as the composite model. However, a case involving two sub-groups will be more accurately represented by equations (7) and (8).

$$U_{aij} = V\left(A_{ij}\left(G_i\right)\right) + \varepsilon\left(A_{ij}\left(G_i\right)\right) \quad (7)$$

$$U_{bij} = V\left(A_{ij}\left(Q_i\right)\right) + \varepsilon\left(A_{ij}\left(Q_i\right)\right) \quad (8)$$

where A_{ij} is the vector of attributes in different scenarios and G_j the vector of respondents' characteristics. Note that in this case, despite G_i and Q_i are $\in$ of Z_i in (6), it is common to observe results yielding values such that $U_{aij} \neq U_{bij} \neq U_{ij}$ (Birol et al., 2009). This implies that average preferences for A_{ij} differs across sub-groups. Therefore, if the difference that defines sub-groups into distinct units is related to between-groups, divergence in average demographic characteristics, a separate experimental design may be required depending on DARII's result.

An application of choice set based on the same experimental design to sub-groups could bias estimates. This is because the set of attributes with the highest preferences within-groups might not be the same as the most preferred subset across groups. Furthermore, attribute subsets most preferred within and across groups may not be the same as the most preferred composite subset obtainable by pooling the sub-groups. This is evident in RII studies (Chan & Kumaraswamy, 1997; El-Sayegh, 2008).

Application of DARII to Solid Waste Management Improvement

This study began with the identification of relevant design-attributes through a literature survey, discussion with experts, and regulatory officials. In addition, a few households from the target population were interviewed. Attribute compilation from the literature was

limited to past valuation studies on solid waste management improvement. The different sources yielded twenty-three (23) attributes, including five attributes specific to solid waste management service provision in Lagos. These included enforcement on defaulting tenements, waste containerisation, pre-collection services, waste evacuation from canals, and door-to-door collection services.

However, three attributes were deemed irrelevant based on interview feedback from stakeholders. The irrelevant attributes included water pollution and psychological fears initially obtained from Pek and Jamal (2011), as well as changes in the mix of collection trucks adopted from Afroz et al. (2009), and Afroz and Masud (2011). Following the procedure outlined in Coast and Horrocks (2007) and Hanley et al. (1998), the attributes deemed irrelevant were finally deleted, leaving twenty attributes. The remaining attributes were synthesised into four broad groups for organisation purposes. The breakdown structure is as shown in Table 1.

Table 1
Solid waste management services design-attributes breakdown structure

S/N	**Solid waste Management Service Attributes**	**Sources**
1.	Waste Charges	Jin et al. (2006), Othman (2007), Karousakis and Birol (2008), Pek and Jamal (2011)
2.	Schedule and Frequency of collection	Das, et al. (2010), Othman (2007), Afroz, and Masud (2011), Othman (2007), Jin et al. (2006)
3.	Bill Discount	Basili, et al. (2006), Caplan, et al. (2007), Adam et al. (2015)
4.	Free Container	Adam et al. (2015), Afroz and Masud (2011), Jin et al. (2006)
5.	Door-to-Door Collection and Pre-Collection	Adam et al. (2015), Afroz and Masud (2011)
6.	Waste Categories	Adam et al. (2015)
7.	Waste Separation and Waste storage	Afroz and Masud (2011), Jin et al. (2006), Othman (2007)
8.	Water pollution	Pek and Jamal (2011)
9.	Disposal Method	Afroz and Masud (2011)
10.	Waste Transport	Othman (2007), Afroz and Masud (2011)
11.	Collection Trucks Mix	Afroz and Masud (2011)
12.	Psychological Fear	Pek and Jamal (2011)
13.	Changes in Franchisee	Adam et al. (2015)
14.	Defaulters Enforcement	Adam et al. (2015)
15.	Land Use	Pek and Jamal (2011)
16.	Services Provider (Private/Public)	Jin et al. (2006), Afroz and Masud (2011), Adam et al. (2015)
17.	Air pollution	Pek and Jamal (2011)
18.	Noise pollution	Jin et al. (2006)
19.	Canal Evacuation	Adam et al. (2015)

Source: Authors' solid waste management service attributes compilation from literature

Design-Attributes in Questionnaire

Both the monetary and non-monetary design-attributes were included in the questionnaire (Table 1). This pre-design analysis caters to our upcoming CE study that will estimate the monetary compensation households are willing to accept to source-separate the solid waste they generate. Therefore, a bill discount is considered as a policy-relevant monetary design-attribute. Our choice of this monetary attribute was motivated by interview feedback from regulatory officials. A top executive member of the Lagos state waste management authority (LAWMA) noted that LAWMA proposes to subsidise the effort of households to segregate their solid waste into designated recyclable categories. LAWMA will collect the separated recyclables, while the source-separator will be given a discount of 50% on the monthly bill (Adam et al., 2015). Due to this policy consideration, other potential monetary design-attributes in Table 1 were deemed policy-irrelevant, reducing the list from 23 to 17 attributes, including other non-monetary attributes.

One of the motivations of this study is to examine the possible differences in DARII for attributes across two solid waste management service market segments. Intuitively, we expected pre-collection service and door-to-door collection to have different demand structures across the market segments. In Lagos, pre-collection service involves the collection of waste from households using lightweight vehicles (motorized tricycles). These vehicles have the advantage of accessing roads in urban slum areas which are usually narrow with no bituminous treatments, making it inaccessible to heavy compactor trucks. These wastes will then be transferred to compactor trucks for final transportation to landfills. Meanwhile, the most common mode of waste collection in affluent areas is door-to-door collection using heavy trucks.

Questionnaire Structure and Measure

The questionnaire used in this study is divided into two sections. The first section elicits demographic information of the respondents, while the second section presents a list of solid waste management service improvement attributes. Respondents were asked to rate each of the attributes to determine the most important subset using a Likert-type rating scale for scoring their perceived importance for each attribute. The response anchors for the rating scale are properly worded to ensure reliable responses. To guarantee that, a prior interview was conducted whereby respondents were asked to explain service attributes that "affect" their satisfaction. In expressing their opinions, they frequently expressed the degree to which attributes' inclusion affected their utility using the words: 'importance', 'effect', and 'impact'.

Based on that, we chose to use a response anchor we defined as, "degree of impact' on respondents' satisfaction with the inclusion of an attribute in improved service provision. This conforms to the anchor used in engineering literature. Kartam and Kartam (2001) and El-Sayegh (2008) used 'degree of impact', while Kangari (1995) and Hwang et al.

(2013) used 'degree of importance'. Meanwhile, Chan and Kumaraswamy (1997), and Aziz (2013) used 'degree of effect'. These response anchors are usually applied to five-point or seven-point Likert scales. Kartam and Kartam (2001), Kangari (1995), Hwang et al. (2013), Chan and Kumaraswamy (1997), Aziz (2013), and El-Sayegh (2008) all used a five-point Likert scale, but Kometa et al. (1994) used a seven-point Likert scale. Accordingly, this study employs a five-point Likert scale where the lowest response anchor (1) denotes "*low impact on satisfaction*", while the highest response anchor (5) denotes "*high impact on satisfaction*".

Sampling and Questionnaire Administration

The provision of solid waste management services slightly differs across affluent and poor neighborhoods (Adepitan, 2010). This discrepancy is not a direct consequence of government policy, but was due to inadequate infrastructure in urban slum areas, specifically accessible roads (Adam et al., 2015). Therefore, the population can be stratified into affluent neighborhoods with accessible roads, and urban slum areas with often inaccessible roads.

Due to the apparent difference in service provision across affluent and poor urban areas, a stratified cluster sampling method was considered appropriate. This was due to the absence of a sample frame arising from non-availability of information. One community was randomly selected from each stratum. Finally, 100 questionnaires were administered in each stratum, yielding a total of 200 observations. The Surulere local government area represented the affluent stratum while the Apapa-Iganmu community development area constituted the selected poor neighborhood stratum. Data was collected through face-to-face questionnaire interviews of household representatives in the selected areas from September to November, 2012. The interviews were conducted by ten trained enumerators. A total of 200 interviews were finally conducted with 100 respondents in each stratum.

RESULT AND DISCUSSION

Socioeconomic Characteristics of Households

A response rate of up to 80% was achieved during data collection. We expected this since the questionnaire was kept very brief (occupying only one page) and was administered via face-to-face interviews. Interviewers were also specifically instructed to remind respondents to revisit missing answers and this yielded up to 99% usable questionnaire responses where only two questionnaires from the affluent stratum were excluded from analysis on account of incomplete responses. The number of respondents included in our final sample was 198. Table 2 shows a summary of the surveyed sample characteristics.

Male and female respondents constituted 55% and 45% of the sample, respectively. This approximates the state's gender distribution (based on the 2006 Census) where males and females account for 51.8% and 48.2% of the population. The average age of the sample

was 35.6 years, with the youngest being 18 and the oldest being 61. Respondents were grouped according to reported ages into three cohorts of 18−24, 25−40 and above 40. These cohorts were respectively labeled young adult, middle-aged adult and older adults. The majority of these respondents are middle-aged adults (67.2%), followed by older adults (24.7%), and young adults (8.1%). About 80% of respondents were married while the rest were either single or divorced. The highest percentage of households (73.7%) had a formal education ranging from primary (10.1%), secondary (22.2%) to tertiary (41.4%). While the remaining 26.3% had no formal education. This literacy rate is slightly higher than the national average of 71.6%. This is expected since a nation-wide literacy survey report showed that the literacy rate was higher in Lagos than in other Nigerian states (NBS, 2010). Most households worked in the private sector (55.1%), followed by the public sector (23.7%) and the remaining 21.2% were either pensioners or unemployed. Households

Table 2
Summary statistics on households' socio-economic characteristics

Variables	Categories	Household Strata			
		Affluent		Poor	
		Frequency	Mean (Std. Dev)	Frequency	Mean (Std. Dev)
Age	18−24	9	35.69 (9.831)	7	35.59 (8.341)
	25−40	65		68	
	>40	24		25	
Gender	Female	46		43	
	Male	52		57	
Marital Status	Single	23		15	
	Married	73		85	
	Separated	2		0	
Education	Never	11	12.57 (5.07) years	41	6.77 (6.27) years
	Primary	5		15	
	Secondary	19		25	
	Tertiary	63		19	
Employment Type	Public	33		14	
	Private	42		67	
	Pension	7		12	
	Unemployed	16		7	
Income	₦10,000−₦50,000	-	85,940 (61,589) 71.6%*	50.5	44,946 (5,590.55) 12.4%*
	₦51,000−₦100,000	69		34.8	
	₦101,000−₦200,000	21		10.6	
	>₦200,000	8		4	
Sample	Affluent Stratum	98		-	
	Poor Stratum	-		100	

**Denotes percentage of relative standard deviations.*

within the low income stratum earn between ₦10,000–₦50,000 monthly while the majority of households in the affluent stratum earned income ranging from ₦51,000–₦100,000. However, it is worth noting that at the time of the study's field survey in 2012 USD/Naira exchange rate hovered around US$1 to ₦160 against US$ 1 to ₦ 387 in the third quarter of 2020.

Composite DARII Computation for both Communities

The composite DARII values were calculated using equation (3). The result shown in Table 3 conforms to prior expectations given our previous interview results that showed that all attributes finally included in this survey are important. This is evidenced by DARII >0.5 for all attributes considered. However, to maintain model parsimony, not all of these important attributes can be included in a CE model. Previous CE studies did not report how this problem can be resolved quantitatively at the pre-design stage. The few studies that attempted to address this problem use a qualitative procedure, which allows surveying only limited opinions via interviews (Coast & Horrocks, 2007; Kløjgaard et al., 2012). Applying a composite DARII technique employed in this study offers an alternative quantitative approach that allows surveying wider opinions with limited subjectivity, since it is not constrained by coding and developing themes peculiar to its qualitative counterpart.

Table 3
Design-attributes relative importance index for both communities with dimensions

Category Name	Attribute ID	Attribute Label	≤2	3	≥4	DARII	Ranking
Pollution-Related Attributes	1	Source-separation	11.1	18.7	70.2	0.78	4
	2	Disposal Method	12.6	39.9	47	0.67*	10
	3	Storage Material	10.1	22.2	67.7	0.75*	6
	4	Transport Method	32.3	36.9	30.8	0.58	14
	5	Canal Evacuation	22.7	24.7	52.5	0.65	12
	6	Air Pollution	41.4	23.7	34.8	0.57*	15
	7	Noise Pollution	48	28.3	23.7	0.51	17
Regulatory Issues	8	Separation Categories	28.8	28.8	42.4	0.62	13
	9	Designated Collector	40.9	25.8	33.3	0.57*	16
	10	Non-Payment Penalty	6.1	15.7	78.3	0.79	3
	11	Land Use	23.2	30.3	46.5	0.67*	11
	12	Franchisee Rotation	10.6	36.4	53	0.70*	9
Service Quality	13	Door-to-Door Collection	19.7	11.1	69.2	0.75*	5
	14	Pre-Collection	17.7	20.7	61.6	0.70*	8
	15	Frequency	6.6	16.2	77.3	0.81	2
	16	Schedule	17.7	23.7	58.6	0.71	7
Monetary	17	Bill Discount	2	15.7	82.3	0.82	1

**Attributes with equal magnitudes of DARII are ranked according to the percentage of respondents scoring 4 or more.*

Attribute ranking shows that a waste bill discount in compensation for household effort and cost for separating waste into designated categories is the most important attribute (Table 3). Generally, this implies that households will be encouraged to vote for improvements in solid waste management services with source-separation if they know they can get a discount on their monthly bill. In terms of importance, this attribute is followed by frequency of waste collection, and a non-payment penalty, which denotes enforcement on defaulting tenements and adoption of source-separation. The ranking continues until the least important, which for the current sample are concerns regarding noise pollution during waste collection.

Table 4 shows the ten most important design-attributes for solid waste management improvement in Lagos. This does not suggest that all ten attributes could be included in a subsequent experimental design in any subsequent CE study. Rather, to achieve model parsimony and reducing CE task complexity, most studies include a maximum of about 4 to 6 attributes (Bekker-Grob et al., 2012; Marshall et al., 2010 in Johnson et al., 2013). This could be achieved with minimal subjectivity on the researcher's part using DARII. However, as important as these findings are, a composite DARII might not make much sense when applied to heterogeneous groups. This is because the magnitude of DARII may not reflect the degree of attributes' preferences within groups. One feasible way to disentangle this is through the exploration of possible differences in households' perceived relevance of attributes across sub-samples. This approach is suitable when an affected population is clustered or stratified by some characteristics. This is the main weakness of the composite DARII, so long as it is true that $\mathrm{D\ddot{A}RII}_{\forall \mathrm{A_i}} \not\equiv \mathrm{D\ddot{A}RII}_{\forall \mathrm{A_i}}$ and both are distinct from $\mathrm{CDARII}_{\forall \mathrm{A_i}}$. Therefore, a realistic alternative under that scenario is to separately compute $D\ddot{A}RII_{\forall A_i}$ and $D\ddot{A}RII_{\forall A_i}$ as shown in equations (4) and (5).

Table 4
Design-attributes relative importance index for both communities

Design−Attribute Label	≤2	3	≥4	DARII	Ranking
Waste Bill Discount	2	15.7	82.3	0.82	1
Frequency	6.6	16.2	77.3	0.81	2
Non-Payment Penalty	6.1	15.7	78.3	0.79	3
Source-separation	11.1	18.7	70.2	0.78	4
Door-to-Door Collection	19.7	11.1	69.2	0.75*	5
Storage Material	10.1	22.2	67.7	0.75*	6
Schedule	17.7	23.7	58.6	0.71	7
Pre-Collection	17.7	20.7	61.6	0.70*	8
Franchisee Rotation	10.6	36.4	53	0.70*	9
Disposal Method	12.6	39.9	47	0.67*	10

**Attributes with equal magnitudes of DARII are ranked according to the percentage of respondents scoring 4 or more.*

Since differentiated markets exist for low-income and high-income communities (Adepitan, 2010), we needed to examine whether pre-design ranking of attributes remain the same across sub-groups. For this case, we assumed that the same underlying choice-determining attributes in CE for both strata would be too restrictive and that imposition could create a problem of attribute non-attendance. This is because although respondents face the same set of attributes, on average, preference varies across groups and leads to including design attributes that may be preferred only by a market segment. The composite DARII is only appropriate for homogeneous samples (Adam et al., 2013).

To justify this stance, we used the independent-samples t-test to inferentially test the potential for significant differences in the relative importance rating of design attributes across the two strata of affluent and poor respondents. The result obtained is shown in Table 5. The result confirms that the market segment within which respondents belong significantly influences their perceived relative importance of solid waste management service attributes. This is evident by the statistical significance of the mean-difference scores of attributes across both segments of the market. In addition, we used effect size based on 'Eta squared' to provide a glimpse of the magnitude of percentage variance in the perceived rating of the importance of attributes induced by the differences in the market segment designation of respondents.

Table 5
Effect of market segment designation on perceived importance of attributes

Attributes	t-test for Equality of Means		Effect Size (% Eta^2)
	Mean Difference	t-Statistic	
Source-separation	0.330	2.297**	2.6
Disposal Method	0.892	7.803***	23.9
Storage Material	0.399	3.607***	6.3
Transport Method	0.521	3.115***	4.7
Canal Evacuation	1.068	6.568***	18.2
Air Pollution	0.035	0.191	0
Noise Pollution	0.987	6.321***	17.2
Separation Categories	0.208	1.230	0.8
Designated Collector	0.359	2.267**	2.6
Non-Payment Penalty	0.806	7.474***	22.5
Land Use	0.801	5.170***	12.3
Franchisee Rotation	0.604	5.285***	12.5
Door-to-Door Collection	0.894	5.206***	12.1
Pre-Collection	0.582	3.603***	6.2
Frequency	0.374	2.974***	4.3
Schedule	1.515	12.04***	42.5
Bill Discount	0.544	5.503***	13.4

*** *and* ** *respectively denote statistical significance at 1% and 5% levels.*

The interpretation of Eta^2 is based on the explanations provided by Cohen (1988), where a percentage variation above 14% is perceived to constitute a large effect of variation in perceived importance due to the difference in respondents' designation of market segment. Based on this indicator, service attributes that include disposal method, canal evacuation, noise pollution, non-payment penalty, and waste collection schedule were largely rated differently across market segments. This suggests a further examination of DARII for each of the market segments.

Comparison of DARII across Poor and Affluent Communities

CE studies such as Naz and Naz (2005) were cautious regarding the existence of sub-markets for the same commodity. Yet a sizeable number of CE studies have attempted comparing agents' utility for certain commodities or contracts across different strata of respondents, assuming the same set of relevant design-attributes (Birol et al., 2009; Christiadi and Cushing, 2007). These studies did not consider that each stratum might, on average, hold different relative importance ratings for attributes. The difference in priorities for design attributes might result in scenarios where a portion of the sample is forced to make choices based on relatively less important attributes. One known consequence of omitting a relevant explanatory variable in a regression model is biased estimates of parameters (Studenmund, 2005). An earlier pre-design computation of DARII for sub-groups could help detect this. Tables 5 and 6 exemplify the case for the two major strata (poor and affluent neighborhoods) in Lagos state solid waste management services provision. Respondents were presented with the same questionnaire containing a similar ordering of attributes to avoid ordering effect.

Ranking of attributes based on DARII in Table 6 and Table 7 are similar, but not the same. The attributes most preferred by the two sub-groups (Tables 6 and 7) are also different from the ones obtained under composite DARII (Table 4). This indicates that $\ddot{DARII}_{\forall A_i} \neq \ddot{DARII}_{\forall A_i} \neq CDARII_{\forall A_i}$. Two important conclusions are implied by this result. First, since $\ddot{DARII}_{\forall A_i} \neq \ddot{DARII}_{\forall A_i}$, we may conclude that design-attribute preferences in addition to the design-attribute subset deemed most preferred varies across-groups. Secondly, the design-attribute sub-set deemed most preferred within each sub-group is not the same as that obtained in the composite case. For instance, in an extreme case, there are findings that the *evacuation of waste from canal* and *land use,* which were all not in Table 4 (composite DARII), turned out to be among the top ten important attributes in different sub-groups (Tables 6 and 7). Furthermore, pre-collection and door-to-door collection services, which are both in Table 4, now seem to be mutually exclusive between Table 6 and Table 7, respectively. This conforms to our prior expectation because earlier interviews with stakeholders revealed that road accessibility is a problem in the urban slum

Table 6
DARII in affluent communities

ID	Design−Attribute Label	≤2	3	≥4	DARII	Ranking
15	Frequency	8.2	9.2	82.7	0.84*	1
13	Door-to-Door Collection	8.2	12.2	79.6	0.84*	2
17	Bill Discount	4.1	27.6	68.4	0.76	3
1	Waste Segregation	8.2	27.6	64.3	0.74*	4
10	Default Enforcement	18.4	34.7	46.9	0.74*	5
3	Storage Material	11.2	22.4	66.3	0.66	6
16	Schedule	17.3	40.8	41.8	0.65	7
12	Franchisee Rotation	16.3	49	34.7	0.63	8
8	Separation Categories	26.5	42.9	30.6	0.59	9
11	Land Use	28.6	46.9	24.5	0.58	10

**Attributes with equal magnitudes of DARII are ranked according to the percentage of respondents scoring 4 or more.*

Table 7
DARII in poor communities

ID	Design−Attribute Label	≤2	3	≥4	DARII	Ranking
17	Bill Discount	0	4	96	0.87	1
14	Pre-Collection	1	3	96	0.85	2
10	Default Enforcement	1	9	90	0.84*	3
3	Storage Material	2	10	88	0.84*	4
1	Waste Segregation	14	10	76	0.82	5
5	Canal Evacuation	5	19	76	0.78	6
16	Schedule	18	7	75	0.77*	7
2	Disposal Method	3	25	72	0.77*	8
15	Frequency	5	23	72	0.77*	9
12	Franchisee Rotation	5	24	71	0.76	10

**Attributes with equal magnitudes of DARII are ranked according to the percentage of respondents scoring 4 or more.*

areas of Lagos. This finding supports assertions that no specific waste management strategy is ideal, even for regions within the same city (Coffey and Coad, 2010; Imam et al., 2008).

It is clear that attributes selection for experimental design based on a qualitative technique has attributable complications that will not permit access to large samples. Such complications include difficulties in coding and developing appropriate themes. While this could be managed by adopting a quantitative technique such as DARII, caution must be taken to understand the composition of the target population. Although we only require within group DARII for homogenous populations or markets, such computation might not be as obvious in a heterogeneous market. In these cases, both within-group and between-group DARII would be required for each market segment, as we demonstrated for the solid

waste management service market in Lagos. If the same set of attributes were designed for all respondents in a heterogeneous market, the CE result might generate biased welfare estimates. This is because, as proven in this study, preferences for design-attributes vary across groups.

CONCLUSION

Our study was motivated by the quest for a less researcher-subjective approach that could be adopted to determine relevant design-attributes that allows access to a large sample at the pre-design stage of CE, while at the same time limiting computational complications. This is aimed at reducing attribute non-attendance at the post-design stage of CE analysis in economic valuation. In order to achieve this, we adopted the relative importance (DARII) computation method. Explanations on the compatibility of DARII to the goals of CE were presented, including how it could be applied. We provided an example on households' pre-design perceived relevance of solid waste management service provision for the case of a market with differentiated services characterised by two segments. The result was found to support a prior interview outcome on the importance of included attributes. This was evidenced by DARII values greater than 0.5 for all attributes.

Our findings also suggest that DARII had the advantage of providing information about the existence or non-existence of segmented markets for consideration in estimating economic value. This is important to explore, especially when the target population is stratified into sub-groups, where prices and other attributes of the service are usually not the same in sub-markets for similar but differentiated goods. Service provision was known to differ slightly across affluent neighborhoods and urban slum areas in prior interview responses (Adam et al., 2015). The key factor noted to be responsible for this was inadequate availability of accessible roads in urban-slum areas populated by the poor relative to the urban-affluent areas. We found that attributes desired in both markets were ranked differently based on varying values of DARII across groups. In addition, certain attributes were mutually exclusive, relevant only in one market, but not both. We further used the independent sample t-test to inferentially test the statistical significance of the difference in DARII value. The mean difference of the ratings was found to be statistically significant. This denotes the presence of segmented markets for solid waste management service provision in Lagos. Therefore, the DARII for each market differs from results assuming homogeneity from the pool response, which we dubbed the composite DARII.

Based on the above exposition on the importance of DARII, we suggest future studies to compute this index for all potential design-attributes obtained through a literature review and interviews. This will be required especially when design-attributes are large. In those cases, researchers' subjectivity would be reduced in prioritising what subset of important

attributes to include in experimental design for CE. If attributes held most important from respondents' purview are selected, responses to CE choice tasks will be genuinely based on trade-offs rather than randomness. This will reduce the risk of observing attribute non-attendance, which has the undesirable effect of biasing welfare estimates. As evidenced in this study, researchers working on stratified or clustered target populations should compute DARII for each sub-group. If attributes ranking based on computed DARII are not the same across groups, especially when the difference between the ratings are statistically different across groups, then imposing the same design as done by some existing studies will be too restrictive.

ACKNOWLEDGEMENT

The authors thank Universiti Putra Malaysia for supporting the publication of this research through the Universiti Putra Malaysia GB-IPB Grant (Vote GP-IPB/ 2017/9542301).

REFERENCES

Adam, S. U., Shamsudin, M. N., Sidique, F. S., Abdul Rahim, K., & Radam, A. (2013). Attribute prioritization in choice experiment pre-design: Suggested method and application to solid waste management service improvement. *Journal of Energy Technologies and Policy, 3*(11), 291-298.

Adam, S. U., Shamsudin, M. N., Sidique, S. F., Abdul, R. K., & Radam, A. (2015). Determinants of privatized solid waste management service provision in Lagos. *Journal of Environmental Planning and Management*, *58(*10), 1804-1826. doi:10.1080/09640568.2014.962126

Adamowicz, W., Louviere, J., & Williams, M. (1994). Combining revealed and stated preference methods for valuing environmental amenities. *Journal of Environmental Economics and Management, 26*(3), 271-292. doi:10.1006/jeem.1994.1017

Adepitan, A. (2010). *Waste management in Nigeria; Lagos state model (1999-2009).* Lagos, Nigeria: Jimsif Limited.

Afroz, R., & Masud, M. M. (2011). Using a contingent valuation approach for improved solid waste management facility: Evidence from Kuala Lumpur, Malaysia . *Waste Management, 31(4)*, 800–808. doi:10.1016/j.wasman.2010.10.028

Afroz, R., Hanaki, K., & Hasegawa-Kurisu, K. (2009). Willingness to pay for waste management improvement in Dhaka city, Bangladesh. *Journal of Environmental Management, 90*(1), 492-503. doi:10.1016/j.jenvman.2007.12.012

Alagabi, A. A., Abdul-Majid, A., Rosemaliza, A. R. (2017). Attribute prioritization in discrete choice experiment: Challenges and suggested approach in a study on Malaysian Islamic Finance talent job choice. *International Journal of Advances in Management and Economics, 6*(5), 54-59.

Alemu, M. H., Mørkbak, M. R., Olsen, S. B., & Jensen, C. L., (2013). Attending to the reasons for attribute non-attendance in choice experiments. *Environmental Resource Economics 54*(3), 333–359. doi:10.1007/s10640-012-9597-8

Andi. (2006). The importance and allocation of risks in Indonesian construction projects. *Construction Management and Economics*, *24*(1), 69-80. doi:10.1080/01446190500310338

Aziz, R. F. (2013). Ranking of delay factors in construction projects after Egyptian revolution. *Alexandria Engineering Journal 52*(3), 387-406. doi:10.1016/j.aej.2013.03.002

Bari, N. A. A., Yusuff, R., Ismail, N., Jaapar, A., & Ahmad, R. (2012). Factors influencing the construction cost of industrialised building system (IBS) projects. *Procedia - Social and Behavioral Sciences 35*, 689 – 696. doi:10.1016/j.sbspro.2012.02.138

Basili, M., Di Matteo, M., & Ferrini, S. (2006). Analysing demand for environmental quality: A willingness to pay/accept study in the province of Siena (Italy). *Waste Management*, *26*(3), 209–219. doi:10.1016/j.wasman.2004.12.027

Basiru, H. A., Yacob, M. R., Radam, A., and AbdManaf, F. (2017). Design-attributes relative importance index (DARII) analysis for improve solid waste collection services among households in Kano Metropolis, North-Western, Nigeria. *IOSR Journal of Humanities and Social Science*, *22*(4), 104-111. doi:10.9790/0837-220405104111

Bateman, I. J., Carson, R. T., Day, B., Hanemann, M., Hanley, N., Hett, T., … & Swanson, J. (Eds.) (2002). *Economic valuation with stated preference pechniques: A manual.* Cheltenham, United Kingdom: Edward Elgar.

Birol, E., Das, S., & Bhattacharya, N. R. (2009). Estimating the value of improved wastewater treatment: The case of River Ganga, India. *Environmental Economy and Policy Research Discussion Paper Series, 43*, 1-20. doi:10.1016/j.jenvman.2010.05.008

Blamey, R., Gordon, J., & Chapman, R. (1999). Choice modelling: Assessing the environmental values of water supply options. *Australian Journal of Agricultural and Resource Economics, 43*(3), 337–357. doi:10.1111/1467-8489.00083

Caplan, A. J., Grijalva, T. C., & Jakus, P. M. (2002). Waste not or want not? A contingent ranking analysis of curbside waste disposal options. *Ecological Economics, 43*(2-3), 185–197. doi:10.1016/s0921-8009(02)00210-0

Carlsson, F., & Martinsson, P. (2008). Does it matter when a power outage occurs? — A choice experiment study on the willingness to pay to avoid power outages. *Energy Economics, 30*(3), 1232–1245. doi:10.1016/j.eneco.2007.04.001

Chan, D. W. M., & Kumaraswamy, M. M. (1997). A comparative study of causes of time overruns in Hong Kong construction projects. *International Journal of Project Management, 15*(1), 55-63. doi:10.1016/s0263-7863(96)00039-7

Christiadi, & Cushing, B. (2007, March 29-31). Conditional logit, IIA, and alternatives for estimating models of interstate migration. In *46th Annual Meeting of the Southern Regional Science Association*, (pp. 1-29). Charleston, South Carolina.

Christie, M., Hanley, N., Murphy, K., Wright, R., & Hyde, T. (2006). Valuing the diversity of biodiversity. *Ecological Economics, 58*(2), 304–317. doi:10.1016/j.ecolecon.2005.07.034

Coast, J., & Horrocks, S. (2007). Developing attributes and levels for discrete choice experiments using qualitative methods. *Journal of Health Services Research & Policy 12*(1), 25–30. doi:10.1258/135581907779497602

Coffey, M., & Coad, A. (2010). *Collection of municipal solid waste in developing countries.* Malta, Europe: Gutenberg Press.

Das, S., Ekin, B., and Bhattacharya, N. R. (2010). Informing efficient solid waste management to improve local environmental quality and public health in West Bengal, India. In J. Bennett, & E. Birol (Ed.), *Choice experiments in developing countries; Implementation, challenges and policy implication* (pp. 171-185). Massachusetts, USA: Edward Elgar.

De Bekker-Grob, E. W., Ryan, M., & Gerard, K. (2012). Discrete choice experiments in health economics: A review of he literature. *Health Economics, 21*(2), 145–172. doi:10.1002/hec.1697

Dibb, S., & Simkin, L. (2009). Bridging the segmentation theory/practice divide. *Journal of Marketing Management, 25*(3), 219–225. doi:10.1362/026725709X429728

El-Sayegh, S. M. (2008). Risk assessment and allocation in the UAE construction industry. *International Journal of Project Management 26*(4), 431–438. doi:10.1016/j.ijproman.2007.07.004

Hanley, N., Wright, R. E., & Adamowicz, V. (1998). Using choice experiments to value the environment. *Environmental and Resource Economics 11*(3–4), 413–428.

Hensher, D. A., Rose, J. M., & Greene, W. H. (2005). *Applied choice analysis: A primer*. Cambridge, England: Cambridge University Press.

Hess, S. (2012, January 22-26) Impact of unimportant attribute in stated choice surveys. In *Transportation Research board 9^{1st} Annual Meeting* (pp. 1-13). Washington, USA.

Hess, S. (2014) Impact of unimportant attributes in stated choice surveys. *European Journal of Transport and Infrastructure Research*, *14*(4), 349 - 361. doi:10.18757/ejtir.2014.14.4.3041

Hess, S., & Hensher, D. A. (2010). Using conditioning on observed choices to retrieve individual-specific attribute processing strategies. *Transportation Research Part B: Methodological, 44*(6), 781-790. doi:10.1016/j.trb.2009.12.001

Hwang, B.-G., Zhao, X., & Gay, M. J. (2013). Public private partnership projects in Singapore: Factors, critical risks and preferred risk allocation from the perspective of contractors. *International Journal of Project Management, 31*(3), 424–433. doi:10.1016/j.ijproman.2012.08.003

Imam, A., Mohammed, B., Wilson, D., & Cheeseman, C. (2008). Country Report: Solid waste management in Abuja, Nigeria. *Waste Management , 28*(2), 468–472. doi:10.1016/j.wasman.2007.01.006

Jin J., Wang Z., & Ran S. (2006). Solid waste management in Macao: Practices and challenges

Waste Management, *26*(9), 1045-1051. doi:10.1016/j.wasman.2005.08.006

Johnson, F. R., Lancsar, E., Marshall, D., Kilambi, V., Muhlbacher, A., Regier, D. A., ... & Bridges, J. F. P. (2013). Constructing experimental designs for discrete-choice experiments: Report of the ISPOR conjoint analysis experimental design good research practices task force. *Value in Health, 16*(1), 3-13. doi:10.1016/j.jval.2012.08.2223

Jones, S., Rees, L., Hall, D., & Tang, A. (2005, December 5-7). Using market segmentation theory to select target markets for sun protection campaigns. In *Proceedings for the ANZMAC Conference* (pp. 144-149). Fremantle, Australia.

Kaffashi, S, Shamsudin, M.N., Sidique, S. F., Bazrbachi, A., Radam, A. Abdul Rahim, K., Adam, S. U. (2016) Choice experiment attributes selection: Problems and approaches in a modal shift study in Klang Valley, Malaysia. *Asian Social Science*, *12*(1), 75-83. doi:10.5539/ass.v12n1p75

Kangari, R. (1995). Risk management perceptions and trends of US construction. *Journal of Construction Engineering and Management, 121*(4), 422-429. doi:10.1061/(asce)0733-9364(1995)121:4(422)

Karousakis, K., & Birol, E. (2008). Investigating household preferences for kerbside recycling services in London: A choice experiment approach. *Journal of Environmental Management*, *88*(4), 1099–1108. doi:10.1016/j.jenvman.2007.05.015

Kartam, A. N., & Kartam, A. S. (2001). Risk and its management in the Kuwaiti construction industry: A contractors' perspective. *International Journal of Project Management, 19*(6), 325-335. doi:10.1016/s0263-7863(00)00014-4

Kløjgaard, M. E., Bech, M., & Søgaard, R. (2012). Designing a stated choice experiment : The value of a qualitative process. *Journal of Choice Modeling 5*(2), 1–18. doi:10.1016/s1755-5345(13)70050-2

Kometa, S. T., Olomolaiye, P. O., & Harris, F. C. (1994). Attributes of UK construction clients influencing project consultants' performance. *Construction Management and Economics, 12*(5), 433-443. doi:10.1080/01446199400000053

Lancaster, K. J. (1966). A new approach to consumer theory. *Journal of Political Economy, 74*(2)*,* 132–157. doi:10.1086/259131

Leithead, A. (2017). The city that won't stopp growing; How can Lagos cope with its spiraling population. *British Broadcasting Corporation (BBC).* Retrieved August 21, from https://www.bbc.co.uk/news/resources/idt-sh/lagos

Louviere, J. J., Pihlens, D., & Carson, R. (2011). Design of discrete choice experiments: A discussion of issues that matter in future applied research. *Journal of Choice Modelling, 4*(1), 1-8. doi:10.1016/s1755-5345(13)70016-2

Mangham, L. J., Hanson, K., & McPake, B. (2009). How to do (or not to do) ... Designing a discrete choice experiment for application in a low-income country. *Health Policy and Planning, 24*(2), 151–158. doi:10.1093/heapol/czn047

Naz, A. C., & Naz, M. T. (2005). *Modeling choices for ecological solid waste management in suburban municipalities: User fees in Tuba, Philippines.* Tanglin, Singapore: Economy and Environment Program for Southeast Asia.

Olukanni, D. O., & Nwafor, C. O. (2019). Public-private sector involvement in providingeEfficient solid waste management services in Nigeria. *Recycling, 4*(2), 1-9. doi:10.3390/recycling4020019

Othman J. (2007) Economic valuation of household preference for solid waste management in Malaysia: a choice modeling approach. *International Journal of Management Studies*, *14*(1), 189-212

Pek, C. K., & Jamal, O. (2011). A choice experiment analysis for solid waste disposal option: A case study in Malaysia. *Journal of Environmental Management*, *92*(11), 2993–3001. doi:10.1016/j.jenvman.2011.07.013

Ramanathan, C., Narayanan, S., & Idrus, A. B. (2012b). Construction delays causing risks on time and cost – a critical review. *Australasian Journal of Construction Economics and Building, 12*(1), 37-57. doi:10.5130/ajceb.v12i1.2330

Smith, R. W. (1956). Product differenciation and market segmentation as alternative marketing strategies. *Journal of Marketing, 21*(1), 3-8. doi:10.1177/002224295602100102

Studenmund, A. H. (2001). *Using econometrics: A practical guide* (4th Ed.). Boston, Massachusetts: Addison-Wesley.

Wind, Y. (1978). Issues and advances in segmentation research. *Journal of Marketing Research*, *15*(3), 317-337. doi:10.1177/002224377801500302

REFEREES FOR THE PERTANIKA

PERTANIKA JOURNAL OF SCIENCE AND TECHNOLOGY

VOL. 28 (S2) 2020

The Editorial Board of the Pertanika Journal of Science and Technology wishes to thank the

Ahmad Sabry
(UniKL, Malaysia)

Ashraf K. Nazir
(Tanta University, Egypt)

Aweng A. L. Eh Rak
(UMK, Malaysia)

Chan Chow Khuen
(UM, Malaysia)

Chew Bee Lynn
(USM, Malaysia)

Daljit Singh A/L Karam Singh
(UPM, Malaysia)

Daniel Klapper
(Humboldt University Berlin, Germany)

Eida Nadirah Roslin
(UniKL, Malaysia)

Farah Nadia Mohd Padzil
(UPM, Malaysia)

Hafiz Rashidi B Harun @ Ramli
(UPM, Malaysia)

Hairol Nizam bin Mohd Shah
(UTeM, Malaysia)

Hassan Ashktorab
(Howard University College of Medicine, Washington)

Herryawan Ryadi Eziwar Dyari
(UKM, Malaysia)

Imane Kouadri
(University of Guelma, Algeria)

Jahwarhar Izuan Abdul Rashid
(UPNM, Malaysia)

Jia-Hong Kuo
(National United University, Taiwan)

Junhua Zhang
(China National Rice Research Institute, Zhejiang, China)

Khairul Nizar Ismail
(UNIMAP, Malaysia)

Lai Chin Wei
(UM, Malaysia)

Liew Rock Keey
(UMT, Malaysia)

Liew Sook Yee
(UM, Malaysia)

Lim Yat Yuen
(UM, Malaysia)

Lim Yat Yuen
(UM, Malaysia)

Loh Su Peng
(UPM, Malaysia)

Mardiana Mohd. Ashaari
(IIUM, Malaysia)

Mas Rina Mustaffa
(UPM, Malaysia)

Mior Ahmad Khushairi bin Mohd Zahari
(UMP, Malaysia)

Mohamad Helmi Hidthiir
(UUM, Malaysia)

Mohd Nizar Hamidon
(UPM, Malaysia)

Mohd Nor Faiz Norrrahim
(UPNM, Malaysia)

Mohd Shahneel bin Saharudin
(UniKL, Malaysia)

Mohd Termizi Yusof
(UPM, Malaysia)

Muhammad Fauzi Daud
(UniKL, Malaysia)

Muhammad Moniruzzaman
(UTP, Malaysia)

Murni Marlina Abd Karim
(UPM, Malaysia)

Nasri Sulaiman
(UPM, Malaysia)

Nazlina Haiza Mohd Yasin
(UKM, Malaysia)

Nazrul Anuar Nayan
(UKM, Malaysia)

Ng Siew Cheok
(UM, Malaysia)

Nor Azman Kasan
(UMT, Malaysia)

Nor'aini Abdul Rahman
(UPM, Malaysia)

Norhisham Razi
(UPM, Malaysia)

Norkhairunnisa Mazlan
(UPM, Malaysia)

Nur Fatihah Mohd Yusuf
(UPM, Malaysia)

Nurina Anuar
(UKM, Malaysia)

Nurul Ain binti Mohd Said
(UTeM, Malaysia)

Nurul Iman Aminudin
(IIUM, Malaysia)

P. Susthitha Menon
(UKM, Malaysia)

Ridhwan Jumaidin
(UTEM, Malaysia)

Rifqi Irzuan Abdul Jalal
(UPM, Malaysia)

Saleha Shamsudin
(UNIMAP, Malaysia)

Salih Ökten
(Kirikkale University, Turkey)

Sarah Abdul Razak
(UM, Malaysia)

Siti Efliza Ashari
(UPM, Malaysia)

Soheli Farhana
(UniKL, Malaysia)

Soon Jan Jan
(UUM, Malaysia)

Suraya Mohammad
(UniKL, Malaysia)

Syahida Ahmad
(UPM, Malaysia)

Syamsiah Mashohor
(UPM, Malaysia)

Takayuki Tsukegi
(Kanazawa Institute of Technology Japan, Japan)

Teh Ooi Kock
(Hokkaido University, Japan)

Toshinari Maeda
(Kyushu Institute of Technology, Japan)

Wan Norhidayah Wan Mohammad
(UPM, Malaysia)

Zulfahmi Ali Rahman
(UKM, Malaysia)

IIUM	- International Islamic University Malaysia
UKM	- Universiti Kebangsaan Malaysia
UM	- Universiti Malaya
UMK	- Universiti Malaysia Kelantan
UMP	- Univiersiti Malaysia Pahang
UMT	- Universiti Malaysia Terengganu
UniKL	- Universiti Kuala Lumpur
UNIMAP	- Universiti Malaysia Perlis
UPM	- Universiti Putra Malaysia
UPNM	- Universiti Pertahanan National Malaysia
USM	- Universiti Sains Malaysia
UTeM	- Universiti Teknikal Malaysia Melaka
UTP	- Universiti Teknologi PETRONAS
UUM	- Universiti Utara Malaysia

While every effort has been made to include a complete list of referees for the period stated above, however if any name(s) have been omitted unintentionally or spelt incorrectly, please notify the Chief Executive Editor, *Pertanika* Journals at executive_editor.pertanika@upm.edu.my

Any inclusion or exclusion of name(s) on this page does not commit the *Pertanika* Editorial Office, nor the UPM Press or the University to provide any liability for whatsoever reason.

Pertanika Journals

Our goal is to bring high-quality research to the widest possible audience

INSTRUCTIONS TO AUTHORS

(SPECIAL ISSUES)
(Manuscript Preparation & Submission Guide)

Revised: November 2020

Please read the *Pertanika* guidelines and follow these instructions carefully. The Chief Executive Editor reserves the right to return manuscripts that are not prepared in accordance with these guidelines.

MANUSCRIPT PREPARATION

Manuscript Types

Pertanika accepts submission of regular articles for peer-review.

Regular article

Regular article is a full-length original empirical investigation, consisting of introduction, materials and methods,results and discussions, conclusions. Original research work should present new and significant findings that contribute to the advancement of the research area. Analysis and Discussion must be supported with relevant references.

Size: Generally, each manuscript is **not to exceed 6000 words** (excluding the abstract, references, tables, and/or figures)**,** a maximum of **80 references**, and **an abstract of less than 250 words.**

Language Accuracy

Pertanika **emphasises** on the linguistic accuracy of every manuscript published. Articles must be in **English** and they must be competently written and presented in clear and concise grammatical English. Contributors are strongly advised to have the manuscript checked by a colleague with ample experience in writing English manuscripts or a competent English language editor.

Author(s) **may be required to provide a certificate** confirming that their manuscripts have been adequately edited. **All editing costs must be borne by the author(s)**.

Linguistically hopeless manuscripts will be rejected straightaway (e.g., when the language is so poor that one cannot be sure of what the authors are really trying to say). This process, taken by authors before submission, will greatly facilitate reviewing, and thus, publication.

Similarity Index

All articles received must undergo the initial screening for originality before being sent for peer-review. The Guest Editor should check all the manuscripts for possible plagiarism using Turn-It-In before sending them out for review. *Pertanika* does not accept any article with similarity index **exceeding 20%.**

PERTANIKA JOURNALS

MANUSCRIPT FORMAT

The paper should be submitted in one-column format with 1.5 line spacing throughout. Authors are advised to use Times New Roman 12-point font and *MS Word* format.

1. Manuscript Structure

The manuscripts, in general, should be organised in the following order:

- **Page 1:** ***Running title***

This page should **only** contain the running title of your paper. The running title is an abbreviated title used as the running head on every page of the manuscript. The running title **should not exceed 60 characters, counting letters and spaces.**

- **Page 2:** ***Author(s) and Corresponding author's information***

General information: This page should contain the **full title** of your paper **not exceeding 25 words**, with the name(s) of all the authors, institutions and corresponding author's name, institution and full address (Street address, telephone number (including extension), handphone number, and e-mail address) for editorial correspondence. **The corresponding author must be clearly indicated with a superscripted asterisk symbol (*).**

Author's name: The names of the authors should be named **in full without academic titles.** For Asian (Chinese, Korean, Japanese, Vietnamese), please write first name and middle name before surname (family name). The last name in the sequence is considered the surname.

Authors' addresses: Multiple authors with different addresses must indicate their respective addresses separately by superscript numbers.

Tables/figures list: A **list** of the number of **black and white/colour figures and tables** should also be indicated on this page. See ***"5. Figures & Photographs"*** for details.

Example (page 2):

***In vivo* Fecundity Evaluation of *Phaleria macrocarpa* Extract Supplementation in Male Adult Rats**

Sui Sien Leong[1]* and Mohamad Aziz Dollah[2]

[1]Department of Animal Sciences and Fishery, Universiti Putra Malaysia, 97008 Bintulu, Sarawak, Malaysia
[2]Department of Biomedical Sciences, Universiti Putra Malaysia, 43400 Serdang, Malaysia

leongsuisien@upm.edu.my (Sui Sien Leong), Contact number
azizdollah@gmail.com (Mohamad Aziz Dollah), Contact number
**Corresponding author*

List of Table/Figure:
Table 1.
Figure 1.

- **Page 3:** ***Abstract***

This page should **repeat** the **full title** of your paper with only the **Abstract**, usually in one paragraph and **Keywords.**

Keywords: **Not more than 8 keywords in alphabetical order** must be provided to describe the content of the manuscript.

2. Text

A regular paper should be prepared with the headings *Introduction, Materials and Methods, Results and Discussions, Conclusions, Acknowledgements, References,* and *Supplementary data* (if any) in this order. The literature review may be part of or separated from the *Introduction*.

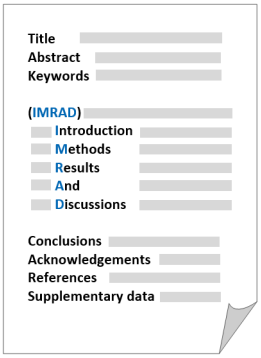

MAKE YOUR ARTICLES AS CONCISE AS POSSIBLE

Most scientific papers are prepared according to a format called IMRAD. The term represents the first letters of the words Introduction, Materials and Methods, Results, And, Discussion. It indicates a pattern or format rather than a complete list of headings or components of research papers; the missing parts of a paper are: Title, Authors, Keywords, Abstract, Conclusions, and References. Additionally, some papers include Acknowledgments and Appendices.

The Introduction explains the scope and objective of the study in the light of current knowledge on the subject; the Materials and Methods describes how the study was conducted; the Results section reports what was found in the study; and the Discussion section explains meaning and significance of the results and provides suggestions for future directions of research. The manuscript must be prepared according to the Journal's instructions to authors.

3. Levels of Heading

Level of heading	Format
1st	**LEFT, BOLD, UPPERCASE**
2nd	**Flush left, Bold, Capitalise each word**
3rd	**Bold, Capitalise each word, ending with .**
4th	***Bold italic*, Capitalise each word, ending with .**

4. Equations and Formulae

These must be set up clearly and should be typed double-spaced. Numbers identifying equations should be in square brackets and placed on the right margin of the text.

5. Tables

- All tables should be prepared in a form consistent with recent issues of *Pertanika* and should be numbered consecutively with Roman numerals (Table 1, Table 2).
- A brief title should be provided, which should be shown at the top of each table **(APA format):**

  Example: Table 1

  PVY infected Nicotiana tabacum *plants optical density in ELISA*

- Explanatory material should be given in the table legends and footnotes.
- Each table should be prepared on a new page, embedded in the manuscript.
- Authors are advised to keep backup files of all tables.

***** Please submit all tables in Microsoft word format only, because tables submitted as image data cannot be edited for publication and are usually in low-resolution.***

6. Figures & Photographs

- Submit an **original** figure or photograph.
- Line drawings must be clear, with a high black and white contrast.

- Each figure or photograph should be prepared on a new page, embedded in the manuscript for reviewing to keep the file of the manuscript under 5 MB.
- These should be numbered consecutively with Roman numerals (Figure 1, Figure 2).
- Provide a brief title, which should be shown at the bottom of each table **(APA format):**

Example: Figure 1. PVY-infected *in vitro* callus of *Nicotiana tabacum*

- If a Figure has been previously published, acknowledge the original source, and submit written permission from the copyright holder to reproduce the material.
- Authors are advised to keep backup files of all figures.

***** Figures or photographs must also be submitted separately as TIFF or JPEG, because figures or photographs submitted in low-resolution embedded in the manuscript cannot be accepted for publication. For electronic figures, create your figures using applications that are capable of preparing high-resolution TIFF files.***

7. Acknowledgement

Any individuals and entities who have contributed to the research should be acknowledged appropriately.

8. References

- References begin on their own page and are listed in alphabetical order by the first author's last name. Only references cited within the text should be included. All references should be in 12-point font and double-spaced.
- If a **Digital Object Identifier (DOI)** is listed on a print or electronic source, it is required to include the **DOI** in the reference list. Use **Crossref** to find a **DOI** using author and title information.

NOTE: When formatting your references, please follow the **APA-reference style** (6th edition) *(refer to the examples)*. Ensure that the references are strictly in the journal's prescribed style, failing which your article will **not be accepted for peer-review**. You may refer to the *Publication Manual of the American Psychological Association* for further details https://apastyle.apa.org/

Examples of reference style are given below:

Books

Books	**Insertion in Text**	**In Reference List**
Book with 1-2 authors	**Information prominent' (the author's name is within parentheses):** … (Cochrane, 2007) … Or **'Author prominent' (the author's name is outside the parentheses):** Cochrane (2007) …	Cochrane, A. (2007). *Understanding urban policy: A critical approach.* Malden, United States: Blackwell Publishing.
Book with 3 or more authors (*Pertanika*'s format)	*For all in-text references, list only the first author's family name and followed by* 'et al.' **Information prominent' (the author's name is within parentheses):** … (Seeley et al., 2011) … Or **'Author prominent' (the author's name is outside the parentheses):** Seeley et al. (2011) …	Seeley, R., VanPutte, C., Regan, J., & Russo, A. (2011). *Seeley's anatomy & physiology*. New York, United States: McGraw-Hill.

Books	Insertion in Text	In Reference List
Book with 6-7 authors	*For all in-text references, list only the first author's family name and followed by* 'et al.' **Information prominent' (the author's name is within parentheses):** … (Bulliet et al., 2011) … Or **'Author prominent' (the author's name is outside the parentheses):** Bulliet et al. (2011) …	Bulliet, R. W., Crossley, P. K., Headrick, D. R., Hirsch, S. W., Johnson, L. L., & Northrup, D. (2011). *The earth and its peoples: A global history* (5th ed.). Boston, United States: Wadsworth.
Book with more than 8 authors	*For all in-text references, list only the first author's family name and followed by* 'et al.' A recent study (Edge et al., 2011) concluded that… Or Edge et al. (2011) concluded that ….	For books with eight or more authors, please follow the guidelines for journal articles with eight or more authors.
Chapter in an edited book	**Information prominent' (the author's name is within parentheses):** … (Richards, 1997) … Or **'Author prominent' (the author's name is outside the parentheses):** Richards (1997) …	Richards, K. C. (1997). Views on globalization. In H. L. Vivaldi (Ed.), *Australia in a global world* (pp. 29-43). Sydney, Australia: Century.
e-book/online book	**Information prominent' (the author's name is within parentheses):** … (Niemann et al., 2004) … Or **'Author prominent' (the author's name is outside the parentheses):** Schiraldi (2001) …	Niemann, S., Greenstein, D., & David, D. (2004). *Helping children who are deaf: Family and community support for children who do not hear well.* Retrieved June 1, 2019, from http://www.hesperian.org/publications_download_deaf.php Schiraldi, G. R. (2001). *The post-traumatic stress disorder sourcebook: A guide to healing, recovery, and growth* [Adobe Digital Editions version]. doi:10.1036/0071393722
Editor	**Information prominent' (the author's name is within parentheses):** … (Zairi, 1999) … Or **'Author prominent' (the author's name is outside the parentheses):** Zairi (1999) …	Zairi, M. (Ed.). (1999). *Best practice: Process innovation management.* Oxford, United Kingdom: Butterworth- Heinemann.

Books	Insertion in Text	In Reference List
Several works by the same author in the same year	**Information prominent' (the author's name is within parentheses):** … (Fullan, 1996a, 1996b) … Or **'Author prominent' (the author's name is outside the parentheses):** Fullan (1996a, 1996b) …	Fullan, M. (1996a). Leadership for change. In *International handbook for educational leadership and administration.* New York, United States: Kluwer Academic. Fullan, M. (1996b). *The new meaning of educational change.* London, United Kingdom: Casell.
Several authors, different years referred to collectively in your work	**List sources alphabetically by the family name in the in-text reference in the order in which they appear in the Reference List.** The cyclical process (Carr & Kemmis, 1986; Dick, 2000) suggests…	Carr, W., & Kemmis, S. (1986). *Becoming critical: Education knowledge and action research.* London, United Kingdom: Falmer Press. Dick, B. (2000). *A beginner's guide to action research.* Retrieved June 1, 2019, from http://www.scu.edu.au/schools/gcm/ar/arp/guide.html

Journals

Journals	Insertion in Text	In Reference List
Journal article with 1-2 authors	**Information prominent' (the author's name is within parentheses):** … (Kramer & Bloggs, 2002) … Or **'Author prominent' (the author's name is outside the parentheses):** Kramer and Bloggs (2002) …	Kramer, E., & Bloggs, T. (2002). On quality in art and art therapy. *American Journal of Art Therapy*, *40*, 218-231.
Journal article with 3 or more authors (*Pertanika*'s format)	*For all in-text references, list only the first author's family name and followed by* 'et al.' **Information prominent' (the author's name is within parentheses):** … (Erlo et al., 2008) … Or **'Author prominent' (the author's name is outside the parentheses):** Erlo et al. (2008) …	Erlo, A., Ervasti, J., Kuosma, E., & Mattila, P. (2008). Evaluation of an organizational stress management program in a municipal public works organization. *Journal of Occupational Health Psychology*, *13*(1), 10-23. doi: 10.1037/1076-8998.13.1.10

Journal article with 6-7 authors	*For all in-text references, list only the first author's family name and followed by* 'et al.' **Information prominent' (the author's name is within parentheses):** … (Restouin et al., 2009) … Or **'Author prominent' (the author's name is outside the parentheses):** Restouin et al. (2009) …	Restouin, A., Aresta, S., Prébet, T., Borg, J., Badache, A., & Collette, Y. (2009). A simplified, 96-well–adapted, ATP luminescence–based motility assay. *BioTechniques, 47*, 871–875. doi:10.2144/000113250
Journal article with more than 8 or more authors	**Information prominent' (the author's name is within parentheses):** … (Steel et al., 2010) … Or **'Author prominent' (the author's name is outside the parentheses):** Steel et al. (2010) …	Steel, J., Youssef, M., Pfeifer, R., Ramirez, J. M., Probst, C., Sellei, R., ... & Pape, H. C. (2010). Health-related quality of life in patients with multiple injuries and traumatic brain injury 10+ years postinjury. *Journal of Trauma: Injury, Infection, and Critical Care, 69*(3), 523-531. doi: 10.1097/ TA.0b013e3181e90c24
Journal article with DOI	**Information prominent' (the author's name is within parentheses):** … (Shaw et al., 2005) … Or **'Author prominent' (the author's name is outside the parentheses):** Shaw et al. (2005) …	Shaw, K., O'Rourke, P., Del Mar, C., & Kenardy, J. (2005). Psychological interventions for overweight or obesity. *The Cochrane database of systematic reviews* (2). doi:10.1002/14651858.CD003818.pub2

Newspapers

Newspapers	Insertion in Text	In Reference List
Newspaper article – with an author	… (Waterford, 2007) ...	Waterford, J. (2007, May 30). Bill of rights gets it wrong. *The Canberra Times*, p. 11.
Newspaper article – without an author	… ("Internet pioneer", 2007) …	Internet pioneer to oversee network redesign. (2007, May 28). *The Canberra Times*, p. 15.
Article in a newsletter	... ("Australians and the Western Front", 2009) ...	Australians and the Western Front. (2009, November). *Ozculture newsletter*. Retrieved June 1, 2019, from http://www.cultureandrecreation.gov.au/newsletter/

Conference / Seminar Papers

Conference / Seminar Papers	Insertion in Text	In Reference List
Print – *If the paper is from a book, use the book chapter citation format. If it is from regularly published proceedings (e.g. annual), use the Journal article citation format.*	… (Edge, 1996) … Or Edge (1996) …	Edge, M. (1996). Lifetime prediction: Fact or fancy? In M. S. Koch, T. Padfield, J. S. Johnsen, & U. B. Kejser (Eds.), *Proceedings of the Conference on Research Techniques in Photographic Conservation* (pp. 97-100). Copenhagen, Denmark: Royal Danish Academy of Fine Arts.
Online	… (Tester, 2008) … Or Tester (2008) …	Tester, J. W. (2008). The future of geothermal energy as a major global energy supplier. In H. Gurgenci & A. R. Budd (Eds.), *Proceedings of the Sir Mark Oliphant International Frontiers of Science and Technology Australian Geothermal Energy Conference*. Canberra, Australia: Geoscience Australia. Retrieved June 1, 2019, from http://www.ga.gov. au/image_cache/ GA11825.pdf

Government Publications

Government Publications	Insertion in Text	In Reference List
Government as author	**First in-text reference: Spell out the full name with the abbreviation of the body.** … (Department of Finance and Administration [DOFA], 2006) … **Subsequent in-text reference/s: Use the abbreviation of the body.** … (DOFA, 2006) …	Department of Finance and Administration. (2006). Delivering Australian Government services: Managing multiple channels. Canberra, Australia: Author.
Government report - online	**First in-text reference: Spell out the full name with the abbreviation of the body.** … (Department of the Prime Minister and Cabinet [PM&C], 2008) … **Subsequent in-text reference/s: Use the abbreviation of the body.** … (PM&C, 2008) …	Department of the Prime Minister and Cabinet. (2008). *Families in Australia: 2008.* Retrieved June 1, 2019, from http://www .....

9. General Guidelines

Abbreviations: Define alphabetically, other than abbreviations that can be used without definition. Words or phrases that are abbreviated in the *Introduction* and following text should be written out in full the first time that they appear in the text, with each abbreviated form in parenthesis. Include the common name or scientific name, or both, of animal and plant materials.

Authors' Affiliation: The primary affiliation for each author should be the institution where the majority of their work was done. If an author has subsequently moved to another institution, the current address may also be stated in the footer.

Co-Authors: The commonly accepted guideline for authorship is that one must have substantially contributed to the development of the paper and share accountability for the results. Researchers should decide who will be an author and what order they will be listed depending upon their order of importance to the study. Other contributions should be cited in the manuscript's *Acknowledgements*.

Copyright Permissions: Authors should seek necessary permissions for quotations, artwork, boxes or tables taken from other publications or other freely available sources on the Internet before submission to *Pertanika*. The acknowledgement must be given to the original source in the illustration legend, in a table footnote, or at the end of the quotation.

Footnotes: Current addresses of authors if different from heading may be inserted here.

Page Numbering: Every page of the manuscript, including the title page, references, and tables should be numbered.

Spelling: The journal uses American or British spelling and authors may follow the latest edition of the Oxford Advanced Learner's Dictionary for British spellings. Each manuscript should follow one type of spelling only.

SUBMISSION OF MANUSCRIPTS

1. **MANUSCRIPT**:

   Ensure your manuscript has followed the *Pertanika* style particularly the first three pages as explained earlier. The article should be written in a good academic style and provide an accurate and succinct description of the contents ensuring that grammar and spelling errors have been corrected before submission. It should also not exceed the suggested length.

2. **DECLARATION FORM:**

   The corresponding author has to sign a declaration form. In signing the form, authors declare that the work submitted for publication is original, previously unpublished, and not under consideration for any publication elsewhere.

Note:

COPYRIGHT FORM: Author will be asked to sign a copyright form when the paper is accepted. In signing the form, it is assumed that authors have obtained permission to use any copyrighted or previously published material. All authors must read and agree to the conditions outlined in the form and must sign the form or agree that the corresponding author can sign on their behalf. Articles cannot be published until a signed form *(original pen-to-paper signature)* has been received.

Visit our Journal's website for more details at http://www.pertanika.upm.edu.my/

ACCESS TO PUBLISHED MATERIALS

Under the Journal's open access initiative, authors can choose to download free material (via PDF link) from any of the journal issues from *Pertanika*'s website. Under "**Browse Journals**" you will see a link, "*Regular Issue*", "*Special Issue"* or "*Archives*". Here you will get access to all current and back-issues from 1978 onwards. No hard copy of journals or offprints are printed.

Visit our Journal's website at
http://www.pertanika.upm.edu.my/regular_issues.php for "Regular Issue"
http://www.pertanika.upm.edu.my/cspecial_issues.php for "Special Issue"
http://www.pertanika.upm.edu.my/journal_archives.php for "Archives"

Cellulose Nanofibers from Waste Paper and their Utilization as Reinforcement Materials in Poly((*R*)-3-Hydroxybutyrate-*co*-(*R*)-3-Hydroxyhexanoate Bionanocomposite 259
Tengku Arisyah Tengku Yasim-Anuar, Nur Sharmila Sharip, Liana Noor Megashah, Hidayah Ariffin and Nor Azlin Muhamad Nor

Nutritional Characteristics of Biochar from Pineapple Leaf Residue and Sago Waste 273
Norshidawatie Bohari, Hasmah Mohidin, Juferi Idris, Yoshito Andou, Sulaiman Man, Hushairy Saidan and Suraiya Mahdian

Static Mechanical, Thermal Stability, and Interfacial Properties of Superheated Steam Treated Oil Palm Biomass Reinforced Polypropylene Biocomposite 287
Muhammad Nazmir Mohd Warid, Tengku Arisyah Tengku Yasim-Anuar, Hidayah Ariffin, Mohd Ali Hassan, Yoshito Andou and Yoshihito Shirai

Parameters Optimization in Compression Molding of Ultra-high Molecular Weight Polyethylene/Cellulose Nanofiber Bio-nanocomposites by using Response Surface Methodology 299
Nur Sharmila Sharip, Hidayah Ariffin, Yoshito Andou, Ezyana Kamal Bahrin, Mohammad Jawaid, Paridah Md Tahir and Nor Azowa Ibrahim

Reducing Attribute Non-Attendance Risk in Choice Experiment: An application of Design Attribute Relative Importance Index for Waste Management Service Provision in Segmented Markets 317
Shehu Usman Adam, Shaufique F. Sidique and Mad Nasir Shamsudin

Cholinesterase from the Liver of *Diodon hystrix* for Detection of Metal Ions 107
Noreen Nordin, Ronaldo Ron Cletus, Mohd Khalizan Sabullah, Siti Aishah Muhammad Khalidi, Rahmath Abdulla and Siti Aqlima Ahmad

Isolation and Characterisation of Thermophilic *Bacillus licheniformis* SUNGC2 as Producer of α-Amylase from Malaysian Hot Spring 121
Marwan Jawad Msarah, Ayesha Firdose, Izyanti Ibrahim and Wan Syaidatul Aqma

Effect of Steam and Bleaching Treatment on the Characteristics of Pineapple Leaves Fibre Derived Cellulose 135
Surenthiran Gnanasekaran, Siti Nur Najihah Muslih, Jun Haslinda Shariffuddin, and Noor Ida Amalina Ahamad Nordin

Physical and Mechanical Study of Palm Oil Fuel Ash (POFA) based Geopolymer as a Stabilizer for Soft Soil 149
Isam Adnan Khasib and Nik Norsyahariati Nik Daud

Deep Learning Object Detector Using a Combination of Convolutional Neural Network (CNN) Architecture (MiniVGGNet) and Classic Object Detection Algorithm 161
Asmida Ismail, Siti Anom Ahmad, Azura Che Soh, Mohd Khair Hassan and Hazreen Haizi Harith

Integrated Braking Force Distribution for Electric Vehicle Regenerative Braking System 173
Anith Khairunnisa Ghazali, Mohd Khair Hassan, Mohd Amran Mohd Radzi and Azizan As'arry

Design and Synthesis of a New Amphipathic Cyclic Decapeptide with Rapid, Stable, and Continuous Antibacterial Effects 183
Hisham N. Farrag, Khaled Metwally, Shinya Ikeno and Tamaki Kato

Enzyme Kinetics Study for Heterogeneous System of Pretreated Kenaf Hydrolysis 197
Nur Izyan Wan Azelee, Norhafiza Nordin, Rosli Md Illias, Nor Hasmaliana Abdul Manas and Mohd Nazlee Faisal Md Ghazali

Effect of Reaction Temperature on the Growth of Carbon Nanotubes from Waste Natural Rubber Glove 217
Mohammad Adib Hazan, Syazwani Mohamad, Mohamad Amin Hamid, Shahira Liza, Md Shuhazlly Mamat, Kar Fei Chan and Yazid Yaakob

Secured Electrocardiograph (ECG) Signal Using Partially Homomorphic Encryption Technique–RSA Algorithm 231
Muhammad Umair Shaikh, Wan Azizun Wan Adnan and Siti Anom Ahmad

Dark Fermentative Biohydrogen Production from Palm oil Mill Effluent: Operation Factors and Future Progress of Biohydrogen Energy 243
Fatin Sakinah Rosman, Mohd Zulkhairi Mohd Yusoff, Mohd Rafein Zakaria, Toshinari Maeda and Mohd Ali Hassan

Pertanika Journal of Science & Technology
Vol. 28 (S2) 2020

Applied Engineering and Sciences

Preface
Hidayah Ariffin, Norhayati Ramli and Suhaidi Shafie i

Detection of Muscle Activities in the sEMG Signal by Using Frequency Features and Adaptive Decision Threshold 1
Husamuldeen Khalid Hameed, Wan Zuha Wan Hasan, Suhaidi Shafie, Siti Anom Ahmad and Haslina Jaafar and Liyana Najwa Inche Mat

Proposal of Blood Glucose Control and Exercise Therapy Support System Using Non-invasive Blood Glucose Meter 13
Ryo Takeuchi, Kazuhiko Nagao and Hiroyuki Miyamoto

Application of Ecological Indices using Macroinvertebrate Assemblages in Relation to Aquaculture Activities in Rawang Sub-basin, Selangor River, Malaysia 25
Nadeesha Dilani Hettige, Rohasliney Binti Hashim, Ahmad Bin Abas Kutty, Nor Rohaizah Binti Jamil and Zulfa Hanan Binti Ash'aari

The Construction of Plant Expression Vector harbouring *Carica Papaya* L. *WRKY* Gene in *Escherichia coli* 47
Fauziah Abu Bakar, Pavitra Paramalingam and Kamariah Hasan

Regression Equation Between Required Force and Lumbar Load of Caregiver in Supporting Standing-up Motion via Computational Musculoskeletal Simulation 59
Kodai Kitagawa, Yoshiki Nishisako, Takayuki Nagasaki, Sota Nakano, Mitsumasa Hida, Shogo Okamatsu and Chikamune Wada

Linear Regression Technique for Improvement of Feet Position Estimation during Standing Balance Using a Cane with Millimeter Wave Radar 71
Ibai Gorordo Fernandez, Kodai Kitagawa, Kawthar Abdul Rahman, Azura Che Soh, Alpha Agape Gopalai, Siti Anom Ahmad and Chikamune Wada

Acetylcholine Receptor-based Biosensor Derived from Asian Swamp Eel, *Monopterus Albus* for Heavy Metals Biomonitoring 83
Siti Aishah Muhammad Khalidi, Mohd Khalizan Sabullah, Suraya Abdul Sani, Mohd Yunus Abd Shukor, Ain Aqilah Basirun, A'aishah Abd Gafar, 'Izazy Nur Mohd Jaafar and Noreen Nordin

Profiling of Cholinesterase Extracted from The Brain Tissue of Diodon hystrix and Its Inhibition Reaction Towards Carbamates 95
Akid Haris, Noreen Nordin, Nur Azizah Mustapa, Suraya Abd. Sani, Mohd Yunus Shukor and Mohd Khalizan Sabullah

Pertanika Editorial Office, Journal Division
Office of the Deputy Vice Chancellor (R&I),
1st Floor, IDEA Tower II,
UPM-MTDC Technology Centre
Universiti Putra Malaysia
43400 UPM Serdang
Selangor Darul Ehsan
Malaysia

http://www.pertanika.upm.edu.my/
E-mail: executive_editor.pertanika@upm.edu.my
Tel: +603 9769 1622

PENERBIT UPM PRESS
http://penerbit.upm.edu.my
E-mail : penerbit@upm.edu.my
Tel : +603 9769 8855

ISSN 0128-7680